

# Polymer Gels



ACS SYMPOSIUM SERIES **833**

# Polymer Gels

## Fundamentals and Applications

**Himadri B. Bohidar**, Editor

*J. N. University*

**Paul Dubin**, Editor

*Indiana–Purdue University*

**Yoshihito Osada**, Editor

*Hokkaido University*



American Chemical Society, Washington, DC

**Polymer gels: fundamentals  
and applications.**

**Library of Congress Cataloging-in-Publication Data**

Polymer gels : fundamentals and applications / Himadri B. Bohidar, editor, Paul Dubin, editor, Yoshihito Osada, editor.

p. cm.—(ACS symposium series ; 833)

Includes bibliographical references and indexes.

ISBN 0-8412-3761-1

1. Polymer colloids—Congresses.

I. Bohidar, Himadri B. II. Dubin, Paul. III. Osada, Yoshihito. IV. American Chemical Society. Meeting. (219<sup>th</sup> : 2000 : San Francisco, Calif.). V. American Chemical Society. Division of Polymer Chemistry, Inc. VI. Series.

QD509.2.P64 P653 2002  
547.7045513—dc21

2002074706

The paper used in this publication meets the minimum requirements of American National Standard for Information Sciences—Permanence of Paper for Printed Library Materials, ANSI Z39.48–1984.

Copyright © 2003 American Chemical Society

Distributed by Oxford University Press

All Rights Reserved. Reprographic copying beyond that permitted by Sections 107 or 108 of the U.S. Copyright Act is allowed for internal use only, provided that a per-chapter fee of \$22.50 plus \$0.75 per page is paid to the Copyright Clearance Center, Inc., 222 Rosewood Drive, Danvers, MA 01923, USA. Republication or reproduction for sale of pages in this book is permitted only under license from ACS. Direct these and other permission requests to ACS Copyright Office, Publications Division, 1155 16th St., N.W., Washington, DC 20036.

The citation of trade names and/or names of manufacturers in this publication is not to be construed as an endorsement or as approval by ACS of the commercial products or services referenced herein; nor should the mere reference herein to any drawing, specification, chemical process, or other data be regarded as a license or as a conveyance of any right or permission to the holder, reader, or any other person or corporation, to manufacture, reproduce, use, or sell any patented invention or copyrighted work that may in any way be related thereto. Registered names, trademarks, etc., used in this publication, even without specific indication thereof, are not to be considered unprotected by law.

PRINTED IN THE UNITED STATES OF AMERICA

**American Chemical Society  
Library**

**1155 16th St., N.W.**

**Washington, D.C. 20036**

In Polymer Gels, Bohidar, H., et al.;  
ACS Symposium Series, American Chemical Society: Washington, DC, 2002.



# Foreword

The ACS Symposium Series was first published in 1974 to provide a mechanism for publishing symposia quickly in book form. The purpose of the series is to publish timely, comprehensive books developed from ACS sponsored symposia based on current scientific research. Occasionally, books are developed from symposia sponsored by other organizations when the topic is of keen interest to the chemistry audience.

Before agreeing to publish a book, the proposed table of contents is reviewed for appropriate and comprehensive coverage and for interest to the audience. Some papers may be excluded to better focus the book; others may be added to provide comprehensiveness. When appropriate, overview or introductory chapters are added. Drafts of chapters are peer-reviewed prior to final acceptance or rejection, and manuscripts are prepared in camera-ready format.

As a rule, only original research papers and original review papers are included in the volumes. Verbatim reproductions of previously published papers are not accepted.

## ACS Books Department

# Preface

Polymer gels, which have both solid and liquidlike properties, are a novel state of matter. Once cross-linked, either chemically or non-covalently, the polymer chains lose their individual identity and become part of a large three-dimensional interconnected network pervading through the entire solution volume. Such a system has both fluidity and elasticity, and the dynamics of such a phase is quite revealing. For physical gels, which are interconnected via noncovalent linkages, the fluidity and elasticity become a matter of the time scales of the observations relative to the lability of those interconnections. Such intriguing considerations have given rise to great activity in gel theory and experimentation, which are further motivated by the development of novel uses for polymer gels.

Gels have applications in numerous fields, including food and chemical processing, pharmaceuticals, biotechnology, agriculture, civil engineering, and electronics. Chemomechanical systems, soft actuators, drug delivery systems (DDS), permselective membranes for selective extraction, and chemical valves are examples of applications of stimuli-responsive polymer gels. Modulation of swelling forces in gels by chemical or physical stimuli enables dynamic control of the gel hydration and desirable diffusion and permeability of solutes can be thereby obtained. Because a polymer gel can absorb water up to several thousands times its original weight (depending on the chemical structure of the gel and number of charges) disposable diapers, sanitary napkins, and perfumes are everyday-life examples of the applications of highly water-absorbing hydrogels.

Considerable interest and activity exists in the application of synthetic and biological polymer gels in medicine, particularly hydrogels for biomedical applications. The bulk property of swelling is of interest for “swelling implants,” which can be implanted in a small dehydrated state via a small incision and then swell to fill a body cavity and/or to exert a controlled pressure. The wide range of biomedical applications for hydrogels can be attributed both to their satisfactory performance

upon either blood- or tissue-contact in vivo implantation and to their fabrication in a wide range of morphologies. In this book, Chapter 16 by Ravi et al. describes hydrogels as potential soft-tissue substitutes. Amphiphilic gels capable of containing active pancreatic beta cells are described by Kennedy et al. (Chapter 19); and alkylthioacrylate hydrogels prepared for possible contact lens development are covered by Mukkamala et al. in Chapter 11. The use of hydrophilic systems for drug delivery provides the motivation for the preparation of hylauronate gels by Yomota and Okada (Chapter 22), and of biodegradable insulin-releasing injectables utilized by Young Jin Kim and Sung Wan Kim (Chapter 20).

Gels can be considered to be formed of a macromolecular network consisting of a number of small cavities that are filled with the fluid. Chemical gels are cross-linked by covalent bonds, whereas physical gels are cross-linked by weak forces such as hydrogen bonds, hydrophobic, or ionic interactions or combinations of them. The formation of polymer gels can thus proceed by conventional synthesis or by physical gelation. Polymer gel synthesis is addressed here from such various perspectives. Allcock and Ambrosio (Chapter 6) describe novel gels based on radiation cross-linking of organophosphazene polymers, and gels with inorganic constituents but formed through multifunctional siloxane monomers are also discussed by Kajiwara and co-workers (Chapter 5). Hydrogels can also be formed through photocrosslinking, as shown by Kuckling et al. (Chapter 21) who prepared gels at the sub-micrometer size range.

Physical gelation processes are usually reversible and are called sol-gel transitions. An overview of physical gelation is provided by Ross-Murphy (Chapter 4) with special focus on biopolymers. Kressler and co-workers (Chapter 8) describe gelation of amphiphilic block copolymers in water. Gels with a wide range of properties result from the relaxation time scale of these physical cross-linkages, as discussed by Morishima et al. (Chapter 2), and by Tribet and co-workers (Chapter 18). Argüelles-Monal et al. (Chapter 7) present the viscoelastic behavior of physical gels from alkali-soluble chitin. That physical gelation can take place for less polar polymers also is shown by the network formation of block copolymers in nonaqueous solution presented by Spontak and co-workers in Chapter 17.

Gels, in general, are considered to be composed of heterogeneous domains from a few angstroms to several micrometers. Because of this heterogeneity and the swelling property that gives the network

motion, detailed gel structures have been difficult to visualize satisfactorily. Scattering techniques such as small-angle neutron scattering (SANS), small-angle X-ray scattering (SAXS), light scattering have been extensively employed to characterize polymer networks as discussed by Candau in 1982. The structure factors, proportional to the scattered intensity, for gels are usually discussed by classifying gels into two categories: non-ionic neutral gels and ionic gels. Here, Oppermann et al. (Chapter 3) use static light scattering to probe the spatial inhomogeneities of networks formed from both ionic and nonionic gels. Water-swelling gels can also possess hydrophobic domains creating yet another form of inhomogeneity. Such gels are the subject of the chapters by Gitsov et al. (Chapter 15), by Ravi et al. (Chapter 16), and by Kressler and co-workers (Chapter 8).

The volume of a polyelectrolyte gel is a manifestation of the competition among three osmotic pressures acting on the polymer network: positive pressure of counterions, negative pressure due to the affinity among polymers, and the rubber elasticity that keeps the network in a state of moderate expansion. The combined effect of these three pressures determines the equilibrium volume. Temperature, pH, and salt ions affect both positive and negative pressures, whereas solvent composition influences only the negative pressure. For some hydrophilic gels, the volume change is discontinuous, as observed by Tanaka in 1980. Here, Harmon and Frank (Chapter 1) describe the kinetics of LCST volume transitions in gels. Several other chapters, in addition to the contribution by Morishima and co-workers (Chapter 2), deal with polyelectrolyte gels. Kudaibergenov et al. (Chapter 10) examine the response of polyampholyte gels to electrical fields, and also the ability of these hydrogels to bind proteins. Tribet's gels arise in part from charge interactions between amphiphilic polyacids and proteins. Opperman describes the response of ionic gels to added salt.

Several contributions point to the importance of dynamic studies for the investigation of gel structure. Rheological methods are featured in the chapters by Eloundou et al. (Chapter 14) who compared gelation and vitrification of epoxyamine systems with percolation theory, and by Dutta and co-workers (Chapter 13) who offer rheological examination of physical gels. Rheology is also central to the studies by Ravi et al. (Chapter 16), who measured creep-recovery in hydrogels; and by Tribet and co-workers (Chapter 18), who used proteins to cross-link amphiphilic polyacids.

The chapters in this volume are derived from a symposium on *Polymer Gels* held by the American Chemical Society (ACS) at their Spring National Meeting in San Francisco, California, March 26–30, 2000 in which 40 authors from 10 countries contributed oral and poster presentations. Support for the travel of overseas speakers was supplied by The Petroleum Research Fund, the ACS Division of Polymer Chemistry, Inc., Rohm & Haas Company, and GelTex, Inc.

### **Himadri B. Bohidar**

School of Physical Sciences  
J. N. University  
New Delhi 11067, India

### **Paul Dubin**

Chemistry Department  
Indiana-Purdue University  
Indianapolis, IN 46202

### **Yoshihito Osada**

Division of Biological Science  
Hokkaido University  
Sapporo, Japan

# Introduction

The history of gels goes back for many centuries, probably even many millennia. Some scientists would even claim that life itself is based on gels. Their scientific study, however, is more recent, dating essentially from the work of Thomas Graham in the nineteenth century. The saying that the gel state is easier to recognize than to define still holds true today, because the term is used by different communities to describe a host of seemingly different objects. These include networks formed by long flexible polymers (e.g., neutral polymers such as poly(dimethylsiloxane), natural rubber, polyacrylamide, or polyelectrolytes such as sodium polyacrylate) cross-linked by permanent covalent bonds and containing a mobile solvent. They include as well quasi-rigid structures (agarose, caragheenan, and so on) in which the connecting struts are bundles of stiff macromolecules. The latter are frequently thermoreversible and the constituent molecules are generally of biological origin. Other gel systems are formed from smaller molecules in solution that, under appropriate conditions of temperature and composition, self-assemble into columns and thence into a three-dimensional network. A further category that is often classified among the genus gels includes arrays of molecular units undergoing fleeting associations and that therefore flow over time. Yet another category is aerogels and xerogels, in which no solvent is present in the pores. The common characteristic of all these systems is that their shear elastic modulus is several orders of magnitude smaller than their bulk modulus: This condition is met in structures where the sequence of molecules that connect cross-links is much longer than the size of the cross-links themselves. The ability of such structures to absorb large amounts of solvent makes them ideal vehicles for the storage or transport of active ingredients. Applications of gels have become extraordinarily widespread, notably in food processing, cosmetics, and paint manufacturing. Polyelectrolyte gels have been developed as superabsorbent materials in diapers and for moisture control for arid soils. Active research is being conducted into these systems for use as

decontaminants for heavy metals and organic pollutants. Recently biomedical applications have taken on immense importance, not only for soft contact lenses, eye implants or for gel chromatography, but in many other fields, such as biosensors, drug release vectors, encapsulating media, and so on.

In the 1940s and 1950s, the study of gels was dominated by the pioneering contributions of Flory, Stockmeyer, Gee, Treloar, and others who established the basic statistical concepts governing the macroscopic elastic and osmotic properties of these systems. At that time, details of the structure at a local scale could only be guessed at, with even less being known about the dynamics. Subsequent investigations by Dusek, Prins, Silberberg, and others based on a variety of techniques, such as classical light scattering or permeability measurements, demonstrated that gels are intrinsically inhomogeneous in their structure. The innovative work of Tanaka, who used quasi-elastic light scattering to study the dynamics of gels, was an important stimulus for theoreticians, notably Edwards and de Gennes, to seek a more local description of these systems. The contemporaneous development of small-angle neutron scattering (SANS) techniques with the possibility of using partial deuteration opened totally new horizons, enabling measurements to be made of the properties of individual marked coils inside networks. In these advances the contributions of several French groups, notably inspired by Benoit, were outstanding. Although many other techniques, such as NMR or fluorescence spectroscopy, have also helped in reaping a rich harvest of knowledge on gels, scattering techniques in general have proved outstandingly successful in resolving the structure and the dynamics of swollen networks. It has been demonstrated for example, that the thermodynamic response of these systems is the same, whether it is measured by SANS, by dynamic light scattering, or by macroscopic osmotic observations. It has also been shown that the intrinsic nonuniformities in concentration are governed by the same thermodynamic forces. Lists of scientific advances such as this, however, are necessarily partial and can reflect only one individual's personal view.

In the past few years significant progress has been made in the understanding of gels. It is fair to say, however, that in spite of considerable effort, several areas still remain poorly understood. Polyelectrolyte systems fall into this category, owing to the many length scales that govern their properties. Also, our knowledge of gels containing filler particles, whether as reinforcing agents or as molecules for drug

release, is incomplete, particularly with respect to their dynamics and their structural response to external forces. Sophisticated experimental techniques, such as neutron spin echo, anomalous small-angle X-ray scattering, or even X-ray photon correlation spectroscopy, are opening promising avenues, whereas computer simulation techniques are also beginning to be able to handle such complex systems.

Recently, the potential of these disordered systems for performing complex functions in biomedical applications has become increasingly visible, whether as drug-release systems, biosensors, or biocompatible encapsulation devices. It seems likely that biomedicine will become the focus for major developments and the driving force for research into gels in the coming years. It is for this reason that this volume is particularly timely.

## **Erik Geissler**

Laboratoire de Spectrometrie Physique  
Universite de Joseph Fourier de Grenoble  
B.P. 87, 38402 St. Martin D'Herès  
France



## Chapter 1

# Kinetics of the *N*-Isopropylacrylamide Gel–Volume Phase Transition in the Presence of Free Polymer Chains

Marianne E. Harmon and Curtis W. Frank

Department of Chemical Engineering, Stanford University, 381 North–South Mall,  
Stanford, CA 94305–5025

The incorporation of free polymer chains into thermoresponsive *N*-isopropylacrylamide gels alters the kinetics of the LCST volume phase transition. The free polymers investigated were a series of *N*-alkyl-substituted polyacrylamides, and the kinetics was observed as a function of crosslinking density and free polymer chain concentration. It was determined that a majority of the free chains diffuse out of the gel, acting as a porogen, but a smaller fraction of the chains remain trapped in the gel matrix. Faster kinetics was associated with higher concentrations of free polymer chains and more hydrophilic polymers. Free polymers that are hydrophilic at all temperatures showed slower kinetics with decreased molecular weight, which has been attributed to increased overlap between the free chains and a more interconnected porous structure. Free polymers that undergo an LCST transition showed faster kinetics with decreased molecular weight, which has been attributed to increased polymer mobility relative to the gel network.

## Introduction

N-isopropylacrylamide (NIPAAm) gels undergo a volume phase transition at the lower critical solution temperature (LCST) of the polymer (1). Much attention has been focused on the nature of this transition because of its potential applications in thermoresponsive drug delivery systems (2), artificial muscles (3), membrane separations (4), and surfaces in biomaterials (5). However, the kinetics of the volume phase transition is diffusion limited, and the slow response has been a significant limitation in the application of these systems. One approach to faster gel response has been to graft hydrophilic or thermoresponsive oligomers to the gel network (6). This method has been successfully applied but is limited to low molecular weights and low concentrations of the grafted chains.

The following experiments explore a similar phenomenon by using high molecular weight, freely mobile polymers in the gel matrix. This allows a much wider range of molecular weights and concentrations to be used. The free polymers investigated were a series of N-alkyl-substituted polyacrylamides, and the kinetics was observed as a function of crosslinking density and free polymer chain concentration.

## Experimental

**Materials.** NIPAAm (Aldrich) was recrystallized from n-hexane, and dimethylacrylamide (DMAAm; Aldrich) and diethylacrylamide (DEAAm; Polysciences, Inc.) were distilled to remove inhibitor. Methylacrylamide (MAAm; ABCR), ethylacrylamide (EAAM; ABCR), acrylamide (AAm; Life Technologies), ammonium persulfate (APS, Aldrich), N,N'-methylenebisacrylamide (BIS; Aldrich), N,N,N',N'-tetramethylethylenediamine (TEMED, Aldrich), allylamine (Aldrich), and fluorescein isothiocyanate (FITC, Sigma) were all used as received.

**Polymer Synthesis.** 700 mM monomer and 6  $\mu\text{L}/\text{mL}$  TEMED were dissolved in water. The solution was bubbled with nitrogen and 0.4 mg/mL APS was added to initiate the reaction. Lower molecular weight polymers were synthesized as above except 0.8 mg/mL APS was added. The molecular weight of the polymer was calculated using intrinsic viscosity measurements (7) as shown in Table I.  $C^*$  values were calculated using  $C^* = N / [(4/3)\pi R_F(N)^3]$ , where  $N$  is the number of monomer units in the polymer chain and  $R_F(N)$  is the radius of the polymer chain. The fluorescently labeled acrylamide polymer chains were synthesized by the addition of 1% allylamine monomer, and the resulting polymer was fluorescently labeled with FITC by standard methods (8).

**Table I. Free Polymer Samples Used**

<i>Polymer</i>	<i>Molecular Weight</i>	<i>C* [mM monomer]</i>	<i>LCST [°C]</i>
AAm	600,000	66	
(AAm)	500,000	88	
MAAm	1,000,000		
EAAm	400,000		
DMAAm	300,000		
NIPAAm	500,000	34	32
(NIPAAm)	300,000	42	32
DEAAm	200,000		25

**Gel Synthesis.** NIPAAm monomer (700 mM to 600 mM), polymer chains (0 mM to 100 mM), BIS (0.5 mol% to 2 mol%) and TEMED (6  $\mu\text{L/mL}$ ) were dissolved in water. The pregel solution was poured in a test tube containing glass capillaries (inside diameter 0.95 mm). The solution was bubbled with nitrogen, and 0.4 mg/mL APS was added to initiate the reaction. After 24 hours, the gels were removed from the capillaries and allowed to equilibrate in a large volume of MilliQ water to remove any unreacted reagents.

**Kinetic Experiments.** Each gel was placed in a water-filled sample holder, and the diameter of the gel was observed using an optical microscope with an Instec HCS400-STC200 stage to control the temperature. The kinetics was observed in response to step changes in temperature. The temperature was changed from 22°C to 50°C for deswelling experiments and from 50°C to 22°C for swelling experiments.

**Diffusion Experiments.** A known volume of gel (approximately 0.05 mL) was placed in a known volume of water (10 mL), and an SLM-Aminco 8100 spectrofluorometer was used to measure the fluorescence intensity of the resulting aqueous solution of eluted chains. The fluorescence was related to the total concentration of polymer chains that have diffused out of the gel and into solution. The final fluorescence measurement was taken after 28 days, and it was assumed that any remaining polymer chains at this point are permanently trapped in the gel network. The measurements at different time intervals were fit to Fick's law of diffusion in a cylindrical geometry (9). The resulting equation is an infinite series of Bessel functions, which was numerically integrated, and the diffusion coefficient was determined through a least squares fit. These values are compared to calculated diffusion coefficients for reptation in a gel or fixed mesh with reptation time (10) of  $\tau_r \sim [\eta_s R_F^3 (N')/T](N/N')^3$ , where  $\eta_s$  is the solvent viscosity,  $N'$  is the number of monomers units between crosslinks in the gel network,  $N$  is the number of monomer units in the reptating free chains, and  $T$  is

temperature. The exact numerical prefactor (11) for the above scaling argument assumes that the free polymer chains are uniformly distributed throughout a regular gel network.

## Results and Discussion

Because the polymer chains are able to move independently of the gel network, it is possible that the chains diffuse out of the gel during the equilibration step. In order to investigate this possibility, we used fluorescently labeled polymers to observe the diffusion of the polymer chains within the gel. The resulting data show that between 60 and 80% of the polymer chains diffuse out of the gel while the remaining chains remain trapped within the gel (Figure 1). This appears to be independent of the starting polymer concentration within

### Diffusion of Free Polymer Out of Gel 2% BIS and AAm Polymer Chains

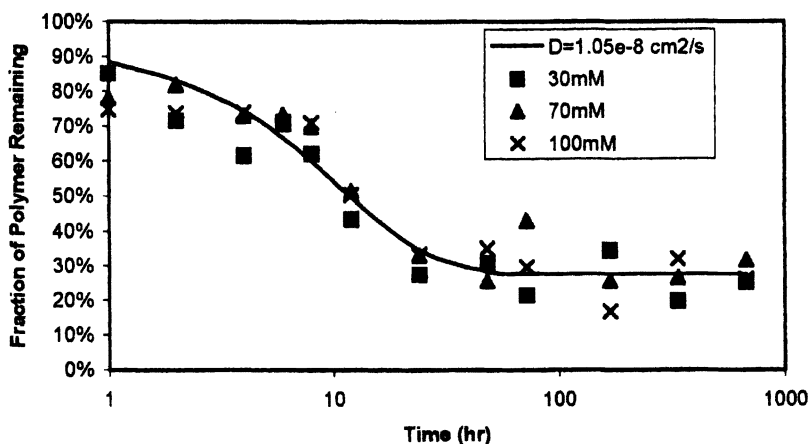


**Figure 1.** Fraction of polymer remaining in the gel as a function of time. The diffusion coefficient is determined through a fit to Fick's law of diffusion in a cylindrical geometry, and the resulting solution is shown as a solid line.

the gel, and the diffusion constants calculated from this data are given in Table II. The diffusion constants are larger than that calculated for the reptation of a polymer chain in a fully crosslinked network but smaller than free diffusion in

solution ( $1.55 \times 10^{-7} \text{ cm}^2/\text{sec}$ ) (7). The diffusion constants decrease with increasing crosslinking density as expected, but it is apparent from these calculations that the gel network is not fully crosslinked. This suggests that the diffusion of polymer chains out of the gel leaves a porous structure in the gel, similar to the use of a porogen. The remaining polymer chains have most likely been activated, through chain transfer or other related mechanisms, during the gel polymerization step and are covalently linked to the gel network.

**Table II. Diffusion Constants**

<i>% BIS</i>	<i>D (measured)</i> <i>/10<sup>-8</sup> cm<sup>2</sup>sec<sup>-1</sup></i>	<i>D (reptation)</i> <i>/10<sup>-10</sup> cm<sup>2</sup>sec<sup>-1</sup></i>
0.5	2.65	4.50
1	2.15	1.75
2	1.05	0.89

The polymers used can be classified into two groups: hydrophilic and thermoresponsive. AAm, MAAm, EAAM, and DMAAm are hydrophilic at temperatures from 22°C to 50°C. NIPAAm and DEAAm have an LCST transition and are hydrophobic at temperatures above the LCST. The free polymer chain concentrations used were 30, 70, and 100 mM, and the resulting kinetics was compared to those of pure NIPAAm gels. We determined that the kinetics of the deswelling transition increased as a function of free polymer chain concentration for all polymers except AAm (Figure 2). The gels containing AAm free polymer chains showed slower deswelling kinetics for 30mM AAm but faster kinetics at higher concentrations of AAm. This supports the idea of the free polymer chains acting as a porogen, forming isolated pores at low concentrations of free polymer chains and interconnected pores at higher concentrations. However, the concentration at which the pores become interconnected appears to be lower than the calculated C\* concentration of the AAm polymer as listed in Table I. The kinetics was also somewhat affected by the crosslinking density (% BIS) with faster kinetics for samples with high crosslinking density.

The fastest kinetics for each set of experiments was for samples with 100 mM free polymer chains and 2% BIS. The deswelling kinetics changed as a function of which free polymer chains were added (Figure 3), while the swelling kinetics was relatively unaffected (Figure 4). For the hydrophilic polymers, the

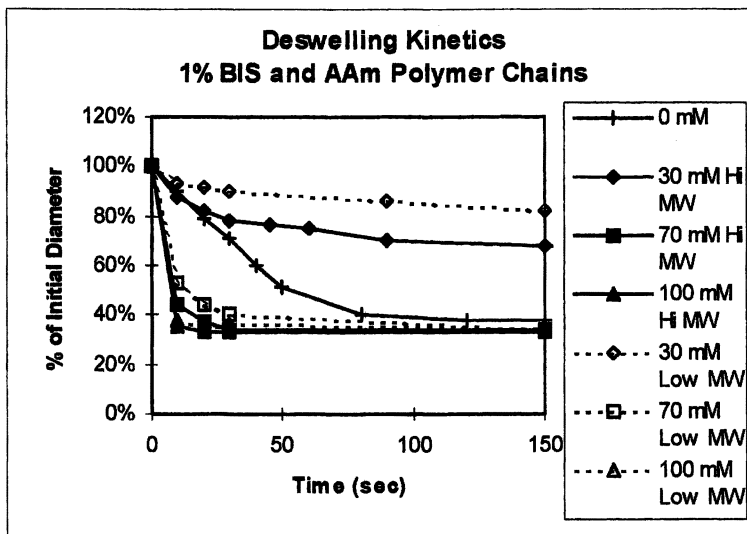


**Figure 2.** Gel kinetics for samples containing AAm free polymer in response to a temperature change from 22°C to 50°C.

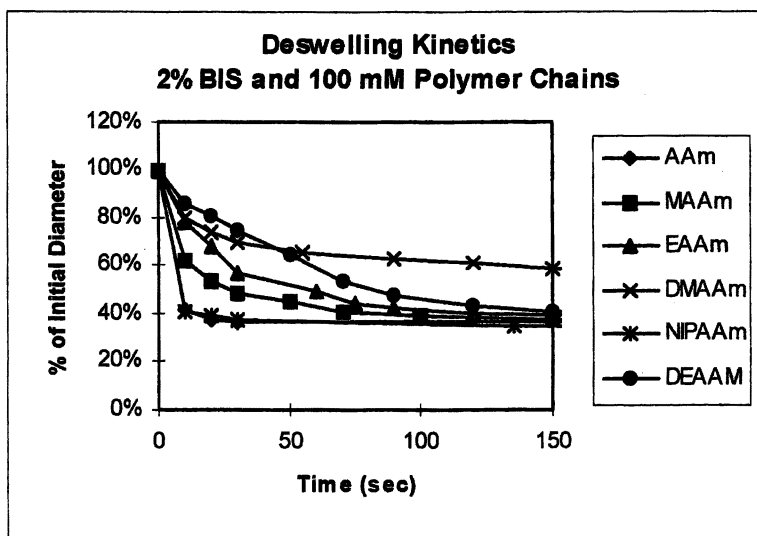


**Figure 3.** Gel kinetics in response to a temperature change from 22°C to 50°C.

initial rate of the deswelling transition decreased as the size of the hydrophobic alkyl group on the free polymer chain increased. This general trend can also be extended to include DEAAm, but NIPAAm is surprisingly fast, considering the relatively large hydrophobic component. These data can be explained in terms of two related mechanisms in the volume phase transition, both of which are a result

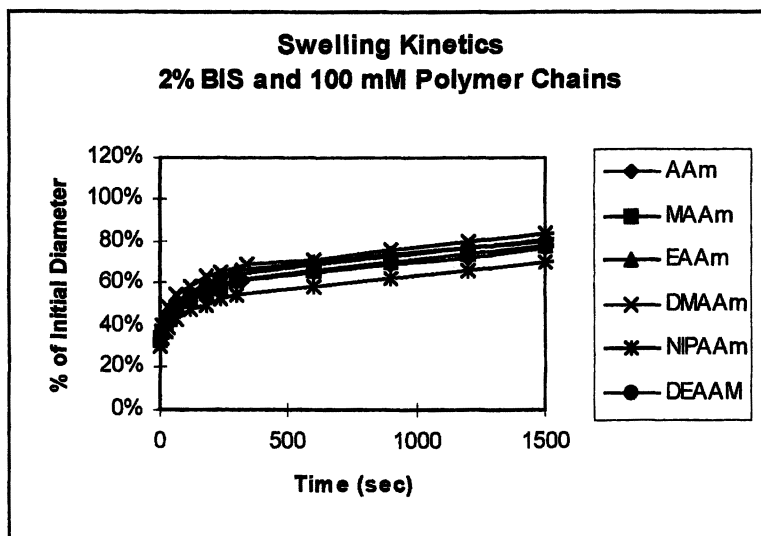


**Figure 4.** Gel kinetics in response to a temperature change from 50°C to 22°C.

of the polymer chains being able to move independently of the gel network. For the hydrophilic polymers, the gel network contracts in response to the increased temperature, while the polymer chains remain swollen. In sufficiently high concentrations, these hydrophilic pockets within the hydrophobic gel can create channels for the water to diffuse out of the gel more quickly (12). The effect of the alkyl group is to make the polymer chain more hydrophobic, which can either slow the diffusion of water through these channels or significantly alter their structure by affecting micro-phase separation within the gel network.

For NIPAAm free polymers in NIPAAm gel, the polymer chains also contract in response to the increased temperature, but they do so more quickly because they are not constrained by the gel network. The slow kinetics of the NIPAAm volume phase transition has been explained in terms of a non-uniform collapse of the gel network (6). The gel near the surface collapses first, forming a dense layer of hydrophobic gel, and it is the diffusion of water through this layer that is responsible for the slow kinetics. The NIPAAm free polymer can produce

local areas of collapsed polymer that serve as nucleation sites for the deswelling of the gel, and this could allow for a more uniform collapse of the gel network. Experiments with networks containing grafted oligo-NIPAAm have shown that the deswelling kinetics no longer scale with the square of the gel dimensions (6). This indicates that the deswelling mechanism is different from the collective diffusion of the network, and a similar phenomenon could be responsible for the fast kinetics of our gels containing free NIPAAm chains.

In order to test this model, we repeated the two fastest systems, AAm and NIPAAm, with lower molecular weight polymer chains (shown in parentheses in Table I). NIPAAm samples showed faster kinetics with decreased molecular weight (Figure 5). This supports the idea that the thermoresponsive polymer chains affect the kinetics because of their high mobility relative to the gel

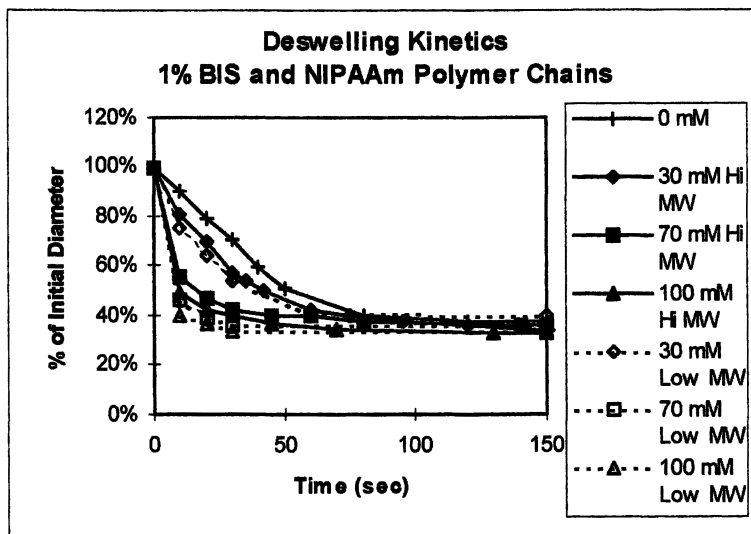


**Figure 5.** Gel kinetics for samples containing NIPAAm free polymer in response to a temperature change from 22°C to 50°C.

network. Lower molecular weight polymers have a higher mobility and should be more effective in initiating the collapse of the gel network. The AAm samples showed slower kinetics with decreased molecular weight (Figure 2). This supports the idea that the hydrophilic polymer chains affect the kinetics by creating effective water channels for the diffusion of water out of the system. In terms of the critical overlap concentration ( $C^*$  in Table I), the higher molecular weight polymer chains have a higher degree of overlap for the same polymer



concentration. This should aid in the formation of water channels, and the diffusion of water out of the system will be more effective with higher molecular weight polymer chains.

## Conclusions

The incorporation of free polymer chains into thermoresponsive N-isopropylacrylamide gels alters the deswelling kinetics of the volume phase transition. The free polymers investigated were a series of N-alkyl-substituted polyacrylamides which can be classified as either hydrophilic or thermoresponsive. Hydrophilic polymers showed slower deswelling kinetics with decreased molecular weight, which has been attributed to increased overlap between the free chains. Thermoresponsive polymers showed faster kinetics with decreased molecular weight, and this has been attributed to increased polymer mobility. A series of diffusion experiments were used to determine the fraction of the polymer chains that diffuse out of the gel during the equilibration step. We have shown that the increased kinetics are in part due to the free polymer chains acting as a porogen, but a significant fraction of the polymer chains does remain trapped within the gel network. For the case of NIPAAm free polymer in a NIPAAm gel network, the kinetics are surprisingly fast, and it is possible that the remaining polymer chains somehow affect the mechanism of the deswelling transition. We have interpreted these results while assuming that the free polymer chains are uniformly distributed throughout the gel network. Further studies will include the use of confocal microscopy to observe the fluorescently labeled chains, and the distribution of the free polymer chains will be determined directly.

**Acknowledgments.** This work was supported by an NSF Graduate Research Fellowship and the Center on Polymer Interfaces and Macromolecular Assemblies (CPIMA) sponsored by the NSF-MRSEC program. The authors also wish to thank Robert M. Dirks for his assistance in carrying out these experiments.

## References

1. Shibayama, M.; Tanaka, T. *Advances in Polymer Science* **1993**, *109*, 1.
2. Dong, L.C.; Hoffman, A.S. *Journal of Controlled Release* **1990**, *13*, 21.
3. Kato, N.; Yamanobe, S.; Takahashi, F. *Materials Science and Engineering C* **1997**, *5*, 141.
4. Reber, N.; Spohr, R.; Wolf, A.; Omichi, H.; Tamada, M.; Yoshida, M. *Journal of Membrane Science* **1998**, *140*, 275.

5. Okano, T.; Yamada, N.; Okybara, M.; Sakai, H.; Sakurai, Y. *Biomaterials* **1995**, *16*, 297.
6. Kaneko, Y.; Nakamura, S.; Sakai, K.; Kikuchi, A.; Aoyagai, T.; Sakurai, Y.; Okano, T. *Polymer Gels and Networks* **1998**, *6*, 333.
7. Brandrup, J., Immergut, E. H., Eds. *Polymer Handbook*, 3<sup>rd</sup> ed.; Wiley: New York, NY, **1989**.
8. Hermanson, G.T. *Bioconjugate Techniques*; Academic Press: New York, 1996.
9. Cussler, E. L. *Diffusion Mass Transfer in Fluid Systems*, 2<sup>nd</sup> ed.; Cambridge University Press: Cambridge, UK, **1997**.
10. DeGennes, P. G. *Scaling Concepts in Polymer Physics*, Cornell University Press: New York, NY, **1979**.
11. Doi, M., Edwards, S. F. *The Theory of Polymer Dynamics*, Oxford University Press, Oxford, UK, **1986**.
12. Hirotsu, S. *Japanese Journal of Applied Physics Part 2-Letters* **1998**, *37*, L284.

## Chapter 2

# Transient Network of Random Copolymers of Sodium 2-(Acrylamido)-2-methylpropanesulfonate and Associative Macromonomers

Yotaro Morishima, Tetsuya Noda, and Akihito Hashidzume

Department of Macromolecular Science, Graduate School of Science,  
Osaka University, Toyonaka, Osaka 560-0043, Japan

Micelle formation and rheological behavior in water of a sodium polysulfonate with  $C_{12}E_m$  surfactant moieties,  $HO(CH_2CH_2O)_mC_{12}H_{25}$  where  $m = 6$  or  $25$ , pendent to the polymer are discussed. The polymer-bound  $C_{12}E_m$  moieties (contents ranging 10 – 30 mol %) undergo side-chain micellization through intra- and interpolymer associations, forming polymer networks. Aggregation numbers of the polymer-bound  $C_{12}E_m$  moieties in one micelle unit are similar to those of free  $C_{12}E_m$  surfactants. The degree of crosslinking by the side-chain micellization was significantly greater for larger  $m$ , increasing with polymer concentration ( $C_p$ ). Arising from the dynamic nature of micelles as junctions, polymer solutions exhibit viscoelastic behavior, concentrated solutions showing gel-like behavior characteristic of transient networks.

Amphiphilic water-soluble polymers and their hydrophobically driven self-associations have been studied extensively because of their potentials in industrial and biological applications (1–10).

There is a class of hydrophobically modified water-soluble polymers known as associative thickeners (AT polymers) that are used in commercial applications for rheology control (11–22). AT polymers and their model polymers include copolymers of acrylamide or (meth)acrylic acid with associative comonomers containing an oligomeric ethylene oxide (EO) chain as a spacer between a polymerizable moiety and terminal hydrophobe (11–16, 23). Associative comonomer units in such copolymers play a role as “stickers” in aqueous solutions. The content of associative comonomers in AT copolymers is usually very low (< 2 mol %) because AT polymers are

designed, for a practical reason, so that interpolymer association can be achieved with a minimum number of hydrophobes incorporated in the polymer.

Associative properties of hydrophobically modified polyelectrolytes strongly depend on polymer architecture. Polymer-bound hydrophobes can associate within the same polymer chain (intrapolymer association) or between different polymer chains (interpolymer association). In most cases, hydrophobically modified random copolymers undergo both intra- and interpolymer associations concurrently. The balance of intra- and interpolymer associations depends on polymer structures including the type and number of hydrophobes per polymer chain, distribution of hydrophobes along polymer chain, and distance of hydrophobe from the backbone (i.e., spacer) (20,24–36). In particular, spacer between hydrophobe and polymer backbone is an important parameter that controls the associative behavior of polymer-bound hydrophobes (30–36). This is due to the fact that in the event of self-association of polymer-bound hydrophobes, polymer chains impose steric constraints to the hydrophobes, restraining their motions. Interpolymer association is likely to occur more easily when the number of hydrophobes per polymer chain is smaller, whereas intrapolymer association becomes more favorable as the number of hydrophobes increases (31,32). In a polymer possessing a larger number of hydrophobes per chain, hydrophobes are located closer to others, and thus there is more chance for them to associate on the same polymer chain. As intrapolymer association proceeds, polymer-bound hydrophobes form clusters (i.e., hydrophobic microdomains). Thus, the intrapolymer association forces a polymer chain to collapse into a “closed” structure in which hydrophobes may no longer be available for association with other hydrophobes on different polymer chains. In a polymer with a small number of hydrophobes, on the other hand, hydrophobes are located far apart from others on the same polymer chain, a circumstance where intrapolymer hydrophobe association is unfavorable, and hence hydrophobes are available for interpolymer association.

This chapter deals with copolymers of sodium 2-(acrylamido)-2-methylpropanesulfonate (AMPS) and a methacrylate substituted with  $\text{HO}(\text{CH}_2\text{CH}_2\text{O})_m\text{C}_{12}\text{H}_{25}$  ( $\text{C}_{12}\text{E}_m$ ) (DE $m$ MA) where  $m = 6$  or  $25$  (Chart 1). A structural feature of these copolymers, comparing to AT polymers mentioned above, is that a much larger number of surfactant comonomer units are incorporated into a strong polyelectrolyte.

Since the  $(\text{CH}_2\text{CH}_2\text{O})_m$  spacer is a flexible chain, the  $\text{C}_{12}$  group at an end of the spacer may be able to move freely depending on its length ( $m$ ). In addition, the polyAMPS backbone and the EO spacer chain are highly hydrated in water and thus the terminal  $\text{C}_{12}$  should be excluded from hydrophilic macromolecular surroundings. Therefore,  $\text{C}_{12}$  chains may easily associate, forming micelles. Micelles may be formed from associations of the surfactant moieties not only on the same polymer chain but also on different polymer chains, and therefore the micelles formed may be connected with polymer chains, forming a network structure.

This chapter describes the side-chain micellization of polyAMPS-bound  $\text{C}_{12}\text{E}_m$  moieties and rheological properties of solutions of the polymer network.

## Experimental

### Synthesis and Characterization of Polymers.

The surfactant monomers were synthesized by reacting  $C_{12}E_m$  ( $m = 6$  or  $25$ ) with methacryloyl chloride in the presence of triethylamine in benzene (36,37).

Copolymerization of a water-soluble monomer and a surfactant monomer can be performed in organic solution or in aqueous media in the presence or absence of nonpolymerizable surfactants (19,38–41). In aqueous media, “micelle” or “emulsion” polymerization may occur, by which copolymers with a blocky sequence distribution of the surfactant comonomer unit may be obtained (19,22,38–40,42). In contrast, homogeneous polymerization in organic solution may yield copolymers with a random distribution. The association behavior of the copolymer depends strongly on the sequence distribution of surfactant comonomer units (19,20,26,39,43,44). To obtain copolymers with a random distribution of AMPS and  $DE_mMA$  (Chart 1), homogeneous solution polymerization was adopted using  $N,N$ -dimethylformamide (DMF) as a solvent in the presence of 2,2'-azobis(isobutyronitrile) at 60 °C (36). Copolymer compositions, determined by  $^1H$  NMR spectroscopy, were virtually the same as monomer feed compositions (36). Apparent number- and weight-average molecular weights of the copolymers, roughly estimated by gel permeation chromatography (GPC), are listed in Table 1. Numbers of surfactant units per polymer chain roughly calculated from copolymer compositions and number-average molecular weights are also given in Table 1.

**Table I. Characteristics of AMPS- $DE_mMA$  Copolymers**

<i>EO length</i>	<i>mol %<sup>a</sup></i>	<i>M<sub>w</sub> × 10<sup>4b</sup></i>	<i>M<sub>w</sub>/M<sub>n</sub><sup>b</sup></i>	<i>Hydrophobe per polymer chain</i>	<i>cmc<sup>c</sup> (g/L)</i>
<i>m = 6</i>	10	4.8	2.4	6.5	0.012
	20	6.9	2.7	17	0.022
<i>m = 25</i>	10	7.0	3.0	7	0.006
	15	6.9	1.9	13	0.018
	20	7.6	2.9	15	0.021
	30	8.3	2.8	16	0.024

<sup>a</sup> Comonomer content determined by  $^1H$  NMR in  $D_2O$ .

<sup>b</sup> Determined by GPC using a 0.1 M  $LiClO_4$  methanol solution as eluent. Standard PEO samples were used for molecular weight calibration.

<sup>c</sup> Determined from steady-state fluorescence excitation spectra of pyrene probes.

## Measurements.

Steady-state fluorescence spectra were recorded on a Hitachi F-4500 fluorescence spectrophotometer. Emission spectra of pyrene probes were measured with excitation at 337 nm at room temperature. Excitation spectra were monitored at 372 nm. Sample solutions were prepared by dissolving a predetermined amount of polymer in an aqueous pyrene solution of a known concentration, and the solutions were allowed to stand for 1 day for equilibration.

Fluorescence decay data were collected on a HORIBA NAES 550 system equipped with a flash lamp filled with H<sub>2</sub>. Sample solutions were excited at 337 nm, and pyrene fluorescence was monitored at 400 nm. Sample solutions were purged with Ar for about 30 min prior to measurement.

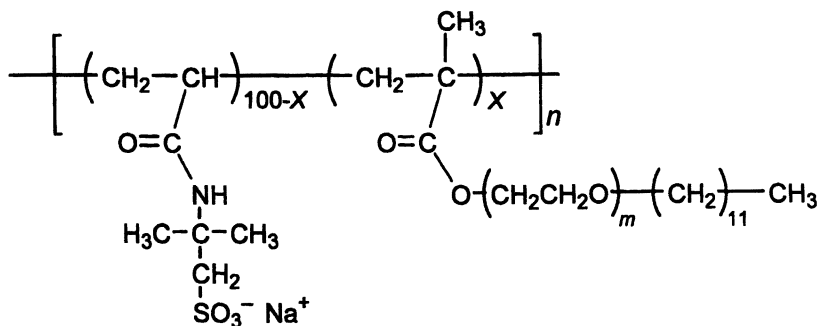
Quasielastic light scattering (QELS) measurements were performed with an Otsuka Electronics Photal DLS-7000 light scattering spectrometer equipped with a 65-mW Ar ion laser ( $\lambda = 488$  nm). Data were collected using an ALV-5000 wide-band multi- $\tau$  digital autocorrelator. All measurements were performed at 25 °C. Sample solutions were filtered prior to measurement using a 0.45- $\mu$ m pore size membrane filter. Relaxation time distributions were obtained by an inverse Laplace transform analysis by conforming the REPES algorithm (36,37). Apparent hydrodynamic radii were calculated using the Einstein-Stokes equation.

The rheological behavior of the copolymers was measured with a DynAlyser 100 stress-control rheometer (RheoLogica) equipped with a cone and plate at 25 °C. The radius of the cone is 40 mm, and the angle between the cone and plate is 4.0°. Steady shear and oscillatory flow measurements were conducted to obtain the steady shear viscosity and dynamic viscoelastic properties of polymer solutions.

## Results and Discussion

### Apparent Critical Micelle Concentration (cmc) and Aggregation Number for Polymer-Bound Micelles.

Since the micelle formation of polyAMPS-bound C<sub>12</sub>E<sub>m</sub> moieties in aqueous solutions is mainly due to interpolymer association, an apparent "cmc" is observed. Here, the apparent "cmc" is defined as a polymer concentration for the onset of interpolymer association. Apparent cmc for polyAMPS-bound C<sub>12</sub>E<sub>m</sub> moieties was estimated using fluorescence excitation spectra of pyrene probes (35,36). This method is based on the fact that the 0–0 absorption maximum for pyrene in water at 334 nm shifts to 337 nm when pyrene is solubilized in a micellar phase (45–48). The ratio of the intensity at 337 nm relative to that at 334 nm ( $I_{337}/I_{334}$ ), estimated from excitation spectra, increases with polymer concentration ( $C_p$ ). As illustrated in Figure 1 for copolymers of  $m = 25$  with varying C<sub>12</sub>E<sub>25</sub>

Chart 1. AMPS-DE $m$ MA Copolymers.

AMPS-DE6MA:  $m = 6$ ,  $X = 10$  and  $20$

AMPS-DE25MA:  $m = 25$ ,  $X = 10, 15, 20$ , and  $30$

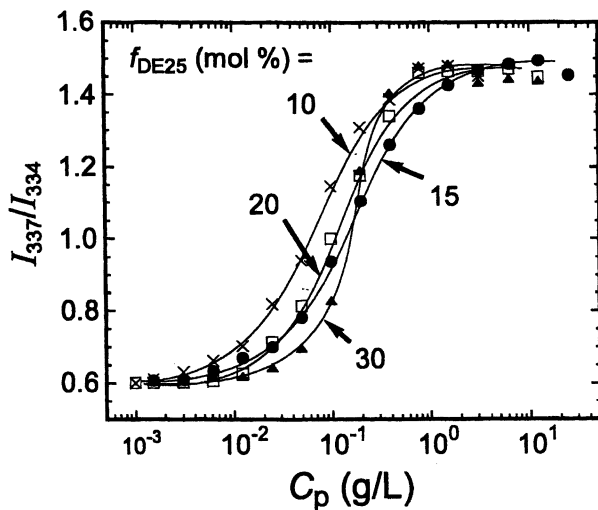


Figure 1. Plots of  $I_{337}/I_{334}$  as a function of the polymer concentration for the copolymers of  $m = 25$  with varying  $f_{\text{DE25}}$ .

surfactant comonomer contents ( $f_{DE25}$ ) (Chart 1),  $I_{337}/I_{334}$  starts to increase more significantly at a certain  $C_p$  with increasing  $C_p$ . A similar tendency was observed for copolymers of  $m = 6$ . From  $I_{337}/I_{334}$  at a given  $C_p$ , along with minimum and maximum  $I_{337}/I_{334}$  values observed at low and high  $C_p$ , respectively, one can calculate the ratio of pyrene concentrations in the micellar and aqueous phases ( $[Py]_m/[Py]_w$ ) at a given  $C_p$ . Figure 2 exhibits an example of  $[Py]_m/[Py]_w$  vs  $C_p$  plots for copolymers of  $m = 6$  with varying  $C_{12}E_6$  surfactant comonomer contents ( $f_{DE6}$ ) (37). The plots comprise two linear lines with a smaller slope at lower  $C_p$  (inset of Figure 2) and a larger slope at higher  $C_p$ . Transition from the small to large slope is sufficiently abrupt to be able to define an apparent cmc. At low  $C_p$ , surfactant moieties associate within the same polymer chain independent of  $C_p$ , forming intrapolymer hydrophobic domains. Upon increase in  $C_p$  to a certain level, however, interpolymer association commences to occur. From a break observed in the  $[Py]_m/[Py]_w$  vs  $C_p$  plot, apparent cmc was estimated, as listed in Table 1. The slope of the linear line corresponds to partition coefficient ( $K_v$ ) for pyrene solubilization; the steeper the slope, the stronger ability to solubilize pyrene in the micellar phase (35–37). Thus, micelles formed at  $C_p > \text{cmc}$  are very different from intrapolymer hydrophobic domains formed at  $C_p < \text{cmc}$  in ability to solubilize pyrene, probably arising from a difference in the size of hydrophobic cores (i.e., aggregation number).

In Figure 3, cmc and  $K_v$  values are plotted against  $f_{DE6}$  and  $f_{DE25}$  for the copolymers of  $m = 6$  and 25, respectively (37). Values of cmc are represented as the molar concentration of  $C_{12}E_m$  residues in the copolymers. Values of cmc for free  $C_{12}E_6$  and  $C_{12}E_{25}$  surfactant molecules in 0.1 M NaCl aqueous solutions were estimated to be  $6.0 \times 10^{-5}$  and  $3.0 \times 10^{-4}$  M, respectively by the same method based on the excitation spectra of solubilized pyrene probes (36,37). Values of cmc for the copolymers are smaller than cmc for the corresponding free  $C_{12}E_m$  surfactants by more than 1 order of magnitude. The cmc values for the copolymers show a tendency to increase with increasing content of surfactant units in the copolymers (Figure 3). A plausible cause is that as the content of the surfactant units in the copolymer increases, the polymer-bound surfactants are more prone to associate on the same polymer chain and thus the number of surfactants available for interpolymer association decreases. This idea is supported by the fact that the slope of the  $[Py]_m/[Py]_w$  vs  $C_p$  plot at lower  $C_p$  increases with increasing surfactant content in the copolymer (inset of Figure 2).  $K_v$  values are fairly constant on the order of  $10^5$  for the two copolymers (Figure 3). These values are a slightly smaller than  $K_v$  values for the corresponding free  $C_{12}E_m$  micelles.

Aggregation numbers ( $N_{\text{agg}}$ ) of dodecyl groups in one core of polymer-bound  $C_{12}E_m$  micelles were determined by a fluorescence technique based on the excimer formation of pyrene probes solubilized in the polymer-bound micelles (49–52). When the concentration of solubilized pyrene is sufficiently low, pyrene emits only monomeric fluorescence, exhibiting a single-exponential decay. However, if pyrene concentration is increased to a certain level, pyrene emits excimer fluorescence, showing a fast decay component because the probability of finding two or more pyrene molecules in the same micelle core increases. In this situation, fluorescence decay



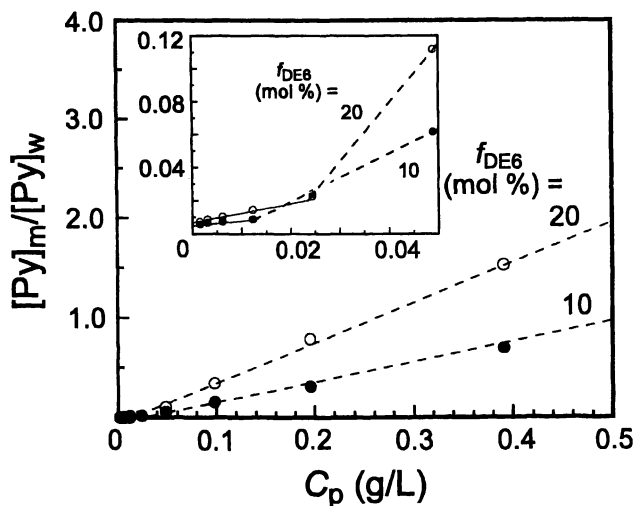


Figure 2. Plots of  $[Py]_m/[Py]_w$  as a function of the polymer concentration for the copolymers of  $m = 6$  with  $f_{DE6} = 10$  and 20 mol %.

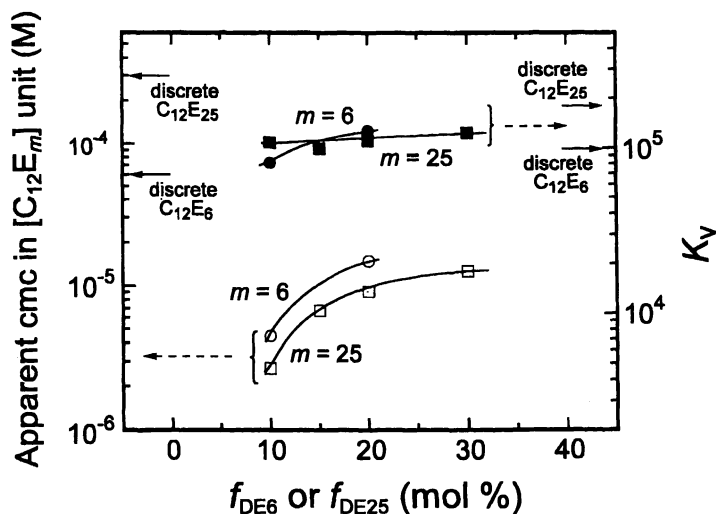


Figure 3. Plots of apparent cmc and partition coefficient ( $K_v$ ) for the copolymers of  $m = 6$  and 25 as a function of macromonomer content in the copolymers. The apparent cmc is represented in terms of the molar concentration of the  $C_{12}E_m$  unit.

profiles may follow a kinetic model developed by Infelta (53) and Tachiya (54);

$$\ln[I(t)/I(0)] = A_3 [\exp(-A_4 t) - 1] - A_2 t \quad (1)$$

$$A_2 = k_0 + n_Q k_Q \bar{k} / (k_Q + \bar{k}) \quad (2a)$$

$$A_3 = n_Q k_Q^2 / (k_Q + \bar{k})^2 \quad (2b)$$

$$A_4 = k_Q + \bar{k} \quad (2c)$$

where,  $I(t)$  and  $I(0)$  are the fluorescence intensities at time  $t$  and 0 following pulse excitation, respectively,  $k_Q$  is the pseudo-first-order rate constant for fluorescence quenching,  $k_0$  is the fluorescence decay rate constant (i.e.,  $\tau_0^{-1}$ ) for pyrene inside the micelle without excimer formation,  $n_Q$  is the average number of quenchers in a micelle, and  $\bar{k}$  is the first-order rate constant for exit of pyrene molecules from a micelle.  $n_Q$  can be expressed as  $[Q]_m/[M]$ , where  $[Q]_m$  is the molar concentration of quencher inside micelle and  $[M]$  is the molar concentration of the micelle. Because the quenching of pyrene monomer fluorescence is due to the excimer formation of pyrene,  $n_Q$  is the average number of pyrene molecules solubilized in a micelle. Assuming complete solubilization of pyrene, one can calculate the molar concentration of micelles from which one can calculate  $N_{agg}$  using  $n_Q$  determined from best fit of fluorescence decay data to eq 1 (35–37).

Values of  $N_{agg}$  thus estimated are plotted in Figure 4 as a function of the molar concentration of the surfactant unit in the copolymers (36,37). In Figure 4,  $N_{agg}$  values for micelles formed from free  $C_{12}E_m$  molecules are also plotted against the surfactant concentration. The values of  $N_{agg}$  for the copolymer of  $m = 6$  range from ca. 170 to ca. 270, increasing with the concentration of the surfactant unit in the copolymer (i.e., polymer concentration). A similar trend was observed for free  $C_{12}E_6$  surfactant molecules. On the other hand, the values of  $N_{agg}$  for the copolymer of  $m = 25$  are nearly constant at ca. 57. A similar trend was observed for free  $C_{12}E_{25}$  surfactant molecules. These  $N_{agg}$  values for the two copolymers are fairly close to those of the corresponding discrete micelles of free  $C_{12}E_m$  surfactant molecules, and the  $N_{agg}$  values for the copolymer of  $m = 25$  are much smaller than those for the copolymer of  $m = 6$ .  $N_{agg}$  values for polymer-bound  $C_{12}E_6$  micelles are either smaller or larger than those for free  $C_{12}E_6$  micelles depending on the polymer concentration, whereas  $N_{agg}$  values for polymer-bound  $C_{12}E_{25}$  are slightly larger than those of free  $C_{12}E_{25}$  micelles over the range of the surfactant concentrations studied.

These aggregation numbers for the polymer-bound micelles are much larger than the numbers of surfactant units per polymer chain (Table 1). Therefore, it is evident that micelles are formed from associations of the surfactant moieties not only on the same polymer chain but also on different polymer chains. For example, in the case of the copolymer of  $m = 6$  with

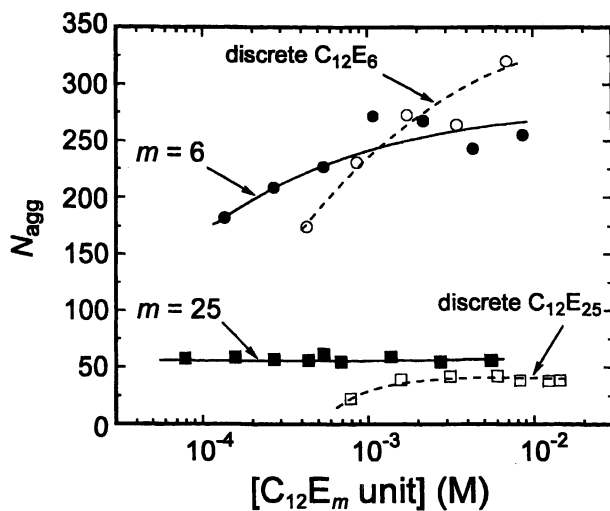


Figure 4. Plots of  $N_{agg}$  as a function of the molar concentration of the  $C_{12}E_m$  unit for the copolymers of  $m = 6$  and 25 with  $x = 20$  mol % in 0.1 M NaCl aqueous solutions.  $N_{agg}$  for discrete  $C_{12}E_m$  surfactants are also presented.

$f_{\text{DE6}} = 20$  mol %, 1 polymer chain possesses 17  $\text{C}_{12}\text{E}_6$  units (Table 1) while  $N_{\text{agg}}$  is 243 at  $C_p = 6.25$  g/L. Thus, 1 micelle is formed by at least 14 polymer chains assuming an extreme case where all the  $\text{C}_{12}\text{E}_6$  units on the same polymer chain belong to the same micelle. In the case of the copolymer of  $m = 25$  with  $f_{\text{DE25}} = 20$  mol %, 1 micelle is formed by at least 4 polymer chains assuming the same extreme case. As is evident from QELS and rheology data, polymer chains are crosslinked by micelles, as will be discussed later. The occurrence of crosslinking indicates that surfactant units on the same polymer chain occupy different micelles. Therefore, each micelle is formed from a larger number of polymer chains than those calculated above.

### Hydrodynamic Size of Polymers Crosslinked by Micelles.

In the case of the copolymer of  $m = 25$  ( $f_{\text{DE25}} = 20$  mol %), distributions of QELS relaxation times in 0.1 M NaCl aqueous solutions are bimodal at  $C_p \leq 18.8$  g/L but they become unimodal at higher  $C_p$  (Figure 5). A similar tendency was observed for the copolymer of  $m = 6$  ( $f_{\text{DE6}} = 20$  mol %) but the presence of a fast mode persists to higher  $C_p$  than for the copolymer of  $m = 25$  (Figure 5). The slow relaxation mode observed in the semidilute regime shown in Figure 5 is attributed to polymers crosslinked by  $\text{C}_{12}\text{E}_m$  micelles, and the fast-mode component may be attributed to a unimer (single polymer state) or an aggregate of a small number of polymer chains ("oligomeric" micelle). There is a clear trend that peak top for the slow mode shifts toward longer relaxation times with increasing  $C_p$ . Apparent hydrodynamic radius ( $R_h$ ) for the crosslinked polymer chains estimated from QELS data increases gradually with increasing  $C_p$  in a low  $C_p$  region but  $R_h$  increases markedly with  $C_p$  in a higher  $C_p$  region. Although polymer-bound  $\text{C}_{12}\text{E}_m$  micelle cores conserve their size over a significant range of  $C_p$  (Figure 4), hydrodynamic size of the crosslinked polymer chains increases significantly with increasing  $C_p$ . This means that the degree of crosslinking increases with  $C_p$  whereas the size of micelles formed from polymer-bound  $\text{C}_{12}\text{E}_m$  moieties (i.e.,  $N_{\text{agg}}$ ) remains unchanged.

### Steady Shear Solution Viscosities of Polymers Crosslinked by Micelles.

Zero-shear viscosities of the copolymers of  $m = 6$  ( $f_{\text{DE6}} = 20$  mol %) and 25 ( $f_{\text{DE25}} = 20$  mol %) in 0.10 M NaCl aqueous solutions are plotted in Figure 6 as a function of  $C_p$  (37,55). The viscosity increases gradually with  $C_p$  in a low  $C_p$  region. In this low  $C_p$  region, the degree of crosslinking of polymer chains by micelles is relatively small. However, viscosity starts to increase sharply as  $C_p$  is increased to ca. 10 g/L for  $m = 25$  and to ca. 30 g/L for  $m = 6$ . In this  $C_p$  region, the degree of crosslinking increases greatly with  $C_p$ , yielding a macroscopic network. Viscosities for the copolymer of  $m = 25$  are roughly 2 orders of magnitude higher than those of the copolymer of  $m = 6$  at a given  $C_p$  in this region; the size of the network of the copolymer of  $m = 25$  is much larger than that of the copolymer of  $m = 6$ .

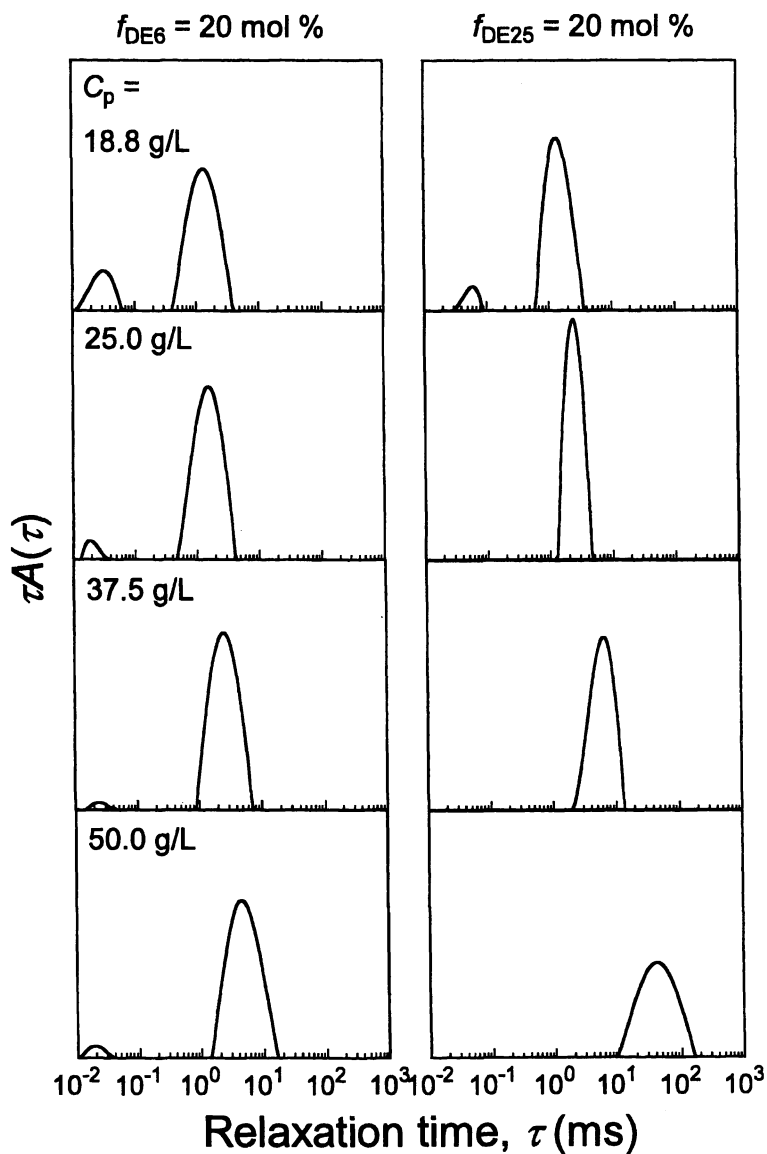


Figure 5. Relaxation time distributions in QELS at  $\theta = 90^\circ$  for the copolymers of  $m = 6$  and  $25$  with  $x = 20 \text{ mol \%}$  in  $0.1 \text{ M NaCl}$  aqueous solutions at varying polymer concentrations.

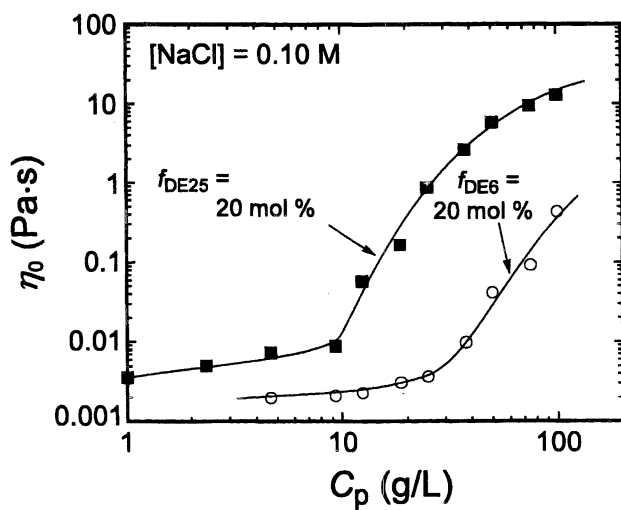


Figure 6. Plots of zero shear viscosity at 25 °C for the copolymers of  $m = 6$  and 25 with  $x = 20 \text{ mol } \%$  in 0.1 M NaCl aqueous solutions as a function of the polymer concentration.

Zero-shear viscosity depends on the concentration of added salt, and salt-dependent viscosity profiles for the copolymers with  $m = 6$  and 25 are greatly different (Figure 7). In the case of  $m = 6$ , viscosity increases rather gradually with increasing salt concentration ( $[\text{NaCl}]$ ) at  $C_p \leq 125$  g/L, but it shows a more significant increase at  $C_p = 150$  g/L with increasing  $[\text{NaCl}]$  at  $[\text{NaCl}] > 0.2$  M. In the case of  $m = 25$ , in contrast, viscosity shows a maximum at a certain salt concentration depending on  $C_p$  (36b). The viscosity first increases with  $[\text{NaCl}]$ , reaching a maximum and then decreases with further increasing  $[\text{NaCl}]$ . The viscosity maximum occurs at  $[\text{NaCl}] = 0.10 - 0.15$  M at  $C_p \leq 50.0$  g/L, and the maximum shifts toward higher salt concentrations at higher polymer concentrations ( $C_p \geq 75.0$  g/L) (Figure 7b). This viscosity increase with  $[\text{NaCl}]$  is more significant at higher  $C_p$ , followed by a sharp drop in viscosity after passing through a maximum. These observations may be explained as follows (36b). Polymer chains are crosslinked when surfactant groups on the same polymer chain occupy concurrently two or more micelles formed from surfactant groups on different polymer chains. This process is an interpolymer association that occurs competing with interpolymer electrostatic repulsion and hence occurs more favorably at higher salt concentrations because of increased electrostatic shielding. Association of surfactant groups on the same polymer chain (i.e., intrapolymer associations) also becomes more favorable at higher salt concentrations because of an increased short range electrostatic shielding within the same polymer chain. Thus, these two kinds of salt effects, competing in the process of micelle formation, may give rise to a maximum degree of crosslinking at a certain salt concentration. In the case of  $m = 6$ , the second salt effect appears to be less pronounced than in the case of  $m = 25$  because surfactant groups in the copolymer of  $m = 6$  are more prone to associate within the same polymer chain than in the copolymer of  $m = 25$  as indicated by QELS and viscosity data. Therefore, only the first salt effect is visible in the viscosity data (Figure 7a). In contrast, for  $m = 25$ , intrapolymer association becomes more pronounced at higher salt concentrations and therefore the second salt effect predominates over the first salt effect at higher salt concentrations showing a maximum in viscosity vs  $[\text{NaCl}]$  plots.

### Shear-Rate-Dependent Solution Viscosities of Polymers Crosslinked by Micelles.

Copolymers with  $m = 6$  and 25 exhibit shear-rate-dependent viscosities in the presence of salt. Steady-shear viscosities of the copolymers of  $m = 6$  ( $f_{\text{DE6}} = 20$  mol %) and 25 ( $f_{\text{DE25}} = 20$  mol %) in aqueous solutions containing different concentrations of NaCl are plotted in Figure 8 as a function of shear rate (36b). Figure 8a is an example for the copolymer of  $m = 6$  at  $C_p = 125$  g/L. The polymer solutions exhibit Newtonian behavior at shear rates  $<$  ca.  $100$   $\text{s}^{-1}$ , and viscosity in the Newtonian region increases with increasing  $[\text{NaCl}]$  due to an increased degree of crosslinking with increasing  $[\text{NaCl}]$ , as discussed above. At shear rates  $>$  ca.  $100$   $\text{s}^{-1}$ , however, polymer solutions undergo shear thinning. The extent of the shear thinning is more pronounced for solutions with higher Newtonian viscosities at higher salt

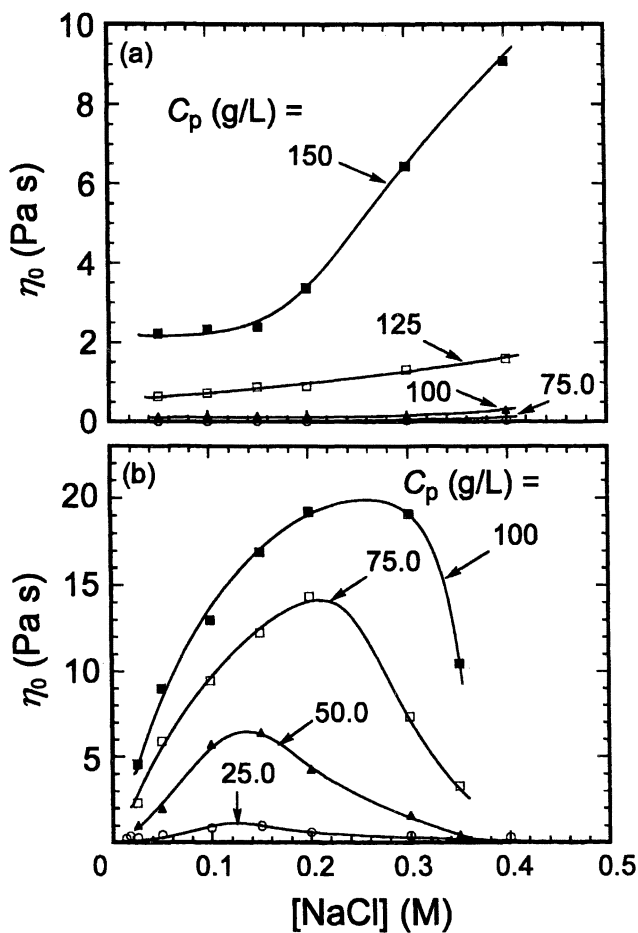


Figure 7. Zero shear viscosities at 25 °C for the copolymers of  $m = 6$  and 25 with  $x = 20$  mol % at varying polymer concentrations plotted against salt concentration.



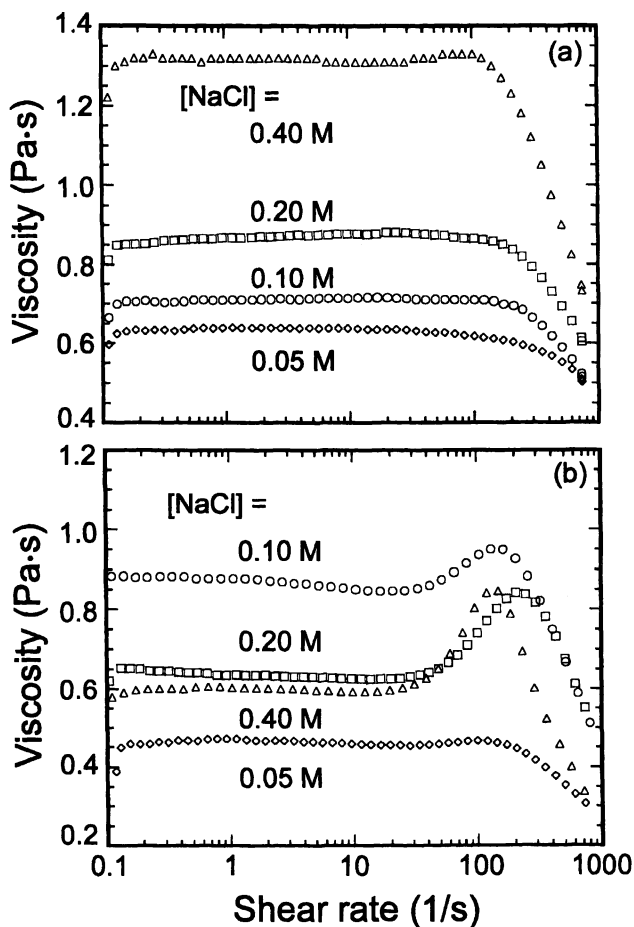


Figure 8. Dependence of viscosity on the shear rate at varying salt concentrations; (a) copolymer of  $m = 6$  with  $f_{DE6} = 20 \text{ mol } \%$ ,  $C_p = 125 \text{ g/L}$ ; (b) copolymer of  $m = 25$  with  $f_{DE25} = 20 \text{ mol } \%$ ,  $C_p = 25.0 \text{ g/L}$ .

concentrations but the viscosities seem to converge at a small value at a shear rate higher than  $1000 \text{ s}^{-1}$ . This shear thinning can be explained by shear-induced disruption of crosslinks.

Figure 8b shows an example for the copolymer of  $m = 25$  at  $C_p = 25.0 \text{ g/L}$  which shows a similar viscosity range as that for the copolymer of  $m = 6$  at  $C_p = 125 \text{ g/L}$  in Figure 8a (36b). Solutions of the copolymer of  $m = 25$  behave as a Newtonian fluid at shear rates  $< 30 \text{ s}^{-1}$ . Viscosity in this Newtonian region at  $C_p = 25.0 \text{ g/L}$  depends on the salt concentration, showing a maximum at  $0.10 - 0.15 \text{ M [NaCl]}$  (Figure 7b). The Newtonian behavior is followed by shear thickening at intermediate shear rates, the thickening behavior persisting up to a shear rate of  $100 - 200 \text{ s}^{-1}$ . Shear thickening is only observed at  $[\text{NaCl}] > \text{ca. } 0.1 \text{ M}$ , and the extent of the shear thickening increases as  $[\text{NaCl}]$  is increased. When the shear rate is further increased beyond  $200 \text{ s}^{-1}$ , shear thinning occurs.

Given that shear-thickening is derived by a shear-induced increase in the density of mechanically active chains, a plausible cause for the observed shear thickening is a shear-induced increase in the degree of crosslinking (50,56). When shear stress is applied to polymer chains crosslinked by micelles at a shear rate beyond the Newtonian region, polymer chains may be stretched out causing some surfactant groups to be pulled out of the micelle and become available for associations with other surfactant groups on different polymer chains, leading to an increase in crosslinking sites and hence a viscosity increase. A further increase in the shear rate may cause the crosslinking site to fragment, resulting in a decrease in the size of network structures and hence a viscosity decrease.

The viscosity restored instantly when applied shear stress was removed, indicating that the shear-induced disruption and re-formation of crosslinking are reversible, as conceptually illustrated in Figure 9. This is a characteristic feature for reversible transient networks (36b). When a polymer network is sheared at a high shear rate, crosslinks are disrupted at a faster rate than the rate of their re-formation, leading to a decrease in steady shear viscosity.

### Viscoelastic Behavior of Polymer Networks.

Figure 10 shows plots of storage modulus ( $G'$ ) and loss modulus ( $G''$ ) as a function of angular frequency ( $\omega$ ) for the copolymers of  $m = 6$  ( $f_{\text{DE6}} = 20 \text{ mol } \%$ ) and  $25$  ( $f_{\text{DE25}} = 20 \text{ mol } \%$ ) at varying polymer concentrations at  $[\text{NaCl}] = 0.1 \text{ M}$  (36b,37). In the case of the copolymer of  $m = 6$ , solutions exhibit viscoelastic properties at  $C_p < 125 \text{ g/L}$ , and the  $G'-\omega$  and  $G''-\omega$  plots can be fitted reasonably well to a Maxwell model with  $G''$  and  $G'$  being proportional to  $\omega$  and  $\omega^2$ , respectively. As  $C_p$  is increased, both  $G'$  and  $G''$  increase and they become close to each other, and solutions exhibit significantly elastic properties.

In the case of the copolymer of  $m = 25$ , solutions behave as a viscoelastic liquid,  $G'$  and  $G''$  data following a Maxwell model at  $C_p \leq 25.0 \text{ g/L}$ . When  $C_p$  is increased to  $50.0 \text{ g/L}$ , both  $G'$  and  $G''$  increase by about 1 order of magnitude, and the  $G'-\omega$  and  $G''-\omega$  plots deviate from the Maxwell model. As  $C_p$  is further increased to  $150 \text{ g/L}$ ,  $G'$  and  $G''$  become the same

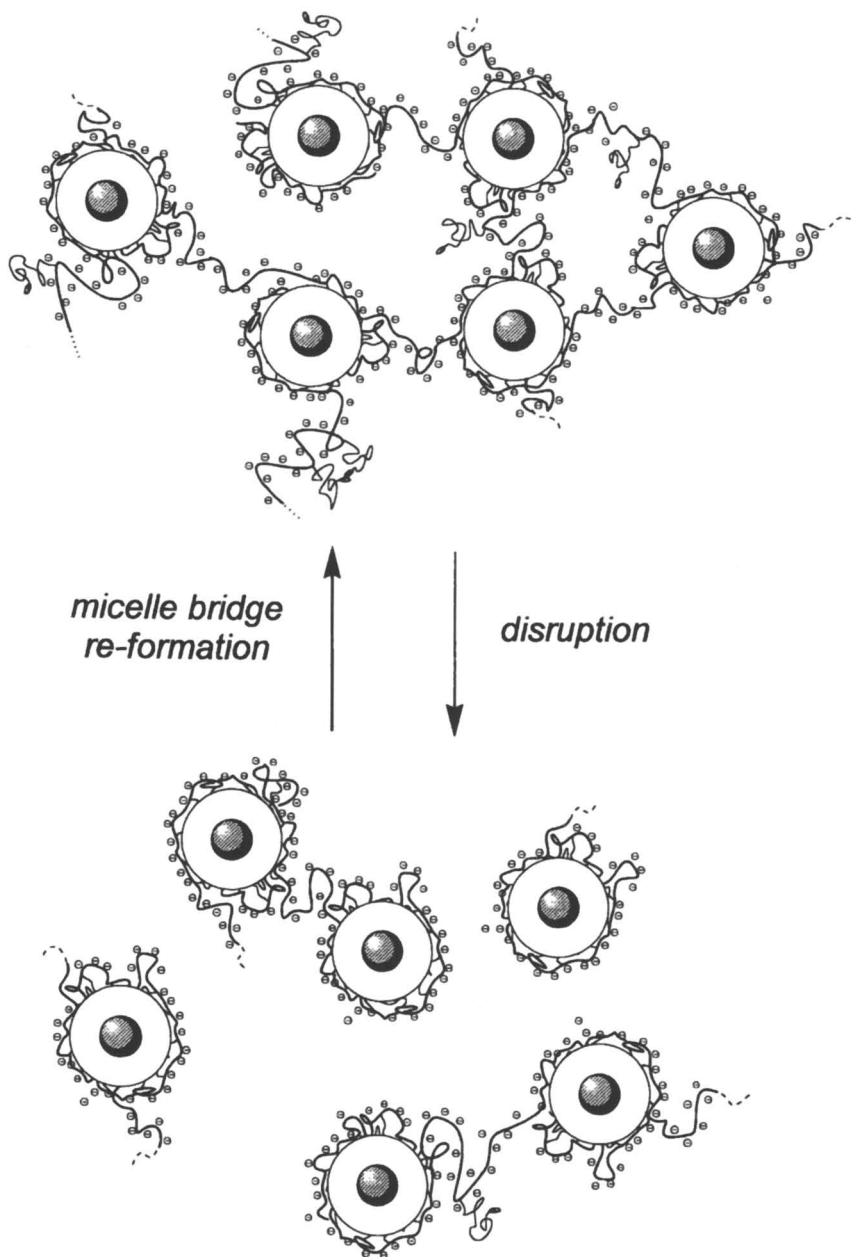


*Figure 9. Conceptual illustration of reversible disruption and re-formation of crosslinks under shear conditions.*

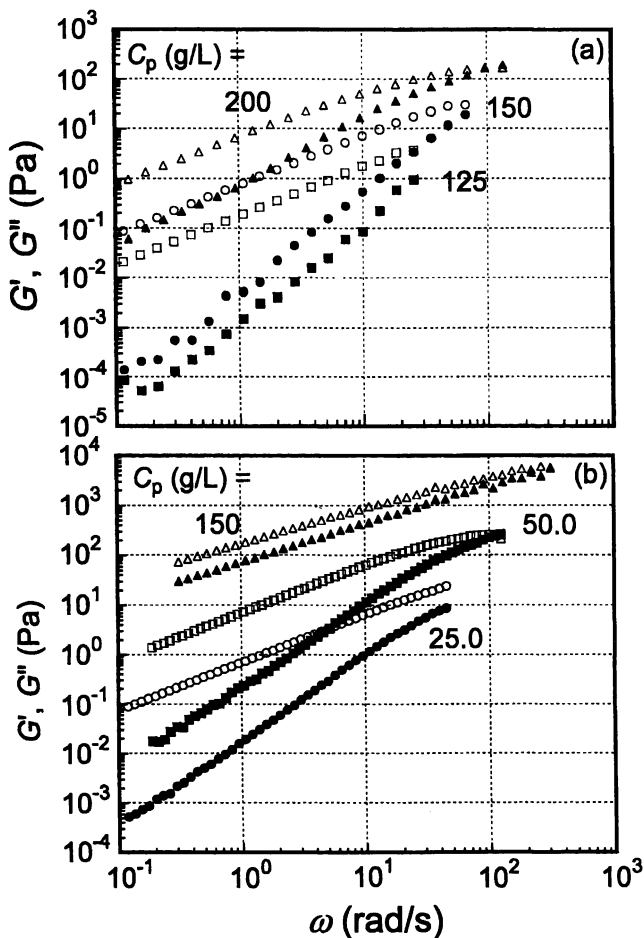


Figure 10. Plots of storage ( $G'$ ) and loss ( $G''$ ) moduli as a function of angular frequency ( $\omega$ ) for the copolymers of  $m = 6$  and  $25$  with  $x = 20$  mol % at varying polymer concentrations in  $0.1$  M NaCl. Closed and open symbols represent  $G'$  and  $G''$ , respectively. Shear stress applied is  $1.0$  Pa at  $25$  °C.

order of magnitude, and they are nearly parallel at low and intermediate frequencies, solutions exhibiting significant elastic properties.

According to a simple theory of rubber elasticity extended to transient networks or reversible physical crosslinks (57), the magnitude of  $G'$  at a moderate  $\omega$  value is related to the density of mechanically reversible physical crosslinks. On the other hand, an increase in  $G''$  indicates an increase in effective volume occupied by polymer networks in solution. At  $C_p = 150$  g/L for the copolymer of  $m = 25$ , the slope of the  $G'-\omega$  plot is rather flat over the  $\omega$  range in Figure 10b, exhibiting gel-like behavior (58). The dominant elastic properties in the concentrated regime arise from a large number of crosslink junctions by  $C_{12}E_{25}$  micelles.

According to the Maxwell model,  $G'$  and  $G''$  are described by a plateau modulus ( $G_0$ ) and a terminal relaxation time ( $\lambda$ ) (58) as

$$G' = G_0 \omega^2 \lambda^2 / (1 + \omega^2 \lambda^2) \quad (3)$$

$$G'' = G_0 \omega \lambda / (1 + \omega^2 \lambda^2) \quad (4)$$

$G_0$  and  $\lambda$  for the copolymer of  $m = 6$  at  $C_p = 100$  g/L at varying salt concentrations were estimated by fitting  $G'$  and  $G''$  data to eqs 3 and 4. At a higher polymer concentration ( $C_p = 150$  g/L), at which  $G'$  and  $G''$  data do not follow the Maxwell model,  $G_0$  and  $\lambda$  were roughly estimated from the intersection of extrapolated lines for  $G'$  and  $G''$  plots. Figure 11 shows plots of  $G_0$  and  $\lambda$  thus estimated as a function of salt concentration. Values of  $G_0$  at  $C_p = 150$  g/L are more than 1 order of magnitude larger than those at  $C_p = 100$  g/L.  $G_0$  increases with increasing salt concentration, and this tendency is more significant at the higher polymer concentration. In contrast, values of  $\lambda$  at  $C_p = 100$  and 150 g/L are close to each other on the order of 40 ms and slightly decrease with increasing salt concentration.

Values of  $G_0$  and  $\lambda$  for the copolymer of  $m = 25$  at  $C_p = 25.0$  and 75.0 g/L at varying salt concentrations were also estimated from  $G'$  and  $G''$  data and plotted as a function of the salt concentration in Figure 12 (36b). At  $C_p = 25.0$  g/L,  $G_0$  increases with increasing salt concentration passing through a maximum at a salt concentration near 0.13 M and then decreases (Figure 12a). A similar tendency is observed for  $C_p = 75.0$  g/L but the maximum shifts toward higher salt concentrations ( $[\text{NaCl}] \approx 0.2$  M) and  $G_0$  drops sharply at  $[\text{NaCl}] > 0.2$  M (Figure 12b). On the other hand, values of  $\lambda$  at  $C_p = 25.0$  and 75.0 g/L are on the order of 10 ms decreasing only slightly with salt concentration.

Zero shear viscosity can be related to  $G_0$  and  $\lambda$  as  $\eta_0 = G_0 \lambda$ . The profiles of  $\eta_0$  vs  $[\text{NaCl}]$  plots in Figure 7 are quite similar to those of  $G_0$  vs  $[\text{NaCl}]$  plots in Figure 12. Furthermore, viscosity values calculated from  $\eta_0 = G_0 \lambda$  at varying salt concentrations are in fair agreement with experimental values. Therefore, it is obvious that viscosity is essentially governed by  $G_0$ , and  $\lambda$  has little or no effect on viscosity. The simple theory for transient networks (57) suggests that the magnitude of  $G_0$  is proportional to the number density of mechanically active chains in the network. Crosslinks formed by micelles act as transient junctions for a network structure, the junctions being in equilibrium between disruption and re-formation (Figure

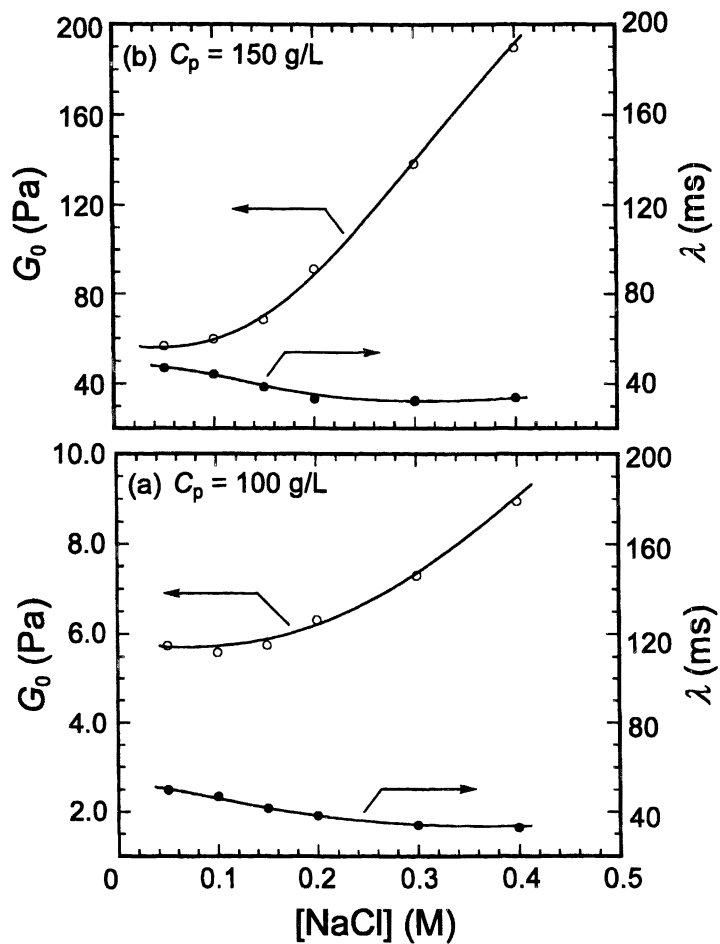


Figure 11. Dependence of plateau modulus ( $G_0$ ) and terminal relaxation time ( $\lambda$ ) on salt concentration for the copolymer of  $m = 6$  with  $f_{\text{DEG}} = 20$  mol % at (a)  $C_p = 100$  g/L and (b)  $C_p = 150$  g/L.

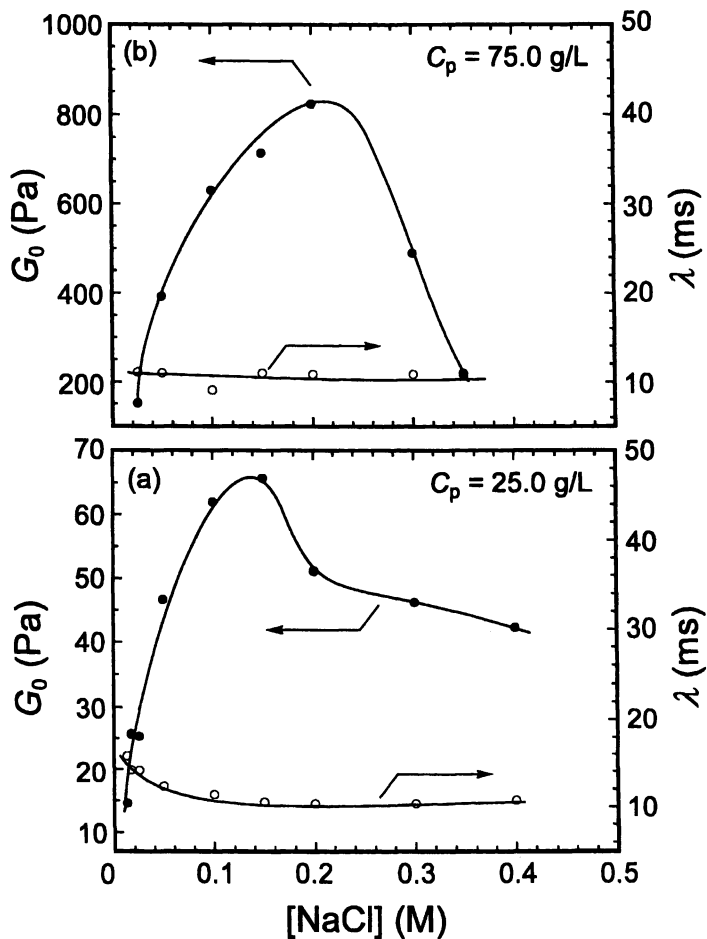


Figure 12. Dependence of plateau modulus ( $G_0$ ) and terminal relaxation time ( $\lambda$ ) on salt concentration for the copolymer of  $m = 25$  with  $f_{\text{DE}25} = 20$  mol % at (a)  $C_p = 25.0$  g/L and (b)  $C_p = 75.0$  g/L.

9). The lifetime of the crosslinks may depend on the residence time for a polymer-bound surfactant unit in a micelle. The terminal relaxation times may be related to the residence lifetime of the surfactant unit in the micelle under shear conditions.

Consequently, in the case of the copolymer of  $m = 6$ , the number of crosslinking junctions increases with increasing salt concentration, leading to an increase in zero shear viscosity. In the case of the copolymer of  $m = 25$ , however, the number of junctions increases with increasing salt concentration in a region of low salt concentrations (e.g.,  $[\text{NaCl}] < \text{ca } 0.13 \text{ M}$  for  $C_p = 25.0 \text{ g/L}$ ), but with a further increase in the salt concentration beyond a certain level, the number of junctions decreases with salt concentration. In both the cases, the lifetime of the junction remains practically the same independent of the polymer concentration over the salt concentrations examined. Micelles formed from  $C_{12}E_{25}$  may be more dynamic in nature than micelles formed from  $C_{12}E_6$  because the hydrophilic EO chain in  $C_{12}E_{25}$  is more than 4 times longer than that in  $C_{12}E_6$ . The longer EO chain in  $C_{12}E_{25}$  is responsible for the higher cmc (Figure 3) and smaller  $N_{\text{agg}}$  for  $C_{12}E_{25}$  micelles (Figure 4) than those for  $C_{12}E_6$  micelles. The relaxation times for the copolymer of  $m = 6$  are about 4 times longer than those for the copolymer of  $m = 25$ . This is probably due to the nature of  $C_{12}E_6$  micelles as compared to  $C_{12}E_{25}$  micelles.

### Concluding Remarks

Because of their relevance in molecular organization in biological systems and also to various practical applications, functionalization of polyelectrolytes with various hydrophobes has been and will continue to be an area of great scientific and technological interest. A key to designing a hydrophobically modified polyelectrolyte for a given application is a fundamental understanding of the structure-property relationship. This chapter has focused on micelle formation of  $C_{12}E_m$  surfactant moieties covalently linked to polyAMPS and rheological behavior in water of polymer networks crosslinked by micelles. The degree of crosslinking and the terminal relaxation time depend strongly on the length of EO chain in the  $C_{12}E_m$  surfactant moieties. The transient nature of the crosslinking junctions originating from the dynamic nature of the micelles dictates dynamic viscosity and viscoelastic behavior of solutions of the polymer networks.

### Literature Cited

1. Zhang, Y. X.; Da, A. H.; Hogen-Esch, T. E.; Butler, G. B. In *Water Soluble Polymers: Synthesis, Solution Properties and Application*; Shalaby, S. W., McCormick, C. L. and Butler, G. B., Eds.; ACS Symposium Series 467; American Chemical Society: Washington, DC, 1991; pp 159.



2. (a) Varadaraj, R.; Branham, K. D.; McCormick, C. L.; Bock, J. In *Macromolecular Complexes in Chemistry and Biology*; Dubin, P., Bock, J., Davis, R. M., Schultz, D. N. and Thies, C., Eds.; Springer-Verlag: Berlin, 1994, pp 15–31 and references cited therein. (b) Bock, J.; Varadaraj, R.; Schulz, D. N.; Maurer, J. J. In *Macromolecular Complexes in Chemistry and Biology*; Dubin, P., Bock, J., Davis, R. M., Schultz, D. N. and Thies, C., Eds.; Springer-Verlag: Berlin, 1994, pp 33–50 and references cited therein.
3. Schmolka, I. R. *J. Am. Oil. Chem. Soc.* **1991**, *68*, 206.
4. Almgren, M.; Bahadur, P.; Jansson, M.; Li, P.; Brown, W.; Bahadur, A. *J. Colloid Interface Sci.* **1991**, *151*, 157.
5. Malmsten, M.; Lindman, B. *Macromolecules* **1992**, *25*, 544.
6. (a) Linse, P.; Bjorling, M. *Macromolecules* **1991**, *24*, 6700. (b) Linse, P.; Malmsten, M. *Macromolecules* **1992**, *25*, 5434. (c) Linse, P. *J. Phys. Chem.* **1993**, *97*, 13896. (d) Linse, P. *Macromolecules* **1993**, *26*, 4437. (e) Linse, P. *Macromolecules* **1994**, *27*, 2685. (f) Malmsten, M.; Linse, P.; Zhang, K.-W. *Macromolecules* **1993**, *26*, 2905.
7. Webber, S. E. *Chem. Rev.* **1990**, *90*, 1469.
8. Webber, S. E. *J. Phys. Chem. B* **1998**, *102*, 2618.
9. Glatter, O.; Gunther, S.; Schilen, K.; Brown, W. *Macromolecules* **1994**, *27*, 6046.
10. Hurter, P. N.; Scheutjens, J. M. H. M.; Hatton, A. T. *Macromolecules* **1993**, *26*, 5592.
11. Hwang, F. S.; Hogen-Esch, T. E. *Macromolecules* **1995**, *28*, 3328.
12. Schultz, D. N.; Kaladas, J. J.; Maurer, J. J.; Bock, J.; Pace, S. J.; Schultz, W. W. *Polymer* **1987**, *28*, 2110.
13. Kumacheva, E.; Rharbi, Y.; Winnik, M. A.; Guo, L.; Tam, K. C.; Jenkins, R. D. *Langmuir* **1997**, *13*, 182.
14. Horiuchi, K.; Rharbi, Y.; Spiro, J. G.; Yekta, A.; Winnik, M. A.; Jenkins, R. D.; Bassett, D. R. *Langmuir* **1999**, *15*, 1644.
15. (a) Tirtaatmadja, V.; Tam, K. C.; Jenkins, R. D. *Macromolecules* **1997**, *30*, 1426. (b) Tirtaatmadja, V.; Tam, K. C.; Jenkins, R. D. *Macromolecules* **1997**, *30*, 3271.
16. Tam, K. C.; Farmer, M. L.; Jenkins, R. D.; Bassett, D. R. *J. Polym. Sci., Part B: Polym. Phys.* **1998**, *36*, 2275.
17. McCormick, C. L.; Nonaka, T.; Johnson, C. B. *Polymer* **1988**, *29*, 731.
18. Biggs, S.; Selb, J.; Candau, F. *Polymer* **1993**, *34*, 580.
19. Volpert, E.; Selb, J.; Candau, F. *Macromolecules* **1996**, *29*, 1452.
20. Regalado, E. J.; Selb, J.; Candau, F. *Macromolecules* **1999**, *32*, 8580.
21. Klucker, R.; Candau, F.; Schosseler, F. *Macromolecules* **1995**, *28*, 6416.
22. Branham, K. D.; Davis, D. L.; Middleton, J. C.; McCormick, C. L. *Polymer* **1994**, *35*, 4429.
23. (a) Horiuchi, K.; Rharbi, Y.; Yekta, A.; Winnik, M. A.; Jenkins, R. D.; Basst, D. R. *Can. J. Chem.* **1998**, *76*, 1779. (b) Dai, S.; Tam, K. C.; Jenkins, R. D. *Macromolecules* **2000**, *33*, 404. (c) Ng, W. K.; Tam, K. C.; Jenkins, R. D. *Eur. Polym. J.* **1999**, *35*, 1245. (d) Guo, L.; Tam, K. C.; Jenkins, R. D. *Macromol. Chem. Phys.* **1998**, *199*, 1175.
24. Kramer, M. C.; Welch, C. G.; Steger, J. R.; McCormick, C. L. *Macromolecules* **1995**, *28*, 5248.

25. Hu, Y.; Kramer, M. C.; Boudreaux, C. J.; McCormick, C. L. *Macromolecules* **1995**, *28*, 7100.
26. Branham, K. D.; Snowden, H. S.; McCormick, C. L. *Macromolecules* **1996**, *29*, 254.
27. Kramer, M. C.; Steger, J. R.; Hu, Y.; McCormick, C. L. *Macromolecules* **1996**, *29*, 1992.
28. Hu, Y.; Smith, G. L.; Richardson, M. F.; McCormick, C. L. *Macromolecules* **1997**, *30*, 3526.
29. Hu, Y.; Armentrout, R. S.; McCormick, C. L. *Macromolecules* **1997**, *30*, 3538.
30. Morishima, Y.; Nomura, S.; Ikeda, T.; Seki, M.; Kamachi, M. *Macromolecules* **1995**, *28*, 2874.
31. Yamamoto, H.; Morishima, Y. *Macromolecules* **1999**, *32*, 7469.
32. Hashidzume, A.; Yamamoto, H.; Mizusaki, M.; Morishima, Y. *Polym. J.* **1999**, *31*, 1009.
33. Yusa, S.; Kamachi, M.; Morishima, Y. *Langmuir* **1998**, *14*, 6059.
34. Yusa, S.; Hashidzume, A.; Morishima, Y. *Langmuir* **1999**, *15*, 8826.
35. Noda, T.; Morishima, Y. *Macromolecules* **1999**, *32*, 4631.
36. (a) Noda, T.; Hashidzume, A.; Morishima, Y. *Macromolecules* **2000**, *33*, 3694. (b) Noda, T.; Hashidzume, A.; Morishima, Y. *Langmuir*, **2000**, *16*, 5324.
37. Noda, T.; Hashidzume, A.; Morishima, Y. *Macromolecules* **2001**, *34*, 1308.
38. Ezzell, S. A.; Hoyle, C. E.; Greed, D.; McCormick, C. L. *Macromolecules* **1992**, *25*, 1887.
39. Hill, A.; Candau, F.; Selb, J. *Macromolecules* **1993**, *26*, 4521.
40. Dowling, K. C.; Thomas, J. K. *Macromolecules* **1990**, *23*, 1059.
41. (a) Ito, K.; Tanaka, K.; Tanaka, H.; Imai, G.; Kawaguchi, S.; Itsuno, S. *Macromolecules* **1991**, *24*, 2348. (b) Ito, K.; Kobayashi, H. *Polym. J.* **1992**, *24*, 199.
42. Branham, K. D.; Shafer, G. S.; Hoyle, C. E.; McCormick, C. L. *Macromolecules* **1995**, *28*, 6175.
43. Chang, Y.; McCormick, C. L. *Macromolecules* **1993**, *26*, 6121.
44. McCormick, C. L.; Chang, Y. *Macromolecules* **1994**, *27*, 2151.
45. Kalyanasundaram, K.; Thomas, J. K. *J. Am. Chem. Soc.* **1977**, *99*, 2039.
46. Nakajima, A. *J. Mol. Spectrosc.* **1976**, *61*, 467.
47. Ham, J. S. *J. Chem. Phys.* **1953**, *21*, 756.
48. Wilhelm, M.; Zhao, C.-L.; Wang, Y.; Xu, R.; Winnik, M. A.; Mura, J.-L.; Riess, G.; Croucher, M. D. *Macromolecules* **1991**, *24*, 1033.
49. Alami, E.; Almgren, M.; Brown, W. *Macromolecules* **1996**, *29*, 2229.
50. Yekta, A.; Xu, B.; Duhamel, J.; Adiwidjaja, H.; Winnik, M. A. *Macromolecules* **1995**, *28*, 956.
51. Xu, B.; Zhang, K.; Macdonald, P. M.; Winnik, M. A.; Jenkins, R. D.; Bassett, D. R.; Wolf, D.; Nuyken, O. *Langmuir* **1997**, *13*, 6896.
52. Vorobyova, O.; Yekta, A.; Winnik, M. A.; Lau, W. *Macromolecules* **1998**, *31*, 8998.
53. (a) Infelta, P. P.; Gratzel, M.; Thomas, J. K. *J. Phys. Chem.* **1974**, *78*, 190. (b) Infelta, P. P. *Chem. Phys. Lett.* **1979**, *61*, 88.

54. (a) Tachiya, M. *Chem. Phys. Lett.* **1975**, *33*, 289. (b) Tachiya, M. In *Kinetics of Nonhomogeneous Processes*; Freeman, G. R., Ed.; John Wiley & Sons: New York, 1987; Vol. **Chapter 11**, pp 575–650.
55. Noda, T.; Hashizume, A.; Morishima, Y. *Polymer* **2001** in press.
56. Tam, K. C.; Jenkins, R. D.; Winnik, M. A.; Bassett, D. R. *Macromolecules* **1998**, *31*, 4149.
57. Green, M. S.; Tobolsky, A. V. *J. Chem. Phys.* **1940**, *14*, 80.
58. Ferry, J. D. *Viscoelastic Properties of Polymers*; 3rd ed.; Wiley: New York, 1980.

## Chapter 3

# Network Inhomogeneities in Polymer Gels

Wilhelm Oppermann, Brigitte Lindemann, and Bettina Vögerl

Institute of Textile and Fiber Chemistry, University of Stuttgart, Pfaffenwaldring 55,  
D-70550 Stuttgart, Germany

Spatial inhomogeneities present in ionic and nonionic hydrogels depend systematically on network density and on the degree of swelling. To obtain a quantitative measure, the mean-square fluctuation of the refractive index,  $\langle \eta^2 \rangle$ , and the correlation length,  $\xi$ , were determined by static light scattering. Upon increase of the network density,  $\langle \eta^2 \rangle$  rises markedly while  $\xi$  remains essentially unchanged. When ionic gels are swollen in aqueous solutions containing various salt concentrations, a series of different degrees of swelling is obtained. In such a series,  $\xi$  rises with increasing swelling while  $\langle \eta^2 \rangle$  decreases, as expected due to three-dimensional expansion and dilution. The data determined in the state of formation of the network, however, deviate strongly from this tendency with  $\langle \eta^2 \rangle$  being some decades lower than in the swollen state.

Hydrogels made by crosslinking copolymerization are interesting materials for a variety of pharmaceutical and hygienic applications. The macroscopic properties such as swelling behavior and elasticity are quite well understood (*1*). However, little information is available on the internal structure and network topology.

One feature of particular interest is the presence of network inhomogeneities. These can be visualized as strongly crosslinked regions in a less densely crosslinked environment. The degree of such spatial inhomogeneities depends strongly on the conditions at preparation of the network and on the chemistry of the crosslinker. It was shown previously that there is a clear correlation between the reactivity of the crosslinker, the efficiency of the cross-linking reaction, and the size and density of network inhomogeneities (2). In this paper we report on the influence of the degree of swelling on the structural parameters as determined by static light scattering experiments.

## Experimental

### Materials

Hydrogels were prepared by copolymerizing acrylic acid or 50%-neutralized acrylic acid with N,N'-methylenebisacrylamide in aqueous solution. The monomer concentration was 10 or 15 % (weight/volume). Great care was taken to avoid dust particles in the samples. Therefore, appropriate starting solutions were filtered through Nalgene cellulose acetate filters into the light scattering cuvettes in a glove box, where polymerization took place. The polymerization reaction was initiated by the redox system tetramethyl ethylenediamine (72 mg/100 ml) / Na<sub>2</sub>S<sub>2</sub>O<sub>8</sub> (80 mg/100 ml).

To study gels in the swollen state, the samples were removed from the cuvettes and immersed in NaCl solutions of different concentrations for several days. After attainment of swelling equilibrium, the weight gain was determined and the degree of swelling,  $Q$ , was calculated as mass of swollen gel per mass of dry polymer. Cylindrical specimens of appropriate diameter were punched out of the swollen gels and brought back into the cuvettes. The small space between sample and glass was filled with the corresponding salt solution to reduce light reflections.

### Light scattering experiments

The measurements were carried out in a modified Sofica apparatus equipped with a HeNe-laser and a computerized data acquisition system. It was calibrated against a toluene standard. The cuvette was rotated to several positions and an ensemble average of scattering intensity was taken to account for the fixed structure of the gels.

The scattering intensity expressed as the Raleigh ratio  $R(q)$  is assumed to be due to thermal concentration fluctuations (ergodic contribution) and to

inhomogeneities resulting from the crosslinking of the chains by which a certain inhomogeneous structure is frozen in (non-ergodic contribution) (3,4).

$$R_{\text{gel}}(q) = R_{\text{th}}(q) + R_{\text{cr}}(q)$$

We are interested in the latter contribution. The experimental means to determine this quantity rests on the assumption that  $R_{\text{th}}(q)$  of a gel is practically identical to that of a solution of linear macromolecules under the same conditions,  $R_{\text{sol}}(q)$ . This is not exactly the case, but applies within 20% error. In particular, the thermal scattering of a gel should never become appreciably larger than that of the corresponding solution. A detailed discussion of this point is given in (3), where the relevant literature is thoroughly reviewed. When the total scattering of the gel exceeds that of the solution to a significant extent, the error in  $R_{\text{th}}(q)$  has no big effect, and  $R_{\text{cr}}(q)$  can be determined safely as the so-called excess scattering intensity:

$$R_{\text{cr}}(q) \cong R_{\text{E}}(q) \equiv R_{\text{gel}}(q) - R_{\text{sol}}(q)$$

by subtracting the scattering intensity measured on an uncrosslinked sample of the same polymer (and salt) concentration from the scattering intensity of the gel.

The Debye-Bueche analysis (5,6) was employed to obtain the correlation length,  $\xi$ , and the mean-square refractive index fluctuation,  $\langle \eta^2 \rangle$ , of the gels from the relationship:

$$R_{\text{E}}(q) = 4\pi K \xi^3 \langle \eta^2 \rangle / (1 + q^2 \xi^2)^2$$

Here  $K = 8\pi^2 n_0^2 \lambda_0^{-4}$ , and  $q$  is the scattering vector amplitude,  $q = 4\pi n / \lambda_0 \sin(\theta/2)$ . (Since  $q\xi \ll 1$ , an Ornstein-Zernicke type function is equally suitable to fit the data. This would only shift the parameters by a constant factor.)

## Results and Discussion

### Influence of Network Density on $\xi$ and $\langle \eta^2 \rangle$ for As-Prepared Gels

In one series of measurements, the crosslinker concentration was varied in gels based on 15 % acrylic acid. The pH in these systems is around 2.3, hence they are essentially nonionic with only around 0.25 % of the carboxylic acid groups being dissociated. Figure 1 gives an overview on the macroscopic properties of the gels. The shear modulus,  $G$ , measured by small uniaxial compression of the gel cylinders as reported elsewhere (7) is plotted versus the theoretical network density,  $\nu_{\text{th}}$ .  $\nu_{\text{th}}$  is twice as large as the molar concentration of

methylenebisacrylamide in the solution used to make the gels, because tetrafunctional crosslinks are formed. The data points correspond to crosslinker concentrations ranging from 0.9% to 4% with respect to acrylic acid. A straight line is obtained the slope of which can be used to calculate the crosslinking efficiency by comparison to the result of rubber elasticity theory (8,9):  $G = (1 - 2/f)\nu RT$ . For tetrafunctional crosslinks ( $f = 4$ ), the theory predicts a slope of  $RT/2 = 1200$  J/mol, while the experiments yield a slope of 340 J/mol. This means that the crosslinking efficiency is only about 30%. Generally, the lower the concentration at the synthesis of the gels, the smaller is the crosslinking efficiency (7,10,11) and the more pronounced is the heterogeneity.

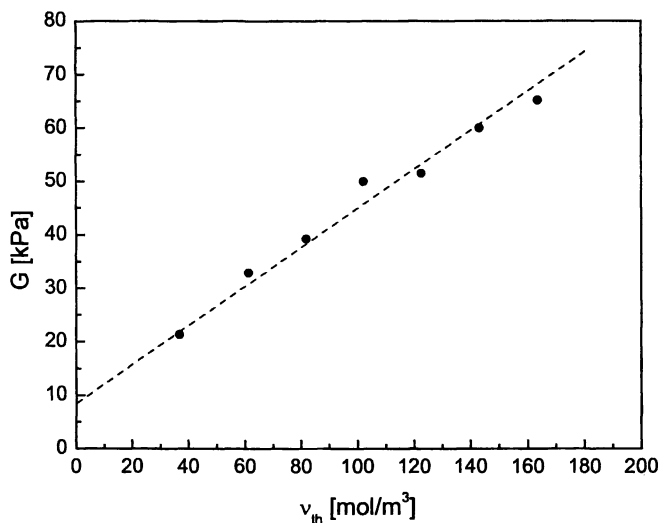


Figure 1. Shear modulus  $G$  versus nominal network density  $\nu_n$ .

The light scattering results obtained on these gels are shown in Figure 2. Additionally, the data for a solution prepared in the same way as the gels but without crosslinker are included (filled circles). The scattering intensity rises markedly with increasing network density.

The determination of the intrinsic viscosity of the polymer in the solution showed that the concentration where the light scattering data were taken is far above the overlap concentration; hence there is no appreciable molar mass dependence.

To determine the parameters  $\xi$  and  $\langle \eta^2 \rangle$ , the excess scattering intensity  $R_E(q)$  is calculated, and the inverse square root of this quantity is plotted versus

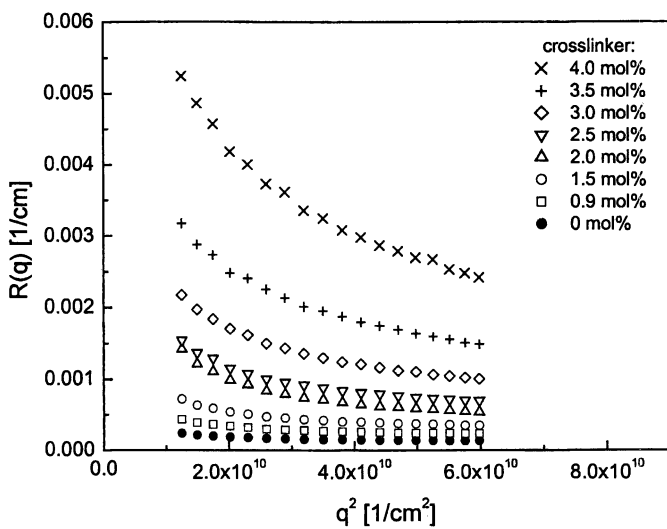


Figure 2. Rayleigh ratio as a function of  $q^2$ , gels with 15% polymer in the as-prepared state.

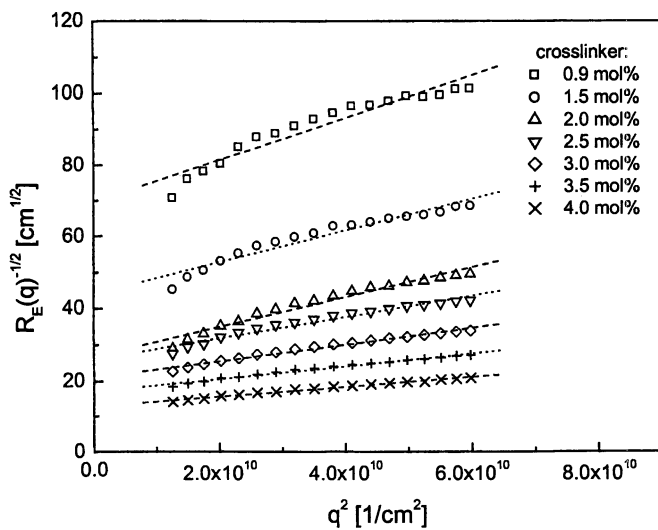


Figure 3. Debye-Bueche plot of data in Figure 2.



$q^2$  in Figure 3. According to the Debye-Bueche approach straight lines should be obtained. This is actually observed for the most heavily crosslinked samples containing 3-4% crosslinker. The lower the network density, the more pronounced is the curvature of the graphs. Nevertheless, straight lines as indicated in Figure 3 are drawn through the data points in order to obtain an estimate of the characteristic parameters.

Note that with the small network densities, the difference between the scattering intensities of the gel and the solution becomes rather small, hence small errors in measured values show up rather exaggerated. Also, an unexpected upturn of scattering intensities at small  $q$  was reported for semi-dilute polymer solutions (12). If this is also present in gels, it could be one reason for the observed curvature seen in the Debye-Bueche plots. To estimate the error resulting from the curvature, the evaluation of  $\xi$  and  $\langle \eta^2 \rangle$  was repeated by taking only the high- $q$  portion of the curve or the low- $q$  portion into account. This changes the slope and intercept of the line appreciably. The data so obtained were used to construct the error bars in Figure 4, where  $\xi$  and  $\langle \eta^2 \rangle$  are given as a function of network density. The correlation lengths are in the range 30 – 40 nm, fairly independent of network density. They are by far larger than the average spacing between crosslinks (3-5 nm). On the other hand,  $\langle \eta^2 \rangle$  rises markedly with increasing network density.

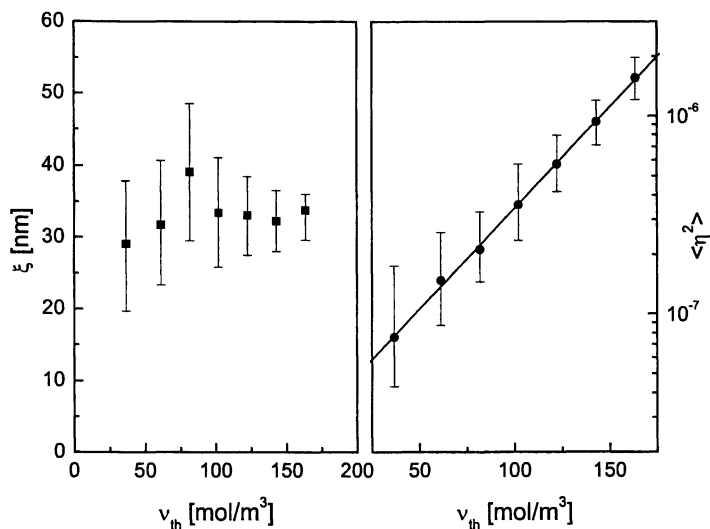


Figure 4. Correlation length and mean-square fluctuation of refractive index versus network density.

## Influence of Swelling

To study the changes brought about by swelling of the gels, a second series of experiments was made on another set of gels based on partially (50 %) neutralized acrylic acid crosslinked in a 10 % solution by 2 % N,N'-methylene-bisacrylamide. The acrylic acid was neutralized in part by NaOH in order to obtain polyelectrolyte gels whose degree of swelling could be adjusted over a wide range by immersing them in NaCl-solutions of different concentration (e.g. 13). The degree of swelling,  $Q$ , ranges from 30 to 200 as shown in Figure 5. Also shown are the shear moduli measured on these gels. Note that they increase strongly when the salt concentration is lowered and the degree of swelling rises. This rise of  $G$  despite of the dilution of the system is a proof of the marked non-Gaussian behavior of the network chains under these conditions (1, 14).

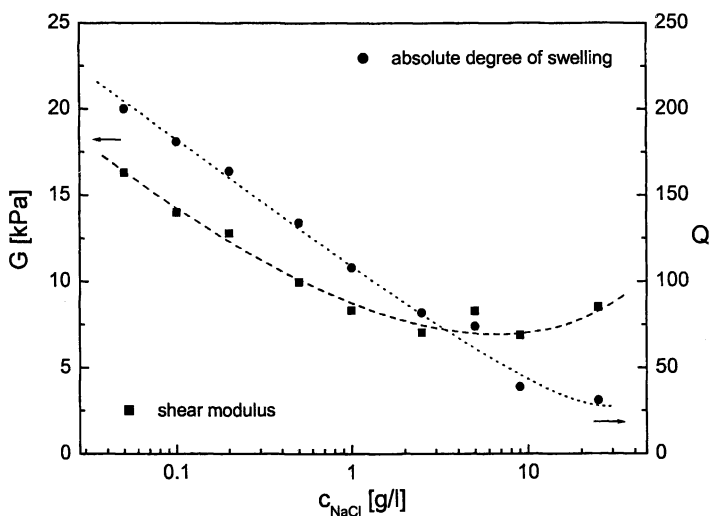


Figure 5. Variation of degree of swelling and shear modulus with salt content of swelling solution.

The results of the light scattering experiments performed on these gels are shown in Figure 6a. The scattering intensity rises strongly when going from the state of formation of the networks ( $Q = 10$ ) to  $Q = 31$ , and then decreases steadily upon further swelling. To apply the evaluation procedure as before, solutions of the linear polymer were prepared with concentrations chosen to match the polymer concentration within the gels. The salt concentration was also adjusted to equal that of the corresponding swelling solutions. Light scattering intensities

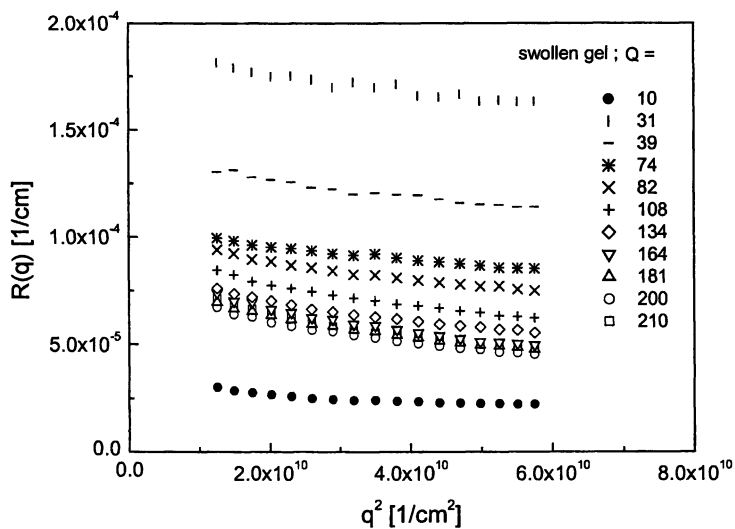


Figure 6a. Rayleigh ratio of gels at different degrees of swelling.

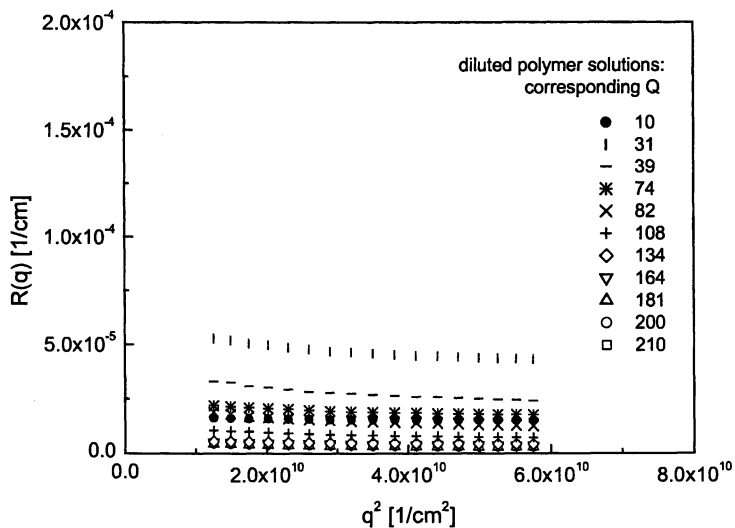


Figure 6b. Rayleigh ratio of solutions corresponding to gels in Fig. 6a

measured on these solutions are shown in Figure 6b, where polymer concentrations are indicated in terms of  $Q$  for easier comparison to the data in Figure 6a. There is an appreciable increase of the scattering intensity for the first dilution step ( $Q = 10 \rightarrow 31$ ), followed by a steady decrease. The absolute scattering intensities are much lower than those of the gels.

The intrinsic viscosity of the linear polymer determined in 0.1 M NaCl solution is around 200 ml/g. This shows that the concentrations used for the light scattering measurements are generally above the overlap concentration. Note that for the highest degrees of swelling, the salt concentration is far below 0.1 M, and the intrinsic viscosity is expected to become larger than 200 ml/g.

In Figure 7, the corresponding Debye-Bueche plot is shown. The data points are fairly close to straight lines, hence the analysis is quite reasonable. Figure 8 represents the dependence of correlation length and mean-square fluctuation of refractive index on the degree of swelling. It is observed that  $\xi$  rises with increasing swelling for those samples which are in swelling equilibrium (open symbols), as expected due to the three-dimensional expansion. However, the slope of the log-log plot is around 0.5, markedly higher than 0.33 to be anticipated if one considers volume expansion in a very simple way. The correlation length in the state of formation of the network (filled symbol) does not fit on the line and is much higher. This may be attributed to the fact that the gel is not in equilibrium with the free solvent.

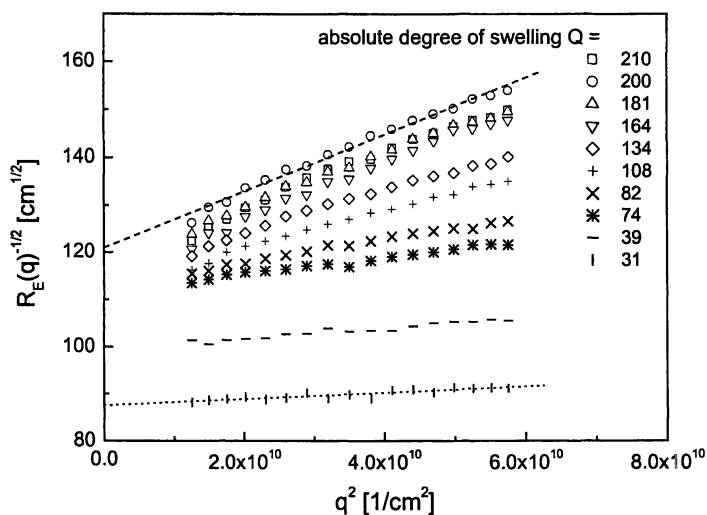


Figure 7. Debye-Bueche plot of gels at different degrees of swelling.

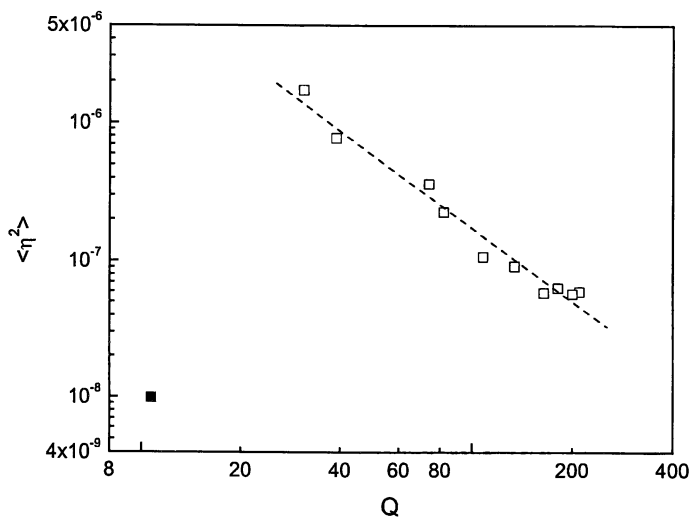
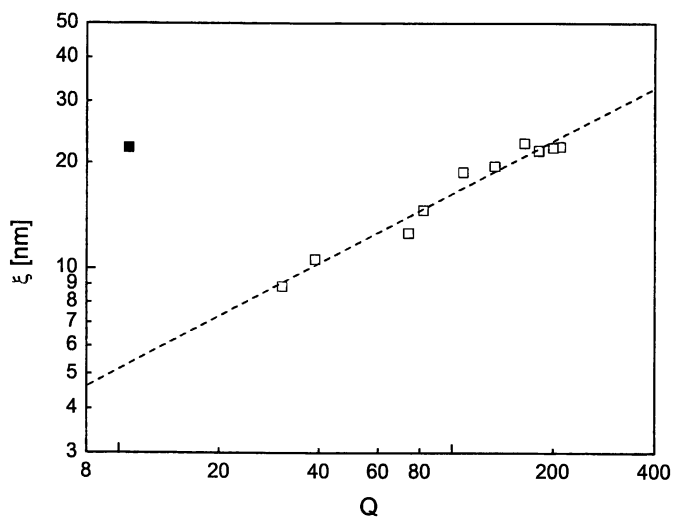


Figure 8. Correlation length (top) and mean-square fluctuation of refractive index (bottom) versus degree of swelling

$\langle \eta^2 \rangle$  shows a corresponding behavior. It decreases with rising degree of swelling due to the dilution of the system. The slope of the log-log plot is close to 2. The data for the state of formation of the network also deviates distinctly from this trend.

### Inspection of the Electrolyte Effect

To discuss the variation of  $\xi$  and  $\langle \eta^2 \rangle$  simply as a function of  $Q$  may be somewhat misleading, because the concentration of added salt is changed simultaneously. It is clear that this significantly affects the thermal contribution of the scattering intensity. However, we had proceeded on the assumption that one would get rid of this effect by considering the difference between gel and solution scattering. The influence of salt on the non-ergodic contribution,  $R_{cr}(q)$ , is less clear. Since it reflects a frozen-in structure, one could argue that it is not affected at all. On the other hand, a coupling between equilibrium and non-equilibrium phenomena cannot be excluded, hence  $R_{cr}(q)$  could be weakened or strengthened by salt.

One striking observation in Fig. 8 is the fact that there is a big change in  $\xi$  and  $\langle \eta^2 \rangle$  when going from the state of preparation of the network to the least swollen equilibrium state ( $Q \cong 30$ ). This also involves going from no added salt to the highest salt concentration. To find out experimentally what is the major cause of the drastic change of the scattering data, a comparison was made between two sets of gels. One set is the one discussed above, the gels being prepared in salt-free solution and brought to different degrees of swelling by immersing them in NaCl solutions of different concentration. For the second set the only difference is that the gels had been prepared in the presence of 2.2% NaCl (0.4 M). This is just the salt concentration used to attain the lowest equilibrium degree of swelling,  $Q \cong 30$ .

The macroscopic properties of the two sets were inspected by looking at the degree of swelling and the pertinent shear moduli. Figure 9 represents the dependence of the degree of swelling on the concentration of NaCl in the swelling solution. It is obvious that the two sets, though being prepared under markedly different conditions, show essentially identical behavior with only negligible offset. The courses of the modulus of the two sets (not shown) are also very similar. Hence there is no appreciable difference with regard to the macroscopic properties.

The scattering power of the gels is illustrated in Figure 10. For simplification, the Rayleigh ratio measured at an angle of  $90^\circ$ ,  $R_{90}$ , is plotted versus the degree of swelling. The course of this quantity is somewhat similar to that of  $\langle \eta^2 \rangle$  (cf. Figure 8). When going from the state of formation of the network ( $Q = 10$ ) to the lowest equilibrium degree of swelling ( $Q = 30$ ),  $R_{90}$  rises strongly, while it decreases gradually upon further swelling. All data for the gels

American Chemical Society  
Library

1155 16th St., N.W.  
Washington, D.C. 20036

In: Polymer Gels; Bohidar, H., et al.; ACS Symposium Series; American Chemical Society: Washington, DC, 2002.

prepared in the presence of NaCl (triangles) are below those of the other set (circles), but the general appearance is similar. Most important, both sets exhibit the sharp rise of  $R_{90}$  in the first swelling step, although there is a considerable rise in salt concentration for the first set, but practically no change in salt concentration for the second one. This clearly indicates that the electrolyte effect is not of major influence.

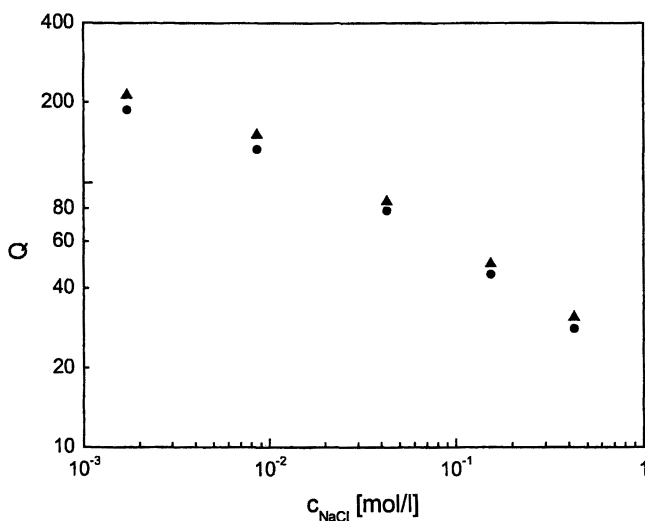


**Figure 9.** Degree of swelling as a function of NaCl concentration  
 ●: gels prepared in salt-free state; ▲: gels prepared in presence of 2.2% NaCl

## Conclusions

The results of the light scattering experiments show that spatial inhomogeneities are present in the gels studied. The fluctuation of the refractive index, presumably equivalent to the fluctuation of local polymer concentration, increases strongly with rising network density, whereas the correlation length does not change significantly. There is a distinct and fundamental difference between inhomogeneities observed in the state of network formation and those observed in gels swollen to equilibrium. It could be shown that this effect is not due to different salt concentrations in the samples. The excess scattering intensity is markedly higher for swollen gels, and the Debye-Bueche analysis traces this back to an even larger increase of the fluctuation of refractive index, while the correlation length surprisingly decreases somewhat.

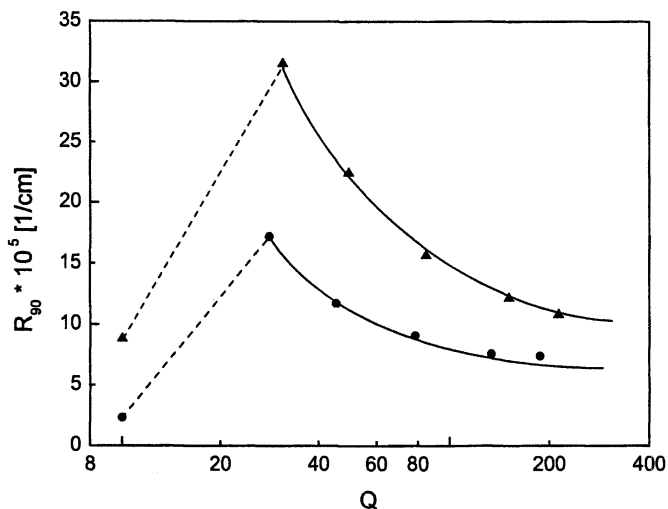


Figure 10.  $R_{90}$  versus degree of swelling; symbols as in Figure 9.

## Acknowledgements

Financial support from the German Science Foundation (DFG) and the Fonds der Chemischen Industrie is gratefully acknowledged.

## References

1. Schröder, U. P.; Oppermann, W. In *Physical Properties of Polymeric Gels*; Cohen-Addad, M., Ed.; Wiley; New York, 1996, pp 19-38.
2. Lindemann, B.; Schröder, U. P.; Oppermann, W. *Macromolecules* **1997**, *30*, 4073.
3. Bastide, J.; Candau, S. J. In *Physical Properties of Polymeric Gels*; Cohen-Addad, M., Ed.; Wiley; New York, 1996, pp 143-308.
4. Shibayama, M. *Macromol. Chem. Phys.* **1998**, *199*, 1.
5. Debye, P.; Bueche, A. M. *J. Appl. Phys.* **1949**, *20*, 518.
6. Soni, V. K.; Stein, R. S. *Macromolecules* **1990**, *23*, 5257.
7. Oppermann, W.; Rose, S.; Rehage, G. *British Polym. J.* **1985**, *17*, 175.



8. Treloar, L. R. G. *The Physics of Rubber Elasticity*, Oxford University Press, Oxford 1975.
9. Flory, P. J. *J. Chem. Phys.* **1977**, *66*, 5720.
10. Geissler, E.; Hecht, A.-M.; Horkay, F.; Zrinyi, M. *Macromolecules* **1988**, *21*, 2594.
11. Oppermann, W. *Angew. Makromol. Chem.* **1984**, *123/124*, 229.
12. Benoit, H.; Picot, C. *Pure Appl. Chem.* **1966**, *12*, 545.
13. Jeon, C. H.; Makhaeva, E. E.; Khokhlov, A. R. *Macromol. Chem. Phys.* **1998**, *199*, 2665.
14. Anbergen, U.; Oppermann, W. *Polymer* **1990**, *31*, 1854.

## Chapter 4

# Thermoreversible and Irreversible Physical Gels from Biopolymers

Simon B. Ross-Murphy

Biopolymers Group, Division of Life Sciences, King's College London,  
Franklin-Wilkins Building, 150 Stamford Street, London SE1 8WA, United Kingdom

### Introduction

In what has subsequently proved to be one of the most quoted articles in gels and gelation, Paul Flory in his introduction (published 1975)<sup>1</sup> to the 1974 "Faraday Discussion on Gels and Gelation" proposed the following classification of gels:

- I. Well-ordered lamellar structures, including gel mesophases.
- II. Covalent polymeric networks; completely disordered.
- III. Polymer networks formed through physical aggregation, predominantly disordered, but with regions of order.
- IV. Particulate disordered structures.

In this article we shall call these Flory I, II, III and IV gels respectively. The majority of synthetic polymer gels are formed by the covalent cross-linking of linear or branched macromolecules using multi-functional cross-linking agents (Flory II). Such gels are networks or true macromolecules with (nominally) infinite molecular weight and consequently they swell rather than dissolve if immersed in a good solvent. The class of materials, nowadays commonly referred to as physical gels, where cross-linking occurs by non-covalent interactions shares much in common with covalent networks, but because these very cross-links are not permanent, they will also show a number of differences. For example, they will tend to show rheological creep behaviour at long times and some will also dissolve rather than swell when placed into a good solvent. Some of these physical gels, such as gelatin gels, and in the case of synthetic polymers, those from certain iso- and syndio-tactic polymers, form on cooling a heated solution, while others form only on heating, as for example those formed from globular proteins and from certain cellulose derivatives. Also some, but by no means all, such gels are thermoreversible<sup>2</sup> i.e. they can be melted out and then will reform without any real hysteresis, since others are formed essentially irreversibly.

As suggested above some physical gels are formed from synthetic polymers, whereas others involve biopolymers.<sup>3,4</sup> In the latter case, non-covalent cross-links often comprise more specific and complex mechanisms involving, rather than point-like cross-links, “junction zones” of known, ordered secondary structure e.g. multiple helices, ion mediated “egg-box” structures etc. – all are Flory III gels. Typically there is a specific, and often intricate, hierarchy of arrangements, a situation which is more familiar to molecular biologists than to polymer physical chemists. We will also introduce the viscoelastic techniques for characterising physical gels, and then relate the properties to the underlying structure at the macromolecular and junction zone level. The parallels between synthetic and biopolymer gels will also be illustrated.

In this chapter, we will also discuss the determination of the gel point in both chemical and physically cross-linked systems, by viscoelastic measurements, and the advantages and possible limitations of this approach. Finally we will describe some of our recent work on the heat-set gelation of globular proteins (Flory IV systems), and on novel cold-set gels of gelatins derived from both mammalian and piscine sources. We will also describe, albeit briefly, models to relate the important parameter of the gelation time,  $t_g$ , to both polymer concentration and temperature for the former system.

### **Rheological Characterisation by Oscillatory Shear Measurements**

Over the last twenty years, the dynamic oscillatory shear experiment has become almost routine. This reflects the improvement in equipment design and computer software, which have turned such experiments from being the realm of the specialist rheologist into becoming a routine procedure. It still remains the best technique for the characterisation of the rheological properties of viscous fluids and soft solids, both of which are by their nature viscoelastic.<sup>5</sup> A sinusoidal oscillation of maximum strain  $\gamma$  and oscillatory frequency  $\omega$  is applied to the sample. If the material is perfectly elastic then the resultant stress wave is exactly in phase with the strain wave. By contrast, for purely viscous systems the rate of change of the sinusoidal oscillation is a maximum and the strain is zero, so the resultant stress wave will be exactly  $90^\circ$  out-of-phase with the imposed deformation. In general the stress wave will have a phase difference  $\delta$  ( $0 < \delta < 90^\circ$ ) and  $\delta$ , or more usually  $\tan \delta$ , is a measure of the viscous/elastic ratio for the material at frequency  $\omega$ . The  $\omega$ -dependent elastic (in-phase) and viscous (out-of-phase) components, the shear storage modulus  $G'$  and the loss modulus  $G''$ , respectively are then separable by software correlation analysis, and the resultant complex viscosity  $\eta^*$  calculated, in the instrument.

Formally this is true only for very small strains. As far as viscoelastic measurements are concerned the coupling of strain and strain rate (frequency) can be a serious problem. This is because only in the small strain limit will the correct  $G'$  and  $G''$  profiles be obtained. The design of an instrument with good minimum strain resolution and good stress detection sensitivity is not, and the purchase of such an instrument can be costly.

If a linear polymer is prepared in the melt above a certain molecular weight (or relative molecular mass) typically  $> 2 \times 10^4$ , it shows enhanced viscosity, due to the presence of entanglements. The same is true for a solution when the product of concentration and molecular weight ( $CM_w$ ) is greater than this figure. Therefore "entanglement networks" are formed by the topological interaction of polymer chains, above some critical value of  $CM_w$ , either in the melt or in solution. These behave as viscoelastic solids at frequencies higher (time-scales shorter) than the lifetime of the topological entanglements. The relevant frequency depends for linear chains on  $M_w^3$ , where  $M_w$  is the (weight average) molecular weight. Such behaviour is described in the book by Doi and Edwards.<sup>6</sup> The classical "mechanical spectrum" of an entangled polymer solution or melt shows a number of features.

At lower frequencies, in the 'terminal zone', it flows as a high viscosity liquid, with  $G' \propto \omega^2$  and  $G'' \propto \omega^1$ . As the frequency is increased there is a "cross-over" in  $G'$  and  $G''$ . At still higher frequencies  $G'$  and  $G''$  are parallel, with  $G' > G''$  and with a largely frequency insensitive spectrum, i.e. both  $G'$  and  $G''$  are  $\propto \omega^0$ . This is commonly referred to as the plateau region.

As implied above, the extent of the low frequency plateau of  $G'$  should depend on  $M_w^3$ . Therefore as the molecular weight increases the plateau region will move to lower and lower frequencies, as illustrated in Figure 1. If the molecular weight becomes extremely large, then the end of plateau frequency can be well below the instrument measurement range (in  $\text{rad s}^{-1}$ ,  $= 2\pi \times \text{frequency}$  in Hertz, typically 0.01 to 50). For a branched cross-linked microgel particle, it is easy to estimate the molecular weight to be of the order of  $10^{12}$ . For a true megamolecule, such as a macroscopic cross-linked network, or a swollen gel, the apparent molecular weight is  $> 10^{16}$ . In this case the longest relaxation time will be well outside any instrument range, and only the plateau modulus or gel spectrum is seen. (The relaxation spectrum for a branched system is much broader than for a linear system, since there are many more "chain paths" for relaxation). A typical mechanical spectrum for a biopolymer hydrogel is illustrated in Figure 2 (although the curvature in  $G''$  may also be more pronounced than is seen here). For lower concentration gels, the slope is slightly greater, although measure close to, or below the critical gel concentration are quite difficult, since such systems usually gel from the dilute, rather than the semi-dilute region.

In the preceding paragraphs we have considered the dynamic mechanical spectra of gels and entangled polymer solutions as a function of frequency, an approach pioneered by J. D. Ferry and co-workers in the 1950s and 60s. However, there is little discussion of the strain dependence in this work, or in his classic monograph.<sup>5</sup> This is because most synthetic polymer solutions, melts,

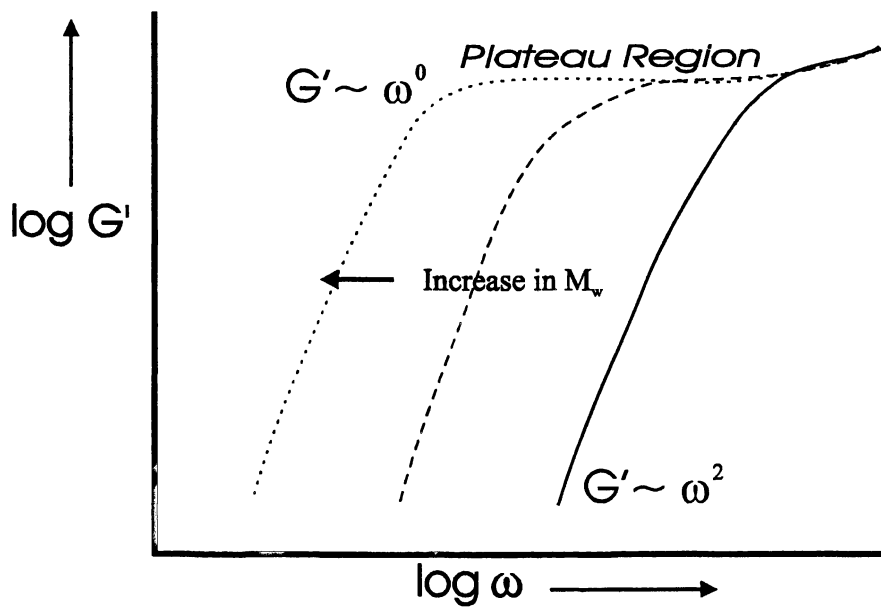


Figure 1 Effect of increase in  $M_w$  for linear polymers on the modulus  $G'$  plotted against frequency. (Reproduced with permission from reference 4. Copyright 2002 Marcel Dekker.)

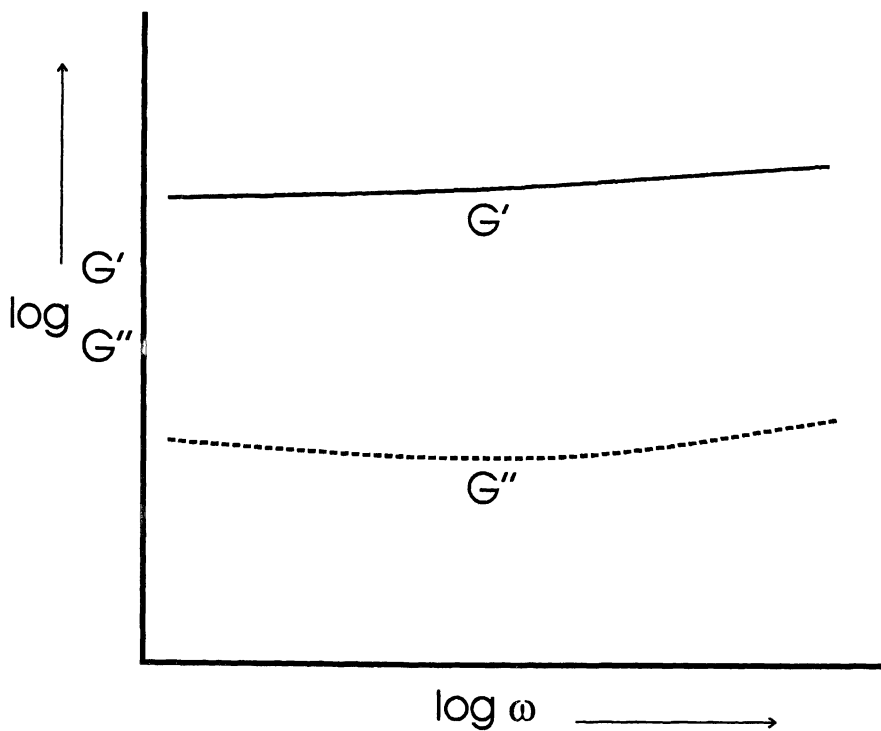


Figure 2 Typical gel spectrum observed, with  $G' > G''$  and both showing little frequency dependence. (Reproduced with permission from reference 4. Copyright 2002 Marcel Dekker.)

rubber networks and glasses are relatively strain insensitive. This is not, however, always the case for biopolymer gels and solutions.

Small and intermediate oscillatory shear strain sweep measurements have enabled a better distinction to be made between what we have defined, albeit qualitatively, as “strong” and “weak” gels.<sup>7</sup> At small enough strains both give essentially the same “gel” mechanical spectrum, with  $G' > G''$ , and with both moduli largely independent of frequency over the breadth of the experimental window. However, the strain dependence of the two classes of materials may be very different. Although no completely hard and fast rules can be stated, not least because such properties are concentration dependent, the moduli, for strong gels are essentially strain independent (linearly viscoelastic) for strains  $\gamma_{lin} \geq 0.25$ , whereas for weak gels they becomes strain dependent when  $\gamma_{lin} \sim 0.05$ . Consequently these behave more like colloidal particle networks (where  $\gamma_{lin}$  may be  $< 0.001$ ). Indeed merely employing the term “weak gel” is liable to generate some confusion, since it is by nature qualitative. (How weak is weak?) It may be safer just to regard such system as structured liquids. Subjecting a sample to large deformations can discriminate further between true gels and these structured liquids. Strong gels will rupture and fail – and it is sometimes asserted (including by this author) that they will never “heal” properly without melting and resetting, although it also appears this hypothesis has never been fully tested!<sup>8</sup> By contrast, and like polymer melts, the so-called “weak gels” will recover given sufficient time. Under appropriate conditions the latter can also be measured, without apparent fracture, under steady shear flow.

A complete characterisation of gel (and gel-like) materials therefore requires both strain and frequency sweeps to be carried out. Indeed since, in general, the two parameters are coupled, the ideal experiment would require a strain sweep to be carried out all frequencies, in order to determine the value of  $\gamma_{lin}$ , prior to making a frequency sweep. In practice it is usually sufficient to choose a frequency in the middle of the experimental range, and then vary the strain. In this case it is important to appreciate that, because of the sample and instrument response,  $\gamma_{lin}$  may decrease at both higher and lower frequencies.

### Kinetic Aspects

Gelation is, of course, a kinetic process, and with modern equipment it is very simple to place an ungelled solution on the instrument and adjust conditions and follow the behaviour of  $G'$  and  $G''$  as a function of time. For physical gels the major control factor is usually the temperature, for chemical gels the amount of cross-linker. The trace observed shows a characteristic shape characteristic “cure” curve of  $\log(G', G'')$  against time. For the fluid state  $G''$  will be greater than  $G'$ . After the start of the cure experiment there is an initial lag time. Subsequently both  $G''$  and  $G'$  begin to increase, but with  $G'$  increasing faster than  $G''$ . Consequently at a given time there is a cross-over where  $G'$  becomes greater

than  $G''$  sometimes associated with the gel(ation) time, (although this does not necessarily occur at the same time). Subsequently  $G'$  continues to increase, before levelling off, while  $G''$  ideally passes through a parabolic maximum, and then decreases to zero. The maximum in  $G''$  is an effect that can be associated with the relaxation of "dangling chain ends". The  $G'$  (strictly  $G$ ) vs. time kinetic behaviour has been calculated by Clark, in terms of the branching model.<sup>9</sup> This form of behaviour is illustrated in Figure 3, in a typical experiment when  $G'$  is monitored at a constant frequency. As the concentration of polymer is increased, the gelation time falls, but the value of  $G'$  at long (actually asymptotic) times increases.

### Critical Gels

Many authors have tried to use dynamic measurements to assess what we may refer to as the rheological gel point. For example, it may be taken when the growth of the modulus ( $G'$ ) on gelling becomes just greater than a pre-assigned threshold value, or when  $G'$  becomes greater than  $G''$ , (i.e. when  $\tan \delta$  becomes just less than 1) sometimes called the cross-over point. The latter method has been employed for decades in the adhesives industry.

The method of Winter and Chambon<sup>10</sup> helps provide a sounder approach. They assumed (and this is a strong assumption, which seems to neglect entanglement effects) that at the gel point the stress relaxation modulus  $G(t)$  could be represented by a power law  $G(t) \sim t^{-n}$ . From the Laplace transform, at the gel point,  $G'(\omega)$  and  $G''(\omega)$  should both be proportional to  $\omega^n$ . We can then pose the question: "What is the value of the common exponent  $n$ ?" It must have some value between the absolute limits of 0 and 2 for  $G'$ , and 0 and 1 for  $G''$ . One simple "guesstimate" would be the arithmetic mean of the two limit exponents  $((0.5 \cdot 2) + (0.5 \cdot 1)) / 2 = 0.75$ . In practice this, and the corresponding geometric mean (0.72), are quite close to a number of (more soundly based, but not necessarily more useful) theoretical estimates. These lie mostly in the range 0.5 to 0.75; corresponding experimental results for a number of systems fall mainly in the range 0.3 to 0.8, with the more extreme values corresponding to non-stoichiometric cross-linking systems.

Work by the present author in collaboration with a major group in Rome, interested in the chemical cross-linking of polysaccharides, can be used both to illustrate the approach, and to display the form of this critical gel spectrum.<sup>11</sup> (We note that while the majority of critical gels do seem to reflect this behaviour, it does not appear to be universal, as shown by Ilavsky and co-workers.<sup>12</sup> There are also systems that can be regarded as critical gels, if at all, only by twisting the definition, which appear to give the same shape of spectrum).

In the work described here,<sup>11</sup> we employed a stoichiometrically "lean" ratio of cross-linker, (1,6-dibromohexane, DBH) to polysaccharide



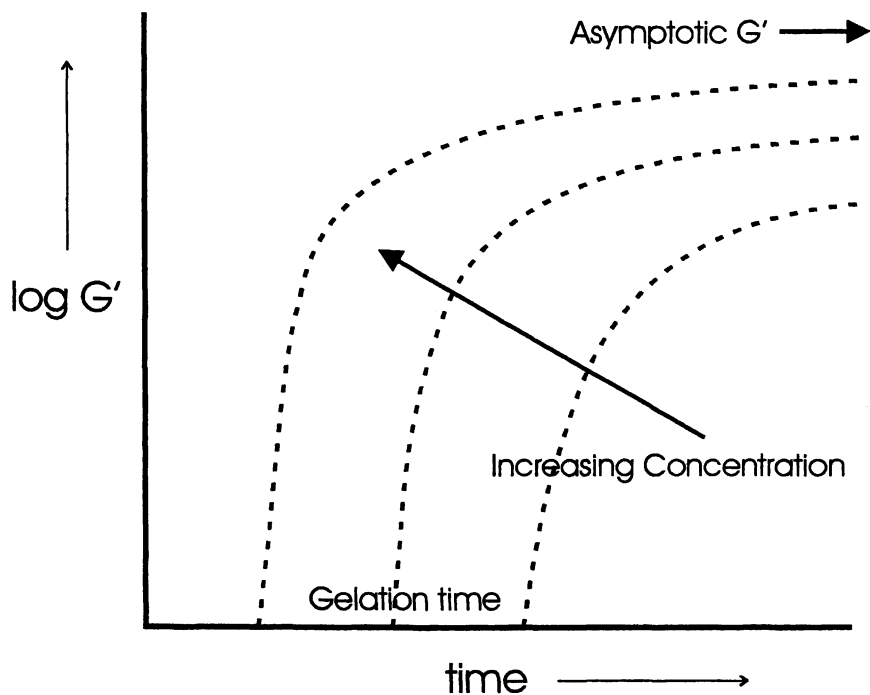


Figure 3 Time dependence of  $G'$  for a gelling system. As the concentration increases, the asymptotic modulus is increased, but the gelation time is decreased. (Reproduced with permission from reference 4. Copyright 2002 Marcel Dekker.)

(polygalacturonic acid, PGA) chains, to prepare systems effectively “frozen” at different ultimate degrees of cross-linking. As the concentrations of the cross-linker and the polymer are varied, the proportion of cross-links involved in elastically effective intermolecular cross-links will alter. This means many cross-links are “wasted” in intramolecular reaction stages. This wastage therefore naturally includes an increasing degree of cycles and other processes leading to cross-link dissipation. This means that by carefully selecting the amount of cross-linker, it should be possible to have the reaction go to completion just as the system reaches the gel point. This means that a stable critical gel can be prepared. Since the Winter-Chambon power-law gelation criterion is assumed to “universal” (even if the precise exponent is not) this should not effect its appropriateness as a determinant of the rheological gel-point.

This was actually the original approach, but some workers have tried to follow the time dependent growth of cross-linking, even employing the “multi-wave” technique, in which a Fourier sum of different frequency sine waves is applied. The idea is to perform a series of mini-frequency sweeps repeated regularly, say every 2 minutes of the reaction. However, the problem with such time dependent (so-called “on-the-fly”) frequency measurements is that the frequency information must become convoluted with the change in moduli from the gelation kinetics. Unfortunately many literature data reflect this (in the author’s view erroneous) approach. Another aspect which could be investigated by this method, and not by any other, is whether or not at (or close to) the rheological gel-point the properties of this chemical gel, based upon polysaccharide chains, becomes noticeably more strain dependent. As suggested above, this might be expected for purely physical polysaccharide gels.

In the experiments, a series of partially esterified PGA systems (tetrabutyl ammonium salt form) were prepared by dissolving the PGA in DMSO, adding cross-linker and reacting for >5000 seconds, until no further change in properties was observed. Then mechanical spectra (frequency and strain sweeps) were taken. Samples were not appreciably strain dependent, at least in the range 0-0.05 strain units, although higher strains did appear to produce some reduction in  $G'$ .

The frequency spectra, illustrated in Figure 4, taken at a strain well within this pre-established linear region, show a sharp transition from pre-gel ( $R = 0.080$ ) to post-gel ( $R = 0.090$ ) behaviour, where  $R$  is the stoichiometric ratio of the DBH cross-linker. At  $R = 0.084$  a clear power law region is seen in both  $G'$  and  $G''$ , with  $G'' \sim 2 \cdot G'$ , extending over 3 decades. The frequency exponents were  $\sim 0.66$  for  $G''$  and  $\sim 0.64$  for  $G'$ . This gives a mean slope of  $\sim 0.65$ , in good agreement with previous results. (Although there is some indication of systematic oscillations, particularly in the  $G'$  trace, this is probably due to minor instrumental artefacts. Certainly the data are statistically highly linear).

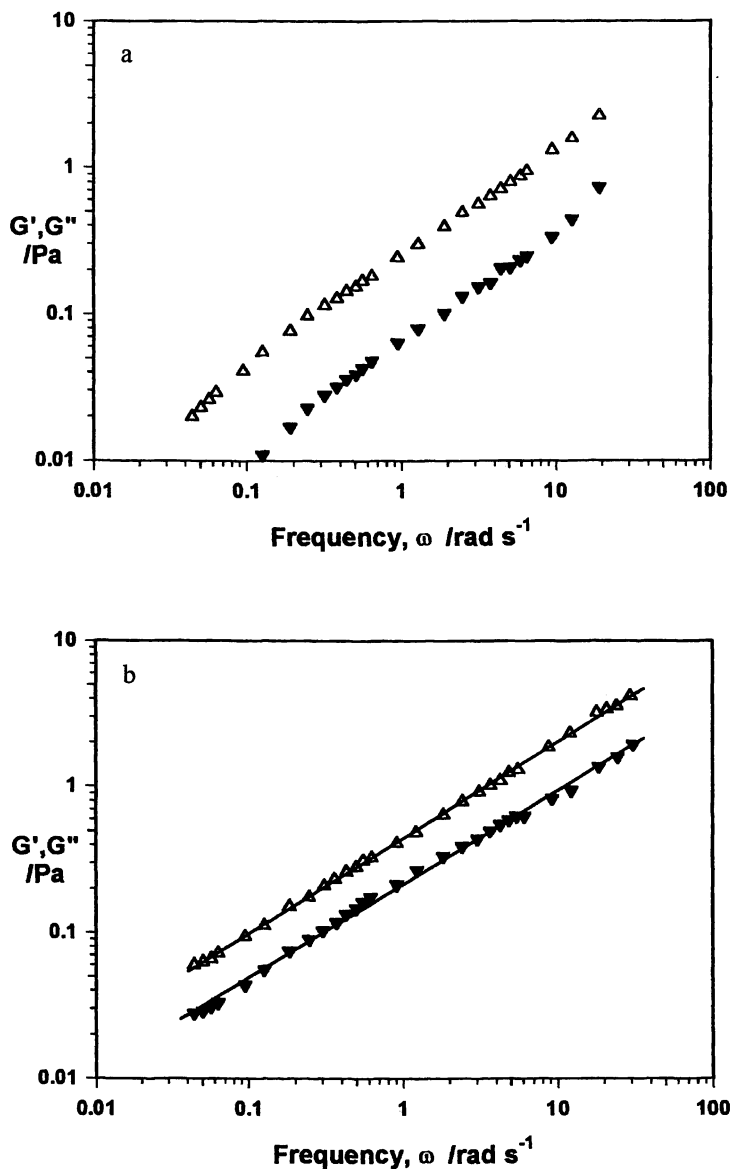
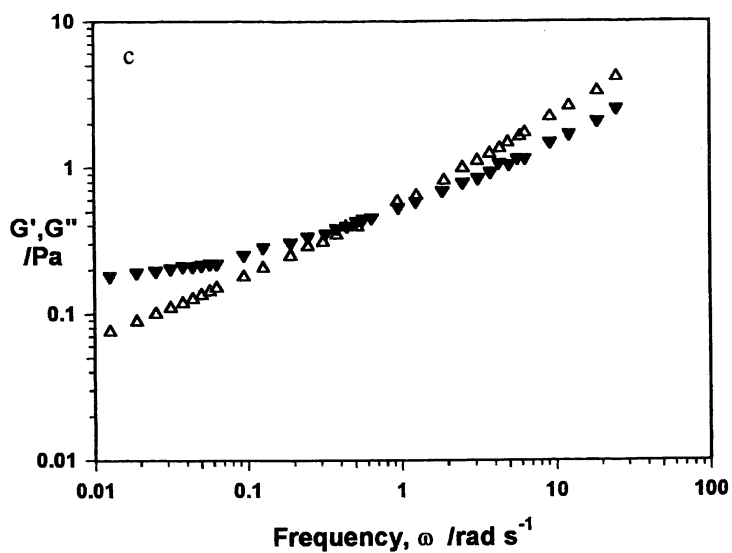


Figure 4 Mechanical spectra of PGA-1,6-dibromohexane cross-linked systems at different cross-linker stoichiometries  $R$ . The polymer is concentration 6% (w/v) in DMSO at 20C.  $G'$ : filled triangles;  $G''$ : open triangles. (a)  $R=0.080$ ; (b)  $R=0.084$ ; (c)  $R=0.090$ . (Adapted with permission from reference 11. Copyright 1995.)

Figure 4. *Continued.*

Some years ago, at a Faraday Meeting on Gels, held in Paris, the author made the suggestion that there should be a cusp-like discontinuity for the linear viscoelastic strain at the gel point, illustrated in Figure 5.<sup>13</sup> This was based on the reasonable hypothesis that  $\gamma_{lin}$  depends upon the reciprocal molecular weight of the sol fraction before gelation, and on the (amount of) gel fraction afterwards shows, this may be vanishingly small. At the time he commented that this region may be so minute that it is of no practical insignificant, although this may not be the case for physical gels, since the structure of these is necessarily more tenuous than that for covalently cross-linked systems. Recent measurements appear to have confirmed some aspects of the behaviour.<sup>14</sup>

### **Cold Set Gelatin Gels from Alternative (Piscine) Sources**

Gelatin-water systems represent the paradigm of a thermoreversible gelling (bio)polymer system. Furthermore, gelatin gels have found widespread use in the food and photographic industries over the years. As far as the scientific literature is concerned, almost all published work has concentrated on gelatins derived from traditional mammalian collagen sources. Consequently, less attention has been given to gelatin from alternative sources. Here we will discuss the properties of gelatin derived from fish, and compare the results obtained with those found for "traditional" samples.<sup>8,15</sup>

It has been known for many years<sup>16</sup> that the melting and gelling temperature of gelatin has been found to correlate with the proportion of imino acid residues in the original collagen. This is typically ~24% for mammals and 16 - 18% for most fish species. Cold water fish, for example cod, have a very low hydroxyproline content and coupled with this is a very low gelling and melting temperature. Consequently a 10% mammalian gelatin forms a gel at ~room temperature, whereas 10% cod will just about gel at ~2°C. The aim of this work is to examine single component fish gelatins as well as some blends and to investigate how the properties of the single systems are altered in the blends. Rheological measurements have been used to characterise the gelling and melting temperatures and the gel modulus. Such measurements have benefited greatly by improvements in instrumentation in recent years. Fish samples studied were tilapia, tuna, megrim and cod, ranging in order from tropical to cold water. The overall results are of great interest, but we summarise only the main details, since a more extensive account is in press.

Gelatin samples prepared from the collagen of cold water fish, such as cod, display much lower melting behaviour than typical mammalian (bovine and porcine) samples and presumably due to the lower imino acid content (although there is also a small molecular weight effect). The melting behaviour fits the Takahashi model for both mammalian and fish samples. The former data are illustrated in Figure 6.<sup>17</sup> This is a useful extension of the classical Eldridge-Ferry<sup>18</sup> (van't Hoff-like model) which enables both molecular weight and

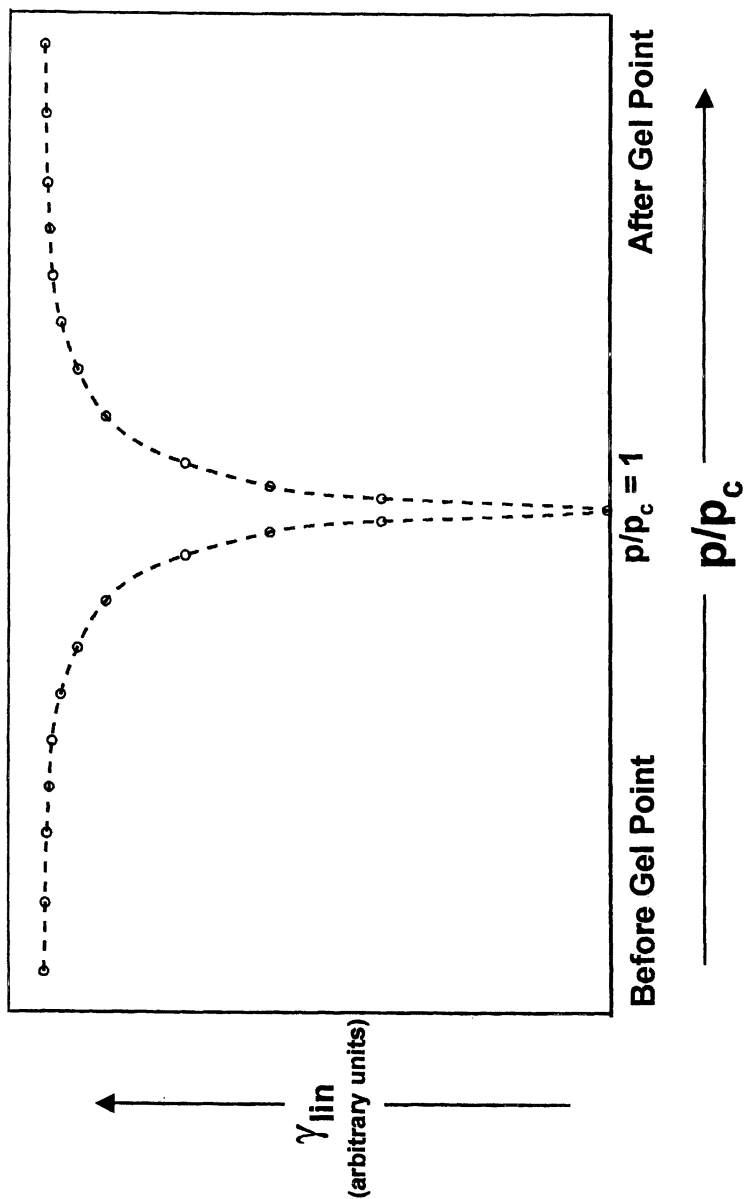


Figure 5 Linear viscoelastic strain (arbitrary units) plotted against  $p/p_c$  (arbitrary scale), where  $p_c$  is the gel point conversion (percolation threshold). (Adapted with permission from reference 13. Copyright 1995.)

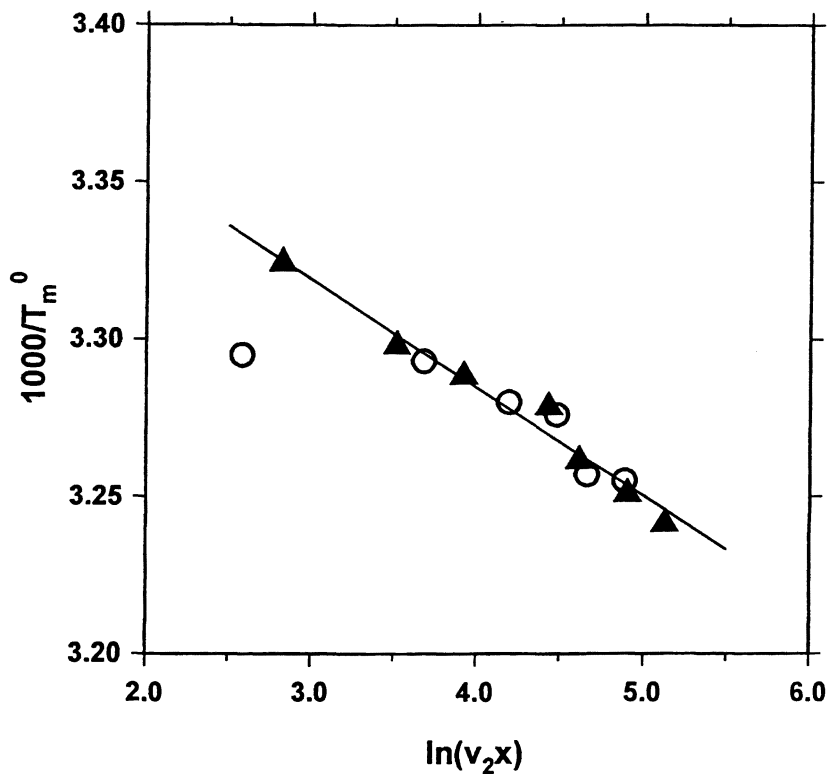


Figure 6 Takahashi plot for bovine (open circles) and porcine (filled triangles) gelatin samples, ordinate is the product of polymer concentration and chain length. (Adapted with permission from reference 8. Copyright 2000.)

concentration dependence to be related to the melting temperature of the gels. The frequency dependence for cod gelatin samples, and to a lesser extent bovine gelatin samples do, on closer examination, show some features qualitatively more similar to an entangled melt than those of a cross-linked polymer network with an equilibrium modulus. This, we suggested, has potentially profound consequences for our understanding of gelatin gels, and also suggests the prospect of performing healing experiments on such gels.

### Heat Set Gels from Globular Proteins

Globular protein gels have been extensively investigated over many years, although the great majority of studies have used rather crude and/or mixed samples of protein. Moreover, most previous work has concentrated on examining structural and rheological properties of fully cured gels. Here we will discuss heat-induced gelation of the globular proteins, bovine serum albumin (BSA) and  $\beta$ -lactoglobulin ( $\beta$ -Lg) not far from critical gel conditions together with aspects of kinetic gelation theory. For systems heated to temperatures not much greater than for initial protein unfolding,  $T_c$  ( $\sim 60$ - $80^\circ\text{C}$ ), many studies, using electron microscopy, X-ray scattering and spectroscopic techniques, have confirmed that the globular conformation of the native protein is only slightly perturbed.<sup>19-21</sup> It appears that denaturation partially disrupts the protein without modifying the overall shape very significantly, but exposes some intra-globular hydrophobic residues. At low enough concentrations these can refold all but reversibly, but above a certain concentration there is competition between intra- and intermolecular  $\beta$ -sheet formation. If the latter predominates, gels are formed which are fibrillar, and whose fibrils are approximately 1-2x the width of the original globule. The parallels between these fibrils and the insoluble protein fibrils being formed and laid down in disease states (so-called  $\beta$ -amyloid fibrils) are of considerable interest.<sup>22</sup> The latter exist, as one example, in the brains of patients with Alzheimer's disease, although similar structures are formed in other dementias such as Huntington's chorea.<sup>23</sup>

The balance between linear and branched chain growth depends upon both pH and ionic strength  $I$ , and a range of "gels" can be prepared ranging from transparent through translucent to biphasic gels and turbid coagulates without macroscopic strength. Experimental "phase" diagrams can be constructed showing the boundary between sols, clear gels and turbid gels as a function of protein concentration, pH and  $I$ . In fact boiled "egg white" is only white because of the concentration of salt in the ovalbumin solution, suitable dialysis can produce a transparent "white". Prolonged heating of protein gels to  $>85^\circ\text{C}$  produces a more drastic change, and some intermolecular covalent disulphide bonds are formed; these gels can no longer be regarded as merely physical networks.<sup>3</sup>



In the experimental work described here, gel formation is achieved by isothermal heating, and the changes in rheological properties during the gelation process monitored by dynamic shear rheometry as a function of time.<sup>24-29</sup> The measurements were carried out at different temperatures and protein concentrations to clarify their effects on the gelation, and the concentration and temperature dependence of the gelation time for heat set gels of the globular proteins BSA and  $\beta$ -Lg determined. What we have established is that the gelation time,  $t_c$  (however precisely measured and defined) is a unique kinetic variable. Further,  $t_c$  can prove of great value in understanding the behaviour of gels prepared under a wide range of conditions such as concentration, pH, I, heating rate, final heating temperature etc. Indeed samples prepared under a wide range of conditions can be scaled to a universal form. Our work has concentrated on developing a simple model that can describe both the temperature and concentration dependence of this gel time. By assuming an Arrhenius form for the dependence of temperature ( $T$ ) and the simple kinetic behaviour for concentration ( $C$ ) an equation was derived to relate  $t_c$  to  $T$  and  $C$  in the form

$$\ln(t_c) = a_1 + a_2 \ln(C) + a_3 / T + a_4 \ln(C)/T \quad (1)$$

(We note here that in this original publication<sup>24</sup> the terms in  $1/T$  were given erroneously as simply as  $T$ . We take this opportunity to correct the oversight. Fortuitously, since  $T$  refers to temperature in Kelvin, and the range employed was 330K to 365K,<sup>25</sup> the expressions in terms of both  $T$  and  $1/T$  are themselves almost linear).

By interpolating the geltime determined at a range of concentrations it is possible to construct a phase diagram (strictly a state diagram) of gelation temperature versus concentration, Figure 7. Recently, the author has begun referring to this novel presentation as a “Tobitani diagram”. This clearly illustrates the qualitative similarity between thermal gelation of globular proteins and the upper critical solution temperature (LCST) type phase diagram seen for certain fluid (and polymer solution) systems. We await theoretical developments to confirm whether or not this apparent behavioural similarity can be made formal.

### Acknowledgements

The author would like to acknowledge a number of collaborators including Dr. A. Tobitani and Dr. P. Gilsenan of King’s College London and Dr. P. Matricardi of “La Sapienza” University, Rome, for providing much of the data described above.

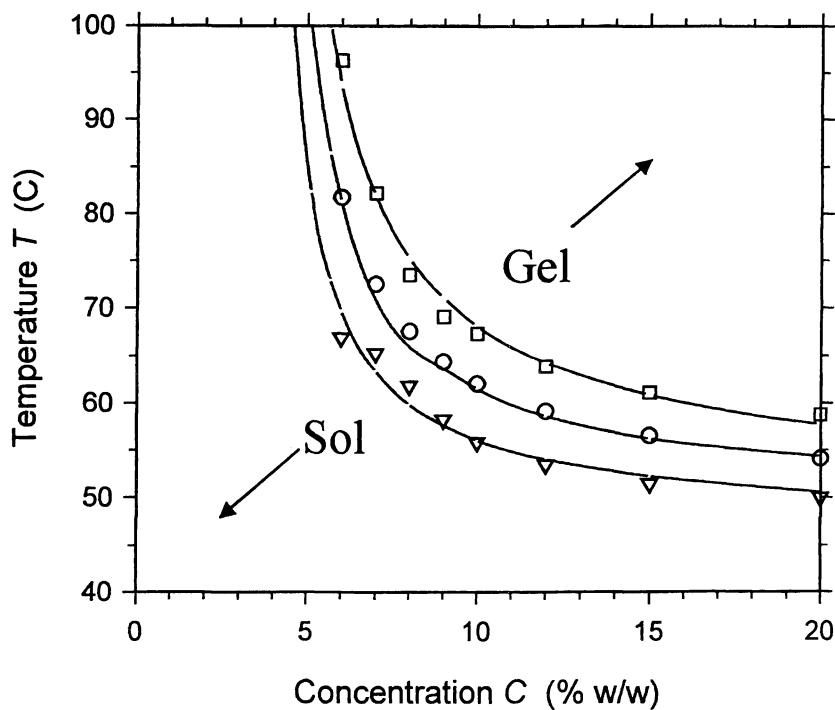


Figure 7 Temperature vs. concentration (Tobitani) sol-gel state diagram for bovine serum albumin (BSA) heat-set gels. Symbols represent interpolated gelation times (squares, 100s; circles, 1000s; triangle down, 10000s) for each concentration and temperature; curves from Equation 1. (Adapted from reference 24. Copyright 1997 American Chemical Society.)

## REFERENCES

1. Flory, P.J. "Introduction" *Farad Discuss* **57**, 7-18 (1974)
2. te Nijenhuis, K. "Thermoreversible networks. Viscoelastic properties and structure of gels" *Advances in Polymer Science* **130**, 1-193 (1997)
3. Ross-Murphy, S.B. "Formation, structure and properties of physical networks", in "Polymer networks: principles of their formation, structure and properties" (Stephens R. F. T., ed.), pp. 290-318. Chapman and Hall, Glasgow, U.K. (1998).
4. Picout, D.R. and S.B. Ross-Murphy "Thermoreversible and irreversible physical gels from biopolymers", in "Polymer gels and networks" (Osada Y. and Khokhlov A. R., eds.), pp. 27-46. Marcel Dekker, Inc., New York, NY. (2002).
5. Ferry, J. D. "Viscoelastic properties of polymers", Wiley Interscience, New York, NY, U.S.A. (1980).
6. Doi, M. and Edwards S. F. "The theory of polymer dynamics", Clarendon Press, Oxford, U.K. (1986).
7. Ross-Murphy, S.B. and K.P. Shatwell "Polysaccharide strong and weak gels" *Biorheology* **30**, 217-227 (1993)
8. Gilsean, P.M. and S.B. Ross-Murphy "Viscoelasticity of thermoreversible gelatin gels from mammalian and piscine collagens" *Journal of Rheology* **44**, 871-883 (2000)
9. Clark, A.H. "Biopolymer gelation - comparison of reversible and irreversible cross-link descriptions" *Polymer Gels and Networks* **1**, 139-158 (1993)
10. Winter, H.H. and F. Chambon "Analysis of linear viscoelasticity of a cross-linking polymer at the gel point" *Journal of Rheology* **30**, 367-382 (1986)
11. Matricardi, P., M. Dentini, V. Crescenzi, and S.B. Ross-Murphy "Gelation of chemically cross-linked polygalacturonic acid-derivatives" *Carbohydrate Polymers* **27**, 215-220 (1995)
12. Ilavsky, M., Z. Bubenikova, K. Bouchal, J. Nedbal, and J. Fahrlich "Violation of the power-law dynamic mechanical behaviour at the gel point threshold in non-stoichiometric epoxide systems" *Polymer Bulletin* **42**, 465-472 (1999)
13. Ross-Murphy, S.B. "General discussion" *Farad Discuss* **101**, 119-120 (1995)
14. Rodd, A.B., D.E. Dunstan, S.B. Ross-Murphy, and D.V. Boger "Dependence of linear viscoelastic critical strain and stress values on extent of gelation for a thermally activated gelling system" *Rheologica Acta* **40**, 23-29 (2001)
15. Gilsean, P.M. and S.B. Ross-Murphy "Shear creep of gelatin gels from mammalian and piscine collagens" *International Journal of Biological Macromolecules* **29**, 53-61 (2001)

16. Veis, A. "The Macromolecular Chemistry of Gelatin", Academic Press, New York, NY, U.S.A. (1964).
17. Takahashi, A. "The melting temperature of thermally reversible gel. I. Poly(vinyl chloride) organic solvent gels" *Polymer Journal* **3**, 207-216 (1972)
18. Eldridge, J.E. and J.D.Ferry "Studies of the cross-linking process in gelatin gels. III. Dependence of melting point on concentration and molecular weight" *Journal of Physical Chemistry* **58**, 992-995 (1954)
19. Clark, A.H. and C.D.Lee-Tuffnell "Gelation of globular proteins", in "Functional Properties of Food Macromolecules" (Mitchell J. R. and Ledward D. A., eds.), pp. 203-272. Elsevier Applied Science, London, U.K. (1986).
20. Aymard, P., J.C.Gimel, T.Nicolai, and D.Durand "Experimental evidence for a two-step process in the aggregation of  $\beta$ -lactoglobulin at pH 7" *Journal de Chimie Physique et de Physico-Chimie Biologique* **93**, 987-997 (1996)
21. Aymard, P., T.Nicolai, D.Durand, and A.H.Clark "Static and dynamic scattering of  $\beta$ -lactoglobulin aggregates formed after heat-induced denaturation at pH 2" *Macromolecules* **32**, 2542-2552 (1999)
22. Gosal, W.S. and S.B.Ross-Murphy "Globular protein gels" *Current Opinion in Colloid & Interface Science* **5**, 209-215 (2000)
23. Sunde, M. and C.C.F.Blake "From the globular to the fibrous state: protein structure and structural conversion in amyloid formation" *Quarterly Reviews of Biophysics* **31**, 1 (1998)
24. Tobitani, A. and S.B.Ross-Murphy "Heat-induced gelation of globular proteins .1. Model for the effects of time and temperature on the gelation time of BSA gels" *Macromolecules* **30**, 4845-4854 (1997)
25. Tobitani, A. and S.B.Ross-Murphy "Heat-induced gelation of globular proteins .2. Effect of environmental factors on single-component and mixed-protein gels" *Macromolecules* **30**, 4855-4862 (1997)
26. Kavanagh, G.M., A.H.Clark, and S.B.Ross-Murphy "Heat-induced gelation of globular proteins: Part 3 Molecular studies on low pH  $\beta$ -lactoglobulin gels" *International Journal of Biological Macromolecules* **28**, 41-50 (2000)
27. Kavanagh, G.M., A.H.Clark, and S.B.Ross-Murphy "Heat-induced gelation of globular proteins: Part 4 Gelation kinetics of low pH  $\beta$ -lactoglobulin gels" *Langmuir* **16**, 9584-9594 (2000)
28. Kavanagh, G.M., A.H.Clark, W.S.Gosal, and S.B.Ross-Murphy "Heat-induced gelation of  $\beta$ -lactoglobulin /  $\alpha$ -lactalbumin blends at pH3 and pH7" *Macromolecules* **33**, 7029-7037 (2000)
29. Kavanagh, G.M., A.H.Clark, and S.B.Ross-Murphy "Heat-induced gelation of globular proteins: Part 5 Creep behaviour of  $\beta$  -lactoglobulin gels" *Rheologica Acta in press* (2002)

## Chapter 5

# Inorganic–Organic Hybrid Gel: Structural Characteristics and Formation Mechanism

Hiroshi Urakawa<sup>1</sup>, Yoshiaki Yuguchi<sup>1</sup>, Yuko Ikeda<sup>1</sup>, Kanji Kajiwara<sup>1</sup>,  
Yoshitaka Hirata<sup>2</sup>, and Shinzo Kohjiya<sup>2</sup>

<sup>1</sup>Faculty of Engineering and Design, Kyoto Institute of Technology, Kyoto,  
Sakyo-ku 606–8585, Japan

<sup>2</sup>Institute for Chemical Research, Kyoto University, Uji 611–0016, Japan

### Introduction

Synchrotron radiation provides a powerful source for X-ray, which enables to observe small-angle X-ray scattering (SAXS) from solutions in a short time. SAXS is suitable for the observation of the spatial correlation in the order of 10 to 1000 Å owing to its wavelength. Thus SAXS has been successfully applied to the structural analysis of enzymes and colloidal particles in solution<sup>1</sup>. The electromagnetic profile (X-ray or light scattering) corresponds to the Fourier transform of the spatial correlation (density distribution function) of the scattering body, so that in principle any structure could be analyzed from the profile. In practice, the range of the observation is not wide enough to elucidate the whole structure of the scattering body, and the conventional method evaluates the size and shape approximately by assuming a homogeneous triaxial body or semi-flexible coil to represent an object<sup>1</sup>.

Here we apply the time-resolved SAXS to observe a structural change during the network formation in the sol-gel process. In order to analyze the observed scattering profiles quantitatively, the Flory-Stockmayer model<sup>2</sup> was adopted to calculate the scattering intensity from the system undergoing gelation, and the results were discussed in terms of the parameters specifying the Flory-Stockmayer model. The Flory-Stockmayer model describes the gelation as trees growing over a space. In this context, gelation is equivalent to the cascade process, and is formulated with the generating function<sup>3,4</sup>. Although the original generating function (the weight-fraction generating function) is based on a simple enumeration of tree branches, the generating function can be extended to include the distance correlation as a path-weighted generating function<sup>5</sup>. The particle scattering function is calculated from this path-weighted generating function for a randomly branched system<sup>6</sup>. A tree-like model of Flory and

Stockmayer has an advantage of its simplicity, but the model corresponds to the state of ideal gas.

The generating function for the real system will be given as a first approximation by introducing the interaction between branches. The inter-branch interaction is incorporated in the particle scattering factor as an interference term due to the finite size of the branch points and the repulsion between branch points.

## Experimental

### Preparation of Hybrid Gel

Organic/inorganic hybrid gels were prepared by the sol-gel process from TEOS (tetraethoxysilane) and ET-PTMO (triethoxysilyl-terminated poly(oxytetramethylene)). ET-PTMO ( $M_n = 1.35 \times 10^3$ ) was synthesized from poly(oxytetramethylene) glycol by end-group modification. The sol-gel process and the preparation of hybrid gel are schematically shown in Figs. 1 and 2, respectively. In the present sol-gel process,  $\text{BuNH}_2$  was employed for catalyst (Series B in Fig. 2), so that the reaction proceeded under the basic condition. The reaction mixture was prepared by mixing and stirring ET-PTMO, TEOS and ethanol (solvent) at room temperature for 2 min. Then hydrochloric acid and water were added to the reaction mixture and stirred for further 10 min. The catalyst was added and the mixed solution was stirred for 1 min. The resulted solution (the reaction mixture) was capsulated in the capillary cell ( $\phi = 2$  mm), inserted in the cell holder maintained at  $50^\circ\text{C}$  and the time-resolved small-angle X-ray scattering was observed immediately from the solution undergoing sol-gel reaction.

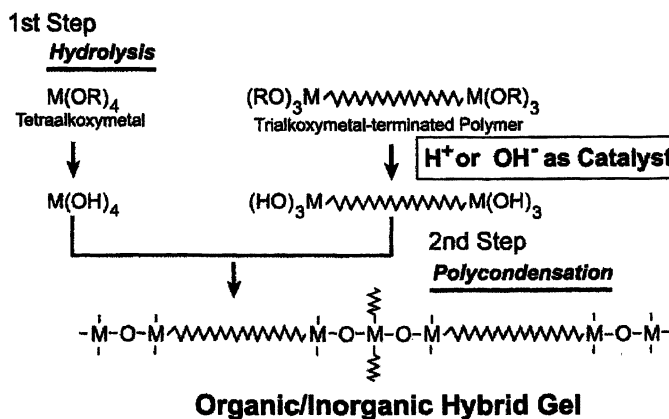


Figure 1. Sol-gel process (schematic)

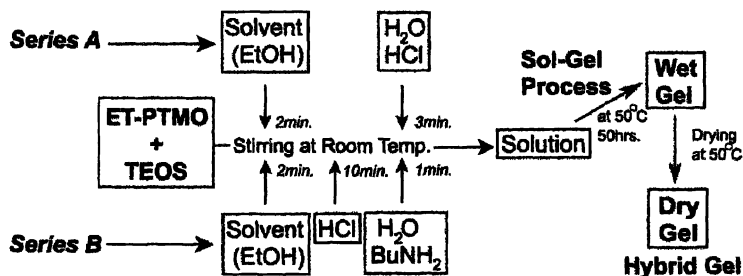


Figure 2 Preparation of hybrid gel

### Small-angle X-ray Scattering

Time-resolved SAXS was observed from a series of the mixed solution of ET-PTMO and TEOS undergoing sol-gel reaction with the SAXES equipment installed at BL-10C in Photon Factory, Tukuba, Japan. The sample code and the reaction conditions are summarized in Table 1. The SAXS measurement was started immediately after the cell was inserted in the cell holder block kept at 50°C. 98 measurements with an appropriate interval were repeated during the course of hydrosilylation, where each measuring time was 3 minutes. The excess scattering intensity at each reaction time was calculated by subtracting the scattering intensity at time 0.

Table 1. Concentration of each component in the reaction mixture (in terms of molar ratio)

Sample code	[(Si)-OEt] <sub>PTMO</sub>	[(Si)-OEt] <sub>TEOS</sub>	EtOH	H <sub>2</sub> O	HCl	BuNH <sub>2</sub>
SGG0	1.0	0	14	13	0.010	0
SGG1	1.0	0	14	13	0.010	0.028
SGG2	1.0	0	14	13	0.010	0.020
SGG3	1.0	0	14	13	0.010	0.015
SGG4	1.0	0	14	13	0.010	0.013
SGG5	1.0	0.23	14	13	0.010	0.013
SGG6	1.0	0.48	14	13	0.010	0.013
SGG7	0.60	1.7	14	13	0.010	0.015
SGG8	0.6	1.7	14	13	0.010	0.013

An incident synchrotron-radiated X-ray was monochromatized to  $\lambda = 1.488$  Å with a double-mirror monochromatizer, and focused to the position of the detector by a focusing mirror. The scattered X-ray was detected by the one-dimensional position sensitive proportional counter (PSPC) of the effective

length 160 mm. The exact camera length was calibrated by using the diffraction peaks of collagen fiber (the long period = 670 Å at the 6th, 9th, and 11th orders).

### Theoretical background

The Flory-Stockmayer model for polyfunctional polycondensation is represented by a tree, which corresponds to the generating function with a dummy variable  $\theta$  as shown in Fig. 3.

The dummy variable corresponds to each branch point (node), and the probability that a branch bears further branches is given by the reactivity  $\alpha$ . That is, the branch would not bear the next generation with the probability  $1 - \alpha$ . The generating function in Fig. 1 is summarized as

$$W(\theta) = \sum_{x=1}^{\infty} w_x \theta^x = \theta(1 - \alpha + \alpha u(\theta))^f \quad (1)$$

$$u(\theta) = \theta(1 - \alpha + \alpha u(\theta))^{f-1} \quad (2)$$

where  $w_x$  denotes the weight fraction of  $x$ -mers in the system. Eq. (1) yields the weight average degree of polymerization before gelation as  $(1 + \alpha)/[1 - (f-1)\alpha]$  by differentiating with respect to  $\theta$  at  $\theta=1$ . The result was first derived by Flory<sup>2</sup> and defines a gel point at  $\alpha = 1/(f-1)$  where the weight average degree of polymerization diverges. The scattering intensity<sup>5,6</sup> is calculated by introducing the random spatial correlation between branch points as a function of the reaction probability  $\alpha$ :

$$I(q) = A^2(q)(1 + \alpha\phi)/[1 - (f-1)\alpha\phi] \quad (3)$$

$$\phi = \exp(-b^2 q^2 / 6) \quad (4)$$

where  $b^2$  denotes the mean-square distance between neighboring scattering units.  $A(q)$  is a scattering amplitude, and is equal to 1 when the scatterer is a point. Eq. (3) holds even when gelation takes place as far as  $1 - (f-1)\alpha\phi < 1$ .<sup>7</sup>  $q$  is the magnitude of the scattering vector defined as  $(4\pi/\lambda)\sin(\theta/2)$  with the wavelength  $\lambda$  of the incident light and the scattering angle  $\theta$ .

In order to analyze the scattering profiles from the gelling system quantitatively, we assume that the random association (in the case of physical gel) or the initial stage of crosslinking reaction (in the case of chemical gel) results in the formation of the multi-functional domains which link together to form a tree-like network. In the case of chemical gel, the domains formed in the initial stage of reaction may be highly branched and broadly distributed in size and shape. The domain formation can be described in general by the Smoluchowski equation<sup>8</sup>, where the forward reaction rate will be given in various ways according to a specified mode of association. That is, the density distribution in the domain will be given by a generalized Ornstein-Zernike form<sup>9,10</sup> as



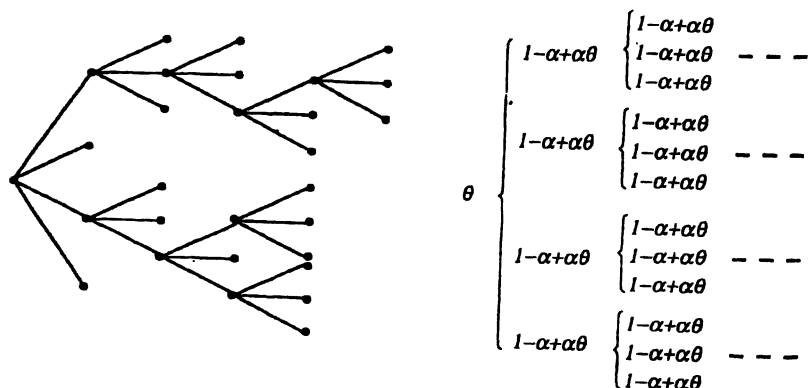


Figure 3. A tree-like model for an  $f$ -functional polycondensation ( $f = 4$ ) and a corresponding stochastic process given in terms of generating function.

$$\gamma(r) \approx (\xi/r)^{3-D} \exp(-r/\xi) \quad (5)$$

where  $D$  ( $1 \leq D < 3$ ) and  $\xi$  denote the fractal dimension and the correlation length specifying the density fluctuation in the domain, respectively. Eq. (5) yields the scattering amplitude in eq. (1) by the Fourier transform<sup>7,11</sup> as

$$A^2(q) \approx \frac{1}{[1 + (D+1)\xi^2 q^2 / 3]^{D/2}} \quad (6)$$

Since  $D = 2$  for a Gaussian chain, eq. (6) reduces to a Lorentzian form<sup>9</sup>:

$$A^2(q) \approx 1/(1 + \xi^2 q^2) \quad (7)$$

The simplest case was given by Debye and Bueche<sup>12</sup> for the correlation function  $\exp(-r/\xi)$  in order to account for the inhomogeneities in solid represented by random associates as

$$A^2(q) \approx 1/[1 + \xi^2 q^2]^2 \quad (8)$$

The Debye-Bueche density correlation function corresponds to the case that  $D = 3$  in eq. (5), which is equivalent to the rigid body having a smooth boundary distinct from the medium. Eq. 8 indicates the  $q^{-4}$  dependence of the scattering intensity (the Porod region<sup>1</sup>) at  $q \rightarrow \infty$ .

## Results and Discussion

Both time-resolved SAXS profiles from the ET-PTMO/TEOS mixtures show the upturn at  $q \rightarrow 0$  in the Kratky plots ( $q^2 I(q)$  plotted against  $q$  with  $I(q)$  and  $q$

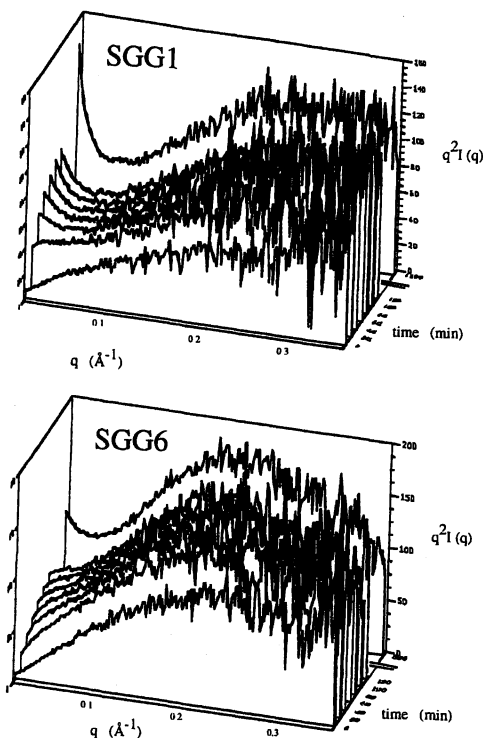


Figure 4. Time-resolved small angle X-ray scattering observed from the ET-PTMO/TEOS mixtures during the sol-gel process

being the scattered intensity and the magnitude of scattering vector, respectively) when the sol-gel reaction proceeds. Two examples (SGG1 and SGG6) are shown in Fig. 4, where the reaction time of the initial upturn corresponds to the gel point of the system as expected from the Flory-Stockmayer tree-like model.

The scattering profiles were analyzed in terms of three parameters  $(f-1)\alpha$ ,  $b^2$  and  $\xi$  by curve fitting. The analyzed results are demonstrated in Figs. 5 and 6, and the results are summarized in Table 2. The reaction time when  $(f-1)\alpha$  exceeds 1.0 is thought to correspond to the gel point. After gelation takes place,  $(f-1)\alpha$  hardly increases in all the series, indicating that further intermolecular reaction is suppressed by gelation.  $b$  and  $\xi$  increase with reaction before the gel point but remain almost constant with the value of  $(f-1)\alpha$  becoming invariant (see Fig. 6). The result implies that the intermolecular reaction is also suppressed

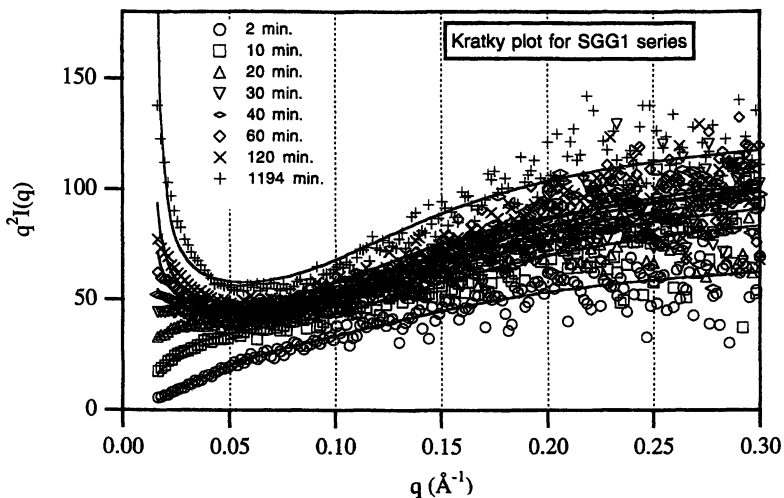


Figure 5. Observed SAXS profiles and calculated profiles according to eqs. (3) and (7) for SGG1 as a function of the reaction time

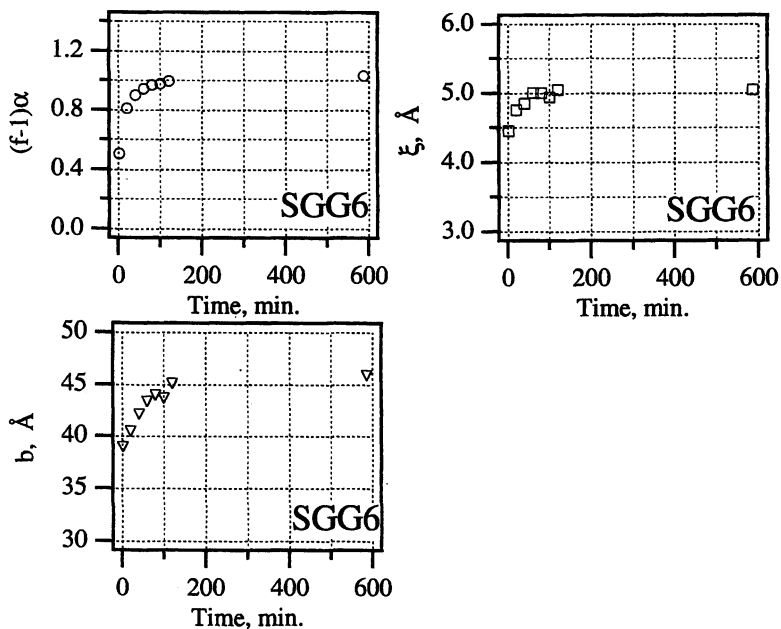


Figure 6. Evaluated parameters  $\xi$ ,  $(f-1)\alpha$  and  $b$  according to eqs. (3) and (8) for SGG6 as a function of the reaction time

**Table 2. Evaluated parameters  $\xi$ ,  $(f-1)\alpha$  and  $b$  in the steady state (at the final reaction time) according to eqs. (3) and (7) (or eqs. (3) and (8)), and the gel point**

<i>Sample code</i>	$\xi$ (Å)	$(f-1)\alpha$	$b$ (Å)	<i>Gel point (min.)</i>
SGG0 <sup>*)</sup>	3.0	0.803	12.0	-
SGG1 <sup>*)</sup>	9.7	1.059	42.2	30
SGG2 <sup>*)</sup>	8.9	1.049	40.9	40
SGG3 <sup>*)</sup>	9.4	1.052	42.1	130
SGG4 <sup>*)</sup>	8.5	1.019	37.2	222
SGG5 <sup>**)</sup>	4.6	1.041	41.9	>120
SGG6 <sup>**)</sup>	5.1	1.036	45.9	120
SGG7 <sup>**)</sup>	8.0	1.018	64.0	90
SGG8 <sup>**)</sup>	8.2	1.021	64.4	>120

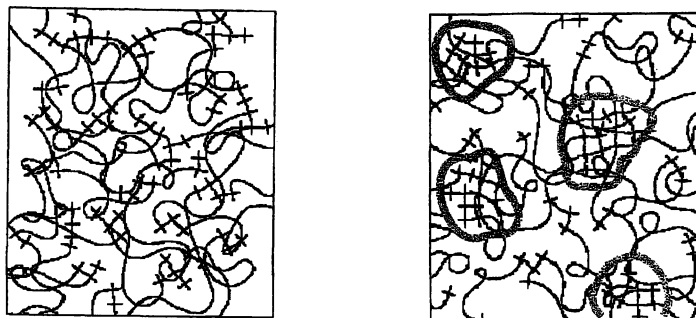
<sup>\*)</sup>Eqs. (3) and (7); <sup>\*\*)Eqs. (3) and (8)</sup>

in the wet state in the hybrid gel once gelation takes place. The result indicates the different situation from the network formation of polysiloxane<sup>13</sup>, where the shrinkage of gel due to the intramolecular reaction was observed after gel point.

The gelation model considered here is similar to the model proposed by Landry et al.<sup>14</sup> Their model comprises a liquid-like arrangement among non-interpenetrating fractal clusters, whereas in the present model non-interpenetrating fractal clusters are distributed and linked as described by the Flory-Stockmayer model. Here a correlation length  $\xi$  specifies the non-interpenetrating fractal clusters according to eq. (7) or eq. (8) in the present instance.

The evaluated parameters by curve fitting were summarized in Table 2. SGG0 (without TEOS under acidic condition) undergoes no gelation. When added no TEOS (SGG1-4), the resulted gel is rather homogeneous and the domain is characterized by a Gaussian type density distribution. Decreasing the amount BuNH<sub>2</sub> (catalyst) reduces the gelation time, but no appreciable change was observed in the gel structure. The formation of relatively hard domain described by the Debye-Bueche type correlation function was observed by adding TEOS in SGG5-8 synthesized under basic condition. The size of the domain increases and the gelation time reduces as increasing the amount of added TEOS. The domain is considered to be composed mainly of inorganic components as illustrated in Fig. 7. The gel structure is schematically shown in Fig. 7.

In conclusion, TEOS promotes the formation of Si-rich domains under the basic condition, but the reaction is suppressed after gelation in the wet state. Further reaction takes place where the intramolecular crosslinking induces the shrinkage of hybrid gel in the drying process.



(a) Without adding TEOS

(b) With adding TEOS

Figure 7: Schematic structure of the PTMO/TEOS hybrid gel

### Acknowledgements

This work was performed under the approval of the Photon Factory Advisory Committee (Proposal No. 91-217). YY thanks JSPS for Research Fellowship for Young Scientists. The part of the work was financially supported by Grant-in-Aid for COE Research No. 10CE2003 (Ministry of Education, Science, Sports and Culture, Japan).

### References

1. See, for example, Glatter, O., Kratky, O., *Small-Angle X-ray Scattering*, Academic P., New York, 1982
2. See, for example, Flory, P. J., *Principles of Polymer Chemistry*, Cornell U.P., Ithaca, 1953
3. Good, I. J., *Proc. Cambridge Phil., Soc.*, **1955**, *51*, 240-242
4. Gordon, M., *Proc. Roy. Soc. (London)*, **1962**, *A268*, 240-259
5. Kajiwara, K., Burchard, W., Gordon, M., *Br. Polym. J.*, **1970**, *2*, 110-115
6. Kajiwara, K., Gordon, M., *J. Chem. Phys.*, **1973**, *59*, 3623-3632
7. Kajiwara, K., Kohjiya, S., Shibayama, M., Urakawa, H. in *Polymer Gels*; De Rossi, D., Kajiwara, K., Osada, Y., Yamauchi, A., Eds.; Plenum: New York, 1991; pp3-19
8. Spouge, J. L. *Macromolecules*, **1983**, *16*, 121-127; Botet, R., Jullien, R., Kolb, M. *Phys. Rev.*, **1984**, *A30*, 2150-2152
9. De Gennes, P.-G. *Scaling Concepts in Polymer Physics*, Cornell U. P., Ithaca, 1979
10. Freltoft, T., Kjems, J. K., Sinha, S. K. *Phys. Rev.*, **1986**, *B33*, 269-275

11. Shibayama, M., Kurokawa, H., Nomura, S., Muthkumar, M., Stein, R. S., Roy, S. *Polymer*, **1992**, 33, 2883-2890
12. Debye, P., Bueche, A. M. *J. Appl. Phys.*, **1949**, 20, 518-525
13. Yamanaka, S., Yuguchi, Y., Urakawa, H., Kajiwara, K., Kohjiya, S. *J. Network Polym.*, **1999**, 20, 157-163
14. Landry, M. R., Coltrain, B. K., Landry, C. J. T., O'Reilly, J. M. *J. Polymer Sci., (Polym. Phys.)*, **1995**, B33, 637-655

## Chapter 6

# Synthesis and Characterization of pH-Responsive Poly(organophosphazene) Hydrogels

Harry R. Allcock and Archel Ambrosio

Department of Chemistry, The Pennsylvania State University, University Park, PA 16802

Water-soluble polyphosphazenes can be crosslinked either by gamma-radiation or by di- or tri-valent cations. The resultant materials imbibe or extrude water in response to changes in temperature, pH, or cations. These hydrogels offer the prospect of uses in responsive membranes, devices for the controlled delivery of drugs, enzyme immobilization and mediation media, and tissue engineering.

### Background and Purpose

The long-range purpose of this work is to develop hydrogels that can be used in switchable membranes - ie. that can exist in a gate-open or gate-closed state. Possible applications include pulsed drug delivery, on-off switching of enzymes or cells, substrates for tissue engineering, or as components in sensors.

In previous work we have developed two different types of hydrogels based on the polyphosphazene platform. Here we demonstrate that the molecular features of these two earlier systems can be combined to generate a third system that offers some advantages over the earlier two.

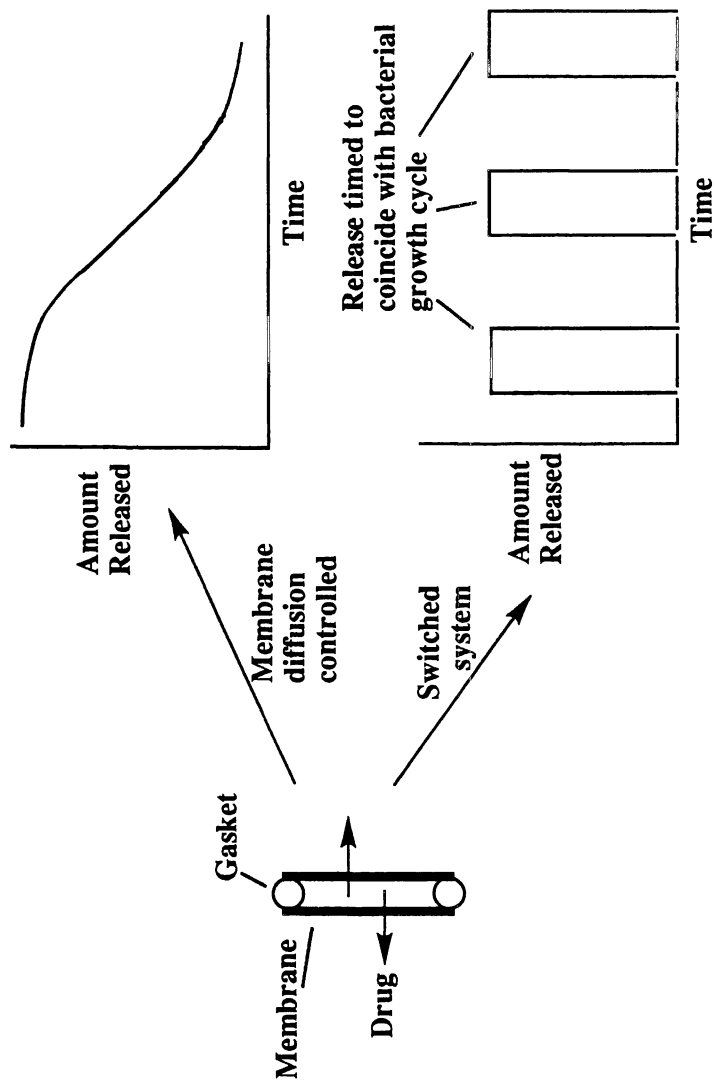


Figure 1. Comparison between normal diffusion-controlling membrane and an on/off switchable hydrogel membrane.



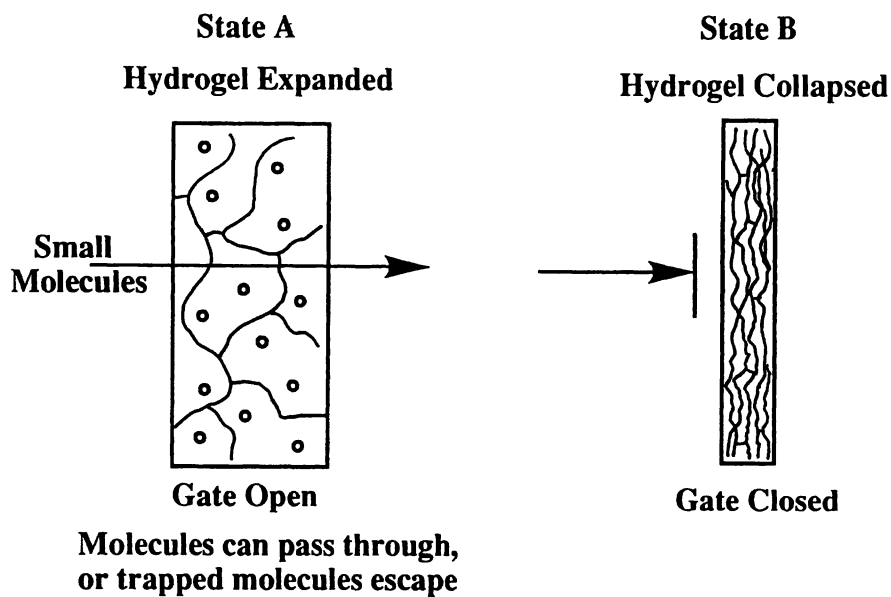


Figure 2. Use of controlled expansion and collapse of a hydrogel to control membrane behavior.

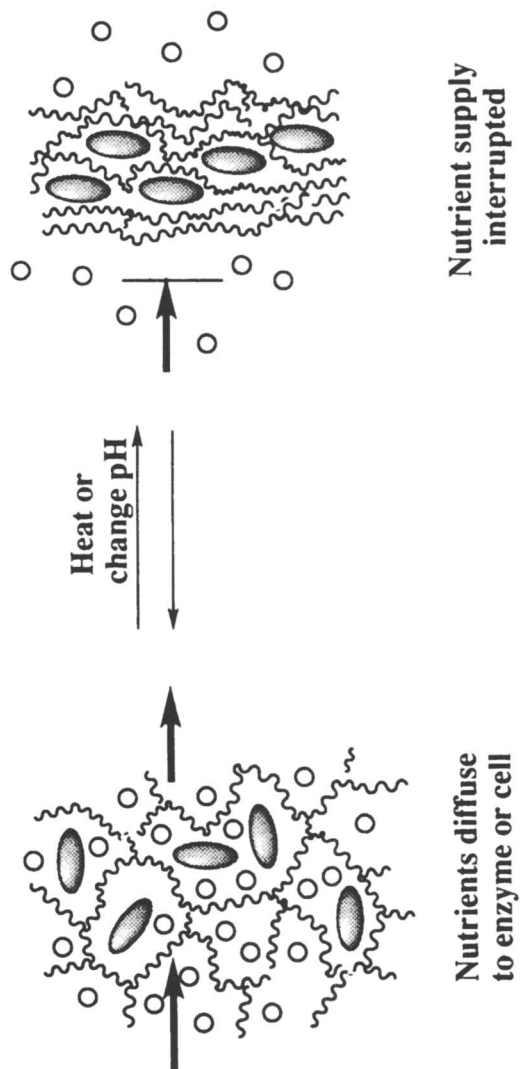
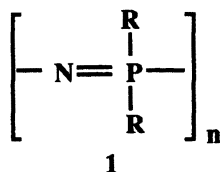


Figure 3. On/off membrane switch for control of enzyme or cell activity.

The polyphosphazene platform is based in the molecular structure shown as **1**.



These polymers can be prepared by several techniques, but the route utilized most in this work is summarized in Scheme I. It is based on the use of a reactive macromolecular intermediate - poly(dichlorophosphazene) (**3**), which can be produced either by the ring-opening polymerization of compound **2** or by the living cationic polymerization of **4**. Replacement of the chlorine atoms in **3** by organic side units is accomplished by treatment of **3** with nucleophiles, such as the sodium salts of alcohols or phenols or with primary or secondary amines. Two or more different side groups can be introduced into the same macromolecule by simultaneous or sequential exposure to the two nucleophiles.

### Alkyl Ether-Substituted Polymers

The use of the sodium salts of alkyl ether alcohols as nucleophiles allows access to a wide range of polymers of the types shown in Table 1. All these polymers are soluble in water, and most show lower critical solution temperature (LCST) behavior, with LCST's that vary with side chain length, with linearity or branching, and with side chain terminating units (*1-3*). Thus, each polymer is soluble in water below the LCST, but becomes insoluble when the solution is heated above that temperature. This behavior is reversible. Particularly important is the polymer with  $\text{OCH}_2\text{CH}_2\text{OCH}_2\text{CH}_2\text{OC}_2\text{H}_5$  side groups, which has an LCST near human body temperature.

All of these polymers can be crosslinked by exposure to  $^{60}\text{Co}$  gamma rays or to ultraviolet light in the presence of a photosensitizer (*4-6*). The crosslinking occurs by a free-radical mechanism (Figure 4) and by cross-combination of the radicals so-formed. Thin films of the hydrogel can be grafted to the surface of other polymers (Figure 5) (*7*). Crosslinking converts a water-soluble polymer into one that absorbs water to form a hydrogel, with the degree of swelling being inversely proportional to the degree of crosslinking, and hence to the radiation dose. (Figure 6).

The hydrogels exhibit LCST behavior at approximately the same temperatures as the uncrosslinked polymers. Thus, maximum swelling in water occurs below the LCST, but the gels contract and extrude water above that temperature. This phenomenon can be used to open or close the membrane to permit or prevent diffusion of a drug or of nutrients to enzymes or cells. For

Scheme I. Macromolecular Substitution Synthesis of Polyphosphazenes.

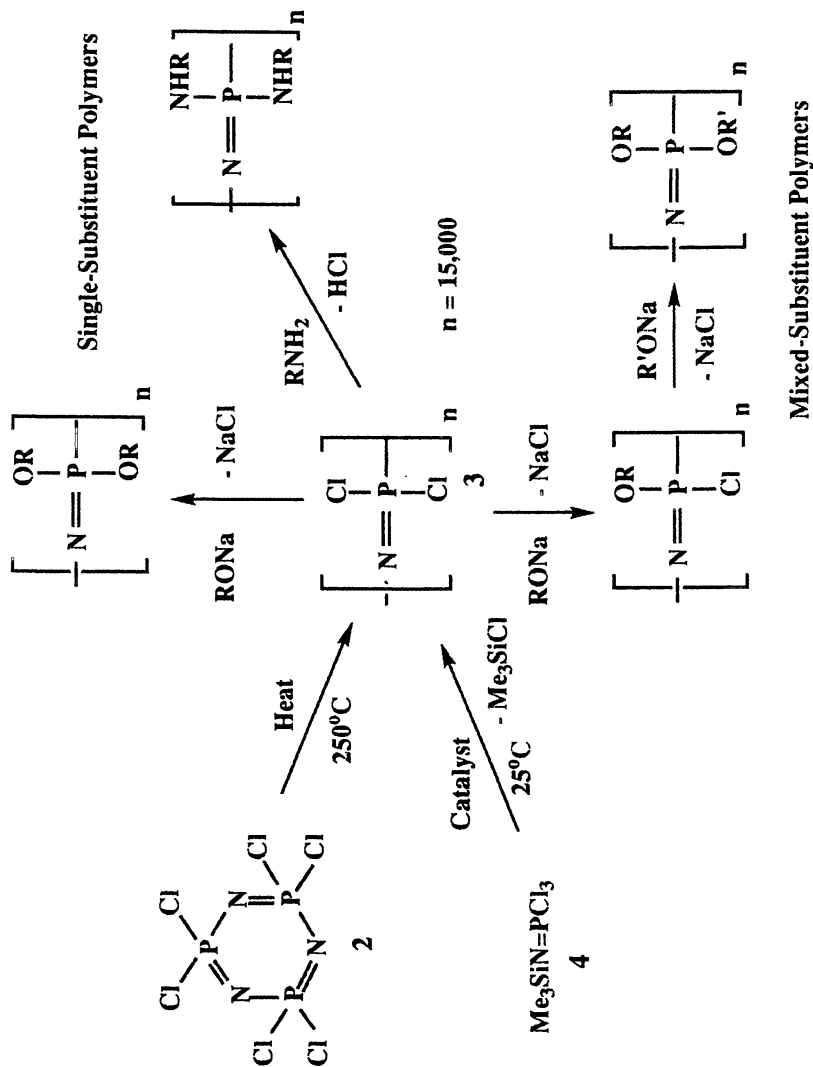
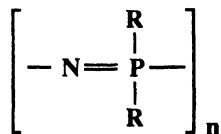


Table I  
Lower Critical Solution Temperature of Water-Soluble Polyphosphazenes



<u>R</u>	<u>LCST (°C)</u>
-OCH <sub>2</sub> CH <sub>2</sub> OCH <sub>3</sub>	30
-OCH <sub>2</sub> CH <sub>2</sub> OCH <sub>2</sub> CH <sub>2</sub> OCH <sub>3</sub>	65
-OCH <sub>2</sub> CH <sub>2</sub> OCH <sub>2</sub> CH <sub>2</sub> OC <sub>2</sub> H <sub>5</sub>	38
-OCH <sub>2</sub> CH <sub>2</sub> OCH <sub>2</sub> CH <sub>2</sub> OC <sub>4</sub> H <sub>9</sub>	51
-OCH <sub>2</sub> CH <sub>2</sub> OCH <sub>2</sub> CH <sub>2</sub> NH <sub>2</sub>	None
$\begin{array}{c} \text{CH}_2\text{OCH}_3 \\   \\ -\text{OCH}_2\text{CHOCH}_3 \end{array}$	44
$\begin{array}{c} \text{CH}_2\text{OCH}_2\text{CH}_2\text{OCH}_3 \\   \\ -\text{OCH}_2\text{CHOCH}_2\text{CH}_2\text{OCH}_3 \end{array}$	38
$\begin{array}{c} \text{CH}_2\text{OCH}_2\text{CH}_2\text{OCH}_2\text{CH}_2\text{OCH}_3 \\   \\ -\text{OCH}_2\text{CHOCH}_2\text{CH}_2\text{OCH}_2\text{CH}_2\text{OCH}_3 \end{array}$	50
$\begin{array}{c} \text{CH}_2\text{OCH}_2\text{CH}_2\text{OCH}_2\text{CH}_2\text{OCH}_2\text{CH}_2\text{OCH}_3 \\   \\ -\text{OCH}_2\text{CHOCH}_2\text{CH}_2\text{OCH}_2\text{CH}_2\text{OCH}_2\text{CH}_2\text{OCH}_3 \end{array}$	61

**Hydrogels derived from these polymers collapse when heated above the LCST**

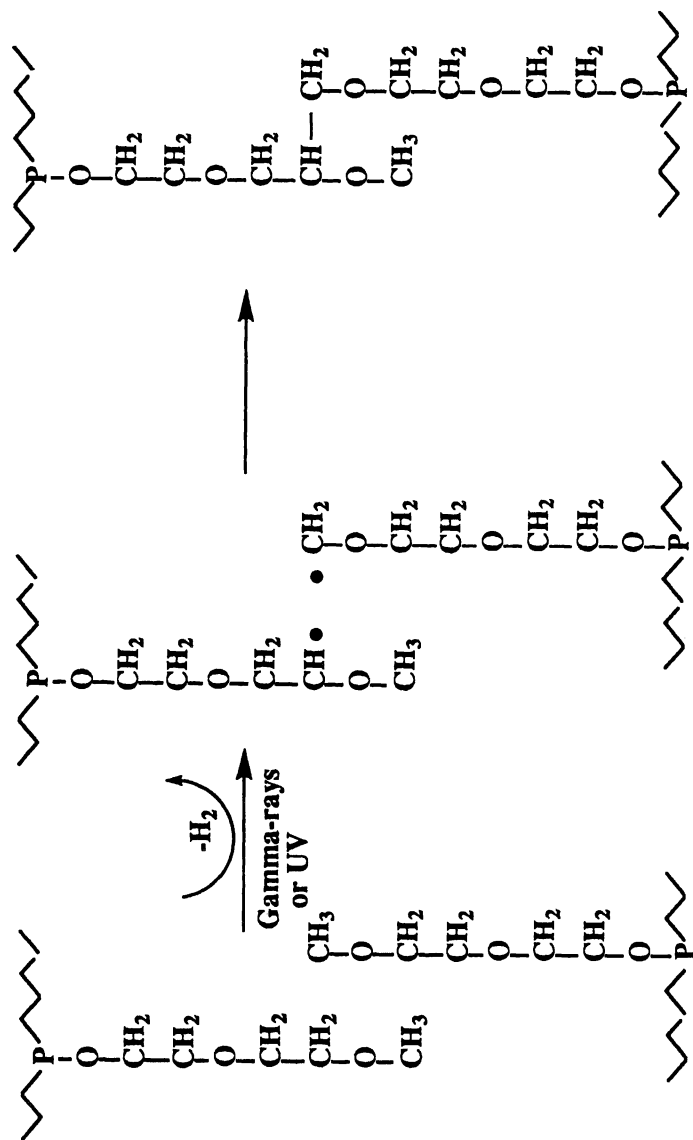


Figure 4. Radiation crosslinking of  $[\text{NP}(\text{OCH}_2\text{CH}_2\text{OCH}_2\text{CH}_2\text{OCH}_3)_2]_n$  to convert a water-soluble polymer to a hydrogel.

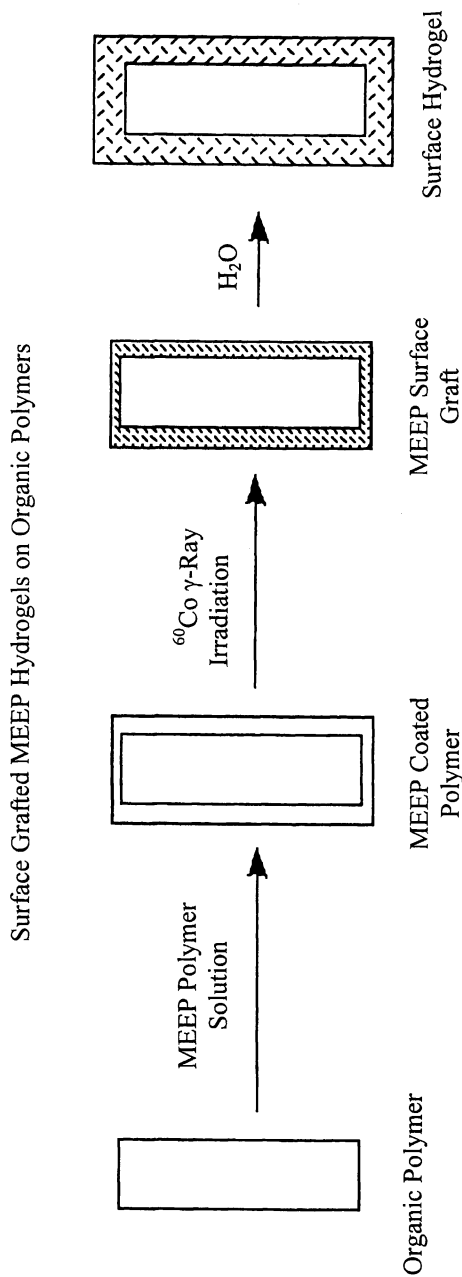


Figure 5. Grafting of  $[\text{NP}(\text{OCH}_2\text{CH}_2\text{OCH}_2\text{CH}_2\text{OCH}_3)_2]_n$  (methoxyethoxyethoxyphosphazene, MEEP) hydrogels to the surfaces of organic polymers.

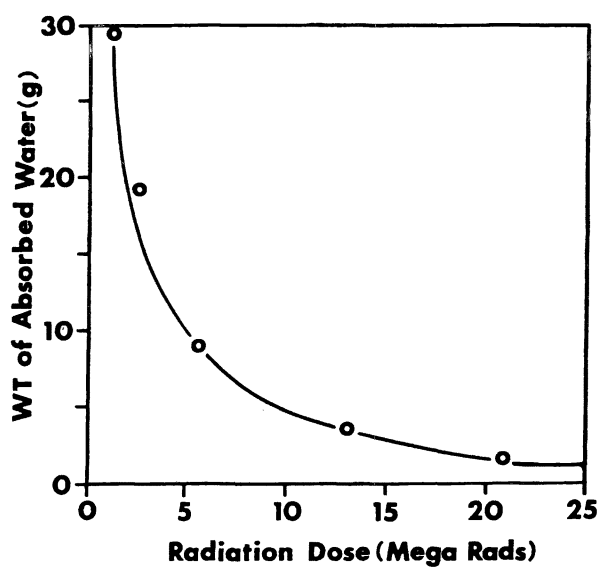


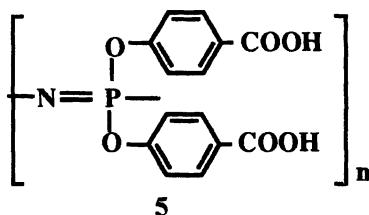
Figure 6. Swelling of MEEP hydrogels by water absorption as a function of crosslinking induced by gamma radiation.



example, the enzyme urease has been immobilized inside membranes of these polymers during the crosslinking step (8), and the enzymic activity can be promoted or inhibited by opening or closing the membrane by small changes in temperature. Some evidence exists that these polymers and their hydrogels show antibacterial properties (9).

## Carboxylate-Bearing Polyphosphazenes

The second hydrogel system developed in our earlier program was based on the polymer shown as 5, and known by the acronym PCPP [poly(carboxyphenoxyphosphazene)].



It is prepared by the sequence of reactions shown in Scheme II, and involves an alkaline deprotection step to yield the free carboxylic acid groups (10).

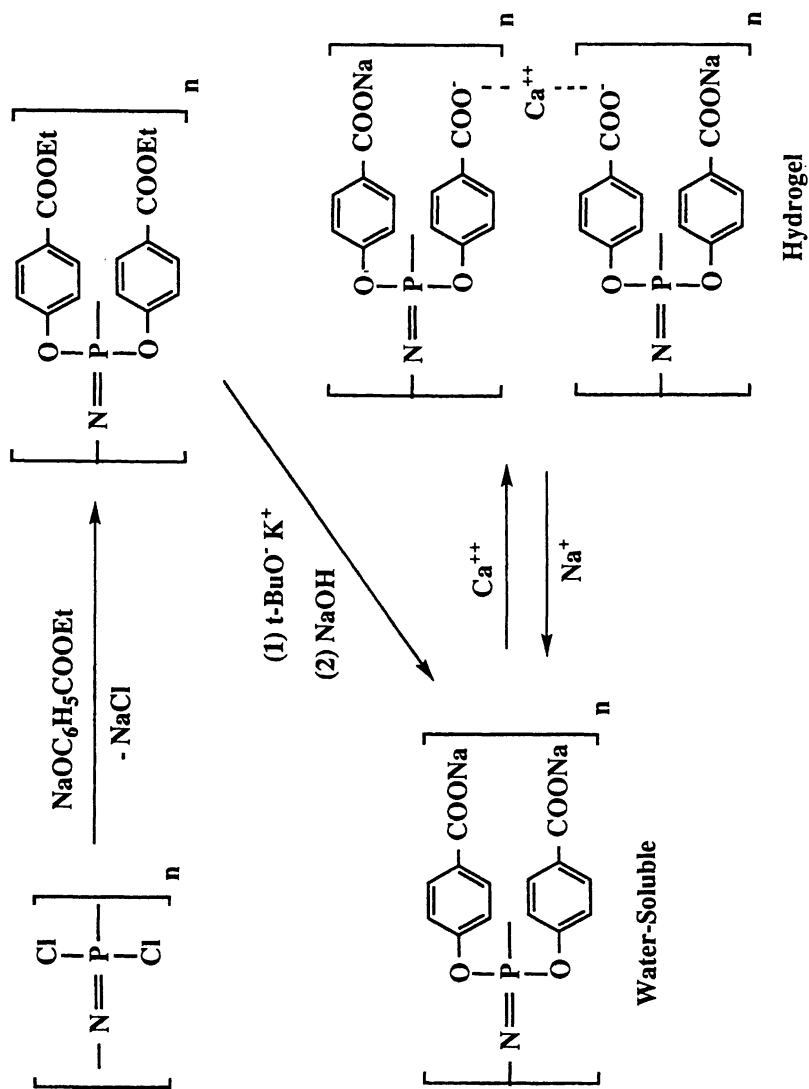
Polymer 5 is insoluble in water, is soluble as its sodium or potassium salt, and is precipitated as a gel by di- or tri-valent cations such as calcium or aluminum ions which form ionic crosslinks between chains. Decrosslinking and redissolving occurs when sodium or potassium ions displace the multivalent cations.

This sequence of property changes has been used to microencapsulate human cells or proteins (11-16), and to provide a vehicle for the delivery of vaccines (17) (Figure 7). PCPP is more useful than naturally occurring polymers such as alginates because of the high loading of carboxylate groups and its availability with precisely controlled molecular weights.

## The Combination Hydrogel System

Numerous advantages can be foreseen for combining the structural features of the alkyl ether phosphazene hydrogels with those of the carboxylate type. For example, specific properties can be tuned into the system by varying the ratios of the alkyl ether to carboxylate units over the range of, say, 95:5 to 5:95 in order to emphasize either the LCST behavior or the reversible ionic crosslinking.

Scheme II. Ionic Crosslinking of a Polyphosphazene Polyelectrolyte



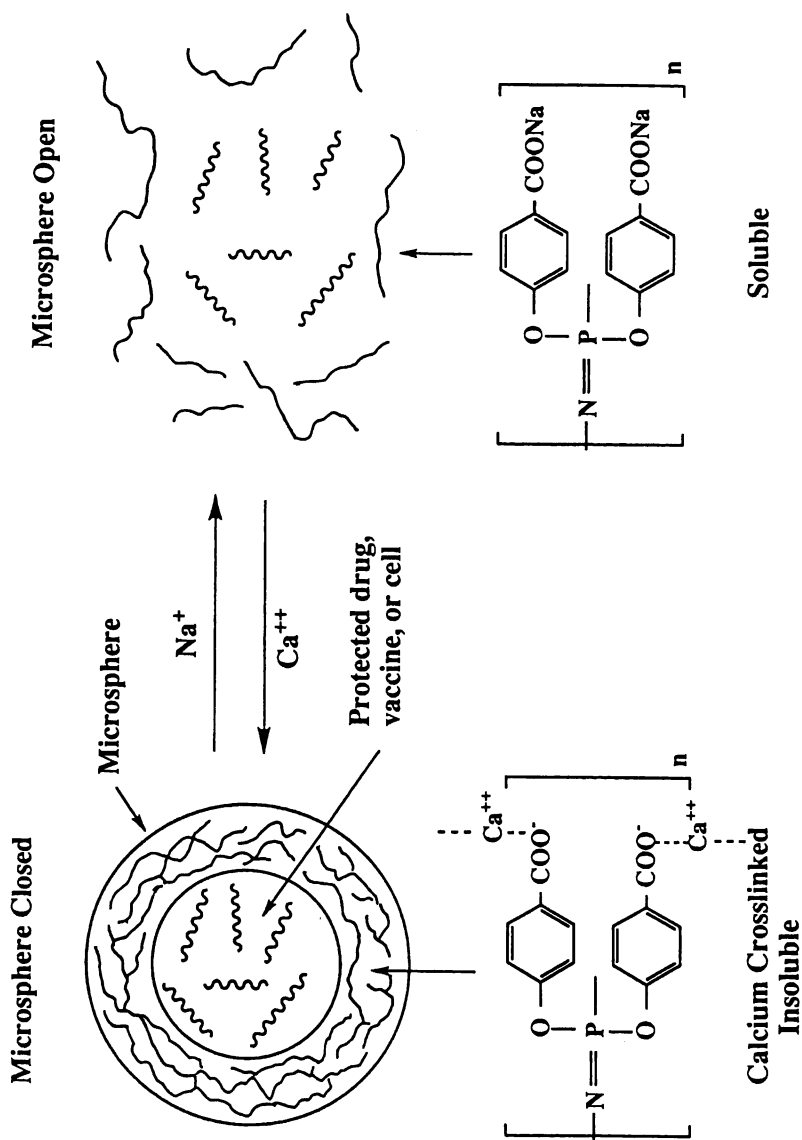


Figure 7. Polyphosphazene microspheres for cell encapsulation or as delivery vehicles.

These polymers are synthesized by the protocol shown in Scheme III (18). In this process, the aryloxy groups were introduced first to define the final side group ratio, followed by the alkyl ether side groups. The ester units were then deprotected by treatment with strong base. Primary crosslinking was then achieved by gamma-ray techniques. Note that the mixed-substituent polymers shown in Scheme III, although represented by an exclusively non-geminal structure, are in fact composed of units which also contain two of the same type of side groups on the same phosphorus atom.

The swelling of these gels is dependent on pH, cation charge, and the ionic strength of the medium, as shown in Figure 8. At low pH values, the gels contract, but swell progressively as the pH is raised from 4 to ~7.5. The actual degree of swelling depends on the ratio of the two side groups, as shown in Figure 8A. The higher the ratio of carboxylate groups, the more dramatic is the effect. Replacement of sodium ions by calcium ions contracts the gels as ionic crosslinks now exert an influence, and the contraction is enhanced as  $\text{Ca}^{2+}$  is replaced by  $\text{Al}^{3+}$  or  $\text{Fe}^{3+}$  (Figure 8C). The higher valency cations presumably increase the density of crosslinking. At low ionic strengths (for example, below 1 M NaCl) increases in salt concentration cause gel contraction as the ionic polymer retracts (Figure 8B).

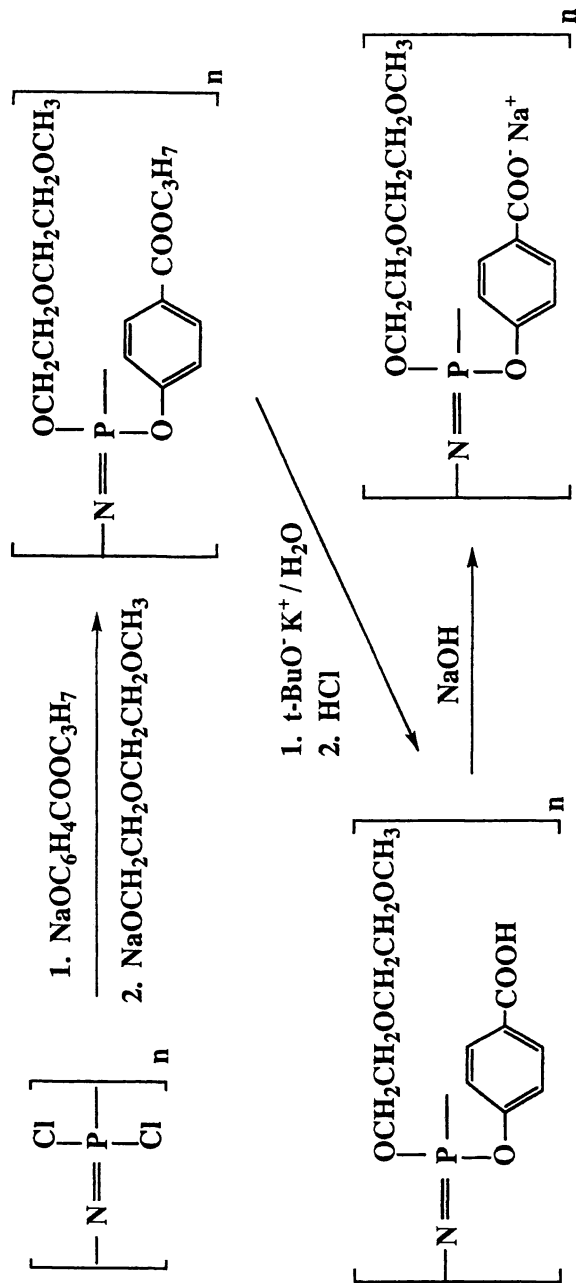
## Bioerosion

The polymers and hydrogels described above are stable in neutral aqueous media for long periods of time. Hydrogels derived from 5 have been maintained in water for more than 5 years without evidence of decomposition. However, certain applications may require bioerodibility to satisfy the requirements for long term biocompatibility. This can be accomplished by the introduction of small amounts of hydrolysis sensitizing side groups of the types shown in Table 2 (19-31). When these side groups are the only ones present in a polyphosphazene, hydrolysis occurs to give the side group alcohol or amine, phosphate, and ammonia. When present in small amounts along the chain, these same side groups can induce slow hydrolysis of the polymer or the gel with hydrolysis rates that depend on the loading of these groups and the precise structure of the sensitizing unit.

## Conclusions

The combination of alkyl ether and carboxylic acid-bearing side groups creates additional opportunities for hydrogel design and behavior over and above those offered by either of the two single-substituent types. Even when not crosslinked through the alkyl ether groups, these polymers offer interesting new possibilities for microencapsulating bioactive molecules or cells. The

Scheme III. Synthesis of Hybrid Hydrogel System



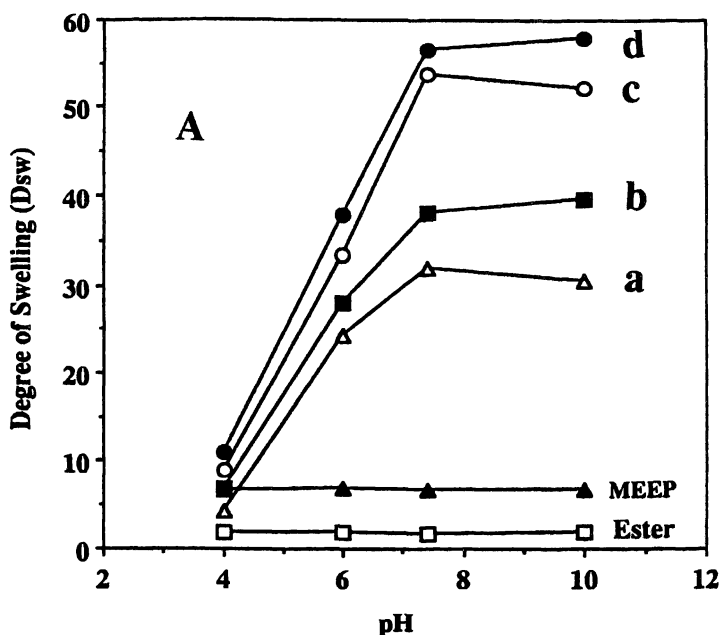


Figure 8. A. Effect of pH on the equilibrium degree of swelling of the hydrogels. B. Influence of sodium chloride concentration on the equilibrium degree of swelling. C. Effect of cation charge on the equilibrium degree of swelling of the hydrogels.

Polymer a=poly[(30% oxybenzoate)(70% methoxyethoxyethoxy)phosphazene].

Polymer b=poly[(50% oxybenzoate)(50% methoxyethoxyethoxy)phosphazene].

Polymer c=poly[(76% oxybenzoate)(24% methoxyethoxyethoxy)phosphazene].

Polymer d=poly[(94% oxybenzoate)(6% methoxyethoxyethoxy)phosphazene].

*Continued on next page.*

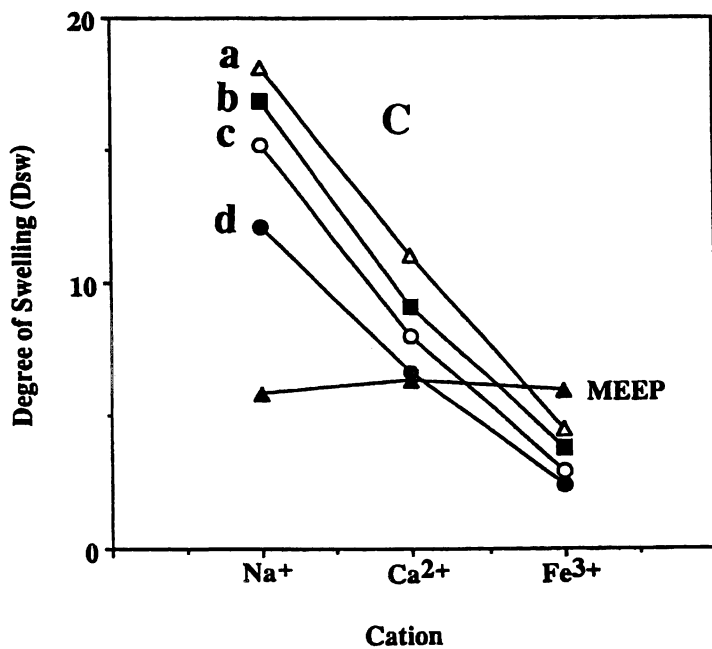
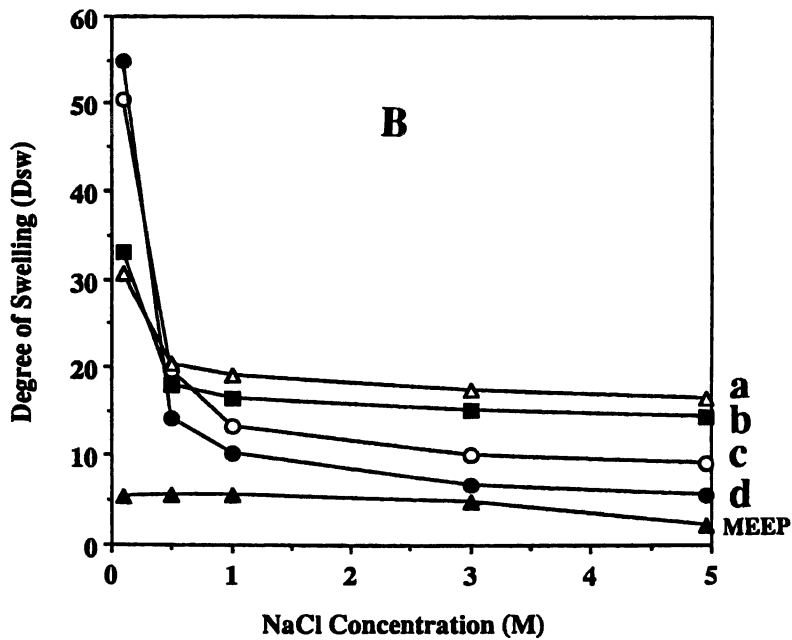
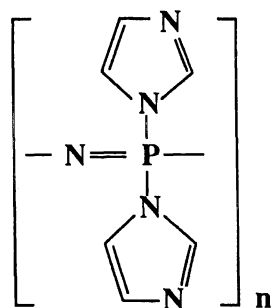
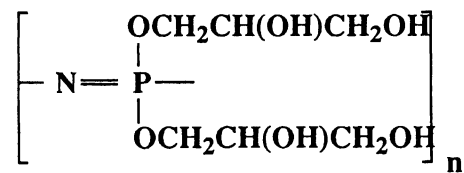
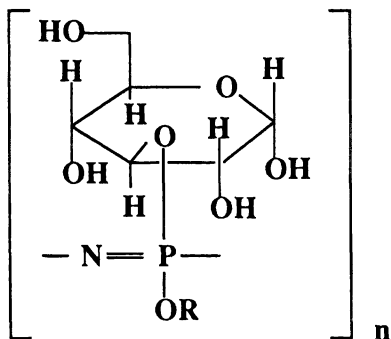
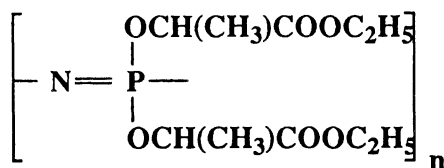
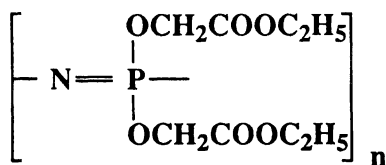
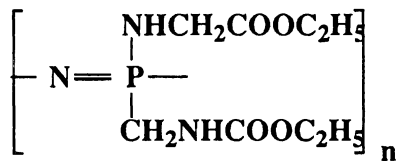
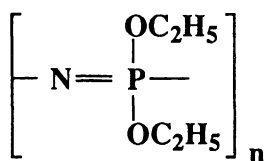
Figure 8. *Continued.*

Table 2. Bioerodible polyphosphazenes





recent access to phosphazene block copolymers (32-36) provides additional opportunities for combining these two types of side groups in ways that could be useful for microencapsulation or for incorporation into controlled diffusion membranes.

## Acknowledgments

This work was supported by Ethicon Inc. (a Johnson & Johnson Company), and by the US Army Research Office.

## References

- (1) Allcock, H. R.; Austin, P. E.; Neenan, T. X.; Sisko, J. T.; Blonsky, P. M.; Shriver, D. F., *Macromolecules* **1986**, *19*, 1508-1512.
- (2) Allcock, H. R.; Pucher, S. R.; Turner, M. L.; Fitzpatrick, R. J., *Macromolecules* **1992**, *25*, 5573-7.
- (3) Allcock, H. R.; Dudley, G. K., *Macromolecules* **1996**, *29*, 1313-19.
- (4) Allcock, H. R.; Kwon, S.; Riding, G. H.; Fitzpatrick, R. J.; Bennett, J. L., *Biomaterials* **1988**, *9*, 509-13.
- (5) Bennett, J. L.; Dembek, A. A.; Allcock, H. R.; Heyen, B. J.; Shriver, D. F., *Polym. Prepr.* **1989**, *30*, 437-8.
- (6) Nelson, C. J.; Coggio, W. D.; Allcock, H. R., *Chem. Mater.* **1991**, *3*, 786-7.
- (7) Allcock, H. R.; Fitzpatrick, R. J.; Visscher, K., *Chem. Mater.* **1992**, *4*, 775-80.
- (8) Allcock, H. R.; Pucher, S. R.; Visscher, K. B., *Biomaterials* **1994**, *15*, 502-6.
- (9) Allcock, H. R.; Pucher, S. R.; Fitzpatrick, R. J.; Rashid, K., *Biomaterials* **1992**, *13*, 857-62.
- (10) Allcock, H. R.; Kwon, S., *Macromolecules* **1989**, *22*, 75-9.
- (11) Cohen, S.; Bano, M. C.; Visscher, K. B.; Chow, M.; Allcock, H. R.; Langer, R., *J. Am. Chem. Soc.* **1990**, *112*, 7832-3.
- (12) Bano, M. C.; Cohen, S.; Visscher, K. B.; Allcock, H. R.; Langer, R., *Biotechnology* **1991**, *9*, 468-71.
- (13) Cohen, S.; Bano, M. C.; Cima, L. G.; Allcock, H. R.; Vacanti, J. P.; Vacanti, C. A.; Langer, R., *Clin. Mater* **1993**, *13*, 3-10.
- (14) Andrianov, A. K.; Cohen, S.; Visscher, K. B.; Payne, L. G.; Allcock, H. R.; Langer, R., *J. Controlled Release* **1993**, *27*, 69-77.
- (15) Cohen, S.; Allcock, H. R.; Langer, R., *Recent Adv. Pharm. Ind. Biotechnol., Minutes Int. Pharm. Technol. Symp., 6th, Meeting Date* **1993**, 36-48.
- (16) Andrianov, A. K.; Payne, L. G.; Visscher, K. B.; Allcock, H. R.; Langer, R., *J. Appl. Polym. Sci.* **1994**, *53*, 1573-8.

- (17) Payne, L. G.; Jenkins, S. A.; Woods, A. L.; Grund, E. M.; Geribo, W. E.; Loebelenz, J. R.; Andrianov, A. K.; Roberts, B. E., *Vaccine* **1998**, *16*, 92-98.
- (18) Allcock, H. R.; Ambrosio, A. M. A., *Biomaterials* **1996**, *17*, 2295-2302.
- (19) Allcock, H. R.; Fuller, T. J.; Mack, D. P.; Matsumura, K.; Smeltz, K. M., *Macromolecules* **1977**, *10*, 824-30.
- (20) Allcock, H. R.; Pucher, S. R.; Scopelianos, A. G., *Biomaterials* **1994**, *15*, 563-9.
- (21) Allcock, H. R.; Pucher, S. R.; Scopelianos, A. G., *Macromolecules* **1994**, *27*, 1071-5.
- (22) Ibim, S. M.; Ambrosio, A. A.; Larrier, D.; Allcock, H. R.; Laurencin, C. T., *J. Controlled Release* **1996**, *40*, 31-39.
- (23) Laurencin, C. T.; El-Amin, S. F.; Ibim, S. E.; Willoughby, D. A.; Attawia, M.; Allcock, H. R.; Ambrosio, A. A., *J. Biomed. Mater. Res.* **1996**, *30*, 133-8.
- (24) Crommen, J. H. L.; Schacht, E. H.; Mense, E. H. G., *Biomaterials* **1992**, *13*, 601-11.
- (25) Crommen, J.; Vandorpe, J.; Schacht, E., *J. Controlled Release* **1993**, *24*, 167-80.
- (26) Vandorpe, J.; Schacht, E.; Dunn, S.; Hawley, A.; Stolnik, S.; Davis, S. S.; Garnett, M. C.; Davies, M. C.; Illum, L., *Biomaterials* **1997**, *18*, 1147-1152.
- (27) Allcock, H. R.; Scopelianos, A. G., *Macromolecules* **1983**, *16*, 715-19.
- (28) Allcock, H. R.; Pucher, S. R., *Macromolecules* **1991**, *24*, 23-34.
- (29) Allcock, H. R.; Kwon, S., *Macromolecules* **1988**, *21*, 1980-5.
- (30) Allcock, H. R.; Pucher, S. R.; Scopelianos, A. G., *Macromolecules* **1994**, *27*, 1-4.
- (31) Allcock, H. R.; Fuller, T. J.; Matsumura, K., *Inorg. Chem.* **1982**, *21*, 515-21.
- (32) Honeyman, C. H.; Manners, I.; Morrissey, C. T.; Allcock, H. R., *J. Am. Chem. Soc.* **1995**, *117*, 7035-6.
- (33) Allcock, H. R.; Crane, C. A.; Morrissey, C. T.; Nelson, J. M.; Reeves, S. D.; Honeyman, C. H.; Manners, I., *Macromolecules* **1996**, *29*, 7740-7747.
- (34) Nelson, J. M.; Primrose, A. P.; Hartle, T. J.; Allcock, H. R.; Manners, I., *Macromolecules* **1998**, *31*, 947-949.
- (35) Allcock, H. R.; Nelson, J. M.; Prange, R.; Crane, C. A.; deDenus, C. R., *Macromolecules* **1999**, *32*, 5736-43.
- (36) Prange, R.; Allcock, H. R., *Macromolecules* **1999**, *32*, 6390-6392.

## Chapter 7

# Chitin and Chitosan in Gel Network Systems

Waldo Argüelles-Monal<sup>1,4</sup>, Francisco M. Goycoolea<sup>2</sup>, Jaime Lizardi<sup>2</sup>,  
Carlos Peniche<sup>3</sup>, and Inocencio Higuera-Ciajara<sup>2</sup>

<sup>1</sup>IMRE, Universidad de La Habana, La Habana 10400, Cuba

<sup>2</sup>Centro de Investigación en Alimentación y Desarrollo, A. C. Apdo. Postal 1735,  
Hermosillo, Sonora 83000, México

<sup>3</sup>Centro de Biomateriales, Universidad de La Habana, La Habana 10400, Cuba

<sup>4</sup> Current address: Unidad Guaymas, CIAD AC, Carretera al Varadero Nacional  
Km 6.6, Apdo. Postal 284, Guaymas, Sonora 85400, México

## 1. Introduction

Gels from natural polymers have received increasing attention over the past years. They display novel physicochemical properties, particularly in aqueous systems, lending themselves valuable for a plethora of advanced applications, particularly in foods, cosmetics, medicine and biotechnology. However, the fundamental mechanisms operating in these gels are still poorly understood in most cases, due to the intrinsic high polydispersity (both in chain size and chemical composition), as opposed to their synthetic counterparts.

Chitin and chitosan are currently at the focus of increasing scientific and economic interest due to their significance in nature and technology. Chitin, poly-*N*-acetylglucosamine (Figure 1a), is ubiquitous in nature, as it is comprised in the microstructure of the exo-esqueleton of crustaceans, insects and in the cell wall of fungi. In animal tissues, chitin exists as a part of a semi-crystalline microfibrillar matrix cemented by protein and inorganic salts while in fungi, it is associated with other polysaccharides such as cellulose, glucan, mannan and polygalactosamine. Chitin supply is currently sourced from crustacean biowaste after removal of protein and inorganic material. Chitosan, the main industrial derivative of chitin, is prepared by controlled deacetylation to yield a linear polymer chain composed mostly of glucosamine residues (Figure 1b).

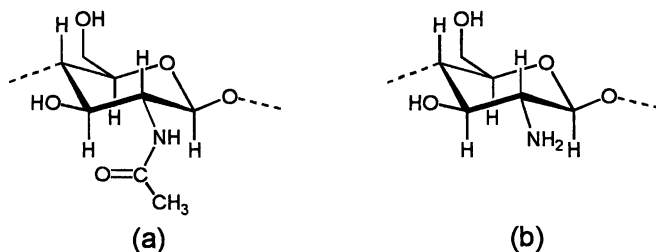


**Fig. 1.**  $\beta(1 \rightarrow 4)$ -Linked monosaccharide repeating units of (a) *N*-acetyl-2-amino-2-deoxy-*D*-glucose in fully *N*-acetylated chitin and (b) 2-amino-2-deoxy-*D*-glucose in fully *N*-deacetylated chitosan.

The scope of this review is centred on the one hand in three-dimensional gel networks embracing in their structure the presence of pre-existing polymer chains of chitin or chitosan in disordered sol state. On the other hand, complex gel networks of carrageenan added with short segments of chitosan are also addressed. Emphasis will be in physicochemical phenomena and exploration of the possible mechanisms underlying the nature of these gel networks. Formally, these gel systems belong either to type II (covalent networks of disordered chains) or type III (networks formed through physical association) according to the nature of the structural connections present as proposed by P. Flory.<sup>1</sup> Mechanisms of creation of the various types of junctions in these gel systems, include permanent chemical cross-linking of chitin/chitosan chains with a wide range of cross-linking agents, physical gelation processes including liquid-liquid segregation in alkali chitin, formation of physical junctions of local order in hydrophobic chitosan derivatives or chitosan/carrageenan co-gels formed by electrostatic association via interpolymeric polyelectrolyte complex formation.

Reference to recent published literature on the subject is included in the various items addressed in this chapter, though the breath of it will embrace recent advances of collaborative research undertaken by our groups over the past three years. In so doing, we aim to provide a picture of the current state of understanding of the above mentioned distinctive chitin/chitosan gel systems.

The characteristics of the samples employed are as follows: Chitin (from shrimp shell of *Peneaeus stylirostris* -70%- and *P. californiensis* -30%-,  $M_v = 2.2 \times 10^5$ , DA = 90%), Chitosan (from lobster *Panulirus argus*,  $M_v = 2.3 \times 10^5$ , DA = 20.1%).

## 2. Chitin Gels

Native chitin itself is known to be insoluble in polar solvents, due to extensive intermolecular hydrogen bonding, however, it dissolves in the aprotic system *N,N*-dimethyl acetamide - 5% LiCl. A sol-gel transition has been documented for chitin 1% (w/w) DMA-LiCl solutions, on heating to  $\sim 110^\circ\text{C}$ .<sup>2</sup> The phenomenon has been attributed to weakening effect of the polymer-solvent

interaction with increasing temperature, however, the precise gelation mechanism has not yet been established.

In aqueous cold alkali, chitin also dissolves and behaves as a macromolecular solution, as verified by its mechanical spectrum when tested by small-deformation oscillatory measurements. At 4°C and 1.5% (w/w) the system could be described as a transparent sol phase with a viscoelastic response characteristic of an entangled concentrated network, which is comparable to the spectrum exhibited by chitosan (in 0.1 mol L<sup>-1</sup> acetic acid),<sup>3</sup> but no yield stress is observed in this case.

Nevertheless, if a gradual increase in temperature is applied, the alkali-chitin solution undergoes phase separation, yielding a dilute (solvent-rich) sol phase and a concentrated (solute-rich) gel phase (see Fig. 2).

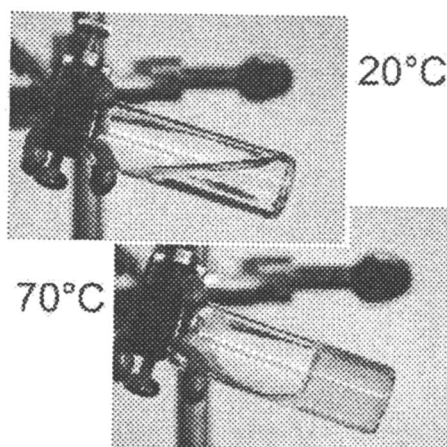


**Fig. 2.** Alkali chitin in aqueous solution at 20°C and after phase separation-gelation upon heating to 70°C

In Fig. 3 are shown the results obtained with a 1% alkali chitin solution. The cloud point can be determined as the temperature at which a very slight increment in the absorbance arises. From optical measurements it could be appreciated that the cloud point is centred at 30°C (Fig. 3a). The appearance of a slight opalescence in the solution at this temperature is in very close correspondence with the onset of changes in  $\eta^*$  equilibrium values. The latter are manifested by a well defined 'break-point' in the Arrhenius-type plots (Fig. 3c). The dependence of the break-point values of each  $\eta^*(T^{-1})$  plot with frequency,  $\omega$ , is also evident. The behaviour of the system was also monitored by the ratio of fluorescence intensities of pyrene at 384 and 372 nm, when excited at 343 nm. From the curve depicted in Fig. 3b, it can be appreciated a decrease in the fluorescence ratio when the system is heated with an inflexion point at 27.5°C (as determined by the first derivative method), signalling the onset of self-aggregation of the polymer.

In order to estimate the cloud point from viscoelastic oscillatory measurements, we propose to extrapolate the critical temperature to  $\omega \rightarrow 0$ ,

*i.e.* infinite relaxation time. The shift in break point values to lower temperatures as the frequency decreases, is a direct consequence of the longer relaxation times expected for larger molecular species bound to be less stable against phase separation.

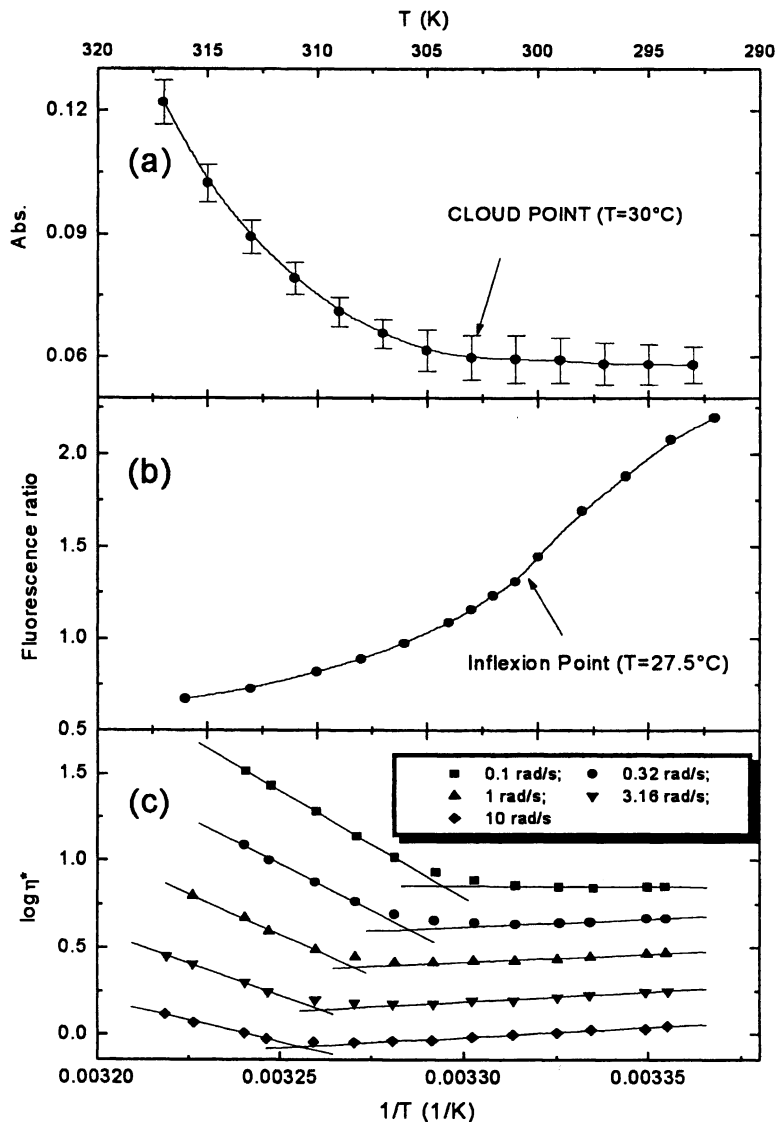


**Fig. 3.** Variation in (a) optical density ( $\lambda = 430$  nm), (b) ratio of intensities of pyrene fluorescence emission at 384 and 372 nm and (c) complex viscosity,  $\eta^*$ , at varying oscillation frequency ( $\gamma = 0.15$ ) during heating to equilibrium of a fresh solution of alkali chitin (*c.* 1% w/w).

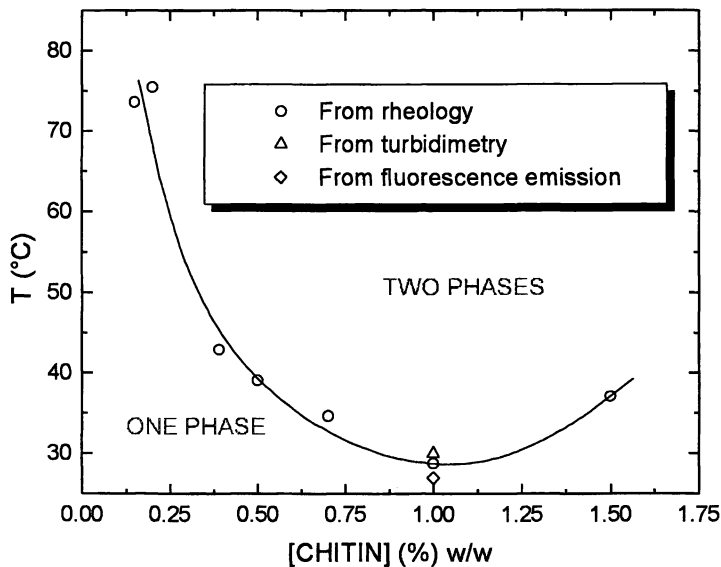


Fig. 4. Cloud point curve for alkali chitin

The cloud point values thus obtained for alkali chitin solutions in the range 0.15 to 1.5%, clearly describe lower limiting phase separation behaviour, as can be observed from Fig. 4. The lower critical solution temperature (LCST) is apparently located at  $T = 30^{\circ}\text{C}$  (1% concentration), where there is a minimum in the cloud point curve. It should be noted the excellent agreement between the three experimental techniques employed at this polymer concentration.

It is well known that the possible causes for the presence of lower critical separation phenomena in polymer solutions have been associated with differences in free volume between the solvent and the macromolecular solute in the vicinity of the solvent critical point.<sup>4,5</sup> Another possible reason for the appearance of lower critical phenomena in aqueous polymer solutions has been identified with the circumstance that at moderate temperatures hydrophobic interactions among polymer chains could be developed. In the later case, the behaviour of phase separation should be related with the existence of hydrogen bonding as well.

Both, natural and synthetic polymers with associative properties arising from hydrophobic interactions give aqueous solutions with LCST.<sup>6,7</sup> Among the most known systems having LCST behaviour should be mentioned polyethylene glycol-water<sup>8</sup> and aqueous solutions of methyl cellulose.<sup>9</sup> Also, in poly(methacrylic) acid, LCST phase diagrams were determined from the change in shear modulus and turbidity.<sup>10,11</sup> For alkali chitin, the main key role played by hydrophobic interactions in LCST is evident from the decrease in the fluorescence ratio observed in Fig. 3b.

A related type of gel network of N-acetyl chitosan has also been prepared in acetic acid-water-propanediol by controlled acetylation of chitosan, where hydrophobic macromolecular association has also been offered as the underlying mechanism of gelation.<sup>12</sup>

### 3. Chitosan Chemical Networks

The rheological investigation of the chemically crosslinked chitosan network has been focused on the evolution of the viscoelastic characteristics of the chitosan/glutaraldehyde system under sensitive dynamic oscillatory testing.<sup>3</sup> The degree of cross-linking of the chitosan chemical network, was controlled by varying the stoichiometric ratio of functional aldehyde groups per mole of amine group (R value), in the range between R=0 to 5 at 35°C (polymer concentration: 1% w/w in 0.1 mol L<sup>-1</sup> acetic acid). A linear viscoelastic response ( $\gamma = 0.15$  to 0.7) in all gels persisted to low R values (R = 0.32), near to the rheological gel point.

The gelation curves of chitosan gels ( $G'$  vs. time at  $\omega = 1 \text{ rad}\cdot\text{s}^{-1}$ ) seem to fall into two “families” with a qualitative change in the rate of increase in  $G'$  during the first 30-40 minutes, which could be interpreted as a consequence of complex network contributions to the storage modulus of physical and chemical type progressively changing in time. The gels were fully cured at 240 min.<sup>3</sup>

Fig. 5 includes five spectra of chitosan gels of progressively higher degree of crosslinking (from R=0.32 to 5) and that of the starting chitosan solution (R=0). All the spectra were recorded after the aforementioned elapsed time when no variation in mechanical moduli with time was observed. For clarity, the spectra are shown in two different scales on the y-axis. The mechanical spectrum of chitosan solution (1% w/w) suggests the presence of a weakly structured network of self-associated chitosan (stabilised by hydrophobic associations of N-acetyl groups) with restricted mobility at high degrees of space occupancy ( $c[\eta] \sim 47$ ). At R=0.4, when glutaraldehyde begins to cross-link chitosan chains, the overall shape of the mechanical spectrum is similar to that of an amorphous vitrified system. This may be consistent with the suggestion that at low degrees of crosslinking, a slight increment in the restriction of chitosan chains mobility (by chemical crosslinking), drastically increases the relaxation time, so segmental motions predominate over long-range ones.<sup>13</sup> As R increases to 0.5, notice that the form of the mechanical spectrum merges the viscoelastic behaviour of a weak gel in the frequency range 0.06 to 6 rad·s<sup>-1</sup> (*i.e.*  $G' > G''$  and both moduli increase with frequency) with that of a dissolved polymer dominated by entanglements of greater lifetime than 6 rad·s<sup>-1</sup>. Presumably at this point the gel network density is just below its percolation point. Hence, this spectrum suggests the existence of a chemically crosslinked gel network ‘dissolved’ in a second entangled network formed by chitosan chains of restricted mobility. Notice that at R=1, the mechanical spectra already corresponds to a ‘lossy’, yet permanent gel network:  $G'(\omega)$  shows almost no dependence with frequency. At high degrees of crosslinking (R=5), it is clear that the  $G'$  values increase by about 3 orders of magnitude, but show hardly any change in frequency dependence with respect to the strong gel. The overall network structure hardening in the spanned region, is accompanied by a gradual change in  $G''$  frequency dependence. The role of associating phenomena due to hydrophobic interactions in highly acetylated chitosan/glutaraldehyde chemical gel has also been noticed.<sup>14</sup>



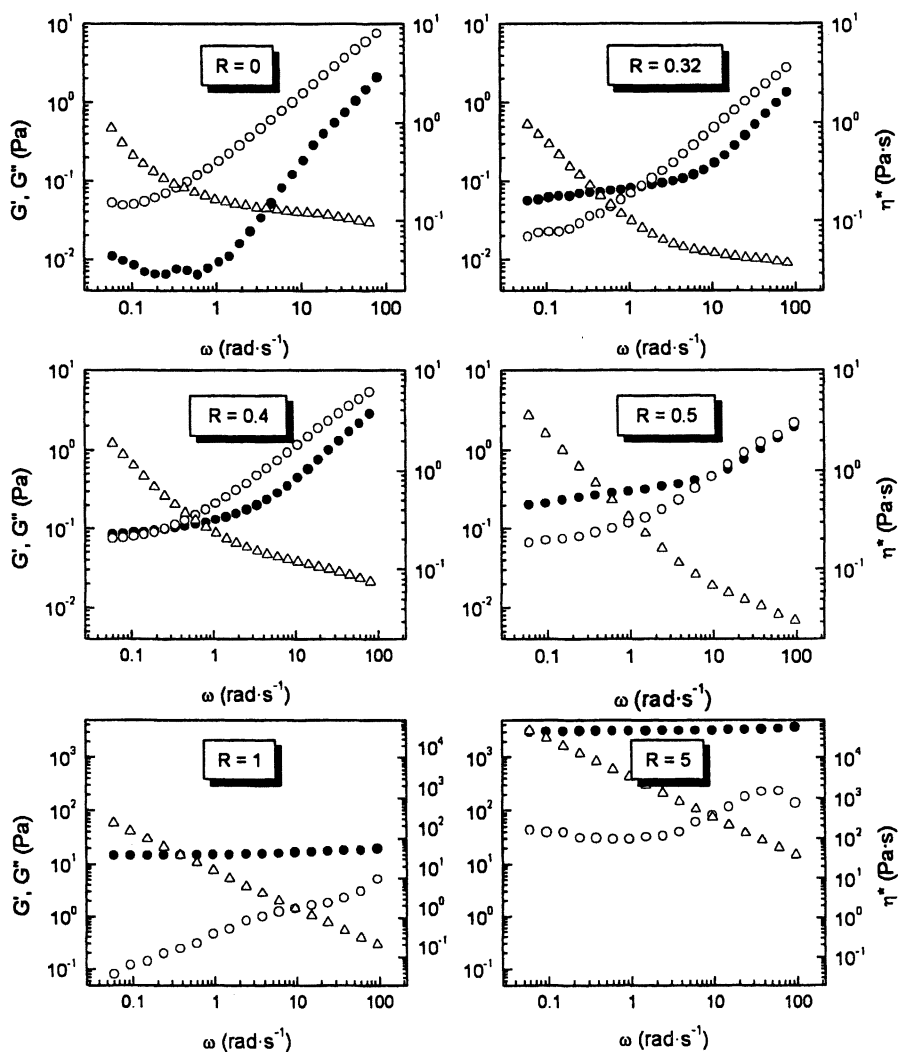


**Fig. 5.** Mechanical spectra of chitosan (1% w/w in 0.1 mol L<sup>-1</sup> acetic acid) chemically cross-linked with glutaraldehyde with stoichiometric ratios,  $R$ , over the range 0.32 - 5 at 35°C.  $G'$ , filled circles;  $G''$ , open circles;  $\eta^*$ , triangles.

The kinetics and rheological properties of chemically crosslinked gels of scleraldehyde-chitosan have also been documented recently. These gels were prepared aiming to achieve enhanced immunostimulating properties of scleroglucan, a neutral water soluble fungal  $\beta(1,3)$ -linked glucan.<sup>15</sup> Here the reaction also proceeds by Schiff-base formation between partly periodate oxidized scleroglucan yielding dialdehyde groups in the side chains (scleraldehyde) and the primary amine functionality of chitosan. Interestingly, in this system, it was noted a change from entropy dominated elasticity at low degree of crosslinking changing to enthalpic elasticity at increasing degree of crosslinking, possibly due to the decreasing length of the elastically active chains. This suggestion seems to agree with the rheological changes observed in chitosan gels at low and high degree of crosslinking.

#### 4. Chitosan in Gel Polyelectrolyte Complexes

Polyelectrolyte complexes (PEC) result from the interaction of oppositely charged polyelectrolytes, giving rise to a complex structure in dependence of various conditions. Experimental results obtained by our laboratories on this topic, were focused on the influence of complexing very short chitosan chains with DP = 20 or 75 regarded here to as CHI-20 or CHI-75, respectively, with  $\kappa$ - or  $\nu$ - carrageenan on their gelation behaviour under various salt environments.<sup>16</sup> Under the conditions used in these series of studies, soluble non-stoichiometric polyelectrolyte complexes (NPEC) were obtained. It is important to point out that soluble NPEC system is formed by the electrostatic association between a strong polyacid (in this case the carrageenan species) and a weak polybase (in this case chitosan), provided that the molecular size of the base is reduced and the stoichiometric ratio of both components is carefully controlled. An experimental proviso worth of mention is that the stoichiometric ratio of chitosan to carrageenan charge equivalents defined as the  $Z$  value, had to be kept under a very narrow range of values and in pronounced favour of the carrageenan component ( $Z = 0.028$  to  $0.084$ ) in order to prevent precipitation of the complex. Indeed, addition of chitosan beyond values of  $Z > 0.084$ , invariably caused onset of precipitation.

The gelation of carrageenan was monitored by strain-controlled small-deformation oscillatory measurements.

##### 4.1 $\kappa$ -Carrageenan in $0.25 \text{ mol}\cdot\text{L}^{-1}$ NaCl

The evolution of the storage modulus at  $\omega = 1 \text{ rad}\cdot\text{s}^{-1}$  during cooling of a  $\kappa$ -carrageenan solution alone and in combination with CHI-20 in NPECs of varying composition ( $Z=0.028$  to  $0.084$ ), at identical carrageenan concentration

in  $0.25 \text{ mol}\cdot\text{L}^{-1}$  NaCl is presented in Fig. 6. Inspection of the individual traces reveals a general elevation of the final  $G'$  values of the NPEC at low temperatures as the proportion of complexed chitosan increases. Moreover, the onset temperature of gelation ( $T_{\text{gel}}$ ) of the NPECs is shifted to higher temperature, regardless of the NPEC composition. It should be noted that in two of the complexes ( $Z = 0.042$  and  $0.084$ ) the  $G'$  moduli registered at temperatures above  $T_{\text{gel}}$  are greater than the rest of the complexes and  $\kappa$ -carrageenan alone.

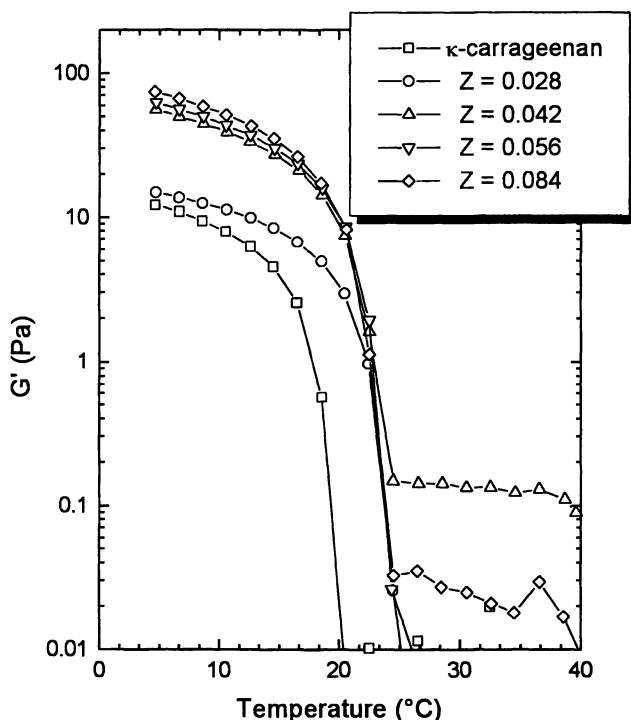


**Fig. 6.** Temperature dependence of  $G'$  ( $1 \text{ rad}\cdot\text{s}^{-1}$ ;  $\gamma = 0.15$ ;  $1^\circ\text{C}\cdot\text{min}^{-1}$ ) for  $\kappa$ -carrageenan in NaCl alone and in complexes with chitosan (CHI-20) of varying  $Z$  (as indicated in label).

The Winter and Chambon criterion<sup>17</sup> was adopted to define the critical rheological *gel point* (i.e. the percolation threshold at the formation of an incipient continuous network of infinite molecular weight). This condition is marked where a power-law variation of  $G'$  and  $G''$  viscoelastic moduli with  $\omega$  is obeyed, hence  $G'(\omega) \propto G''(\omega) \propto \omega^\Delta$ , and irrespectively of  $\omega$ ,  $\tan \delta (=G''/G')$  remains constant.<sup>18</sup>

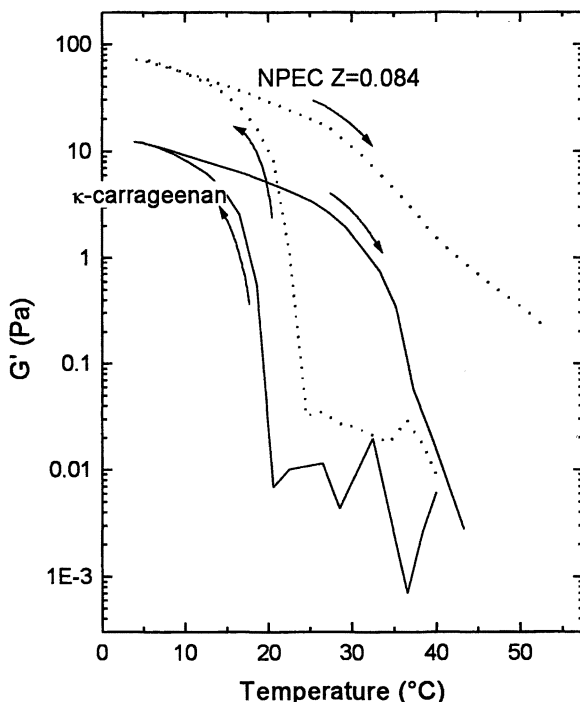


**Fig. 7.** Variation of  $G'$  on cooling and heating (as indicated by arrows;  $1^\circ\text{C}\cdot\text{min}^{-1}$ ) for  $\kappa$ -carrageenan alone and for a complex ( $Z = 0.084$ ) from Fig. 6.

In Fig. 7 is shown the variation in the storage modulus at  $\omega = 1 \text{ rad}\cdot\text{s}^{-1}$  corresponding to gel formation and melting during respectively cooling and heating scans of  $\kappa$ -carrageenan and chitosan/carrageenan NPEC of  $Z = 0.084$ . The difference in the cooling and heating traces reflects the thermal hysteresis expected for helix-helix aggregation of  $\kappa$ -carrageenan in  $0.25 \text{ mol}\cdot\text{L}^{-1} \text{ NaCl}$ <sup>19</sup>. This thermal hysteresis has a greater magnitude in the presence of chitosan in the NPEC of  $Z=0.084$ , and similar results were obtained for the other NPECs. Fig. 8 shows data for  $G'$  and  $G''$  of the gels formed at  $4^\circ\text{C}$  for  $\kappa$ -carrageenan alone and NPECs with CHI-20 and CHI-75 as a function of the amount of complexed chitosan. Notice that in both cases, the NPEC with CHI-20 and CHI-75, there is a plateau level in  $G'$  values the gels tend to at  $4^\circ\text{C}$  as the  $Z$  value in the NPEC increases. NPECs with CHI-20 however, seem to level off at  $Z>0.042$ , whereas NPECs with CHI-75 reach their plateau at  $Z>0.028$ . The mechanical spectra (variation of  $G'$ ,  $G''$  and  $\eta^*$  with  $\omega$ ) recorded on completion of the cooling scans (results not shown) were typical for a polysaccharide gel network. The presence of chitosan resulted in an overall increase in the viscoelastic moduli, but no significant change in the spectral shape of the gels

was observed (*i.e.* no dependence of  $G'$  and  $G''$  and linear decrease of  $\eta^*$  on frequency with a slope close to -1).

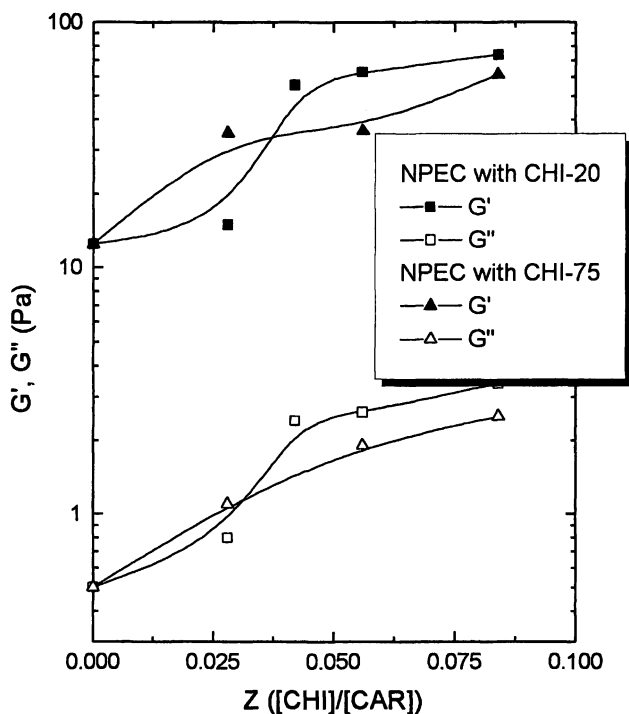


**Fig. 8.** Variation of  $G'$  ( $4^{\circ}\text{C}$ ;  $1 \text{ rad}\cdot\text{s}^{-1}$ ;  $\gamma = 0.15$ ) with  $Z$  for complexes of  $\kappa$ -carrageenan with chitosan (CHI-20 and CHI-75) in NaCl. The value at  $Z = 0$  corresponds to  $\kappa$ -carrageenan alone.

#### 4.2 $\kappa$ -Carrageenan in $0.03 \text{ mol}\cdot\text{L}^{-1}$ KCl

The temperature course of gel formation for  $\kappa$ -carrageenan complexed with chitosan (CHI-20) and alone in  $0.03 \text{ mol}\cdot\text{L}^{-1}$  KCl, was also monitored. The traces of  $G'$  at  $\omega=1 \text{ rad}\cdot\text{s}^{-1}$  are drawn in Fig. 9. Under these conditions, the final  $G'$  moduli values are almost the same within the expected error for the NPECs and for  $\kappa$ -carrageenan. Only a very small elevation in the final  $G'$  values is observed for the NPEC of  $Z=0.028$ , as compared to the rest of the gels. It is evident that there is no detectable change in gelation temperature (*i.e.* the onset of the steep rise in moduli). The sol-gel transition for these systems lied within the range  $32\text{-}34^{\circ}\text{C}$ .

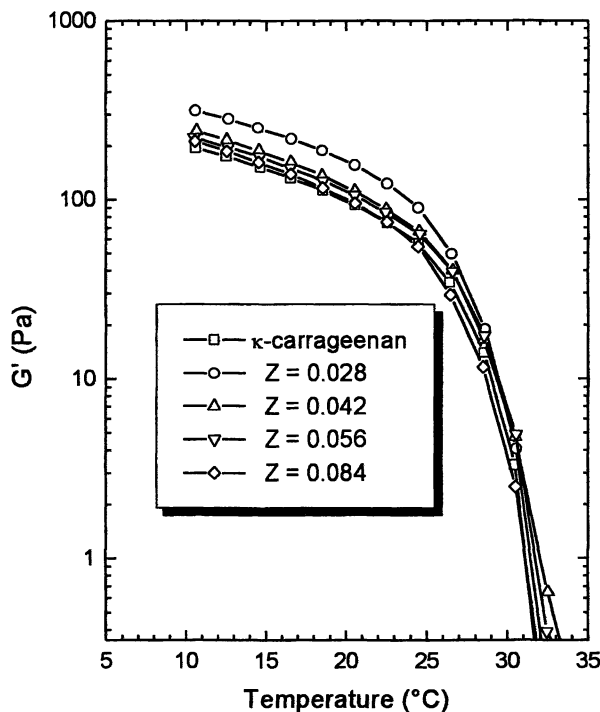


**Fig. 9.** Temperature dependence of  $G'$  ( $1 \text{ rad}\cdot\text{s}^{-1}$ ;  $\gamma = 0.15$ ;  $1^\circ\text{C}\cdot\text{min}^{-1}$ ) for  $\kappa$ -carrageenan in KCl alone and in complexes with chitosan (CHI-20) of varying  $Z$  (as indicated in label).

The storage modulus corresponding to cooling and heating scans of  $\kappa$ -carrageenan and the chitosan/carrageenan NPEC shows also a difference, which reflects again the thermal hysteresis, expected for helix-helix aggregation of  $\kappa$ -carrageenan in KCl.<sup>19</sup> In this case, the ion-driven transition is favoured at significantly lower ionic strength than that in the systems prepared in the presence of NaCl. This is due to the well known specific binding of  $\text{K}^+$  cations to the double-helical form of  $\kappa$ -carrageenan, thus effectively promoting conformational ordering and aggregation at significantly lower concentrations than do non-specific ions, acting solely by charge screening.<sup>20</sup> In contrast with NaCl gels, this thermal hysteresis is unaffected by the presence of chitosan in the NPEC of  $Z=0.028$ , and similar results were obtained for other NPECs of different  $Z$  values.

#### 4.3 $\iota$ -Carrageenan in $0.25 \text{ mol}\cdot\text{L}^{-1}$ NaCl

$\iota$ -Carrageenan bears two  $\text{SO}_3^-$  charges per residue, otherwise it shares a similar idealized structure with  $\kappa$ -carrageenan. As  $\kappa$ -,  $\iota$ -carrageenan also gels

when the ionic strength is high enough to stabilise the ordered helical conformer as a consequence of association of the ordered structure.<sup>21</sup> In 0.25 mol L<sup>-1</sup> NaCl, ι-carrageenan (3 g L<sup>-1</sup>) gels at  $T_{\text{gel}} \sim 47.0^\circ\text{C}$ . Addition of CHI-20 under a similar protocol as that described above for the κ-carrageenan/chitosan system causes no change in  $T_{\text{gel}}$  for NPECs within the range of  $Z$  between 0.028 and 0.056. When CHI-75 replaces CHI-20, the critical gel temperature shifts progressively to lower values (down to 42.2°C) as  $Z$  increased from 0.056 to 0.084 (Fig. 10).

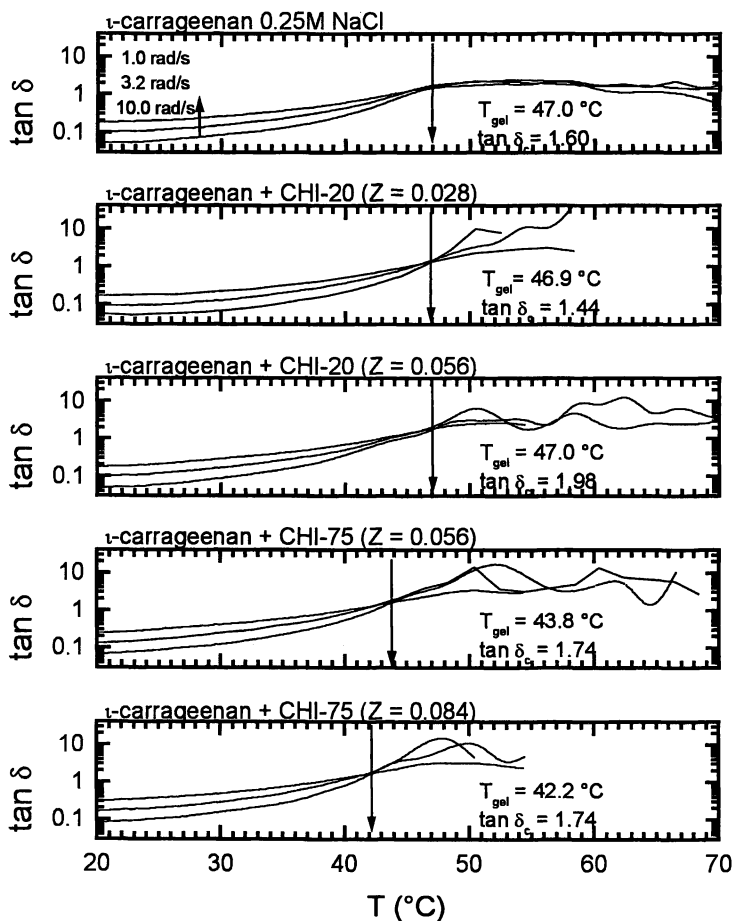


**Fig. 10.** Variation of  $\tan \delta$  with temperature on cooling at varying oscillation frequency (as shown in top frame) for ι-carrageenan in 0.25 M NaCl alone and in complexes with CHI-20 or CHI-75 of varying  $Z$  (as indicated in headings). Rheological critical gel point ( $T_{\text{gel}}$ ) values are indicated in each frame.

Due to the subtle rheological differences observed in this system, a detailed analysis of the ι-carrageenan/chitosan system at the gel point was conducted according to the approach of Winter and Chambon<sup>17,18</sup>. The results are summarised in Table 1.  $G'$  moduli (at 1 rad s<sup>-1</sup>) and the S gel strength parameter values correlated well and were found to vary between ι-carrageenan and the various NPECs perhaps reflecting differences in junctions chain length. It is worth to notice that for the ι-car-CHI 20 complex of  $Z=0.028$ , there is a slight increase in gel strength ( $G'$  and S values) with respect to ι-carrageenan and the rest of the NPECs. Also the differences in the power law exponent (n) values seem to be associated with subtle differences in stoichiometry the consequence of electrostatic complexation of chitosan to the carrageenan chain. A fractal dimension value,  $d_f$ , was calculated according with the theoretical approach developed by Muthukumar.<sup>22</sup> This parameter relates the mass of a cluster to its radius of gyration by  $Rd_f \sim M$  in the absence of excluded volume long-range interactions. In general, there is a tendency of  $d_f$  to decrease as chitosan complexes to ι-carrageenan beyond  $Z=0.028$ . This result indicates that the attachment of chitosan to ι-carrageenan causes a reduction in the overall network density.

**Table 1.** Critical power-law parameters at the rheological gel point for incipient ι-carrageenan and ι-carrageenan /chitosan NPEC gels in 0.25 mol·L<sup>-1</sup> NaCl.

Complex	$G'$ at $T_{gel}$ (Pa) <sup>a</sup>	$T_{gel}$ (°C)	$\tan \delta_{crit}$	n	S (Pas <sup>n</sup> ) <sup>b</sup>	$d_f^c$
ι-carrageenan alone	0.048	47.0	1.60	0.66	0.033	1.79
ι-car-CHI20 $Z=0.028$	0.060	46.9	1.44	0.63	0.042	1.83
ι-car-CHI20 $Z=0.056$	0.022	47.0	1.98	0.77	0.011	1.63
ι-car-CHI75 $Z=0.056$	0.040	43.8	1.74	0.70	0.026	1.74
ι-car-CHI75 $Z=0.084$	0.034	42.2	1.74	0.71	0.022	1.73

<sup>a</sup> Measured at  $\omega = 1.0$  rad s<sup>-1</sup>

<sup>b</sup> Calculated from equation:<sup>17</sup>  $S = G'/\omega^n \Gamma(1-n) \cos \delta$

<sup>c</sup> Calculated from equation:<sup>22</sup>  $n = d(d+2-2d_f)/2(d+2-d_f)$ ; where  $d$  ( $d=3$ ) is the spatial dimension.

Power law relaxation behaviour ( $G' \sim G'' \sim \omega^{-n}$ ) was observed in the frequency range 1 to 10 rad s<sup>-1</sup> (Fig. 11).<sup>17</sup>

The temperature course elevation of  $G'$  as a function of cooling for these systems is shown in Fig. 12. In the plot, it can also be appreciated that final  $G'$  values at 10°C are lower as  $Z$  increased in both CHI-20 and CHI-75 NPECs.



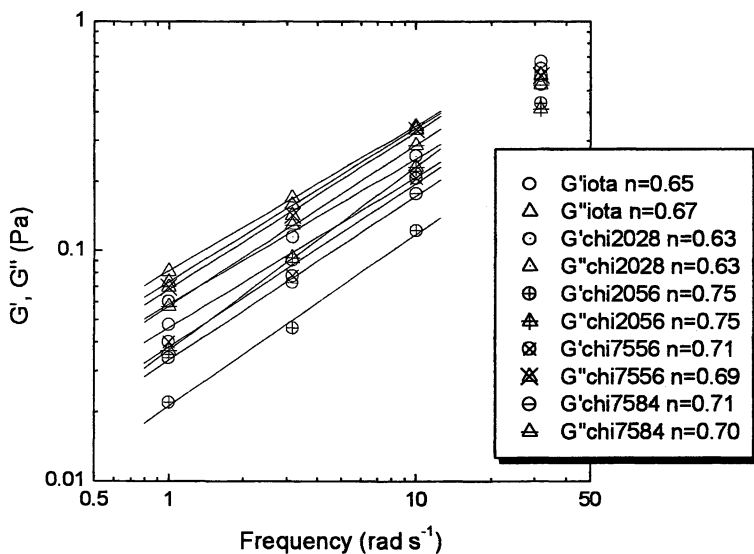


**Fig. 11.** Variation of  $G'$  and  $G''$  with frequency for  $\iota$ -carrageenan alone and  $\iota$ -carrageenan/chitosan NPECs at the critical gel point. Power-law exponent ( $n$ ) for each system is shown in label in  $0.25 \text{ mol} \cdot \text{L}^{-1} \text{ NaCl}$ .

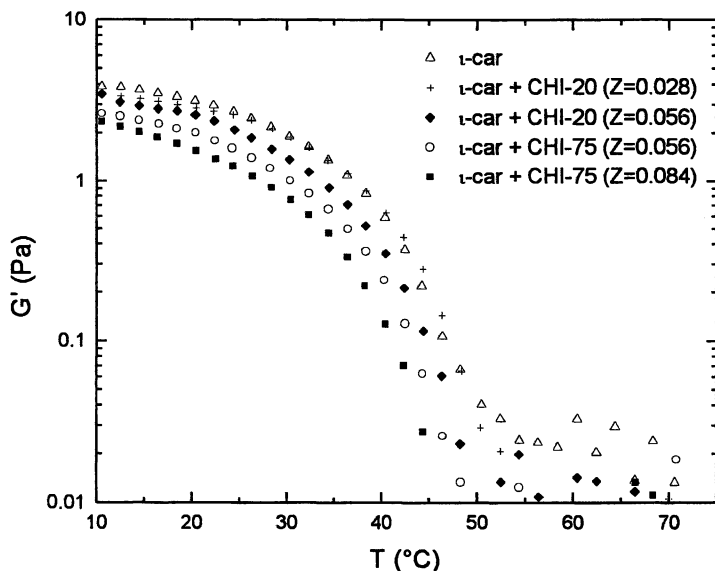


**Fig. 12.** Temperature-dependence of  $G'$  ( $1 \text{ rad s}^{-1}$ ;  $0.15$  strain) for  $\iota$ -carrageenan in  $0.25 \text{ M NaCl}$  alone and in complexes with chitosan (CHI-20 or CHI-75) of varying  $Z$  (as indicated in label).

#### 4.4 $\iota$ -Carrageenan in $0.03 \text{ mol}\cdot\text{L}^{-1}$ KCl

In  $0.03 \text{ mol}\cdot\text{L}^{-1}$  KCl,  $\iota$ -carrageenan (c.  $3 \text{ g}\cdot\text{L}^{-1}$ ), forms a very tenuous gel network on cooling to  $4^\circ\text{C}$ , as can be appreciated from the mechanical spectrum displayed in Figure 13a. There is overall predominance of  $G'$  over  $G''$  but a clear dependence of both moduli with  $\omega$ . However, in the NPEC with CHI-20 ( $Z = 0.084$ ) under identical conditions, gelation of  $\iota$ -carrageenan at  $4^\circ\text{C}$  was completely suppressed (Fig. 13b). Whether the transition of  $\iota$ -carrageenan is shifted to yet lower temperature or else was inhibited completely, cannot be established conclusively at this stage.

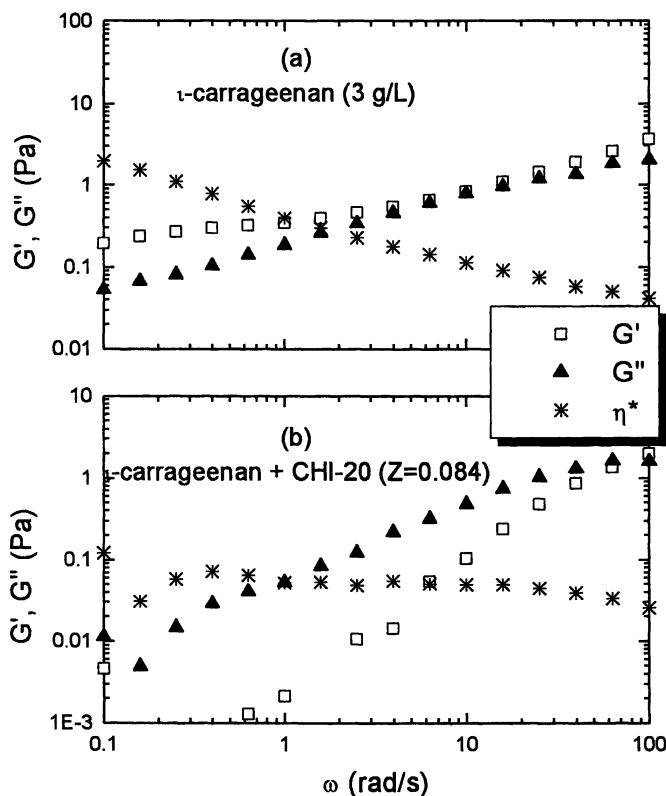


**Fig. 13.** Mechanical spectra ( $4^\circ\text{C}$ ;  $\gamma = 0.15$ ;  $30 \text{ mM}$  KCl) of (a)  $\iota$ -carrageenan alone ( $0.3 \text{ \% w/w}$ ) and (b) NPEC CHI-20,  $Z = 0.084$ .

#### 4.5 Discussion on Chitosan-Carrageenan Polyelectrolyte Complex Gels

The different behaviour for the two main carrageenan species documented in this investigation towards the addition of extremely small amounts of short segments of chitosan to produce non-stoichiometric polyelectrolyte complexes, is definitively linked to the different underlying mechanisms of gel formation on each polyelectrolyte galactan. In the case of  $\kappa$ -carrageenan, gelation takes place as a direct consequence of helical ordering and subsequent aggregation. The process is induced by monovalent cations, both selective and non-selective, but suppressed under non-aggregating conditions (e.g. in the presence of tetramethyl ammonium salts). For  $\iota$ -carrageenan, on the other hand, the situation is much less clear, as it forms weak gels even under conditions when there is no evidence of aggregation. An added difficulty to further rationalise the results in the NPECs studied is that commercial carrageenans are never pure, but normally exist as hybrid structures. In this sense, it has been demonstrated that small additions of  $\kappa$ -carrageenan to  $\iota$ -carrageenan, in the presence of  $K^+$ , triggers gelation at a greater temperature than that of  $\iota$ -carrageenan alone, due to the ordering of the  $\kappa$ -fractions by selective binding of  $K^+$ .<sup>23</sup>

According to the results described throughout this section, it could be argued that the complexation of chitosan with  $\kappa$ -carrageenan coils in presence of  $0.25 \text{ mol}\cdot\text{L}^{-1}$  NaCl leads to a reduction of charge density, due to charge compensation, and hence to the stabilisation of the ordered form of this gelling biopolymer. Besides, the obtained gel network is stronger than that of  $\kappa$ -carrageenan at the same equivalent concentration. This effect is rationalised in terms of the formation and self-association of hydrophobic PEC junction zones<sup>23</sup> at temperatures well above that of the sol-to-gel transition (Fig. 6) -leading to increase in  $G'$  at high temperature-. The slightly greater mechanical strength can be a consequence of secondary aggregation of such PEC hydrophobic 'patches', bound to be reinforced by the addition of NaCl,<sup>24,25,26</sup> a non selective electrolyte for  $\kappa$ -carrageenan.<sup>20</sup> Hence, such complexed regions can be conceived as micro-phase separated inclusions in a sort of block co-polymer gel network.

A further stabilising mechanism mediating in the association of the two polyelectrolytes, is perhaps related to an extra enthalpic (conformational adaptation) advantage of chitosan to bind directly to  $\kappa$ -carrageenan, in a similar manner than other plant  $\beta(1\rightarrow4)$ -linked glycans do, under conditions of moderate aggregation,<sup>27</sup> thus effectively reinforcing the strength of the gel network. These arguments agree well with the presence of wider thermal hysteresis between setting and melting processes (Fig. 7), as well as with greater  $G'$  values recorded for the CHI-20 than for the CHI-75 NPECs as the  $Z$  value increases as illustrated in Fig. 8 (*i.e.* since the number of CHI-20 chain species introduced into the complex is larger than that of CHI-75 at identical

concentration). The differences observed for varying chitosan chain length are a logical consequence of the cooperative nature of the complex formation.

By contrast, in the presence of  $0.03 \text{ mol}\cdot\text{L}^{-1}$  of  $\text{K}^+$  counterions –firmly established to bind specifically to the  $\kappa$ -carrageenan helix– addition of chitosan beyond  $Z=0.028$  and as the chitosan chain length increases, weakens slightly the NPEC gel network. This can be rationalised as a consequence of unscreened repulsion in the complexed PEC regions of uncompensated charges, hence opposing to  $\text{K}^+$ -driven aggregation in the  $\kappa$ -carrageenan network.<sup>28</sup> Charge compensation in this PEC system may be hindered by both the low ionic strength itself and also by site-binding of  $\text{K}^+$  in the host polymer, thus effectively interfering with the overall degree of  $\text{K}^+$ -driven aggregation of the  $\kappa$ -carrageenan network. This mechanism seems to dominate over the possible favourable conformational adaptation advantage effect discussed above.

By difference with NPEC with  $\kappa$ -carrageenan,  $\iota$ -carrageenan/chitosan NPECs in  $0.25 \text{ mol L}^{-1}$  NaCl, grow weaker with  $Z$  with respect to  $\iota$ -carrageenan alone. One could argue that  $\iota$ -carrageenan, bearing twice as many charges than does  $\kappa$ -carrageenan (distance between two charges:  $\iota$ -carrageenan coil,  $b=0.54 \text{ nm}$ ;  $\kappa$ -carrageenan coil,  $b= 0.96 \text{ nm}$ ; chitosan,  $b= 0.515 \text{ nm}$ ), forms a stronger polyelectrolyte complex with chitosan due to better charge compensation. Addition of CHI-20 up to  $Z=0.028$ , seems no to interfere with the equilibrium of the coil-to-helix conformational transition and it even seems that there is a reinforcement of the gel strength, particularly at the incipient stages of gel formation. Further addition of CHI20 and/or introduction of larger chitosan segments, namely of CHI-75, however, reduce slightly the stability of the ordered conformation and also weakens the gel network due to the known effect of increasing the cooperativity of the complexation when the polymer chain length is larger. Only a highly speculative interpretation can be offered thus far: either due to the greater charge density of  $\iota$ -carrageenan or the lack of steric advantage for heterotypic association between the two polymers (or indeed a combination of both effects), NPEC junctions in this system seem to interfere with the helix formation process. Although the role of self-aggregation in  $\iota$ -carrageenan gelation is less clear than in  $\kappa$ -carrageenan, it seems that growth of NPEC regions along the  $\iota$ -carrageenan chain at the expense of local ordered helical carrageenan ones and their branching into new ones, results in a more defective –hence weaker- gel network. The formation of such a defective gel network is the cause of the loss in mechanical properties that chitosan/ $\iota$ -carrageenan NPEC exhibits with respect to  $\iota$ -carrageenan alone

The phenomena observed for chitosan/ $\iota$ -carrageenan in  $0.03 \text{ mol L}^{-1}$  KCl, are still poorly understood. At this stage, we invoke the role of the small  $\kappa$ -carrageenan fraction ( $\sim 8\%$  of the total residues) in the gelation of  $\iota$ -carrageenan itself. Complexing of such  $\kappa$ - sites along with  $\iota$ - ones, seems to interfere with  $\text{K}^+$ -driven aggregation of carrageenan thus suppressing gelation of this NPEC.

As a final remark it should be pointed out that it is becoming increasingly evident that hydrophobic interactions seem to play a key role in many network connecting phenomena of polysaccharides. This kind of interactions have been recognised to be present in chitosan itself in solution,<sup>29,30</sup> but it should be remarked that their effect underlies all the phenomena addressed here in chitin and chitosan gel network systems, giving rise to the unusual behaviour of these systems. The described novel properties of these materials are yet to be thoroughly exploited.

## Acknowledgments

W.A.M. wishes to recognise the financial support from CONACYT, Mexico and his colleagues from CIAD for their kind invitation to collaboration.

## References

1. Flory, P. J. *Faraday Discussions* **1974**, *57*, 7.
2. Terbojevich, M.; Cosani, A.; Bianchi, E.; Marsano, E. in: *Advances in Chitin Science*. Domard, A., Jeuniaux, C., Muzzarelli, R. and Roberts, G., Ed.; Jacques André Publisher: Lyon, **1996**; Vol. I, pp 333.
3. Argüelles-Monal, W.; Goycoolea, F.M.; Peniche, C.; Higuera-Ciagara, I.; *Polym. Gels & Networks* **1998**, *6*, 429.
4. Flory, P.J.; Orwoll, R.A.; Vrij, A. *J. Am. Chem Soc.* **1964**, *86*, 3515.
5. Orwoll, R.A.; Flory, P.J. *J. Am. Chem Soc.* **1967**, *89*, 6822.
6. Tager, A.A.; Safronov, A.P.; Berezyuk, E.A.; Galaev, I.Yu. *Colloid & Polym. Sci.* **1994**, *272*, 1234.
7. Tong, Z.; Zeng, F.; Zheng, X.; Sato, T. *Macromolecules* **1999**, *32*, 4488.
8. Saeki, S.; Kuwuhara, N.; Nakata, M.; Kaneko, M. *Polymer* **1976**, *17*, 685.
9. Hirrien, M.; Chevillard, C.; Desbrieres, J.; Axelos, M.A.V.; Rinaudo, M. *Polymer* **1998**, *39*, 6251.
10. Eliassaf, J.; Silberberg, A. *Polymer* **1962**, *3*, 555.
11. Nakamura, K.; Itoh, T.; Sakuraqi, M.; Nakagawa, T. *Polym. J.* **1992**, *24*, 1419.
12. Domard, A.; Vachoud, L.; Zydowicz, N. *Crabohydr. Res.* **1998**, *302*, 169.
13. Ferry, J. D. *Viscoelastic Properties of Polymers*; 3rd ed.; Wiley: New York, **1980**.
14. Draget, K.I. *Polym. Gels & Networks*, **1996**, *4*, 143.
15. Guo, B.; Elgsaeter, A.; Stokke, B.T. *Polym. Gels & Networks*, **1998**, *6*, 113.
16. Goycoolea F.M., Argüelles-Monal W., Peniche-Covas C. and Higuera-Ciagara I. in: *Hydrocolloids Part 2: Fundamentals and Applications in*

- Food, Biology and Medicine*. K. Nishinari Ed.; Elsevier Science B.V., 2000, pp. 211
17. Winter, H. H.; Chambon, F. *J. of Rheology* **1986**, *30*, 367.
  18. Nijenhuis, K. t.; Winter, H. H. *Macromolecules* **1989**, *22*, 411.
  19. Rochas, C.; Rinaudo, M. *Biopolymers* **1980**, *19*, 1675.
  20. Piculell, L.; Nilsson, S.; Strom P. *Carbohydr. Res.* **1989**, *188*, 121.
  21. Piculell, L. in *Food Polysaccharides*; Stephen, A. M., Ed.; Marcel Dekker, Inc.: New York, **1996**; Vol. 67, pp 205.
  22. Muthukumar, M. *Macromolecules* **1989**, *22*, 4656.
  23. Piculell, L.; Nilsson, S.; Muhrbeck P. *Carbohydr. Polym.*, **1992**, *18*, 199.
  24. Kabanov, V. A.; Zenin, A. B. *Pure Appl. Chem.* **1984**, *56*, 343.
  25. Desbrieres, J.; Martinez, C.; Rinaudo, M. *Int. J. Biol. Macromol.* **1996**, *19*, 21.
  26. Dautzenberg H. *Macromolecules*, **1997**, *30*, 7810.
  27. Goycoolea, F. M.; Richardson, R. K.; Morris, E. R.; Gidley, M. J. *Biopolymers* **1995**, *36*, 643.
  28. Morris, E. R.; Rees, D. A.; Robinson, G. *J. Mol. Biol.* **1980**, *138*, 349.
  29. Amiji, M.M. *Carbohydr. Polym.* **1995**, *26*, 211.
  30. Nystrom, B.; Kjoniksen A.L.; Iversen C. *Adv. Colloid Interface Sci.* **1999**, *79*, 81.

## Chapter 8

# The Behavior of Amphiphilic Block Copolymers in Water and Their Association Behavior

Dirk van Eck<sup>1</sup>, Siegfried Höring<sup>1</sup>, Karsten Busse<sup>2</sup>, and Jörg Kressler<sup>2</sup>

<sup>1</sup>Fachbereich Chemie and <sup>2</sup>Fachbereich Ingenieurwissenschaften, Martin-Luther-Universität Halle-Wittenberg, D-06099 Halle, Saale, Germany

Amphiphilic di- and triblock copolymers containing blocks of the sodium salt of methacrylic acid and a methacrylate with a perfluorinated side chain are water soluble when their content of the hydrophobic block is less than 10 mol%. They form micelles in water that can be detected by electron microscopy or dynamic light scattering. The micelles are able to encapsulate colloidal gold particles. At higher polymer concentrations an intermicellar aggregation as a precursor of gel formation occurs as demonstrated by viscosity measurements. This happens at significantly lower concentrations of triblock copolymers in water compared to the respective diblock copolymers.

Hydrophobically modified water soluble polymers (HMWSP) are gaining importance due to their unique rheological and structural properties. The attention has been focused mainly to HMWSP based on random copolymers or water soluble polymers endcapped with hydrophobic groups (1-6). Furthermore, water soluble amphiphilic block copolymers can be used for numerous applications governed by their structure (7,8) e.g. as surfactants (9,10) and drug delivery systems (11,12). In dilute solutions the surface is covered firstly which leads to a decrease of the surface tension. Above a sometimes rather low critical micelle concentration (c.m.c., 13-15) the formation of micelles occurs. With increasing concentration the number of micelles in the solution increases whereas the size or the aggregation number remains mainly constant (16,17) and the surface is not affected (plateau in surface tension). Besides spherical micelles with a core-shell-structure other types like hollow spheres or rodlike

structures (18,19) may occur. In the case of diblock copolymers the overlap of different micelles at elevated concentrations leads to gelation (20). For A-B-A triblock copolymers in addition bridging by single chains between two micelles may occur which leads to a higher elastic modulus and larger average lifetime (21). Intermicellar associations lead e.g. to a decrease in surface tension (22). Higher concentrated i.e. semidilute solutions of triblock copolymers form network structures as can be seen by rheological measurements (23). For fluorinated units in the hydrophobic blocks the tendency for phase separation is very strong due to the high surface activity (24). In this work, water soluble A-B di- and A-B-A triblock copolymers were synthesized by sequential anionic polymerization of *tert*-butyl methacrylate (tBMA) and 2-(*N*-methylperfluorobutanesulfonamido) ethyl methacrylate (FMA) (Figure 1).

These block copolymers can be transformed into water soluble species when the FMA content is moderate and when tBMA is transferred into the sodium salt of poly(methacrylic acid). The details are discussed below.

The preparation of these block copolymers was extensively investigated by spectroscopic and thermal methods. The block copolymers in the solid state were studied by AFM and SAXS. The solutions of the transformed (amphiphilic) block copolymers in water were characterized by rheology, TEM and dynamic light scattering. Furthermore, the micelle structure of an A-B-A triblock copolymer in water is characterized by SAXS measurements. Finally, the addition of gold colloids was taken into consideration.

## Experimental Part

**Polymerizations.** All polymerizations were carried out at  $-78^{\circ}\text{C}$  (25). The reaction components were added to a previously flamed and argon-purged glass reactor. Di- and triblock copolymers have been synthesized in tetrahydrofuran (THF, Merck) under Ar atmosphere with (1,1-diphenyl-3-methylpentyl) lithium/LiCl and naphthalene potassium as initiator. THF was dried over  $\text{CaH}_2$ , distilled from the purple sodium salt of the benzophenone dianion, stored over K/Na alloy, and finally freshly distilled from the alloy. Naphthalene potassium was prepared through the reaction between naphthalene (Fluka) and sodium (Merck) in THF at  $0^{\circ}\text{C}$  (26). 1,1-diphenyl-3-methylpentyllithium was synthesized by the reaction of 1,1-diphenylethylene (Merck) with *sec*-butyllithium (Merck; dissolved in cyclohexane) at  $25^{\circ}\text{C}$  just before the polymerization. *Tert*-butyl methacrylate (tBMA; Polysciences Europe GmbH) was dried and distilled over  $\text{CaH}_2$ . Prior to use, it was condensed from  $(\text{C}_2\text{H}_5)_3\text{Al}$  under vacuum according to the standard procedure (27). 2-(*N*-methylperfluorobutanesulfamido)ethyl methacrylate (FMA) was kindly supplied by the Bayer AG, recrystallized twice from methanol, and finally sublimated under high vacuum. At first the THF (only in FMA homopolymerization after



preaddition of LiCl) and a solution of the initiator in THF were filled into the reactor through a rubber septum with a stainless steel capillary followed by the dropwise addition of the calculated amount of the first monomer (tBMA). After stirring for 1 h a prechilled THF solution of the second monomer (FMA) was added. The reaction was allowed to last 9 h and then stopped with methanol/water. The polymer was isolated by precipitation in methanol. For the decomposition of the *tert*-butyl ester a certain amount of the block copolymer was heated for 2 h at 200 °C in vacuum. Some polymers obtained by sequential anionic polymerization are listed in Table I.

**Size Exclusion Chromatography (SEC) Measurements.** For determination of molar mass and molar mass distribution, the samples were prepared by dissolving the purified polymer solid in HPLC grade THF. The SEC was performed in THF at 25 °C on a Knauer Chromatograph equipped with styragel columns and refractive index detector at a flow rate of 1.0 ml/min. Poly(methyl methacrylate) standards from Polymer Standard Service were used for calibration.

**Fluorine-19 and Proton NMR measurements.** <sup>1</sup>H- and <sup>19</sup>F-NMR spectra were recorded on a Varian spectrometer operating at 300 MHz (<sup>1</sup>H) and 282 MHz (<sup>19</sup>F) in CDCl<sub>3</sub> at 25 °C.

**Thermolyses.** The thermal ester splitting of the tBMA units was performed at 200 °C under vacuum. For kinetic studies the reactions were recorded with a FTIR spectrometer (Bruker).

**Preparation of Aqueous Polymer Solutions.** In order to convert the anhydride in sodium methacrylate units the samples of the ester splitting (1- 2 g) were refluxed for 1 h with 1 N NaOH. The solutions were purified by dialysis against deionized water using a dialysis membrane tube (Nadir<sup>®</sup>, 2.5-3.0 nm) and then filtered with a 0.8 μm CA membrane filter. The solid polymer obtained by evaporation of the solvent was dried at 40 °C in a vacuum oven and dissolved in deionized water for subsequent measurements.

**Atomic Force Microscopy (AFM) and Transmission Electron Microscopy (TEM).** Measurements were carried out with a MultiMode AFM (Digital Instruments). The tapping mode was applied. The polymer was dissolved in 2,2,3,3-tetrafluoro-1-propanol or THF and a film was formed by slow evaporation of the solvent at ambient temperature. The samples for TEM were dissolved in water and in some cases colloidal gold was added. The solutions were cast onto copper grids covered with a carbon film. A Zeiss-CEM902 was used with an acceleration voltage of 80 kV.

**Small Angle X-ray Scattering (SAXS)** SAXS measurements were performed in an evacuated Kratky compact camera (Anton Paar K.G.) with an 80 μm entrance slit. Cu K<sub>α</sub> radiation with a wavelength of λ=0.154 nm was used. The scattered intensity, *I*, was recorded by a scintillation counter in a step-scanning mode at room temperature. The scattering profiles were corrected for background scattering and desmeared. The cosine Fourier transformation of the scattering curve yields the linear correlation function *K*(*z*) defined by (28)

$$K(z) = \int_0^{\infty} 4\pi s^2 I(s) \cos(2\pi sz) ds \quad (1)$$

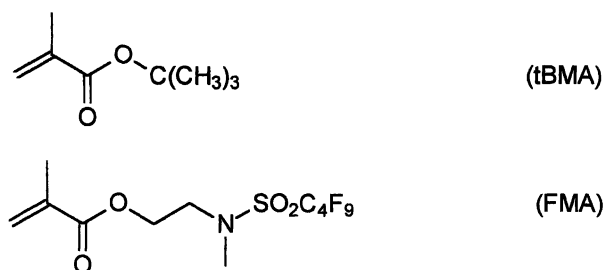


**Figure 1.** Monomers used for sequential anionic polymerization.

**Table I.** Synthesized di- and triblock copolymers of FMA (A) and tBMA (B)

Polymer <sup>a</sup>	$M_w^b$ g/mol	$M_n^b$ g/mol	$M_w/M_n$	FMA <sup>c</sup>	
				mol%	vol%
31Di02	32 600	30 900	1.06	2	3
52Tri07	57 100	51 700	1.10	7	11
57Tri07	62 100	56 100	1.11	7	11
57Tri08	62 400	57 000	1.09	8	14
72Tri26	80 900	72 400	1.12	26	40
49Tri38	56 700	49 400	1.15	38	54

<sup>a</sup>Sample name: first number is the overall  $M_n$ -value, Di is A-B, Tri is A-B-A, second number means mol% FMA.

<sup>b</sup>Determined by SEC in THF using PMMA standards.

<sup>c</sup>Determined by <sup>1</sup>H-, and <sup>19</sup>F-NMR spectroscopy.

$s$  is the scattering vector (sometimes  $q=2\pi s$  is used). The samples under investigation were 49Tri38 in the solid state and dilute solutions of 57Tri07H in water with concentrations between 0.13 and 1.4 wt%.

**Dynamic Light Scattering.** The experimental equipment consists of a DLS-SLS 5000 Laser Light Scattering Goniometer (ALV Langen, Germany), equipped with a 140 mW Nd:YAG laser (diode pumped, frequency doubled; ADLAS Lübeck, Germany) with a wavelength of 532 nm, and an ALV-5000 Multiple Tau digital correlator. The scattered light was detected at an angle of  $90^\circ$  and the measurements were carried out at  $T=25^\circ\text{C}$ . The correlation functions were analyzed with the CONTIN (29) program.

The samples were held in a cylindrical glass vessel. An aqueous solution of 57Tri07H with  $c=0.26$  wt% was filtered through a  $5\text{-}\mu\text{m}$  Millipore filter. The gold colloid is a 0.013 wt% solution. The dilute samples used for dynamic light scattering are (a)  $6.5 \cdot 10^{-4}$  wt% gold colloid in water, (b) 0.26 wt% of 57Tri07H, and (c) a solution with  $4.5 \cdot 10^{-4}$  wt% gold colloid and 0.18 wt% 57Tri07H. The samples are measured some minutes after preparation. Then sample (c) was put for 30 minutes in an ultrasonic bath and kept for some minutes before measuring again (d). The pair correlation function  $g_2(t)$  obtained by dynamic light scattering is analyzed to get effective diffusion coefficients  $D_{\text{eff}}$  of the samples. The hydrodynamic radius of assumed hard spheres is calculated via the Stokes-Einstein equation  $r_{\text{hyd}}=kT/(6\pi\eta D_{\text{eff}})$  where  $k$  is the Boltzmann constant and  $\eta$  is the viscosity of the solvent at temperature  $T$ .

**Rheology and Wilhelmy plate method.** The relative viscosities were determined by using a capillary viscometer (capillary diameter 0.6 mm). The measurements were carried out at  $25^\circ\text{C}$ . For surface tension measurements a digital tensiometer K10T of Krüss was used equipped with a platinum plate.

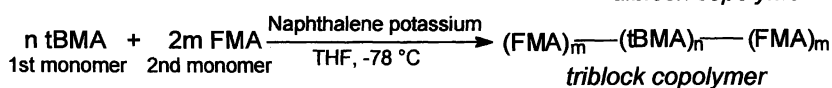
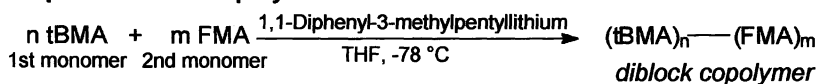
## Results and Discussion

The synthesis of block copolymers of tBMA and FMA is outlined above. Figure 2 shows the transformation mechanism into water soluble species.

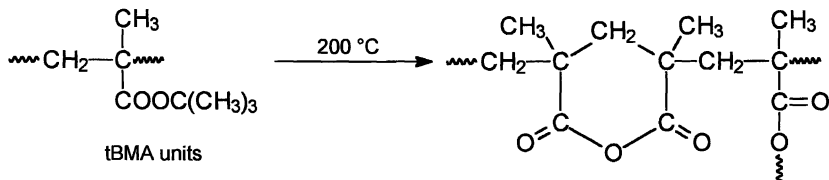
A selective two step transformation of the tBMA block into the water soluble poly(sodium methacrylate) was carried out. Firstly, anhydride, isobutene and water is formed at  $200^\circ\text{C}$  and then the cleavage of the anhydride is done in 1N NaOH under reflux. This procedure does not influence the ester group with the perfluorobutane side chain. The reaction can be followed by FT-IR spectroscopy (30).

In order to verify that block copolymers are formed it is necessary to demonstrate a microphase separation of the respective blocks. This can be done e.g. by atomic force microscopy (AFM) as demonstrated in Figure 3. Figure 3a shows the morphology of the triblock copolymer 49Tri38 after slow evaporation of tetrahydrofuran (THF). The phase contrast mode was employed. There is a microphase separation but the phases do not appear very well ordered. Also thermal annealing above the glass transition did not yield a more perfect structure.

### Sequential block copolymerization



### Thermal treatment



### Alkaline treatment

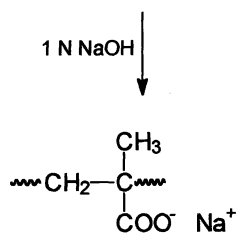


**Figure 2.** Synthesis of amphiphilic di- and triblock copolymers.

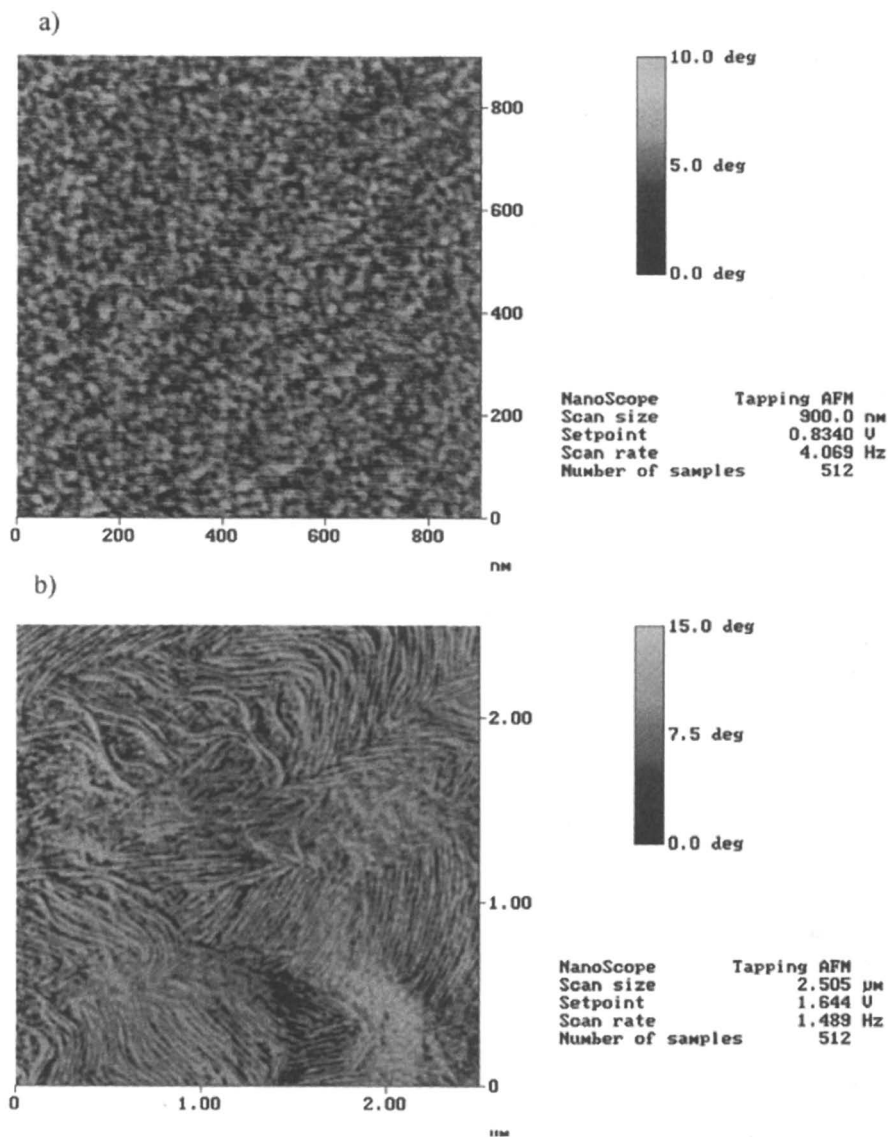


**Figure 3.** AFM measurements on a film of 49Tri38 a) cast from tetrahydrofuran, b) cast from 2,2,3,3-tetrafluoro-1-propanol.

A better order could be achieved by using 2,2,3,3-tetrafluoro-1-propanol (TFP) as a solvent (Figure 3b). Obviously this is due to the fact that TFP is a more selective solvent for the blocks with the perfluoro alkyl side chain. Thus, the tBMA block collapses during the evaporation of the solvent and the lamellar order appears more significant. This is a frequently observed phenomenon that using very selective solvents leads to a better order in cast block copolymer films (31). Since the block copolymer 49Tri38 is symmetrically when assuming

volume fraction it is also reasonable that a lamellar morphology is formed. The same result was obtained by small angle X-ray scattering (SAXS) as shown in Figure 4.

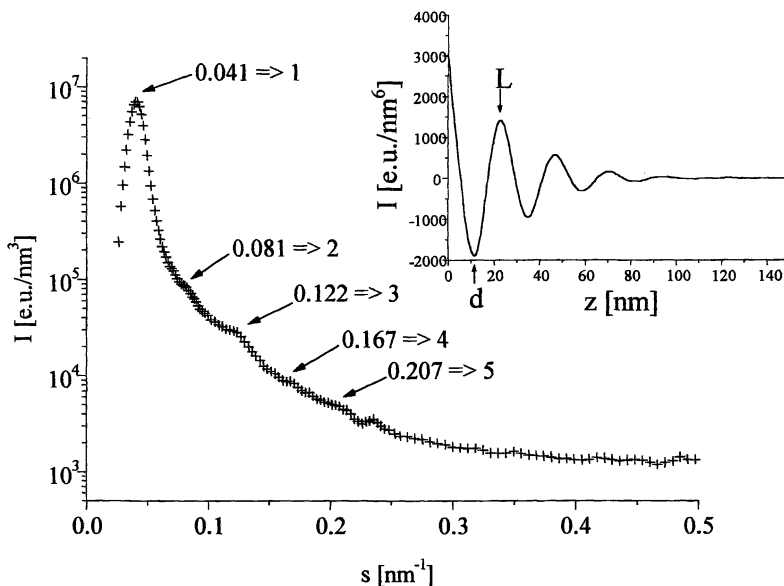


**Figure 4.** Intensity versus  $s$  and correlation function of 49Tri38 slowly cooled from the melt obtained by SAXS.

The SAXS trace has a first order maximum at  $s^* = 0.041 \text{ nm}^{-1}$ . Higher order maximums occur at multiples of  $s^*$ . Thus it is definitively demonstrated that a lamellar order is also achieved in bulk samples which were cooled from the melt. The inset shows the calculated correlation function. The long period is obtained to be 23 nm.

After the characterization of the synthesized block copolymers it is now interesting to analyze the water soluble species. It should be remembered that these species were obtained after transformation of the tBMA blocks into the respective sodium salt of methacrylic acid. We use the codes given in Table I but we add an H in order to make clear that the water soluble species are under consideration. The surface activity of the block copolymers in water was studied by surface tension measurements as demonstrated in Figure 5. Figure 5a shows the decrease of the surface tension of water with increasing amount of the diblock copolymer 31Di02H. This is the classical behavior (32,33) and the concentration where the surface tension stays constant with increasing amount of block copolymer in water is called critical micelle concentration. For this block copolymer the c.m.c. value at room temperature is 67 g/l. This situation is slightly different for the triblock copolymer 52Tri07H (see Figure 5b). The surface tension decreases at much lower concentrations compared to the diblock

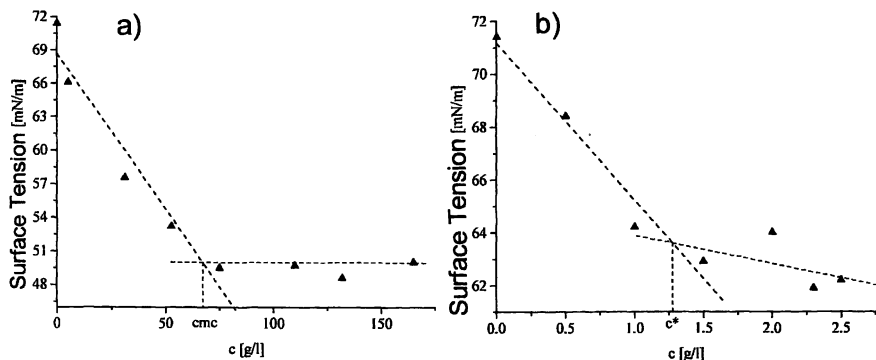


**Figure 5.** Surface tension of block copolymers in water at room temperature. a) 31Di02H b) 52Tri07H.

copolymer. Then the surface tension decreases further after reaching a critical value  $c^*$ . If this overlap concentration, which is at 1.3 g/l for this measurement, coincides with c.m.c. cannot be decided at this point. The low concentration is an indication that the free energy for the formation of micelles and the free energy for the amphiphilic molecules to cover the free surface is in a very similar order of magnitude. This seems to be more relevant to triblock copolymers. For diblock copolymers it is obvious that in a first step the free surface is covered and then the micelles are formed.

This size of the micelles could readily be obtained by dynamic light scattering (34). Intensity fraction distributions of hydrodynamic radii obtained by dynamic light scattering for solutions of the polymer 57Tri07H, the gold colloid, and mixtures of them are depicted in Figure 6.

The polymer concentration was chosen near  $c^*$  in order to reduce the concentration of single chains but without having crosslinking effects between different micelles by single triblock molecules. The hydrodynamic radius of gold particles (sample (a)) was determined to  $r_{hyd}=9\text{ nm}$ . The hydrodynamic radius of micelles obtained from a solution with 0.26 wt% 57Tri07H (sample (b)) is much larger with approximately  $70\text{ nm}$ . Putting both materials together in one sample without destroying the already formed micellar structure, the intensity fraction distribution of the hydrodynamic radius shows two peaks close to the radii distributions of the pure components (c). Caused by the fitting procedure the mean value of the peaks has a larger scattering, but two peaks with nearly the same intensity are always distinguished. Treating the sample with ultrasound, the polymer micelles will be affected. The intensity fraction distribution of the hydrodynamic radius obtained from sample (d) shows clearly a decrease of larger clusters while the other peak now appears with an increased radius of about 22 nm. The covering of gold by the polymer can also be detected by TEM as shown in Figure 7.

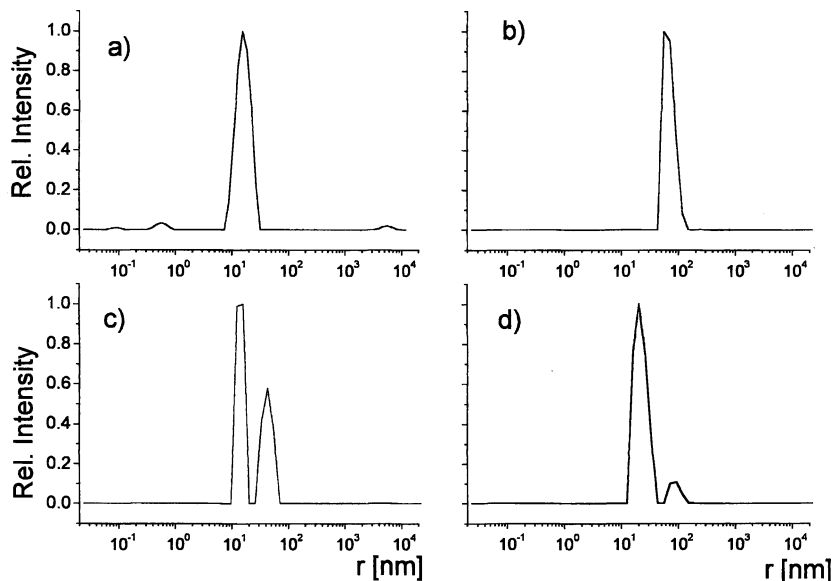


**Figure 6.** The dilute samples used for dynamic light scattering were (a)  $6.5 \cdot 10^{-4}$  wt% gold colloid in water, (b) 0.26 wt% of 57Tri07H, and (c) a solution with  $4.5 \cdot 10^{-4}$  wt% gold colloid and 0.18 wt% 57Tri07H. The samples were measured some minutes after preparation. Then sample (c) was put for 30 minutes in an ultrasonic bath and kept for some minutes before measuring again (d).

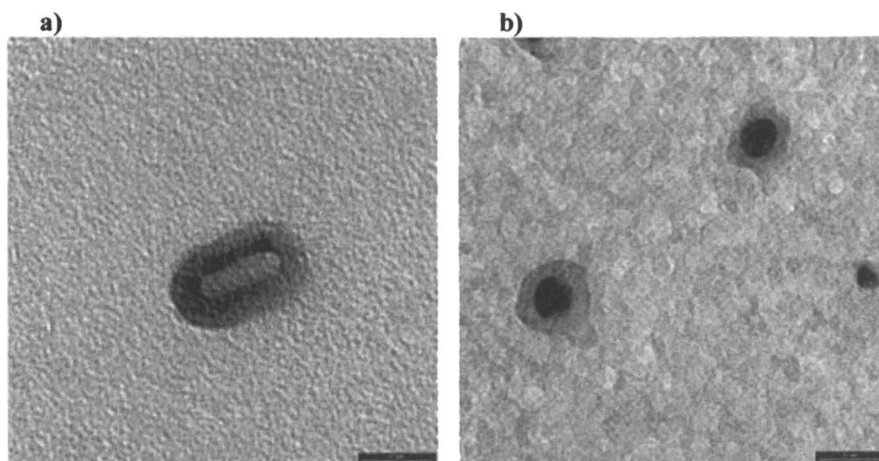


**Figure 7.** TEM pictures, the scale bars are 20 nm a) a micelle of 52Tri07H, b) gold colloid (black particles) covered with 52Tri07H.



Figure 7a shows a typical micelle. The micelles were transferred from a solution in water onto a carbon film. The samples were not stained for TEM. The dark part is the fluorine containing block due to its larger electron density compared to the other block. When colloidal gold particles are present (see Figure 7b) they are surrounded by the block copolymer after ultrasonic treatment. It is obvious that the hydrophobic block is attached to the gold particles (the intermediate gray value). The effect of covering gold particles by amphiphilic block polymers is well known and is used for the formation of nanoparticles (35).

The size of the micelles could also be obtained by SAXS measurements. The background corrected and desmeared intensity distributions are depicted in Figure 8. The intensity is divided by the respective concentration, all curves show the same behavior. Each trace can be approximated by either the Ornstein-Zernicke function (eq 3, Figure 9) or a core-shell structure of spheres (eq 4). The correlation length  $\xi$  and the radii  $R_1$  (core) and  $R_2$  (shell) were determined for several concentrations close to  $c^*$  (Table II).

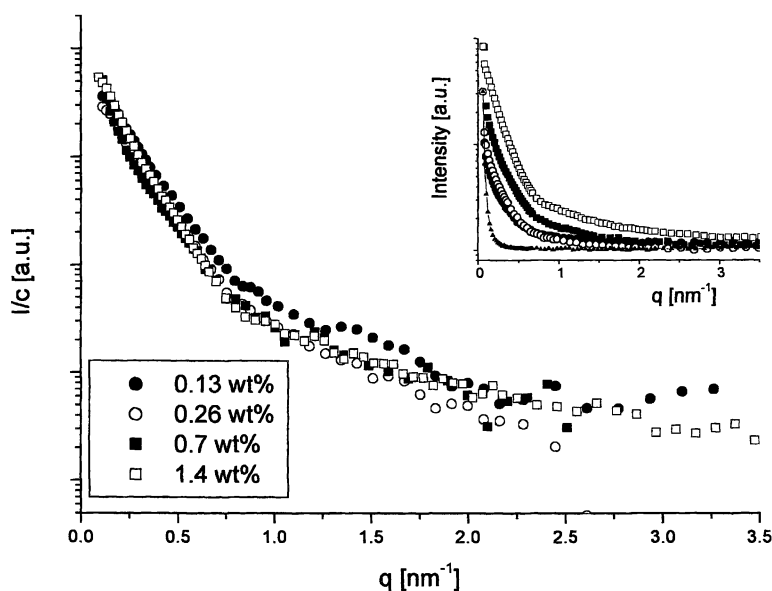


**Figure 8.** The corrected intensity distributions divided by the respective concentration from SAXS measurements (original data in inset, including background) for solutions of 57Tri07H with increasing concentration.

$$I(q) = I_0 \frac{1}{1 + \xi^2 q^2} \quad (3)$$

$$I(q) = I_0 \left( \frac{\sin(R_1 q) - R_1 q \cos(R_1 q)}{(R_1 q)^3} + a \frac{\sin(R_2 q) - R_2 q \cos(R_2 q)}{(R_2 q)^3} \right)^2 \quad (4)$$

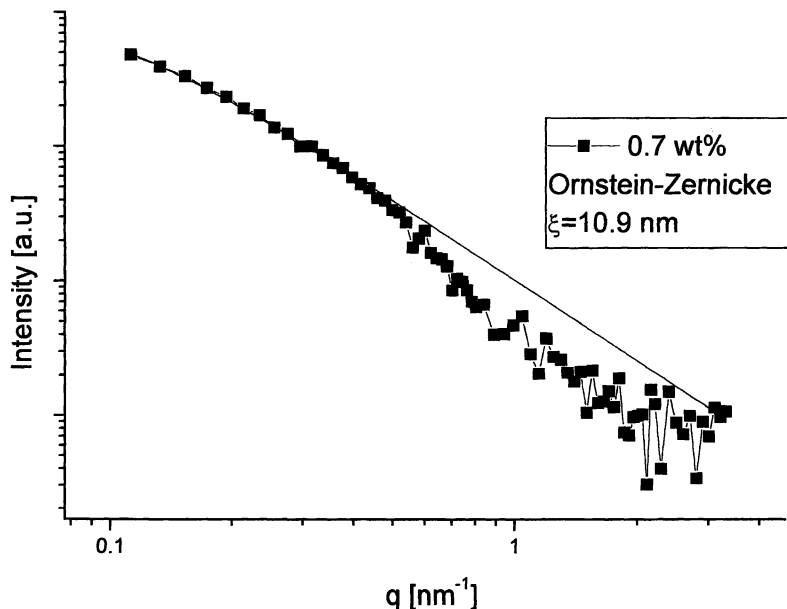


**Figure 9.** Intensity distribution of an aqueous solution with 0.7 wt% 57Tri07H and Ornstein-Zernicke approximation.

The assumption of a spherical core-shell behavior cannot be verified unambiguously, even though the obtained radii (Table II) agree with  $\xi \approx R_2/2$  for small  $Rq$  (eq 5). The outer radius remains nearly constant at about  $18 \pm 2$  nm. This means that the size of the micelles does not depend on the concentration. The structure of the micelles could be worm-like (Figure 7a), as known from other triblock systems (7, 36).

$$I(q) \propto \left( \frac{\sin(Rq) - Rq \cos(Rq)}{(Rq)^3} \right)^2 \approx \frac{1}{9} \left( 1 + \frac{1}{5} (Rq)^2 \right)^{-1} \Rightarrow \xi \approx \frac{R}{\sqrt{5}} \quad (5)$$

**Table II.** Size of 57Tri07H micelles in water at 25°C obtained by SAXS using eqs (3) and (4)

concentration	$R_1$ (nm)	$R_2$ (nm)	$\xi$ (nm)
0.13 wt%	6	15.6	7.3
0.26 wt%	6.4	18.2	9.2
0.7 wt%	5.7	18.1	10.9
1.4 wt%	6.9	17.8	9.5

The SAXS measurements were carried out up to the concentration range where intermicellar association takes place. The change in the rheological behavior was also detected by viscosity measurements. Figure 10 shows the reduced viscosity

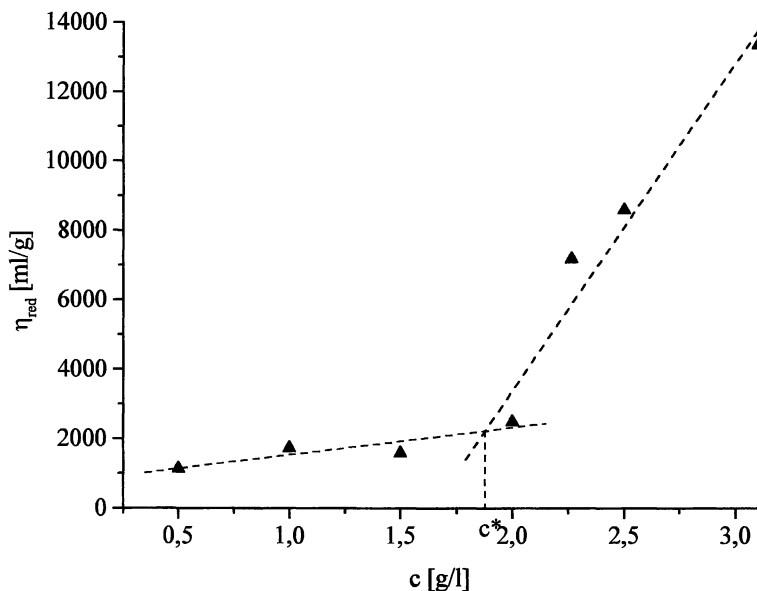


**Figure 10.** Reduced viscosity of the aqueous solution of 52Tri07H as a function of polymer concentration at 25°C.

$\eta_{red}$  of the aqueous solution of 52Tri07H as a function of the polymer concentration.

The concentration  $c^*$  of 1.9 g/l can be considered as the overlap concentration, i.e. the begin of gel formation. The same effect can be observed at the other polymers (25).

### Conclusions

It is demonstrated that amphiphilic di- and triblock copolymers can be obtained by sequential anionic polymerization of tBMA and FMA. A selective transformation of the tBMA block into the respective Na salt of the methacrylic acid is possible. Various experimental methods indicate the nanophase separation in bulk. Micelles formed in water were observed by TEM and dynamic light scattering. Gold colloids added to the amphiphilic hydrogels are coated with the FMA block. Intermicellar associations as indication for the onset of formation of amphiphilic networks were observed by viscosity measurements.

**Acknowledgement.** The authors thank the Deutsche Forschungsgemeinschaft and the Fonds der Chemischen Industrie. Dr. Ralf Thomann (Albert-Ludwigs-Universität Freiburg) carried out the TEM measurements. The AFM measurements did Rameshwar Adhikari.

## Literature

- (1) Petit, F.; Iliopoulos, I.; Audebert, R.; Szönyi, S. *Langmuir* **1997**, *13*, 4229.
- (2) Petit, F.; Iliopoulos, I.; Audebert, R. *J. Chim. Phys.* **1996**, *93*, 887.
- (3) Chen, J.; Jiang, M.; Zhang, Y.; Zhou H. *Macromolecules* **1999**, *32*, 4861.
- (4) Zhang, Y.; Li, M.; Fang, Q.; Zhang, Y.X.; Jiang, M.; Wu C. *Macromolecules* **1998**, *31*, 2527.
- (5) Chassenieux, C.; Nicolai, T.; Durand, D. *Macromolecules* **1997**, *30*, 4952.
- (6) Xie, X.; Hogen-Esch, T.E. *Macromolecules* **1996**, *29*, 1734.
- (7) Förster, S.; Antonietti, M. *Adv. Mat.* **1998**, *10*, 195.
- (8) Kennedy, J.P. *J.M.S. Pure Appl. Chem.* **1994**, *A31(11)*, 1771.
- (9) Cantor, R. *Macromolecules* **1981**, *14*, 1186.
- (10) Annable, T.; Buscall, R.; Ettelaie, R.; Shepherd, P.; Whittlestone, D. *Langmuir* **1994**, *10(4)*, 1060.
- (11) Jeong, B.; Bae, Y.H.; Lee, D.S.; Kim, S.W. *Nature*, **1997**, *388*, 860.
- (12) Park, K. (Ed.) *Controlled Drug Delivery*, American Chemical Society: Washington DC, 1997.
- (13) Everett, D.H. *Pure Appl. Chem.* **1972**, *31(4)*, 577.
- (14) Mysels, K.J.; Mukerjee, P. *Pure Appl. Chem.* **1979**, *51*, 1085.
- (15) Nguyen-Misra, M.; Misra, S.; Wang, Y.; Rodrigues, K.; Mattice, W.L. *Progr. Colloid Polym. Sci.* **1997**, *103*, 138.
- (16) Förster, S.; Zisenis, M.; Wenz, E.; Antonietti, M. *J. Chem. Phys.* **1996**, *104*, 9956.
- (17) Zhang, L.; Barlow, R.J.; Eisenberg, A. *Macromolecules* **1995**, *28*, 6055.
- (18) Nakano, M.; Matsuoka, H.; Yamaoka, H.; Poppe, A.; Richter, D. *Macromolecules* **1999**, *32*, 697.
- (19) Brown, W.; Pu, Z.; Ryndén, R. *J. Phys. Chem.* **1988**, *92*, 6068.
- (20) Adam, M.; Carton, J.P.; Corona Vallet, S.; Lairez, D. *Journal de Physique II* **1996**, *6(12)*, 1781.
- (21) Nguyen-Misra, M.; Mattice, W.L. *Macromolecules* **1995**, *28*, 1444.
- (22) Guenoun, P.; Davis, H.T.; Tirrell, M.; Mays, J.W. *Macromolecules* **1996**, *29*, 3965.
- (23) Raspaud, E.; Lairez, D.; Adam, M.; Carton, J.P. *Macromolecules*, **1996**, *29*, 1269.
- (24) Kissa, E. *Fluorinated surfactants and repellents*, Marcel Dekker: NY, 2001.
- (25) van Eck, D. Ph.D. thesis, Martin-Luther-Universität Halle-Wittenberg, Halle, 2000.
- (26) Smid, J. *J. Am. Chem. Soc.* **1965**, *87 (3)*, 655.
- (27) Allen, R. D.; Long, T. E.; McGrath, J. E.; *Polym. Bull. (Berlin)* **1986**, *15*, 127.
- (28) Strobl, G. *The physics of polymers*; Springer: Berlin, 1997.
- (29) Provencher, S.W. *Comput. Phys. Comm.* **1982**, *27*, 229.

- (30) Arndt, K.-F.; Richter, A.; Ludwig, S.; Zimmermann, J.; Kressler, J.; Kuckling, D.; Adler, H.-J. *Acta Polym.* **1999**, *50*, 383-390.
- (31) Hasegawa, H.; Takana, H.; Yamasaki, K.; Hashimoto, T. *Macromolecules* **1987**, *20*, 1651.
- (32) Yu, G.-E.; Deng, Y.; Dalton, S.; Wang, Q.-G.; Attwood, D.; Price, C.; Booth, C. *J. Chem. Soc. Faraday Trans.* **1992**, *88(17)*, 2537.
- (33) Wanka, G.; Hoffmann, H.; Ulbricht, W. *Macromolecules* **1994**, *27*, 4145.
- (34) Derici, L.; Ledger, S.; Mai, S.-M.; Booth, C.; Hamley, I. W.; Pedersen, J.S. *Phys. Chem. Chem. Phys.* **1999**, *1*, 2773-2785.
- (35) *Nanoparticles and nanostructured films*; Fendler, J. H., Ed.; Wiley-VCH: Weinheim 1998.
- (36) Schillén, K.; Brown, W.; Johnsen, R. M. *Macromolecules* **1994**, *27*, 4825.

## Chapter 9

# Phase Transitions in Interpolymer Complexes of Some Linear and Cross-Linked Polymers

L. A. Bimendina, G. T. Zhumadilova, and S. E. Kudaibergenov

Institute of Polymer Materials and Technology, Satpaev Str. 18a,  
480013, Almaty, Republic of Kazakhstan

Phase transitions in polymer-polymer and gel-linear polymer systems consisting of complexes of acrylic acid/butyl vinyl ether copolymers with linear and crosslinked poly-N-vinylpyrrolidone, 1,2,5-trimethyl-4-vinylethynylpiperidinol-4/N-vinylpyrrolidone copolymer with linear and crosslinked polyacrylic acid, polyacrylic acid with crosslinked poly-N-vinylcaprolactam taking place as a function of internal (composition of copolymers) and external (thermodynamic quality of solvents, degree of ionization, temperature) factors have been investigated. In most cases the analogy in behavior of interpolymer complexes in a solution and gel-polymer complexes is observed.

Interpolymer complexes (IPC) and high swollen polymer gels represent “intelligent” polymer systems that can reversibly respond to insignificant changes of properties of external media (1,2). Fundamentals of IPC have been formulated and at present it is known that the change of the size of complex particles occurs as coil-globule phase transition in a narrow interval of change of both the media properties (pH, temperature, solvent quality, ionic strength etc.) and the properties of interacting polymers (the chain length, microstructure of polymer chains, the content of active groups, hydrophilic-hydrophobic balance, the degree of ionization of polyelectrolyte components etc.) (3,4,5,6).

A sharp decrease of swollen hydrogel volume stimulated by change of pH, temperature, ionic strength, solvent quality, action of electric or magnetic fields is called “collapse” phenomenon (7,8,9,10). Collapse of polymer gels according to theoretical predictions is the result of coil-globule conformational transition taking place in gel network (11,12). Besides the complexation of polymer gels with complementary macromolecules,

surfactants, metal ions, dyes and drugs can also cause collapse or contraction of gels (13,14). These volume-phase transitions occur as phase transitions of the first order and take place in a narrow interval of change of media properties.

Polymer hydrogels due to their unusual properties may be used as sensors, artificial muscles, drug delivery systems. The ability of polymer hydrogels to absorb the huge amounts of water have ensured the successful using of these polymers in medicine, agriculture, membrane technologies. Interpolymer complexes at present are widely used for fabrication of membranes for separation and pervaporation purposes (15,16).

In the present paper we have compared the behavior of polymer-polymer and gel-polymer complex systems consisting of acrylic acid and vinylbutyl ether (AA-VBE) and 1,2,5-trimethyl-4-vinylethynylpiperidinol-4 and N-vinylpyrrolidone (TMVEP-VP) copolymers with the linear (LPVP) and crosslinked (CPVP) poly-N-vinylpyrrolidone and linear (LPAA) and crosslinked (CPAA) polyacrylic acid respectively, LPAA and crosslinked poly-N-vinylcaprolactam (CPVCL).

## Experimental part

### Materials

Copolymers of acrylic acid and vinylbutyl ether (AA-VBE) containing 44; 55; 65; 76; 87 and 97 mol.% of AA were synthesized by radical polymerization of monomer mixtures in ethanol with asoisobutyronitrile ( $C=5 \cdot 10^{-5}$  mol/L) as initiator. Copolymers were purified by three-fold precipitation from ethanol into diethyl ether. The composition of copolymers was determined by potentiometric titration. The number-average molecular weights  $M_n$  of copolymers determined by ebullioscopy are arranged in (20-30)  $\cdot 10^3$  interval. The samples of AA/VBE copolymers are abbreviated as CP-44; CP-55; CP-65; CP-76; CP-87; CP-97 respectively.

Copolymer of 1,2,5-trimethyl-4-vinylethynylpiperidinol-4 and N-vinylpyrrolidone (TMVEP-VP) was synthesized according to (17). The composition of TMVEP-VP sample determined by potentiometric titration is 12:88 mol.% respectively. The intrinsic viscosity  $[\eta]$  of this sample is 0.26 dl/g in 0.002 N HCl.

Linear poly-N-vinylpyrrolidone (LPVP) with molecular weight  $850 \cdot 10^3$  was purchased from BDH (Great Britain).

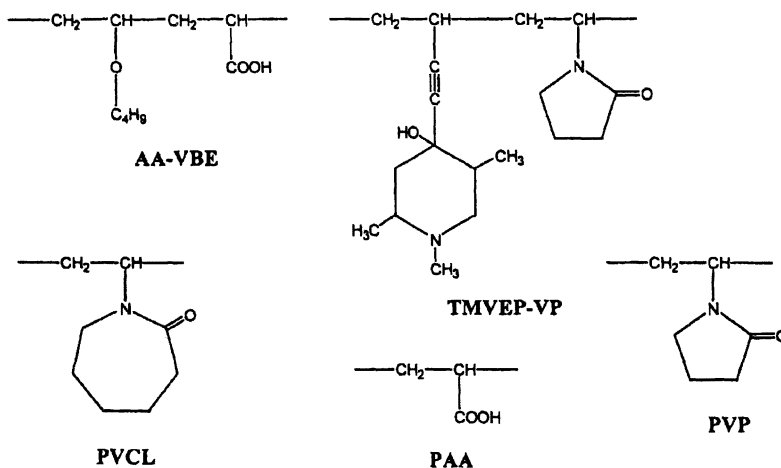
Crosslinked PVP (CPVP) was synthesized at the Institute of High Macromolecular Compounds (Russia).

Linear polyacrylic acid (LPAA) of molecular weight  $450 \cdot 10^3$  was purchased from "Polyscience" (USA).

Crosslinked polyacrylic acid (CPAA) and sodium salt of polyacrylic acid (CPAANA) were synthesized from the corresponding monomers by radical polymerization in the presence of dinitrylazoisobenzoic acid as initiator ( $C=5 \cdot 10^{-3}$  mol/L) at 353 K during one hour. Methylenebisacrylamide ( $C=0.05$  mol.%) was used as crosslinking agent. The three-dimensional polymerization was carried out in an argon atmosphere in a glass tube. Crosslinked samples

were washed out from the sol-fraction and unreacted monomers during 2-3 weeks and then dried in vacuum to constant mass at 398 K.

Crosslinked poly-N-vinylcaprolactam (CPVCL) was purchased from the Institute of Macromolecular Chemistry, Academy of Sciences of the Czech Republic, Prague. All samples of crosslinked polymers were ground to a powder.



### Instrumentation

Potentiometric and conductimetric titrations were carried out on pH/Conductivity Meter "Mettler Toledo MPC 227" (Sweden) at room temperature.

IR-spectra were obtained by "UR-20" spectrophotometer (Germany).

The viscosity of solutions was measured by Ubbelohde viscometer.

The swelling coefficients  $K_s$  were determined gravimetrically as  $K_s = (m - m_0)/m_0$  where  $m_0$  and  $m$  are the masses of dry and swollen gels respectively.

The binding degree of linear polymer with hydrogel is equal to  $\theta = C_{\text{bound}}/C_{\text{total}}$  where  $C_{\text{total}}$  is the concentration of initial AA-VBE (mol/L) calculated for common volume  $V_{\text{gel}} + V_{\text{AA-VBE}}$ ;  $C_{\text{bound}}$  is the concentration of bound carboxyl groups of AA-VBE.  $C_{\text{bound}}$  was calculated as difference between  $C_{\text{total}}$  and  $C_{\text{free}}$ . In its turn  $C_{\text{free}}$  which represents the concentration of uncomplexed carboxyl groups of AA-VBE (mol/L) was obtained by titration of external solution of copolymer with potassium hydroxide.

Complexes of linear polymers were prepared by mixing of dilute solutions ( $C=0.05-0.10$  g/dL) of complementary polymers.

The kinetics of swelling of each hydrogel sample was determined. The coefficient of swelling  $K_s$  gradually increases with time and achieves the constant value during 48 h. One can consider that the system becomes equilibrium at this time.

The gel-polymer complexes were obtained by adding an aqueous solution of linear polymer of definite concentration to the swollen gel. To achieve equilibrium it was allowed to stay the system during 96 h. Gel-polymer



complex formed was then separated from the solution, dried in vacuum at room temperature and ground to a powder for further investigations.

## Results and Discussion

Specific, noncovalent interaction in polycarboxylic acid-nonionic polymer systems is caused by arising of cooperative system of hydrogen bonds (3,4,5). Complexation in studied polymer systems with the participation of linear and crosslinked polymers is confirmed by electrochemical, viscometric and IR-spectroscopic methods. Diagrams property (electroconductivity, pH, intrinsic viscosity, optical density etc.) -composition of binary mixture of interacting polymer components deviate considerably from the additive rule and have extreme character. According to the principles of physico-chemical analysis (18) it indicates the formation of individual compound with the exact composition. The potentiometric and conductimetric titration curves for [CP-97]/[LPVP], [TMVEP-VP]/[LPAA] and [CP-87]/[LPVP] systems do not submit to rule of additivity and discover the bends that indicate the composition of forming complexes. The latter is expressed as molar ratio of active monomer units of copolymer and the second component and is equal to 1:1 (19). Complex formation reaction between linear polymers is accompanied by strong hydrophobization of complex particles and the intrinsic viscosities of interpolymer complexes are close those of globular proteins (0.05-0.10 dl/g).

The formation of H-bonds between interacting macromolecules is confirmed by IR-spectroscopy. IR-spectra of AA-VBE copolymer and LPVP have the characteristic bands of C=O groups at  $\nu=1710\text{ cm}^{-1}$  and  $\nu=1680\text{ cm}^{-1}$  respectively. In IR-spectra of [AA-VBE]/[LPVP] complex the band of C=O groups from LPVP is widened and observed at  $\nu=1660\text{ cm}^{-1}$ . At the same time the absorbance band of C=O group of acrylic acid splits and displaces at higher frequency region that indicates the destruction of intra- and intermolecular H-bonds within acrylic acid molecules. Thus the formation of new of H-bonds leads to shifting of C=O bonds.

Analogous changes are observed for IR-spectra of [TMVEPVP]/[LPAA] complexes. The shifting of the characteristic band of C=O groups of N-vinylpyrrolidone from  $\nu=1672\text{ cm}^{-1}$  to  $\nu=1640\text{ cm}^{-1}$  and C=O groups of LPAA from  $\nu=1710\text{ cm}^{-1}$  to  $\nu=1730\text{ cm}^{-1}$  testifies the formation of polycomplexes stabilized by H-bonds.

It is well known that complex formation reactions depend on the length of interacting polymer chains, the content of active groups in copolymers, the degree of ionization of polyelectrolyte components, and the composition of mixed solvent (3,4,5). Figure 1 represents the dependence of the reduced viscosity of [AA-VBE]/[LPVP] systems on the content of active carboxyl groups in copolymer chains. As seen from Figure 1 the values of viscosity sharply fall in a narrow interval of change of copolymer composition that confirms the cooperative character of complex formation reactions. Only copolymers containing more than 65 mol.% of acrylic acid are able to form stable interpolymer complexes with intrinsic viscosity about 0.10 dL/g.

The stability of [CP-87]/[LPVP] and [TMVEP-VP]/[LPAA] complexes was studied with respect to temperature and ionization degree  $\alpha$  of polyelectrolyte components. For both systems the compact structure of IPC is stable in water at  $T=25-80^{\circ}\text{C}$  because the value of intrinsic viscosity does not change and is about 0.10 dL/g. While the ionization of polyelectrolyte components of IPC destroys the compact complex particles because the viscosity sharply increases and the systems behave as ordinary polyelectrolytes during the ionization. [TMVEP-VP]/[LPAA] complexes preserve a stable compact structure up to  $\alpha=0.02$ .

The composition of [AA-VBE]/[CPVP] and [TMVEP-VP]/[CPAA] gel-polymer complexes was determined from the dependencies of swelling coefficients  $K_s$  on concentration of linear copolymers. The swelling coefficients of gels  $K_s$  sharply decrease at equimolar ratio of interacting components due to complex formation reaction (Figure 2). The dependence of binding degree  $\theta$  of linear polymer by hydrogel on concentration of linear polymer has opposite character (Figure 2, curve 2). The maximal degree of binding  $\theta$  is about 0.6-0.7 for both systems. Reptation of linear polymer within the network causes two effects. One of them is connected with overall hydrophobization of the system, another - with additional crosslinking of network by linear polymers. These two combined effects are responsible for gel collapse.

The stability of interpolymer complexes of linear and crosslinked polymers was studied in water-DMSO mixtures. It is known that DMSO is the acceptor of H-bonds and interpolymer complexes stabilized by H-bonds are usually destroyed in this solvent (3,4). Figures 3 and 4 represent the dependencies of swelling coefficients  $K_s$  and intrinsic viscosities  $[\eta]$  of [AA-VBE]/[CPVP] and [TMVEP-VP]/[LPAA] complexes on water-DMSO mixture.

As there is the correspondence in size of a single polymer chain in a solution and that of subchain in network (20) one can expect the similar behavior of both  $K_s$  and  $[\eta]$  values of corresponding complexes. For [AA-VBE]/[LPVP] and [AA-VBE]/[CPVP] complexes analogous behavior in water-DMSO mixtures is found (Figure 3). For complexes of linear polymers CP-87 and LPVP the phase transition from compact structure to unfolded one occurs in a narrow interval of change of solvent composition and is observed in mixtures containing more than 50 vol.% of DMSO. The same dependence of swelling coefficients  $K_s$  on water-DMSO composition is characteristic for gel-polymer [CP-87]/[CPVP] complexes. The sharp increasing of  $K_s$  values of gel-polymer complexes due to destruction of polycomplexes and reswelling of initial gel occurs in the same region of solvent composition. However, for complexes of TMVEP-VP copolymer with linear and crosslinked poly-N-vinylpyrrolidone some differences are observed.

Probably this is due to participation of tertiary amine groups of piperidinol ring in formation of ionic bonds that additionally strength the stability of complexes. For [TMVEP-VP]/[CPAA] complexes the gradually destruction of structure of gel-polymer complexes is observed (Figure 4, curve 3). It is accompanied by gradually increasing of  $K_s$  values up to  $K_s=100$  being closer to  $K_s$  of initial CPAA that is equal to 122. The further decreasing of  $K_s$  is

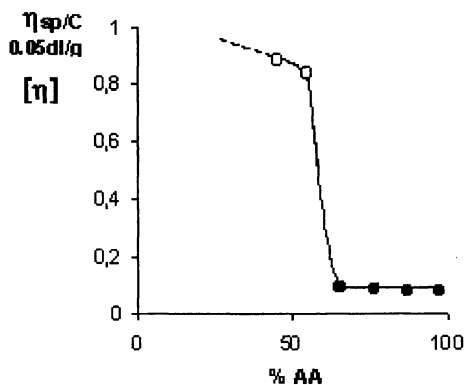


**Figure 1.** Dependencies of the reduced (○) and intrinsic (●) viscosities of [AA-VBE]/[LPVP] systems on the content of AA groups in copolymers.

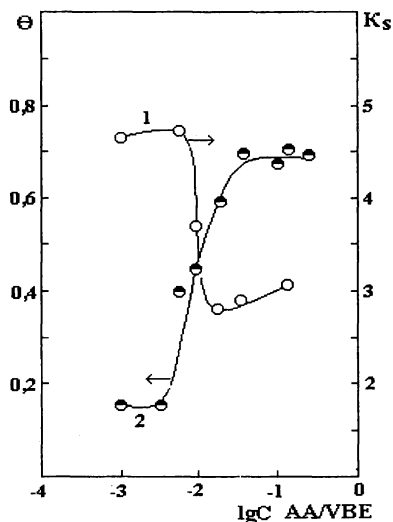


**Figure 2.** Dependencies of swelling coefficients  $K_s$  (1) and binding degree  $\theta$  (2) on the logarithm of concentration of linear [AA-VBE] copolymer.  $[\text{Gel}] = 1,8 \cdot 10^{-2} \text{ mol/L}$ .

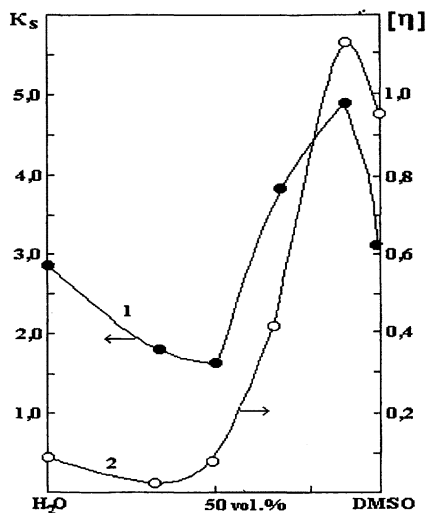


**Figure 3.** Dependences of swelling coefficients  $K_s$  and intrinsic viscosity  $[\eta]$  in [AA-VBE]/[CPVP] (1) and [AA-VBE]/[LPVP] (2) systems on water-DMSO composition.

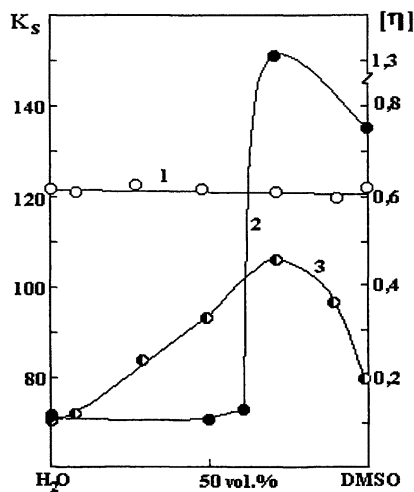


**Figure 4.** Dependences of swelling coefficients  $K_s$  of CPAA (1), intrinsic viscosity  $[\eta]$  of [TMVEP-VP]/[LPAA] (2) and  $K_s$  of [TMVEP-VP]/[CPAA] complexes (3) on water-DMSO composition.

probably connected with contraction of partially destroyed gel-polymer complexes due to change of thermodynamic quality of the solvent. The swelling coefficient of CPAA is about 120 g/g and does not change in water-DMSO mixtures (Figure 4, curve 1). Complexes of linear polymers [TMVEP-VP]/[LPAA] preserve their compact structure up to 60 vol.% of DMSO in the mixture (Figure 4, curve 2), then the cooperative destruction of complex structure takes place. Thus the destruction of polymer-polymer and gel-polymer complexes in mixed solvents is common phenomenon. An analogous volume-phase transitions of gel-polymer and polymer-polymer complexes by changing of the thermodynamic quality of solvent was shown by authors (13,14).

The behavior of CPVP and CPAA hydrogels are different with respect to ionization. CPVP is nonionic gel while CPAA being the polyacid is ionized upon addition of NaOH and forms CPAANa gel. As consequence the swelling coefficients of CPVP are about ten units, while those for CPAANa are about several hundred ones. Dependencies of the reduced viscosity of [CP-87]/[LPVP] and swelling coefficients of [CP-87]/[CPVP] complexes on ionization degree  $\alpha$  are represented in Figure 5.

Complexes of linear polymers are destroyed at insignificant degree of ionization. The dependence of  $K_s$  of gel-polymer complexes on degree of ionization is more complicated: at first the additional contraction occurs, then the gel-polymer complex sharply swells. This is accounted for by appearance of charged macromolecules within CPVP network. In the case of gel-polymer complexes in contrast to polymer-polymer complexes the shifting of phase transition occurs to higher values of ionization degree. One can suppose that the gel structure restricts the ionization of linear polymer component.

For complexes of linear polymers [TMVEP-VP]/[LPAA] the stabilization of compact structure of complex particles up to  $\alpha=0.1$  is observed (Figure 6, curve 3). Then complex particles are cooperatively destroyed at increasing of degree of ionization. For gel-polymer [TMVEPVP]/[CPAA] complexes (Figure 6, curve 2) and CPAA (Figure 6, curve 1) these dependencies have the analogous character, no stabilization of gel-polymer complex structure is observed. At insignificant degree of ionization the swelling coefficients of gel-polymer complexes are changed from 70 to 120 and reached the value of CPAA gel (for CPAA  $K_s$  is equal to 120). The further increasing of ionization degree strongly increases the swelling coefficient of gel matrix up to  $K_s=700-800$  due to its full ionization.

For CP-65 and LPVP systems the possibility of complex formation was also investigated in organic solvents such as ethanol and DMF. It was found that the composition of complex in ethanol is [CP-65]/[LPVP]=3:1, but in DMF there is no any complexation. Complexes are considerably less stable to the action of DMSO in comparison with complexes forming in water and are destroyed at 40 vol.% of DMSO in ethanol-DMSO mixtures. It is probably connected with weakening of hydrophobic interactions in these media.

The interaction of CP-65 with CPVP was also investigated in ethanol. Swelling kinetics of pure CPVP testifies that the equilibrium values of  $K_s$  are reached during 48 h. Therefore the swelling coefficients of gel-polymer

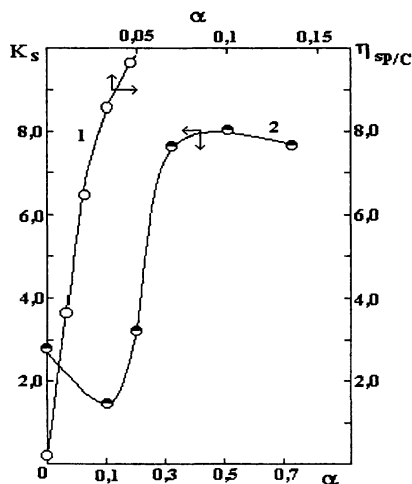


**Figure 5.** Dependencies of the reduced viscosity  $\eta_{sp}/C$  and swelling coefficients  $K_s$  for [AA-VBE]/[LPVP] (1) and [AA-VBE]/[CPVP] (2) systems on the ionization degree  $\alpha$  of polyelectrolyte component.

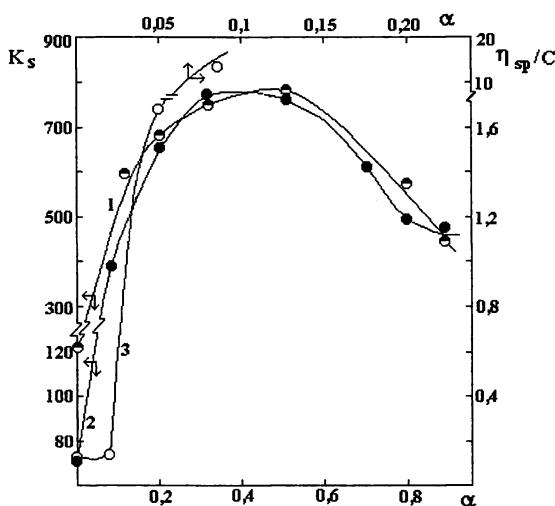


**Figure 6.** Dependencies of swelling coefficients  $K_s$  of CPAA (1), [TMVEP-VP]/[CPAA] complexes (2) and the reduced viscosity  $\eta_{sp}/C$  of [TMVEP-VP]/[LPAA] complexes (3) on the ionization degree  $\alpha$ .

complexes in ethanol were measured after 96 h. The composition of gel-polymer complexes determined from the dependencies of swelling coefficients on concentration of linear copolymer in ethanol is equal to [CP65]:[CPVP]=1:2. The properties of polymer-polymer and gel-polymer complexes forming in ethanol are different in ethanol-DMSO mixtures. The compact structure of complexes of linear polymers is cooperatively destroyed at 40 vol.% of DMSO in ethanol-DMSO mixtures, the intrinsic viscosity sharply increases in a narrow interval of change of composition of mixed solvents. At the same time the structure of gel-polymer complexes slightly changes in ethanol-DMSO mixture.

The composition of polyacrylic acid-crosslinked poly-N-vinylcaprolactam (PAA-CPVCL) complexes determined from the dependence of swelling coefficients of CPVCL on concentration of linear polyacrylic acid is equal to 1:1. The swelling coefficients of pure gel and gel-polymer complex in water-DMSO mixtures are compared in Figure 7. Poly-N-vinylcaprolactam gel undergoes sharp volume-phase transition in dependence of the thermodynamic quality of the solvent. In the case of gel-polymer complex at first the destruction of this complex occurs in mixtures containing up to 30 vol.% of DMSO, then the behavior of the system becomes similar to that for pure crosslinked polymer in water-DMSO mixtures.

The behavior of pure CPVCL was also studied in chloroform-ethanol, chloroform-dioxane, chloroform-DMSO mixtures (Figure 8). In these mixtures the swollen gel only contracts while the volume-phase transition or the collapse of gel occurs in water-DMSO mixture (Figure 7, curve 2). This difference is obviously connected with hydrophilic-hydrophobic balance in these systems.

## Conclusion

1. It is found the volume-phase transition or collapse of some polymer hydrogels (poly-N-vinylpyrrolidone, poly-N-vinylcaprolactam, polyacrylic acid) due to complex formation reaction with complementary linear polymers.
2. The composition of gel-polymer and polymer-polymer complexes are determined and their behavior at change of external factors (thermodynamic quality of the solvent, temperature, degree of ionization) are studied.
3. The properties of gel-polymer and corresponding polymer-polymer complexes are compared. In some cases the absolute analogy in properties of two types of interpolymer complexes is observed.
4. The obtained results confirm the theoretical predictions that the collapse of polymer hydrogels occurs as the result of coil-globule transition taking place in linear parts of gel network.
5. Behavior of crosslinked poly-N-vinylcaprolactam is differed in mixtures of two organic solvents (chloroform-DMSO) and water-organic solvent mixtures (water-DMSO). It is observed the gel contraction in the first case and gel collapse in the second one that is obviously connected with thermodynamic quality of the solvent and hydrophilic-hydrophobic balance in these systems.

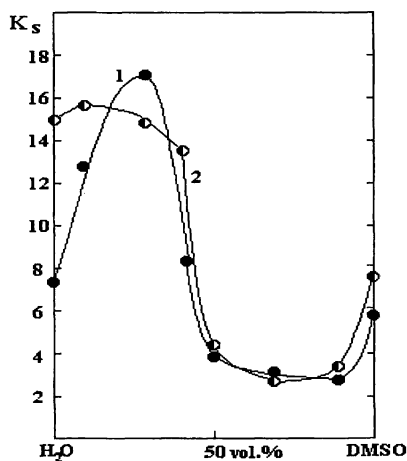


**Figure 7.** Dependencies of swelling coefficients  $K_s$  of polyacrylic acid-crosslinked poly-N-vinylcaprolactam complexes (1) and crosslinked poly-N-vinylcaprolactam (2) on water-DMSO composition.

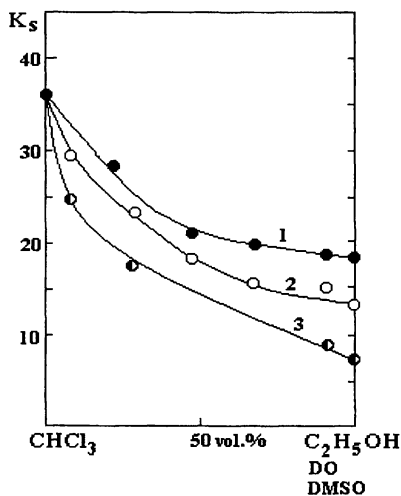


**Figure 8.** Change of swelling coefficients  $K_s$  of crosslinked poly-N-vinylcaprolactam in chloroform-ethanol (1), chloroform-dioxane (2) and chloroform-DMSO (3) mixtures.



**Acknowledgements.** The authors would like to thank INTAS-1746 Grant for financial support.

## References

1. Galaev, I.Yu. *Uspekhi Khimii*, **1995**, *64*, 505.
2. Bixler, H.J.; Michaels, A.S. *Encyclopedia of Polymer Science and Technology*, **1969**, *10*, 765.
3. Tsuchida, E.; Abe, K. *Adv. Polym. Sci.* **1982**, *45*, 1.
4. Bekturov, E.A.; Bimendina, L.A. *Adv. Polym. Sci.* **1981**, *41*, 99.
5. Zezin, A.B.; Kabanov, V.A. *Uspekhi Khimii*, **1982**, *56*, 1447.
6. Philipp, B.; Dautzenberg, H.; Linov, K.J.; Kotz, J.; Dawydoff, W. *Prog. Polym. Sci.* **1989**, *14*, 91.
7. Tanaka, T. *Phys. Rev. Lett.* **1978**, *40*, 820.
8. Responsive Gels. Volume Transitions. *Adv. Polym. Sci.* **1993**, *109*, 110, 275.
9. Osada, Y.; Gong, J. *J. Progr. Polym. Sci.* **1993**, *18*, 1187.
10. Budtova, T.; Suleimenov, I.; Frenkel, S.Ya. *Polymer*, **1995**, *36*, 2055.
11. Khokhlov, A.R.; Dormidontova, E.E. *Uspekhi Fiz. Nauk*, **1997**, *167*, 113.
12. Vasilevskaya, V.V.; Khokhlov, A.R. *Vysokomol. Soed.* **1991**, *A33*, 883.
13. Yu, X.; Tanaka, A.; Tanaka, K.; Tanaka, T. *J. Chem. Phys.* **1992**, *97*, 7805.
14. Bekturov, E.A.; Frolova, V.A.; Bimendina, L.A. *Macromol. Chem. Phys.* **1999**, *200*, 431.
15. Nam, S.Y.; Lee, Y.M. *J. Membr. Sci.* **1997**, *136*, 161.
16. Ageev, E.P.; Vikhoreva, T.A.; Galbraikh, L.S. et al. *Vysokomol. Soed.* **1998**, *A40*, 1198.
17. Shaikhutdinov, E.M.; Kurmanaliev, O.Sh.; Ermagambetov, M.E. *Macromol. Chem., Macromol. Symp.* **1989**, *26*, 297.
18. Anosov, V.Ya.; Pogodin, S.A. *Principles of Physico-Chemical Analysis*. Science, Moscow-Leningrad, 1947.
19. Kudaibergenov, S.E.; Bimendina, L.A.; Zhumadilova, G.T. *Polym. Adv. Technol.*, **2000**, *11*, 506.
20. Shibayama, M.; Uesaka, M.; Inamoto, S.; Mihare, H.; Nomura, Sh. *Macromolecules*, **1996**, *29*, 885.

## Chapter 10

# Structure of Polyampholyte Gels and Their Behavior with Respect to Applied External DC Electric Field

S. E. Kudaibergenov, V. B. Sigitov, A. G. Didukh, and S. B. Moldakarimov

Institute of Polymer Materials and Technology, Satpaev Str. 18a,  
480013, Almaty, Republic of Kazakhstan

Polyampholyte gels based on 1-vinyl-2-aminoethyl ether (VAEE) and sodium salt of acrylic acid (AANa) were synthesized by  $\gamma$ -initiated radical polymerization. Physico-chemical and structural properties of crosslinked polyampholytes have been characterized by elemental analysis, potentiometric titration, gravimetry, IR, NMR, DSC, SAXS and WAXS methods. Amphoteric gels have amorphous structure independently on pH. The amount of non-freezing water and the mesh size of the gel depends on pH being minimal at the isoelectric point (IEP). Structural data have been interpreted in terms of microphase separation phenomenon due to long-ranged electrostatic attraction or repulsion forces. Amphoteric gel mass oscillation and pH oscillation as well as arising of pH gradient within the gel matrix under the externally imposed electric field has been observed. The qualitative explanation of oscillation phenomenon is given in terms of interpretation observed for ultrathin polyelectrolyte complex membranes. The formation of pH gradient across the gel sample stimulated by DC electric field is considered from the polarization of gel matrix point of view. The driving force leading to appearance of pH oscillation in polyampholyte gels is also discussed.

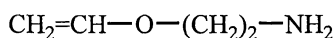
Polyampholytes due to dualistic behavior constantly attract the attention of both theorists and experimentalists (1-4). Particularly the internal structures of amphoteric macromolecules are determined by either polyelectrolyte (repulsive) or polyampholyte (attractive) effects which take place respectively far or near of the IEP. Generally for linear and crosslinked polyampholytes the coil-globule conformational and the swollen-collapsed volume phase transitions have the same nature and are governed by electrostatic interactions. Amphoteric macromolecules can be considered as inhomogeneous microphases separated systems due to either different reactivity of acidic and basic monomers (the static inhomogeneity) or long-ranged electrostatic interactions (the dynamic inhomogeneity). The existence of microphase domains for weakly charged polyelectrolyte gels in poor solvent has been predicted by Khokhlov et al. (5). The collapsing-swelling behavior of quenched amphoteric gels in pure water and saline solution was analyzed by Candau (5) in the light of structural differences between the domains. The first part of the present paper describes the properties of annealed polyampholyte gels and interprets the obtained results from the structural point of view. Considerable attention was paid to the IEP of amphoteric macromolecules where the probability of microphase segregation is to be high.

It is well known that polyelectrolyte gels swell, shrink or bend when an external electric current is applied (7). The authors (8) proposed a semiquantitative theory which describes the swelling and shrinking behavior of polyelectrolyte gel under an applied electric field. An analytically tractable model for the description of polyampholytes in an external electric field has been presented (9). Gel systems demonstrating rhythmically pulsatile motion, i.e. self-oscillative swelling and deswelling (10) and pH oscillations (11) were realized by coupling pH and temperature stimuli and redox reactions. Motion and deformation of Gaussian polyampholytes in free flow electrophoresis, i.e. in an applied external electric field (12) and a biased reptation of polyampholytes within a fixed network (13) were considered. An effective separation of polyampholytes according to their charge distribution has been shown even for polyampholytes that have the same length and the same overall charge. In this connection the second part of this paper concerns with oscillation phenomenon of amphoteric gel (14) as well as appearance of pH gradient and pH oscillation under the action of DC electric field that was observed for the first time. The perspective way of using polyampholyte gels for protein separation and purification is also discussed.

## Experimental part

**Purification and identification of VAEE.** Commercially available monomer vinyl-2-aminoethyl ether (VAEE) containing 99,5% of basic product were dried during 7-8 days with the help of the annealed potash and distilled over calcium hydride three times under the argon atmosphere (15).

Boiling point of VAEE is 387 K at 101,45 kPa, refraction index is 1,4352. The purity of monomer was checked by IR, Raman and NMR spectroscopy. Tables 1 and 2 represent characteristic bands of monomer identified from IR and Raman spectroscopy and chemical shifts derived from NMR spectra.



Acrylic acid was purchased from "Aldrich" and was converted to sodium salt of acrylic acid (AANa) by addition of equimolar amount of NaOH powder.

**Synthesis and characterization crosslinked (co)polymers.** Crosslinked poly(VAEE) and poly(AANa-VAEE) were synthesized by gamma-initiated radical polymerization in the presence of divinyl ether of diethyleneglycol (4 mol.%) as crosslinking agent with the help of  $^{60}\text{Co}$  «RXM- $\gamma$ -20M» at an irradiation dose 170 rad/s during 3-5 h (16). To remove the sol fraction, the gel samples were washed out by distilled water during 2 weeks. The swelling degree of amphoteric gels calculated by the

Table 1. Characteristic bands of VAEE derived from IR and Raman spectroscopy

Bond	Frequency, $\text{cm}^{-1}$	
	IR	Raman
$\nu_s(\text{COC})$	1090	-
$\nu_{as}(\text{COC})$	1210	1210
$\nu(\text{CN})$	1325	1323
$\nu(\text{C}=\text{C})$	1620	1625
$\delta(\text{NH})$	1640	1640
$\nu(\text{CH})$	2880, 2935	2875, 2935
$\nu_s(\text{NH})$	3315	3320
$\nu_{as}(\text{NH})$	3387	-

Table 2.  $^1\text{H}$  NMR and  $^{13}\text{C}$  NMR spectra of VAEE

Groups	$^1\text{H}$ NMR	$^{13}\text{C}$ NMR
Chemical shift, ppm		
$=\text{CH}-\text{O}$	6,3-6,7 quintet	153
$=\text{CH}_2$	3,85-4,3 multiplet	81
$-\text{CH}_2-\text{O}$	3,6-3,8 triplet	70
$-\text{CH}_2-\text{N}$	2,8-3,0 triplet	40
$-\text{NH}_2$	1,7-1,9 singlet	-

formula:  $\alpha = (W - W_0)/W_0$  (where  $W$  and  $W_0$  are the weights of dry and equilibrium-swollen gels) is approximately 60 g/g. Crosslinked sodium salt of poly(acrylic acid) (PAANa) with the swelling degree 300 g/g was synthesized by radical polymerization of AANa in the presence of *N,N*-methylenebisacrylamide. Table 3 shows the content of acid and base groups in copolymer gels determined by potentiometric titration and elemental analysis, the swelling degree as well as the IEP of polyampholyte gels.

FTIR spectra of PA-3 assigned by comparison of the IR and Raman spectra of VAEE and AA show intensive peaks at 3420-3440 and 1710-1730  $\text{cm}^{-1}$  belong to  $\text{NH}_2$  groups of VAEE and  $\text{C}=\text{O}$  groups of AA. The band at 1080-1100 reflects the asymmetrical vibrations of COC groups. The appearance of the band at 1630-1640  $\text{cm}^{-1}$  for all gel samples can be attributed to the terminal double bonds from VAEE. It is probably explained by the fact that during the gamma-irradiation polymerization due to elimination of hydrogen atoms from the side methylene groups of VAEE some amount of  $\text{OCH}_2\text{CH}\cdot$  radicals may be produced that serve as active centers for the formation of branched gel structure. The appearance of small peaks at 153 ppm and 80.6 ppm in  $^{13}\text{C}$  NMR spectra of gels also confirms this statement. Potentiometric titration was carried out on pH/Conductivity meter "Mettler Toledo MPC 227" (Switzerland) at room temperature in thermostated cell. IR spectra of samples were recorded on a JASCO FT/IR-5300 spectrophotometer with KBr pellets. The band resolution is 4  $\text{cm}^{-1}$ . Raman spectra of VAEE were registered with the spectrophotometer «Ramanor HG.2S» (France). The 514,5 nm line of the argon ion laser was used for excitation. NMR spectra were recorded using Varian VCR-300 multinuclear spectrometer in  $\text{D}_2\text{O}$ . Thermograms were measured using Perkin-Elmer DSC-7 at temperatures from +10 to +80 and from -50 to +10 C. WAXS and SAXS experiments were performed at room temperature by S. Strandman at the X-ray laboratory of Department of Physics, University of Helsinki, Finland.

**Measurement of pH gradient.** To measure pH gradient a special rectangular electrochemical cell provided with platinum electrodes was constructed (Fig. 1). Gel sample was placed into the frame with length and width 4 cm, height 2 cm not touching the electrodes. The magnitudes of applied DC electric fields are 5, 10, 15 and 20 V. The gel sample contained 15 cells with diameter of 3 mm and deep of 10 mm. The distance between cells is 10 mm. Glass electrode with diameter 3 mm was placed into the cells to follow by the change of pH during experiments.

## Results and Discussion

### 1. Structure of polyampholyte gels

Crosslinked copolymers of VAEE and AANa belong to annealed polyampholytes where the net charge of whole macromolecule depends on the pH of the solution, e.g. they behave as polycations in acidic solution and polyanions in alkaline region. The swelling degree of PA-3 at the IEP is

Tab.3. Composition of monomers in the feed, composition of copolymers, swelling degree and the IEP of polyampholyte gels

Sample No.	Molar ratio of VAAE:AA in the feed, mol.%	Composition of copolymers, mol.%	Swelling degree	IEP
PA-1	90:10	42:58	57,1	4,8
PA-2	80:20	32:68	57,0	4,4-4,5
PA-3	70:30	28:72	60,3	4,2

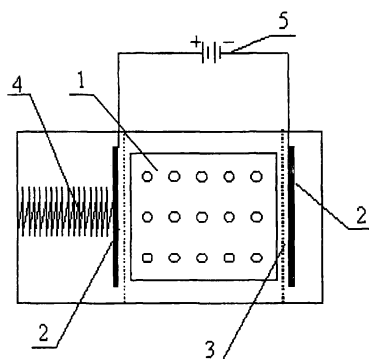


Fig.1. Electrochemical cell for measurement of pH gradient. 1-cellular gel sample, 2-electrodes, 3-capron network, 4-spring, 5-feed source.

minimal at the IEP (14). It is obvious that at this point the electrostatic attraction forces between acidic and basic moieties tend to collapse the chains into compact globules. It should be mentioned that due to enrichment of copolymer composition by carboxylic groups the shape of curves has asymmetric character, e.g the swelling degree decreases sharply at  $\text{pH} > \text{pH}_{\text{IEP}}$  than at  $\text{pH}_{\text{IEP}} < \text{pH}$ . The amount of non freezing water determined by DSC for PA-3 depends on pH of the solution and is equal to 1.57, 0.73 and 0.96 g/g at pH = 3.6, 4.2 (IEP) and 4.8 respectively. The amount of non freezing water is minimal at the IEP because the swollen-collapsed phase transition taking place at this point results in squeezing out of water molecules from the gel volume. Fig.2 shows WAXS data of sample PA-3 measured at different pH. Amphoteric gels are amorphous and have no organized structures. Intensity maxima found at scattering vector values of 1.9 and 2.8  $\text{\AA}^{-1}$  are typical for water molecules. The maximum displaced at scattering vector value of 0.5-0.6 corresponds to gel network. The mesh size of the network calculated from the peak intensity is equal to 10  $\text{\AA}$ , 2-3  $\text{\AA}$  and 5-6  $\text{\AA}$  at pH 3.6, 4.2 and 4.8. The mesh size is largest at pH 3.6 and smallest at pH 4.2 and coincides well with DSC data that also shows the maximal and minimal amount of bound water at these pH. Results of the SAXS measurements are shown in Fig 3. The scattering intensity versus scattering vector may be interpreted by the next approaches.

**a) Power law behavior**

The SAXS intensity curves of the PA-3 obey a power law  $k^{-\alpha}$ . The exponent  $\alpha$  is 1.2 for pH values 3.6 and 4.2. At pH 4.8  $\alpha$  is equal to 1.7 and reflects the state of polymers in good solvents. Possible interpretation for the exponent 1.2 is that the coils are more rodlike at pH 3.6 and 4.2. The existence of rodlike structures has been observed for DNA and poly(styrene sulfonate). Thus a model of a dilute solution of rods is fitted to the intensity curves of crosslinked polyampholytes and a good agreement is obtained at pH 3.6 and 4.2. According to this analysis the length of the rod is about 400  $\text{\AA}$  and the cross sectional radius of gyration of the rod is about 5  $\text{\AA}$  for both pH values.

**b) The model of persistent chains**

The model decomposes the chain structure into two levels, one corresponding to the Gaussian regime and another to the persistence regime. The fitting parameters are the persistence length  $L_p$ , the number of Kuhn segment  $N_k$  and a factor arising from the contrast between the polymer and the solvents as well as from the number of chains in the scattering volume (Tab. 4).

**c) The model for a weakly charged polymer gel**

The results of SAXS experiments may also be analyzed in terms of a model applied to weakly charged polymer gels. According to this model the intensity curve is presented as a linear combination of Ornstein-Zernike model:

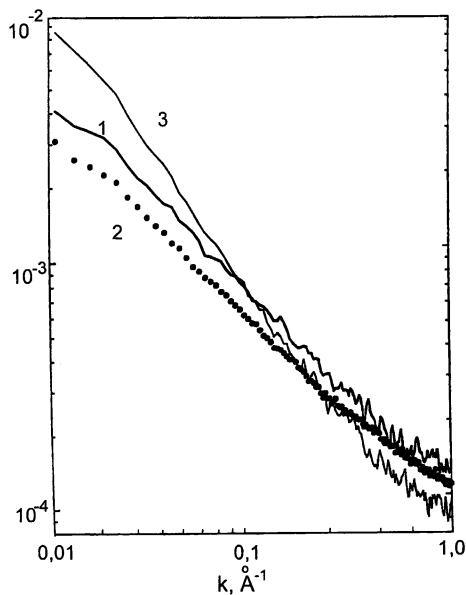


Fig.2. SAXS curves of polyampholyte gel PA-3 at pH=3,6 (1), 4,2 (2), 4,8 (3).

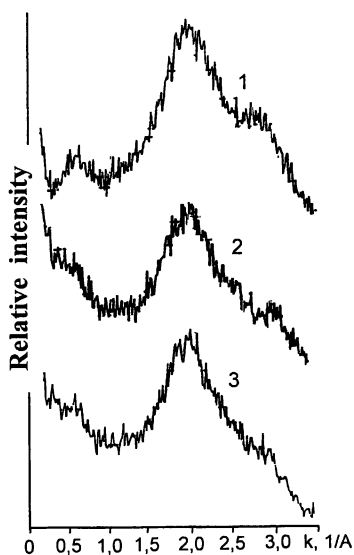


Fig.3. WAXS curves of polyampholyte gel PA-3 at pH = 3,6 (1), 4,2 (2), 4,8 (3).



$$I_{OZ}(k) = (1 + k^2\zeta_{OZ}^2)^{-1}$$

and Debye-Bueche model:

$$I_{DB}(k) = (1 + k^2\zeta_{DB}^2)^{-2}$$

where  $\zeta_{OZ}$  and  $\zeta_{DB}$  are the correlation lengths. The Ornstein-Zernike model is used to describe correlation fluctuations in liquid like systems. The Debye-Bueche model is applied to describe dense crosslinked part of the gel. The correlation lengths  $\zeta_{OZ}$  and  $\zeta_{DB}$  obtained by fitting the model into experimental intensity curves are shown in Table 5. The values of  $\zeta_{OZ}$  and  $\zeta_{DB}$  for crosslinked polyampholyte are minimal at the IEP and sharply increase at pH 4.8 approximately five times.

The internal structure of amphoteric gels as a function of pH can be understood in terms of inhomogeneity arising in gel volume. It is likely that at the IEP microphase separation occurs due to long-ranged electrostatic attraction between the acidic and basic groups. The distance between the domains is in good agreement with the estimated mesh size of amphoteric gel at the IEP (2-3Å). Deviation from the IEP leads to excess of positive or negative charges and a spatial structure of the network tends to be homogeneous. Drastically increasing of the correlation lengths  $\zeta_{OZ}$  and  $\zeta_{DB}$  for amphoteric gel is the result of the electrostatic repulsion between negatively charged carboxylate ions. It is interesting to note that the structural inhomogeneities observed for quenched polyampholyte gel consisting of poly[(2-crylamido-2-ethylpropanesulfonate acrylamide)-*co*-(2-methacryloyloxyethyltrimethylammonium chloride)] as a function of ionic strength (6) and for our system in dependence of pH may have the common nature and can be related to microphase separation phenomenon.

## 2. Formation of pH gradient under the action of DC electric field

To follow by the appearance of pH gradient poly(AANa), and PA-3 gel samples were selected. As seen from Fig 4, pH profiles of poly(AANa) and poly(VAAE) have no any considerable pH deviation in an applied external DC electric field. Whereas as follows from Fig. 5 the applied DC electric field leads to sharp appearance of pH gradient during 1 min for amphoteric gel. Fully stabilization of pH occurs after 10 min. When the electricity switches off, pH of the gel returns quickly to initial state. At the central part of gel specimen the value of pH is close to neutral while near of cathode and anode sides they are more acidic and basic respectively. The sharpness of pH gradient depends on the value of applied DC electric field. The values of  $\Delta pH = pH_0 - pH_{t \rightarrow 0}$  (where  $pH_0$  and  $pH_{t \rightarrow 0}$  are initial value of pH and the value of pH extrapolated to  $t \rightarrow 0$  respectively) is a function of DC electric field. Fig. 6 represents the dependence of pH on distance  $\pm l$  when the glass electrode is placed on cathode or anode sides of gel specimen in comparison with its central section, where  $l=0$ . Without the applied DC electric field pH gradient along the sample is uniform and equal to 7,4. The dependence of

Tab.4. The persistence length and the number of Kuhn segment of CPA-3

pH	$L_{ps}$ , Å	$N_k$
3.6	629	13
4.2 (IEP)	581	15

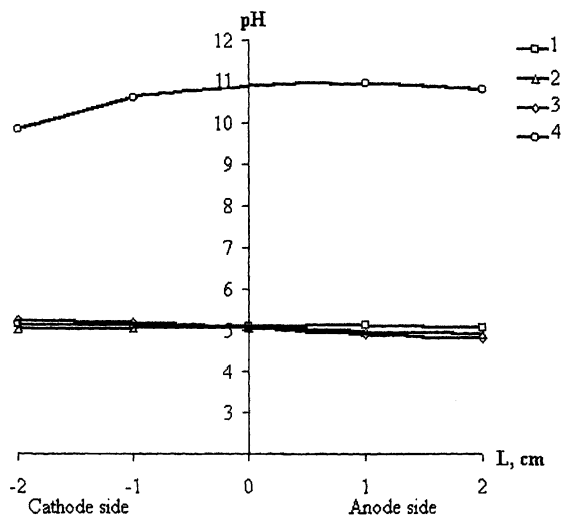


Fig.4. pH dependence of poly(VAEE) ( curve 1) and poly(AANa) (curves 2-4) on distance L at E = 3, (curve 2), 7 (curve 3) and 10 V ( curves 1 and 4).

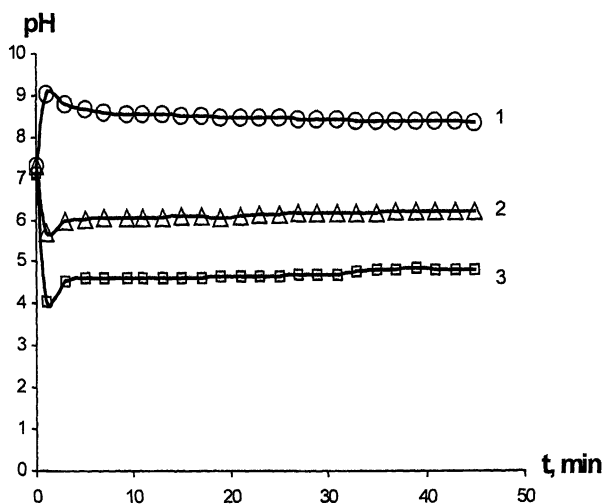


Fig. 5. Change of pH near of anode (curve 1) and cathode (curves 2 and 3) sides in amphoteric gels specimen at E = 10 V.

pH gradient on  $l$  has linear character but the slope of straight lines differs and depends on the magnitude of applied DC electric field. In order to interpret these data the distribution of fixed network charges and counterions along the gel specimen should be considered. Gel specimen can be divided into three major zones **A,B,C** as schematically shown in Fig. 7. The externally imposed potential across the gel causes the polarization effect. A negative fixed charges ( $\text{COO}^-$ ) and mobile ions ( $\text{OH}^-$ ) are accumulated in zone **A** that corresponds to anode side while a positive fixed charges ( $\text{NH}_3^+$ ) and mobile ions ( $\text{Na}^+$ ) are accumulated in zone **C** that corresponds to cathode side. Zone **B** forms a neutral ampholytic space. As a result, zones **A,B,C** have basic, neutral and acidic character. Increasing of DC electric current leads to acidification of gel sample (see Fig.6, curve 5) due to excess of acidic groups in copolymers and narrowing of zones **B** and **C** and expanding of zone **A**.

### 3. Oscillation of mass of polyampholyte gel in an applied external DC electric field

Previously we have observed the ability of amphoteric gels to oscillate periodically under the influence of DC electric field when the salt concentration in external solution does not exceed  $1 \cdot 10^{-2}$  mol/L (14). To explain this effect the redistribution of fixed and mobile ions, the Donnan equilibrium and water electrolysis was taken into account. In our opinion the correct interpretation of this phenomenon can be reached if the oscillation of an ultrathin polyelectrolyte complex (PEC) membrane in the presence of 0,15M NaCl under the action of electric potential will be adopted (16). The membrane material designed from co(acrylic acid-acrylamide) and poly(N,N-dimethylaminoethacrylate) is similar to amphoteric gel and consists of three major zones: a cation selective polyacidic zone (**A**), a anion selective polybasic zone (**B**) and a electroneutral polyampholytic zone (**C**) (see Fig.7). The main difference of PEC and polyampholyte is that the positive and negative charges are replaced respectively on different and in one and the same chain. The qualitative explanation of oscillation mechanism without chemical reaction is that when the externally potential is imposed across the PEC membrane (or polyampholyte gel) the current-carrying cations will flow from left to right. Simultaneously the current-carrying anions will flow opposite side. As a result the accumulation of low molecular weight salt in amphoteric region **C** will take place. This salt accumulation in turn will produce several effects. Since PA-1 is in isoelectric state, the accumulated low molecular weight ions screen the oppositely charged units of network and gel swells. The increased osmotic pressure in amphoteric zone **C** will require water flow with the consequent increase of hydrostatic pressure. At the same time the increased salt concentration will induce the contraction of polyanionic and polycationic zones **A** and **B**. If the point is reached where the increase of hydrostatic pressure with concentration, resulting from the polyelectrolyte conformational change, is greater than the corresponding

Tab.5. Correlation lengths of crosslinked polyampholyte chains

pH	$\zeta_{OZ}, \text{\AA}$	$\zeta_{DB}, \text{\AA}$
3.6	8	20
4.2 (IEP)	8	17
4.8	39	65

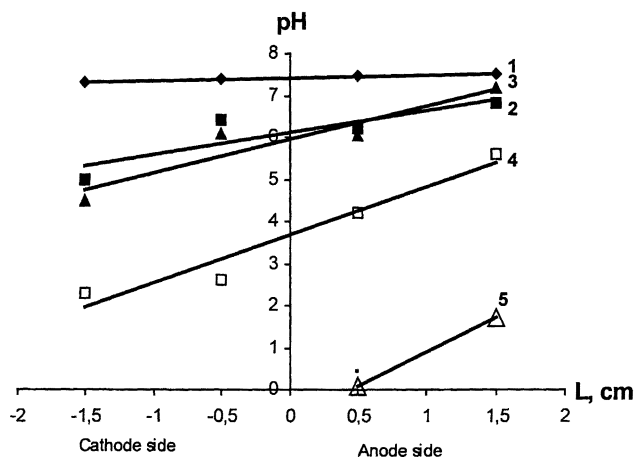
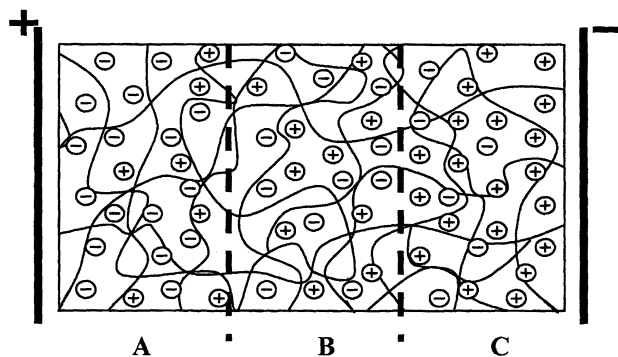
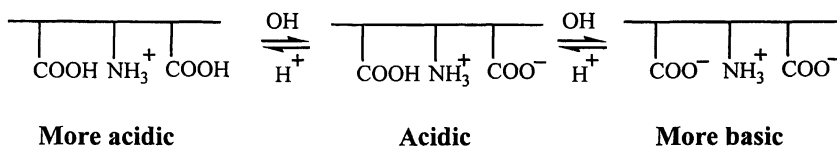
Fig.6. The dependence of pH on distance  $L$  at  $E = 0$  (curve 1), 5 (curve 2), 10 (curve 3), 15 (curve 4) and 20 V (curve 5)

Fig. 7. Schematically representation of three zones in the amphoteric gel matrix.

osmotic pressure increment, the flow of solvent will be reversed. At this stage, then, the process becomes regenerative, with any increase in salt concentration tending to enforce solvent from the zone C, thereby driving the concentration yet higher. During the regenerative process, however, salt will begin to leave the amphoteric region C because of its high concentration gradient, and will continue its flow out after the amphoteric gel has reached the point of maximum contraction. Thus the process enters a phase of decreasing salt concentration, with consequent relaxation of amphoteric gel matrix, and eventual return the gel to its initial state.

#### 4. pH oscillation of amphoteric gel induced by DC electric field

High applied voltage (20 V) generates inside of gel matrix the periodically changing of pH (Fig.8). An average deviation of pH during 7-10 minutes is estimated as  $\pm 0,5$  pH unit. Probably this is accounted for participation of  $H^+$  and  $OH^-$  ions in association-dissociation reactions with functional groups of polyampholytes via intermediate acidic form by the following scheme:



Periodically circulation of  $H^+$  and  $OH^-$  ions within gel matrix is probably the driving force of pH oscillation.

#### 5. Possible application of amphoteric gels for protein separation and purification purpose

Development of simple and efficient protein separation and purification technologies is very important for the biotechnological, food, cosmetic and pharmaceutical industries. Among the various protein analysis and purification technique the isoelectric focusing (IEF) is main tool to separate and purify proteins for analytical and preparative purposes. However the main disadvantage of this method is that it uses expensive carrier ampholytes (mixture of hundreds or thousands low molecular weight amphoteric molecules) and highest applied voltage (up to 200 V/cm). Moreover, amphoteric buffers tend to associate with proteins and often yield irreproducible gradient shapes. In order to avoid these disadvantages we suggest a new approach that could provide a simple method of electrophoretic resolution of proteins. The main idea is to combine both gel matrix and carrier ampholytes in one and the same sample like polyampholyte gel. In practice aqueous solution of protein molecules to be

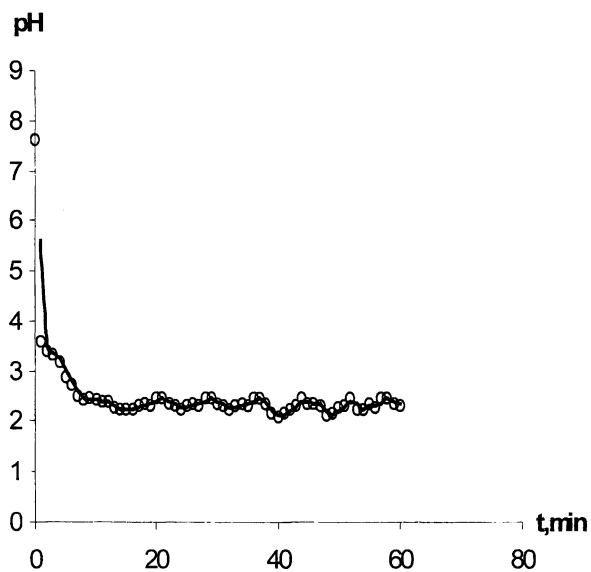


Figure 8. pH oscillation of PA-3 at  $E=20V$  with time.

separated is injected by syringe into central section of polyampholyte gel specimen, then DC electric field switches on. An applied DC electric field will stimulate the formation of linear pH gradient along the gel sample as shown in Fig.6. In its turn, the generated pH gradient will promote to migrate the charged protein molecules until they will be gradually localized at their isoelectric pH. Protein molecules will be separated and concentrated if the isoelectric pHs of proteins will coincide with appropriate pH zones of amphoteric gel. The further experimental works to realize this idea are in progress.

### Acknowledgement

Authors are thankful to S. Strandman from the X-ray laboratory of Department of Physics, University of Helsinki, Finland, and R. Serimaa and Prof. H. Tenhu from the laboratory of Polymer Chemistry, Department of Chemistry, University of Helsinki, Finland for providing of FTIR, NMR, DSC, SAXS and WAXS measurements.

### References

1. Tanford, Ch. *Physical Chemistry of Macromolecules* (in Russian), Mir, Moscow, 1965, 772 p.
2. Candau, F.; Joanny, J.F. *Polymeric Materials Encyclopedia*, (J.Salamone Ed.) CRS Press, Boca Raton, N.Y., London, Tokyo, **1996**, 7, 5476-5488.
3. Higgs, P.G.; Joanny, J.F. *J.Chem.Phys.* **1991**, *94*, 1543.
4. Kudaibergenov, S.E. *Adv.Polym.Sci.* **1999**, *144*, 115-197
5. Khokhlov, A.R.; Dormidontova, E.E. *Uspekhi Fiz. Nauk (Adv.Phys.Sci.)*, **1997**, *167*, 113-128.
6. Nisato, G.; Munch, J.P.; Candau, S.J. *Langmuir* **1999**, *15*, 4236-4244.
7. Osada, Y. *Adv.Polym.Sci.*, **1987**, *82*, 2-46.
8. Doi, M.; Matsumoto, M.; Hirose, Y. *Macromolecules* **1992**, *25*, 5504.
9. Winkler, R.G.; Reineker, P. *J.Chem.Phys.* **1997**, *106*, 2841.
10. Yoshida, R.; Ichijo, H.; Hakuta, T.; Yamaguchi, T. *Macromol.Rapid Commun.* **1995**, *16*, 305.
11. Giannos, S.A.; Dinh, S.M.; Brener, B. *Macromol.Rapid Commun.* **1995**, *16*, 527.
12. Long, D.; Dobrynin, A.V.; Rubinstein, M.; Ajdari, A. *J.Chem.Phys.* **1998**, *108*, 1234-1244.
13. Loomans, D.; Schiessel H.; Blumen, A. *J.Chem.Phys.* **1997**, *107*, 2636-2642.
14. Kudaibergenov, S.E.; Sigitov, V.B. *Langmuir*, **1999**, *15*, 4230-4235.
15. Shostakovskii, M.F. *Vinyl Ethers* (in Russian), Moscow, 1952, 280 p.
16. Katchalsky, A.; Spangler, R. *Quarterly Review on Biophysics* **1968**, *1*, 137-175.

## Chapter 11

# Hydrogel Polymers from Alkylthio Acrylates for Biomedical Applications

Ravi Mukkamala<sup>1,2</sup>, Aaron M. Kushner<sup>1</sup>, and Carolyn R. Bertozzi<sup>1</sup>

<sup>1</sup>Department of Chemistry, University of California and Materials Sciences Division,  
Lawrence Berkeley National Laboratory, Berkeley, CA 94720

<sup>2</sup>Current address: Rohm and Haas Chemical Company, Process Chemistry  
Laboratory, 1900 Tidal Road, Deer Park, TX 77536

We have developed new acrylate monomers having pendent sulfide, sulfoxide and sulfone functional groups, and their cross-linked hydrogel polymers. Herein, the physicochemical characteristics including bulk and surface hydrophilicity, affinity for protein adsorption on the surfaces of these hydrogels are discussed. The sulfoxide hydrogels possess high degree of hydrophilicity and low affinity for *in-vitro* protein adsorption on their surfaces, thus showing potential to be new materials for use in biomedical applications, especially for soft contact lens preparation. Our results show that replacing sulfoxide functionality with sulfide or sulfone groups causes significant changes in polymer properties. Some of the mixed hydrogels derived from sulfide/sulfone acrylates and 2-hydroxyethyl methacrylate (HEMA) exhibit low to moderate hydrophilicity, but exceptional resistance to *in-vitro* protein adsorption.

## Introduction

Hydrogels, the water-swelled cross-linked networks of hydrophilic polymers, have found extensive applications as synthetic biomedical implant



materials (1). One of the most crucial characteristics of such implant materials is 'biocompatibility' or the lack of adverse effects on biological tissue at the material interface. Such biocompatibility of a synthetic material is controlled closely by adsorption of proteins from biological milieu on its surface (2). Consequently, extensive research efforts have been aimed towards developing synthetic polymeric materials with precise bulk and surface properties for controlled protein adsorption and cell adhesion at interfaces (1, 2). Poly(2-hydroxyethyl methacrylate) [p(HEMA)] hydrogels have been the optimal choice of material for use in a variety of artificial implants. Especially, p(HEMA) hydrogels have found extensive utility in the soft contact lens industry, and this is mainly due to their inherently-low protein binding nature and excellent physical properties including optical clarity and high tensile strength (1b-c, 3, 4). However, p(HEMA) hydrogels are also characterized by relatively low levels of hydration (equilibrium water content ~40% at ambient temperature), a feature that must be significantly improved for better performance in various applications, especially when they are fabricated into soft contact lenses. For example, as the hydration level of hydrogel-derived contact lenses increases (up to a certain limit), they become softer and provide better comfort to the wearer. In addition, an increase in water content of hydrogels is also known to improve their permeability to oxygen; eye is an avascular tissue that acquires oxygen directly from the atmosphere, and contact lenses in general impede oxygen supply to the eye. During the use of soft contact lenses, the dissolved oxygen in the water of the hydrogel matrix is supplied to the cornea, and therefore, the oxygen permeability of a hydrogel material is directly related to its equilibrium water content (3). Copolymerization of HEMA with ionic or polar monomers enhances the water content of the resulting mixed hydrogels, but not without compromising the excellent resistance to protein adsorption exhibited by native p(HEMA) hydrogels (3, 4). Thus, an urgent need exists in biomedical polymer industry for developing hydrogels with high water content and minimal bio-adsorption.

Sulfur containing polymers have gained increased attention in recent years because of their novel properties and promising applications in a number of areas (5). Whitesides and co-workers have shown that sulfoxide-derived self assembled monolayers (SAMs) were able to prevent non-specific adsorption of proteins such as RNase A and fibrinogen on their surfaces (6). Their resistance towards protein adsorption was shown to be comparable to that of PEG-derived SAM surfaces (6). This has prompted us to study poly(sulfoxide) hydrogels as possible protein-resistant materials for biomedical applications. We envisaged that hydrogels adorned with highly polar, but non-ionic sulfoxide functionality would be much hydrophilic, and that those derived from monomers with sulfide and sulfone functionalities (reduced and oxidized forms of sulfoxide group,

respectively) would also exhibit interesting physicochemical properties. Herein, we describe the physical properties and *in-vitro* protein adsorption behavior of various polymeric hydrogels from HEMA and acrylates **1**, **2**, **3** or **4** (Chart 1) containing sulfide, sulfoxide or sulfone functional groups (7).

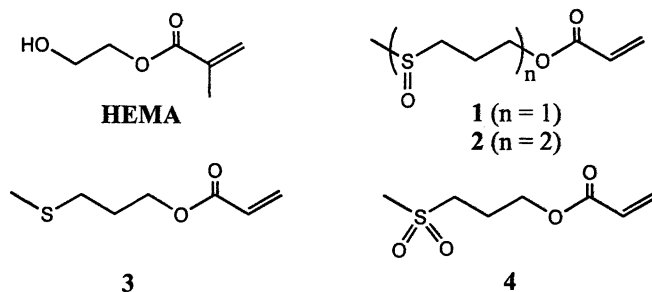


Chart 1

## Experimental

### Materials and Methods

Preparation of monomers **1-4** and hydrogels was described elsewhere (7a). Absorption spectra were recorded on a Shimadzu UV-1601 spectrophotometer. Static contact angles of diiodomethane (99%, Aldrich, 3 microliter droplets) on dry hydrogels in air or on hydrated hydrogels immersed in water were measured using a goniometer (model # 100-00115, Rame-Hart, Inc., Mountain Lakes, NJ). X-ray photoelectron spectroscopy (XPS) on dry hydrogels was performed using a Phi 5300 spectrometer from Perkin Elmer Instruments with Mg K $\alpha$  radiation of 1253.6 eV, operating at 15 kV and 26 mA.

### Protein adsorption study

Artificial tear fluid (ATF) containing a mixture of proteins (lysozyme, albumin, and mucin) and lipids (triolein, cholesteryl linoleate, etc.) was prepared following the procedure published previously (7a). The total protein concentration of the ATF was 3.2 mg/mL as determined using the Pierce BCA protein assay. Hydrogel pieces (1x1 cm<sup>2</sup> in area and ~1 mm in thickness) were immersed and incubated with gentle shaking, for a period of 24h in ATF solution (2 mL per hydrogel piece) in a water bath maintained at 36 °C. After incubation,

hydrogels were removed from the protein solution, quickly rinsed in a gentle flow of deionized distilled water, and shaken for 10 min in 10 mL of PBS solution at room temperature, twice. Washed hydrogel pieces were assayed for the presence of the adsorbed proteins using BCA protein assay reagent (8). As controls, all the hydrogels were treated with buffer solution alone and assayed with BCA reagent.

## Results and Discussion

The amount of water in a hydrogel, generally referred to as equilibrium water content (EWC), at a given temperature is directly related to the hydrophilicity of the functional groups on polymer chains and the degree of cross-linking. Pure HEMA hydrogels at 1-2 wt% cross-linking level typically exhibit equilibrium water contents of ca. 40% at room temperature (1, 3). Incorporation of highly polar sulfoxide functionality into poly(HEMA) matrix has significantly improved the water uptake of the resulting mixed hydrogels. When the concentration of monomer 1 in the pre-polymer mix containing HEMA is increased from 0-100 wt%, the water content of the resulting hydrogels goes up from 40-90%. Interestingly, similar levels of water uptake is observed for hydrogels made from monomer 2 with two sulfoxide moieties (Figure 1). We speculate that the effect of second sulfoxide group in the acrylic ester side chain of 2 is probably compensated by non-polar methylene units that come along with sulfoxide moiety, leaving the total hydrophilicity of the polymers similar to those made from 1. Our previous investigations with carbohydrate-HEMA mixed hydrogels showed that as the number of hydroxyl groups on the hexose unit of the carbohydrate acrylamides increases without increasing the total number of carbon atoms, the equilibrium water content of the resulting hydrogels increases commensurately (7, 9).

Surface properties of hydrogels are known to play a dominant role in their biocompatibility, and it is generally believed that, in the absence of electrostatic interactions, increasing the hydrophilicity of a hydrogel's surface leads to the reduction in protein and bacterial cell adhesion (2, 10). The contact angle of a liquid drop on a solid surface may be used as an indication of the surface polarity or hydrophilicity. Nakame and co-workers have showed by contact angle measurements that increasing 2-(glucosyloxy)ethyl methacrylate content in poly(methyl methacrylate) or poly(styrene) copolymers enhances their surface hydrophilicity (11). Previously, we have observed a similar improvement in the surface hydrophilicity of poly(HEMA)-carbohydrate acrylamide mixed hydrogels when compared to pure poly(HEMA) hydrogels (7, 9). We have examined the surface nature of the sulfoxide hydrogels by contact angle

measurements using diiodomethane. The static contact angles of diiodomethane droplets on the surfaces of swollen hydrogel immersed under water (12) showed a small, but gradual rise (Table I), indicating a moderate enhancement of hydrogels' surface polarity with increasing sulfoxide content.

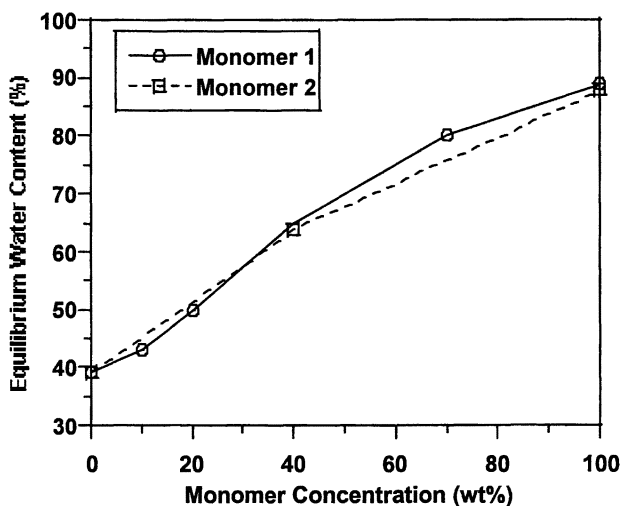


Figure 1. Concentration (wt%) of 1 or 2 in pre-polymer mix versus equilibrium water content (%) of the hydrogels.

Since surfaces of materials play a dominant role in bioadhesion, gaining knowledge of their chemical nature and composition is of paramount importance. X-ray photoelectron spectroscopy (XPS) is a surface analysis technique that has found extensive use in studying the surface properties of synthetic polymers and hydrogels, especially in their dry state (13). We have used XPS to analyze the surface chemical nature of HEMA-40 wt% 1 or 2 mixed hydrogels in their dry state (7a). Since monomers 1 and 2 have sulfoxide functionality, presence of an XPS peak corresponding to sulfur in the mixed HEMA hydrogels can be taken as an evidence for sulfoxide groups being present at materials' surface. In fact, the peaks for sulfur, along with those for carbon and oxygen, were detected in XPS survey scans. And, also the observed surface atomic concentrations matched well with theoretical values at the given mole ratios of HEMA and monomer 1 or 2 (Table II). This indicates complete incorporation of sulfoxide monomers into mixed hydrogels. In addition, no significant changes were observed in C, O or S

atomic concentrations at various sampling depths (reached by different take-off angles of the incident beam; data not shown), and this suggests that the sulfoxide functionality is uniformly distributed throughout the mixed hydrogels (13, 14).

**Table I. Static Contact Angles of Diiodomethane on Hydrated HEMA-1 Hydrogel Surfaces Under Water**

<i>Sulfoxide Concentration (wt%)<sup>a</sup></i>	<i>Contact Angle (deg)</i>
0 [poly(HEMA)]	132±3
10	131±3
20	134±4
40	137±3 (134±6) <sup>b</sup>
70	137±6
100	139±4 (137±6) <sup>b</sup>

<sup>a</sup> In pre-polymerization mix. <sup>b</sup> Values in the parenthesis are for HEMA-2 mixed hydrogels.

**Table II. Surface Atomic Concentrations of Mixed Hydrogels of HEMA and 1 or 2 (40 wt%) as Measured by X-ray Photoelectron Spectroscopy (XPS)<sup>a</sup>**

<i>Polymer</i>	<i>Atomic Concentrations (%)<sup>b</sup></i>		
	<i>C</i>	<i>O</i>	<i>S</i>
HEMA-1	66.7 (65.4)	29.0 (31.2)	4.3 (3.4)
HEMA-2	66.0 (65.1)	29.7 (30.3)	4.2 (4.6)

<sup>a</sup> Obtained on dry hydrogel pieces using Mg K  $\alpha$  radiation of 1253.6 eV and at 45° take-off angle. <sup>b</sup> Average values ( $\pm 0.5$ ) from 3 different samples, and theoretical values are given in the parenthesis.

Protein deposition on materials' surface is dependent on chemical nature of the surface (hydrophilicity, hydrophobicity, charge density) and also on the size and chemical composition of the proteins exposed to the synthetic surface (2). Since different biological media are composed of rather different types of proteins, materials designed for specific implant applications must be tested using those proteins most likely encountered *in vivo*. Materials used in contact lens applications are generally tested for *in vitro* protein adsorption using an artificial tear fluid (ATF) containing mixtures of proteins and lipids that are commonly found in human tear fluid and in contact lens deposits (15, 16). A

major component of both tear proteins and contact lens deposits is lysozyme, and others include albumin, mucins, lactoferrin, IgA and IgG. Our sulfoxide-HEMA mixed hydrogels belong to the high water content-non ionic class of materials, and such materials are useful in the fabrication of soft contact lens. Thus, we were interested in studying the *in vitro* protein adsorption behavior of our sulfoxide-derived hydrogels using the artificial tear fluid.

We have prepared an ATF solution using a protocol similar to those previously reported (7, 15). Our preparation contained three of the major proteins found in tears and lens deposits, namely, lysozyme, albumin and mucin. Hydrogels prepared from HEMA, monomers 1 or 2, or their mixed combinations were incubated in ATF for 24h at 36 °C, and the adsorbed proteins were quantified using the BCA assay (7). The results of the study are presented in Figure 2.

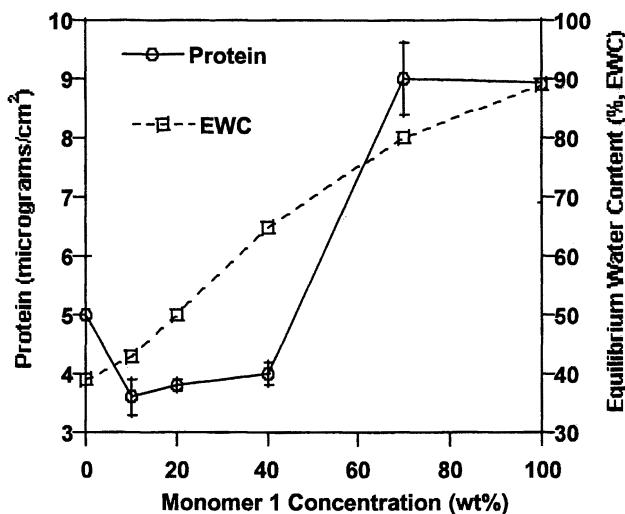


Figure 2. Concentration (wt%) of 1 in pre-polymer mix versus equilibrium water content (%) of the hydrogels, and amount of protein (micrograms/cm<sup>2</sup>) adsorbed after 24h incubation in ATF at 36 °C.

When mixed hydrogels of HEMA-1 (10-40 wt%) were incubated in artificial tear fluid solution for a period of 24h, the amounts of total polymer-bound protein were found to be about the same as that was bound to pure HEMA

hydrogels. More interestingly, however, for mixed hydrogels made from HEMA and  $\geq 70$  wt% of monomers **1** or **2**, the amount of protein adsorbed was nearly twice that of the pure HEMA hydrogels (Figure 2). In another set of experiments with HEMA-40 wt% **1** or **2** mixed hydrogels using individual protein solutions of either albumin or lysozyme, the hydrogels exhibited virtually no affinity for albumin; lysozyme, however, was adsorbed in amounts close to that of the total protein(s) adsorbed on mixed hydrogels that were incubated in ATF (17). Proteins such as lysozyme which are small in size are known to penetrate and be absorbed on hydrogels' inner matrix besides the surface adsorption (18). This may be more facilitated in hydrogels of high water content and large pore sizes (due to high degree of swelling) as in the case of mixed hydrogels with  $\geq 70$  wt% sulfoxide concentration. Interestingly, Yishihara et al. have recently argued that protein adsorption on phosphorylcholin-HEMA hydrogels is dependent not on the total level of hydration, but on the ratio of free versus bound water within the polymer matrix (18). Results from our recent work on HEMA-carbohydrate acrylamide hydrogels suggested that while increasing hydrophilicity (bulk and surface) of hydrogels helps lower protein adsorption in general, specific interactions among various functional groups on synthetic polymers as well as those on biomolecules play a crucial role in determining the final affinity (or lack of it) for each other (9, 10). Thus, it appears from our data presented here and the work of Whitesides and co-workers (6) that sulfoxide functionalized polymer surfaces have lower affinity for RNase A and fibrinogen than for lysozyme, and further work is needed to understand the underlying reasons. Regardless, sulfoxide-derived mixed hydrogels presented here are one of very few mixed poly(HEMA) systems whose equilibrium water content is much higher than pure poly(HEMA) hydrogels (70% versus 40%) but with similar resistance to the deposition of some tear proteins (Figure 2).

### Effect of Sulfur Oxidation State on Hydrogels' Properties

In order to discern the effect of oxidation state of sulfur on hydrogel properties, we have investigated hydrogels of **3** and **4** (acrylate monomers with sulfide and sulfone groups, respectively). Herein, nature of hydrogels of **3**, **4** and their mixed hydrogels of 60 wt% HEMA are discussed. Hydrogels made from of **3** or **4** alone exhibited much lower equilibrium water contents compared to the sulfoxide hydrogels of **1** or **2** (Figure 3), and this may be due to the obvious polarity differences in their respective functional groups. It is, however, interesting to note that the hydration levels of hydrogels of **3** and **4** are rather similar in spite of large polarity differences between sulfone and sulfide groups. The EWC of mixed hydrogels prepared from **4** (40 wt%) and HEMA (60 wt%)

is in fact close to that of pure HEMA hydrogels. On the other hand, mixed hydrogels prepared from 3 (40 wt%) and HEMA (60 wt%) exhibited EWC that is similar to that of hydrogels made from 3 alone.

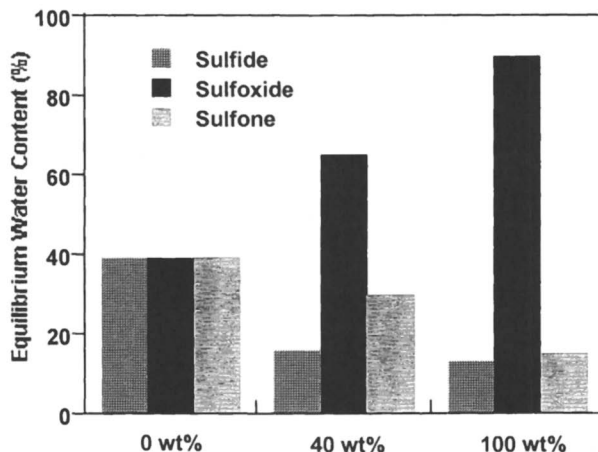


Figure 3. Concentration (wt%) of 1 (sulfoxide), 3 (sulfide) or 4 (sulfone) in pre-polymer mix versus equilibrium water content of the corresponding hydrogels.

Table III. Static Contact Angles of Diiodomethane on Hydrated HEMA-1, 3 or 4 Hydrogel Surfaces Under Water

Monomer Concentration (wt%) <sup>a</sup>	Contact Angle (deg)		
	Sulfoxide (1)	Sulfone (4)	Sulfide(3)
0 [poly(HEMA)]	132 <sub>+3</sub>	132 <sub>+3</sub>	132 <sub>+3</sub>
40	128 <sub>+3</sub>	137 <sub>+3</sub>	132 <sub>+3</sub>
100	116 <sub>+4</sub>	139 <sub>+4</sub>	125 <sub>+3</sub>

<sup>a</sup> In pre-polymerization mix.

Replacing the sulfoxide functionality with either a sulfide or sulfone group resulted not only in the reduction of hydrogels' bulk polarity, but lowered their surface hydrophilicity, as well; diiodomethane contact angles on swollen hydrogel surfaces of 3 and 4 were lower than those obtained for sulfoxide hydrogels (Table III). Not surprisingly, the surface polarity of hydrogels of sulfide monomer 3 was the least among the three polymers compared.



*In vitro* protein adsorption behavior of sulfide and sulfone hydrogels was investigated using ATF, and the results are presented in Figure 4. These results allow us to make distinctions among various hydrogels, and draw correlations between their bulk/surface hydrophilicity and protein adsorption behavior. In spite of their much lower EWC or surface hydrophilicity, sulfide and sulfone hydrogels adsorbed significantly lower amounts of protein (s) when compared to sulfoxide hydrogels. In particular, hydrogels of sulfone-acrylate 4 with an EWC of ca. 15 % adsorbed protein(s) in amounts that are barely detectable. This indicates that high bulk and/or surface polarity may *not* be a necessary requirement for synthetic polymers to resist protein adsorption. Similarly, mixed hydrogels of HEMA-4 (40wt%) posses moderate hydrophilicity (EWC ~30 %), but exhibit much greater resistance (ca. 5 times) to protein adsorption as compared to poly(HEMA) hydrogels. It may be inferred from these results that affinity between biomolecules such as proteins and synthetic polymer surfaces is not controlled by bulk or surface hydrophilicity of the polymers alone, but perhaps by specific interactions between various functional groups present on both proteins and polymers, as well.

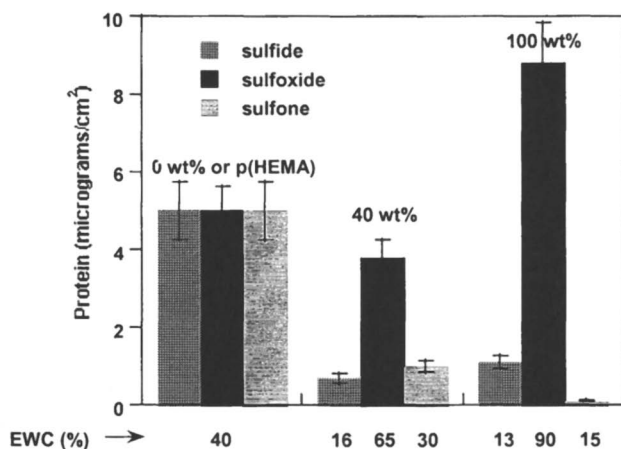


Figure 4. Concentration (wt%) of 1 (sulfoxide), 3 (sulfide) or 4 (sulfone) in pre-polymer mix versus amount of protein adsorbed after 24h incubation in ATF at 36 °C. Equilibrium water contents (EWC, %) of the hydrogels are given at the bottom of each bar.

## Conclusions

Herein, we have described novel sulfur-containing hydrogels whose characteristics are significantly influenced by the oxidation state of sulfur. Some of the sulfoxide-derived hydrogels studied here possess interesting properties such as high hydrophilicity and low affinity for *in-vitro* protein adsorption, and could be useful in the fabrication of biomedical implants such as soft contact lenses. Whereas, sulfone- or sulfide-functionalized hydrogels and their mixed hydrogels with HEMA exhibit rather low hydrophilicity, but exceptionally-high resistance to protein adsorption. Such polymers may be useful in those bio-applications where high hydrophilicity is not a requirement (for example, catheter coatings). Regardless, sulfur-containing hydrogel polymers described here display rather interesting physicochemical properties which appear to arise from an interplay between bulk/surface polarity and functional group interactions, and their role in dictating a given hydrogel's affinity (or lack of it) for proteins. Our future investigations will focus on hydrogels prepared from mixtures of sulfone, sulfoxide and sulfide monomers to achieve further control on tuning hydrogels' characteristics, and to gain better understanding of various functional group interactions in a given hydrogel system.

## Acknowledgments

Authors wish to thank Department of Energy (DOE) and Sunsoft Corporation for financial support of this research.

## References

1. (a) Peppas, N. A. *Hydrogels in Medicine and Pharmacy*; CRC Press: Boca Raton, FL, 1986. (b) Ottenbrite, R. M.; Huang, S. J.; Park, K., Eds.; *Hydrogels and Biodegradable Polymers for Bioapplications*; American Chemical Society: Washington DC, 1996. (c) Wheeler, J. C.; Cox, M. J.; Cantrell, R. W.; Watkins, F. H.; Edlich, R. F. *J. Long Term Eff. Med. Implants*, **1996**, 6, 3.
2. (a) Brash, J. L.; Horbett, T. A., Eds.; *Proteins at Interfaces. Physicochemical and Biochemical Studies*; American Chemical Society: Washington DC, 1987. (b) Andrade, J. D.; Hlady, V. *Adv. Polym. Sci.*, **1986**, 79, 1. (c) Peppas, N. A.; Langer, R. *Science*, **1994**, 263, 1715. (d) Tsuruta, T. *Adv. Polym. Sci.* **1996**, 126, 1.
3. Phillips, A. J.; Stone, J., Eds.; *Contact Lenses*; Butterworths: London, 1989.
4. Garbassi, F.; Morra, M. Occhiello, E., Eds.; *Polymer Surfaces from Physics to Technology*; Chichester: New York, 1994.

5. (a) Ogawa, F.; Endo, T. *Polymer*, **1998**, 39 (22), 5543. (b) Oyama, T.; Ozaki, J.; Chujo, Y. *Polym. Bull.*, **1998**, 40(6), 615. (c) Allcock, H. R.; Olmeijer, D. L. *Macromolecules*, **1998**, 31 (23), 8036. (d) Koyama, E.; Sanda, F.; Endo, T. *Macromolecules*, **1998**, 31 (5), 1495.
6. Deng, L.; Mrksich, M.; Whitesides, G. M. *J. Am. Chem. Soc.* **1996**, 118, 5136.
7. (a) Bertozzi, C. R.; Mukkamala, R.; Chen, Q.; Hu, H.; Baude, D. U.S. Patent 6,107,365, 2000. (b) Mukkamala, R.; Kushner, A. M.; Bertozzi, C. R. *Polymer Preprints*, **2000**, 41 (1), 733.
8. Smith, P. K.; Krohn, R. I.; Hermanson, G. T.; Mallia, A. K.; Gartner, F. H.; Provenzano, M. D.; Fujimoto, E. K.; Goeke, N. M.; Olson, B. J.; Klenk, D. C. *Anal. Biochem.* **1985**, 150, 76.
9. (a) Chen, Q.; Mukkamala, R.; Bertozzi, C. R. Presented in the 214<sup>th</sup> ACS National Meeting, Las Vegas, September 1997. (b) Mukkamala, R.; Chen, Q.; Bertozzi, C. R. Submitted for publication in *Macromolecules*.
10. (a) Hong, Y.; Chirila, T. V.; Vijayasekaran, S.; Dalton, P. D.; Tahija, S. G.; Cuypers, M. J. H.; Constable, I. J. *J. Biomed. Mater. Res.* **1996**, 30, 441. (b) Holly, F. J. *J. Polym. Sci., Polym. Symp.* **1979**, 66, 409.
11. (a) Nakamae, K.; Miyata, T.; Ootsuki, N. *Macromol. Chem. Phys.*, **1994**, 195, 1953. (b) Nakamae, K.; Miyata, T.; Ootsuki, N. *Macromol. Chem. Phys.*, **1994**, 195, 2663.
12. (a) Morra, M.; Occhiello, E.; Garbassi, F. *J. Colloid Interfac. Sci.* **1992**, 149, 84. (b) Adamson, A. W. *Physical Chemistry of Surfaces*; Wiley: New York, 1990. (c) K. Nakamae, T. Miyata, and N. Ootsuki, *Macromol. Chem. Rapid Commun.* **1993**, 14, 413.
13. (a) Briggs, D.; Shea, M. P. *Practical surface analysis, vol.1: Auger and X-ray photoelectron spectroscopy*; Wiley: New York, 1990. (b) Gardella, Jr. J. A. *Appl. Surface Sci.* **1988**, 31, 72. (c) Lewis, K. B.; Ratner, B. D. *J. Coll. Interfac. Sci.* **1993**, 159, 77.
14. Nakamae, K.; Miyata, T.; Ootsuki, N. *Macromol. Chem. Phys.* **1994**, 195, 2663.
15. (a) Mirejovsky, D.; Patel, A.S.; Rodriguez, D. G.; Hunt, T. J. *Optom. Vis. Sci.* **1991**, 68, 858. (b) Prager, M. D.; Quintana, R. P. *J. Biomed. Mater. Res.*, **1997**, 36, 119.
16. (a) Gudmundsson, O. G.; Woodward, D. F.; Flower, S. A.; Allansmith, M. R. *Arch. Ophthalmol.* **1985**, 103, 196. (b) Leahy, C. D.; Mandell, R. B.; Lin, S. T. *Optom. Vis. Sci.* **1990**, 67, 504.
17. Among other factors, competition between various proteins for selective adsorption onto polymers plays an important role when protein mixtures are used. See, Vroman, L.; Adams, A. L. *J. Colloid Interfac. Sci.* **1986**, 111, 391.
18. Refejo, M. F.; Leong, F. L. *J. Polym. Sci. Polym. Symp.* **1979**, 66, 227.
19. Ishihara, K.; Nomura, H.; Mihara, T.; Kurita, K.; Iwasaki, Y. *J. Biomed. Mater. Res.* **1998**, 39, 323.

## Chapter 12

# Stimuli-Responsive Gels Based on Ring-Opened Polyferrocenes: Synthesis, Characterization, and Electrochemical Studies of Swellable, Thermally Cross-Linked Polyferrocenylsilanes

Kevin Kulbaba, Mark J. MacLachlan, Christopher E. B. Evans,  
and Ian Manners\*

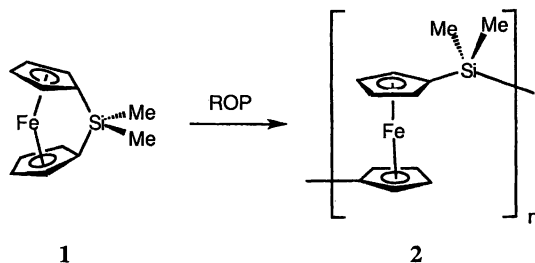
Department of Chemistry, University of Toronto, 80 St. George Street,  
Toronto M5S 3H6, Canada

A series of crosslinked polyferrocenylsilane networks have been prepared via the copolymerization of the silicon-bridged [1]ferrocenophane,  $\text{fcSiMe}_2$  ( $\text{fc} = \text{Fe}(\eta\text{-C}_5\text{H}_4)_2$ ) with controlled amounts of a spirocyclic [1]ferrocenophane  $\text{fcSi}(\text{CH}_2)_3$ . Thermal analysis revealed that the crosslinked polyferrocenylsilanes have improved thermal stability relative to their linear counterparts. Swellability was investigated as a function of temperature, solvent and crosslink density. As expected, the degree of crosslinking had a dramatic effect on the swelling in various media. From swellability measurements in various solvents, it was determined that the best solvents for poly(ferrocenyldimethylsilane) are THF, chloroform, and dichloromethane. The solubility parameter ( $\delta$ ) for the homopolymer was found to be  $18.7(7) \text{ MPa}^{1/2}$ . The redox and spectroscopic properties of the gels were investigated using spectroelectrochemistry in an optically transparent thin-layer electrochemistry (OTTLE) cell. Significant oxidation of the gel was evident at oxidation potentials greater than 450 mV (vs Ag/AgCl), consistent with the first oxidation potential of the linear homopolymer.

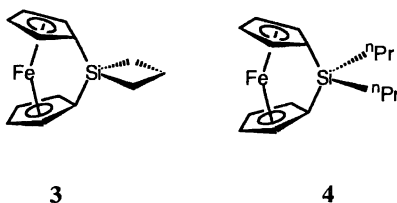
Crosslinked polymers can form gels that swell, but do not dissolve, in a liquid medium. A polymer network changes its volume in response to changes in its environment such as temperature, solvent composition, mechanical strain, electric field, exposure to light etc. (1a). "Smart gels" are crosslinked networks capable of responding to such a stimulus with a rapid swelling or contraction. As a consequence of this fast dimensional change, these materials have potential for applications in drug delivery, chemical sensing, shape memory, and molecular separation devices (1).

The incorporation of transition metals into polymer networks represents an appealing route to gels with electrochemically controllable properties. For example, pendant ferrocene moieties have been incorporated into networks via copolymerization of vinylferrocene with acrylamide and N,N'-methylenebisacrylamide. The resulting random copolymer gels have been investigated for potential use as glucose biosensors (2). An interesting redox-active self-oscillating gel has been synthesized by Yoshida and coworkers by inducing the Belousov-Zhabotinsky reaction within a copolymer gel of N-isopropylacrylamide and tris(2,2'-bipyridine) ruthenium(II). The gel was found to swell and contract at the oxidized and reduced states of  $[\text{Ru}(\text{bpy})_3]^{3+/2+}$ , respectively. The reaction produces periodic redox changes within the gel, which autonomously pulsates like a beating heart (3a). Tatsuma and coworkers have synthesized a redox-active poly-N-isopropylacrylamide-co-vinylferrocene gel and that displays electrochemically and thermally controllable phase transitions (3b).

As a consequence of its high stability and interesting physical properties, ferrocene is an attractive moiety to incorporate into polymeric structures (4). Ring-opening polymerization (ROP) of strained, ring-tilted [1]ferrocenophanes (e.g. 1) provides a well-established route to high molecular weight, soluble polyferrocenes (e.g. 2) (5). For such polymers, metal-metal interactions occur along the polymer backbone, as is illustrated by the cyclic voltammetry of 2 which shows the presence of two reversible oxidation waves which occur at 460 mV and 710 mV respectively vs a Ag/AgCl reference electrode (6).



Recently, we reported the first examples of well-characterized, crosslinked, swellable polyferrocenylsilanes (7). Thermal copolymerization of ferrocenophane **1** with the spirocyclic [1]ferrocenophane **3** allows access to material with controlled crosslink densities. Because of the interesting properties of polyferrocenylsilanes, we identified crosslinked examples as possible candidates for stimuli-responsive gels.



In this Chapter, the synthesis and characterization of polymer networks formed by copolymerization of monomers **1** (fcSiMe<sub>2</sub>) and **4** (fcSiPr<sub>2</sub>) with the spirocyclic [1]silaferrocenophane **3** are reported. The swelling response to changes in temperature, solvent, and substituents at silicon, as well as the effect of crosslinking on the thermal and mechanical properties of the material by thermogravimetric analysis (TGA) and differential scanning calorimetry (DSC) are reported. Lastly, the metal-metal interactions within the polymer network were investigated using spectroelectrochemistry.

## Experimental

Monomers **1**, **3**, and **4** were prepared according to literature procedures (6, 7) and purity was assessed by solution <sup>1</sup>H NMR. A Perkin-Elmer DSC-7 differential scanning calorimeter equipped with a TAC 7 instrument controller was used to study the thermal behaviour of the gels. The thermograms were calibrated with the melting transitions of decane and indium and were obtained at a heating rate of 10°C min<sup>-1</sup> under nitrogen. T<sub>g</sub> values quoted in this study correspond to the inflection point of the heat capacity change. Thermogravimetric analyses were performed at a heating rate of 10°C min<sup>-1</sup> under an atmosphere of prepurified N<sub>2</sub> using a Perkin-Elmer TGA-thermogravimetric analyser calibrated with the Curie points of Perkalloy and Nicoseal standards.

Controlled potential electrolysis of **5b** was effected using a spectroelectrochemistry cell of published design (8, 9). The electrodes consisted of a Pt mesh working electrode, a Pt wire counter electrode and a Ag/AgCl wire reference electrode. The electrolyte solution consisted of 0.1 M

tetrabutylammonium hexafluorophosphate in freshly distilled  $\text{CH}_2\text{Cl}_2$ . Potentials were applied using an AMEL instruments Model 2049 general purpose potentiostat and UV-Vis-NIR spectra were collected with a Perkin-Elmer Lambda900 UV/Vis/NIR spectrophotometer. Data were collected every 0.33 nm between 240 and 2200 nm using an integration time of 0.08 s at a scan rate of 247 nm/min.

### Synthesis of Poly(ferrocenyldimethylsilane)-Polycarbosilane Network **5a**

A solution of 10 mg (0.039 mmol) of  $\text{fcSi}(\text{CH}_2)_3$  (**3**) and 476 mg (1.97 mmol)  $\text{fcSiMe}_2$  (**1**) in 5 mL  $\text{CH}_2\text{Cl}_2$  was added to a Pyrex polymerization tube (approx. 1 cm internal diameter and 10 cm length). Solvent was slowly removed under vacuum over a period of 1 h to leave a red powder. After drying under vacuum for an additional 15 min, the tube was sealed under vacuum. The polymerization tube containing the intimate mixture of monomer and crosslinking agent was heated at 140°C for 4 h then 180°C for 4 h. After cooling to room temperature, the contents of the tube appeared orange with some red polymer. The Pyrex tube was cut into 4 sections and stirred for 16 h under  $\text{N}_2$  in *ca.* 100 mL of dry THF, giving a pale yellow solution and a swollen orange gel. The product was isolated by filtration on a Buchner funnel and dried under vacuum for 24 h. Yield: 379 mg (78%) of orange powder.

Crosslinked networks **5b-e** were prepared using a method analogous to that for **5a**. Table 1 gives the experimental data for **5a-e** including amounts of starting materials used in the preparations, yields, swellability, and ceramic yield determined from thermal analysis.

**Table 1.** Experimental Details for the Preparation of Polymer Networks **5a-e**.

Sample	$\text{fcSi}(\text{CH}_2)_3$ ( <b>3</b> )	$\text{fcSiMe}_2$ ( <b>1</b> )	Mol% <b>3</b>	Yield	Swellability in THF <sup>a</sup>	Ceramic Yield (600°C) <sup>b</sup>
<b>5a</b>	10 mg	476 mg	2	379 mg	260%	31%
	0.039 mmol	1.97 mmol		78%		
<b>5b</b>	28 mg	709 mg	4	383 mg	248%	--
	0.11 mmol	2.93 mmol		52 %		
<b>5c</b>	25 mg	462 mg	5	178 mg	200%	32%
	0.098 mmol	1.91 mmol		37%		
<b>5d</b>	51 mg	436 mg	11	275 mg	170%	37%
	0.20 mmol	1.80 mmol		56%		
<b>5e</b>	76 mg	412 mg	18	344 mg	40%	41%
	0.30 mmol	1.70 mmol		71%		

<sup>a</sup> THF was chosen as a solvent for swellability measurements as the homopolymer **2** is soluble in this solvent. Small pieces of the polymer networks were weighed and immersed in THF under  $\text{N}_2$  for 48 hours. Surface solvent was removed from the pieces and they were reweighed. The swellability given represents the % mass increase. <sup>b</sup> Determined by TGA under  $\text{N}_2$  at 10°C min<sup>-1</sup>.

## Synthesis of Poly(ferrocenyldi-n-propylsilane)-Polycarbosilane Network 6

A crosslinked network, **6** was prepared in a method analogous to **5a**, using 16 mg (0.06 mmol) of  $\text{fcSi}(\text{CH}_2)_3$  (**3**) and 400 mg (1.34 mmol)  $\text{fcSi}^{\text{IPr}}_2$  (**4**). Yield: 103 mg (25 % yield) of an orange-red material **6** with 4 mol % of crosslinker **3**. Samples were washed for a period of 4 weeks with fresh THF daily in an effort to remove unwanted oligomeric species from the gel network. Despite such efforts, discoloration of the THF solution was apparent upon standing for 12 hours. Such discoloration may have been due to the mechanical breakdown of the gel during washing. Additional errors associated with the loss of such material was deemed to be insignificant due to the large changes in weight between the gel in the dry and swollen state (a 2200 % mass increase).

### Theory

The Hildebrand solubility parameter is a fundamental thermodynamic property of polymers and is used extensively for the discussion of the miscibility of polymers in solvents and blends. The process of dissolving an amorphous polymer in a solvent is governed by the free energy of mixing,

$$\Delta G_m = \Delta H_m - T\Delta S_m \quad [1]$$

where  $\Delta G_m$  is the Gibbs free energy change of mixing,  $\Delta H_m$  is the enthalpy change on mixing,  $T$  is the absolute temperature, and  $\Delta S_m$  is the entropy change on mixing. Hildebrand and Scott and Scatchard (10) proposed that the free energy of mixing ( $\Delta H_m$ ) can be related to the energy of vaporization ( $\Delta E^v$ ) by:

$$\Delta H_m = V \left( (\Delta E^v_1 / V_1)^{1/2} - (\Delta E^v_2 / V_2)^{1/2} \right)^2 \phi_1 \phi_2 \quad [2]$$

where  $V$  is the volume of mixture ( $V_1 + V_2$ ),  $\Delta E^v_i$  is the energy of vaporization of species  $i$  and  $\phi_i$  is the volume fraction of species  $i$ .

The solubility parameter,  $\delta_i$ , of a liquid is defined as the square root of the cohesive energy density ( $\Delta E^v_i / V_i$ ) which describes the attraction between molecules of the material.

$$\delta_i = (\Delta E^v_i / V_i)^{1/2} \quad [3]$$

where  $V_i$  is the molar volume of species  $i$ . Equation [2] can be rewritten to give the heat of mixing per unit volume for a binary mixture:

$$\Delta H_m / V = (\delta_1 - \delta_2)^2 \phi_1 \phi_2 \quad [4]$$



In order for the Gibbs free energy of mixing ( $\Delta G_m$ ) to be favourable (i.e. negative) the heat of mixing must be smaller than the entropic term ( $T\Delta S_m$ ). In general  $(\delta_1 - \delta_2)^2$  must be small for the components to be miscible and therefore a good understanding of the solubility parameter of a polymer is of fundamental significance.

### Solubility Parameter Determination Technique

The poly-(ferrocenyldimethylsilane) network **5b** was chosen as a suitable sample for further swelling studies. It should be noted that the simple manipulation of the gel, which was necessary for this study, resulted in mechanical degradation of the polymer network leading to a decrease in the weight of the bulk gel over time. To minimize errors associated with the handling of the gels, the weight of each gel was therefore measured only once before and once after swelling. The formation of linear and oligomeric materials during the synthesis of such networks is unavoidable. To ensure that such species were completely removed from **5b**, the gel was swollen in fresh solutions of THF until no appreciable discoloration of the solution was observed after standing for 12 h.

The solubility parameter range for the poly(ferrocenyldimethylsilane) homopolymer was estimated using the method developed by Gee (11). Initial swelling studies indicated that two days were required for the gels to reach their equilibrium swollen state. To ensure that this equilibrium was reached the samples of the dry gel were cut, weighed, and swollen in the designated solvent for a minimum of five days at room temperature. The samples were then reweighed after removal of excess surface solvent using a kimwipe. The weight gain was used to calculate the swelling of the gel, expressed as mL of liquid absorbed per gram of dry gel for a minimum of 5 different samples. To obtain data which spans a suitable range, the weakly crosslinked gel **5b** (4 mol % of crosslinking agent **3**) was swelled in 14 different solvents with  $\delta$  values ranging from 14.3 to 24.3 MPa<sup>1/2</sup> (12).

## Results and Discussion

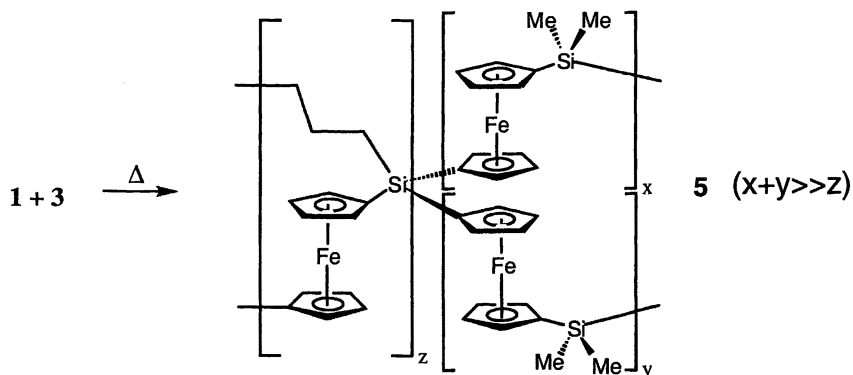
### Crosslinked Poly(ferrocenyldimethylsilane) Networks **5a,c-e**

To initiate our studies of crosslinked polyferrocenyldimethylsilanes, we identified precursors **1** and **3** as candidates to form crosslinked networks consisting of linear segments of polymer **2**. DSC studies of **3** indicated that this monomer undergoes exothermic ring-opening polymerization (ROP) at a fairly similar

temperature to **1** (175 and 130°C, respectively), and might therefore be expected to form random copolymers with **1**. Samples were prepared by dissolving an appropriate amount of **1** and **3** in CH<sub>2</sub>Cl<sub>2</sub> and evaporating the solvent. This permitted intimate mixing of the two monomers, a requirement for homogeneous random copolymer formation. When the samples were treated at 140°C, they were observed to melt then to quickly form an immobile polymer. The temperature was maintained at 140°C for 4 h and then raised to 180°C to increase polymer conversion. The orange-red polymers obtained from the polymerization of **1** with 2-15 mol% (see Table 1) of **3** were insoluble in common organic solvents in which homopolymer **2** is soluble, but were instead observed to swell in THF and CH<sub>2</sub>Cl<sub>2</sub>. The swellability of crosslinked polymers **5a,c-e**, was studied by swelling in THF. The networks properties were also investigated using differential scanning calorimetry (DSC), solid-state NMR, and thermogravimetric analysis.

Crosslinked gels swell rather than dissolve in good solvents for their linear counterparts. Homopolymer **2**, for instance, is completely soluble in THF whereas the corresponding crosslinked networks **5** are insoluble, but swell as they absorb solvent. Measurements of the degree of swelling for samples of networks **5a-e** show an increased swelling in THF with a decrease in the ratio of the monomers, **3:1** (Table 1). As shown previously, this is consistent with controlling the crosslink density of the polymer network (*7a*).

Scheme 1



DSC of **2** shows that this material possesses a glass transition ( $T_g$ ) at 33°C and when annealed, a  $T_m$  at 122-145°C (*6*). In contrast, DSC analysis of **5a,c-e** showed no evidence for melt transitions. Networks **5a** and **5c** have broad  $T_g$ s at 38-40°C, and no  $T_g$  was observed for polymers **5d** and **5e**. These observations are consistent with crosslinked networks in which the ordered interchain packing is disrupted by the presence of crosslink sites.

Crosslinking is a good method to improve the ceramic yield of polymers (13). Whereas homopolymer **2** has a ceramic yield of 22% at 600°C under N<sub>2</sub>, the crosslinked networks **5a,c-e** showed an increased ceramic yield with increased crosslink density (Table 1). All of the samples showed a weight loss of 2-5% between 100 and 250°C, probably resulting from the loss of oligomeric species entangled in the crosslinked network. The polymers then decompose at 400-600°C, as is also observed for homopolymer **2**. Figure 1 shows the TGA traces of **2** and the crosslinked networks **5a,c-e**. It is noteworthy that the addition of only 2% crosslinking agent results in a 50% improvement in the ceramic yield of the polymer at 600°C. The presence of the crosslinking agent serves to reduce decomposition pathways in which volatile depolymerization products are eliminated.

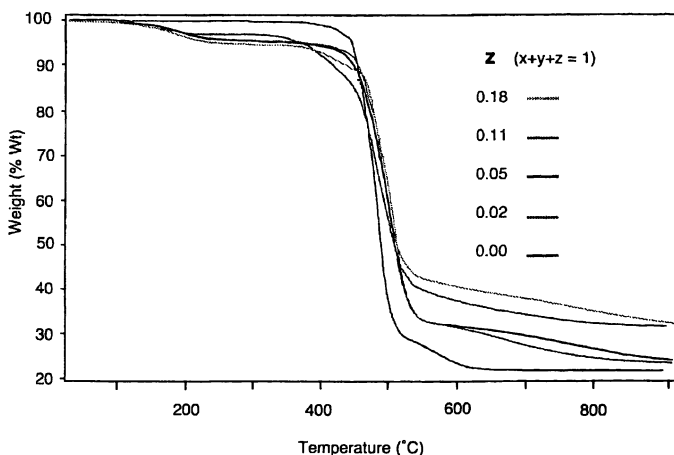


Figure 1. TGA traces of homopolymer **2** and crosslinked networks **5a,c-d**.

### Solubility Parameter of Poly(ferrocenyldimethylsilane) **2**

The solubility parameter ( $\delta$ ) of a polymer provides information about the polymer-solvent interactions, and is quite useful for material processing. It is not possible to directly measure the solubility parameter from a determination of the heat of vapourization thus other indirect methods must be employed such as refractive index (14), intrinsic viscosity (15), turbidimetric titration (16), gas chromatography (17), and swelling measurements (11, 18). Of these, swelling measurements provide a relatively straightforward technique for estimating the solubility parameter of a polymer. By measuring the degree of swelling of a weakly crosslinked polymer in a range of solvents of known  $\delta$ , a graph of

swellability vs  $\delta$  can be created. The degree of swelling should reach a maximum when the polymer network has the same solubility parameter as the solvent. It is assumed that this value corresponds to the solubility parameter of the linear homopolymer.

Swelling data for **5b** have been plotted in Figure 2. Maximum swelling of the gel is observed for solvents with  $\delta$  values of 18.0 to 19.4  $\text{MPa}^{1/2}$ . In such solvents the gel may swell to four times its original size. One exception to this trend was methylethylketone ( $\delta = 19.0$ ) in which there is minimal swelling relative to styrene ( $\delta = 19.0$ ) and chloroform ( $\delta = 19.0$ ). This difference in swelling is not uncommon for polymeric gels in solvents with varying H-bonding characteristics. Unfavourable interactions of the solvent with the polymer network may exist due to the weakly hydrogen bonding character of MEK in comparison with styrene and chloroform. The solubility parameter range for poly(ferrocenyldimethylsilane) is 18.7(7)  $\text{MPa}^{1/2}$  in poorly H-bonding solvents from the swelling characteristics of network **5b**. The best solvents for the homopolymer are THF, chloroform, and dichloromethane.

Samples of **5b** were placed in THF and the swollen gels thermostated to  $-56$ ,  $-20$ ,  $+25$  and  $+40^\circ\text{C}$  to probe the effect of temperature on the degree of swelling. The volume of the gel remained relatively unperturbed over the temperature range studied and the material did not appear to show significant thermal responsivity.

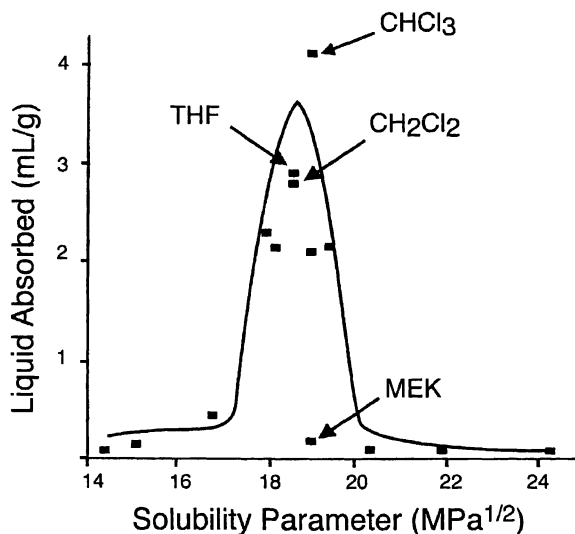


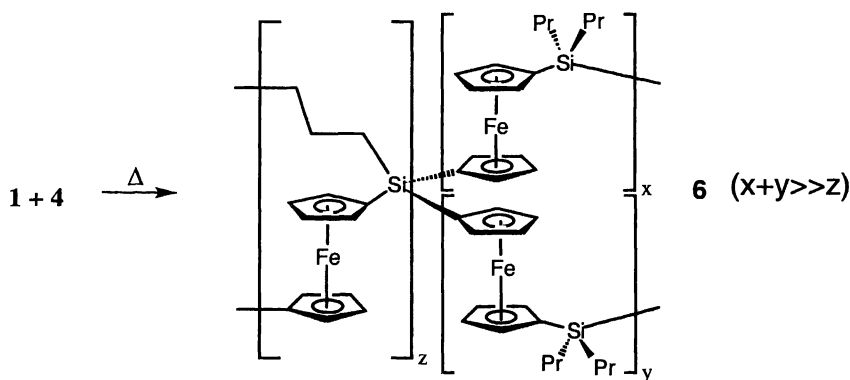
Figure 2. Relationship between the swelling ratio (mL/g) of the poly(ferrocenyldimethylsilane) gel, **5b**, and the solubility parameter of the various solvents. Maximum swelling occurs at  $\delta = 18.7(7) \text{MPa}^{1/2}$ .

## Swelling Studies of 6

Swelling characteristics of polymer networks are highly dependent on the polymer-solvent interactions as well as crosslink density. Altering the polymer architecture (i.e. changing the substituents at Si) may affect the swelling properties of the gel. A longer alkyl chain at silicon should have more favourable interactions with a nonpolar solvent and thus serve to increase the swellability of the gel.

To test this hypothesis, a lightly crosslinked poly(ferrocenyldipropylsilane) gel (4 mol % of 3) was synthesized, and swollen in THF to measure the degree of swelling. The *n*-propyl substituted gel, 6, was found to swell *ca.* 10 times more than the analogous methyl substituted gel 5b (2240% and 248% respectively). It is clear that the swelling of these polymer gels can be dramatically influenced by the substituents at silicon.

Scheme 2



## Electrochemical Studies of 5b

Oxidation of 2 by chemical means has been effected using various redox reagents in solution and in the solid state (19, 20). Such chemical oxidation may lead to cleavage of the polymer backbone due to potential side reactions, e.g. with the products of the oxidation reaction (21, 22). Electrochemical oxidation of the polymer allows for finer control over the degree of oxidation, and the potential applied. As noted above, oxidation of polyferrocenyldipropylsilanes occurs in two discrete steps at  $\approx 460$  mV and  $\approx 710$  mV vs a Ag/AgCl reference electrode (6, 20).

Controlled potential electrolysis was used to investigate the redox properties of the gels. With the gel placed on the Pt mesh working electrode, the spectrum of the deep red-orange material in the fully reduced state was recorded (Figure 3). The lowest energy visible band has previously been assigned to a d-d transition in substituted ferrocenes (23). Weak absorptions at 1650 nm and 1680 – 1720 nm were attributed to the overtones of trace amounts of water and to

$\text{CH}_2\text{Cl}_2$ , respectively. Upon oxidation, two new features were observed in the spectrum. A band centred near 640 nm and a broad band centred at 1300 nm were observed at potentials greater than 400 mV. The former is assigned to a ligand-to-metal charge transfer (LMCT) of ferrocenium centers, and the latter is assigned as an intervalence transition (IT) due to the formation of a mixed-valent polymer (20). At potentials of 450 mV and greater, the intensity of both these bands was observed to increase rapidly. This corresponds well, qualitatively, with the first oxidation potential of the homopolymer ( $\approx 460$  mV) (24). The color of the gel was observed to darken to deep blue with increasing oxidation, particularly where it was in intimate contact with the electrode surface. With time, the blue color diffused throughout the gel, and when left overnight the bulk gel became entirely blue. This indicates that charge diffusion in the bulk gel is very slow, which is further observed in the long times necessary for the gel to come to equilibrium ( $i \approx 0$ ) even at potentials far below  $E^\circ$ . (In a solution experiment, a thin-layer cell will usually come to equilibrium within a few seconds.) Due to the possibility of unwanted side reactions at higher oxidation potentials, a maximum of 500 mV was applied to the sample. At this potential, in theory 50% of the Fe sites along the backbone would be oxidized to Fe(III) states and the IT band should be at a maximum in intensity.

Reversibility was investigated by stepwise reduction over a potential range from 500 mV to  $-100$  mV. A gradual change in color from dark blue to red-orange was observed upon reduction. The spectroelectrochemical spectra reflect this change by a decrease in the intensity of both the LMCT band at 640 nm and the IT band at 1300 nm. The gel demonstrated good reversibility as shown by the complete disappearance of the LMCT and the IT bands. It must be noted, however, that the spectrum obtained upon reduction of the oxidized gel had fairly poor overlap with the spectrum of the reduced gel prior to oxidation. It is possible these changes are due to the Pt mesh shifting as the gel is oxidized.

## Conclusions

Here we have investigated a series of thermally crosslinked polyferrocenylsilane networks. TGA analysis revealed that the crosslinked polyferrocenes have improved thermal stability relative to their linear counterparts. Swellability was found to be affected by solvent, crosslink density and the substituents at silicon. From measurements of swellability in various solvents, it was determined that the best solvents for poly(ferrocenyldimethylsilane) are THF, chloroform, and dichloromethane. The solubility parameter ( $\delta$ ) for the homopolymer 2 is  $18.7(7)$   $\text{MPa}^{1/2}$ . The redox and spectroscopic properties of the gel were investigated using spectroelectrochemistry. Significant oxidation of the gel is evident at potentials greater than 450 mV (vs Ag/AgCl), corresponding well with the oxidation potential of the homopolymer. Such gels represent interesting materials, with reversible redox properties and ultimately are of interest for possible applications such as electrochemical actuators or switches.

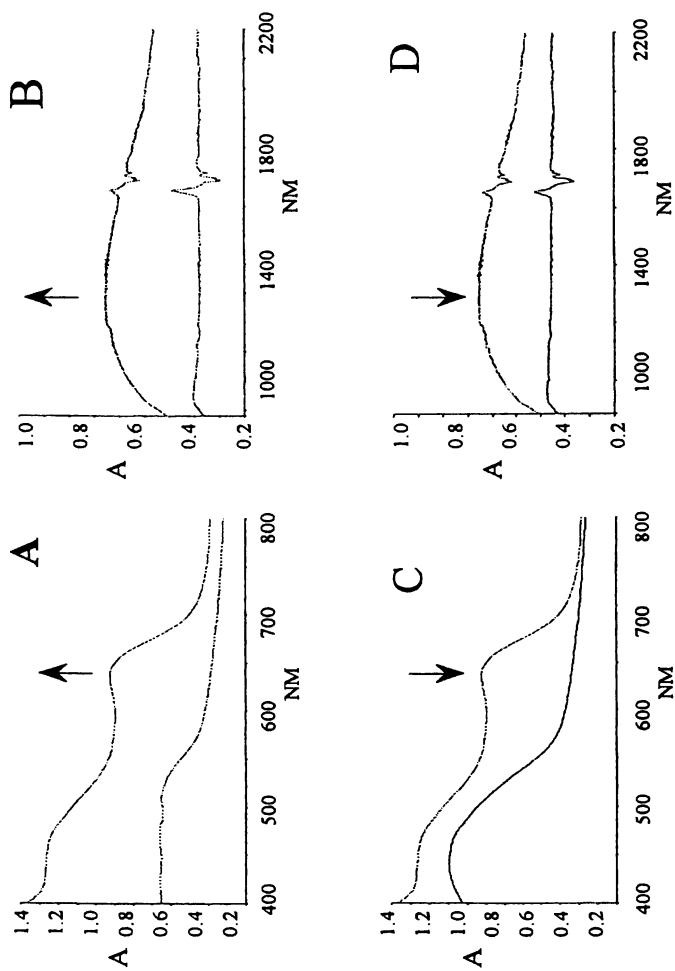


Figure 3. Oxidation of **5b** at 500 mV; (a) Visible spectrum, (b) NIR spectrum.  
Reduction of **5b** at -100 mV; (c) Visible spectrum, (d) NIR spectrum.

**Acknowledgements.** The authors would like to thank Fazila Seker and Prof. A. B. Ellis for helpful discussions, Professors A. Yudin and R. Morris for the use of their electrochemical equipment. We would also like to thank the Natural Sciences and Engineering Research Council of Canada (NSERC) for a Postdoctoral Fellowship for C.E. and Postgraduate Scholarships for K.K. and M.M. and a E.W.R. Steacie Fellowship (1997-1999) for I.M. In addition I.M. is grateful to the Alfred P. Sloan Foundation for a Research Fellowship (1994-1998), the University of Toronto for a McLean Fellowship (1997-2003), and the Ontario Government for a PREA Award (1999-2004).

## References

1. See for example: (a) Osada, Y.; Gong, J.-P. *Adv. Mater.* **1998**, *10*, 827. (b) Suzuki, A.; Tanaka, T. *Nature* **1990**, *346*, 345. (c) Holtz, J.H.; Asher S.A. *Nature* **1997**, *389*, 829.
2. (a) Bu, H.-Z.; Mikkelsen, S. R.; English, A. M. *Anal. Chem.* **1995**, *67*, 4071. (b) Bu, H.-Z.; English, A. M.; Mikkelsen, S. R. *J. Phys. Chem. B* **1997**, *101*, 9593.
3. (a) Yoshida, R.; Takahashi, T.; Yamaguchi, T.; Ichijo, H. *J. Am. Chem. Soc.* **1996**, *118*, 5134. (b) Tatsuma, T.; Takada, K.; Matsui, H.; Oyama, N. *Macromolecules* **1994**, *27*, 6687.
4. Manners, I. *Angew. Chem. Int. Ed. Engl.* **1996**, *35*, 1602.
5. Foucher, D. A.; Tang, B. Z.; Manners, I. *J. Am. Chem. Soc.* **1992**, *114*, 6246.
6. Manners, I. *Chem. Commun.* **1999**, 857.
7. (a) MacLachlan, M. J.; Lough, A. J.; Manners, I. *Macromolecules* **1996**, *29*, 8562. (b) MacLachlan, M. J.; Lough, A. J.; Geiger, W. E.; Manners, I. *Organometallics* **1998**, *17*, 1873.
8. Evans, C. E. B.; Naklicki, M. L.; Rezvani, A. R.; White, C. A.; Kondratiev, V. V.; Crutchley, R. J. *J. Am. Chem. Soc.* **1998**, *120*, 13096.
9. Krejcik, M.; Danek, M.; Hartl, F. *J. Electroanal. Chem.* **1991**, *317*, 179.
10. (a) Hildebrand, J. H.; Scott, R.L. *The Solubility of Nonelectrolytes*, 3<sup>rd</sup> ed. Rienhold Publishing Corporation, New York, 1950; Dover Publications Inc., New York, **1964** pp 123 – 133. (b) Scatchard, G. *Chem. Rev.* **1931**, *8*, 321.
11. Gee, G. *Trans. Inst. Rubber Ind.* **1943**, *18*, 266.
12. solvent ( $\delta$  in MPa<sup>1/2</sup>); pentane (14.4), diethyl ether (15.1), cyclohexane (16.8), xylenes (18.0), toluene (18.2), tetrahydrofuran (18.6), dichloromethane (18.6), chloroform (19.0), methylethyl ketone (19.0), styrene (19.0), chlorobenzene (19.4), acetone (20.3), hexanol (21.9), acetonitrile (24.3). All solubility parameter values were taken from Grulke, E. A. *Polymer Handbook*, 3<sup>rd</sup> ed., J. Brandrup and E. H. Immergut, Eds., John Wiley and Sons, Inc., New York, **1989**, p 519.



13. Visscher, G. T.; Nesting, D. C.; Badding, J. V.; Bianconi, P. A. *Science* **1993**, *260*, 1496.
14. Koenhen, D. M.; Smolders, C. A. *J. Appl. Polym. Sci.* **1975**, *19*, 1163.
15. (a) Mieczkowski, R. *Eur. Polym. J.* **1992**, *28*, 53. (b) Siemann, U. *Eur. Polym. J.* **1992**, *28*, 293.
16. Marco, C.; Bello, A.; Fatou, J. G.; Garza, J. *Macromol. Chem.* **1986**, *187*, 177.
17. (a) DiPaola-Baranayi, G. *Macromolecules* **1982**, *15*, 622. (b) Ashworth, A. J.; Price, G. J. *Macromolecules* **1986**, *19*, 362.
18. (a) Yagi, Y.; Inomata, H.; Saito, S. *Macromolecules* **1992**, *25*, 2997. (b) Hamurcu, E. E.; Baysal, B. M. *J. Polym. Sci., Polym. Phys.* **1994**, *32*, 591.
19. (a) Rulkens, R.; Resendes, R.; Verma, A.; Manners, I.; Murti, K.; Fossum, E.; Miller, P.; Matyjaszewski, K. *Macromolecules* **1997**, *30*, 8165. (b) Nguyen, M.T.; Diaz, A.F.; Dement'ev, V.V.; Pannell, K.H. *Chem. Mater.* **1994**, *6*, 952.
20. Rulkens, R.; Lough, A. J.; Manners, I.; Lovelace, S. R.; Grant, C.; Geiger, E. *J. Am. Chem. Soc.* **1996**, *118*, 12683.
21. Connelly, N. G.; Geiger, W. E. *Chem. Rev.* **1996**, *96*, 877.
22. Oxidation studies of homopolymer **2** in solution show significant  $M_w$  decline using very strong chemical oxidants (e.g.  $\text{NO}^+$ ) or in cases where nucleophilic counter ions are present (e.g.  $\text{I}^-$ ), Perry, R.; Manners, I., unpublished results.
23. Sohn, Y.S.; Hendrickson, D. N.; Gray, H. B. *J. Am. Chem. Soc.* **1971**, *93*, 3603.
24. The first oxidation potential of the homopolymer has been previously reported as 460 mV vs SCE (see reference 19). Note, however, that the potential of the AgCl reference electrode is known to be not very well-defined in organic solvents, particularly  $\text{CH}_2\text{Cl}_2$ . See Sawyer, D. T.; Roberts Jr., J. L. *Experimental Electrochemistry for Chemists*, John Wiley and Sons, New York, **1974** pp 34-60.

## Chapter 13

# Hydrocarbon Gels: Rheological Investigation of Structure

Nov Markovic<sup>1</sup>, Naba K. Dutta<sup>1,\*</sup>, David R. G. Williams<sup>2</sup>,  
and Jani Matisons<sup>1,3</sup>

<sup>1</sup>Ian Wark Research Institute, University of South Australia, Mawson Lakes,  
South Australia SA 5095, Australia

<sup>2</sup>Chemical Engineering Department, University of Adelaide, North Terrace Adelaide,  
South Australia, SA 5005 Australia

<sup>3</sup>Current address: Chair of Nanotechnology, Flinders University, G.P.O. Box 2100,  
Adelaide, South Australia SA 5001, Australia

This review focuses light on the complex rheological behavior of physical gels formed by the addition of aluminium soap based gelator to aliphatic, non-polar hydrocarbons. Rheological investigations were carried out in steady flow, creep and dynamic oscillation modes over a wide range of shear rates, frequencies, temperatures and times. It is observed that the rheological behavior is very sensitive to the concentration of gelator, however, in general they exhibit viscoelastic, thixotropic, shear reversible behavior. The gel network structure results from polar interaction and strongly polar contaminants have a deleterious effect on the formation of the gel.

## Introduction

There is considerable commercial and environmental interest in being able to safely manage highly flammable hydrocarbon fuels. One option is to convert the fuel from a low viscosity fluid to a gel. The decision on how the gel is formed now depends upon the ultimate purpose, for example, if it were intended that the fuel be discarded, then one would consider adding an organo-gelator system that would produce a chemically cross-linked structure. The chemical gel would remain in that state despite any unforeseen changes in the environment such as an increase in temperature. If it intended that the fuel be used later, then a satisfactory choice would be to produce a physical gel where the physical bonds could be disrupted by either temperature or shear. An example would be the gelling of hydrocarbon fuel to allow safe transport and later dispersion by pumping for the controlled burning of grasslands etc. Clearly an understanding of the flow properties of the physical gels in this application is important [1-4].

There were some early studies on the gelling action of soaps from heavy metals [5] with the primary interest centered on the formation of greases and lubricants [6]. However, there has been a recent upsurge in interest in organo-gelators with the discovery that there are many classes of compound capable of forming gels in organic solvents [7-9]. Furthermore, the applications have expanded with interest in biocatalysis, biomimetics, extraction processes and the preparation of micro particles. Surprisingly, however, there have been very few studies of the rheological behavior of these physical gels.

In contrast the rheological properties of gels formed from both natural and synthetic polymers have been thoroughly studied [10-14]. The overall character of the physical gel is dominated by both the labile nature of the physical bond between the polymer chains and the molecular weight of the polymer. The physical bond may be due to dispersion forces, polar groups or more specifically hydrogen bonding. The junctions so formed between the chains act as pseudo-crosslinks that allow the development of a supramolecular structure that is now well defined and understood. In contrast very little is known about the supramolecular structure of gels based on the low molecular weight organo-gelators.

This review will concentrate on the rheological properties of gels formed by the addition of an aluminium soap gelator to aliphatic, non-polar hydrocarbon fuels typically used in gasoline engines. More recent studies by the authors have shown that similar results are obtained with diesel and other non-polar fuels and solvents.

It is known that the supramolecular structure formed by the aluminium soaps relies upon hydrogen bonding between the molecule [15-16] and that rigid gels are only formed in non-polar organic solvents. It was realized therefore that the formation of aluminium soap/hydrocarbon gels would be susceptible to contamination by highly polar solvents. The extent of this disruption will also be discussed in this review.

To be commercially viable it was necessary to identify organogelators that could economically be employed to gel large quantities of hydrocarbon. A satisfactory group of candidates was identified as mixture of the aluminium soaps of organic (fatty) acids with addition of fillers.

## Experimental

### Sample Preparation

The hydrocarbon tested in this study was a highly volatile, low boiling point fuel (commercially available) used in combustion engines and typically composed of a mixture of non-polar aliphatic and aromatic organic compounds. It will be referred to as HCF. The aluminium soap of hexanoic acid was prepared [17] but was found to be less effective compared to a commercial compound based on mixed organic acids. Gels could be formed with as little as 0.5% wt. aluminium soap to volume of hydrocarbon fuel. The gelling agent was a commercially available powder consisting of the aluminium soap of mixed organic acids and will be referred to as ALSP (H. L. Blachford LTEE, Montreal, Canada).

Gels were prepared by dispersing the gelling agent powder in the hydrocarbon solvent (conveniently expressed as weight percent ALSP to volume of HCF). All gels were prepared by dispersing the gelling agent ALSP into the hydrocarbon HCF at 25°C. Gelation was achieved in a few minutes but to complete the reaction, samples were placed in solvent tight glass jars for 24 hours prior to testing. All runs were performed in triplicate and the average reported. The rheological properties of the gels were investigated over the range of ALSP content from 0.5% to 3%, with some measurements extending to 5%. Below 0.5% ALSP, the sample remained liquid like with little indication of the formation of a contiguous gel, whilst at concentrations greater than 5% ALSP the gels became rigid.

To determine the effect of contamination the following polar co-solvents were chosen to represent a wide range of polarity: hexanol, acetone, methanol and water. The method of preparation of the gels with co-solvents was similar. The weight to volume ratio of gelator to co-

solvent was 1:1. The gelator/co-solvent solution was then added to the liquid hydrocarbon and the gel transferred to a stoppered container.

## Rheological Investigation

Rheological properties of the gels were performed with a constant stress rheometer (Rheolyst AR1000 N, TA Instruments) with a cone and plate geometry (cone diameter 40 mm and  $2^\circ$  angle). Rheological experiments were carried out in steady flow, creep and dynamic oscillation modes over a wide range of shear rates, frequencies, temperatures and time. To prevent evaporation of the hydrocarbon a solvent trap (as supplied by TA Instruments) was installed for all experiments.

## Results and Discussion

### Steady Shear Measurements

Typical flow curves for some representative gels are illustrated in Figure 1. Note that to accommodate the wide range of values, both axes are plotted on log scales. All flow curves except that for 0.5% ALSP are non-linear and therefore can be described as exhibiting non-Newtonian behavior. It can be seen that the rheological behavior is very sensitive to the concentration of ALSP for values from 0.5% ALSP to 2.0% ALSP. Higher concentrations of ALSP had little effect ( $> 3\%$  ALSP).

The gels are also sensitive to the shear strain rate and this is depicted in Figure 2 where the data from Figure 1 is replotted in the form of viscosity (ratio shear stress to shear strain rate) versus the shear strain rate. Note again the sensitivity of the viscosity to small changes in ALSP concentration - an increase in ALSP of 1.5% produces a 40-fold increase in viscosity.

The experimental data revealed that soap based hydrocarbon gels are shear-thinning in nature, that is, there is a steady decrease in viscosity with increase in shear rates for all concentrations of the gelling agent indicating that there has been a change in the structure as a result of the shear stress.

At low shear rates ( $< 0.2\text{s}^{-1}$ ) and at high shear rates ( $> 2\text{-}3\text{s}^{-1}$ ), the viscosity tends to plateau and it is convenient to define these values as  $\eta_0$ , the viscosity at the initial condition (maximum) and  $\eta_\infty$ , the viscosity at the final condition (minimum). In structural terms, the viscosity at zero

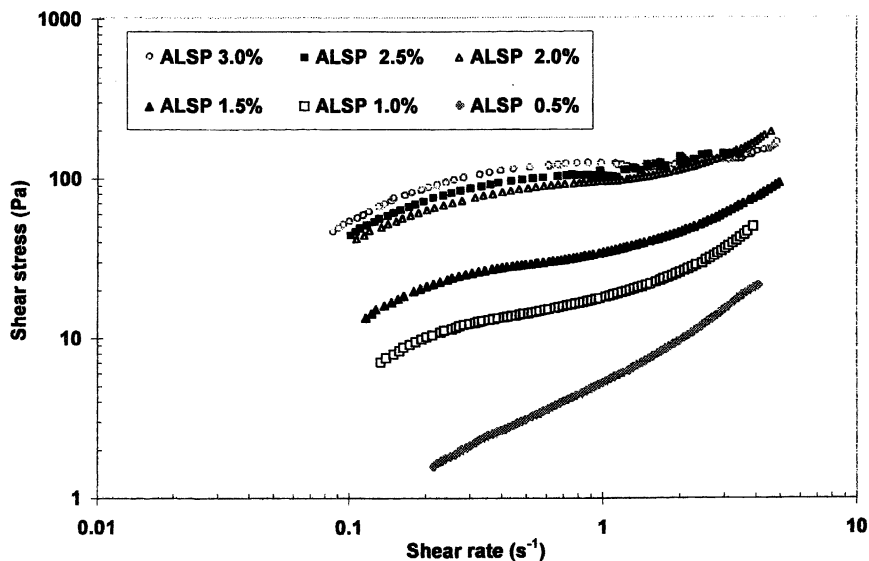


**Figure 1.** *The effect of ALSP concentration on the flow properties of ALSP/HCF gels at 20<sup>o</sup>C.*

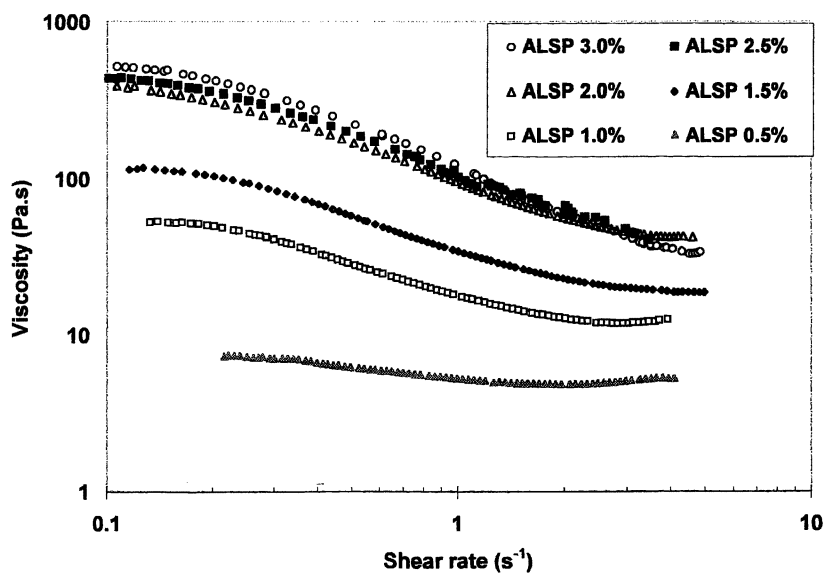
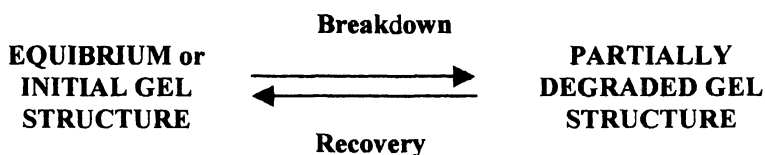


**Figure 2.** *The effect of ALSP concentration on the viscosity of ALSP/HCF gels at 20<sup>o</sup>C.*

shear is an indication of the fluidity of the gel under near static conditions, and as will be discussed later, there are other techniques that allow measurement of gel properties at near zero shear strain. The viscosity,  $\eta_{\infty}$  or more particularly the quantity  $(\eta_0 - \eta_{\infty})$ , indicates the extent of the breakdown of the structure as a result of shear.

For those gels in which shear thinning occurs (ALSP 1-3%), the process can be reversed by either the removal or the reduction of the shear strain rate. That is, the breakdown process is reversible. Each point on the non-linear zone of the flow curve corresponds to a state of dynamic equilibrium between the processes of deformation and recovery of structure of the matrix. The situation can be represented by the following equation:



This behavior is typical of a thixotropic substance where the structure is a function of the shear strain and the shear strain rate. It is imperative therefore that cognizance be taken of any pre-shearing prior to an experimental observation. Furthermore evidence will be presented later confirming that shearing can alter the initial or equilibrium state. A technique of investigating the rate of recovery of the structure will also be discussed.

It is informative to plot the values  $\eta_0$  and  $\eta_{\infty}$  as a function of the ALSP concentration (Figure 3). At low values of ALSP where a discontinuous gel is only beginning to form, the values of  $\eta_0$  and  $\eta_{\infty}$  are relatively close, indicating that the effect of shear strain rate on the structure is minimal. As the concentration of ALSP increases there is a rapid divergence between  $\eta_0$  and  $\eta_{\infty}$  up to an ALSP concentration of 2%, indicating that a substantial supramolecular structure has been formed but has been broken down by shear. Above 2% ALSP there are now relatively small changes in  $\eta_0$  and  $\eta_{\infty}$ .

The plot in Figure 3 can be divided into three regions. In Region I, below an ALSP concentration of 0.5%, the gel is not contiguous, that is, there are gelled volumes separated by low viscosity fluid. The result is best described as a “lumpy” or discontinuous gel. In Region II, (ALSP 0.5 – 2%), the supramolecular structure has grown to encompass the entire volume so that the structure can be described as contiguous and meets one of the definitions of a gel [1]. However, in this condition it is also susceptible to the action of shear strains and can be broken down to yield

a markedly lower viscosity. In Region III, for an ALSP concentration greater than 2%, the three-dimensional structure is complete and the additional ALSP molecules apparently do not add to the viscosity of the structure.

It has been suggested [15] that the structure of the aluminium soap in the hydrocarbon solvent is based on the formation of a linear assembly of aluminium soap molecules as shown in Figure 4. The molecules are bound together by hydrogen bonds to form linear chains which presumably stack to form supramolecular structures similar to that found for the divalent or trivalent metal salts of fatty acids. Because the ALSP form large assemblies by hydrogen bonding, the presence of other polar additives such as polar co-solvents can noticeably affect the rheological properties. For example, ALSP is unable to gel methanol at any concentration. The effect of the presence of different co-solvents on the viscosity behavior of the gels formed with a concentration of ALSP 2% is shown in Figure 5. The gels formed continued to show non-Newtonian and shear-thinning behavior, however, there is a reduction in viscosity that relates directly to the capacity of the co-solvent to disrupt the hydrogen bonding of the ALSP. The order of the effectiveness of the co-solvent follows the values of the polar component of the solubility parameter  $\delta_p$  with hexanol  $\delta_p=2.5$ , acetone  $\delta_p=5.1$ , and methanol  $\delta_p=6$  [18]. The viscosity values for water ( $\delta_p=7.8$ ) are an exception and probably relate to the lack of miscibility of water in the hydrocarbon fuel.

This problem of contamination can be turned to advantage by eliminating the practical difficulty of handling the powder ALSP. It could be more convenient to dissolve the ALSP in a non-gelling polar solvent and then add this solution to the hydrocarbon that one desires to gel. Appropriate candidates in this example would be hexanol, acetone and water.

## Dynamic Oscillation Measurements

Polymer gels exhibit viscoelastic behavior and probing by dynamic oscillation techniques has yielded valuable information on the structure. However, very few equivalent studies have been conducted on low molecular weight organo-gels.

When a gel is subjected to sinusoidal shear oscillation with an angular frequency  $\omega$  and amplitude  $\gamma_0$ , the real  $G'$  and imaginary part  $G''$  of complex shear modulus,  $G^*$  ( $G^* = (G' + iG'')$ ) - known as storage shear modulus and loss modulus respectively- may be obtained. The storage modulus ( $G'$ ) is proportional to the elastic energy that is stored in



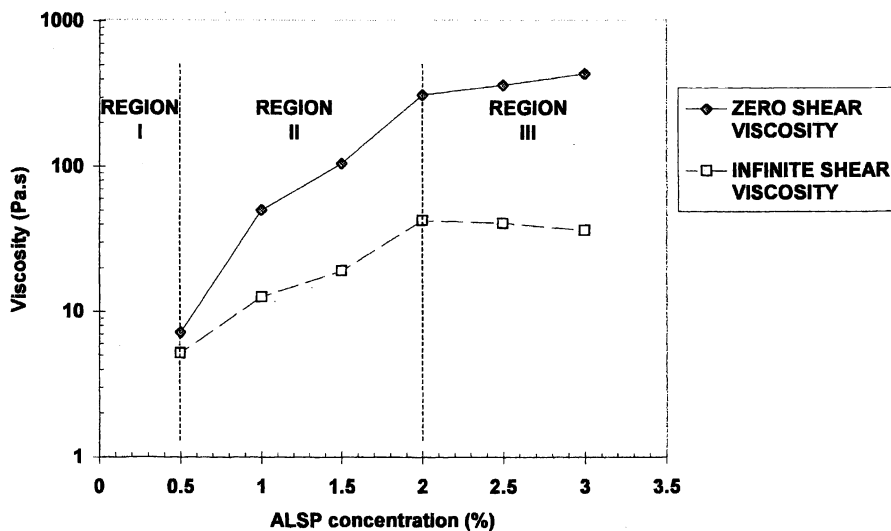


**Figure 3.** Effect of gelator (ALSP) concentrations on zero shear viscosity, and infinite shear viscosity.

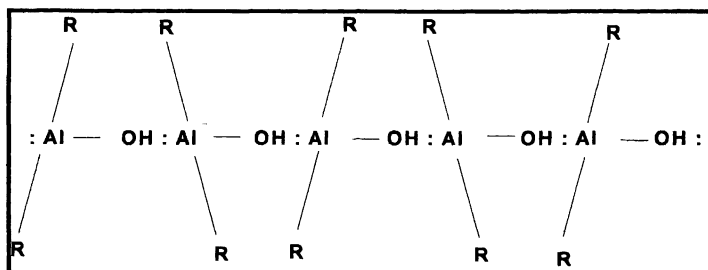


**Figure 4.** Proposed supramolecular structure of aluminum soaps (ALSP) in gels.

viscoelastic material during the period of oscillation, while the loss modulus ( $G''$ ) is proportional to the dissipated or lost energy as heat during oscillation process. The ratio,  $G''/G'$  ( $= \tan\delta$ ), provides an indication of the elastic or viscous nature of the material. For  $\tan\delta < 1$  the structure is more elastic in nature and for  $\tan\delta > 1$  the product is more viscous [19].

The effect of gelator concentration as a function of the angular frequency on storage modulus  $G'$  is shown in Figure 6. The gels with ALSP concentration ranging from 1.0 to 5.0% illustrate that  $G'$  is almost independent of frequency over three decades of frequency. This observation clearly indicates that the relaxation time for these gels is sufficiently small for the molecular rearrangement to occur within the time frame of the experiment. However, the gel with ALSP 0.5% demonstrates a pronounced frequency dependency in 10 to 300  $\text{rads}^{-1}$  range of frequency. The shift in the slope of this plot from positive at low values of ALSP (0.5 – 1%) through to almost zero slope at higher values of ALSP is also seen in many other gel systems, for example, in the gelation of a polymer by cross-linking.

The increase in storage modulus (measured at 1 Hz) is shown as a function of ALSP concentration in Figure 7 for measurements taken with and without preshearing. While there is a general, almost linear increase in modulus with ALSP concentration, there is a noticeable improvement in modulus over a narrow ALSP concentration range where preshear must have the effect of consolidating the structure.

A further complication arose when shearing during the test measurement induced further changes in the modulus. Despite initial thorough dispersion of the gelator in the solvent followed by standing for 24hr, the gels appear to undergo further change if they are pre-sheared and allowed to stand again for 24 hr. Shearing of the gel for ALSP concentrations less than 2% appears to induce a modification of the structure with an increase in modulus. At concentrations of ALSP greater than 2%, a reverse effect occurs where the shearing must disrupt the structure.

The effect of polar contaminants is presented in Figure 8. The gels with ALSP only have the lowest  $\tan\delta$  over the whole range of experimental frequencies indicating that the structure is the most elastic of all samples. On the other hand, values for  $\tan\delta$  for the other systems, at low frequency, are closer to 1 (or is higher than 1) indicating dominance of the viscous part of structure. These findings agree with the steady flow measurements for both the ALSP/HCF gels and those contaminated with co-solvents.

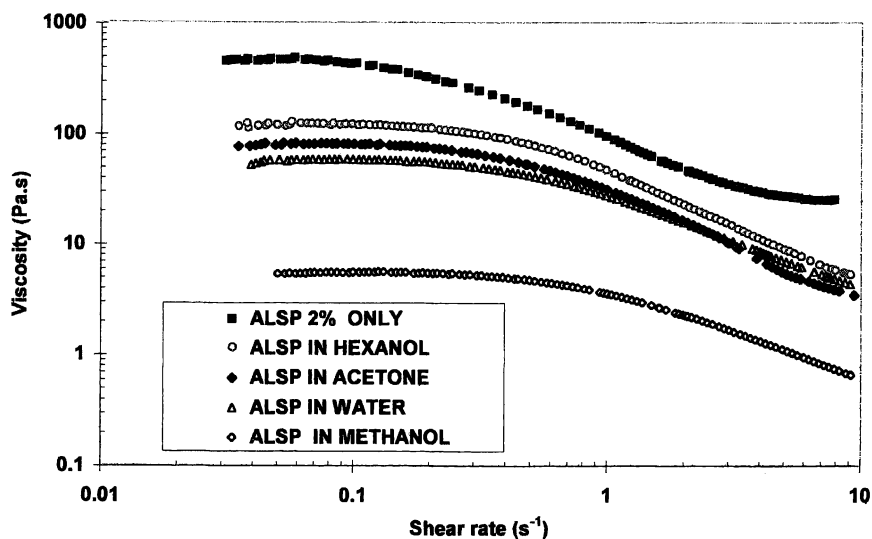


**Figure 5.** *The effect of the addition of polar co-solvents on the viscosity of 2% ALSP/HC gels at 20°C.*

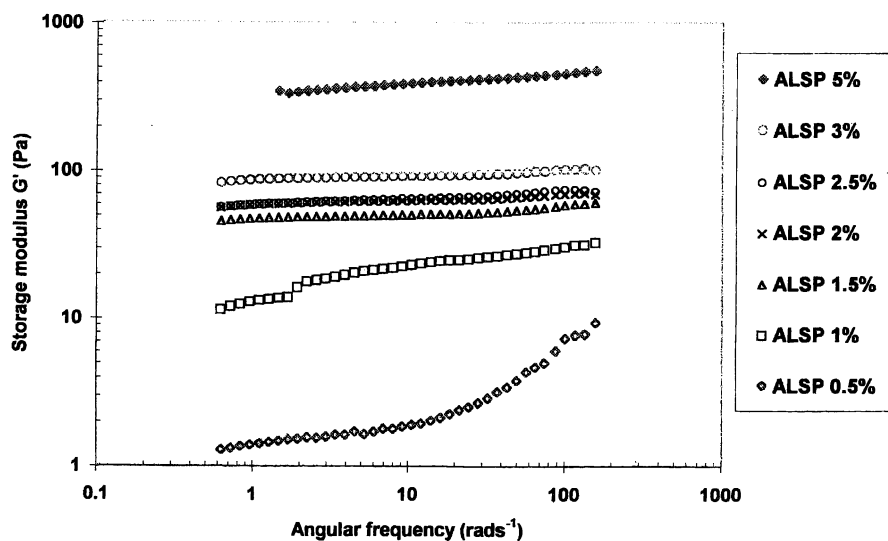


**Figure 6.** *Storage modulus  $G'$  as a function of ALSP concentration and frequency.*

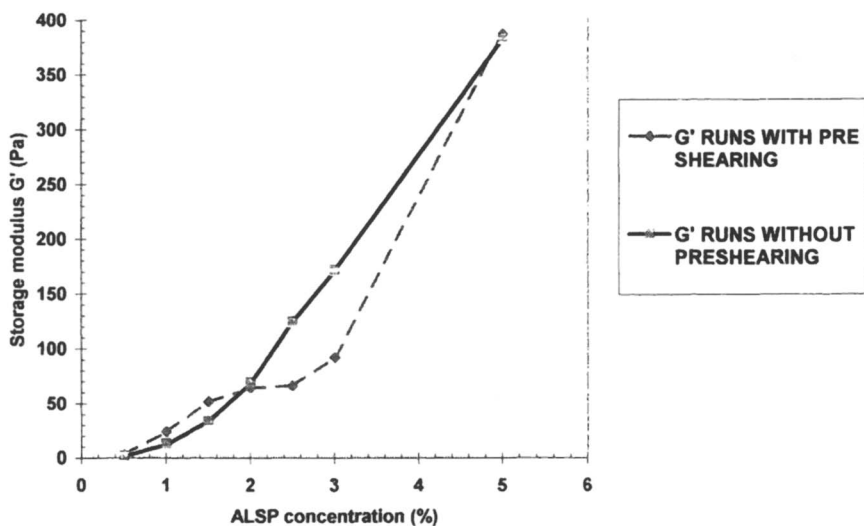


**Figure 7.** *The effect of ALSP concentration on the storage modulus  $G'$  of ALSP/HCF gels.*

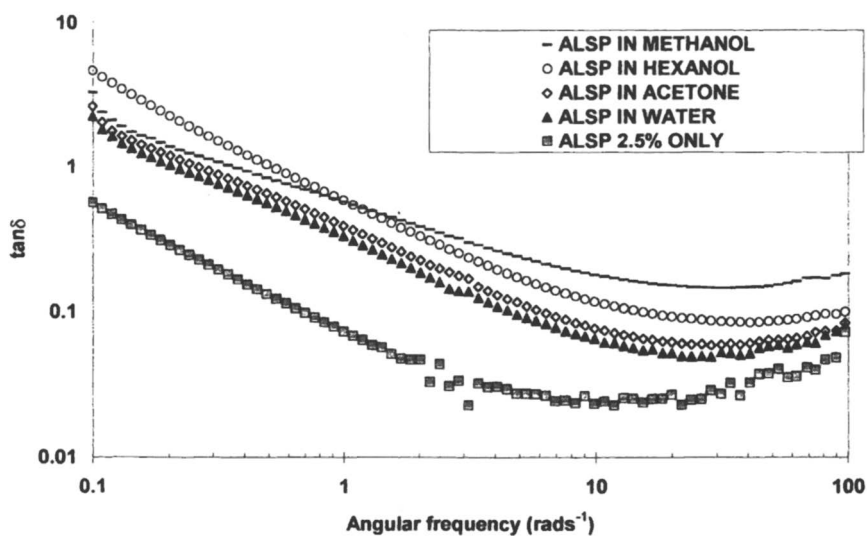


**Figure 8.** *The effect of frequency and co-solvent on  $\tan \delta$  for 2.5 % ALSP/HCF gels at 20 C.*

## Effect of Temperature on the Elasticity of the Gels

Most physical gels are thermoreversible, that is, a rise in temperature can cause the gel to collapse and a decrease in temperature will then allow the gel to reform, in fact, this is how most thermoreversible gels are formed. In the present system however, the gel rapidly forms at room temperature on dispersion of the ALSP.

The 2% ALSP /HCF gel were observed in the dynamic mode as the test temperature was varied from 10 – 40°C, with the maximum (40°C) being dictated by the closeness of the boiling point of the HCF (Figure 9). Surprisingly, the storage modulus increased monotonically from 10 to 40°C. One suggestion is that the increased diffusion at higher temperatures may allow the gel to adopt a more efficient packing of the structure.

## Creep Measurements

In creep measurement a constant tensile stress ( $\sigma$ ) is applied to the sample and the time-related strain  $\epsilon(t)$  is measured. Stress and strain are related by:

$$\epsilon(t) = J(t) \sigma$$

where,  $J(t)$  is the time dependent compliance with units [ $\text{Pa}^{-1}$ ]. This is a material constant similar to that of viscosity ( $\eta$ ) in steady state flow.

The time dependent tensile strain measured for a range of gels of different ALSP concentration is shown in Figure 10. The creep strain curves decrease systematically with an increase in ALSP concentration corresponding to an increase in the rigidity of the structure with further development of the ALSP hydrogen bonded assemblies. It is interesting to note that creep strain continues to slowly increase at long times; another characteristic of physical gels containing labile polar bonds.

## Reversibility of the Gels

From the earlier flow studies it was noted that the structure degraded (reduced  $\eta$ ) under the action of a shear strain, that is, the viscosity  $\eta_0$  was reduced to  $\eta_\infty$ . Constant shear stress studies revealed that this could occur in approximately 10 seconds. If the shear strain was removed, the viscosity  $\eta_0$  could be recovered. To measure the rate of recovery of the structure the following two-step experiment was devised.

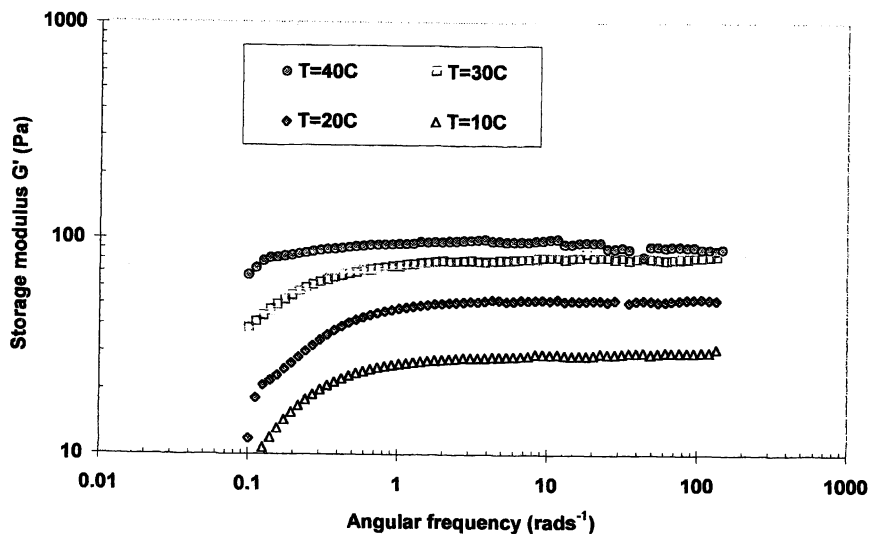


**Figure 9.** *The effect of temperatures on storage modulus  $G'$  for 2% ALSP/HCF gels.*

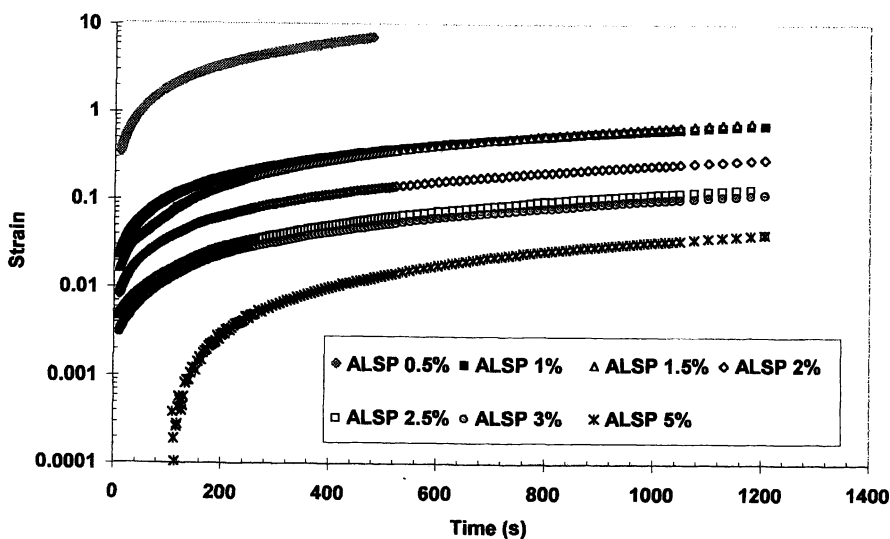


**Figure 10.** *Tensile creep strain behavior of ALSP/HCF gels for different ALSP concentrations at a constant stress of 0.2 Pa and at 20°C.*

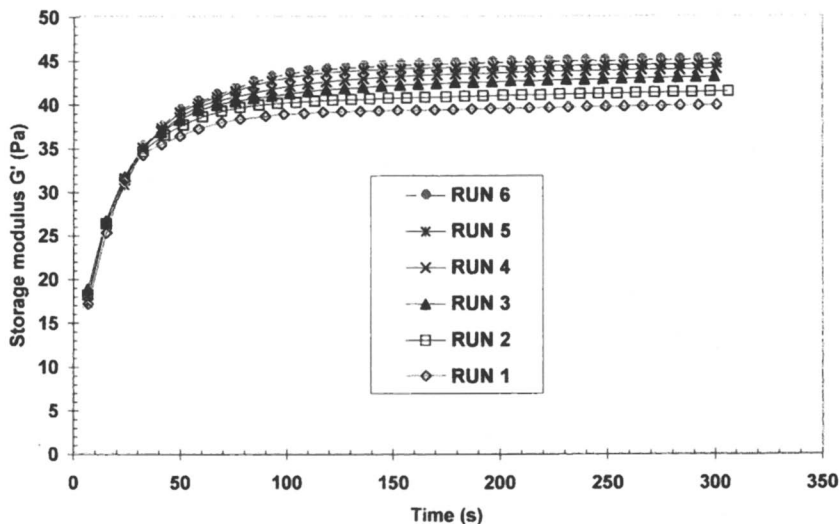


**Figure 11.** Recovery behavior of a 2% ALSP/HCF gel after pre-shearing for 2min with shear strain  $5s^{-1}$ . Six consecutive runs are plotted. Temperature= $20^{\circ}C$ .

The gel was first pre-sheared at a shear strain rate of  $5s^{-1}$  for two minutes in the flow mode. Shearing was then stopped and the dynamic mode (frequency 6Hz and shear stress 1Pa) immediately commenced allowing the recovery in the storage modulus to be measured as function of time. The advantage of the dynamic experiment over the flow experiment is that the shear strain is sufficiently small to prevent significant structure breakdown.

The recovery of storage modulus  $G'$  for a typical gel (ALSP 2.0% concentration) with time is presented in Figure 11. The result indicates that recovery of the structure is a slower process than the breakdown. Additionally, five sets of similar runs were performed on the sample in consecutive order (after finishing of the current run the next one was started immediately and completed automatically). Comparing the consecutive runs from 1 to 6, a marginal but systematic increase in plateau value of  $G'$  (beyond six consecutive runs no further increase was observed) suggesting that some further development of the structure was occurring with additional shearing of the sample. For the gels with ALSP concentrations greater than 2%, recovery behavior was similar.

## Conclusions

Gels formed as result of the addition of small quantities of the gelator ALSP to non-polar hydrocarbon fuel possess complex rheological

properties. The gels are thixotropic and shear thinning and cover a range from liquid-like discontinuous gels through to rigid gels. As a consequence, care must be taken in designing testing regimes that produce reliable and pertinent data. Because the gels possess a structure involving polar bonds, the addition of strongly polar contaminants can have a deleterious effect on the formation of the gel.

## Acknowledgments

The authors would like to thank RITE, Japan for the financial support to carry out this research work.

## References

1. Terech, P.; Weiss, R.G. *Chem. Rev.* **1997**, *97*, 3133-3159.
2. Stepto, R.F.T. In *Comprehensive Polymer Science*; Allen G., Ed, Pergamon Press: New York, 1992; First Supplement.
3. Djabourov, M. *Pol. Inter.* **1991**, *25*, 135.
4. Kavanagh, G.M.; Ross-Murphy, S.B. *Prog. Polym. Sci.* **1998**, *23*, 533.
5. Moghadam, P.E. *Bull. Iranian Petroleum Institute* **1968**, *33*, 112.
6. Bauer, W.H.; Shuster, D.O.; Wiberley, S.E. *Trans. Soc. Rheol.* **1960**, *IV* 315.
7. Terech, P. In *Specialist Surfactants*; Robb, I.D., Ed.; Blackie Acad. and Prof., London, 1996, 209.
8. Lin, Y.; Kachar, B.; Weiss R.G. *J. Am. Chem. Soc.* **1989**, *111*, 5542.
9. Te Nijenhuis, K. *Thermoreversible Networks*; Adv. Pol. Sci. 130, Springer-Verlag: Berlin, 1997.
10. Dokic', P.; Sefer, I.; Sovilj, V. *Progr. Col. Pol. Sci.* **1996**, *102*, 71.
11. Nishinari, K. *Col. Pol. Sci.* **1997**, *275*, 1093.
12. Abdallah, D.J.; Weiss R.G. *Langmuir* **2000**, *16*, 352.
13. Criddle, D.W.C. *J. Rheol.* **1965**, *9*(2), 287.
14. Beerbower, A.; Nixon, J.; Wallace, T.J. *J. Aircraft* **1968**, *5*(4), 367.
15. Beerbower, A.; Philipoff, W. *Aircraft Fluids Fire Hazard Symposium Proceedings*, Ft. Monroe, Va., June 7-8 1966, 86.
16. Teng, J.; Lucas, J.M. *Fed. Av. Admin.*; Washington D.C. 1971.
17. Cohen, L. U.S. Patent 2,741,629, 1956.
18. *Directory of Solvents*; Whim, B.P.; Johnson P.G., Eds.; Blackie Acad. and Prof., London, 1996.
19. Macosko, C.W. *Rheology Principles, Measurements and Applications*, Wiley-VCH: N.Y., 1994.



## Chapter 14

# Rheology of Epoxy–Amine Systems Near the Gel Point

Jean Pascal Eloundou<sup>1</sup>, Jean François Gérard<sup>2</sup>, and Jean Pierre Pascault<sup>2</sup>

<sup>1</sup>Laboratoire de Mécanique des Matériaux et Construction, Ecole Nationale Supérieure Polytechnique, B.P. 8390, Yaoundé, Cameroun

<sup>2</sup>Laboratoire des Matériaux Macromoléculaires, Institut National des Sciences Appliquées de Lyon, 20 Avenue Albert Einstein, 69 621, Villeurbanne Cédex, France

The behavior of epoxy - amine systems was studied by rheology near the gel point. At the gel point, the moduli  $G'$  and  $G''$  verify the equation  $G'(\omega) \propto G''(\omega) \propto \omega^4$ . Near the gel point, viscosity,  $\eta$ , and elastic modulus,  $G'$ , follow power laws of the relative distance from the gel point ( $\eta \propto \varepsilon^{-k}$ ;  $G' \propto \varepsilon^z$ ). The exponents  $\Delta$ ,  $k$  and  $z$  are related one another by the percolation theory and found to be the same as those found in the Rouse model for temperatures higher than  $T_{g\infty}$ .

Many authors have studied theoretically (1-5) and experimentally (6-14) the rheological behavior of physical of and chemical gels. Chemical gels, like epoxy - amine systems, formed of covalent bonds, are irreversible. In this case, polymerization produce a three - dimensional network when one monomer have a functionality greater than 2.

This paper describes theory of percolation and the rheological behavior of

two epoxy – amine systems near the gel point. A low- $T_g$  (flexible) epoxy – amine system based on diglycidyl ether of 1,4 butanediol (*DGEBD*) with 4,9-dioxo-1,12-dodecanediamine (*4D*) and a high- $T_g$  (rigid) epoxy – amine system based on diglycidyl ether of bisphenol A (*DGEBA*) with 4,4'-methylenebis [3-chloro, 2,6-diethylaniline] (*MCDEA*) were considered. The maximum glass transition temperature of the fully cured network,  $T_{g\infty}$  is low for *DGEBD/4D* system, which presents only gelation transition at curing temperatures considered (15).  $T_{g\infty}$  is high for *DGEBA/MCDEA* system, which exhibits gelation and vitrification below  $T_{g\infty}$  (16,17), but only gelation above  $T_{g\infty}$ . The kinetics of these systems is well known (15-17).

## Background

The percolation model (18-20) was developed to describe the properties of branched polymers near the gel point. In the bond percolation model, the monomers that occupied the sites of dimension,  $d$ , are randomly linked with the probability,  $x$ . In the case of epoxy - amine systems,  $x$  is the degree of conversion of epoxy functions. At the first step of the curing, when  $x$  is low, some dimers and trimers develop with chains of low molar masses. As  $x$  increases progressively, larger clusters appear (branched polymers). A low increase of viscosity,  $\eta$ , and of weight average molar mass,  $M_w$ , is then observed as amine and epoxy functions disappear. For a critical value,  $x_{gel}$  the viscosity quickly increases leading to an elastic behavior, which can be observed in rheological measurements. An infinite cluster appears, having a size and a mass that diverge at the gel point. The gelation phenomenon is characterized by the presence of two phases in the reaction medium: the soluble one (small clusters) and the non-soluble one (infinite cluster). Beyond the gel, the soluble fraction decreases while the gel fraction,  $n_g$ , increases. Above  $x_{gel}$ , very large clusters connect to the infinite one to form a network. The finite clusters with an average size decreasing as the reaction proceeds, are included in these very large clusters.

### Structural Parameters

The size distribution of the clusters (number of clusters of mass  $m$ ) is  $N(m) \propto m^{-\tau} f(m/M_z)$  where  $M_z$  is the z-average molar mass, which has the same critical behavior as the mass of the larger cluster before the gel point.  $f(m/M_z)$  is a cut-off function, which implies that, a mass greater than  $M_z$  has a zero probability to exist. In the mean field theory,  $f(m/M_z) = e^{-m/M_z}$ . Beyond the gel point,  $M_z$ , is equivalent to the gel fraction,  $n_g$ . The mass  $m$  is expressed as

a function of the radius of gyration by  $m \propto R^{d_f}$  where  $d_f$  is the fractal dimension of the polymer. The radius,  $\xi$ , of  $M_z$  is called the correlation length. Near the gel point, several quantities diverge as power laws of the relative distance to the gel point,  $\varepsilon$  ( $\varepsilon = |x - x_{gel}| / x_{gel}$ ). This is the case of  $\xi$  ( $\xi \propto \varepsilon^{-\nu}$ ), of  $M_z$  ( $M_z \propto \xi^{d_f} \propto \varepsilon^{-1/\sigma}$ ) and of the mass average molar mass  $M_w$  ( $M_w \propto \varepsilon^{-\gamma}$  with  $\gamma = (3 - \tau)/\sigma$ ). Then,  $d_f = 1/(\sigma\nu)$ . The dimensions  $d$  and  $d_f$  are associated by the hyperscaling law  $d = d_f(\tau - 1)$ . Beyond the gel point, the gel fraction varies as  $n_g = \varepsilon^\beta$  with  $\beta = (\tau - 2)/\sigma$ . Table 1 give the values of critical exponents in three-dimensional percolation ( $d = 3$ ) and in classical or mean field theory.

**Table 1. Critical exponents in three-dimensional percolation and classical or mean field theory**

Exponent	Percolation 3D	Classical theory	Scaling law
$\gamma$	1,74	1	$\overline{M}_w \propto \varepsilon^{-\gamma}$
$\beta$	0,45	1	$n_g \propto \varepsilon^\beta$
$\tau$	2,2	2,5	$N(m) \propto m^{-\tau} f(m/M_z)$
$\sigma$	0,46	0,5	$\overline{M}_z \propto \varepsilon^{-1/\sigma}$
$\nu$	0,88	0,5	$\xi \propto \varepsilon^{-\nu}$
$d_f$	2,5	4	$m \propto R^{d_f}$

## Rheological Behavior

Before the gel point ( $x < x_{gel}$ ), the steady state shear viscosity,  $\eta$ , follows a power law ( $\eta \propto \varepsilon^{-k}$ ). Beyond the gel point ( $x > x_{gel}$ ), the equilibrium modulus,  $G$ , varies as  $G \propto \varepsilon^z$ .

Considering the electrical analogy  $\eta$  corresponds to the conductivity of a mixture of superconductors and conductors, and  $x_{gel}$  is the supraconduction threshold.  $G$  corresponds to the conduction of a mixture of conductors and insulators and  $x_{gel}$  is the conduction threshold. In this way, three-dimensional simulations lead to  $k = 0.75 \pm 0.04$  (18) and  $z = 1.94 \pm 0.01$  (19).

In the Rouse model approach, the macromolecule is considered as a bead spring free of any hydrodynamic interaction with the solvent, which then can be of the same nature as the polymer. This approach can be applied to the case of a

reaction proceeding in bulk. Then, the viscosity is purely entropic and varies as the mass-average square of the radius of gyration,  $\langle R^2 \rangle_w$  (18). The calculations made in this case lead to  $\eta \propto M_z^{2-\tau+2/d_f} \propto \varepsilon^{(2-\tau+2/d_f)/\sigma} \propto \varepsilon^{\beta-2\nu}$ . In three-dimensional percolation model,  $k = \beta - 2\nu$ , thus  $k = 1.33$ .

Close to the gel point, the equation  $m \propto R^{d_f}$  shows that the clusters forming the "polymolecular medium" are described in terms of fractal geometry. The fractal domain corresponds to scaling lengths included between the monomer size and the correlation length,  $\xi$ , which varies as the size of the largest cluster (20). If the fractal dimension describes the way the object occupies the volume, however, it gives no indication on the connectivity. Then, a spectral dimension,  $d_s$ , was introduced (1,2) which reflects connectivity and takes into account the diffusion as well as the transfer phenomena in the network. This spectral dimension is given by  $N_i \propto t^{d_s/2}$  where  $N_i$  is the number of distinct sites visited during a random walk in the network.

The number of steps executed is proportional to the time,  $t$ , of the random walk and is connected to the average radius,  $R_w$ , of the visited space by means of the fractal dimension of the random walk in the network ( $t \propto R_w^{d_w}$ ). The three dimensions  $d_f$ ,  $d_s$  and  $d_w$  verify the relation  $d_s = 2d_f / d_w$ .

By comparing the percolating system with a mixture of conductors and insulators beyond the gel point, we obtain (1)  $d_s = 2d_f / [2 + (z - \beta) / \nu]$ . Alexander and Orbach (1) have observed, from various simulations, that the spectral dimension is always close to 4/3 in the case of percolation with a space dimension,  $d$ , between 1 and 6. For  $z = 1.94$ , the value  $d_s = 1.35$  was found.

The existence of a fractal domain is expressed by a distribution of relaxation times,  $\lambda$  (time taken by a cluster to diffuse on a length equal to its own radius), from a lower limit,  $\lambda_0$ , to an upper limit  $\lambda_z$  (20). The upper limit eliminates the problem of the divergence of the largest cluster size when approaching the gel point, and the lower limit takes into account the similarity loss for very small dimensions.

The viscoelastic measurements showed that, at the gel point, the distribution of relaxation times obeys a power law  $H(\lambda) d \ln \lambda \propto \lambda^{-A} d \ln \lambda$  (6-8). The shear relaxation modulus, which describes the relaxation strain proceeding from a constant shear deformation, can be obtained by  $G(t) = \int_0^\infty [H(\lambda) / \lambda] e^{-t/\tau} d\lambda$  with  $\lambda_0 < t < \lambda_z$  (21). When applying the Fourier transform to this equation, we obtain  $G(\omega) \propto \omega^A$  with  $1/\lambda_z < \omega < 1/\lambda_0$  (21). It appears, then, that  $G'$  and  $G''$  vary according to a power law of the angular frequency,  $\omega$

( $G'(\omega) \propto G''(\omega) \propto \omega^4$  with  $\omega^* < \omega < \omega_0$ ) between two limits  $\omega^* = 1/\lambda_z$  and  $\omega_0 = 1/\lambda_0$ . The measurement frequencies are generally very low compared to  $\omega_0$ , which corresponds to the monomer size. Generally, only  $\omega^*$  is taken into account. Thus, as the frequency is lower than  $\omega^*$ , (i) before the gel point, the medium can be considered as a Newtonian liquid for which  $G'$  and  $G''$  are proportional to  $\omega^2$  and to  $\omega$ , respectively; (ii) after the gel point, the medium is equivalent to an elastic solid for which  $G'$  is constant and  $G''$  are proportional to  $\omega$ ; (iii) at the gel point, when an infinite macromolecule appears,  $\omega^*$  tends towards 0 (21). Using the Kronig-Kramers relations at the gel point,  $G''/G' = \tan \delta = \tan(\pi\Delta/2)$  (21).

### Relations between Static and Dynamic Exponents

Many authors (1-5) successfully connect the exponents  $\Delta$ ,  $k$ ,  $z$ ,  $\sigma$ ,  $\tau$ , and  $\nu$  with the dimensions  $d$ ,  $d_f$ ,  $d_s$ , and  $d_w$ .

In the Rouse model, for which the hydrodynamic interactions are totally screened, the relaxation time,  $\lambda_n$ , of a cluster of mass,  $M'$ , is proportional to  $M'$  (20,22). The surroundings of a molecule of mass  $M$  are based on smaller fractals, which relax at times,  $\lambda_i < \lambda' \propto M'$ , and of larger clusters considered as immobile in the time scale of the testing (5). The diffusion factor  $D_i$  ( $D_i \propto R^2/\lambda$ ) is then inversely proportional to the mass. In the Zimm limit of the excluded volume, where the hydrodynamic interactions are strong, the diffusion factor is given by the Stokes-Einstein relation and varies as  $R^{2-d}$ . Martin et al (5) showed that the exponent  $k$  must be between a lower limit (Zimm) and an upper limit (Rouse) ( $0 < k < \nu(d_f + 2 - d)$ ). Then,  $d/(d_f + 2) < \Delta < 1$  and as  $\Delta = d\nu/(d\nu + k)$  and  $z = d\nu$ , we obtain  $\Delta = z/(z + k)$ . Restricting their approach to the Rouse model, Rubinstein et al. (4) proposed  $d_s = 2d_f/(d_f + 2)$ ,  $k = 2/\sigma d_s - (\tau - 1)/\sigma$  and  $z = (\tau - 1)/\sigma$ . It can be showed that these equations are the same as those found by Martin et al (5). Then, in a three-dimensional percolation,  $d_s$ ,  $k$  and  $z$  are found to be equal to 1.11, 1.33 and 2.67, respectively. The expression  $\Delta = d/(d_f + 2)$  was also established by Muthukumar (2), who studied the dependence of the dynamic viscosity on the frequency in dense media ( $\eta^* \propto \omega^{4-d}$ ), where the hydrodynamic interactions are completely screened (Rouse model).

The value  $d_s = 1.11$  found by Rubinstein et al (4) is different from that presented by Alexander and Orbach ( $d_s = 1.33$ ) (1). However, it can be noticed that  $d_s = 1.11$  is obtained in three-dimensional percolation if the value  $z = 2.67$  in

equation  $d_s = 2d_f / [2 + (z - \beta) / \nu]$ . Both values of  $d_s$  lead to  $\Delta = 0.67$ . In the electrical analogy, the equation  $\Delta = z / (z + k)$  lead to  $\Delta = 0.72$ .

In the case of an ideal gel, where the crosslinks are linked each other by "phantom chains" (i.e., there is no interaction with the adjoining chains), the elastic modulus is inversely proportional to the number,  $N$ , of units that constitute these chains ( $G \propto kT / N$  where  $k$  is the Boltzman constant and  $T$  the absolute temperature). Each of these effective chains, included in a correlation volume  $\xi^d$ , constitutes a fractal cell of dimension  $d_f$ , thus,  $N$  and  $G$  are proportional to  $\xi^{d_f}$  and  $\xi^{-d_f}$  respectively. As  $\omega \propto 1/t \propto R_w^{-d_w}$ , then  $G \propto \omega^{d_f/d_w} \propto \omega^{d_f/2} \propto \omega^\Delta$ . For  $d_s = 4/3$ ,  $\Delta = 0.66$ .

Table 2 gives the theoretical values of critical exponents in the Rouse model and the electrical analogy.

**Table 2. Theoretical values of critical exponents in the Rouse model and the electrical analogy**

<i>Exponent</i>	<i>Rouse model</i>	<i>Electrical analogy</i>	<i>Scaling law</i>
$d_s$	1,11	1,33	$N_t \propto t^{d_s/2}$
$k$	1,33	0,75	$\eta \propto \varepsilon^{-k}$
$z$	2,67	1,94	$G \propto \varepsilon^z$
$\Delta$	0,67	0,72	$G^* \propto \omega^\Delta$

For Martin et al. (5), the modulus, which is purely entropic, is proportional to the density of correlation blobs in the gel ( $G \propto kT / \xi^d$ ). As  $\omega \propto 1/t \propto R_w^{-d_w}$ , then  $G \propto \omega^{d/d_w} \propto \omega^{(d/2)(d_f/d_f)} \propto \omega^\Delta$ . Taking  $d_s = 1.11$ , the value  $\Delta = 0.67$  is found in three-dimensional percolation.

The approach developed by Martin et al (5) seems more realistic. Using the equations in the text, we can find that  $G \propto \xi^{-d}$ ,  $d\nu = d_f\nu + \beta = 1/\sigma + \beta$  and  $G \propto kTn_g / M_z$ . In this way, it can be connected with the rubber elasticity theory, in which the elastic modulus is proportional to the density of the elastically active network chains (23).

## Experimental Part

Experimental procedures have been described earlier (12-14). All reagents are used as received from supplier. The measurements were done for a stoichiometric ratio of epoxy to amino hydrogens equal to 1.

Steady state measurements of viscosity were performed at constant temperature with a Searle Contraves Rheomat 115 type viscosimeter. Unfortunately, the maximum temperature allowed with this apparatus is 90°C.

Dynamic mechanical spectra of both systems were obtained using a Rheometrics Dynamic Analyser (RDA 700 or RDA II) equipped with a parallel plates tool during isothermal curings. For *DGEBD/4D* system, the shear strain was fixed to 5% and a small frequency range was used in frequency sweep mode, due to the very low viscosity of the initial monomer mixture. For *DGEBA/MCDEA* system, the shear strain varies from 50% in the liquid state to 1% in the solid state. The high value of the deformation in the liquid state allows us to obtain accurate values of the real part of the dynamic viscosity,  $\eta'$ . The frequency range depends on the curing temperature. The low limit of the frequency range must be sufficiently low to consider the change of modulus negligible during testing. Then, at the gel time for which the derivative of the logarithm of the complex modulus,  $G^*$  is close to its maximum value, we must have  $(1/G^*)(\partial G^*/\partial t)(2\pi/\omega) < 0.1$ .

## Experimental Curves

The dependence of the viscosity,  $\eta$  as a function of time is given in *Figure 1*. A very rapid increase of  $\eta$  can be observed for times close to 140 min. *Figure 2* shows a curve of the real part of the complex viscosity,  $\eta'$  versus time.

### Temperatures Greater than $T_{g\infty}$ (Gelation Only)

At curing temperatures greater than  $T_{g\infty}$  the curves of elastic modulus,  $G'$ , loss modulus,  $G''$  and loss factor,  $\tan\delta$  versus time exhibit the same behavior for both systems (*Figures 3 and 4*):

- The greater the frequency is, the earlier  $G'$  appears before the gel point; then  $G'$  varies quickly close to the gel point, takes a value independent on the frequency beyond the gel point and reaches a constant value at the rubbery plateau (*Figure 3*).

- The appearance of  $G''$  well before the gel point allows us to obtain the real part,  $\eta'$  of the complex viscosity ( $\eta^* = G''/\omega$ );  $G''$  depends on the frequency beyond the gel point (Figure 3).
- There exists a time for which the value of  $\tan\delta$  is independent on the frequency as indicated by the crossover of  $\tan\delta$  versus time curves; beyond the gel point, the evolution of  $\tan\delta$  is slower, leading to a constant value depending on the frequency (Figure 4).

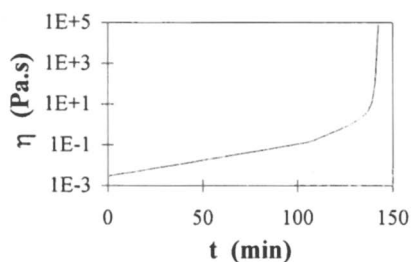


Figure 1. Viscosity versus time at 50°C (DGEBD/4D) (12)

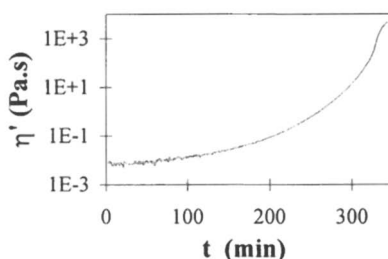


Figure 2. Real Part of complex viscosity versus time at 135°C (DGEBA/MCDEA) (13)

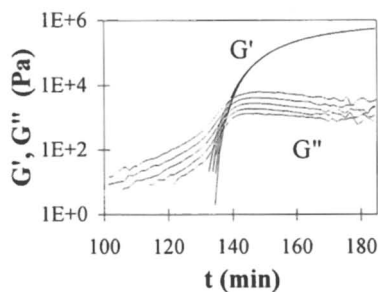


Figure 3. Moduli  $G'$  and  $G''$  versus time curves at 50°C (DGEBD/4D) (12)

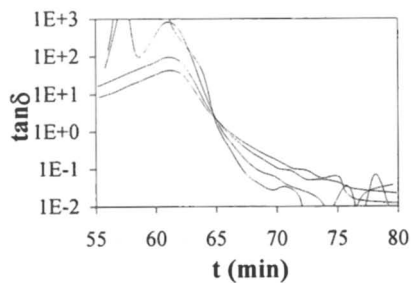


Figure 4. Loss factor versus time curves at 180°C (DGEBA/MCDEA) (13)

### Temperatures Lower than $T_{g\omega}$ (Gelation and Vitrification)

The DGEBA/MCDEA system was also investigated at temperatures below  $T_{g\omega}$  (Figures 5, 6). It can be observed:



- An increase of  $G'$  after the rubbery plateau.
- A maximum on  $G''$  and  $\tan\delta$  versus time curves; the time of the maximum is all the greater than the frequency is low.

The behavior of  $G'$ ,  $G''$  and  $\tan\delta$  beyond the gel point is characteristic of the vitrification ( $\alpha$  relaxation).

The crossover on  $\tan\delta$  versus time curves still exists, even at low curing temperatures near  $_{gel}T_g$ , temperature at which gelation and vitrification occur simultaneously. Nevertheless, at these temperatures, gelation is strongly disrupted by vitrification, as higher frequencies no longer participate to the gelation.

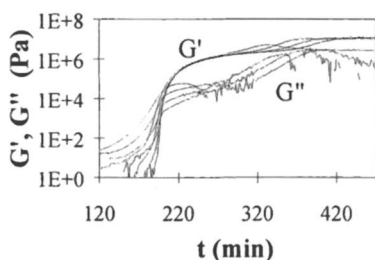


Figure 5. Moduli  $G'$  and  $G''$  versus time curves at 150°C (DGEBA/MCDEA) (13)

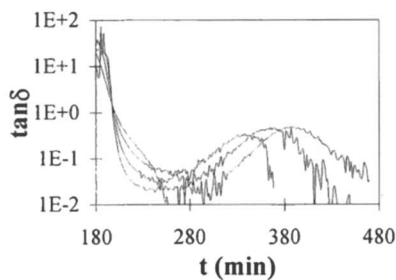


Figure 6. Loss factor versus time curves at 150°C (DGEBA/MCDEA) (13)

## Behavior at the Gel Point

The times,  $t_1$  (DGEBD/4D system only) and  $t_2$  corresponding respectively to  $\eta = 1000$  Pa.s and the crossover of  $\tan\delta$  versus time curves are measured. On the other hand, the representation of  $\log G'$  and  $\log G''$  as function of  $\log\omega$  shows that there exists a time,  $t_3$  for which these curves are parallel straight lines (Figure 7), i.e. the equation  $G'(\omega) \propto G''(\omega) \propto \omega^4$  is verified. Time  $t_3$  can be measured at all the curing temperatures for both systems, except at 80°C for DGEBA/MCDEA. At this temperature close to  $_{gel}T_g$ , gelation is strongly disrupted by vitrification. Times  $t_1$ ,  $t_2$  and  $t_3$  are found to be very close to those obtained by the method of insoluble fractions in tetrahydrofuran (15-17). Then the three methods allow measuring the gel time. Moreover, these times follow an

Arrhenius law (Figure 8). The activation energies are close to those found for the rate constants in kinetics equations ( $60.3 \text{ kJ}\cdot\text{mol}^{-1}$  and  $58.3 \text{ kJ}\cdot\text{mol}^{-1}$  for *DGEBD/4D* (15);  $56.1 \text{ kJ}\cdot\text{mol}^{-1}$  and  $59.4 \text{ kJ}\cdot\text{mol}^{-1}$  for *DGEBA/MCDEA* (16)).

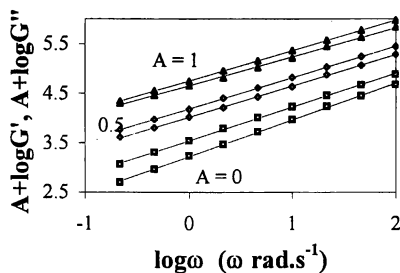


Figure 7.  $\log G'$  and  $\log G''$  versus  $\log \omega$  near the gel point (*DGEBA/MCDEA*) (13)

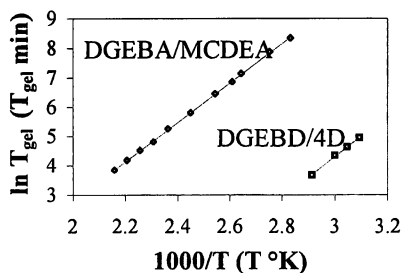


Figure 8 Arrhenius plot of gel times (12, 13)

## Behavior near the Gel Point

From kinetics equations (15-17),  $\eta$ ,  $\eta'$  and  $G'$  can be expressed in terms of conversion of epoxy functions,  $x$ . Figures 9 and 10 represent the  $\log \eta$  versus  $\log \varepsilon$  curves and the  $\log \eta'$  versus  $\log \varepsilon$  curves, respectively ( $\varepsilon$  is the relative distance to the gel point). These curves are straight lines at all the curing temperatures for both systems. Likewise, the  $\log G'$  versus  $\log \varepsilon$  curves are represented by straight lines in Figure 11.

Straight lines in Figures 9, 10 and 11 show that equations  $\eta \propto \varepsilon^{-k}$  and  $G \propto \varepsilon^z$  are verified. Exponents  $k$  and  $z$  are the slope of these straight lines. Exponent  $z$  depends of the frequency, following the equation  $z = z_0 + a \log \omega$  where  $z_0$  corresponds to the angular frequency  $\omega = 1 \text{ rad}\cdot\text{s}^{-1}$  (Figure 12). The gel times used to calculate the relative distance from the gel point  $\varepsilon$  are indicated in each figure.

## Discussion and conclusion

Figure 13 contains the variations of exponents  $\Delta$ ,  $k$  and  $z_0$  as functions of curing temperatures. Two cases must be considered.

### Temperatures Greater than $T_{g\infty}$ (Gelation Only)

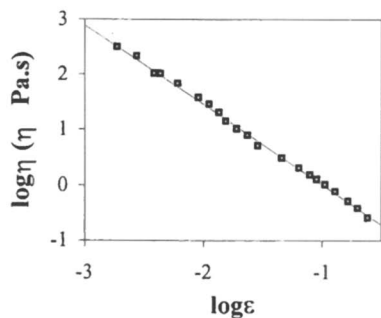


Figure 9.  $\log \eta$  versus  $\log \epsilon$  at 50°C (DGEBD/4D) (gel time  $t_1$ ) (12)

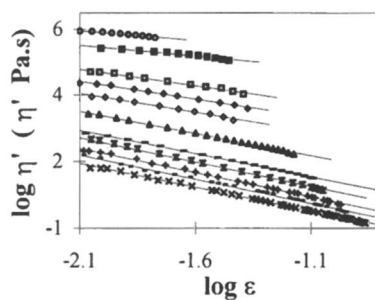


Figure 10.  $\log \eta'$  versus  $\log \epsilon$  (DGEBA/MCDEA) (gel time  $t_2$ ) (13)

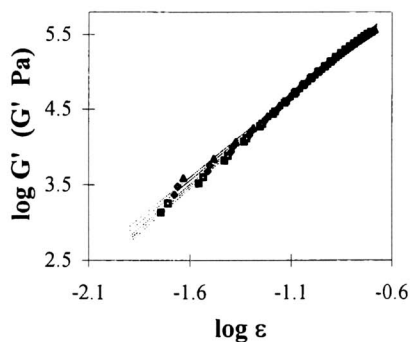


Figure 11.  $\log G'$  versus  $\log \epsilon$  (DGEBD/4D) (gel time  $t_2$ ) (12)

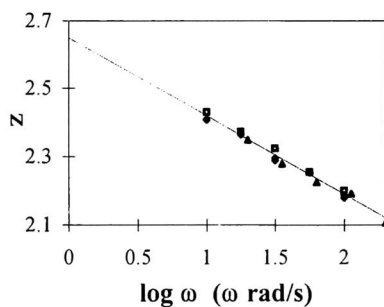


Figure 12. Exponent  $z$  versus  $\log \omega$  (DGEBD/4D) (12)

*DGEBD/4D* and to 180°C and 190°C for *DGEBD/MCDEA* system. Exponents  $\Delta$ ,  $k$  and  $z_0$  remain constant with temperature and their values are close to those predicted by the percolation theory in the Rouse model (Table 3). Some authors find similar values for other epoxy - amine system studied at curing temperatures greater than  $T_{g\infty}$  ( $\Delta = 0.72 \pm 0.02$  (9),  $\Delta = 0.70 \pm 0.03$  (10) and  $k = 1.3 \pm 0.2$  (10) for *DGEBA/Jeffamine D400* system;  $\Delta = 0.70 \pm 0.05$ ,  $k = 1.4 \pm 0.2$  and  $z_0 = 2.8 \pm 0.2$  for *DGEBA/diethanolamine* system (11)).

**Table 3. Exponents  $\Delta$ ,  $k$  and  $z_0$  at Temperatures Greater than  $T_{g\infty}$ .**

Systems	$\Delta$	$k$	$z_0$
DEBD/4D	$0.70 \pm 0.01$	$1.44 \pm 0.02$	$2.65 \pm 0.02$
DGEBA/MCDEA	$0.69 \pm 0.01$	$1.43 \pm 0.02$	$2.51 \pm 0.04$
Rouse model	0.67	1.33	2.67

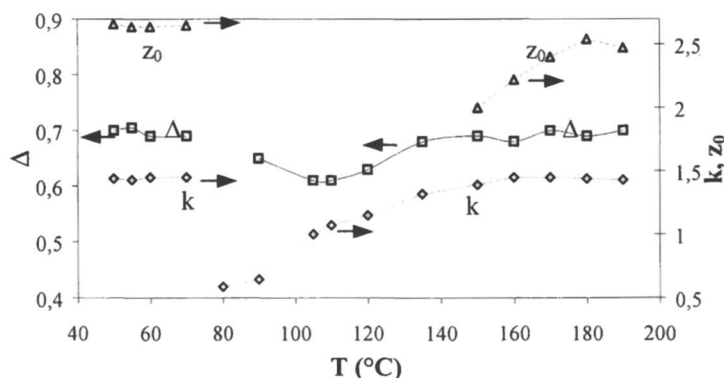


Figure 13. Exponents  $\Delta$ ,  $k$ ,  $z_0$  versus temperature (12, 13)

### Temperatures Lower than $T_{g\infty}$ (Gelation and Vitrification)

These temperatures concern only the *DGEBA/MCDEA* system.

From 170°C to 150°C,  $z_0$  decreases while  $\Delta$  and  $k$  remain almost constant. This variation means that  $z_0$ , which governs the behavior of the reaction bath after the gel point, is more sensitive to the vitrification than  $\Delta$  and  $k$ . Mean values of  $\Delta$  and  $k$  ( $0.69 \pm 0.01$  and  $1.43 \pm 0.03$  respectively) show that the reaction bath still follows the Rouse model before the gel point.

disturbed by vitrification. Motions of molecular chains become slow with relaxation times larger and larger. This behavior favors the elastic modulus  $G'$  to the detriment of the loss modulus  $G''$ . The consequence is the decrease of the loss factor  $\tan\delta$  and exponent  $\Delta$  with the temperature. Then the molecular bath is no longer a polymolecular distribution of fractals at temperatures slower than 150°C.

## References

1. Alexander, S.; Orbach, R. *J. Phys. (Paris) Lett.* **1982**, *43*, L625
2. Muthukumar, M. *J. Chem. Phys.* **1985**, *83*, 3162
3. Hess, W.; Vilgis, T. A.; Winter, H. H. *Macromolecules*, **1988**, *21* 2536
4. Rubinstein, M.; Colby, R.; Gillmor, J. R. *Polym. Prepr., Am. Chem. Soc. Div. Polym. Chem.* **1989**, *30*, 81
5. Martin, J. E.; Adolf, D.; Wilconxon J. P. *Phys. Rev.* **1989**, *A39*, 1325
6. Durand, D.; Delsanti, M.; Adam, M.; Luck, T. M. *Europhys. Lett.* **1987**, *3*, 277
7. Chambon, F.; Winter, H. H. *J. Rheol.* **1987**, *31*, 683
8. Izuka, A.; Winter, H. H.; Hashimoto, T. *Macromolecules*. **1994**, *27*, 6883
9. Matjeka, L. *Polym. Bull.* **1991**, *26*, 109
10. Miaoling, L. H.; Williams, J. G. *Macromolecules* **1994**, *27*, 7423
11. Adolf, D.; Martin J. E. *Macromolecules* **1990**, *23*, 3700
12. Eloundou, J. P.; Fève, M.; Gérard, J. F.; Harran, D.; Pascault, J. P. *Macromolecules* **1996**, *29*,6907
13. Eloundou, J. P.; Gérard, J. F.; Harran, D.; Pascault, J. P. *Macromolecules* **1996**, *29*,6917
14. Eloundou, J. P.; Ayina, O.; Noah Ngamveng, J. *Eur. Polym. J.* **1998**, *34*, 1331
15. Eloundou, J. P.; Fève, M.; Harran, D.; Pascault, J. P. *Angew. Makromol. Chem.* **1995**, *220*, 13
16. Girard-Reydet, E.; Riccardi, C. C.; Sautereau, H.; Pascault, J. P. *Macromolecules* **1995**, *28*, 7599
17. Eloundou, J. P.; Ayina, O.; Ntede, N. G.; Gérard, J. F.; Pascault, J. P.; Boiteux, G.; Seytre, G. *J. Polym. Sci. Part B: Polym. Phys.* **1998**, *36*,2911
18. de Gennes, P. G. *C. R. Acad. Sci. Ser. B* **1978**, *286*, 131
19. Derrida, B.; Stauffer, D.; Hermann, H. J.; Vannimenus, J. *J. Phys. (Paris) Lett.* **1983**, *44*, L701; **1984**, *45*, L913
20. Stauffer, D.; Coniglio, A.; Adam, M. *Adv. Polym. Sci.* **1982**, *44*, 103
21. Ferry, J. D. *Viscoelastic properties of Polymers*, 3<sup>rd</sup> ed.; Wiley: New York, 1980
22. Hodson, D. F.; Amis, E. J. *Phys. Rev. A* **1990**, *41*, 1182
23. Graessley, W. W. *Macromolecules* **1975**, *8*, 186

## Chapter 15

# Amphiphilic Hydrogels with Highly Ordered Hydrophobic Dendritic Domains

Ivan Gitsov, Thomas Lys, and Chao Zhu

Faculty of Chemistry, College of Environmental Science and Forestry,  
State University of New York, Syracuse, NY 13210

This chapter describes the synthesis of amphiphilic hydrogels with highly organized crosslink junctions based on the reaction of poly(ethylene) glycol, PEG, and perfectly branched (dendritic) macromolecules. The synthetic strategy employs linear PEG with isocyanate end-groups as the hydrophilic component and hydrophobic dendritic poly(benzyl ethers) with amino-groups at the periphery. It is found that the crosslinking reaction proceeds fast at room temperature the efficiency being governed by the stoichiometric ratio of the two building blocks. The swelling of the gels formed is affected by the relative PEG content, by the polarity of the medium and the temperature.

## Introduction

The remarkable biocompatibility of poly(ethylene glycol), PEG, and its good solubility in organic and aqueous media enabled the widespread use of this hydrophilic polymer as one of the major components in the formation of

synthetic hydrogels (1). These water-swollen networks find increasing usage as phase-transfer agents (2), supports for catalysts in different organic reactions (3), as devices for controlled release of pharmacological substances (4), materials for cell immobilization and encapsulation (5), as size-selective polymerization media (6) and others.

The procedures used in the formation of PEG hydrogels can be divided in three main groups: 1) Formation of physical networks by specific interactions of designated segments in the polymer chains or by entanglement of macromolecules with very high molecular weight (7). This method yields materials that are usually free of impurities like residual cross-linking agents – an important requirement for any biomedical application. The deficiencies of the physical gels are in their easy disruption by relatively small mechanical forces or by changes in temperature and solvents. 2) Radiation induced cross-linking of PEG and PEG derivatives and copolymers (8). This approach also produces pure hydrogels and their degree of cross-linking can be conveniently controlled by the dose of irradiation. The disadvantages of the method are in the high limits in polymer molecular weights ( $M_w > 500,000$ ) and the relatively high occurrence of defects in the network with pending linear chains. 3) Chemical cross-linking by copolymerization of PEG macromonomers and selected bifunctional comonomers or by modification of preformed functionalized polymers and copolymers (9). In this method the network density can be controlled by the concentration of the cross-linking agent, but additional purification of the gel is necessary to remove the unreacted cross-linker. It should be mentioned that all three methods yield gels with a random distribution of cross-links (junctions) and interjunction molecular weights. Another common disadvantage of the hydrogels formed by all three methods is the relatively small size of their hydrophobic junctions and the ill-defined macromolecular organization of these junctions. Both drawbacks ultimately affect not only the encapsulation and release rates into and from the gels, but also their binding capacity. While the randomness in the interjunction molecular weights could possibly be eliminated by a reaction of telechelic PEGs and multifunctional cross-linking agents, very few studies have been published on the incorporation of large well-structured hydrophobic domains in amphiphilic hydrogels despite the obvious advantages they might offer (10). It was found, for example, that hydrogels containing linear or cyclic siloxane segments exhibit a much stronger affinity towards various hydrophobic molecules in comparison to conventional linear and crosslinked PEGs (10).

Dendritic macromolecules would be ideal candidates for cross-linking agents (11). They have highly symmetrical, perfectly branched structure and multiple reactive sites placed in the interior and at the periphery of the macromolecules. The number (density) of the junctions and their chemical composition can be easily controlled by the generation of the dendrimer (*i.e.* the number of reactive groups therein) and the chemistry used in the construction.

The fractal character of the dendritic interior provides unique possibilities for size-selective encapsulation, manipulation and release of different substrates. Surprisingly, publications on dendrimer networks are rather scarce (12). In addition, in all known studies only small molecules have been used to form the links between the dendritic fragments (network junctions).

The goal of this study is to explore the synthesis of amphiphilic hydrogels using telechelic PEG and surface-functionalized poly(benzyl ether) dendrimers. The networks formed should have randomly distributed linear (hydrophilic) and globular (hydrophobic) segments, but with precisely engineered size and chemical composition of both components.

## Experimental section

**Materials.** Poly(ethylene glycol) diisocyanate with PEG molecular weight 3,400 and  $M_w/M_n = 1.03$  was obtained from Shearwater Polymers and was stored at  $-10^\circ\text{C}$  under nitrogen atmosphere prior to use. Triethylamine, 3,5-dihydroxybenzylalcohol, 18-crown-6 and 1,1,1-tris(4-hydroxyphenyl) ethane - all from Aldrich;  $\alpha$ -bromo-*p*-tolunitrile,  $\text{LiAlH}_4$  and  $\text{K}_2\text{CO}_3$  from ACROS (Fisher Scientific), were used without further purification. Dichloromethane and tetrahydrofuran (THF) were dried over  $\text{P}_2\text{O}_5$  and benzophenone-sodium, respectively, and distilled immediately before use.

**Instrumentation.** FT-IR analyses were performed on a Nicolet 410 spectrophotometer from 500 to  $4\,000\text{ cm}^{-1}$ . The materials were analyzed as thin films on disposable IR cards (3M, Type 62 TPEF films).  $^1\text{H-NMR}$  spectra were recorded in  $\text{CDCl}_3$  or  $\text{DMSO-d}_6$  when necessary (also used as internal standards) at room temperature on a Bruker Avance 300 instrument operating at 300 MHz. Size-exclusion chromatography (SEC) analyses were performed on a SEC line consisting of a 510 pump, U6K universal injector, 486 tunable UV detector (all Waters) and a Refractomonitor IV (Milton-Roy). The separations were achieved at  $40^\circ\text{C}$  across a set of three  $5\ \mu\text{m}$  SDV columns (Polymer Standards Service) with THF eluting at 1 mL/min. DSC data were acquired on a Seiko DSC 220 calorimeter in a heating/cooling/heating cycle between  $-100^\circ\text{C}$  and  $100^\circ\text{C}$  with a scanning rate  $10^\circ\text{C}/\text{min}$ .

**Synthesis.** Poly(benzyl ether) dendrimers with amino groups at the periphery were obtained from cyano-terminated precursors by modifications of known methods (13).

*Preparation of the protected monomer  $(\text{NC})_2\text{-[G-1]-OH}$ .* In a three-neck round-bottom flask,  $\text{K}_2\text{CO}_3$  (4 equiv.) was added to 150 ml of acetone under nitrogen. 1 equiv. of 3,5-dihydroxybenzylalcohol and 2.05 equiv. of  $\alpha$ -bromo-*p*-tolunitrile were added to the solution under stirring, followed by 0.3 equiv. of 18-crown-6. The solution was kept under vigorous stirring, nitrogen and reflux



for 24 hours, the evolution of the reaction being checked by thin layer chromatography (TLC). The mixture was allowed to cool down and was filtered to remove  $K_2CO_3$ . The solvent was evaporated to dryness, the crude product was extracted three times with water and  $CH_2Cl_2$  and the combined organic layers were dried with  $MgSO_4$ . The solvent was evaporated to dryness, a white-brown solid was recovered and then analyzed by  $^1H$ -NMR.  $^1H$ -NMR ( $CDCl_3$ ):  $\delta$  7.7 (4H, d, ArCH), 7.55 (4H, d, ArCH), 6.65 (2H, s, ArCH), 6.5 (1H, s, ArCH), 5.1 (4H, s,  $CH_2$ ), 4.6 (2H, s,  $CH_2$ ), 1.75 (1H, s, OH).

#### General Procedure for the Synthesis of Dendritic Benzyl Bromides.

These reactions were carried out on a scale of 0.5 - 10g, depending on generation number. To a solution of the corresponding dendritic benzyl alcohol (1.000 equiv.) in the minimum amount of tetrahydrofuran were added  $CBr_4$  (1.25 equiv.) and triphenylphosphine (1.25 equiv.) and the reaction mixture was stirred at room temperature under nitrogen. Typically, the reaction mixture changed from a transparent to a white solution with a precipitate forming over time (1 to 5 minutes depending on the generation). The progress of the reaction was monitored by TLC and additional amounts of carbon tetrabromide and triphenylphosphine were added at 15-min intervals until reaction was complete. Decomposition was observed when the mixture was turning bright yellow, followed by green and then brown if the reaction was not stopped. The reaction was quenched by addition of a large amount of water and  $CH_2Cl_2$ . The aqueous layer was extracted with  $CH_2Cl_2$  (3x), the combined  $CH_2Cl_2$  extracts were dried and concentrated under reduced pressure.

$(NC)_2$ -[G-1]-Br. This was prepared from  $(NC)_2$ -[G-1]-OH and 1.25 equiv. of  $CBr_4$  and  $PPh_3$ . The product was recrystallized in MeOH to give white crystals.  $^1H$ -NMR ( $CDCl_3$ ):  $\delta$  7.7 (4H, d, ArCH), 7.55 (4H, d, ArCH), 6.65 (2H, s, ArCH), 6.5 (1H, s, ArCH), 5.1 (4H, s,  $CH_2$ ), 4.4 (2H, s,  $CH_2$ )

#### General procedure for the synthesis of cyano-terminated tridendrons.

A mixture of the particular dendritic cyano-benzyl bromide (3.10 equiv.), 1,1,1-tris(4-hydroxyphenyl)ethane (1.00 equiv.), dry  $K_2CO_3$  (4.0 equiv.) and 18-crown-6 (0.3 equiv.) in acetone was heated at reflux and stirred vigorously under nitrogen for 36 h. The reaction mixture was allowed to cool down and evaporated to dryness under reduced pressure. The residue was partitioned between water and  $CH_2Cl_2$  (3x), the combined organic layers were then dried and the solvent was distilled off. The crude product was purified by flash chromatography, eluting with 1:4 hexane/ $CH_2Cl_2$  to give a colorless glass.

$\{(NC)_2$ -[G-1] $\}_3$ -C- $CH_3$ . Selected spectral data:  $^1H$ -NMR ( $CDCl_3$ ):  $\delta$  7.66 (12H, d, ArCH), 7.51 (12H, d, ArCH), 7.02 (6H, d, ArCH), 6.8 (6H, d, ArCH), 6.7 (6H, s, ArCH), 6.5 (3H, s, ArCH), 5.1 (12H, s,  $CH_2$ ), 4.95 (6H, s,  $CH_2$ ), 2.1 (3H, s,  $CH_3$ ). FT-IR:  $\nu$ : 2908, 2230, 1606, 1505, 1166, 827  $cm^{-1}$

#### General Procedure for the synthesis of amino-terminated tridendrons.

To a solution of  $LiAlH_4$  (2 equiv. per CN function) in dry THF was added dropwise under vigorous stirring a solution of THF containing the appropriate

cyano-terminated tridendron. The reaction mixture was heated under reflux overnight. The mixture was allowed to cool down and then quenched with sodium hydroxide. After filtration, the solvent was evaporated to dryness. The glassy product was then purified by flash chromatography, eluting with 1:4 hexane/CH<sub>2</sub>Cl<sub>2</sub> to give a yellow glass. The amino-terminated tridendron was characterized by <sup>1</sup>H-NMR, and FT-IR.

$\{(H_2NCH_2)_2-[G-1]\}_3-C-CH_3$ . Selected spectral data: <sup>1</sup>H-NMR (DMSO-d<sub>6</sub>): δ 7.4 (24H, d, ArCH), 6.9 (12H, d, ArCH), 6.7 (6H, s, ArCH), 6.6 (3H, s, ArCH), 5.1 (12H, s, CH<sub>2</sub>), 5 (6H, s, CH<sub>2</sub>), 3.7 (12H, s, CH<sub>2</sub>), 2.8 (12H, s broad, NH<sub>2</sub>), 2.05 (3H, s, CH<sub>3</sub>). FT-IR: ν: 3370, 3297, 3025, 2859, 1600, 1155, 830 cm<sup>-1</sup>

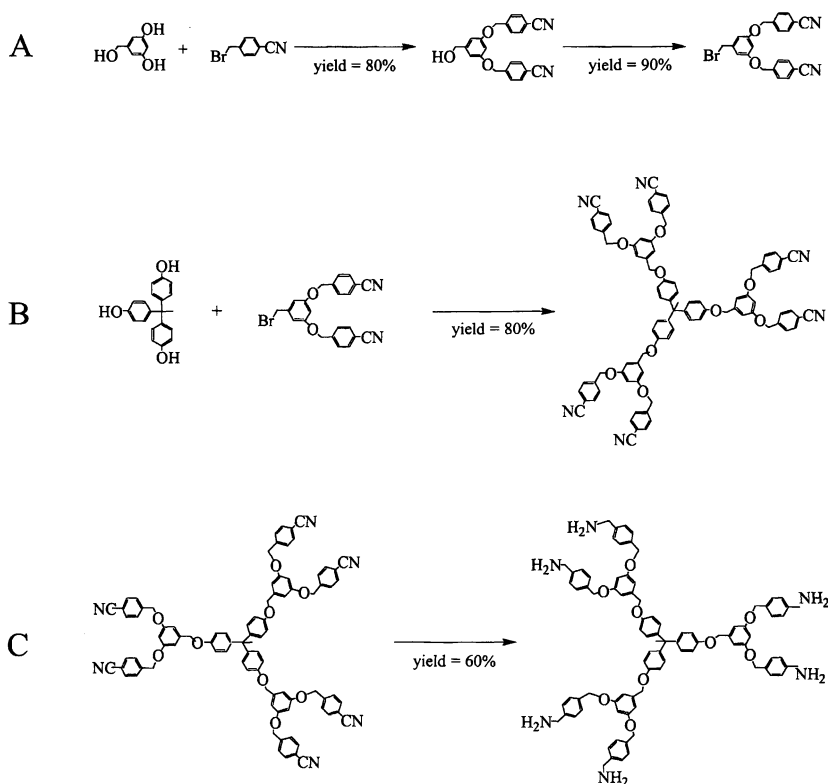
**General Procedure for Gel synthesis.** To a solution of the appropriate amino-terminated tridendron in DMF was added at 0°C the solution of the diisocyanate PEG in dry CH<sub>2</sub>Cl<sub>2</sub> and a small amount of triethylamine. The solution was allowed to warm up to room temperature under stirring within 1 hour. The solvent was removed under reduced pressure. Selected spectral data: <sup>1</sup>H-NMR (DMSO-d<sub>6</sub>): δ 7.4 (24H, d, ArCH), 6.9 (12H, d, ArCH), 6.7 (6H, s, ArCH), 6.6 (3H, s, ArCH), 5.1 (12H, s, CH<sub>2</sub>), 5 (6H, s, CH<sub>2</sub>), 3.7 (12H, s, CH<sub>2</sub>), 3.5 (H, s, CH<sub>2</sub>CH<sub>2</sub>O), 2.05 (3H, s, CH<sub>3</sub>). FT-IR: ν: 3370, 2866, 1971, 1679, 1467, 837, 532 cm<sup>-1</sup>

## Results and Discussion

**Synthesis of amino-terminated tridendrons.** The preparation of the cyano-terminated monodendrons of different generation is achieved by the convergent growth method (13) using 3,5-dihydroxybenzyl alcohol as shown in Scheme 1A. The purity of the products formed is checked by <sup>1</sup>H-NMR (Figure 1a). The subsequent step is a coupling of the dendritic wedges to a core molecule - 1,1,1-tris(4-hydroxyphenyl)ethane using chemistry similar to the dendrimers' growth (Scheme 1B). The product is purified by conventional flash chromatography. The efficiency of the coupling and the purity of the final product are estimated by SEC and <sup>1</sup>H-NMR techniques. SEC eluograms contain only one peak with a polydispersity of 1.04. In the <sup>1</sup>H-NMR spectra (Figure 1, b), the protons of the aromatic rings in the core can be observed clearly as a pair of doublets at 6.98-7.02 and 6.81-6.84 ppm, well separated from the signals due to protons of the aromatic rings in the dendritic wedges. The protons of the methyl group in the core show as a singlet peak at 2.12 ppm. The ratio of the aromatic protons in the core to those of the dendritic wedges provides useful information for the extent of the coupling reaction. In the final step, the cyano-terminated tridendrons can be reduced by LiAlH<sub>4</sub>, Scheme 1C. It should be mentioned that, up to this time, we are not able to produce the amino-terminated tridendrons in a satisfactory yield. The difficulties arise during the isolation of

the final product due to the strong polarity of the amino-terminated tridendrons. For example, the first generation amino-terminated tridendron has 6 amino groups at the periphery of the molecule. The flash chromatography, used traditionally to purify dendrimers of this type, is not very effective to elute quantitatively the amino-terminated tridendron out of the column. Despite the relatively low yield, amino-terminated first generation tridendrons can still be obtained by  $\text{LiAlH}_4$  reduction in pure form.

Scheme 1



The  $^1\text{H-NMR}$  spectrum of the product is recorded in  $\text{DMSO-d}_6$  (Figure 1c). The fine structure of the peaks due to the aromatic protons disappears, but the integration corresponds to the expected number of protons. The new peak at 3.70 ppm is due to the protons of the benzylic  $\text{CH}_2$ -group next to the peripheral amino-groups. The broad peak of the protons in these groups can be seen between 2.5 and 3.0 ppm. The integration of the peaks corresponds to 12 protons (*i.e.* 6  $\text{NH}_2$  groups) – a good indication for the complete reduction of the

6 cyano-groups. The presence of the amino-groups in the tridendron is also evidenced by the absorption bands at 3370 and 3297  $\text{cm}^{-1}$  in the IR-spectrum of the isolated compound, Figure 2b.

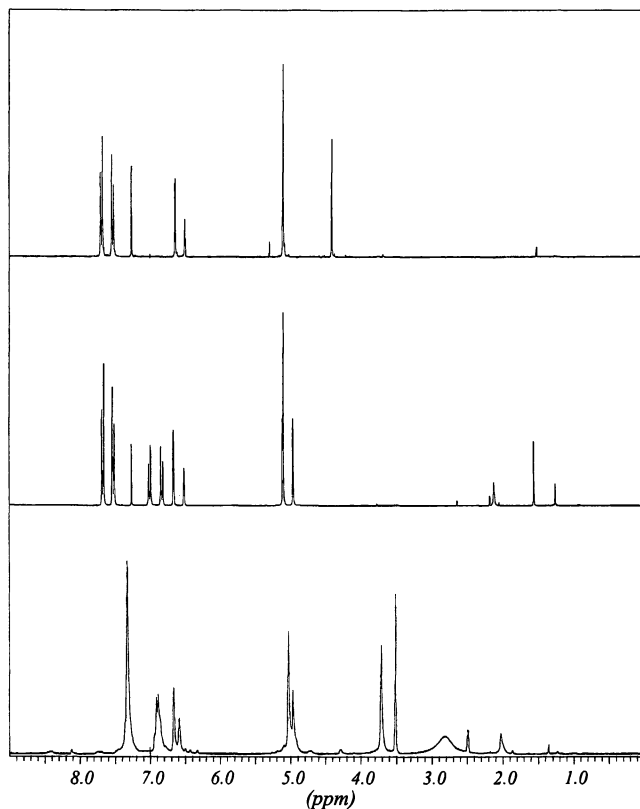
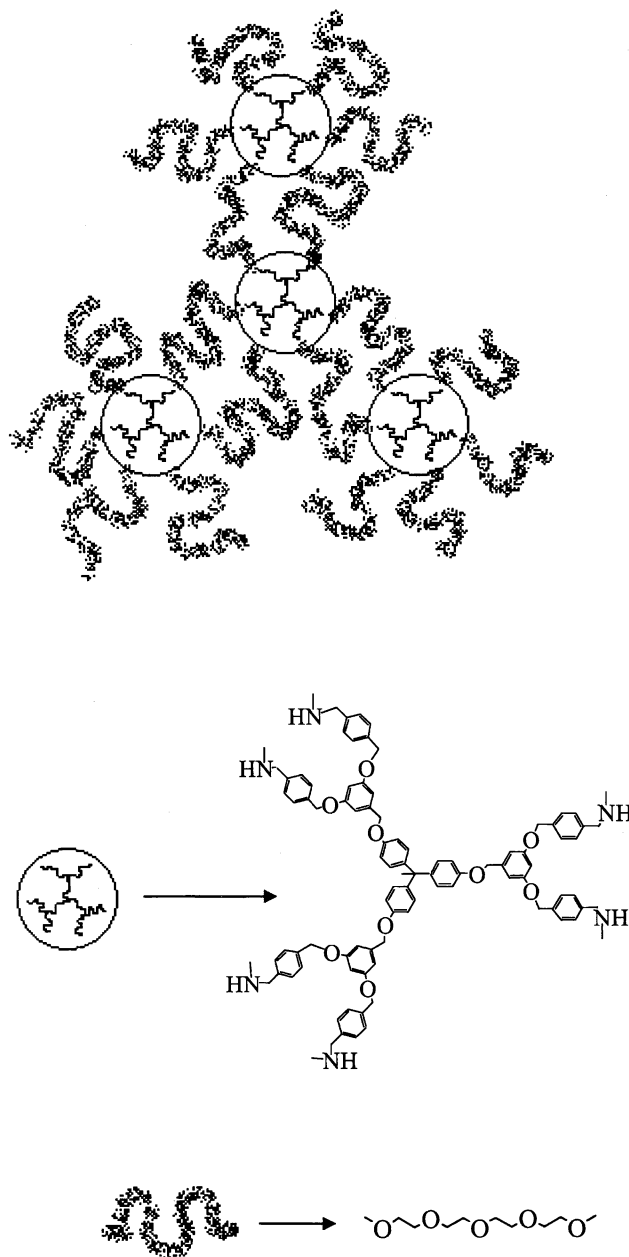
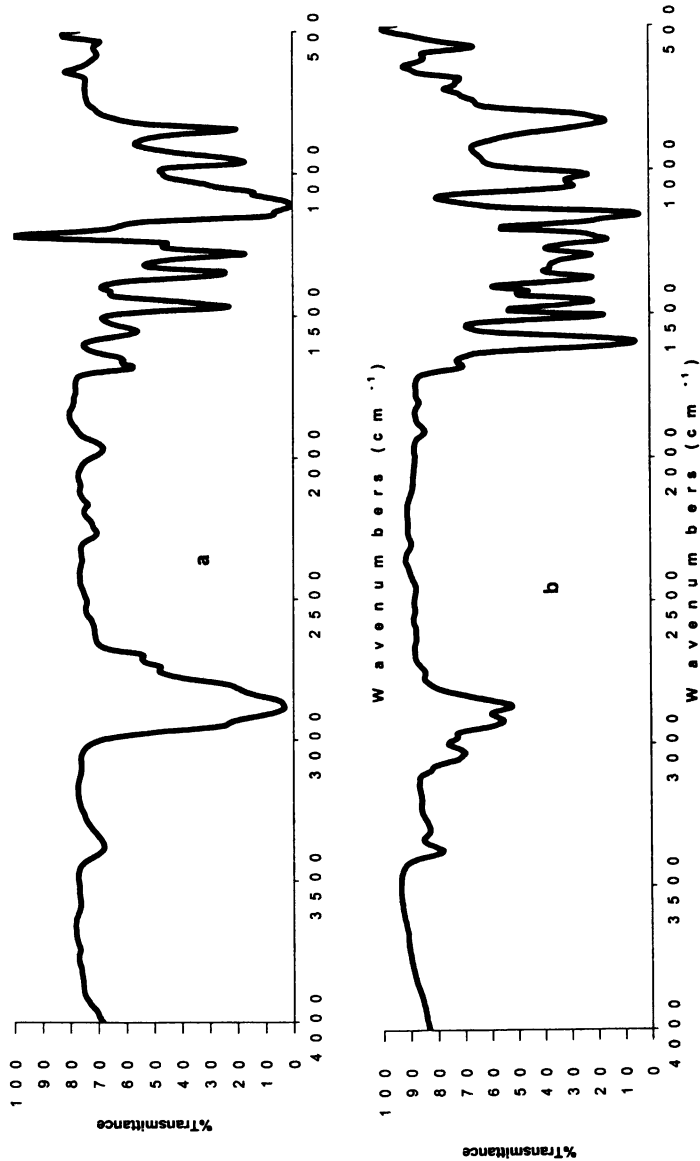


Figure 1.  $^1\text{H-NMR}$  spectra of: a)  $(\text{NC})_2\text{-[G-1]-Br}$  in  $\text{CDCl}_3$ ; b)  $\{(\text{NC})_2\text{-[G-1]}\}_3\text{-C-CH}_3$  in  $\text{CDCl}_3$ ; c)  $\{(\text{H}_2\text{NCH}_2)_2\text{-[G-1]}\}_3\text{-C-CH}_3$  in  $\text{DMSO-d}_6$

**Synthesis of the hydrogels.** The formation of the amphiphilic hydrogels is achieved by a surface-to-surface connection of the dendritic fragments. The synthetic strategy is based on the interaction of two macromolecules – a hydrophilic linear PEG with reactive groups at the extremities of the chain and a hydrophobic dendritic poly(benzyl ether) with reactive sites placed at the periphery (surface) of the molecule, Scheme 2.

Scheme 2





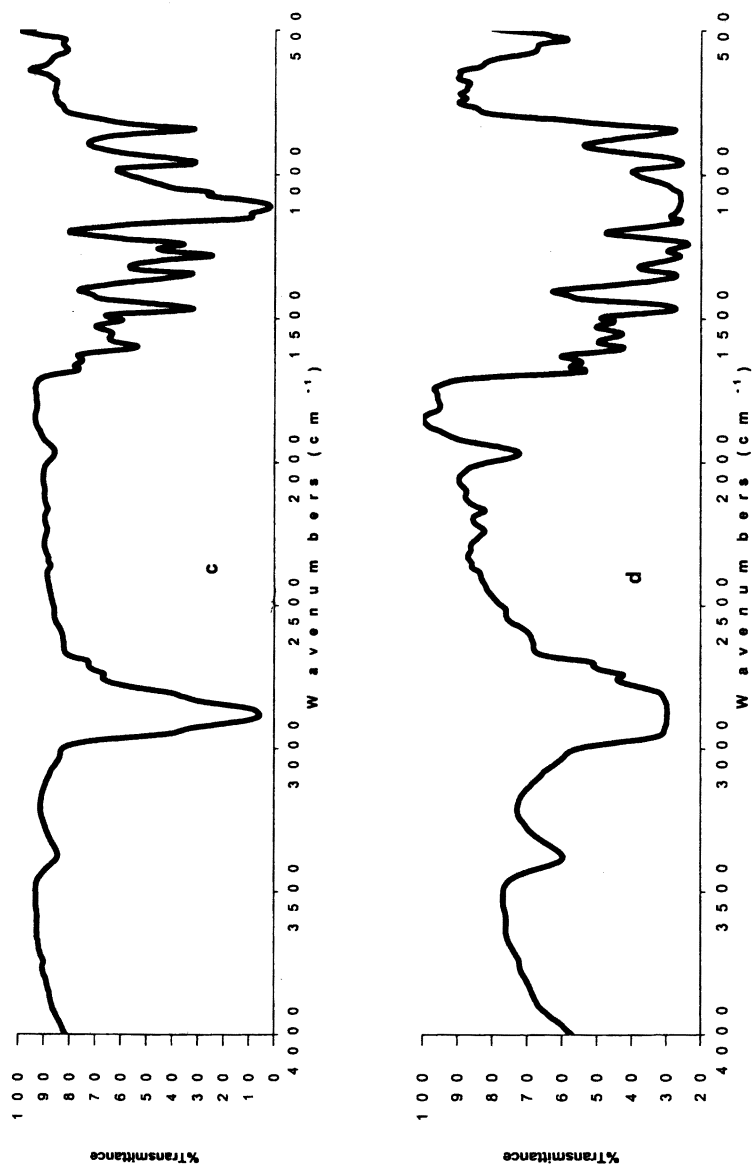


Figure 2. FT-IR spectra of: a) (OCN)-PEG3400-(NCO); b)  $\{(H_2NCH_2)_7[G-1]\}_3-C-CH_3$ ; c) cross-linked product (PEG/dendrimer = 1.5); d) cross-linked product (PEG/dendrimer = 3)

The network can be formed by several different chemistries depending on the nature of the participating reactive groups. In this report we concentrate on a single type of linkage, but several other scenarios are also possible. Initially we explored the gel formation based on the interaction of PEG diisocyanate with amino-terminated tridendrons. Solution of the amino-terminated tridendron in dry DMF and solution of the PEG diisocyanate in dry dichloromethane are introduced into a reaction flask at 0°C, then the resulting clear homogeneous mixture is allowed to warm up to room temperature in the presence of the trace of triethylamine. The reaction mixture turns milky with the increase in temperature, and the viscosity also increases. After the solvents' removal, the hydrogel forms a white film with good mechanical strength and adhesion to glass.

The cross-linking reaction can be conveniently monitored by FT-IR spectroscopy. The conversion is assumed complete after the disappearance of the characteristic isocyanate and the primary amino group bands at 2265 cm<sup>-1</sup> and 3370 - 3297 cm<sup>-1</sup>, respectively (Figure 2a and b).

To test the influence of the steric hindrance on the coupling efficiency, we performed the reaction with the two different ratios of the amino-terminated tridendrons to the PEG diisocyanate - 1:1.5 and 1:3. These ratios correspond to full cross-linking (1:3) and 50% reaction (1:1.5). In the IR spectra of the cross-linked products, the distinctive peaks for the NH<sub>2</sub> groups are transformed almost quantitatively into absorptions characteristic for secondary amino groups, which proves that the cross-linking reaction took place (Figure 2c and d). Interestingly, the gels' IR spectra still contain a very weak peak at 2265 cm<sup>-1</sup> for the stoichiometric feeding ratio of dendrimer:PEG = 1:3 (Figure 2d), while for the other feeding ratio (1:1.5), this absorption disappears completely, Figure 2,c. The possible reason, for the incomplete reaction, is the steric hindrance experienced by the approaching macromolecular PEG reagent. Due to the crowded periphery of the dendritic wedges, not all NH<sub>2</sub> functions are accessible for the isocyanate groups at the extremities of the PEG chain. Therefore, for the stoichiometric feeding ratio, some of the isocyanate groups will remain in the gel, and show the weak peak in the IR. <sup>1</sup>H-NMR spectroscopy is not so useful in the quantitative evaluation of the cross-linking process (Figure 3). The signal of CH<sub>2</sub> protons in the PEG is rather strong and prevents the accurate integration of protons in the dendritic wedges, Figure 3c. It is seen that the aromatic protons from the dendrimer are still present in the gel while the broad peak for the amino groups disappears in the region from 2.50 to 3.00 ppm.

**Characterization of the Hydrogels.** The swelling behavior of both networks formed with first-generation dendrimers shows clearly their hydrophilic properties due to the PEG as the dominant component. It also reflects the differences in their crosslinking density and the solubility of the two distinct building blocks in solvents of various polarity (Tables I and II). In water the gels form stable flocculates regardless of the cross-linking ratio and can be split under a weak external mechanic force, such as stirring. The volume swelling ratio in this solvent goes up to 3 while the weight swelling is significantly higher ranging between 5.5 and 7.8, respectively. It is interesting to



note that the swelling ratio is visibly affected by heating the solvents where PEG has limited solubility at room temperature (Tables I and II).

The thermal behavior of the gel is also strongly influenced by the PEG as revealed by DSC, Figure 4. The melting transition ( $T_m$ ) of the gel occurs at 48.3°C, which is very close to  $T_m$  of the initial PEG (48.7°C).

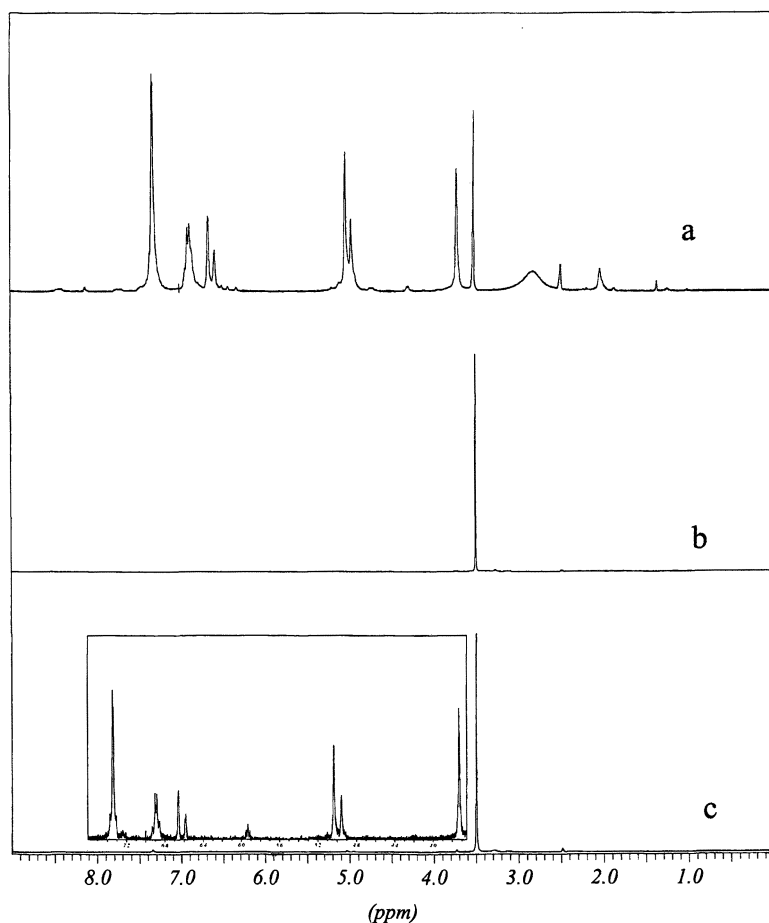


Figure 3.  $^1\text{H-NMR}$  spectra in  $\text{DMSO-}d_6$  of: a)  $\{(H_2NCH_2)_2-[G-1]\}_3\text{-C-CH}_3$ ; b)  $(\text{OCN})\text{-PEG3400-(NCO)}$ ; c) cross-linked product (PEG / dendrimer = 1.5)

**Table I. Weight Swelling Ratio of Hydrogels Formed by Crosslinking of First Generation Amino-terminated Tridendron with PEG-diisocyanate (feeding ratio of tridendron to PEG = 1: 1.5)**

Solvent	Temperature, (°C)			
	Room Temperature (20)	40	60	80
Water	5.5	5.8 (4.8) <sup>1</sup>	5.2 (4.9)	4.1 (4.1)
Toluene	1.3	5.0 (4.3)	4.7 (4.7)	5.0 (5.5)
THF <sup>2</sup>	1.9	6.2 (5.4)	6.5 (6.0)	-
Methylenechloride <sup>3</sup>	16.2	-	-	-

<sup>1</sup> The data in the parentheses were obtained by rapid heating of the swelling system to the desired temperature and subsequent equilibrating for at least 12 h; the other data were recorded by gradual increase in the temperature starting from 20 °C followed by extended equilibrating for at least 12 h.

<sup>2</sup> The boiling temperature for THF is 65°C.

<sup>3</sup> The boiling temperature for methylenechloride is 40°C.

**Table II. Weight Swelling Ratio of Hydrogels Formed by Crosslinking of First Generation Amino-terminated Tridendron with PEG-isocyanate (feeding ratio of tridendron to PEG = 1: 3)**

Solvent	Temperature, (°C)			
	Room Temperature (20)	40	60	80
Water	7.8	6.9 (7.6) <sup>1</sup>	5.7 (5.4)	4.4 (4.7)
Toluene	1.7	6.0 (6.6)	5.8 (6.2)	5.9 (5.3)
THF <sup>2</sup>	2.1	5.5 (5.9)	5.8 (6.7)	-
Methylenechloride <sup>3</sup>	16.7	-	-	-

<sup>1</sup> The data in the parentheses were obtained by rapid heating of the swelling system to the desired temperature and subsequent equilibrating for at least 12 h; the other data were recorded by gradual increase in the temperature starting from 20 °C followed by extended equilibrating for at least 12 h.

<sup>2</sup> The boiling temperature for THF is 65°C.

<sup>3</sup> The boiling temperature for methylenechloride is 40°C.

It should be noted that the gels show a single glass transition ( $T_g = -38.7^\circ\text{C}$ ), which is far below the  $T_g$  of the first generation amino-terminated tridendrons ( $20.2^\circ\text{C}$ ), but above the  $T_g$  of the pure PEG,  $-52^\circ\text{C}$  (14). It is also seen that even the addition of a relatively small quantity of low generation dendrimer decreases the crystallinity of the resulting gel ( $\Delta H_{\text{PEG}} = 122.6 \text{ J/g}$ ,  $\Delta H_{\text{gel}} = 105.3 \text{ J/g}$ ).

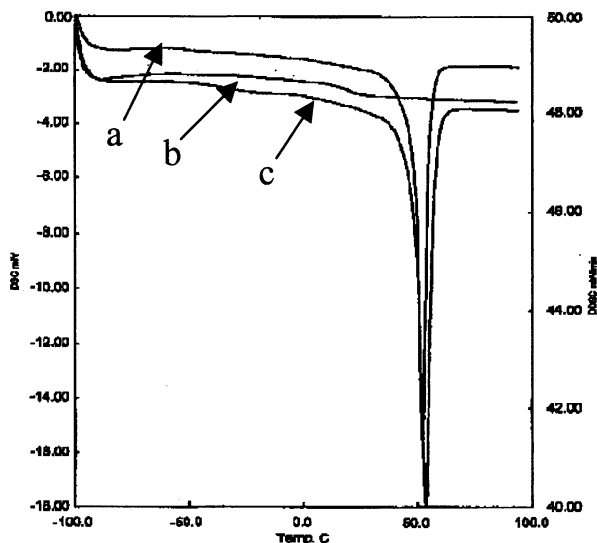


Figure 4. DSC traces of: a) (OCN)-PEG3400-(NCO); b)  $\{(H_2NCH_2)_2-[G-1]\}_3-C-CH_3$ ; c) cross-linked product (PEG/dendrimer = 1.5)

## Conclusions

Our preliminary results show that poly(benzyl ether) dendrimers with different functional groups at the periphery can be successfully applied in the construction of amphiphilic hydrogels with highly organized hydrophobic junctions. Their swelling behavior is affected by the polarity of the medium, the relative content of the PEG and the temperature. The binding properties towards various substrates in different media are currently under investigation.

## Acknowledgements

The financial support for this project provided by Cornell Center for Materials Research (CCMR) and the State of New York/United University Professions (Individual Development Award to I.G.) is gratefully acknowledged. Part of the analyses were carried out in the Polymer

Characterization Facility at CCMR supported by NSF (DMR-9632275). The authors are particularly indebted to Professor N. Ashcroft (Cornell University) for his kind support in the initial stages of this research.

## References

1. McNeill, M.E.; Graham, N.B. *J. Controlled Release* **1984**, *1*, 99
2. Tsanov, T.; Stamenova, R.; Tsvetanov, C.B. *Polymer* **1993**, *34*, 616
3. Ivanova, P.; Eliyas, A.; Stamenova, R.; Petrov, L.; Tsvetanov, C. *Appl. Cat.* **1989**, *53*, 41
4. See for example: a) *Hydrogels in Medical and Related Applications*, Andrade, J.D., Ed.; ACS Symp. Ser., Am. Chem. Soc., Washington, DC, 1976, Vol. 31; b) *Hydrogels in Medicine and Pharmacy*, Peppas, N.A., Ed.; CRC Press, Boca Raton, 1987, Vol. 1 – 3; c) Belcheva, N.; Stamenova, R.; Tsvetanov, C.B.; Lambov, N.; Tsankov, S.; Smid, J. *Macromol. Symp.* **1996**, *103*, 193 and references therein
5. a) Jen, A.C.; Wake, M.C.; Mikos, A.G. *Biotechnol. Bioeng.* **1996**, *50*, 357; b) Li, R.H.; Altreuter, D.H.; Gentile, F.T. *ibid.* **1996**, *50*, 365
6. Tsvetanov, C.B.; Novakov, C.P.; Dotcheva, D.T.; Gitsov, I. *Macromol. Symp.* **1993**, *67*, 157
7. Ross-Murphy, S.B. In *Polymer Gels*, DeRossi, D., Ed., Plenum Press, New York, 1991, p.21
8. a) Griffith Cima, L.; Lopina, S.T. *Macromolecules* **1995**, *28*, 6787; b) Tsvetanov, C.B.; Stamenova, R.; Dotcheva, D.; Doytcheva, M.; Belcheva, N.; Smid, J. *Macromol. Symp.* **1998**, *128*, 165
9. a) Belcheva, N.; Zlatkov, T.; Panayotov, I.M.; Tsvetanov, C. *Polymer* **1993**, *34*, 2213; b) Mathur, A.M.; Moorjani, S.K. Scranton, A.B. *J. Macromol. Sci. – Rev. Macromol. Chem. Phys.* **1996**, *C36*, 405
10. Xu, W.Y.; Sein, A.; Xia, D.W.; Smid, J. *Polym. Mat. Sci. Eng.* **1992**, *66*, 11 and references therein
11. Newkome, G.R.; Moorefield, C.N.; Vögtle, F. *Dendritic Molecules. Concepts, Syntheses, Perspectives*, VCH, Weinheim, **1996**
12. a) Tomalia, D.A. *U.S. Pat.* 4,737,550, **1998**; b) Watanabe, S.; Regen, S. *J. Am. Chem. Soc.* **1994**, *116*, 8855
13. Wooley, K.L.; Hawker, C.J.; Fréchet, J.M.J. *J. Chem. Soc., Perkin Trans. 1* **1991**, 1059
14. *Alkylene Oxides and Their Polymers*, Bailey, Jr. F.E.; Koleske, J.V., Eds.; Marcel Dekker, Inc., New York, 1991, p. 190

## Chapter 16

# The Effect of Hydrophobicity on the Viscoelastic Creep Characteristics of Poly(ethylene glycol)–Acrylate Hydrogels

N. Ravi<sup>1-3</sup>, A. Mitra<sup>3</sup>, L. Zhang<sup>4</sup>, P. Kannan<sup>2</sup>, and B. A. Szabó<sup>4</sup>

<sup>1</sup>Department of Surgery, VA Medical Center, St. Louis, MO 63106  
Departments of <sup>2</sup>Ophthalmology and Visual Sciences, <sup>3</sup>Chemical Engineering,  
and <sup>4</sup>Mechanical Engineering, Washington University, St. Louis, MO 63110

The creep behavior of hydrophobic poly(ethylene glycol)-acrylate hydrogels was well characterized by two Kelvin units in series, compared to the other various combinations of the linear viscoelastic elements investigated. The hydrogels were synthesized by reacting acrylate derivatives of poly(ethylene glycol) [PEG] with PEG-diacrylate as the crosslinking agent. By using different amounts of  $\omega$ -phenoxy-PEG-acrylate in the monomer feed ratio, the hydrophobicity was varied. The extent of monomer conversion was greater than 95%, as determined by Raman spectroscopy. With increasing hydrophobicity, the elastic modulus of the hydrogels increased from 10.92 kPa to 35.10 kPa, and the density increased from 1.0004 g/cm<sup>3</sup> to 1.0091 g/cm<sup>3</sup>, while the dimensional stability decreased from 1.55 to 1.48. Two Kelvin units in series well characterized the creep curve for various loads and time durations. The time constants were in the range of 1-2 s and approximately 300 s for the two Kelvin units. These hydrophobic hydrogels may be used as model tissues to determine the viscoelasticity of the human lens.

## Introduction

Hydrogels are extensively used as biomaterials in biology and medicine (1-5), scaffolds in tissue engineering (6), and adjuvants in drug delivery (7-9). In ophthalmology, hydrogels are not only used for soft contact lenses, but also as vitreous, corneal, and lenticular substitutes (10-14). We plan to use hydrogels as model tissues for understanding the biomechanics of accommodation and presbyopia (15).

The function of the normal eye is to form clear retinal images of objects, irrespective of the distance. To form focussed images requires the molding of the lens substance by several tissues. This process of altering the lenticular refractive power to see clearly at near is referred to as accommodation (16). However, by the fourth decade of life, accommodation begins to fail and the condition known as presbyopia sets in. Age-related changes in the ciliary body (17,18), lens capsule (19,20), neuro-sensory system (21), and the lens substance (22-25) have all been implicated in the pathogenesis of presbyopia. Recent evidence however indicates that the lens may be the primary cause of presbyopia (23). The lens fiber matrix, enclosed within the capsular bag, is a collection of well-organized lens fibers whose cytoplasm is rich in proteins. Thus, the whole lens is analogous to a fiber-reinforced viscoelastic composite within an elastic aspheric biconvex capsular bag. The elastic modulus of the lens has been determined to range from 0.75 kPa to 10.9 kPa depending on the age of the lens and the technique used (19,25-29).

Our ultimate goal is to develop a robust axisymmetric finite element model for accommodation and presbyopia. However, one must first determine the biomechanical characteristics of the tissues involved in accommodation, particularly of the lens. The lens itself has a complex geometry, which makes determination of the stress difficult. Hence, to determine the stress deformation characteristics of a system with simpler geometry, cylindrical disc shaped synthetic hydrogels with comparable elastic properties were investigated.

PEG-based hydrogels assume importance due to their unique solubility characteristics and biocompatibility (30,31). Furthermore, they are readily available commercially and can be easily modified. In our earlier work (15), we determined that  $\omega$ -hydroxy-PEG-methacrylate hydrogels exhibit an elastic modulus of 8-20 kPa. In this study, we hypothesized that the replacement of the  $\omega$ -hydroxy pendant group would result in a lower elastic modulus due to the absence of hydrogen bonding. Thus, we investigated hydrogels derived from  $\omega$ -methoxy-PEG-acrylate with PEG-diacrylate as the crosslinking agent. In order to evaluate the effect of hydrophobicity, we incorporated  $\omega$ -phenoxy-PEG-acrylate

in this system. The effect of monomer feed ratio on the creep-recovery and dimensional stability of hydrogels equilibrated in water was evaluated.

## Experimental

### Materials

The monomers used were  $\omega$ -methoxy-poly(ethylene glycol)-acrylate [ $\omega$ -CH<sub>3</sub>-PEG-Ac] and  $\omega$ -phenoxy-poly(ethylene glycol)-acrylate [ $\omega$ -Ph-PEG-Ac]. The crosslinking agent was poly(ethylene glycol)-diacrylate [PEGDAc]. The reagents used were N, N, N', N' tetramethylethylenediamine [TEMED] and ammonium persulfate [APS].  $\omega$ -CH<sub>3</sub>-PEG-Ac was received from Polysciences and TEMED from Sigma Chemicals. The rest of the chemicals were purchased from Aldrich Chemical Corp. All of the chemicals were used as received.

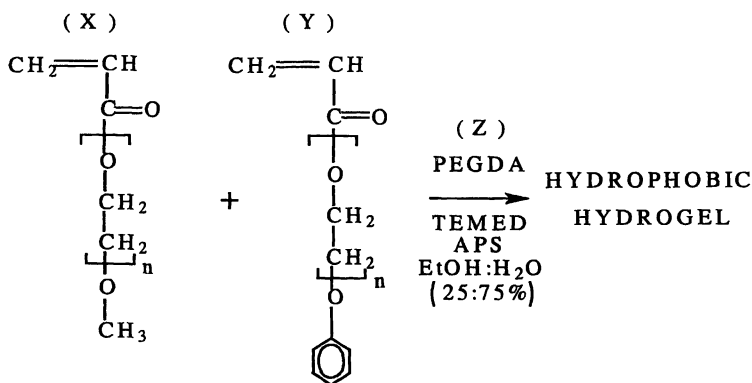
### Characterization of Monomers

The number average molecular weights [ $M_n$ ] of the PEG segment in  $\omega$ -CH<sub>3</sub>-PEG-Ac,  $\omega$ -Ph-PEG-Ac, and PEGDAc were 400, 340, and 400 Daltons respectively (as reported by the supplier). The molecular weight distribution of the monomers was obtained by mass-spectroscopy (MALDI -TOF MS) using a 377 nm nitrogen laser for desorption of ions adsorbed onto  $\alpha$ -cyano-4-hydroxycinnamic acid matrix. The amount of sample added was 0.1-1% and was varied to maximize the signal. Acetonitrile-water mixture served as the solvent for both the sample as well as the matrix. The masses of the oligomeric peaks obtained from the calibrated spectra, combined with their relative intensities (height or counts), allowed for the calculation of  $M_n$  and  $M_w$ . The monomers were characterized by FTIR and Raman spectroscopy (LabRam; Horiba Group).

### Hydrogel Preparation

The gels were prepared using varying amounts of the two monomers, keeping the total weight constant at 2 g. Three grams of solvent (EtOH : H<sub>2</sub>O at 25 : 75 w/w ratio) was added to this mixture. Therefore, all of the samples were

at 40% w/w solids. The final hydrogels [HG] were described by HG-X-Y-Z where X, Y, and Z are the initial monomer weight percent of  $\omega$ -CH<sub>3</sub>-PEG-acrylate,  $\omega$ -Ph-PEG-acrylate, and PEG-diacrylate respectively. The process for synthesizing the hydrophobic hydrogels is represented below:



*Scheme 1. Synthesis of hydrophobic hydrogels.*

As an example, the synthesis of the hydrogel HG-83-15-02 was carried out as follows: To  $\omega$ -CH<sub>3</sub>-PEG-Ac (1.66 g), the crosslinking agent [PEGDAc (0.04 g)] was added, followed by the addition of  $\omega$ -Ph-PEG-Ac (0.30 g). The contents were thoroughly mixed until a uniform mixture was obtained. Three grams of the solvent [EtOH:H<sub>2</sub>O::1:3] was added slowly with continuous stirring to form a 40% w/w clear solution. TEMED (10  $\mu$ l) and freshly prepared APS (10% w/w solution) were added to this solution and mixed thoroughly. No attempts were made to remove oxygen or inhibitors. The solution was poured into a glass mold (10 x 8 x 0.45 cm) formed by two glass sheets separated with spacers along three sides and securely held in position with clamps. Polymerization and gelation was carried out for 24 hours. The hydrogel was subsequently removed from the mold and carefully submerged in MilliQ water (200 ml). The water was changed twice a day for 5 days to remove the unreacted monomer.

### Characterization of Hydrogels

The density of the hydrogel was calculated using a high precision weighing balance equipped with a density measurement kit. After measuring the weight of



the sample in air and in dodecane, and using the density of dodecane, the density of the sample was obtained as described by Peppas (7). Measurements were carried out on five samples and the average and standard deviation were determined.

## Raman Spectroscopy

Aliquots of the monomers (neat) were placed on microscope slides. A Raman spectrometer (LabRam) equipped with a He-Ne laser and coupled to an optical microscope was used to obtain the Raman signals. GRAMS/32 (Galactic Industries) software was used to analyze and display the spectra.

## Mechanical Properties

Mechanical properties were determined using a dynamic mechanical analyzer (Perkin Elmer DMA 7e). A cylindrical disc shaped sample, 1 cm in diameter and 0.6 cm thick was placed between parallel plates in an environment chamber containing 3 ml of MilliQ water, maintained at 37°C. The sample was allowed to equilibrate at zero load for 300 s and its height was measured. A constant load was then applied rapidly and the sample was allowed to creep for 300 s to 2700 s. By this time, the sample strain was assumed to have reached equilibrium. The experiment was performed with varying loads using a new sample for each test. The instrument compliance was less than 0.01% of the sample's compliance and hence no correction was required. The strain at the end of 60 s was considered for the stress-strain plot, the slope of which gives the elastic modulus (E). The shear modulus, G, for low strains (<5%), was obtained from the slope of the plot of stress ( $\sigma$ ) versus  $\lambda-\lambda^{-2}$ , where  $\lambda$  is the deformation ratio. For high strains (5-20%), G was verified using the Mooney-Rivlin equation:

$$\sigma = 2C_1(\lambda-\lambda^{-2}) + 2C_2(1-\lambda^{-3}) \quad (1)$$

In the above equation,  $2C_1$  approximates G. The creep data (for 900 s) was fitted to a generalized linear viscoelastic model, consisting of 'n' Kelvin units either alone or in series with a spring or a dashpot as represented below:

$$D(t) = \sum_{i=1}^n D_i [1-\exp(-t/\tau_i)] + \{(t/\eta)_{\text{Dashpot}} \text{ or } D_{\text{Spring}}\} \quad (2)$$

where  $D$  is the spring compliance,  $\eta$  is the viscosity of the dashpot and  $\tau$  is the retardation time constant. A combination of viscoelastic elements was chosen and an initial guess of the retardation time constant was given. The unconstrained optimization fit was performed using a quasi-Newton method with the formula proposed by Broyden (32)-Fletcher (33)-Goldfarb (34)-Shanno (35) (BFGS). The quasi-Newton methods (as opposed to the Newton methods) avoid the large amount of computation needed to calculate the Hessian matrix numerically. The BFGS formula is considered as the most effective for use in a general-purpose method. The relative error was determined as follows:

$$\% \text{ Error norm} = \frac{\sqrt{(\sum(\epsilon_c - \epsilon_e)^2)}}{\sqrt{(\sum(\epsilon_e)^2)}} \times 100 \quad (3)$$

where  $\epsilon_c$  and  $\epsilon_e$  are the calculated and experimental strain values respectively. The summation is carried out over data points taken at constant time intervals.

## Results and Discussions

The monomers were essentially free from acidic impurities, giving rise to non-ionic hydrogels. The molecular weight of the poly(ethylene glycol)-acrylate monomers was determined using MALDI-TOF MS. The mass difference between adjacent peaks was 44 Da, which corresponds to the mass of the ethylene glycol repeat unit in the monomers. However, the molecular weight of both the groups were not consistent with the theoretically calculated masses, and instead showed a shift of 23 and 39 mass units. Several other investigators (36,37) have also observed this mass shift. They attributed it to the cationic complexation of the glycol units to the  $\text{Na}^+$  and  $\text{K}^+$  cations usually present as adventitious impurities in either the sample and/or the matrix (36). Wytenbach et al., (37) using computational techniques, have shown that PEG coordination of  $\text{Na}^+$  in the gas phase is structurally similar to the coordination with crown ethers, but in a less constrained way. The  $M_n/M_w$  for  $\omega$ -methoxy-PEG-acrylate,  $\omega$ -phenoxy-PEG-acrylate, and PEG-diacrylate were 495/515, 434/446, and 325/410 respectively.

### Raman Spectra of Monomer and Hydrogels

Raman spectroscopy was preferred over IR, due to the presence of water in the polymerization media and in the hydrogels. The monomers and the crosslinking agent show signals at  $850 \text{ cm}^{-1}$ ,  $1260 \text{ cm}^{-1}$ ,  $1286 \text{ cm}^{-1}$  characteristic

of the trans-gauche trans-helical conformation of the oxyethylene unit (Figure 1) (38, 39). The bands at 1407 and 1470  $\text{cm}^{-1}$  correspond to the wagging (in plane) and bending (out of plane) vibrations of methylene (40). The C=C bond is characteristically strong in the Raman spectrum (in contrast to IR). The C=C and the carbonyl group of the ester bond  $-\text{COOCH}_2-$  scatter at 1640 and 1720  $\text{cm}^{-1}$  respectively. The spectral frequency of the ester bond is influenced by inter- or intra-molecular hydrogen bonding with the carbonyl oxygen as well as intra-molecular resonance effects. Figure 1 shows a marked decrease in the C=C bond at 1640  $\text{cm}^{-1}$  in the hydrogel. In addition, the band at 1710  $\text{cm}^{-1}$ , characteristic of the ester group, decreases. The carbonyl ester groups are usually not strong Raman scatterers, but when an  $\alpha$ -C=C group exists, a coupled harmonic oscillation between the two functional group can occur. However, this oscillation is lost upon polymerization.

## Mechanical Properties

The age-related viscoelastic properties of the ocular lens have not been fully characterized. Most of the attempts have been at elucidating only the elastic modulus, since the lens has been treated as an elastic substance (19,26). The process of accommodation however is mechanically analogous to a stress-relaxation experiment, where the stress is allowed to decay at constant strain (refractive power). Hence, the lens is truly viscoelastic. Researchers investigating the viscoelastic characteristics of the lens performed creep-recovery or frequency scan techniques *ex-vivo* (27,28). Ejiri et al. (28) investigated creep properties of a decapsulated dog lens by compression and fitted the time-displacement curve with three Kelvin units. The time constants for the three units were 0.09 s, 7.0 s, and 106 s. The elastic modulus could not be obtained, as the applied stress was unknown due to the aspheric geometry of the lens. In this article, we have investigated the creep behavior of cylindrical disc shaped hydrogels in order to obtain the time constants as well as the elastic modulus of the viscoelastic units.

Figure 2 is a representative plot of the stress-strain curve (at 60 s) for various loads. The slope of this plot gives the elastic modulus (E). All three hydrogels behave as linear viscoelastic materials under these conditions. The correlation coefficient of stress versus strain, in the linear region, is usually greater than 0.99. The shear modulus also exhibits linearity in the range of loads investigated (Figure 3). Figure 4 is a Mooney-Rivlin plot indicating a value of  $C_2$  close to zero, while  $2C_1$  approximates G. The elastic modulus (E) of the sample is approximately three times the shear modulus (G). Thus, the material can be considered as nearly incompressible with a Poisson's ratio ( $\mu$ ) close to 0.5. The Poisson's ratio,  $\mu$ , relates E and G by the equation:

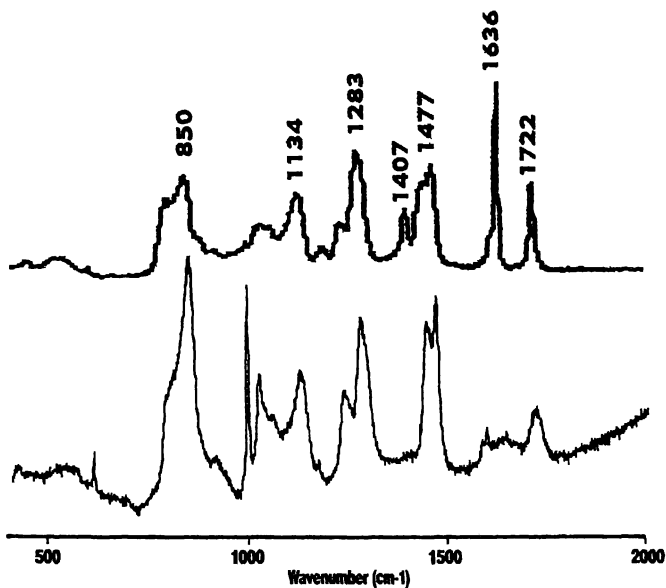


Figure 1. Raman spectra of monomer and hydrogel.

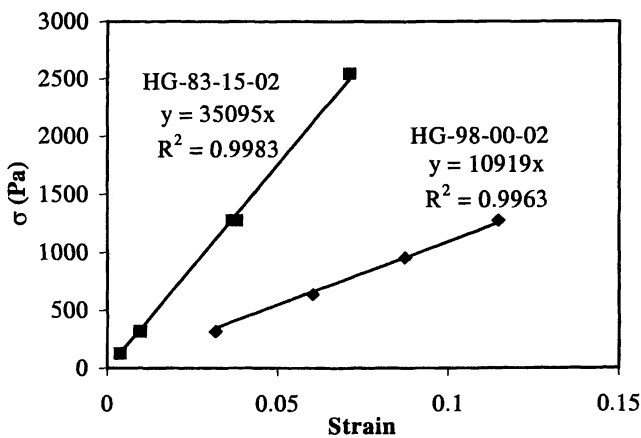


Figure 2. Determination of elastic modulus ( $E$ ).

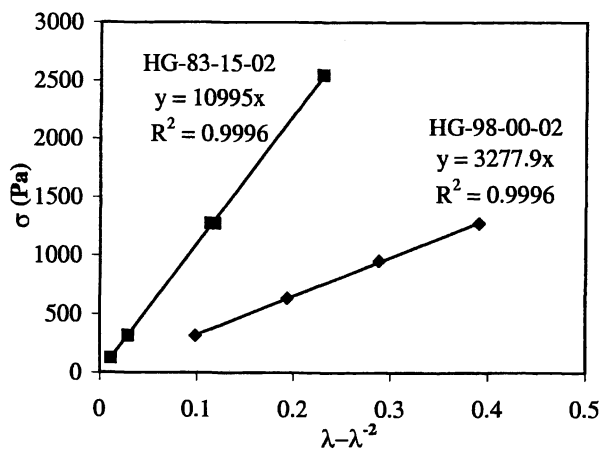


Figure 3. Determination of shear modulus ( $G$ ).

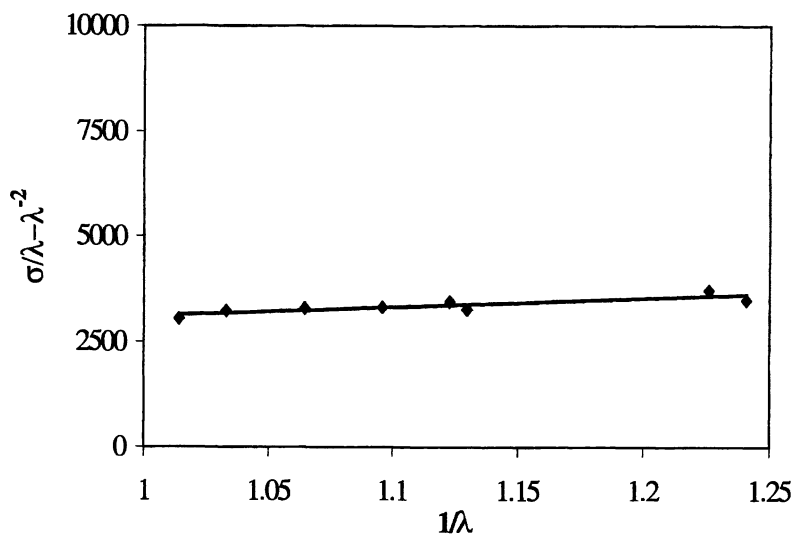
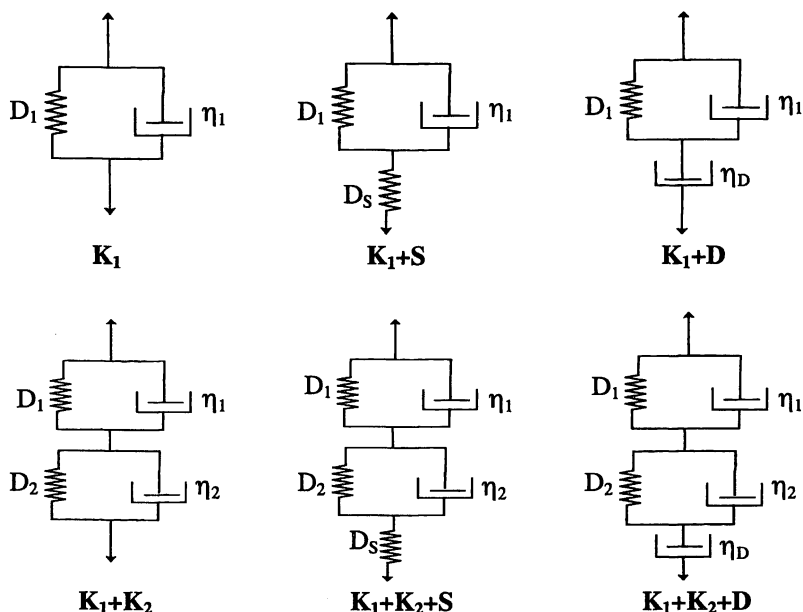


Figure 4. Mooney Rivlin plot for HG-98-00-02.

$$E = 2(1+\mu) G \quad (4)$$

As seen for HG-98-00-02 in Figure 5, the loads yielding strains close to 5% were chosen for all the other compositions as well. This was because the lens does not strain more than 5%. Furthermore, the signal obtained at this strain is relatively free of noise and is within the linear viscoelastic regime.

The creep portion of the creep-recovery curve was fitted to various combinations of linear viscoelastic elements illustrated in Scheme 2.



where for model nomenclature :  $K_1$  = first Kelvin model;

$K_2$  = second Kelvin model; S = Spring; D = Dashpot.

for parameters:  $\eta_1, \eta_2, \eta_D$  = Dashpot constants (Viscosity);

$D_1, D_2, D_S$  = Spring constants (Compliance).

*Scheme 2. Various combinations of the viscoelastic elements.*

The single Kelvin unit ( $K_1$ ) has a compliance,  $D_1$ , of  $9.49E-05 \text{ Pa}^{-1}$  and viscosity,  $\eta_1$ , of  $19.44 \text{ kPa}\cdot\text{s}$ . The time constant,  $\tau_1$ , which is a product of the compliance and the viscosity, is approximately 2 s and represents the time taken by the Kelvin unit to achieve 63% of its final deformation. On addition of a

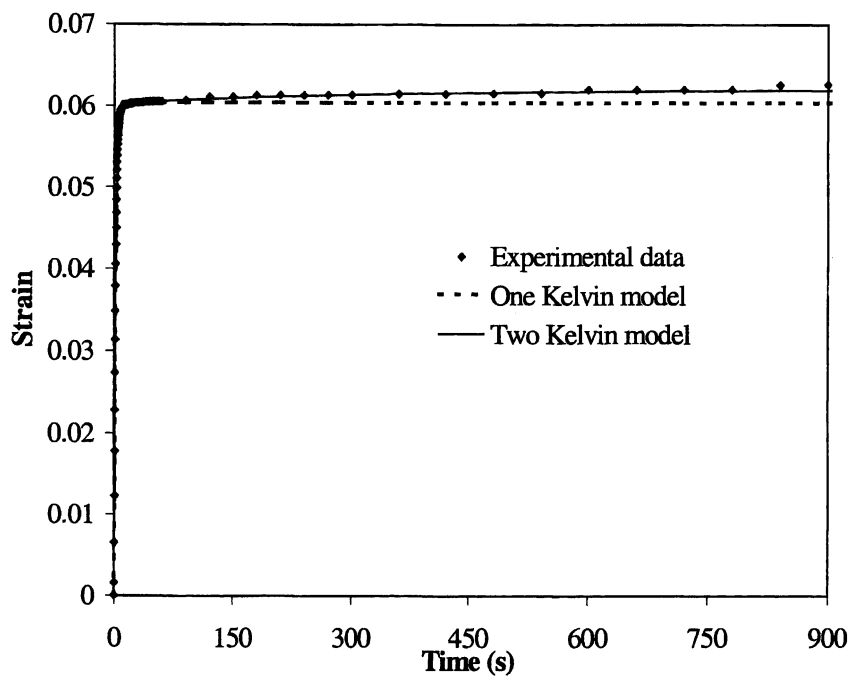


Figure 5. Creep experimental data of HG-98-00-02 at 50mN and 5% strain fitted to one Kelvin and two Kelvin models.

single spring ( $K_1+S$ ), the compliance and the viscosity values of the Kelvin unit remain unchanged (Table 1). The additional spring displays nearly zero compliance, indicating that the single spring does not participate in the creep behavior of the hydrogel. On replacing the spring with a single dashpot ( $K_1+D$ ), it is observed that the dashpot exhibits an extremely low viscosity (lower than that of water). The error norm values ranged from 1.49 to 0.43 and generally decreased with an increase in the number of parameters. In the case of a dashpot connected in series with a Kelvin unit ( $K_1+D$ ), the decrease in the error norm could be attributed to the fitting of the slow drift in the baseline arising from the deswelling of the hydrogel (41), rather than the actual creep phenomenon. Therefore, the addition of a single spring or dashpot does not enhance significantly the ability of the single Kelvin unit to describe the viscoelastic creep behavior of the hydrogel.

**Table 1. Various viscoelastic elements fitted to creep data for HG-98-00-02**

Model	Dashpot Constant (kPa.s)			Spring Constant (1/Pa)		
	$\eta_1$	$\eta_2$	$\eta_D$	$D_1$	$D_2$	$D_s$
$K_1$	19.44	-	-	9.49E-05	-	-
$K_1 + S$	19.44	-	-	9.49E-05	-	0.0
$K_1 + D$	19.38	-	6.57E-12	9.47E-05	-	-
$K_1 + K_2$	19.37	1.06 E+05	-	9.46E-05	2.82E-06	-
$K_1+K_2+S$	19.37	1.06 E+05	-	9.46E-05	2.82E-06	0.0
$K_1+K_2+D$	19.38	inf	6.57E-12	9.47E-05	0.00	-

On fitting the creep data (for 900 s) to a model comprising of two Kelvin units ( $K_1+K_2$ ), a decrease in the error norm is observed when compared with a single Kelvin unit. The two Kelvin units ( $K_1+K_2$ ) have two retardation time constants,  $\tau_1$  and  $\tau_2$ . The shorter time constant,  $\tau_1$ , is in the range of 1-2 s while the longer one,  $\tau_2$ , is approximately 300 s. The second Kelvin unit ( $K_2$ ) has a compliance,  $D_2$ , of 2.82E-06 Pa<sup>-1</sup> and a viscosity,  $\eta_2$ , of 1.06E+05 kPa.s. On performing similar experiments, Westman et al. (42) observed that the viscosity of the dashpot was in the range of 5-20 GPa.s.

At longer time intervals (900 s < t < 3000 s), the strain, in the model comprised of two Kelvin units, reaches equilibrium. The addition of the spring or the dashpot to the two Kelvin units does not affect the descriptive ability of the two Kelvin model. This is due to the zero compliance exhibited by the single



spring and the extremely low viscosity displayed by the single dashpot, as observed in the previous case. Similar to HG-98-00-02, the other hydrophobic hydrogels also demonstrated the best fit with a two Kelvin model. The elastic modulus of the hydrogel prepared using  $\omega$ -hydroxy-PEG-methacrylate instead of  $\omega$ -CH<sub>3</sub>-PEG-Ac in HG-98-00-02, was 22.7 kPa, almost twice that of the HG-98-00-02. This increased elastic modulus (E) may be not only due to the lack of H-bonding, but also perhaps due to the presence of difunctional impurities in the  $\omega$ -hydroxy-PEG-methacrylate monomer. As the hydrophobicity was increased by incorporating  $\omega$ -Ph-PEG-acrylate, the modulus also increased indicating that the intermolecular hydrophobic interactions act as effective crosslinkers. Additionally, with the increased hydrophobicity of the gel, the degree of swelling, which is the ratio of the height of the water-equilibrated specimen to the height of the initial network (0.45 cm), was observed to decrease. As seen from Table 2, an increase of the hydrophobic component in the pre-gel composition is also associated with a decrease in the time constant of the first Kelvin unit. The density of the hydrogel also increased with an increase in the hydrophobicity.

**Table 2. Four parameter model for the hydrophobic hydrogels**

Pre-gel composition	Dashpot constant (kPa.s)		Spring Constant (1/Pa)		E (k Pa)	D.S.*	Density (g/cm <sup>3</sup> )
	$\eta_1$	$\eta_2$	D <sub>1</sub>	D <sub>2</sub>			
HG-98-00-02	19.37	1.06 E+05	9.46 E-05	2.82 E-06	10.92	1.55	1.0004
HG-90.5-7.5-02	29.62	9.33 E+04	5.27 E-05	3.22 E-06	19.58	1.51	1.0046
HG-83-15-02	47.62	2.61 E+05	3.17 E-05	1.15 E-06	35.10	1.48	1.0091

\*D.S. = Dimensional stability

## Conclusions

Hydrophobic hydrogels synthesized from  $\omega$ -methoxy and  $\omega$ -phenoxy derivatives of PEG exhibit an elastic modulus in the range of 11-30 kPa with the shorter time constant being approximately 2 s. Decreasing the H-bonding or the hydrophobic interactions decreases the modulus of the hydrogels. The above hydrogels exhibit viscoelastic properties comparable with those of the aged

natural lens. An aging lens has an elastic modulus between 0.75-10.9 kPa and the time constants are in the range of 0.05-100 s. Hence, in future work, hydrogels with lower modulus and with time constants representative of the youthful eye need to be identified.

### Acknowledgements

This research was supported by the Veterans Affairs Merit Review grant and in part by an unrestricted Educational Research grant from Pharmacia Inc. to N. Ravi. Mass spectrometry was provided by the Washington University Mass Spectrometry Resource with support from the NIH National Center for Research Resources (Grant No. P41RR0954). The authors would like to thank Mr. P. Hamilton for his support with the dimensional stability measurements.

### References

1. Griffith, L. G. *Acta Material* 2000, 48, pp 263-277.
2. Rosiak, J.; Yoshii, F. *Nucl. Instrum. Methods Phys. Res., Section B*. 1999, 151, pp 56-64.
3. Park, H. and Park, K. In *Hydrogels in Bioapplications*. ACS Symp. Ser. 1996, 627, pp 2-10.
4. Tighe, B. *Macromol. Rep.* 1994, 31A, pp 707-713.
5. Hoffman, A. *Materials Research Bull.* 1991, 16, pp 42-46.
6. Langer, R.; Vacanti, J.P. *Science* 1993, 260, pp 920-926.
7. Peppas, N. A.; Barr-Howell B. D In *Hydrogels in Medicine and Pharmacy*; Graham, N. B., Ed.; CRC Press: Boac Raton, FL, 1987; pp 27-56.
8. Park, K.; Shalby, W. S. E.; Park, H. In *Biodegradable Hydrogels for Drug Delivery*; Technomic: Lancaster, Pa, 1993.
9. Gehrke, S. H. In *Transport Process in Pharmacy Systems*; Gordon L. Amidon, Lee, P.J., Totp, E.M., Eds.; Marcell Decker: New York, 2000; pp 473-546.
10. Giordano, G. G.; Refojo, M. In *Human Biomaterials Application*; Humana: Totowa, N. J., 1996; pp 301-317.
11. Liang, D.; Chen, J.; Li, Y.; Lin, J.; Chen, Z. *Eye Sci.* 1999, 15, pp 246-249.
12. Legeais, J.; Renard, G. *Biomaterials* 1998, 19, pp 1517-1522.
13. Chirila, T.; Hicks, C. R.; Dalton, P.; Vijayasekaran, S.; Lou, X.; Hong, Y.; Clayton, A. B.; Ziegelaar, B.; Fitton, J. H.; Platten, S.; Crawford, G.; Constable, I. *Prog. Polym. Sci.* 1998, 23, pp 447-473.
14. Trinkaus-Randall, V.; Capecchi, J.; Leibowitz, H.; Franzblau, C. *Investigative Ophthalmology & Visual Sciences* 1988, 29, pp 393-400.

15. Shanmugananda Murthy, K.; Ravi, N. *Polymer Preprints* 1999, 40, pp 630-631.
16. Koretz, J. F.; Handelman, G. H. *Vision Research* 1982, 22, pp 917-927.
17. Tamm, E.; Croft, M. A.; Jungkunz, W.; Lutjen-Drecoll, E.; Kaufman, P. L. *Archives of Ophthalmology* 1992, 110, pp 871-876.
18. Koretz, J. F.; Cook, C. A.; Kaufman, P. L. *Investigative Ophthalmology & Visual Science* 1997, 38, pp 569-578.
19. Fisher, R.F. *Journal of Physiology* 1969, 201, pp 1-19.
20. Krag, S.; Olsen, T.; Andreassen, T. T. *Investigative Ophthalmology & Visual Science* 1997, 38, pp 357-363.
21. Gilmartin, B. *Ophthalmic & Physiological Optics* 1986, 6, pp 23-37.
22. Fisher, R. F. *Experimental Eye Research* 1971, 11, pp 143-143.
23. Glasser, A.; Campbell, M. C. W. *Vision Research* 1999, 39, pp 1991-2015.
24. Glasser, A.; Campbell, M. C. W. *Vision Research* 1998, 38, pp 209-229.
25. Soergel, F.; Meyer, C.; Eckert, G.; Abele, B.; Pechhold, W. *Journal of Refractive Surgery* 1999, 15, pp 714-716.
26. Van Alphen, G. W.; Graebel, W. P. *Vision Research* 1991, 31, pp 1417-1438.
27. Kikkawa, Y.; Sato, T. *Experimental Eye Research* 1963, 2, pp 210-215.
28. Ejiri, M.; Thompson, H. E.; O'Neill, W. D. *Vision Research* 1969, 9, pp 233-244.
29. Beers, A. P.; Van der Heijde, G. L. *Vision Research* 1994, 34, pp 2897-2905.
30. Harris, J. M.; Zalipsky, S. In *Polyethylene Glycol - Chemistry and Biological Applications*; ACS symposium series: Washington D.C, 1997.
31. Harris, J. M. In *Poly(ethylene glycol) Chemistry- Biotechnical and Biological Applications*; Plenum Press: New York, 1992.
32. Broyden, C. G. *J. Inst. Maths. Applics.* 1970, 6, pp 76-90.
33. Fletcher, R. *Computer Journal* 1970, 13, pp 317-322.
34. Goldfarb, D. *Mathematics of Computing* 1970, 24, pp 23-26.
35. Shanno, D. F. *Mathematics of Computing* 1970, 24, pp 647-656.
36. Montaudo, G.; Montaudo, M. S.; Puglisi, C.; Samperi, F. *Macromolecules* 1995, 28, pp 4562-4569.
37. Wytenbach, T.; Helden, G. V.; Bowers, M. T. *Int. J. of Mass Spectrometry and Ion Processes* 1997, 165/166, pp 377-390.
38. Masatoki, S.; Takamura, M.; Matsuura, H.; Kamagawa, K.; Kitagawa, T. *Chemistry letters* 1995, pp 992.
39. Matsuura, H.; Fukuhara, K.; Masatoki, S.; Sakakibara, M. *J. Am. Chem. Soc* 1991, 113, pp 1193-1202.
40. Urban, M. W. *Adv. Chem. Ser.* 1989, 223, pp 295-314.
41. Horkay, F.; Zrinyi, M. *Macromolecules* 1988, pp 3260-3266.
42. Westman, L.; Lindstrom, T. *J. Applied Polymer Science* 1981, 26, pp 2533-2544.

## Chapter 17

# Gel Network Development in AB, ABA, and AB/ABA Block Copolymer Solutions in a Selective Solvent

Elizabeth A. Wilder<sup>1</sup>, Scott A. White<sup>2</sup>, Steven D. Smith<sup>3</sup>,  
and Richard J. Spontak<sup>4,5,\*</sup>

<sup>1</sup>Department of Chemical Engineering, North Carolina State University,  
Raleigh, NC 27695–7905

<sup>2</sup>Medical Device Technologies Department, Becton Dickinson Technologies,  
Research Triangle Park, NC 27709–2016

<sup>3</sup>Corporate Research Division, The Procter and Gamble Company,  
Cincinnati, OH 45239–8707

<sup>4</sup>Institut für Makromolekulare Chemie, Albert Ludwigs Universität Freiburg,  
D–79104 Freiburg I. Br., Freiburg, Germany

<sup>5</sup>Permanent corresponding address: Department of Chemical Engineering, North  
Carolina State University, Raleigh, NC 27695–7905

### Abstract

In the presence of a selective solvent, ordered block copolymers form micelles that, at sufficiently high copolymer concentrations, serve to stabilize a three-dimensional network and promote physical gelation. This study examines the steady and dynamic rheological properties of micellar solutions composed of AB diblock, ABA triblock and bidisperse mixtures of AB and ABA copolymer molecules. Of particular interest is the unexpected improvement in network development upon addition of an AB copolymer to an ABA copolymer at constant solution composition. This behavior is observed for ABA/solvent systems above and below the critical gelation concentration, and is interpreted in terms of the volume exclusion that occurs in bidisperse mixture of grafted chains.

### Introduction

At sufficiently high thermodynamic incompatibility, AB diblock and ABA triblock copolymers order into several periodic nanostructures, the curvature of which is governed by a combination of interfacial area minimization and packing considerations (1,2). Comparable nanostructures are likewise generated in concentrated solutions of block copolymers in the presence of either a neutral (3) or at least one selective (4–6) solvent. At high solvent concentrations, block copolymer molecules behave as surfactants and micellize in a selective solvent (see Fig. 1). If the copolymer is an ABA triblock copolymer and the solvent is B-selective, the B blocks of the copolymer are capable of adopting looped,

bridged and dangling-end conformations (7,8). These conformations affect the rheological properties of the solution and promote the formation of physical gels above the critical gelation concentration (cgc). We consider a physical gel as a bi- or multicomponent system possessing a liquid matrix and exhibiting two characteristic rheological properties (9): (i) the dynamic storage modulus ( $G'$ ) is independent of oscillatory frequency ( $\omega$ ); and (ii)  $G'$  exceeds the dynamic loss modulus ( $G''$ ). Recent rheological studies of block copolymer micellar solutions have focused on elucidating the effects of composition (10,11), temperature (10,12,13) and shear (14,15) on gel characteristics. In this work, we use steady and dynamic rheology to examine micellar solutions of an AB copolymer, an ABA copolymer and a bidisperse mixture of the two to establish the roles of molecular conformation and coronal packing in gel network development.

### Experimental

Two copolymers, a poly(styrene-*b*-isoprene-*b*-styrene) (SIS) triblock (60 wt% S;  $M_n=100,000$ ,  $M_w/M_n=1.04$ ) and a poly(styrene-*b*-isoprene) (SI) diblock (70 wt% S;  $M_n=50,000$ ,  $M_w/M_n=1.05$ ), were synthesized by anionic polymerization. The selective solvent used here was an aliphatic white mineral oil (MO) produced by Witco (380PO). Specific masses of each copolymer and MO were dissolved in cyclohexane and cast into molds. Upon solvent evaporation, the resultant films were vacuum-dried for up to 7 h at 120°C. Steady-shear tests were performed on a Rheometrics dynamic stress rheometer (DSR) as a function of shear stress ( $\tau$ ) to measure the solution viscosity ( $\eta$ ), while dynamic tests were performed here to discern  $G'$  and  $G''$  as functions of  $\tau$ ,  $\omega$  and temperature.

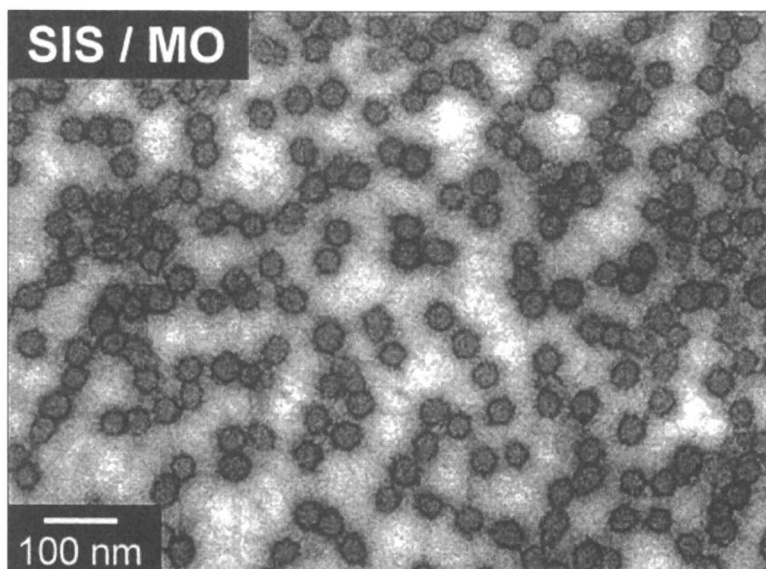


**Figure 1.** Transmission electron micrograph of a micellar SIS triblock copolymer gel containing MO. The stained I blocks comprising the coronae are dark.

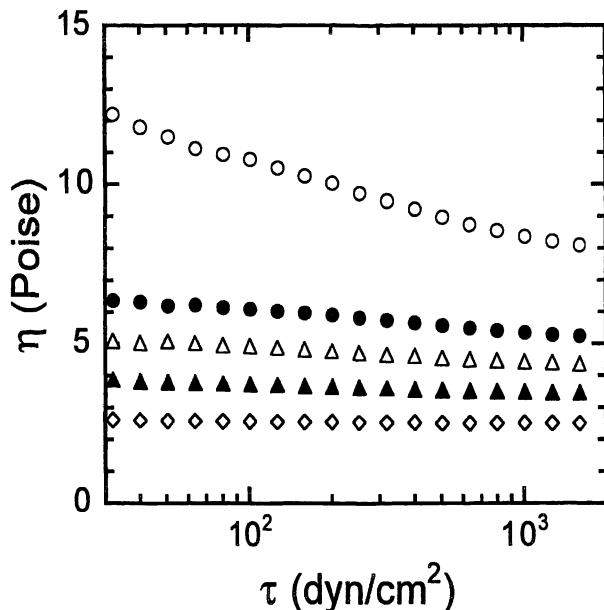


**Figure 2.** Steady-shear viscosity ( $\eta$ ) evaluated at ambient temperature and presented as a function of shear stress ( $\tau$ ) for SI diblock copolymer/MO micellar solutions differing in  $\phi_{SI}$  (in wt%): 15 (○), 13 (●), 11 (△), 9 (▲) and 5 (◇).

## Results and Discussion

### A. Pure Copolymer Solutions

In this section, we first address micellar solutions composed of either the SI or SIS copolymer, but not both. The concentration (expressed here in wt%) of copolymer in these solutions is designated by  $\phi_i$  ( $i=SI$  or  $SIS$ ). Shown in Fig. 2 is the dependence of steady-shear  $\eta$  on  $\tau$  for SI copolymer solutions differing in  $\phi_{SI}$ . These solutions consist of glassy micellar cores surrounded by a swollen brush of I tails. Intermicellar interactions may occur only through entanglement of the tails comprising the coronae of adjacent micelles. As seen in Fig. 2, an increase in  $\phi_{SI}$  promotes a monotonic increase in  $\eta$ , which is weakly dependent on  $\tau$  for solutions with  $\phi_{SI}$  up to 13 wt%. As  $\phi_{SI}$  is increased further to 15 wt%, however,  $\eta$  is found to increase substantially and become more dependent on  $\tau$ . This abrupt change in viscosity behavior suggests that a more highly correlated micellar morphology develops within the solution. Values of  $\eta$  evaluated at two arbitrary  $\tau$  are presented for comparison as a function of  $\phi_{SI}$  in Fig. 3. The regressed solid lines included in this figure reveal that  $\eta$  increases exponentially with increasing copolymer concentration.

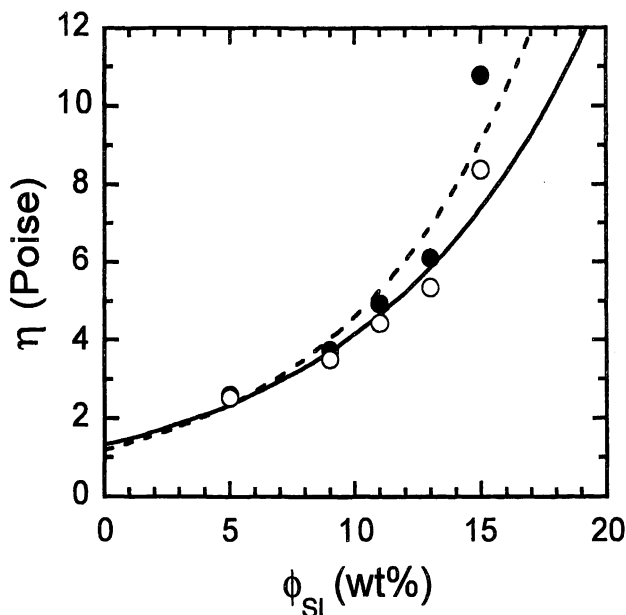


**Figure 3.** Dependence of  $\eta$  evaluated at shear stresses of  $10^2$  (●) and  $10^3$  (○) dyn/cm<sup>2</sup> on composition in the SI diblock copolymer/MO solutions presented in Fig. 2. The solid and dashed lines are exponential fits to the two data sets.

Dynamic rheological measurements of the SI copolymer solutions described in Fig. 2 indicate that these solutions are not physical gels, according to the criteria specified earlier. In marked contrast, the SIS copolymer solutions behave as physical gels, in which the S-rich micelles serve as physical crosslink sites for highly swollen I midblocks. Frequency measurements (not shown here for brevity) confirm that  $G'$  is both independent of  $\omega$  (from  $10^{-1}$  to  $10^2$  rad/s) and always greater than  $G''$  in these solutions. Figure 4 displays the dependence of  $G'$  on  $\tau$  for four SIS solutions differing in  $\phi_{SIS}$ . In all these solutions, two trends are apparent: (i)  $G'$  increases with increasing  $\phi_{SIS}$ , and (ii)  $G'$  exceeds  $G''$  by at least an order of magnitude. Solutions in which  $\phi_{SIS}$  is less than 9 wt% do not exhibit gel behavior, implying that the cgc in this series lies between 7 and 9 wt% at ambient temperature.

According to the data in Fig. 4,  $G'$  is invariant with respect to  $\tau$  over a  $\phi_{SIS}$ -dependent range, which identifies the linear viscoelastic (LVE) regime. Within this regime, the dynamic moduli are independent of  $\tau$ , and the properties of the gel network existing in each solution can be probed without irreversibly damaging the nanostructure. The LVE regime, denoted by  $\tau_{LVE}$  and presented as a function of  $\phi_{SIS}$  in Fig. 5, increases with increasing  $\phi_{SIS}$ . Such dependence

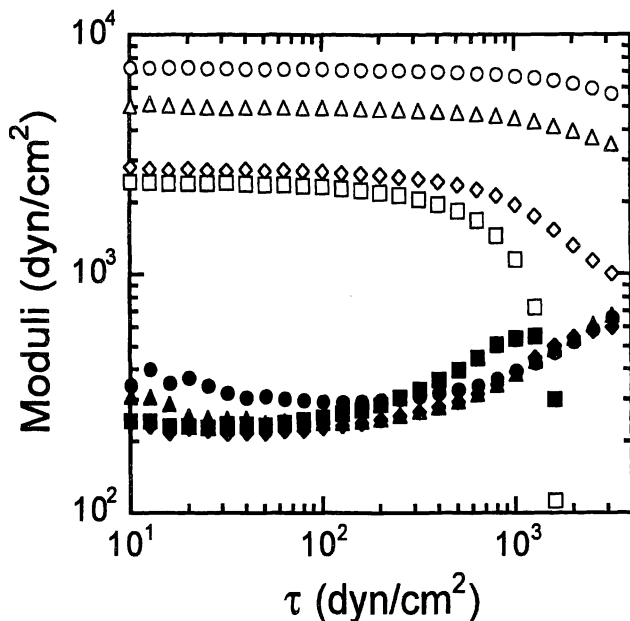


**Figure 4.** Dynamic storage moduli ( $G'$ , open;  $G''$ , filled) displayed as functions of  $\tau$  for SIS diblock copolymer/MO micellar solutions differing in  $\phi_{\text{SIS}}$  (in wt%): 15 (circles), 13 (triangles), 11 (diamonds) and 9 (squares). In these and later dynamic stress measurements,  $\omega$  is maintained constant at 1 rad/s.

is representative of more highly connected networks in gels with high copolymer content. Values of  $G'$  measured in the LVE regime are also displayed in terms of  $\phi_{\text{SIS}}$  in Fig. 6. These data, acquired from both  $\omega$  and  $\tau$  measurements, are accurately fitted by a power-law expression (represented by the solid line in Fig. 6), indicating that  $G' \sim \phi_{\text{SIS}}^n$  with  $n \approx 2.3$ . This relationship, with  $n > 1$ , is consistent with theoretical predictions (16) and experimental evidence (6,10,11) for flowered block copolymer micelles. In this case, both the looped and bridged midblocks of triblock copolymer micelles contribute to the measured modulus. As  $\phi_{\text{SIS}}$  is reduced, the intermicellar distance increases, eventually inhibiting entanglements (due to looped midblocks) between neighboring coronae. In this limit,  $G'$  only depends on the network formed by bridged midblocks. Another composition-dependent feature of the moduli in Fig. 4 is the dynamic yield stress ( $\tau_y$ ), the stress at which the gel network is disrupted. Values of  $\tau_y$  identified either as the stress at which a catastrophic reduction in  $G'$  occurs or from the point at which two tangent lines (reflecting the data) intersect are included in Fig. 5. In similar fashion as  $\tau_{\text{LVE}}$ ,  $\tau_y$  increases with increasing  $\phi_{\text{SIS}}$  due to reduced intermicellar distance and improved network development.



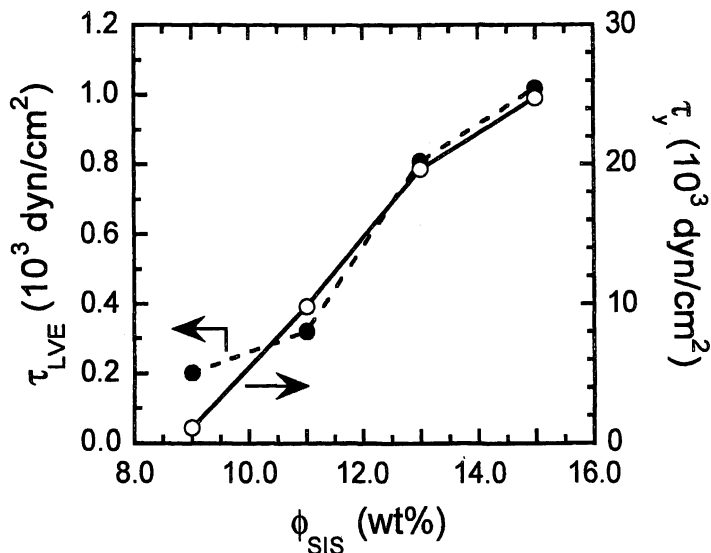


**Figure 5.** Dynamic stresses identifying the linear viscoelastic regime ( $\tau_{LVE}$ , ●) and yield ( $\tau_y$ , ○) as a function of  $\phi_{SIS}$ . Solid and dashed lines connect the data.

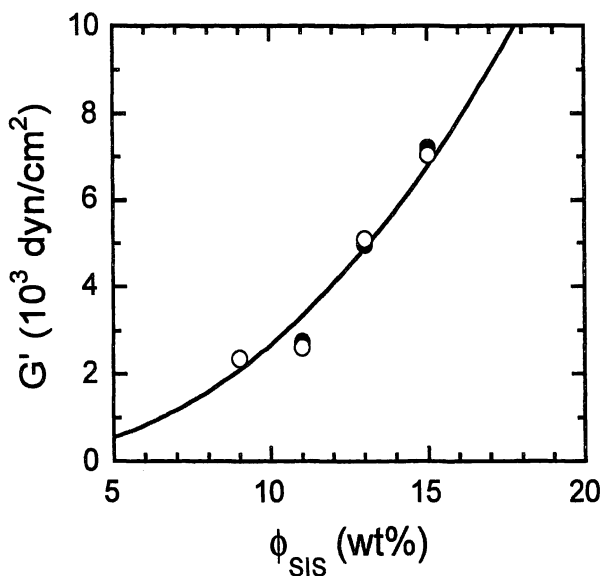


**Figure 6.** Variation of  $G'$  from  $\omega$  (○) and  $\tau$  (●) measurements with  $\phi_{SIS}$  in the micellar solutions shown in Fig. 4. The solid line is a power-law fit to the data.

## B. Bidisperse Copolymer Solutions

In the previous section, each micellar solution consisted of one copolymer (either the SI diblock or SIS triblock) at a specified composition. Here, we turn our attention to micellar solutions composed of bidisperse mixtures of both the SI and SIS copolymers. Three solution series with fixed copolymer compositions ( $\phi_{BC}$ ) of 15, 11 and 7 wt% are examined. The concentration of the SI copolymer in each of these blends, expressed relative to the solution, is designated by  $\phi_{SI}$ . The maximum value attainable by  $\phi_{SI}$  is  $\phi_{BC}$ , which occurs in solutions containing only the SI copolymer. To facilitate comparison between the three series, we also introduce  $w_{SI}$  as the concentration (in wt%) of SI copolymer in each SI/SIS blend used to prepare a bidisperse copolymer solution. This blend composition is related to  $\phi_{SI}$  by  $w_{SI}=100\%*\phi_{SI}/\phi_{BC}$ .

Values of the steady-shear  $\eta$  of the two solution series with 15 and 7 wt% copolymer are presented as a function of  $\tau$  in Figs. 7a and 7b, respectively. In Fig. 7a,  $\eta$  for the pure SI copolymer solution ( $\phi_{SI}=15$  wt%,  $w_{SI}=100$  wt%) varies relatively little with increasing  $\tau$ , in agreement with the data presented earlier in Fig. 2. A reduction in  $\phi_{SI}$  is accompanied by a rather abrupt (*ca.* 5 orders-of-magnitude) increase in the terminal  $\eta$  (at low  $\tau$ ). As  $\tau$  is increased, however,  $\eta$  generally decreases to a high- $\tau$  limit on the order of  $10^3$  P. The manner by which this  $\eta$  reduction occurs is composition-dependent. In the solution with  $\phi_{SI}=9$  wt%, this occurs gradually over a broad  $\tau$  range. This is clearly not the case for the three remaining solutions shown in Fig. 7a. In these SIS-rich solutions, the transition from high- to low- $\eta$  appears relatively sharp, and the value of  $\tau$  responsible for the onset of the transition is sensitive to  $\phi_{SI}$ .

Figure 7b corresponds to the solution series with  $\phi_{BC}=7$  wt% and reveals two very interesting features. The first is that both the pure SI ( $\phi_{SI}=7$  wt%) and the pure SIS ( $\phi_{SI}=0$  wt%) copolymer solutions exhibit comparable magnitudes of  $\eta$ , on the order of about 3 P. In both cases,  $\eta$  is virtually independent of  $\tau$ , as was evident for only the SI solution in Fig. 2. This behavior does not change substantially if  $\phi_{SI}$  is reduced to 6 wt% or increased to 1 wt%. Within these bounds, however,  $\eta$  is seen to increase dramatically, and its shear dependence becomes sensitive to solution composition. Consider the solution with 3 wt% SI copolymer. Its steady-shear  $\eta$  increases by up to  $\sim 5$  orders of magnitude at low  $\tau$ , and then decreases by  $\sim 2$  orders of magnitude over the range of  $\tau$  shown in Fig. 7b. Comparison of Figs. 7a and 7b reveals that, between 3 and 5 wt% SI, the  $\eta$  curves displayed in Fig. 7b resemble the curves for SIS-containing solutions in Fig. 7a. Such similarity suggests that solutions ( $\phi_{BC}=7$  wt%) lying within this composition window may possess copolymer nanostructures that are comparable to those found in the solutions with  $\phi_{SI}=15$  wt%. To compare further the  $\eta$  data in Fig. 7, Fig. 8 displays  $\eta$  at  $\tau=10^2$  dyn/cm<sup>2</sup> as a function of SI/SIS blend composition ( $w_{SI}$ ) and demonstrates that  $\eta$  generally decreases with increasing  $w_{SI}$  when  $\phi_{BC}=15$  wt%. In contrast,  $\eta$  for bidisperse copolymer

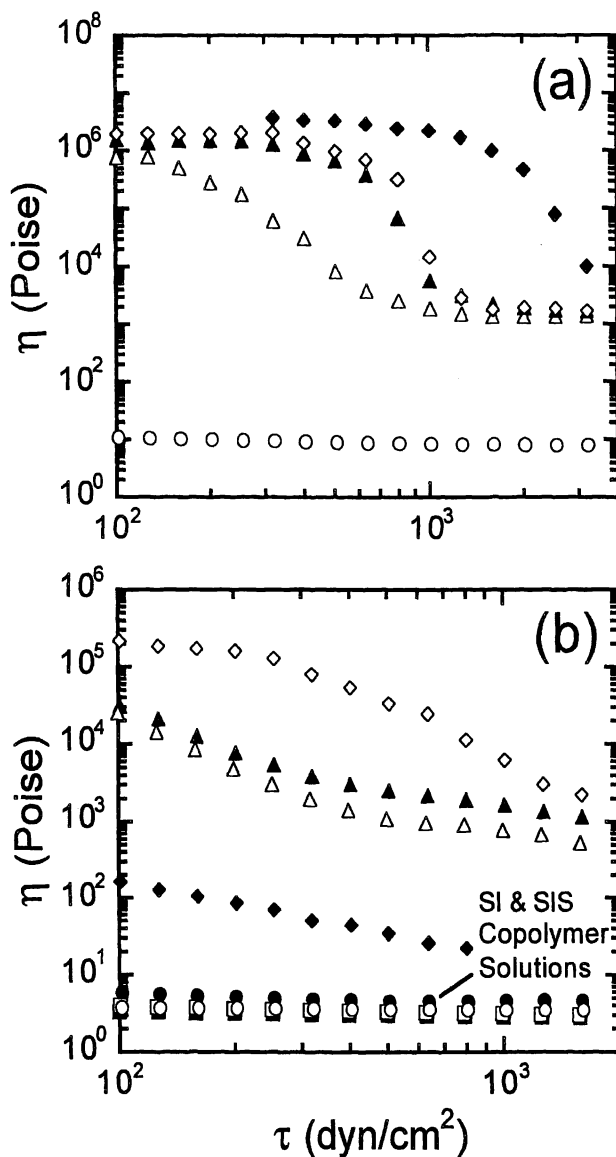


**Figure 7.** Dependence of  $\eta$  on  $\tau$  for bidisperse SI/SIS block copolymer gels with different  $\phi_{BC}$  (in wt%): (a) 15 and (b) 7. In (a), values of  $\phi_{SI}$  (in wt%) are 0 ( $\blacklozenge$ ), 3 ( $\diamond$ ), 6 ( $\blacktriangle$ ), 9 ( $\triangle$ ) and 15 ( $\circ$ ). In (b), values of  $\phi_{SI}$  (in wt%) are 0 ( $\blacksquare$ ), 1 ( $\square$ ), 2 ( $\blacklozenge$ ), 3 ( $\diamond$ ), 4 ( $\blacktriangle$ ), 5 ( $\triangle$ ), 6 ( $\bullet$ ) and 7 ( $\circ$ ).

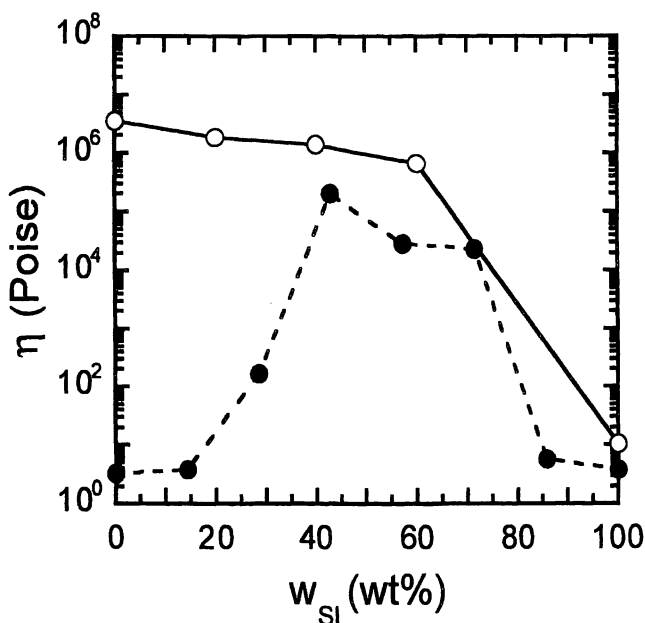


**Figure 8.** Variation of  $\eta$  with blend composition ( $w_{SI}$ ) at ambient temperature for the two blend series shown in Fig. 7 in which  $\phi_{BC}$  is equal to either 15 (O) or 7 (●) wt%. The solid and dashed lines connect the data.

solutions with  $\phi_{BC}=7$  wt% clearly exhibits a maximum between 20 and 80 wt% SI (in the blends used to prepare the solutions). This maximum in  $\eta$  cannot be attributed to differences in micelle size, since the S blocks of the SI and SIS copolymers possess comparable masses (35,000 and 30,000, respectively). Moreover, solutions of the pure copolymers exhibit almost identical  $\eta$ .

While the  $\eta$  data in Figs. 7 and 8 strongly suggest that bidisperse block copolymer solutions exhibit synergistic rheological behavior, Mortensen and co-workers (14) and Hamley and co-workers (15) have conclusively established that the nanostructure of block copolymer solutions is highly sensitive to shear. To minimize shear-induced artifacts in the solutions examined here, we turn our attention again to dynamic rheological testing. Figure 9 shows the stress dependence of the dynamic moduli ( $G'$  and  $G''$ ) for bidisperse block copolymer solutions with three different  $\phi_{BC}$  (in wt%): 15 (Fig. 9a), 11 (Fig. 9b) and 7 (Fig. 9c). Only data in which  $G'$  is independent of  $\omega$  in complementary  $\omega$  measurements (not shown) are presented in Fig. 9. In Fig. 9a,  $G'$  clearly exceeds  $G''$  (by about an order of magnitude) and exhibits a considerable LVE threshold, which generally decreases as  $\phi_{SI}$  increases. The same is true for the magnitude of  $G'$ , except for the solution in which  $\phi_{SI}=3$  wt%. This solution shows a diblock-

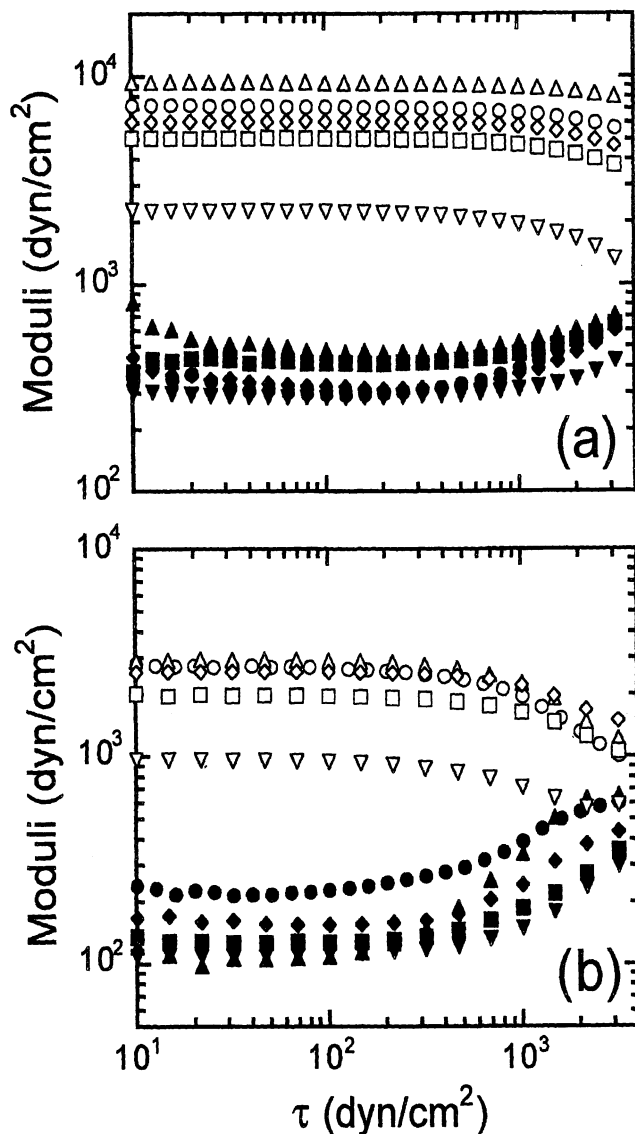


**Figure 9.** Dependence of  $G'$  (open) and  $G''$  (filled) on  $\tau$  for SI/SIS copolymer gels with different  $\phi_{BC}$  (in wt%): (a) 15, (b) 11 and (c) 7. In (a), values of  $\phi_{SI}$  (in wt%) are 0 (circles), 3 (triangles), 6 (diamonds), 9 (squares) and 12 (inverted triangles). In (b), values of  $\phi_{SI}$  are 0 (circles), 2 (triangles), 5 (diamonds), 6 (squares) and 9 (inverted triangles).

*Continued on next page.*

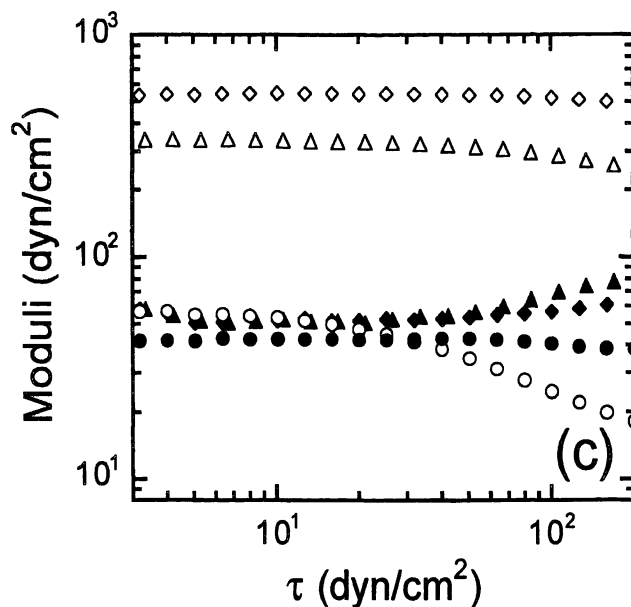


**Figure 9 (cont.).** Dynamic moduli ( $G'$ , open;  $G''$ , filled) presented as a function of  $\tau$  for bidisperse SI/SIS block copolymer gels with  $\phi_{BC}$  equal to 7 wt%. In this figure, values of  $\phi_{SI}$  (in wt%) are 2 (circles), 3 (triangles) and 4 (diamonds).

induced increase of about 30% in  $G'$  beyond that of the pure SIS solution at constant copolymer concentration. The reproducibility in  $G'$  of the micellar solutions examined here is estimated to be about 10%, which means that the increase in  $G'$  evident in Fig. 9a is beyond experimental uncertainty. Similar, but less pronounced, behavior is observed for the solutions with  $\phi_{BC}=11$  wt% in Fig. 9b. Values of  $G'$  do not differ substantially with solution composition up to  $\phi_{SI}=5$  wt%. In the series with 7 wt% block copolymer (Fig. 9c), only solutions possessing intermediate blend compositions are found to exhibit a measurable viscoelastic response. This observation indicates that the solutions composed of either the pure SI or pure SIS copolymer are below the  $c_{gc}$  and do not form physical gels in MO under the present conditions, a finding that agrees with the results presented in the first section of this study. Values of  $G'$  extracted from Fig. 9, as well as from  $\omega$  measurements (not shown), are provided as a function of  $w_{SI}$  in Fig. 10. The maxima discussed above with regard to the three bidisperse copolymer solution series are more clearly evident in this figure. The dashed lines identify values of  $G'$  corresponding to the pure SIS solutions, whereas the dotted lines denote linear fits to the data beyond  $G'_{max}$ . In the series with copolymer concentrations of 15 and 11 wt%, these fits correctly extrapolate to vanishing  $G'$  (for the pure SI copolymer solutions).

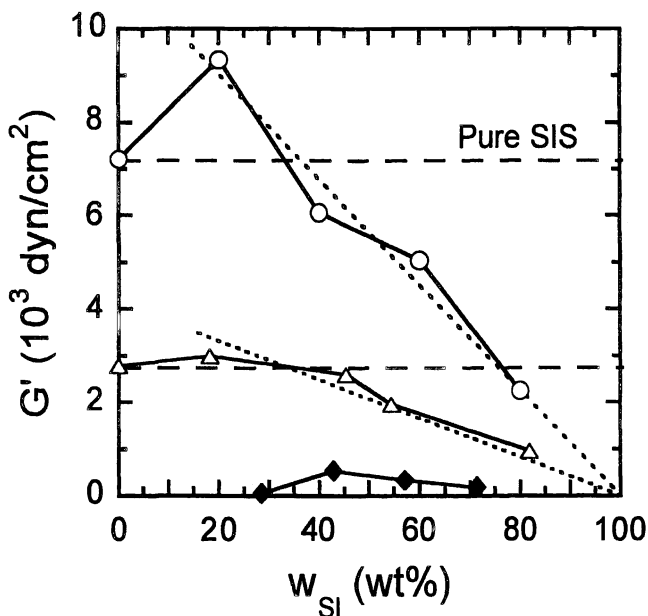


**Figure 10.** Variation of  $G'$  with blend composition for bidisperse SI/SIS block copolymer micellar solutions with  $\phi_{BC}$  of 15 (O), 11 ( $\Delta$ ) and 7 ( $\blacklozenge$ ) wt%. The solid lines connect the data, and the horizontal dashed lines identify  $G'$  for the solutions composed of only the SIS copolymer. Dotted lines are linear fits to the data beyond  $G'_{max}$ . All data have been acquired at ambient temperature.

According to the data presented in Fig. 10, incorporation of SI copolymer molecules within S-rich micelles composed of SIS molecules either *improves* or *promotes* physical gelation at constant copolymer concentration, implying that bidisperse copolymer mixtures synergistically enhance network development. Results from mixtures of polymer chains differing in length and grafted at one end to an impenetrable surface (17) reveal that monolayer stratification induces extension of the longer chains. In the present study, the looped midblocks of the SIS copolymer are further extended relative to the corresponding tails of the SI copolymer (the molecular weight of the I block in the SI copolymer is 15,000, while the half molecular weight of the I block in the SIS copolymer is 20,000). Such extension is expected to inhibit the formation of midblock loops due to coronal volume exclusion of the SIS molecules, thereby favoring the formation of intermicellar bridges and, hence, improving network connectivity (18). Note that at constant copolymer concentration, two SI molecules replace each SIS molecule upon substitution, which is consistent with coronal volume exclusion in bidisperse block copolymer micellar solutions. We recognize, however, that other explanations for the rheological behavior observed here may exist (19).

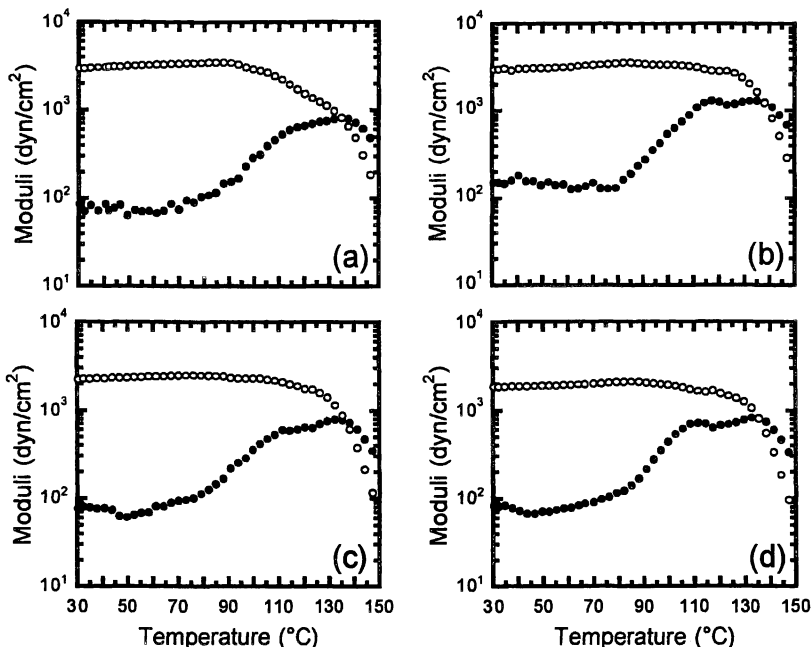


**Figure 11.** Dependence of  $G'$  (O) and  $G''$  (●) on temperature for the SI/SIS block copolymer solution series with  $\phi_{BC}=11$  wt% at four different  $\phi_{SI}$  (in wt%): (a) 0, (b) 2, (c) 5 and (d) 6. These tests have been performed at 1 rad/s.

The results presented thus far demonstrate that bidisperse copolymer solutions influence gel network development. Figure 11 shows the thermal response of the bidisperse solutions with  $\phi_{BC}=11$  wt%. These data exhibit two characteristics with increasing temperature: (i) a two-step reduction in  $G'$  and (ii) a maximum in  $G''$ . The first reduction in  $G'$  occurs near 100 °C and is attributed to the glass transition temperature ( $T_g$ ) of the S blocks of the constituent copolymers. As seen in Fig. 12, which displays temperature as a function of blend composition, this  $T_g$  does not vary with  $w_{SI}$ , as expected. The second reduction in  $G'$  coincides with the high-temperature maximum in  $G''$ . This transition, which is presumed to correspond to lattice disordering (10,12), is weakly composition-dependent, decreasing slightly with increasing diblock content. It is important to recognize that this thermal transition reflects a difference in intermolecular correlation, *not* a change in intermolecular connectivity (associated with gelation).

#### Acknowledgments

This study was partially supported by the Video-Based Engineering Education program at North Carolina State University. R.J.S. is grateful to the Alexander von Humboldt Stiftung for a research fellowship.



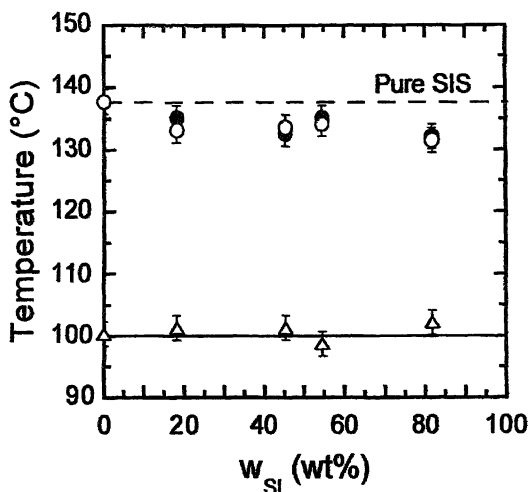


**Figure 12.** Transition temperatures presented as a function of  $w_{SI}$ . The initial reduction in  $G'$  ( $\Delta$ ) reflects the  $T_g$  of the S blocks. A disordering transition is identified by a second reduction in  $G'$  (O), as well as a maximum in  $G''$  ( $\bullet$ ).

## References

1. Hamley, I.W. *The Physics of Block Copolymers*; Oxford Univ.: NY, 1998.
2. Jinnai, H.; *et al.*, *Phys. Rev. Lett.* **2000**, *84*, 518.
3. Hanley, K.J.; Lodge, T.P. *J. Polym. Sci. B: Polym. Phys.* **1998**, *36*, 3101.
4. Hamley, I.W.; *et al.*, *Macromolecules* **1998**, *31*, 1188.
5. Alexandridis, P.; Olsson, U.; Lindman, B. *Langmuir* **1998**, *14*, 2627.
6. Laurer, J.H.; *et al.*, *Langmuir* **1999**, *15*, 7947.
7. Watanabe, H.; *et al.*, *Macromolecules* **1997**, *30*, 5877.
8. Nguyen-Misra, M.; Mattice, W.L. *Macromolecules* **1995**, *28*, 1444.
9. Kavanagh, G.M.; Ross-Murphy, S.B. *Prog. Polym. Sci.* **1998**, *23*, 533.
10. Laurer, J.H.; *et al.*, *J. Polym. Sci. B: Polym. Phys.* **1998**, *36*, 2379, 2513.
11. Raspaud, E.; *et al.*, *Macromolecules* **1996**, *29*, 1269.
12. Soenen, H.; *et al.*, *Polymer* **1997**, *38*, 5653.
13. Yu, J.M.; *et al.*, *Macromolecules* **1997**, *30*, 4619.
14. Mortensen, K.; *et al.*, *Physica B* **1997**, *241*, 1025.
15. Daniel, C.; *et al.*, *Macromolecules* **2000**, *33*, 2163.
16. Semenov, A.N.; *et al.*, *Macromolecules* **1995**, *28*, 1066.
17. Levicky, R.; *et al.*, *Macromolecules* **1998**, *31*, 2616.
18. Spontak, R.J.; *et al.*, *Langmuir* **2001**, *17*, 2294.
19. Vega, D.A.; *et al.*, *J. Polym. Sci. B: Polym. Phys.* **2001**, *39*, 2183.

## Chapter 18

# Photoresponsive Thickening in Polyamphiphile-Based Physical Gels: The Examples of Micelle, Protein, and Cyclodextrin Cross-Linkers

G. Pouliquen<sup>1</sup>, I. Porcar<sup>1</sup>, C. Tribet<sup>1</sup>, and C. Amiel<sup>2</sup>

<sup>1</sup>Laboratoire de Physico-chimie Macromoléculaire, CNRS UMR 7615, ESPCI,  
10 rue Vauquelin, F-75005 Paris, France

<sup>2</sup>Laboratoire de Recherche sur les Polymères, CNRS UMR 7581, 2-8 rue H. Dunant,  
F-94320 Thiais, France

### Introduction:

Macromolecules that can form transient associations via their end-groups or pendant groups have found increasing interest because of their unique rheological properties. They are receiving attention as replacement for high molecular weight viscosifiers in applications such as paints, coating, oil recovery, or controlled drug release. Such systems can flow under shear like a viscous fluid, but recover rapidly gel-like behaviors at low shear rate or at rest. Owing to the formation of reversible connections between the polymer chains, these physical gels also exhibit self-heal capacity, and sensitivity to stimuli that can modify the strength of the connections (pH, salt, and temperature...). In water-based media, hydrophobe-bearing polymers (HP) have been recognized for their striking thickening efficiency due to the self-association of pendant hydrophobes groups (1-2, 3). One difficulty, however, in handling such polymers is the slow dissolution rate, and possible gel blocking of the concentrated stock solutions. These drawbacks are significantly reduced if the association and correlatively the viscosity enhancement are obtained by mixing complementary components. Stimulated by the development of HP, much research has been conducted on additives that can rapidly strengthen -or induce-connections between polymers. Well-documented examples are mixtures of HP and surfactants (4). Obvious advantages of such mixed systems include the reduction of polymer concentration (and of the viscosity of this initial stock solutions), the rapid adjustment of viscosity by supplementation with the additives, and the possible development of responsive-systems modulated by changes of the affinity between polymer and additives. It is the aim of this chapter to present the essential features of these mixed polymer/additive

systems with special emphasis on the case of colloidal additives and HP. Many studies have been dealing with particles being able to form complexes with several hydrophobic side-groups of HP. Although surfactant/HP systems have been more extensively considered (4, 5, 6), promising effects have been reported using colloid additives such as proteins (7), cyclodextrine polymers (8, 9), vesicles (10). Without seeking at a comprehensive review of the couples of (particle, modified polymer) that were devised to form gels, the first part of this paper will point out recent progress in the field. Beyond the differences in the chemical nature of the systems, it is aimed here at a basic view of their common behaviors.

In a second part, the practical benefits that can be taken from the specificity of polymer/particle association will be exemplified by the recent results obtained in our groups on photo-responsive thickeners. It is shown how association can be sensitive enough to small changes occurring on the side-groups of polymers, at the molecular level, and resulting in a macroscopic response of the viscosity or eventually a gel-sol transition. The presence of a few molar percent of responsive groups (such as weak acids for pH-responsiveness) or sensitive chains along the backbone (e.g. chains exhibiting a lower critical solution temperature LCST) has been shown to modulate the self-associating propensity or the conformation of polymers (11). Potential applications of responsive mixed gels have been first proposed by Lee and Park using a neutral polyvinylpyrrolidone-allylglucose copolymer cross-linked by the protein: concanavalin A (12). The formation of reversible and glucose sensitive gels, at some optimal protein/allylglucose ratio has demonstrated the possibility of cross-links formation upon recognition by a protein of a few pendant groups along the polymer chain (here up to 4 glucose groups per protein). For practical developments of highly viscous (>1 Pa.s) or gelified responsive fluids, however, a supplementation with salt or other additives, such as glucose, is fraught with technical difficulties. Except in the case of temperature-sensitive systems, such stimuli seem unlikely to propagate rapidly through thick materials. The photo-responsiveness could provide an excellent alternative to switch rapidly the viscosity of a solution without the need for stirring or mixing. The properties of polymers have been triggered by light due to the presence of chromophores in the macromolecules (13, 14). In recent years, several photo-stimulations of physical or chemical properties have been examined although not yet with self-associating chains. Volume changes (15, 16), solubility (17), chain extension (18), enzymatic activity (19) or gelation in liquid crystal systems (20) have been reversibly switched between two states upon irradiation at two different wavelengths. In such systems, the initial change induced by light (for instance the *trans* to *cis* transconversion of a double bond in a pendant chromophore group) is located at molecular scale and it needs therefore to be amplified up to a supramolecular or macroscopic scale. In the known polymer-based systems, this amplification has been achieved by the critical transition between an

extended and a collapsed state of the modified macromolecules, resulting either in the precipitation or in a volume change of a chemical gel. To our knowledge, the sol-gel transition in reversible polymer networks was not exploited to date although recognition phenomena together with criticality should efficiently amplify the transconversion. We present in the part 2 a generic route toward reversible photomodulation, in systems containing hydrophobically modified water-soluble polymer and various colloidal particles. A chromophore, namely the azobenzene molecule, was grafted as a pendant group along polyacrylic acid backbones. Rheological experiments were conducted to show the formation of cross-links and their modulation upon UV irradiation using three different connector particles such as SDS micelles, a protein (bovine serum albumin) or  $\beta$ -cyclodextrin polymers.

## Part I: principles and systems

### Thickening scenario:

The thickening of copolymer solutions as induced by addition of another colloidal species such as micelle, protein or cyclodextrin clusters, is essentially based on the idea of forming cross-links when the colloids exhibit some affinity toward a few pendant groups along the polymer chains (figure 1a). For the sake of simplicity, the added colloidal objects shall be referred to as “particle” in the following chapter. Provided that the host particle can bind several groups, cross-links may be formed. Since the early stage of development of mixed HP/surfactant mixtures, a simple scenario has been proposed to interpret the visual observation of the dramatic increase and decrease in viscosity obtained upon supplementation of a fluid polymer solution with near-micellar solutions of surfactant (21). As proposed in figure 1b, the initial solution (absence of particles) corresponds to conditions in which the polymer chains do not self-associate: the viscosity of this state would be rather low and similar to the viscosity of a solution of polymer without pendant groups. Upon addition of particles, the formation of mixed hydrophobic clusters (figure 1a) would connect the polymers provided that they are comprised of several pendant groups from at least two macromolecules. At both high enough a polymer concentration (close to a semi-dilute regime) and high enough physical cross-links per chain, gelation could occur. Further increase of the particle concentration would saturate all the side groups. In excess of particles, the macromolecules would finally appeared as “necklaces” of particles that cannot stick together: this situation, essentially similar to the initial state, corresponds to a low viscosity. This sketch matches with the reported initial thickening at increasing surfactant concentration followed, at constant polymer concentration, by a drop of the viscosity (figure 2B). In principle, such a scenario should also

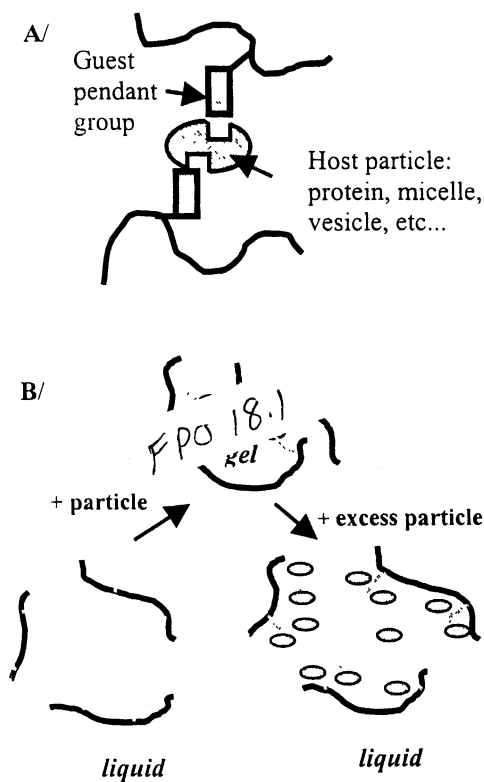
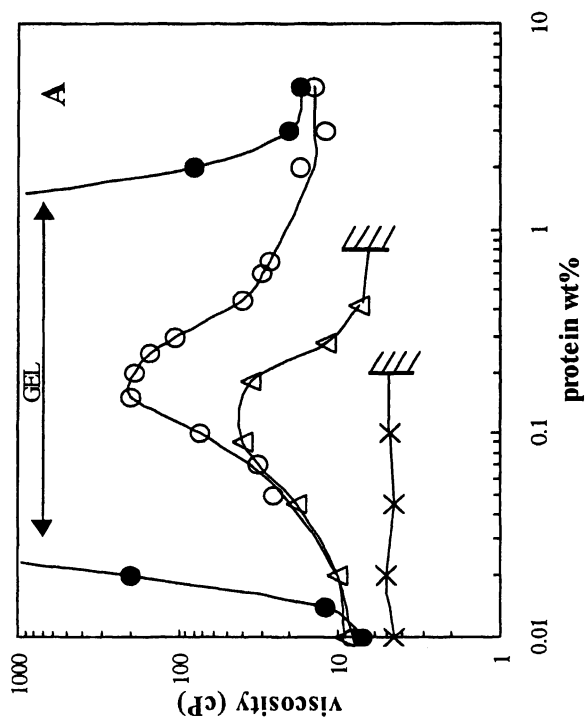


Figure 1: Possible scenario of gelation in mixed particle/polymer systems. A/ host-guest like formation of cross-links. B/ gelation-fluidification scheme upon increasing the host particle concentration.



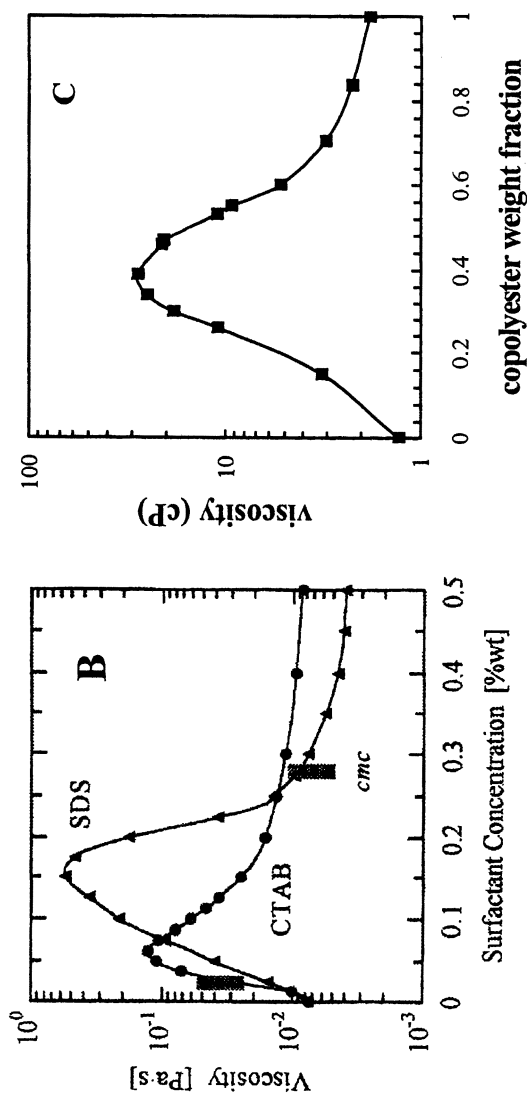


Figure 2: Low-shear viscosity of hydrophobically modified polymer / cross-linkers mixtures. *A/* 0.5 wt% C18-grafted poly(acrylic acid) and protein. ( $\times$ ) lysozyme + ungrafted polymer, ( $\Delta$ ) lysozyme + 1 mol%-modified polymer, ( $\circ$ ) BSA + 1 mol%-modified polymer, ( $\bullet$ ) BSA + 3 mol%-modified polymer *B/* 0.5 wt% C16-modified Hydroxyethylcellulose (0.9 mol% of C16 groups along the chain) + surfactant. SDS: sodium dodecyl sulfate, CTAB: cetyltrimethylammonium bromide. *C/*  $\beta$ -CD-EP cluster + poly( $\beta$ -malic acid-co-ethyladamantyl  $\beta$ -malate) having an adamantyl content of 7.5 mol%. In this case, the total concentration (both  $\beta$ -CD-EP and copolyester) was kept constant at 10 g/L, varying the weight fraction of the two macromolecules.

remain essentially unmodified by the replacement of the micelles for another particle of nanometric size by exhibiting some affinity for the pendant groups. As judged by the variety of mixed systems that gelified the essential qualitative behaviors are likely to be captured in the sketch in figure 1. Similar tentative interpretations were indeed proposed for HP/rod-like micelles mixtures (22), cholesterol-modified pullulan/surfactant (23), HP/protein (7, 24, figure 2A), sugar-modified polymer/lectin (12), cyclodextrin clusters/aromatic- or adamantane-bearing polymer chains (8, 9, figure 2C). All these mixtures exhibited the characteristic bell-shaped variation of viscosity as a function of particle concentration (figure 2). The amplitude of the thickening was sometimes of the order of a 3-decade variation of the viscosity at a fixed polymer concentration of about 1 wt%. Other mixtures of a linear HP with colloids, such as vesicles (10), linear copolymer with pendant cyclodextrin (25), or microemulsion (26), although not characterized in that way, are suspected to belong to the same class of systems.

The generality of this simple picture is however limited to a qualitative view and to systems that do not undergo complex phase transition. Reversible gelation demands two seemingly contradictory behaviors: interpolymer associations must be strong enough to stabilize the network of macromolecules, yet the chains cannot exclude the solvent or they will precipitate. This might be a reason for the absence of reversible gelation in many mixed systems that prefer to form soluble complexes (for instance, when highly hydrophobic polymer wrap around a single particle) or phase separate (27, 28, 29). The polymer structures, shown to form mixed gels, appear very often to be copolymers comprised of a majority of water-soluble monomers and only a few side groups that could bind to a particle. Within the above limitations, HP of polyelectrolytes nature seem generic systems in which both a reversible and strong gel formation has been observed in a wide range of composition and with different particle additives such as protein, surfactant micelles, or clusters of cyclodextrin.

### **Particle/polymer stoichiometry:**

More quantitative considerations on the latter systems emphasize their similitude in term of association mode, and possibly network structure. From the rheological data, we can identify two characteristic points in the formation/disruption processes of inter-polymer contacts. Firstly, the maximum of associativity corresponds to the maximum viscosity at a fixed polymer concentration (maximum of the bell-shaped curve such as figure 2). Secondly,



the almost complete disruption of interpolymer connections could be defined as the point where the viscosity at high particle concentration becomes equal to the value measured in the absence of particle. The corresponding values of the ratio of pendant groups to particles should reveal the typical stoichiometries for either the optimal connection or for the breakage of interchain contacts respectively. A strong homogeneity emerged from the typical examples given in table 1. Note that the present values were calculated from the total particle, or pendant group concentrations. They would reflect an average composition of cross-links only if the unbound species were almost absent in the mixtures. In most cases, however, neither the fraction of free or bound groups, nor the concentration of free particles were studied. The composition at the optimal thickening efficiency of any mixture reflected, nevertheless, the need for an excess of pendant groups (bound or free) compared to the number of particles (table 1). Usually, this excess corresponded to several tens of pendant groups per “connector” particle. An excess as large as 100, estimated for polycyclodextrin-based particles, was however attributed by Moine and coll. (30) to the need for saturation of about all the accessible cyclodextrin (about 500 CD sites per particle in that example). If the particle would display a large number of binding sites at its surface, it is not surprising that multiple binding of a single polymer chain takes place, recruiting therefore a large number of pendant groups. This remark also agrees with the conclusions published by Piculell (6) reviewing several surfactant/HP mixtures (neutral or charged polymers, cellulose derivatives, various surfactants). In the language of Piculell, the data points out large similarities in the stoichiometry of mixed micelles that are formed at the maximum of viscosity. Although it has been often written that the peak in viscosity occurred at (or very close to) the critical micellar concentration (CMC) of the surfactant, some examples, contradict this view (figure 2b). As pointed out by Piculell, the distance from the CMC has no absolute meaning due to the change of the effective CMC and aggregation number in the presence of polymer. Using a relevant model of binding isotherms of surfactants to the polymer, Piculell has determined a characteristic ratio of 1-4 bound pendant groups/surfactant at the maximum of the thickening effect (6). The value of a few tens of groups per particle is recovered assuming an aggregation number in the range 30-50 for micellar aggregates (in the presence of polymer, the aggregation number was found to be lower than in absence of macromolecules). These relatively high numbers of putative links/particle were significantly higher than the minimum functionality of a cross-link, i.e. 2-3 pendant groups/particle. Being calculated from the total composition, this does not indicate whether a high ratio reflects a high functionality of the cross-links, or the absence of binding of most among the pendant groups, or the formation of a cluster comprised of several pendant groups close to the particle. The minimum experimental values, about 2-3 pendant groups per particle, were however obtained with polymers comprised of highly hydrophobic pendant groups (hexyl-cholesterol), and/or of a not too stiff

and neutral backbone, which probably induced an unusually tight binding with the added micelles.

As expected from the scenario in figure 1, the breakage of the connections took place when the number of pendant groups per added protein or micelle felt down to 1-4 (table 1). In all particle/HP systems, the exact value of the composition at vanishing connectivity should be regarded as a rough estimate owing to the arbitrary criterion chosen (based on the viscosity returning to its initial value in absence of particle). In addition, at such a large excess of added particles, the viscosity did not markedly decrease upon further addition of particles entailing some uncertainty in the determination of this ratio. Nevertheless the present data matches very well with a correlation between the saturation of the polymer pendant groups and the breakage of the associativity. In a few micelle/HP systems, the breakage of interpolymer associations were corresponding to just 1 pendant group/micelle. They corresponded to the cases of tight association where the maximum viscosity was reached at about 3 pendant groups/micelles –close to the minimum functionality of 2. Saturation and gel breakage may however been reached despite the binding onto a single particle of a several pendant groups belonging to the same polymer chain (table 1). This remark is consistent with the saturation plateaus determined from binding isotherms of proteins to HP (31). In dilute mixtures, it has been shown that either C18 or C12-modified polyacrylic acid chains were in equilibrium with an excess of free proteins while polymer/protein complexes contained 2.5-3.5 alkyl group per bound protein. The multipoint attachment of the polymer onto a colloid particle, in the presence of excess particles, is likely to depend on both the strength of association and the chain stiffness (if the formation of loops is needed to wrap the chain around the particle). Although not extensively studied, the polymers/ $\beta$ -CD ratios available appeared of the same order of magnitude (8, 9, 30). Recent works on adamantane-modified poly  $\beta$ -malic macromolecules also suggested that a minimum number of pendant group per polymer chain was required for large polymer clusters to be formed via cyclodextrin connectors (30). The presence of only 5 pendant groups per macromolecules was not enough to obtain networks and 42 adamantyl side groups/macromolecule enabled them to form strong gels, providing indirect evidence that the presence of 1-5 pendant group/CD cluster was not enough to cross link the polymers.

The discussion above is consistent with thickening effects being essentially controlled by the molar ratio of cross-linker “hosts”/pendant guest groups. In that sense, any reorganization of the supramolecular assemblies of surfactant is expected to have a major influence on the viscosity (10, 22). The amplitude of the effect has also been shown to exhibit dramatic dependency on the affinity of pendant groups for the particle. Not unexpectedly, the higher the affinity between the partners, the stronger the thickening. In mixtures of hydrophobically modified polymer and amphiphilic particles, this affinity is modulated by both the length of the pendant groups (i.e. its hydrophobicity) and the density of grafting. Small increase in the polymer grafting rate with C18 pendant groups (ranging from 1mol% to 7mol%) has been shown to result in dramatic differences in the rheology of protein/HP mixtures: At a low

Table 1: Examples of pendant groups/particle molar ratios at the following characteristic points: optimum of thickening effect (at a fixed polymer concentration) and disruption of the connectivity.

Backbone monomer(s)	Pendant guest	Host particle	Optimal molar ratio	Disruptive molar ratio
Sodium acrylate (from 7)	n-octadecyl	Lysozyme	18-22	3-5
		Bovine albumin	21-27	2-4
DMA/HEMA (from 27)	Adamantane	$\beta$ -CD cluster <sup>a/</sup>	~ 500	30-40
Malic acid (from 8)	Adamantane	$\beta$ -CD cluster <sup>a/</sup>	~ 210	n.d.
Sodium acrylate (from 32)	Dodecyl	Dodecyltrimethylammonium micelles <sup>c/</sup>	10-15	6
Ethylenoxide (from 33)	Octadecyl	SDS micelles <sup>c/</sup>	3	1
Pullulan (from 23)	Hexamethylenediurethane-cholesterol	SDS micelle <sup>b/</sup>	~2.7	~1

<sup>a/</sup> number of cyclodextrin particles estimated from the average Mn equal to  $1.10^6$ . <sup>b/</sup> estimates obtained by assuming an aggregation number of 60 for SDS micelles. <sup>c/</sup> estimation obtained from the measurement of the number of micelles by fluorescence techniques.

DMA/HEMA: dimethylacrylamide/hydroxyethylmethacrylate, n.d.: not determined

hydrophobicity -1mol% of C18 groups along the backbone- slightly viscous solutions were obtained upon addition of bovine serum albumin; the maximum viscosity of a 0.5wt% polymer solution was about 200 cP (7). On the contrary, beyond 3mol% of C18 groups, the same solutions gelified ( figure 2a, 7, 24) exhibiting viscosity well above 5000 cP (and strong shear thinning). Similarly, the change from a slightly hydrophobic protein (lysozyme, papain) to a more hydrophobic one (bovine serum albumin) led to more than one decade increase of the maximum elastic modulus of the gels (figure 2a, 24). Although the same trend was reported for surfactant/HP systems, the possible reorganizations of mixed micelles (depending on the length of the alkyl chain) made it difficult to distinguish among all the modifications induced by changes of the hydrophobicity. Possible reorganizations of such micellar systems include variation of the size of the cross-links, or change of the concentration of the mixed micelles, together with changes of the association strength of the pendant groups.

In conclusion, molar stoichiometry dominates the bell-shape variation of the viscosity whereas local affinity between a polymer side group and the particle surface dominates the amplitude of the effect. It is worth to keep in mind that the “local” affinity may involve a few pendant groups per particle, being therefore dependent on the density of these groups along the polymer chain. The current view, well supported by the data above, is that solutions owe their viscoelasticity to the formation of a 3D network with polymers connected on a particle in a reversible manner. The transient nature of the bonds adds further complexity to this simple picture in that concentration may modulate the composition of the cross-links and shear-rate or frequency dependence of the network response should appear. Many theories of self-associating HP have been developed to account for shear thickening, shear thinning and strong effect of concentration on viscosity or elastic modulus. In summary, the first class of models refers to essentially unentangled macromolecules that self-associate to form bridged micelles (34, 35, 36). A transient network would be formed above critical values of both the number of micelles and the number of bridge per micelle. Close to this sol-gel transition, the viscosity and elastic modulus of such solutions would grow very steeply with any change of either the strength of the association or the concentration. The second category of models has been developed for entangled networks in which the chain motion is a reptation modulated by transient tie points (37). The shear-modulus and viscosity would be controlled by the slowing down of the reptation due to the transient sticky contacts with other chains. Near-perfect agreement with theoretical predictions of structure/concentration effects has been obtained recently with linear polymers having both a high molecular weight and alkyl pendant groups distributed along their backbone (38). It is beyond the scope of this introduction to discuss on the results of these models and their pertinence for mixed systems.

Nevertheless, some recent advances on the rheological studies of micelle/HP systems have given convincing evidence for their behavior being captured by the reptation approach (39, 40). On the other hand, the sol-gel transition determined in protein/HP mixtures, together with the absence of changes in the frequency of  $G'$ ,  $G''$  crossover in the gel domain, were consistent with a description in term of the transient network approach (24). It is still unclear whether this difference stem from the nature of the systems or from range of polymer length and concentration that have been considered. Studies on the micelle/HP systems were conducted at relatively high polymer concentrations and with long chains, in order to reach the regime of high entanglement between the macromolecules. Both assumptions of the reptation model were fulfilled, namely entangled structure and a low number of interchain "sticky" associations as compared to the interchain contacts. On the contrary, studies on protein/HP systems were carried out at as low a polymer concentration as possible in the absence of polymer self-association (absence of self-micellisation of the pendant hydrophobes). In practice, the presence of a critical sol-gel transition in protein/HP systems could be regarded as a promising hint for their use as very sensitive responsive systems. This was a reason for studies being launched on the development of light-responsive thickeners based on particle/polymer recognition using systems as close as possible to the protein/HP ones.

## Part 2: Photo-responsive Systems

### *Photoresponsive and Associating Polymers*

Associating water soluble polymers were derived from a precursor chain, poly(acrylic acid) in its sodium form. Two different precursor batches were used; they had an average molecular weight of 150.000 and 225.000 according to the supplier (Polysciences Inc, Warrington, PA). SEC analyses gave  $M_w$  of 130.000 and 370.000 respectively with polydispersity indexes of about 4 and 6. A minor fraction of acid groups along the precursors were grafted in an organic solvent by hydrophobic amines using a procedure already described (41). It enabled us to synthesize sets of random co- or ter-polymers comprising a large majority of carboxylic groups and a few mol % of pendant chromophore or alkyl groups. As compared to the copolymers, terpolymers contained additional octadecyl side groups that increased the affinity of the polymers for the particle without changing its photosensitivity. An example of the chemical structure of those amphiphilic polymers is shown in Figure 3. Their composition, determined by  $^1\text{H-NMR}$ ,  $^{13}\text{C-NMR}$  and by UV-visible spectroscopy is given in table 2.

Table 2: Composition and code of the azo-modified poly(acrylic acid) as determined by  $^1\text{H-NMR}$ ,  $^{13}\text{C-NMR}$  and by UV-visible spectroscopy.

Code	Mol % of octadecylamine "C18"	Mol % of azobenzene "azo"	Mol % of dodecylamido-phenyl-azobenzene: "C12azo"
150-1.1azo	0	1.1±0.1	0
150-4.5azo	0	4.5±0.3	0
150-7azo	0	7±0.5	0
225-3c18	2.9±0.3	0	0
150-1c18-0.5azo	0.5±0.1	1.2±0.1	0
150-1c18-4.5azo	1.3±0.2	4.5±0.2	0
150-1c18-1c12azo	1	0	1
225-0.9c12azo	0	0	0.9±0.1

The structure are denoted in the following with a code reflecting both the  $\overline{M}_w$  of the precursor poly (acrylic acid) and the grafting rate. For instance, 150-yC18-zAZO is a polymer that contains y mol % of C18, and z mol % of azobenzene groups. The grafted chromophores were either the aminophenylazobenzene (shown in figure 1) denoted "azo" or the aminododecylamidophenylazobenzene (i.e. the latter chromophore separated from the backbone via a "spacer" n-dodecyl chain) denoted c12azo.

Upon irradiation by UV or visible light, the azobenzene molecule has the particularity to undergo a reversible transconformation of the NN double bond from its trans isomer to the cis form. Its absorption spectrum is known to reflect this isomerization in water. The ungrafted trans azobenzene exhibits a main band in the visible range centered at about 320nm (42, 43). In the case of copolymers and terpolymers, this maximum of absorption was shifted to 347nm, due to the presence of an amide substituent (figure 4). The spectra of the modified polymers, however, were not sensitive to their grafting rate, neither to the presence of C18 along the polymer backbone. Upon irradiation at a wavelength close to the main absorption band, most of the trans azobenzene are expected to undergo isomerization to the cis conformation. This transconversion is accompanied by a marked drop of the absorption band at 347 nm, the cis form having a molar extinction coefficient equal to about 5% those of the trans conformation (44). Experiments were conducted on dilute polymer solutions in water (<0.1 wt%), which were submitted to UV irradiation at 365 nm. The rapid decrease of the main absorption band upon irradiation confirmed the rapid transconversion (Figure 4). All the polymers in table 2 reached a final stationary state, within two minutes, that was found to correspond to about 80% of transconversion (45). The presence of two tight isosbestic points (at 296 nm and 426 nm, figure 4) during the irradiation indicated that the phenomenon was not accompanied by any photodegradation. Upon a subsequent irradiation at 436nm, the initial spectrum was partially recovered, indicating the back-isomerization of cis isomers to the trans form. Almost 80% of azobenzene was found to be under its trans isomer form in the stationary state reached upon irradiation at 436 nm. It was finally possible to cycle the solutions by a regular change of the wavelengths used to irradiate the samples (figure 5). From the cycling values of the absorbency of the solutions, it was estimated that the two stationary states obtained steadily at each cycle corresponded to residual low or high fractions of trans isomer equal to about 20% or 75-80% respectively. Similar experiments were also performed in dilute mixtures containing both an azo-modified polymer and a colloid (SDS micelles and proteins (45), and unpublished data of  $\beta$  Cyclodextrin polymers). The absence of marked changes, as compared to the solutions of the sole polymer, showed that it was possible to

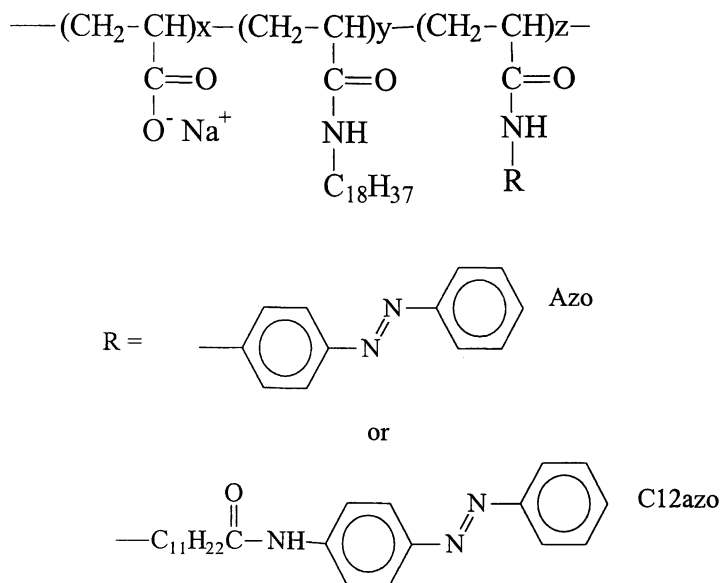


Figure 3: Typical structure of an azo-modified polymer.

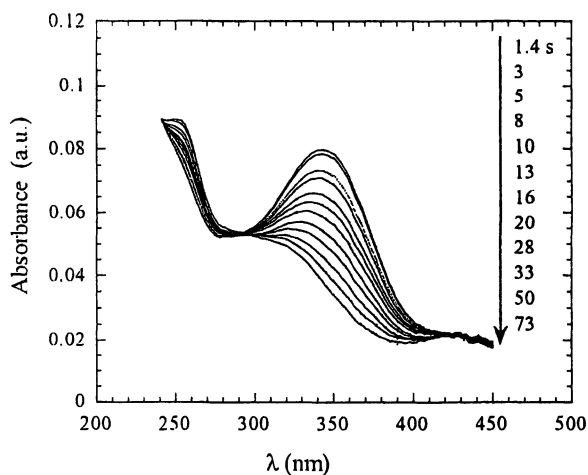


Figure 4: Change upon irradiation of the UV-visible spectrum of 150-1c18-0.5azo at 0.01 wt% in water. Irradiation wavelength = 365 nm  $\pm$  10 nm.



trigger similarly the cis-trans isomerization process in spite of the binding of the polymer to a particle. It was therefore attempted to study more concentrated mixture aiming at the formation of photosensitive gels.

To this aim, gels or highly viscous mixtures were obtained by supplementing azo-modified polymer solutions with one among the following “connector “ particles: SDS micelle (a 99% pure Sodium Dodecyl Sulfate, from Poly Labo), Bovine Serum Albumin (BSA, fraction V, 95% pure, from Sigma Chemical Co), or a  $\beta$ -cyclodextrin polymer ( $\beta$ CD-EP). The preparation of the latter water soluble  $\beta$ -cyclodextrin cluster was achieved by polycondensation of two monomers,  $\beta$ -cyclodextrin and epichlorohydrin using a procedure described in details by Renard et al (46). In this study we used a polymer with a  $\beta$ -cyclodextrin weight fraction of 55% and  $a = 29.900 \text{ g}\cdot\text{mol}^{-1}$ . This conferred to the  $\beta$ CD-EP an average number of CD cavities per particle equal to 15, each cavity being a putative site for the binding of a pendant group of the modified polymers. Measurements were initially conducted on the viscosity of mixtures kept in the dark. Although giving only indirect evidence for polymer/particle association, these experiments were convincing evidence for the formation of cross-links involving both polymer chromophores and the added particles. The figure 6 shows the viscosity of samples kept in the dark (all trans chromophores) at constant polymer concentration as a function of the colloid/polymer ratio (wt/wt). As discussed in part 1, when supplementation by a connector particle induced the formation of cross-links, the association was revealed by a marked increase of the viscosity as compared to the viscosity in absence of additive (usually more than 1-decade increase). Such a dramatic variation cannot be attributed to a change of the polymer extension. From these rheological measurements, it was established that SDS micelles, BSA, or  $\beta$ CD-EP bind some pendant groups along the terpolymers, that contained both C18 and the trans-azobenzene chromophore. Supplementation of an azo-modified copolymer solution, in the absence of C18 pendant group along the chain, did not result in any significant change using either SDS micelles or BSA additives (e.g. figure 6 with BSA/150-4.5azo and other data not shown). On the contrary the addition of  $\beta$ CD-EP clusters in azo-modified copolymers induced a pronounced variation of viscosity for the 150-4.5azo (figure 6), similar to the variations of bell shape curve in figure 2. However this behavior was not found again either with a lower or a higher grafting rate, namely 150-3azo and 150-7azo. The case of C12azo-modified copolymers has not been extensively considered to date, although gelification was observed in 150-1C18-1C12azo/BSA solutions and in 225-0.9C12azo/ $\beta$ CD-EP. Altogether our observations gave convincing evidence for the strong association between C18 side chains and all the particle additives, whereas the trans-azobenzene chromophores were only shown to bind  $\beta$ CD-EP, presumably via the expected formation of host/guest cross-links between the

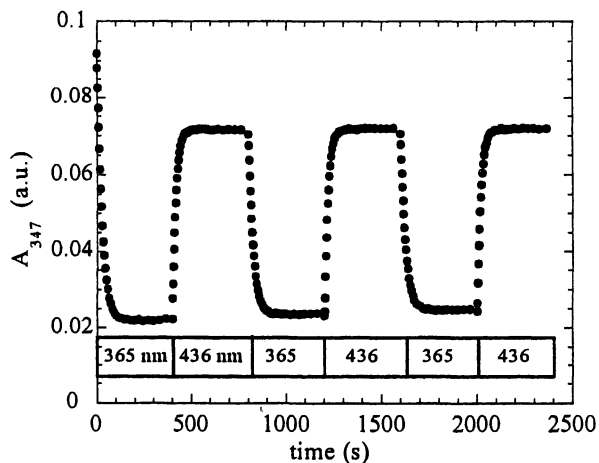


Figure 5: UV absorption at 347 nm of a 0.01 wt% 150-1c18-0.5azo solution in water as a function of the irradiation time. The irradiation wavelength was sequentially changed as indicated above the x-axis.

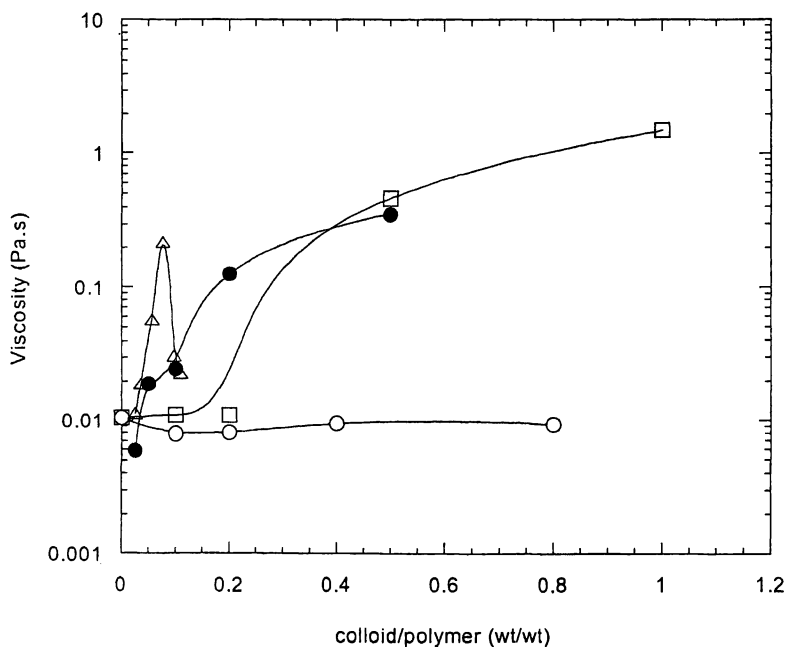


Figure 6: Variation of the viscosity as a constant polymer concentration, as a function of the colloid/azo-modified polymer ratio; (○) BSA + 1% 150-4.5azo, (□)  $\beta$ CD-EP + 1% 150-4.5azo, (●) BSA + 1% 150-1c18-4.5azo, ( $\Delta$ ) SDS + 2% 150-1c18-0.5. (Shear rate  $10s^{-1}$ ).

hydrophobic cavities of CD and the chromophore. Whether the chromophore was involved in the association of C18-containing polymer was not established from experiments carried out in the dark. However all samples that exhibited thickening effect were sensitive to irradiation, which reflected the influence of the chromophores on the formation of any type of cross-links.

### ***Photo-responsive viscosity in BSA- or SDS-based systems.***

In a typical experiment, a polymer/colloid mixtures was kept in water at least 24 hours in the dark, before being loaded in a transparent couette cell. It was then sheared at a constant shear rate and subjected to sequential irradiation (alternating the wavelength between 365nm and 436 nm). A complete description of the instrumentation was reported in a previous paper (45). As judged by the characteristic times of c.a. 2 min estimated from spectrophotometry (figure 5), the irradiation cycles were long enough (10-30 min) to let the system reach the stationary states of photo-isomerization. The initial value of viscosity in figure 7 corresponded to the measurements performed during the first 100 or 200 seconds where the samples were maintained in the dark. Therefore the initial value indicates the viscosity in the absence of cis isomers along the polymer backbone. In the examples displayed in Figure 7, the rapid drop of the viscosity was correlated with the increase of the fraction of cis pendant groups ( irradiation at 365 nm). A value close or slightly smaller than the initial viscosity was recovered upon the increase of the fraction of trans isomer during the irradiation at 436 nm. Similar viscosity cycles were obtained in a wide variety of azo-modified polymer/colloid mixtures, although the amplitude of the effect was strongly system-dependent. For systems, which were supplemented with BSA or SDS, no effect was noticed in the solutions of 150-xazo copolymers ( $x < 7\%$  as given in table 2). The photoresponse effect emerged for the terpolymers, comprised of both C18 and azo side groups. In these cases, the maximum relative variation of viscosity, between the initial viscosity in the dark and after irradiation at 365 nm, was rather small. Typical values of the relative changes were in the range 11%-25%. The effect was essentially independent of the grafting rate of azobenzene (in the range 0.5-3mol%) and also of the composition of the mixture. The substitution of the short azobenzene by C12azo enhanced significantly the amplitude of the effect. As shown on figure 7a, a photo-induced variation of the viscosity by a factor 2 became possible in the presence of BSA. Although the latter system was not studied extensively, it enabled us to observe a decrease of the viscosity by a factor as high as 3 upon irradiation at 365 nm (polymer 150-1C18-1C12azo 0.25% + BSA 0.3% in water). Its sensitivity to light was found to be strongly modulated by the BSA/polymer ratio, in the range 0.2–0.8 wt/wt.. Altogether, the results on BSA or SDS-based mixed systems were consistent with the photo thickening being correlated with the formation of cross-links involving both

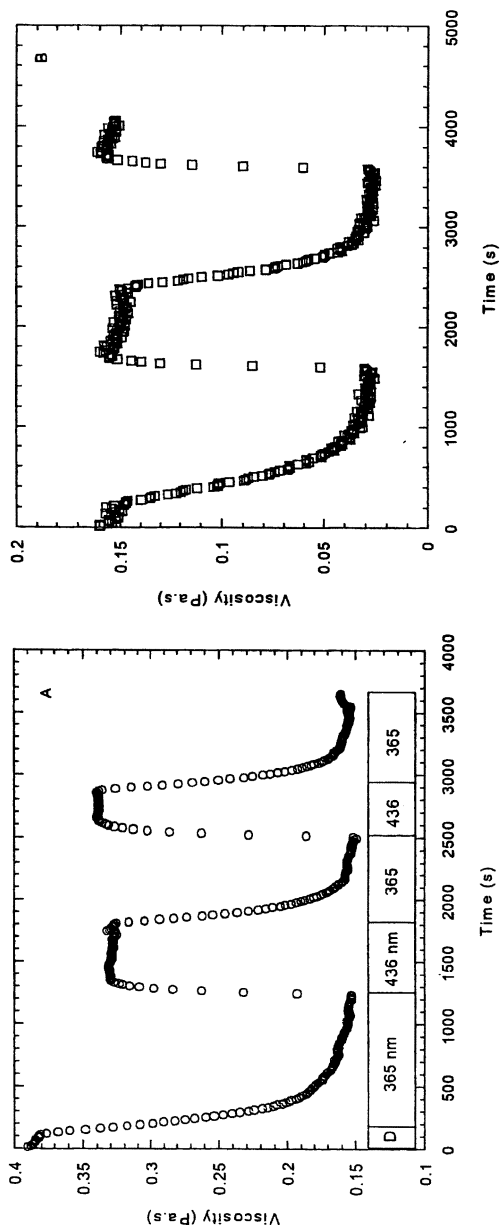


Figure 7 : Variation of viscosity as a function of the irradiation time at 365 and 436 nm for (A) 150-1c18-1c12azo + 0.3% azo and for (B) 225-0.9c12 azo + 0.25%  $\beta$ CD-EP. D stands for the initial period during which the sample is kept in the dark. (Shear rate  $10 \text{ s}^{-1}$ ).

C18 and azo benzene groups. Upon irradiation, the increase of the polarity of the chromophore and/or its change in shape would affect the stability of these cross-links. Both SDS and BSA can bind hydrophobic molecules. It was not surprising to find that an increase of the polarity was resulting in a decrease of the association. The latter polymer was the only one to exhibit marked photoresponse in the presence of BSA. A complete study has now confirmed that the presence of interpolymer associations was required for the photoresponsiveness to emerge (45).

### Systems containing $\beta$ -cyclodextrin polymers

The supplementation of copolymers and terpolymers solutions with  $\beta$ CD-EP polymer gave more complex phenomena that need more detailed explanations. Using  $\beta$ -cyclodextrin clusters, we noticed the thickening effect in the dark and the presence of photoresponse for both azo-modified copolymers and terpolymers. Moreover, all these mixtures allowed us to obtain easily marked photo-induced variation (Figure 7b and data not shown on 150-4.5 azo showing decreases by a factor higher than 2).  $\beta$ CD-EP clusters appeared in that sense as a more responsive and more versatile cross-linkers than BSA or SDS. Although it was observed that the variation of viscosity versus the concentration of  $\beta$ CD-EP showed a common bell shape curve (see for example fig 8), the maximum of this curve was found at a fixed value of  $\beta$ CD-EP/amphiphilic polymer ratio. This optimal ratio, close to 3-4 g/g (table 3), did not depend on either the grafting rate and the type of the pendant groups. The number of pendant group per  $\beta$ CD cluster was therefore strongly varying from one polymer to another. Additionally, the number of pendant group per particle, usually higher than 3 (cf table 1), was as low as 1 pendant group per particle at the optimal viscosity enhancement. A possible explanation would be the presence of a large fraction of unbound CD-EP particles that do not contribute to cross-links. Under such an assumption, the affinity of azo groups for CD cavities should be extremely low, as judged by the large excess of CD cavities at the optimal thickening effect (table 3).

Like the samples containing BSA or SDS, all polymers that were found to associate with  $\beta$ CD-EP gave also mixtures sensitive to irradiation. Figure 8 shows the difference in viscosity at different mixture compositions (sweeping through all the bell-shaped curve) as induced by irradiation at 365nm. Owing to the huge dependence of viscosity on the composition, a relative scale was needed for a comparison of the light-sensitivity among different samples. An

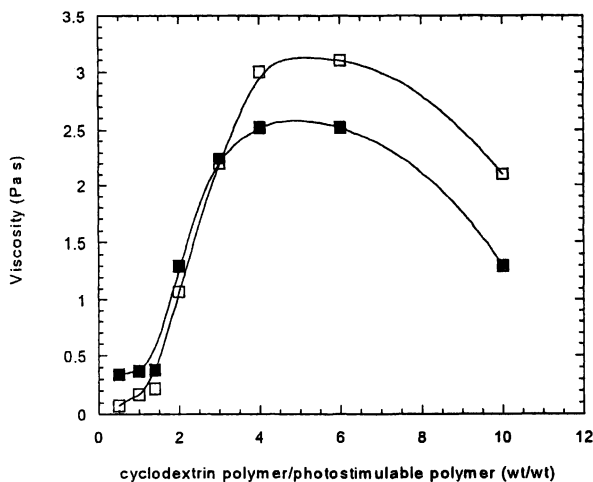


Figure 8: Variations of viscosity of 0.5% solutions of 150-0.9C12azo as a function of the  $\beta$ CD-EP/ polymer ratio ( $\square$ ) in the dark (all trans conformation) and ( $\blacksquare$ ) after a 1000s irradiation at 365 nm. (shear rate  $10s^{-1}$ ).

Table 3: Characteristic features of water solutions of modified polymer at the viscosity maximum reached upon supplementation with  $\beta$ CD-EP particles.

Polymers	225-1c12azo	225-1c12azo	150-1c18-4.5azo	225-3c18	150-4.5azo
<b>Polymer Concentration (wt %)</b>	0.5	0.7	0.7	1	1
<b>Maximum viscosity (Pa.s)</b>	2.5	7.1	0.23	128	~ 2
<b>Optimum ratios CD-EP/ polymer (wt/wt)</b>	3.4 - 6.7	2.5 - 4.3	4 - 5.9	3.0 - 4.0	~ 2 - 3
<b>Pendant group/CD particle (mol/mol)</b>	0.5 - 1.0	0.8-1.4	3 - 5	3 - 4	~ 6 - 8

index of photoresponsiveness was defined as the ratio  $\frac{\Delta\eta}{\eta_a}$  where  $\Delta\eta$  and  $\eta_a$

were respectively the difference and the average value of viscosity between the two plateaus measured in the dark and after irradiation. Figure 9 shows the relative variation of viscosity, between the initial value (dark-adapted mixtures), and after irradiation at 365nm, as a function of the composition. Positive or negative ratios mean an increasing or a decreasing viscosity upon irradiation respectively. For the 225-0.9c12azo the index was negative at low concentration of  $\beta$ CD-EP and became positive at higher concentration. The maximum value of 1 of the index corresponded to a variation by a factor of 3. The index of 150-4.5azo was found to present a negative sign at low concentration and a maximum value of 1.2. On the contrary, with 150-1c18-4.5azo, the sign of the index was reversed even though the amplitude of the effect was similar to the latter cases.

The simple origin proposed to interpret the behavior of SDS or BSA-based systems cannot explain the change of the sign of the index of photoresponsiveness. If the azobenzene groups in their trans conformation would have the possibility to penetrate inside the hydrophobic cavity of cyclodextrin, whereas the cis form would stay outside due to the steric hindrance or loss of hydrophobicity, it is expected that irradiation in the presence of low cross-linkers concentration always decreases the viscosity. Moreover it appeared that the index (positive or negative) was maximum for samples well below or beyond the optimal composition of highest viscosity. A high concentration of interpolymer links was therefore unfavorable to the response to light. These apparently conflicting results may be rationalized in the framework of the transient network model. Provided that a critical sol-gel transition would occur, it would involve the percolation of polymer/particle clusters at some critical composition. Any light-induced variation of the affinity of the pendant groups to the particle, changing slightly the fraction of cross-links in the sample, would result close to this critical composition to important variations of the number of elastically active chains. This might explain how the photoresponsiveness should be low in gelified sample, while it is high at both low or high particle concentrations, close to the composition that either induce gelation or break the gel. In other terms, the criticality of sol-gel transition should amplify small variations of the binding density of particle. In azo-modified copolymer solutions, the expected decreasing affinity upon formation of cis isomers would result in a retardation of the gelation. At low particles concentration, the viscosity would thus decrease upon irradiation. On the contrary, at high particle concentration, when the interpolymer connections are broken through increasing binding of particle, the same release of bound pendant group upon irradiation would induce an increase of the viscosity. The

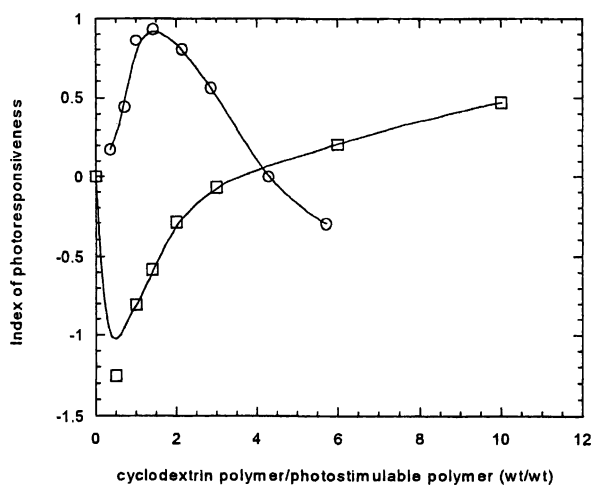


Figure 9: Relative amplitude of variation of the viscosity upon irradiation at 365 nm as a function of the  $\beta$ CD-EP/polymer ratio in (□) 225-0.9C12 azo 0.5%, (○) 150-1c18-4.5azo 0.7%. (shear rate  $10s^{-1}$ ).



sign of the photoresponsiveness index would be the inverse as that observed at low particle concentration. An interpretation of the dependence sign inversion due to modification of structure of polymers is also possible. It needs however to assume that the apparent affinity of azobenzene groups for the cyclodextrine would be modulated by the presence of C18. The association with terpolymers should involve a competition between the 2 different pendant groups C18 and azobenzene, that both could be accommodated by the cyclodextrin cavity. If the azo groups were able to displace bound C18, their transconversion from trans to cis would be accompanied by an apparent strengthening of C18 binding. As a result, the effect of irradiation could be inverted as compared to azo-modified copolymers, provided that the C18 play the major role in the viscosity enhancement. Collecting data to settle on the mechanism of photoresponsiveness will deserve further works being conducted for instance on the estimation of binding, and competitions of the various pendant groups (and isomers) on cyclodextrin clusters. The low affinity of benzene derivatives as compared to long alkyl chain has been reported for monomer of CD (47,48). The known binding constant of molecules similar to the present pendant groups are thus consistent with the preferential binding of C18 along terpolymers.

### Conclusion:

An association of polymer with particles has appeared a general principle to adjust the viscosity or the elastic modulus of water-based systems. Their sensitivity to many structural parameters (polymer composition, type of particle...) and system parameters (particle concentration, pH, molecular competitors...), together with the facile mixing of the two fluid solutions of the separated partners confer to such mixture a high versatility. Viscous fluids, or gels exhibiting a shear modulus as high as 100 Pa, were obtained at polymer concentrations of the order of 1 wt%. In addition, simple arguments (stoichiometry, association strength) can be used to predict the behavior of unknown mixtures.

Playing with recognition phenomena opened new avenues to develop responsive systems on that basis. This work showed the good sensitivity of such mixtures to very tenuous modifications such as a cis-trans isomerization of one among hundred monomers along the polymer backbone. From the present results, it is expected that a simple irradiation under UV or visible light should trigger the flow rate, and possibly the rate of release of trapped compounds, by a factor higher than three. The strength and life-time of particle/polymer association is likely to influence significantly this photo-responsiveness. Future works will aim at the optimization of the sensitivity to light. Many parameters are still largely unexploited, including the accessibility of pendant chromophores (via a

spacer group), the chemical nature of the chromophore, possible competition between two different pendant groups...Among the various connector particles that were considered, the clusters of cyclodextrins offer the interesting advantage that both their size and specificity can be varied by synthesis. Protein-based systems should also find applications when sensitivity to biomolecules is required.

### Acknowledgments:

The authors would like to thank C.Prata for her assistance in the synthesis of the alkyl spacer. This project was mainly supported by the Ministère de la Recherche (France), CNRS, and TMR Marie Curie grant n°ERBFMBICT983300.

### Literature Cited:

- <sup>1</sup> Winnick, M.; Yekta, A.; *Curr. Opin. Colloid Interface Sci.* **1997**, *2*, 424-436.
- <sup>2</sup> Annable, T.; Buscall, R.; Ettelaie, R. *Colloids and Surfaces A* **1996**, *112*, 97-116
- <sup>3</sup> Magny, B.; Iliopoulos, I.; Audebert, R.; In *Macromolecular complexes in chemistry and biology*, Dubin, P.; Bock, D.; Schulz D.N.; Thies, C. Eds; Springer-Verlag, Berlin **1994**; pp 51-62.
- <sup>4</sup> Goddard E.D.; Ananthapadmanabhan K.P.; Application of polymer-surfactant systems, In *Polymer-surfactant systems surfactant science series Kwak J.C.Ed; M. Dekker Inc, vol77 (1998)*, pp22-64
- <sup>5</sup> Magny, B.; Iliopoulos, I.; Zana, R.; Audebert, R. *Langmuir* **1994**, *10*, 3180-3187
- <sup>6</sup> Piculell, L.; Thuresson, K.; Ericsson, O. *Faraday Discuss.* **1995**, *101*, 307-318
- <sup>7</sup> Petit, F.; Audebert, R.; Iliopoulos, I.; *Colloid Polymer Sci.* **1995**, *273*, 777-781
- <sup>8</sup> Moine, L.; Cammas, S.; Amiel, C.; Renard, E.; Sebille, B.; Guérin, P. *Macromol. Symp.* **1998**, *130*, 45-52.
- <sup>9</sup> Amiel, C.; Sandier, A.; Sébille, B.; Valat, P.; Wintgens, V. Associations between end-capped polyethylene oxide and water-soluble  $\beta$ -cyclodextrin polymers, *Int. J. polymer Analysis Characterisation* **1995**, *1*, 289-300.

- <sup>10</sup> Sarrazin-Cartalas, A.; Iliopoulos, I.; Audebert, R.; Olsson, U.; *Langmuir* **1994**, *10*, 1421-1426.
- <sup>11</sup> Hourdet, D.; L'Alloret, F.; Audebert, R. *Polymer* **1994**, *35*, 2625-2630
- <sup>12</sup> Lee, S.J.; Park, K. Synthesis and characterisation of sol-gel phase reversible hydrogels sensitive to glucose, *Polym. Preprints* **1994**, *35*, 391-392
- <sup>13</sup> Eisenback, C. D. *Polymer* **1980**, *21*, 1175-1179
- <sup>14</sup> Irie, M.; Hirano, Y.; Hashimoto, S.; Hayashi, K. *Macromolecules* **1981**, *14*, 262-267
- <sup>15</sup> Mamada, A.; Tanaka, T.; Kunwatchakun, D.; Irie, M. *Macromolecules* **1990**, *23*, 1517-1519
- <sup>16</sup> Irie, M. in *Advances in Polymer Science*, vol. 110, K. Dusek Ed., Springer Verlag, **1993**, 50-65
- <sup>17</sup> Irie, M.; Tanaka, H. *Macromolecules* **1983**, *16*, 210-214
- <sup>18</sup> Irie, M.; Schnabel, W. *Macromolecules* **1985**, *18*, 394-398
- <sup>19</sup> Willner, I.; Rubin, S. *Angew. Chem. Int. Ed. Engl.* **1996**, *35*, 367-385
- <sup>20</sup> Murata, K., Aoki, M., Suzuki, T., Harada, T., Kawabata, H., Komori, T., Ohseto, F., Ueda, K., Shinkai, S., *Journal of the American Chemical Society* **1994**, *116*, 6664-6676
- <sup>21</sup> Sau, A.C.; Landoll, L.M.; in Glass J.E. Ed, *Polymer in aqueous media: performance through association*, ACS Adv. Chem. Ser. (**1986**), Vol 213, 343-
- <sup>22</sup> Panmai, S.; Prud'homme, R.K.; Peiffer, D. *Rheology of HP with spherical and rod-like surfactant micelles*, *Colloids and surfaces A* **1999**, vol 147, 3-15
- <sup>23</sup> Deguchi, S.; Kuroda, K.; Akiyoshi, K.; Lindman, B.; Sunamoto, J. *Gelation of cholesterol-bearing pullulan by surfactant and its rheology*, *Colloid and surfaces A* **1999**, vol 147, 203-211.
- <sup>24</sup> Borrega, R.; Tribet, C.; Audebert, R., *Macromolecules* **1999**, *32*, 7798-7806
- <sup>25</sup> Weickenmeier, M.; Wenz, G.; Huff, J. *Macromol. Rapid Commun.* **1997**, *18*, 1117-1123
- <sup>26</sup> Filali, M.; Aznar, R.; Svenson, M.; Porte, G.; Appell, J. *J. Phys. Chem. B* **1999**, *103*, 7293-7301
- <sup>27</sup> Gosselet, N.M.; Borie, C.; Amiel, C.; Sébille, B. *J. dispersion sci. And Technol.* **1998**, *19* (6-7), 805-820.
- <sup>28</sup> Borrega, R.; Tribet, C.; Audebert, R. *Gelation and demixing in HP/protein mixtures*, Proc. Yamada Conf. On Polyelectrolytes, Noda, J.; Kokufuta, E.; Ed (**1999**) Japan, pp 311-314
- <sup>29</sup> Piculell, L.; Lindman, B.; Karlstroem, G. *Phase behavior of polymer-surfactant systems*, In Kwak, J.C. Ed, *Polymer-surfactant system*, *Surfactant science series* **1998**, vol 77 pp 65-141
- <sup>30</sup> Moine, L.; Amiel, C.; Brown, W.; Guerin, P. in preparation
- <sup>31</sup> Porcar, I.; Cottet, H.; Tribet, C.; Gareil, P. *Macromolecules* **1999**, *32*, 3922-3929
- <sup>32</sup> Magny, B., Ph. D Dissertation Thesis, University Paris 6, Paris, France, 1992.

- <sup>33</sup> Heitz, C.; Prud'homme, R.K.; Kohn, J.; *Macromolecules* **1999**, *32*, 6658-6667.
- <sup>34</sup> Annable, T.; Buscall, R.; Ettelaie, R.; Whittlestone, D. *J. Rheol.* **1993**, *37*(4), 695-726.
- <sup>35</sup> Tanaka, F.; Edwards, S.F. *J. Non-Newtonian fluid mech.* **1992**, *43*, 247-309.
- <sup>36</sup> Semenov, A.N.; Joanny, J-F.; Khokhlov, A. *Macromolecules* **1995**, *28*, 1066-1075
- <sup>37</sup> Leibler, L.; Rubinstein, M.; Colby, R.H. *Macromolecules* **1991**, *24*, 4701-4707
- <sup>38</sup> Regalado E.; Selb, J.; Candau, F. *Macromolecules* **1999**, *32*, 8580-8588.
- <sup>39</sup> Guillemet, F. Thesis University Paris 6, Paris, France, **1995**
- <sup>40</sup> Candau, F. Personal communication.
- <sup>41</sup> Wang T.K.; Iliopoulos I.; Audebert R.; *Polymer Bulletin* **1988**, *20*, 577-585
- <sup>42</sup> Zimmerman, G.; Chow, L.Y.; Paik, U.J.; *J. Am. Chem. Soc.* **1958**, 3528-3531
- <sup>43</sup> Bullock, D.J.W.; Cumper, C.W.N.; Vogel, A.I.; *J. Chem. Soc.* **1965**, *XLIII*, 5316
- <sup>44</sup> Morishima, Y.; Tsuji, M.; Kamachi, M.; Hatada, K.; *Macromolecules* **1992**, *25*, 4406-4410
- <sup>45</sup> Porcar, I.; Sergot Ph.; Tribet C.; *A.C.S. Adv. Chem. Series*, Stimuli reponsive and amphiphilic polymers, C. Mc Cormick Ed.; **2001**, 82-100
- <sup>46</sup> Renard, E.; Deratani, A.; Vollet, G.; Sebille, B.; *Eur. Polym. J.* **1997**, *33*, 49-57
- <sup>47</sup> Bertrand, G.L.; Faulkner, J.R.; Han, S.H., Armstrong, D.W, *J. Phys. Chem* **1989**, *93*, 6863-6867
- <sup>48</sup> Park, J.W.; Soong, H.J.; *J. Phys. Chem.* **1989**, *93*, 6454-6458

## Chapter 19

# Amphiphilic Gels with Controlled Mesh Dimensions for Insulin Delivery

J. P. Kennedy<sup>1</sup>, G. Fenyvesi<sup>1</sup>, S. Na<sup>1</sup>, B. Keszler<sup>1</sup>, and K. S. Rosenthal<sup>2</sup>

<sup>1</sup>Institute of Polymer Science, The University of Akron, Akron, OH 44325-3909

<sup>2</sup>Northeastern Ohio Universities College of Medicine, Box 95, Rootstown, OH 44272

### Introduction

Our ultimate goal is the development of a functioning bioartificial pancreas to provide long term correction of blood glucose levels in individuals with Type 1 diabetes. Our device consists of porcine islets or islet fragments enclosed in a fully synthetic precision designed polymer membrane that is flexible, biocompatible and permeable to glucose, insulin, and oxygen, but impermeable to immune cells and proteins greater than  $\sim 60,000$  g/mol, e.g. immunoglobulins. The membranes are designed such that upon implantation, the encapsulated porcine islets are able to sense and regulate the glucose level in the blood of diabetic individuals and at the same time are isolated from the onslaught of the immune system. In this manner, the bioartificial device can remain functional for an extended period of time and then be readily removed and replaced.

Encapsulation of islets has been investigated by various groups of researchers employing a variety of materials. A thorough analysis of the requirements discussed in the scientific and patent literature leads us to suggest that the optimum membrane of an implantable biohybrid device for immunoisolating islets should exhibit the following characteristics:

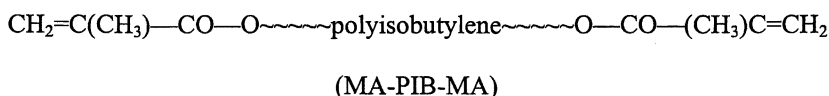
1. Biocompatible, biostable, sturdy, rubbery with properties maintained for long periods ( $\sim 1$  year) of implantation
2. Nonthrombogenic, hemocompatible, avascular, nonclogging, smooth, immunologically "invisible" surfaces

3. Membranes with designed pore sizes (i.e., molecular weight cut-off ranges) for controlled permeability
4. Physiologically satisfactory bi-directional fluxes of glucose, insulin, nutrients and metabolites, with exclusion of immunoglobulins
5. Thin membrane walls to ensure rapid oxygen diffusion
6. Good mechanical properties (strength, modulus, elongation) maintained for long implantation times
7. Easily manufactured into sealable transparent tubules of well-defined volumes
8. Easily retrievable after long implantation
9. Sterilizable (with steam or ethylene oxide)
10. Reasonable cost

Available implantable devices for the correction of diabetes have several but not all of these properties. Many researchers utilize alginate gels to microencapsulate individual islets (1-3). The fundamental disadvantage of microencapsulation, however, is that the microcapsules enveloping the islets cannot be completely and reliably retrieved.

Our research started some 10 years ago after the development of designed controlled release devices when we recognized that the material requirements for a drug delivery device and that of an implantable macro-immunoisulatory membrane are quite similar. For both applications the devices must be biocompatible ("bioinvisible") and biostable, must have smooth non-clogging surfaces even after long implantation times, must allow the diffusion of desirable well-defined molecules, must have controlled pore sizes, must be sterilizable, and must have robust mechanical properties for implantation, use, and easy retrieval.

Upon analysis of the requirements for an ideal immunobarrier membrane we concluded that the synthesis of such a membrane was feasible by our recently discovered/patented "living" polymerization technique (4,5). By this technique we have synthesized polyisobutylene-based, novel, hydrophobic crosslinking agents, e.g., methacrylate-ditelechelic polyisobutylene (MA-PIB-MA), which has become a key ingredient for our membranes:



Immunoisulatory amphiphilic networks have been prepared by crosslinking water-soluble acrylate (e.g., N,N-dimethyl acrylamide) chains with MA-PIB-MA (6). Figure 1 helps to visualize the microarchitecture of a network that changes its microstructure depending upon the medium with which it is in

contact, i.e. water, hydrocarbon (HC), or amphiphilic solvent e.g., tetrahydrofuran (THF) (“smart” networks) (7,8). This conformational isomerization upon contact with various media is virtually instantaneous and may account for the biocompatibility of our networks. The hydrophilic polyacrylate moiety in our networks give rise to slipperiness while the hydrophobic PIB moiety ensures elasticity, softness, and strength.

The physical-chemical-mechanical-biological properties of our amphiphilic networks have been characterized by a battery of various techniques (9-16). The hydrophilic/hydrophobic content of our network is 50/50, and the diameter of the hydrophobic domains is 2-8 nm diameter (12). These membranes can be formed into rubbery 3-5 cm long, 0.5 cm diameter tubules with very thin walls of defined thickness (0.15-0.2 mm). The tubules can be sealed with methyl cyanoacrylate (“superglue”) by crimping or by inserting a plug of the same amphiphilic material. The tubules are optically clear, heat resistant and can be sterilized by autoclaving at 120°C.

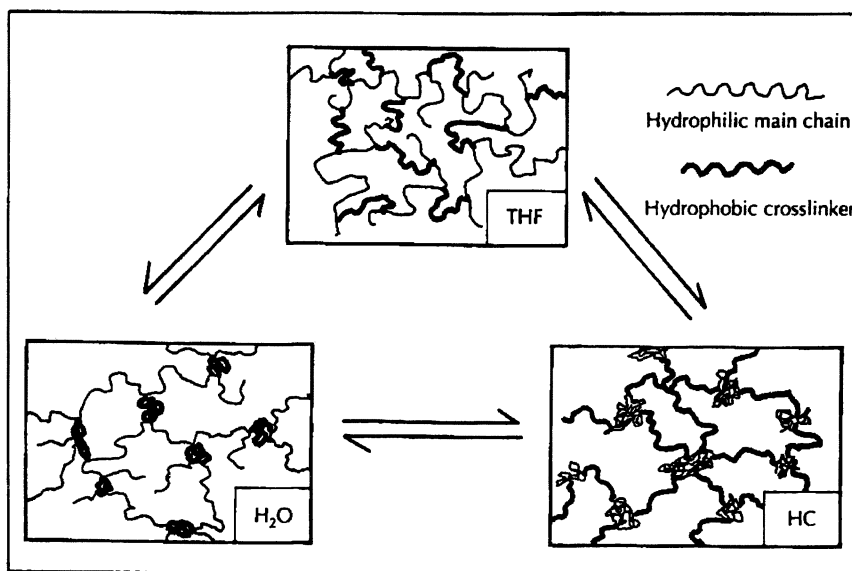


Figure 1. Microarchitecture of Amphiphilic Networks in Various Media

The biocompatibility of the membranes was demonstrated by *in vivo* implantation in rats for longer than 120 days. The absence of inflammation and fibrous cell growth at the site of implantation, and lack of adherence or abnormal vascularization on or near the device was demonstrated by histology and scanning electron microscopy of explants. These membranes adsorb less fibrinogen, albumin and Hageman factor (factor XII) than glass, polyethylene or silicone rubber (12). Reduced protein adsorption and cell adhesion also indicated hemocompatibility at blood contacting surfaces (9,14).

The present research concerned investigations to elucidate the molecular weight cut-off (MWCO) ranges of the membranes intended for use in our bioartificial pancreas and the diffusional characteristics of glucose and insulin through the membranes. The MWCO ranges were compared to the hydrodynamic (or Stokes) radii ( $R_s$ ) of the various protein markers capable of permeating through the membranes as descriptors of membrane permeability characteristics.

## Experimental

**Network Synthesis:** The synthesis of methacrylate ditelechelic polyisobutylene (MA-PIB-MA) has been described (6,10,17-19). The hydrophilic monomer N,N-dimethylacrylamide, (DMMAm) (Aldrich) was copolymerized/crosslinked with MA-PIB-MA in THF solution. Active copolymerizing charges together with azo-bis(isobutyronitrile) (AIBN) were rotated in 20-25 cm long and ~4.0 mm inner diameter glass tubes at ~60°C. The centrifugal force moves the active polymerizing charges to the wall of the revolving tube and thus tubular membranes can be prepared. The tubes were removed from the reactor, washed sequentially by hexanes, ethanol and distilled water, and conditioned with a physiological buffer solution. The inner diameter (~0.25 cm) and wall thickness (~0.02 cm) of the tubules were determined with a hemocytometer using a light microscope. The hydrophilic/hydrophobic ratios of the tubules were 40/60, 50/50, and 60/40 wt%. The amphiphilic networks are identified by a three character name, e.g. A-10-50 in which the letter refers to the hydrophilic component; A: N,N-dimethyl acrylamide; the 10 refers to the molecular weight of the PIB component; and the 50 refers to the weight percentage of hydrophobic component in the membrane.

**Pore Size Diameter:** The molecular weight cut-off (MWCO) and pore size ranges of tubules were studied by determining the permeability of the membranes by the use of a series of commercially available protein markers of known molecular weight and size, i.e., aprotinin (MW=6,500 g/mol,  $R_s$  = 1.5 nm), cytochrome C (MW = 12,400 g/mol,  $R_s$  = 1.63 nm), carbonic anhydrase (MW = 29,000 g/mol,  $R_s$  = 2.01 nm), and albumin (MW = 66,000 g/mol,  $R_s$  = 3.62). Tubules were loaded with a mixture of four different proteins, and were sealed by crimping and cementing with cyanoacrylate. The protein-filled tubules were incubated in 5 mL of phosphate buffered saline at 37 °C with



shaking, and aliquots of the surrounding buffer were removed at different times. The aliquots were then analyzed by sodium dodecyl sulfate-polyacrylamide gel electrophoresis (SDS-PAGE) to identify the proteins that had permeated the tubes. The proteins were electrophoresed in tris-glycine 4-20% bis-polyacrylamide gels (20) and then stained with coomassie blue.

**Permeability and Diffusion Studies:** Tubules of different composition were filled with sterile glucose (40mg/mL) and insulin (40mg/mL) solutions in phosphate buffered saline, pH 7.4 (PBS). The tubules were sealed and then incubated with shaking at 37° C in 5 mL of PBS. Aliquots were removed at different time intervals and the concentration of glucose determined colorimetrically by the glucose oxidase method (21) and insulin by the protein dye binding assay (22).

## Results and Discussion

### Pore Size Determination:

The permeability of tubules with networks ranging from A-10-50 to A-2.5-60 were compared (Figure 1 and Table 1). A molecular weight cut-off range (MWCO) was obtained by determining which of a series of globular proteins was capable of permeating the membrane of the tubule. This is the conventional parameter which is used to describe the pore size of membranes. In this study we also assessed the permeability of the membranes with regard to the Stokes radius ( $R_s$ ) of the proteins capable of passing into the surrounding medium. This parameter provides a better description of the shape and size of the molecules which permeate the network membrane and hence, its porosity.

In Figure 1, the  $M_{c,hydrophilic}$  for a set of membranes was plotted with respect to either MWCO (Figure 2A) or Stokes radius (Figure 2B). The  $M_{c,hydrophilic}$  is the molecular weight of the hydrophilic segment. The lines are drawn to indicate the ranges of proteins which were capable of permeating through the membrane such that the area between the lines includes the proteins which were capable of permeating the membrane. The membranes are transparent to proteins with molecular weights or  $R_s$  below the upper line. The upper line is indicative of the cut-off range for permeability of proteins and hence, opacity. The MWCO or  $R_s$  cut-off are represented as ranges because these membranes do not have well defined pores.

The  $M_{c,hydrophilic}$  of the membranes provides the best correlation with the permeability cut-off ranges of the membranes. This parameter can therefore be used to select the appropriate membrane for an insulin delivery biodevice. The membrane should provide optimal permeability to glucose (too small to be of concern) and insulin (~5,700g/mol) but restrict the entry of immunoglobulins (>60,000g/mol). With this criterion, the A-10-50, A-10-60 or A-4.5-40

membranes should be appropriate to immunoisolate encapsulated islet cells but still allow optimal permeability of glucose and insulin.

#### Permeability and diffusion studies:

Amphiphilic network tubules varying in composition and  $M_{c,hydrophilic}$  were evaluated further for permeability and diffusion coefficients for glucose, insulin and albumin (Table II). There was some variability in thickness of the membranes due to experimental conditions but this was factored into the calculations.

As expected, glucose was freely permeable through the membranes while insulin was somewhat less permeable and albumin was impermeable. The membranes exhibited superior permeability characteristics. Membranes with higher  $M_{c,hydrophilic}$  were more permeable to insulin. In comparison, the diffusion coefficients of glucose and insulin through membranes prepared with poly(hydroxyethylmethacrylate) as the hydrophilic segment were only 0.042 and  $0.009 \times 10^6$  (cm<sup>2</sup>/sec) respectively (15). Earlier diffusion studies performed with different MA-PIB-MA membranes formed into flat membranes (15,18) gave very similar results as described herein for tubules. Our results for insulin permeability and diffusion indicate that the membranes and the tubules are satisfactory for use in an artificial pancreas biodevice. On the basis of these results the A-10-40 network was chosen for further *in vitro* and *in vivo* experiments.

**TABLE 1. Molecular Weight Cut-Offs and Pore Size Ranges**

Amphiphilic Network	$M_{c,hydrophilic}$ g/mol	Molecular Weight Range g/mol	Stokes Radii ( $R_s$ ) Range nm
A-10-50	5000	29,000 – 66,000	2.01 - 3.62
A-10-60	3333	29,000 – 66,000	2.01 - 3.62
A-4.5-40	3375	29,000 – 66,000	2.01 - 3.62
A-4.5-50	2250	12,400 - 29,000	1.63 – 2.01
A-4.5-60	1500	12,400 - 29,000	1.63 – 2.01
A-2.5-40	1875	12,400 - 29,000	1.63 – 2.01
A-2.5-50	1250	6,500 – 12,400	1.50 – 1.63
A-2.5-60	833	6,500 – 12,400	1.50 – 1.63

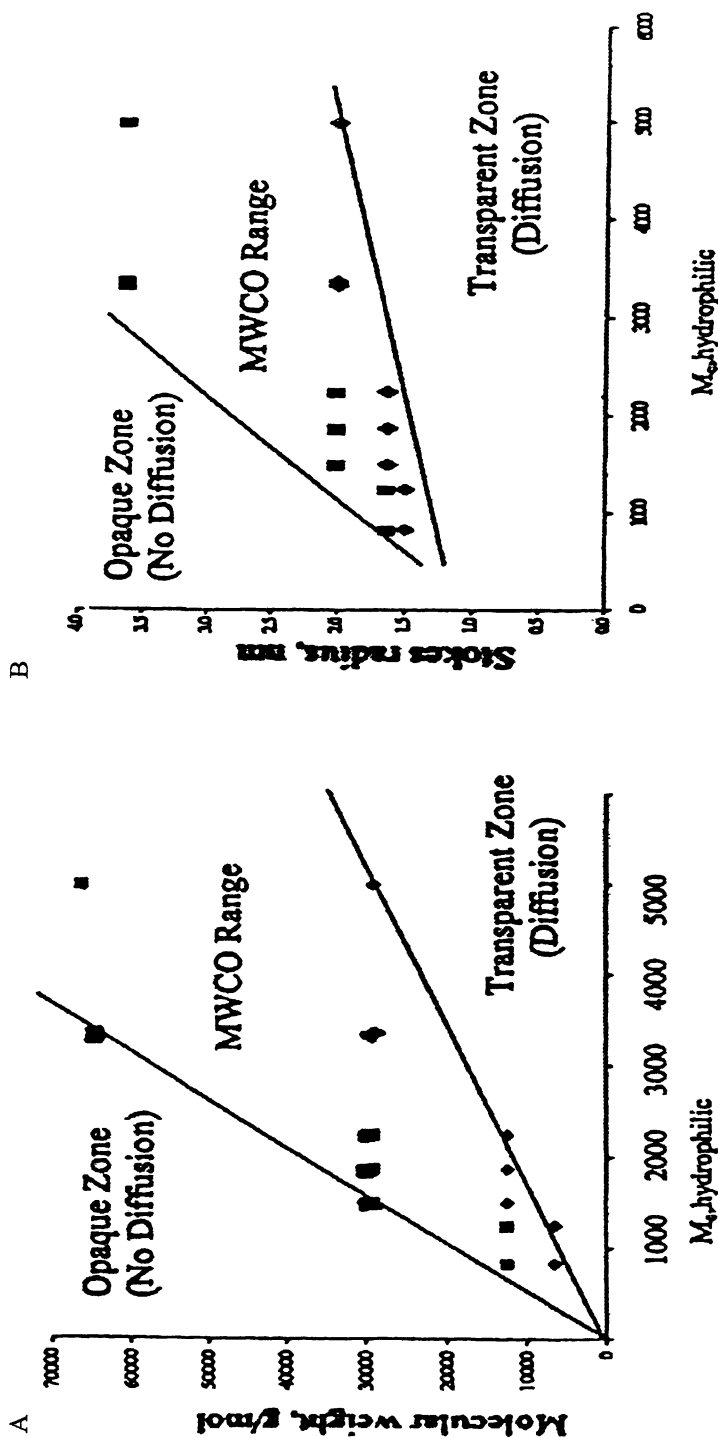


Figure 2. Correlation between  $M_{c,hydrophilic}$  and MW (A), and  $M_{c,hydrophilic}$  and Stokes radius (B). The symbols  $\blacklozenge$  and  $\blacksquare$  respectively indicate molecular weights and radii of the protein markers that have or have not diffused through the membrane.

**Table 2. Diffusion and Permeability of Glucose and Insulin Through Tubular Amphiphilic Networks**

Amphiphilic Network <sup>1</sup>	M <sub>w,hydrophilic</sub> g/mol	Diffusion Coefficient		Permeability	
		Glucose x10 <sup>6</sup> cm <sup>2</sup> /s	Insulin x10 <sup>6</sup> cm <sup>2</sup> /s	Glucose x10 <sup>7</sup> cm <sup>2</sup> /s	Insulin x10 <sup>7</sup> cm <sup>2</sup> /s
A-10-50	5500	1.34±0.03	0.19±0.04	1.03±0.02	0.26±0.02
A-10-60	3333	1.18±0.02	0.16±0.03	1.06±0.02	0.10±0.01
A-4.5-40	3375	1.01±0.01	0.14±0.03	1.71±0.02	0.14±0.03
A-4.5-50	2250	1.01±0.01	0.10±0.01	1.66±0.02	0.065±0.02
A-4.5-60	1500	1.03±0.03	0.187±0.01	1.56±0.02	0.026±0.01
A-2.4-40	1875	1.06±0.02	0.076±0.02	1.13±0.01	0.036±0.01
A-2.4-50	1250	1.25±0.03	0.057±0.01	1.12±0.02	0.022±0.01
A-2.4-60	833	1.34±0.02	0.047±0.01	1.12±0.02	0.015±0.01

<sup>1</sup> Wall thickness of tubule was approximately 0.02 cm.

## Summary

A series of amphiphilic networks, poly(N,N-dimethylacrylamide)-l-polyisobutylene, with different hydrophilic to hydrophobic ratios were synthesized and thin-walled tubular membranes were prepared. The molecular weight cut-off ranges and the insulin and glucose diffusion coefficients and permeabilities were determined. Our results show a direct correlation between the  $M_{c,\text{hydrophilic}}$  and the permeability of the membrane. According to these studies,  $M_{c,\text{hydrophilic}}$  is the significant parameter that correlates with permeability, allowing selection of the appropriate membrane for development of a bioartificial pancreas.

## Acknowledgements

This research was supported by grants from the National Science Foundation (DMR-99-88808), the Summa Health System Foundation and a Research Challenge Grant from Northeastern Ohio Universities College of Medicine. We thank Drs. R.P.Levy and A. Sokolov for stimulating discussions.

## References

1. C.F. Chen, H.T. Chern, F.J. Leu, T.M. Chang, L.R. Shian, A.M. Sun, *Artif. Organs*, **18**, 193, 1994.
2. P. Brunetti, G. Basta., A. Falorni, F. Calcinaro, M. Pietropaolo, R. Calafiore, *Int. J. Artif. Organs*, **14**, 789, 1991.
3. R.P. Lanza, W.M. Kuhlreiber, D. Ecker, J.E. Staruk, W. Chick, *Transplantation*, **59**, 1377, 1995.
4. J.P. Kennedy, and R. Faust, U.S. Patent 5,122,572, June 16, 1992.
5. J.P. Kennedy, B. Ivan, *Designed Polymers by Carbocationic Macromolecular Engineering*, Theory and Practice, Hanser Publishers, Munich Vienna, New York, Barcelona, p. 35, 1992.
6. D. Chen, J.P. Kennedy, A.J. Allen, *J. Macromol. Sci. Chem.*, **A25(4)**, 389, 1988.
7. B. Keszler, J.P. Kennedy, P.W. Mackey, *J. Controlled Release*, **25**, 115, 1993.
8. D. Park, B. Keszler, V. Galiatsatos, J.P. Kennedy, *Macromolecules*, **28**, 101, 1995.
9. D. Chen, J.P. Kennedy, M.M. Kory, D.L. Ely, *J. Biomed. Mat. Res.*, **23**, 1327, 1989.
10. B. Ivan, J.P. Kennedy, P.W. Mackey, *Polymeric Drugs and Delivery Systems*, R.L. Dunn and R.M. Ottenbrie, eds. ACS Symposium Series No. 469, Chapter 18, 194, 1991.

11. B. Ivan, J.P. Kennedy, P.W. Mackey, *Polymeric Drugs and Delivery Systems*, R.L. Dunn and R.M. Ottenbrie, eds., ACS Symposium Series No. 469, Chapter 19, 203, 1991.
12. B. Keszler, J.P. Kennedy, N.P. Ziats, M.R. Brunstedt, S. Stack, J.K. Yun, J.M. Anderson, *Polym. Bull.*, **29**, 681, 1992.
13. B. Keszler, J.P. Kennedy, *J. Polym. Sci. Part A, Polym. Chem.*, **32**, 3153, 1994.
14. R. Blezer, T. Lindhout, B. Keszler, J.P. Kennedy, *Polym. Bull.*, **34**, 101, 1995.
15. S. Shamlou, J.P. Kennedy, R.P. Levy, *J. Biomed. Mat. Res.*, **35**, 157, 1997.
16. D. Park, B. Keszler, V. Galiatsatos, J.P. Kennedy, *Macromolecules*, **66**, 901, 1997.
17. P.W. Mackey, Ph.D. Thesis, University of Akron, 1991.
18. S. Shamlou, Ph.D. Thesis, University of Akron, 1996.
19. S.Na, Thesis, The University of Akron 1999.
20. B.D. Hames., B.D. Hames, in: *Gel Electrophoresis of Protein*, Rickwood, D. ed., 1990, Ch.1.
21. E.Raabo, T.C. Terkildsen, *Scand.J.Clin.Lab. Invest.* **12**, 402, 1960.
22. M.M.Bradford, *Analytical Biochemistry*, **72**, 248-254. 1976.

## Chapter 20

# Controlled Drug Delivery from Injectable Biodegradable Triblock Copolymer

Young Jin Kim and Sung Wan Kim

Center for Controlled Chemical Delivery, University of Utah,  
30 So. 2000 E., Room 201, Salt Lake City, UT 84112-5820

The ABA and BAB triblock copolymers composed of poly(DL-lactide-co-glycolide) (PLGA) and poly(ethylene glycol) (PEG) were used in this study. It is a new biodegradable and injectable implant system, which has sol to gel transition behavior. It is a sol between 5 and 30 °C but forms a gel at the body temperature in an aqueous solution. Two model drugs, ketoprofen and spironolactone, which have different hydrophobicities, were released from the PEG-PLGA-PEG triblock copolymer hydrogel. Ketoprofen was released over 2 weeks while spironolactone was released over more than 2 months with a sigmoid release profile. Human insulin was released from the PLGA-PEG-PLGA triblock copolymer hydrogel in a sink condition of phosphate buffer saline solution. We tried to modify the association states of insulin by zinc in order to inhibit the initial burst effect and obtain a constant release rate. Insulin associated from monomer and dimer to hexamer with increasing zinc concentration. The insulin release profile showed the constant release rate over more than 2 weeks.

Thermosensitive polymers have been developed extensively over the past years [1-4]. In particular, polymers showing a sol-gel transition by temperature change have been proposed for an injectable drug delivery depot [5,6]. As an example of temperature sensitive polymers, aqueous solutions of commercially available poly(ethylene oxide)-poly(propylene oxide)-poly(ethylene oxide) (PEO-PPO-PEO; Pluronic (BASF) or Poloxamers (ICI)) demonstrated sol-gel phase transitions with increasing temperature.

Hydrogel of triblock copolymers consisting of poly(DL-lactic acid-co-glycolic acid) (PLGA) and poly(ethylene glycol) (PEG) were used in this study. It is a new injectable implant system, which has thermosensitivity and biodegradability. It is a free flowing sol below 15 °C but it forms a high viscosity gel at body temperature in an aqueous solution. In addition to biodegradability of the polymers, the in-situ formed gel maintains for more than one month, where as the known gelling polymer, Poloxamer, is not biodegradable and the formed gel is dissolved out in a days at best.

Hydrogels are useful in biomedical and pharmaceutical applications because of their biocompatibility, high water content, and rubbery state. Additionally, as carriers of bioactive agents, they can also provide protection for the proteins or drugs [7]. Generally, protein and peptide drugs have different properties like biological half-life and conformational stability from the conventional ones. One way to increase the therapeutic efficiency of these polypeptides is encapsulating them in a sustained dosage form that is capable of releasing the macromolecule continuously, at a controlled rate [8]. Most hydrogel-based drug delivery systems are designed as implants that release drug locally at a predetermined rate.

Drug release from a hydrogel can be affected by several factors, such as pore size, degradability of the hydrogel, size, hydrophobicity, concentration of a drug, and presence of specific interactions between hydrogels and the incorporated drugs. Typically, the release mechanism from a biodegradable hydrogel follows the diffusion at an initial stage and then a combination of diffusion and degradation at a later stage [9].

## ABA triblock copolymer

An ABA (hydrophilic-hydrophobic-hydrophilic) triblock copolymer has been studied extensively because of its ability to form a hydrogel. As an example, aqueous solutions of commercially available PEO-PPO-PEO polymers (Pluronic (BASF) or Poloxamers (ICI)) demonstrate phase transitions from sol to gel (low temperature sol-gel boundary) and gel to sol (high temperature gel-sol boundary) as monotonically increasing temperature when the polymer concentration is above a critical value [4,10]. Continuous heating the polymer solutions in a temperature range above the high temperature boundary makes the



solution opaque. The sol-gel transition behavior of PEO-PPO-PEO triblock copolymers have been utilized for the delivery of labile drugs such as polypeptides and proteins because such drugs can be formulated in an aqueous solution [6,11]. The formulation forms a gel depot in situ when exposed to body temperature via subcutaneous injection. The incorporated drug is then released into the body in a controlled manner. The gel depot of PEO-PPO-PEO triblock copolymer dissolved from its surface within 1 day into soluble unimers, which may cause a harmful or toxic effect in the body, thus resulting in difficulties in sustained release in a long-term base.

In this report, we use PEG-PLGA-PEG triblock copolymers as an ABA type phase transition polymer. It also showed sol-gel phase transition by increasing the temperature of aqueous solutions. The transition temperature monotonically increased as concentration increased. The formed gels of PEG-PLGA-PEG in rats maintained their integrity longer than 1 month [12,13]. In addition to their biodegradability, longer duration of PEG-PLGA-PEG gels is clearly distinguished from PEO-PPO-PEO gels. PEG-PLGA-PEG gels are not erodible by dilution and are more beneficial for the carriers of polypeptide, proteins, and other pharmaceuticals for long-term delivery. The ABA triblock copolymer is good for hydrophilic drugs. In this study, we discuss the effect of the hydrophilicity on the drug release in PEG-PLGA-PEG triblock copolymers .

### Sol-gel transition

Ring-opening polymerization of lactide and glycolide onto monomethoxy poly(ethylene glycol) was performed to synthesize PEG-PLGA diblock copolymers. Diblock copolymers were then coupled using hexamethylene diisocyanate to produce the PEG-PLGA-PEG (Mn:550-2810-550) triblock copolymers.

The sol-gel transition temperature was determined by a test tube inverting method with temperature increments of 1 °C per each step [12,14,15]. Each sample with a given concentration was prepared by dissolving the polymer in distilled water in a 4 ml vial. After equilibration at 4 °C for 12 h, the vials containing samples were immersed in a water bath at a constant designated temperature for 20 min. Inverting the vial determined a gel state when no fluidity in 1 min was visually observed. A minimum shear stress of 62 Pa is needed for the system to flow in vial [15]. The sol-gel transition temperature determined by this method has a precision of  $\pm 0.5$  °C. Figure 1 shows the sol-gel transition of PEG-PLGA-PEG triblock copolymer in aqueous solution. The viscosity of PEG-PLGA-PEG triblock aqueous solution at 33 wt% concentration at room temperature was 10 cP, which makes it easy to formulate and inject through a syringe needle. The viscosity abruptly increased at the sol-gel

transition temperature. With further increasing temperature, the transparent gel became turbid.

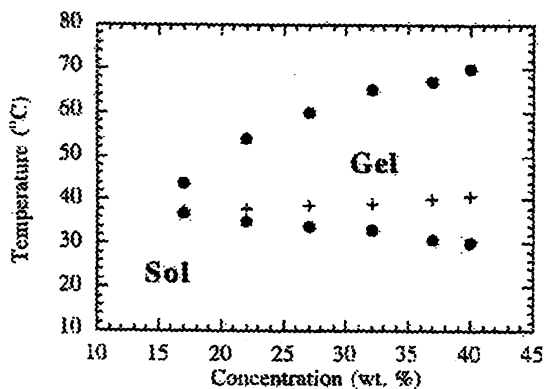


Figure 1. Sol-gel transition of PEG-PLGA-PEG triblock copolymer aqueous solution. Cross bar indicates the temperature at which the gel becomes turbid. (Reproduced with permission from reference 13. Copyright 2000 Elsevier.)

## Drug delivery

PEG-PLGA-PEG (550-2810-550) triblock copolymers were studied for drug release of ketoprofen (Sigma) and spironolactone (Sigma). Ketoprofen or spironolactone was dissolved in a PEG-PLGA-PEG triblock copolymer solution at a concentration of 10 mg/ml (ketoprofen) or 2.5 mg/ml (spironolactone), respectively. An aqueous polymer solution containing the model drug (0.4 ml) was injected into 4 ml vials, which were thermostated in a shaking water bath (16 strokes/min) at 37 °C, to form a clear gel. After 2 min, 3.5 ml of release medium at 37 °C was added to the formed gel. A 10 mM phosphate buffer (pH 7.4) was used as a drug release medium to improve drug solubility. All release medium was replaced with the same amount of fresh medium at designated sampling intervals to mimic a sink condition and subjected to reversed-phase high performance liquid chromatographic (RP-HPLC; Shimadzu) analysis with a C<sup>18</sup> reversed-phase column (Phenomenex). Mobile phases were acetonitrile and water with a feed ratio of 50:50 for Ketoprofen and 70:30 for spironolactone with a total flow rate of 1.0 ml/min. UV-Vis detection at 260 nm and 254 nm was used for the analysis of Ketoprofen and spironolactone, respectively.

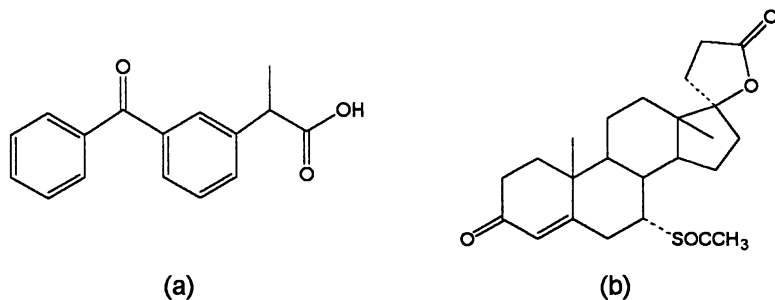


Figure 2. Structure of the model drugs, (a) ketoprofen and (b) spironolactone. (from Ref. 13).

The PEG-PLGA-PEG triblock copolymer hydrogel system is thought to have a domain (core-shell micelle) structure in aqueous environments. The hydrophilic PEGs occupy the outer shell region and hydrophobic PLGAs constitute the inner core in order to decrease free energy of hydration. Two drugs differing in hydrophobicity were studied as model drugs. Figure 2 shows the structure of the two model drugs. Ketoprofen (KP) has a carboxyl group ( $pK_a=5.0$ ) which is ionized at pH 7.4, making it hydrophilic [16]. Spironolactone is relatively hydrophobic [17]. The difference in hydrophobicity may force the drug to partition into different polymer domains, resulting in different release profiles. The more hydrophobic the drug, the more it will partition into the PLGA micellar core in the hydrogel, and consequently have a sustained drug release profile. Figure 3 shows KP release from the PEG-PLGA-PEG (550-2810-550) triblock copolymer hydrogel. The ketoprofen release rate was controlled by changing initial polymer solution concentration. The release rate decreased to near zero after 5 days. The higher initial polymer solution concentration, the slower was the drug release rate observed, due to tighter polymer-polymer contacts among the gel at higher concentrations of the polymer. In case of spironolactone, the release profile (Figure 4) shows an sigmoid release profile typical of a biodegradable polymer, with diffusion followed by a degradation/diffusion mechanism [9,18]. The more hydrophobic and the smaller the water content in the gel, the slower the degradation rate, resulting in a slower drug release rate in the degradation dominant stage. Drug release from the hydrophobic domain mainly comes from the degradation. With degradation of the core polymers, the number of end groups increases, and free volume increases.

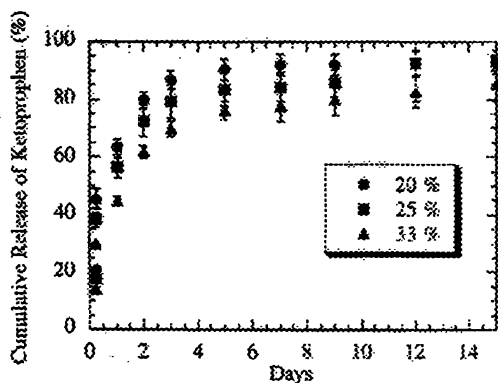


Figure 3. Ketoprofen release from PEG-PLGA-PEG triblock copolymer hydrogel. The legend indicates initial concentration of the polymers in PBS buffer.

(Reproduced with permission from reference 13. Copyright 2000 Elsevier.)

When drug hydrophobicity and release profile are compared, important conclusions can be drawn about the gel structure. The more hydrophilic drug (ketoprofen) tends to be more partitioned into the hydrophilic domain, with easier diffusion out of the hydrogel system into the release medium. There is continuous dynamic repartitioning between the two polymer phases during the release of the drug from the hydrogel, resulting in a single stage-like drug release profile for the hydrophilic drug. In this case, the major mechanism of drug release is diffusion. Hydrophobic drugs (spironolactone) tend to be more partitioned into the PLGA core of the micelles. However, there is some small release of drug by diffusion at the first stage, which comes predominantly from the drug partitioned into the hydrophilic region. At a later stage, the drug is released by the core degradation and diffusion from the hydrophobic component [13].

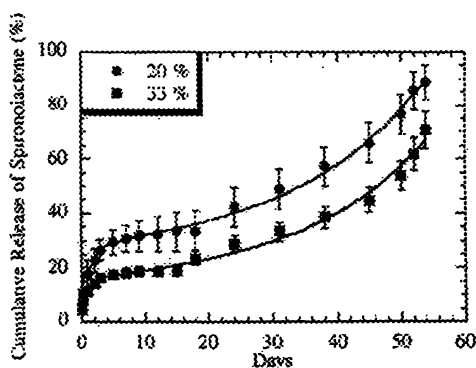


Figure 4. Spironolactone release from PEG-PLGA-PEG triblock copolymer hydrogel. The legend indicates initial concentration of the polymers in PBS buffer.

(Reproduced with permission from reference 13. Copyright 2000 Elsevier.)

## BAB triblock copolymer

A BAB (hydrophobic-hydrophilic-hydrophobic) triblock copolymer was also studied because it could form the hydrogel in certain conditions. It shows the similar properties of the ABA triblock copolymer that is water soluble, biodegradable, and thermosensitive. In this study, we used the PLGA-PEG-PLGA (1500-1000-1500) triblock copolymer that also showed the sol-gel transition in an aqueous solution. The gelation mechanism is somewhat different and the gelation temperature (15 – 25 °C) is lower than PEG-PLGA-PEG triblock copolymer (30 °C). The BAB triblock copolymer was good for the hydrophobic drugs as a new injectable implant system that possesses both thermosensitivity and biodegradability [19].

Insulin is a hydrophobic peptide drug for diabetes. Diabetes mellitus is a serious pathologic condition responsible for major health care problems all around the world costing billions of dollars annually. In the United States, it represents the fourth leading cause of death. Diabetes also leads to severe complications such as kidney disease, retinopathy, neuropathy, leg or foot amputations and heart disease [20]. As a consequence of poor oral bioavailability and current lack of alternative delivery routes, insulin is presently administered parentally. The subcutaneous route, requiring single or multiple daily injections, is the main stay of conventional insulin therapy [21].

In this study, we designed the sustained release system, which provides basal line insulin release for duration of over several weeks by one injection. Human insulin was entrapped in the hydrogel in order to sustain its release as a subcutaneous insulin delivery system. We tried to modify the association states of insulin by zinc in order to inhibit the initial burst effect and obtain constant release rate. At otherwise equivalent conditions, insulin associated from monomer and dimer to hexamer with increasing zinc concentration [22]. Insulin samples with different zinc contents exhibited different release profiles due to association-state differences within the hydrogel.

### Sol-gel transition

PLGA-PEG-PLGA (1500-1000-1500) triblock copolymers (ReGel™) were made by ring-opening polymerization. The composition of the PLGA block was 75/25 (LA/GA) in molar ratio. ReGel™ has hydrophilic-hydrophobic groups inside the copolymer. Considering the enhanced hydrophobic interactions at elevated temperatures, the hydrophobic domain of the copolymer forms a physical crosslink (or aggregate) which makes the gelation state (Figure 5).

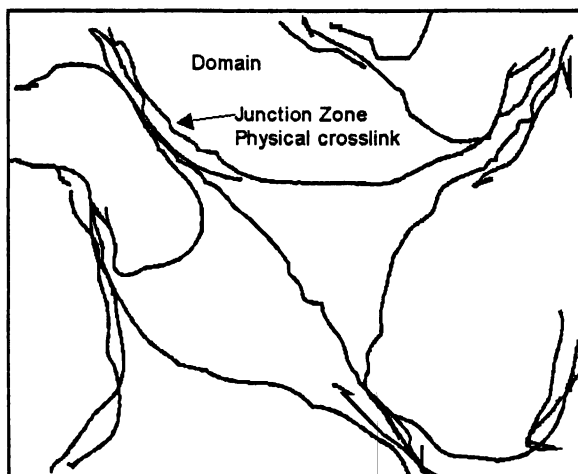


Figure 5. Schematic diagram of hydrogel formation in PLGA-PEG-PLGA triblock copolymer.

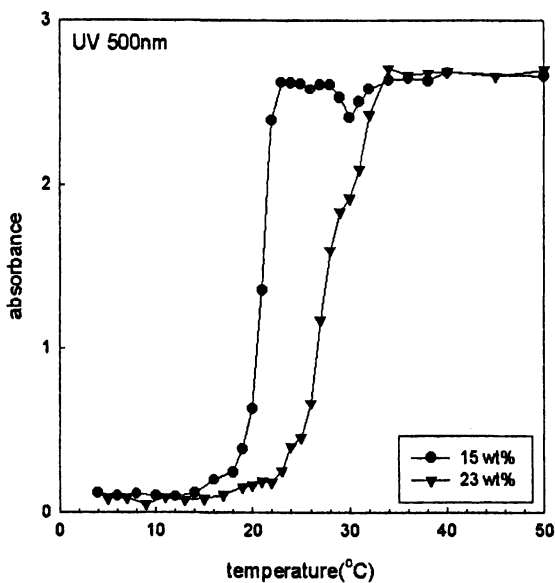


Figure 6. Sol-gel transition curve of ReGel™ aqueous solution by UV spectrometer.

(Reproduced with permission from reference 19. Copyright 2001 Kluwer Academic.)

The aqueous solution of ReGel<sup>TM</sup> was investigated by UV spectroscopy to determine the sol-gel transition temperature. The triblock copolymer aqueous solutions were prepared by dissolving the polymers in the cold water at 4°C to make 15 and 23 wt% solutions. The sol-gel transition temperature was measured by increasing the temperature at 2°C increments. The UV cuvet was immersed in a water/glycerol bath at each temperature for 5 min. The sol-gel transition was monitored by UV spectrophotometer (Lambda 19, Perkin Elmer) at 500 nm. Figure 6 shows the sol-gel transition temperature at 15 – 20 °C with the concentration variation of ReGel<sup>TM</sup> solution. The ReGel<sup>TM</sup> solution is a free flowing sol below 15°C and forms a high viscosity gel at body temperature in aqueous solutions. At low temperature (< 15 °C), the solution can be formulated with a labile drug such as a bioactive protein, and the formulated solution can be injected into the body for the controlled release of macromolecular drugs.

## Drug delivery

The PLGA-PEG-PLGA triblock copolymer was dissolved in the cold water at 5 °C to make a 23 wt% solution. Insulin solutions were prepared in buffer (isotonic 10 mM PBS, pH 7.4) to a concentration of 5.04 mg/ml and zinc was added (0.0, 0.2 wt%) to the hydrogel solution. Then 2 ml of each formulation were placed in vials, incubated at 37 °C until forming gels, and 10 ml of PBS solution was added as a release medium. Release medium samples were withdrawn and replaced immediately to keep the sink condition. They were analyzed by reversed-phase high performance liquid chromatography (RP-

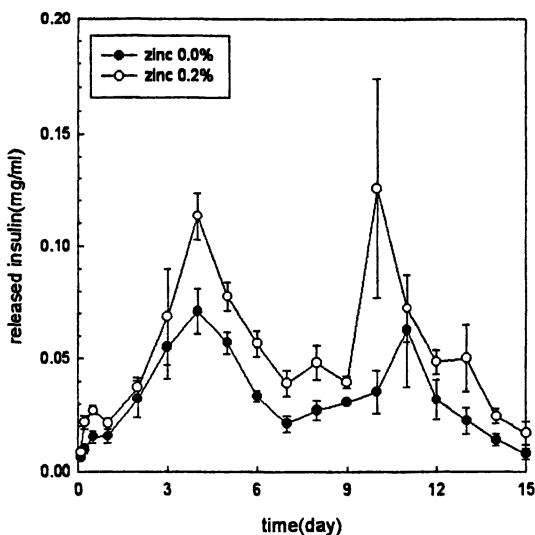


Figure 7. Daily release amount of insulin from ReGel<sup>TM</sup> formulation *in vitro* test.

HPLC) to measure the concentration of insulin. RP-HPLC (SCL-10Avp, Shimadzu) was equipped with a C<sub>4</sub> column (Vydac), which was previously equilibrated. The mobile phases were water and acetonitrile with a gradient flow and the flow rate is 1.2 ml/min.

Figures 7 and 8 show the result of insulin release from the hydrogel in an *in vitro* test. Different associations of insulin were entrapped in the gelatinized hydrogel with various zinc contents. First of all, there were no initial burst effects of the insulin release from ReGel™ formulation. Two release stages were shown in the release profile. The ReGel™ hydrogel system is thought to have a core-shell structure in an aqueous environment. The hydrophilic PEG occupies the shell region and hydrophobic PLGA hides into the core in order to decrease the free energy. Insulin is a hydrophobic drug and may locate inside the hydrogel network. The release mechanism from the hydrogel follows the diffusion at an initial stage and then a combination of diffusion and degradation at a later stage.

Generally, insulin forms a hexamer with zinc. The insulin association resulted from the zinc content in the insulin [22]. However, without zinc, insulin formed various association states such as monomer, dimer, hexamer, and aggregate. It is thought that insulin without zinc formed the aggregation state inside the gel. The aggregated insulin may not diffuse fast from the ReGel™ formulation, which presented a slower release (60% after 15 days). Insulin with 0.2 wt% zinc formed the hexameric state. The release profile of the insulin with

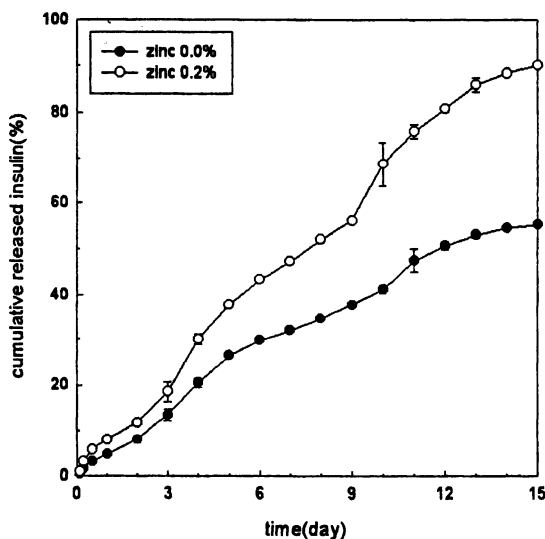


Figure 8. Cumulative amount of released insulin from ReGel™ formulation *in vitro* test.

(Reproduced with permission from reference 19. Copyright 2001 Kluwer Academic.)



zinc showed a constant release rate and almost 90 % of the initial amount was released over 15 days. We verified the result with an animal study using Sprague-Dawley rats with insulin (0.2 wt% zinc)/ReGel™ formulation.

## Conclusions

ABA and BAB triblock copolymers composed of PLGA and PEG were used as a drug delivery carriers for the continuous release of drugs. The triblock copolymers in aqueous solutions are free-flowing sols at room temperature and become gels at body temperature. These are water soluble, biodegradable, thermosensitive polymers for an injectable drug delivery depot. The release of hydrophilic drug (ketoprofen) shows 5 day release profile from a PEG-PLGA-PEG triblock copolymer. Comparing a more hydrophobic drug (spitonalactone) shows an sigmoid release profile from a PEG-PLGA-PEG triblock copolymers because the drug located inside the hydrophobic part of the hydrogel and showed two release stages, diffusion and diffusion/degradation. The release of human insulin from PLGA-PEG-PLGA triblock copolymers showed no initial burst and a constant release (zero-order) rate *in vitro*. It was necessary to modify the insulin's zinc content to 0.2 wt% in order to get a maximum release rate. Insulin with 0.2 wt% zinc showed a constant release rate over more than 2 weeks.

The PLGA-PEG-PLGA triblock copolymer is the ideal injectable biodegradable phase transition polymer.

## References

- (1) Bae, Y. H.; Okano, T.; Kim, S. W. *Pharm. Res.* **1991**, *8*(5), 624.
- (2) Mukae, K.; Bae, Y. H.; Okano, T.; Kim, S. W. *Polym. J.* **1990**, *22*, 250.
- (3) Gutowska, A.; Bae, Y. H.; Jacobs, H.; Feijen, J.; Kim, S. W. *Macromolecules* **1994**, *27*, 4167.
- (4) Jeong, B.; Lee, D. S.; Shon, J. I.; Bae, Y. H.; Kim, S. W. *J. Polym. Sci.: Part A: Polym. Chem.* **1999**, *37*, 751.
- (5) Jeong, B.; Bae, Y. H.; Lee, D. S.; Kim, S. W. *Nature* **1997**, *388*, 860.
- (6) Bhardwaj, R.; Blanchard, J. J. *Pharm. Sci.* **1996**, *85*(9), 915.
- (7) Keys, K. B.; Andreopoulos, F. M.; Peppas, N. A. *Macromolecules* **1998**, *31*, 8149.
- (8) Cohen, S.; Yoshioka, T.; Lucarelli, M.; Hwang, L. H.; Langer, R. *Pharm. Res.* **1991**, *8*(6), 713.
- (9) Baker, R. *Controlled release of bioactive materials*; Academic Press: New York, **1980**, 15.

- (10) Malmsten, M.; Lindman, B. *Macromolecules* **1992**, *25*, 5440.
- (11) Miyazaki, S.; Ohkawa, Y.; Takada, M.; Attwood, D. *Chem. Pharm. Bull.* **1992**, *40*(8), 2224.
- (12) Jeong, B.; Bae, Y. H.; Kim, S. W. *Macromolecules* **1999**, *32*, 7064.
- (13) Jeong, B.; Bae, Y. H.; Kim, S. W. *J. Control. Rel.* **2000**, *63*, 155.
- (14) Gilbert, J. C.; Richardson, J. L.; Davies, M. C.; Palin, K. J.; Hadgraft, J. *J. Control. Rel.* **1987**, *5*, 113.
- (15) Tanodekaew, S.; Godward, J.; Heatley, F.; Booth, C. *Macromol. Chem. Phys.* **1997**, *198*, 3385.
- (16) *PDR Generics*, 3<sup>rd</sup> edn.; Medical Economics: New Jersey, **1997**, 1845.
- (17) *British Pharmacopoeia*, Vol. 1, Constable & Co.: London, **1988**, 531.
- (18) Youxin, L.; Volland, C.; Kissel, T. *J. Control. Rel.* **1994**, *32*, 121.
- (19) Kim, Y.J.; Choi, S.; Koh, J.J.; Ko, K.S.; Kim, S.W. *Pharm. Res.* **2001**, *18*, 548.
- (20) Baudys, M.; Kim, S. W. *Adv. Drug Delivery Rev.* **1999**, *35*, 141.
- (21) Hinchcliffe, M.; Illum, L. *Adv. Drug Delivery Rev.* **1999**, *35*, 199.
- (22) Brange, J.; Langkær, L. in: *Stability and Characterization of Protein and Peptide Drugs: Case Histories*; Wang, Y. J.; Pearlman R.; Ed.; Plenum Press: New York, **1993**, 315.

## Chapter 21

# Poly(*N*-isopropylacrylamide) Copolymers: Hydrogel Formation via Photocrosslinking

Dirk Kuckling<sup>1</sup>, Hans-Jürgen P. Adler<sup>1</sup>, and Karl-Friedrich Arndt<sup>2</sup>

Institutes of <sup>1</sup>Macromolecular Chemistry and Textile Chemistry, and <sup>2</sup>Physical Chemistry and Electrochemistry, Dresden University of Technology, D-01062 Dresden, Germany

Recent results on the photocrosslinking of temperature sensitive polymers are reviewed. Polymers with temperature dependent degrees of swelling, especially polymers which exhibit lower critical solution temperature (LCST) behaviour in aqueous solutions, are of interest for applications in micro-systems, e. g. in microvalves. For these applications it is necessary to form and pattern thin films in the  $\mu\text{m}$ -range. This has been achieved through the photocrosslinking of linear prepolymers. Copolymers based on *N*-isopropylacrylamide (NIPAAm) were modified with a stilbazolium salt or acridizinium salt chromophore to yield photocrosslinkable temperature sensitive polymers. The photocrosslinking properties of the two chromophores were compared. Patterned networks in the  $\mu\text{m}$ -range (20  $\mu\text{m}$  space width and > 50  $\mu\text{m}$  line width) were prepared through irradiation of thin films using a mask. The polymers exhibited LCST, which was measured using DSC. The patterned networks had temperature dependent swelling properties in aqueous media.

## Introduction

The swelling behaviour of smart hydrogels make them very attractive for microactuator applications (1-3). Poly(N-isopropylacrylamide) (PNIPAAm) was chosen as a basis for smart hydrogels, which exhibits a sharp phase transition at 34 °C (4). Most of the PNIPAAm systems were prepared via free radical polymerizations yielding voluminous gel samples (5). However, it is rather difficult using this method to prepare the thin films which are necessary for applications in microsystems, e. g. with integrated valves or pumps based on polymeric actuators. One solution to this problem is the preparation of a gel film from narrowly distributed spherical microgel particles (6) or the branching of the sensitive polymer onto the surface (7). The photocrosslinking of a polymer film is a more suitable method for microsystem technology and increasing interest is being shown in this method (8). There exists only a few reports on the preparation of hydrogels via photocrosslinking of water-soluble polymers (9-13) and their photolithographic patterning (14-17).

One key point in the employment of smart polymers is their adaption to microsystems with its standard techniques. The adaption of hydrogels for microsystem technology requires the following:

- crosslinking in the applied state (e. g. by photocrosslinking)
- high resolution and contrast
- influence on the patterning through the irradiation process (adjustment of the crosslinking density and generation of a crosslinking gradient)
- fast crosslinking reaction
- good adhesion to the substrate.

Another advantage of the application of smart polymers in microsystems is the decrease of the transition times which are known to be relatively large for bulk objects. Due to the fact that the swelling/deswelling of these networks is a diffusion controlled process, the macroscopic size of the gel is important for the kinetic of swelling. The rate of swelling is inversely proportional to the square of the characteristic length of the gel. To improve the response time to external stimuli to a usable level it is necessary to reduce the gel size dramatically. This can be achieved by using thin films and micropatterns.

In order to design microactuators containing these gels the gel sizes must be reduced to the  $\mu\text{m}$ -range (gel thickness and gel extension) (18). Therefore, materials with both a high aspect ratio through patterning and a strong adhesion to semiconductor or microchannel substrates have to be developed. This can not be achieved with the simple polymer as it is and, therefore requires the chemical modification of the material itself. In order to pattern the original gel PNIPAAm copolymers have been developed which can be photocrosslinked (19-21). This

allows not only photopatterning of the material with a technique widely used in semiconductor technology, but also gel film deposition by crosslinking the initial polymer at a substrate surface. The changes in the gel properties, necessary for actuator use, accompanied with this material modification proved to be acceptable as shown below.

## Synthesis

Most of the research on sensitive networks has been focused on bulk gels like disks and rods or microgels. However, for applications in microsystems, the gel size must be reduced to the micrometer range in order to shorten the gel response time to external stimuli. Therefore, methods have to be developed to prepare such gels supported on Si-wafers. This can be achieved through the UV induced crosslinking of thin films of linear macromolecules with photodimerizable moieties in the side chains. The UV induced crosslinking of temperature sensitive PNIPAAm copolymers with photodimerizable styrylpyridinium chromophores in thin polymer films for potential use in microelectronic as actuators has recently been conducted (19).

The balance between hydrophobic/hydrophilic interactions plays a major role in determining the LCST behaviour of the thermosensitive polymers and their gels, the introduction of the hydrophobic substituents into the polymer system can cause a dramatic decrease of the critical temperature ( $T_c$ ). Due to the fact that it is not possible to cool the desired microsystem only smart polymers with  $T_c$  higher than room temperature are applicable. A positive charge on the stilbazolium and acridizinium ion, should compensate for its hydrophobic character. Hence, the modification of the prepolymers with the chromophore should not lead to a significant decrease of  $T_c$ .

A lot of the research on the photocrosslinking of hydrophilic polymers has been focused on the UV-induced crosslinking of photosensitive polymers in which the pendant chromophores undergoing two competing photoreactions: photodimerization and *cis-trans* isomerization. It is known that the acridizinium ion only undergoes reversible photodimerization reactions upon irradiation: it dimerizes through a [4+4]-cycloaddition, and the dimers split into their monomers on photolysis at lower wavelengths or thermolysis. Thus, by choosing this chromophore to synthesize hydrophilic, temperature-responsive, photosensitive polymers we expected a higher photoreactivity (a faster crosslinking), in comparison with the polymers containing, e. g. styrylpyridinium salts as the photocrosslinkable moiety.

Prepolymers were prepared by free radical copolymerization of NIPAAm with a carboxylic acid bearing group and their composition was determined by

acid-base titration. It has been shown by  $^{13}\text{C}$  NMR spectroscopy that the copolymerization reactivities of NIPAAm and the selected comonomers are comparable (22), and therefore, copolymerizations can be carried out to high conversions. For the selected polymer samples the weight average molecular weights were obtained by GPC analysis and were around 70 000 g/mol (19, 23).

The prepolymers were then modified by polymer analogous reactions with chromophores to yield photochemically reactive polymers (Figure 1) (19, 23). The compositions and thermal data of two selected pre- and photopolymers are summarized in Table 1.

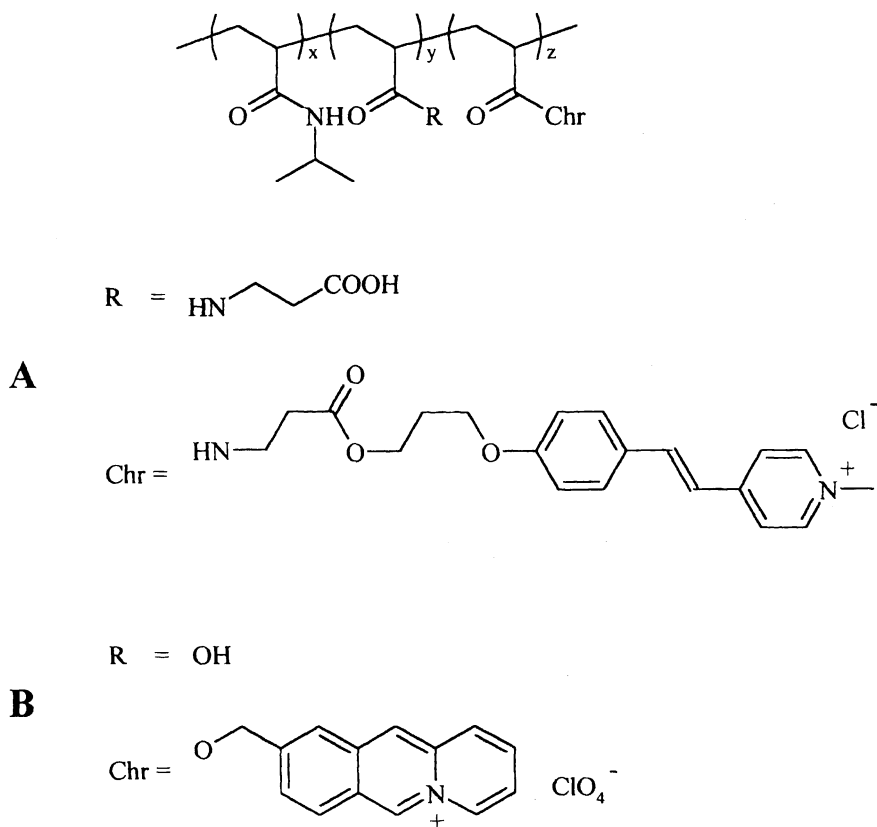


Figure 1: General structure of the photocrosslinkable temperature sensitive polymers

**Table 1: Composition and thermal properties of prepolymers and photopolymers**

	<i>prepolymer</i>			<i>photopolymer</i>		
	<i>COOH content</i> [mol-%]	$T_g$ [°C]	$T_c$ [°C]	<i>chromophore content</i> [wt.-%]	$T_g$ [°C]	$T_c$ [°C]
<b>A</b>	5.3	146	31.9	3.2 % stilbazolium	134	17.6
<b>B</b>	4.4	144	31.4	3.5 % acridizinium	138	26.8

The synthesized photopolymers, **A** and **B**, have glass transition temperatures ( $T_g$ ) of 134 °C and 138 °C, respectively. Due to the thermal radiation of the lamp the polymer films were heated to approx. 80 °C, nevertheless during irradiation the photocrosslinking was still carried out in the glassy state. The  $T_g$  of the polymers plays an important role in the photocrosslinking of polymer films. When the irradiation was performed at temperatures below  $T_g$  the rate of crosslinking decreased due to the reduced mobility of the chromophores.

The chromophore has an important influence on the phase transition temperature ( $T_c$ ) of the photopolymers (19) A decrease of  $T_c$  was observed with an increase of the chromophore content. But in contrast to the stilbazolium chromophore, where a chromophore content of 3.2 wt-% led to a  $\Delta T_c$  of -14.3 °C, the introduction of the acridizinium group with a content of 3.5 wt-% resulted in a  $\Delta T_c$  of only -4.6 °C. Hence a photopolymer with high chromophore content and a  $T_c$  above room temperature was obtained. A  $T_c$  above room temperature is indispensable for microsystem technology due to the lack of possibilities for cooling the microsystems.

## Photocrosslinking

Photocrosslinking experiments were carried out with thin polymer films, which were prepared from dilute polymer solutions in different solvents and poured onto quartz plates. The reactions were monitored by observing the change in the UV spectra. The photostimulated crosslinking of the polymers occurs via photodimerization reactions of chromophores under UV irradiation. The stilbazolium salts are known to undergo competing photoreactions under illumination (24, 25). With light at wavelengths below 460 nm,  $[2\pi+2\pi]$ -cycloaddition (photodimerization) and *trans-cis* isomerization may occur. At

shorter wavelengths, i.e. about 280-320 nm, the dimers may split into monomers. For the acridinium chromophore no *trans-cis* isomerization is possible.

The changes in the UV spectra of irradiated films of the polymer samples (prepared from a butanone and THF solution) are displayed in Figure 2. For photopolymer A a decrease of absorbance at the absorption maximum at 383 nm with irradiation time is observed, accompanied by a slight shift of the maximum to shorter wavelengths (Figure 2a). The latter feature indicates a *trans-cis*-isomerization rather than dimerization which should also lead to a more complete bleaching of the sample (26). Different spectral features are observed when the films were prepared from polymers dissolved in chloroform and THF. In these two systems the blue shift of the absorption maximum indicating isomerization does not occur. A more complete bleaching of the films was also found, i.e. the photodimerization was more exhaustive. For photopolymer B a complete bleaching of the polymers could be obtained within 80 min, indicating the complete conversion of the chromophores (Figure 2b). Thus this reaction is approximately hundred times faster than those with photopolymer A (Figure 3). Both photopolymers are able to form solid networks within several minutes of exposure (depending on the irradiance of the UV lamp) which swelled in water. The gel point of these systems is reached well in advance of complete conversion of the chromophore.

Since photodimerization constitutes the photocrosslinking reaction it is necessary that an excited photochrome comes in contact with a ground state photochrome within the lifetime of the former. The crosslinking efficiency is thus affected by the mean distance between the chromophores, and by their mobility (in fluid systems) or order (in solid or highly viscous systems). For real crosslinking it is further required that chromophores attached to different macromolecules react with each other rather than chromophores in the same macromolecule. Consequently, for crosslinking in the films, the macromolecules should preferably assume an elongated thread-like structure on the quartz surface and undergo crosslinking at entanglements of the threads. An adsorption in the form of single coils, on the other hand, can be considered disadvantageous for crosslinking.

The different crosslinking behaviours of photopolymer films formed from different solvents can be explained with the help of different polymer conformations in these solvents. Studies were performed with one selected photopolymer (27). The second virial coefficients ( $A_2$ ), determined by light scattering, revealed the most coiled photopolymer structure in THF solution. This is to be expected since the magnitude  $A_2$  (found to be lowest in THF solution) is related to the Flory-Huggins constant  $\chi_1$ , widely used in fundamental polymer studies as measure for the polymer-solvent interactions. If  $A_2 > 0$ , the interactions between polymer molecules and solvent molecules are more attractive than the solvent-solvent interactions. Such solvents are considered to be thermodynamically „good“ for the polymer. Thus, the low value for THF means that this solvent can be considered to be „poor“, leading to a more



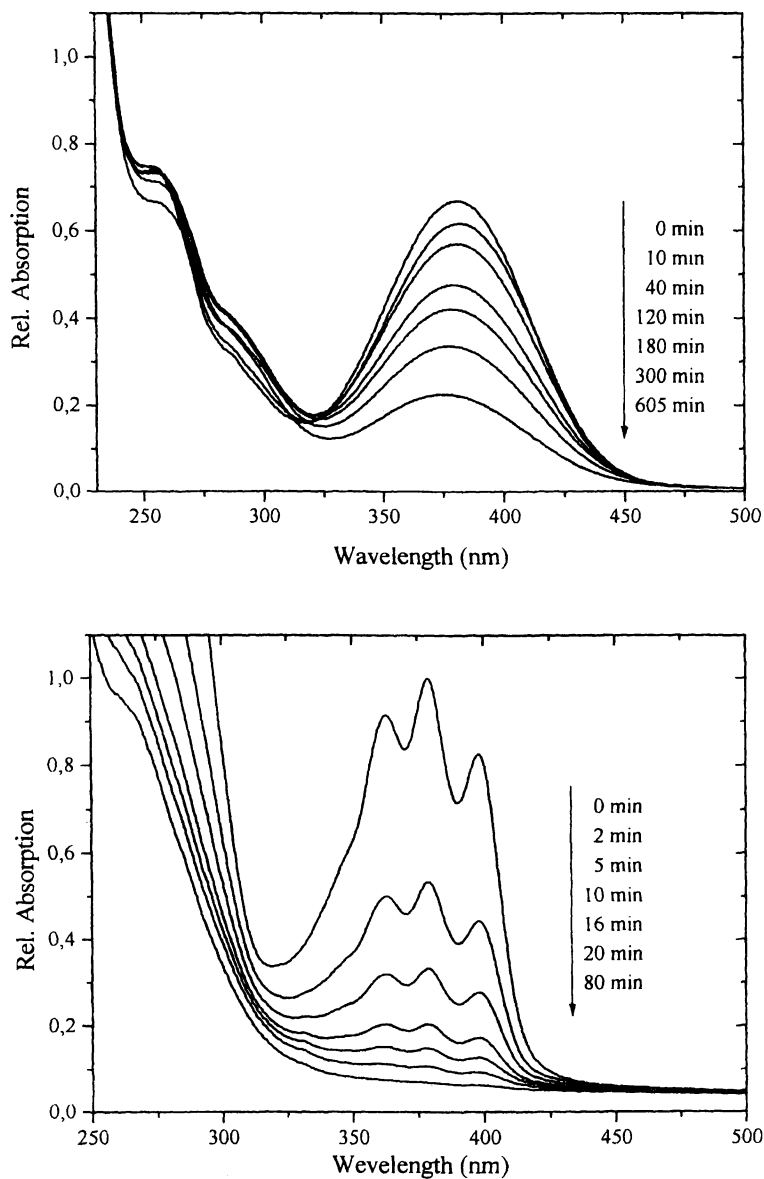


Figure 2: Variation of UV absorption spectrum during photoinduced gelation of a film of photopolymer A (prepared from butanone) (upper diagramm (21)) and of photopolymer B (prepared from THF) (lower diagramm (23))

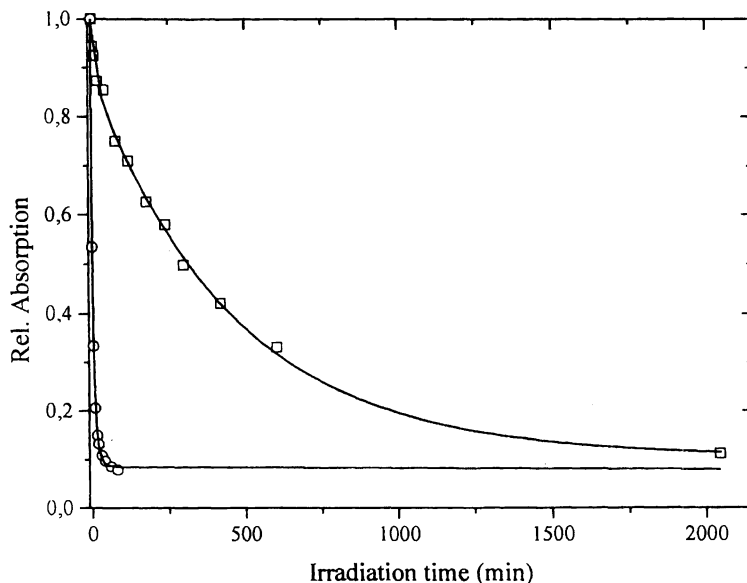


Figure 3: Relative UV absorption at ca. 380 nm vs. irradiation time of (□) photopolymer A and (○) photopolymer B

compact conformation of the macromolecules in the solution in accordance with the comparatively small volume determined. If this conformation remains after formation of the polymer films, both a high rate of photodimerization and the predominance of intra(macro)molecular crosslinking in the solid state are likely. General features of the influence of the solvent on the crosslinking behaviour are summarized in Table 2.

**Table 2: General features of the influence of the solvent on the crosslinking behaviour**

<i>THF</i>	<i>water</i>
no spectral shift	blue shift
faster photoreaction	slower photoreaction
higher conversion	lower conversion
slower gel formation	faster gel formation
smaller $r_g$	larger $r_g$
worse solvent	better solvent

## Patterning Results

The starting point of the patterning studies was the preparation of blanket polymer films with a high thickness ( $> 10 \mu\text{m}$ ). One main feature of the photocrosslinkable copolymers are their suitability for spin coating. Both ethanol and butanone were used as solvents. In order to obtain thicker films spinning velocities ( $n$ ) of 250 to 2000 rpm were applied revealing the commonly known  $(1/n)^{1/2}$  dependency. The introduction of an additional adhesion promoter (hexamethyl disilazane, HMDS) did not only increase the adhesion, but also improved the initial wetting behaviour of the polymer solution. The resulting film thickness could be increased from 3 to 12  $\mu\text{m}$  on bare surfaces and from 10 to 40  $\mu\text{m}$  on HMDS treated surfaces using a 20 wt.% polymeric solution. The given variation corresponds to the range of spinning velocities mentioned above. The change from ethanol as solvent to butanone also caused an increase in the film thickness.

The crosslinking is initiated by UV light. The irradiation of the dry polymer films was performed using a common mask aligner with a Hg lamp and an irradiance at the wafer plane of approximately 8 to 12  $\text{mW}/\text{cm}^2$ . Exposure times between 2 and 20 min were applied yielding total exposures of 1 to 14  $\text{J}/\text{cm}^2$ . By changing the irradiation time the crosslinking ratio can be adjusted leading to different dot heights after development. During the development of the layer in water the unirradiated part and the sol part of the irradiated segments of the polymer film are dissolved. Therefore, the feature height strongly depends on the density of crosslinked polymer chains before development and therefore on the exposure. Figure 4 shows the results of experiments using 20 wt.% polymeric solutions in butanone on HMDS treated  $\text{SiO}_2$  surfaces with exposures through a mosaic like patterned mask.

The development of the micropatterns involves rinsing the irradiated polymer films in water whereby the non-crosslinked, i.e. the unirradiated polymer segments are dissolved. The patterning results given in Figure 5 were obtained using an exposure time of 16 min. Figure 5 shows a patterning example with a 30 wt.% polymeric solution in ethanol on a Al film yielding a polymer thickness of about 1.6  $\mu\text{m}$  with a patterning resolution of greater than 10  $\mu\text{m}$ . Especially in the cases of thicker films ( $> 10 \mu\text{m}$ ) the lateral resolution of the photopatterning is limited by the swelling of the gels during development. In these cases a minimum line width of about 20  $\mu\text{m}$  can ultimately be formed. Smaller features – both spaces and lines – lose their shape during swelling and do not return to their original geometry due to proximity effects of features in the region or substrate interaction.

The adhesion of the micropatterned features at the substrate is one main criterion for their application in microactuators. The characterization of the adhesion behaviour involved measurements of the force required by a shearing tool to peel them off and normalized to the area of the gel dot. At gel dots crosslinked with a exposure time of 16 min (i.e approx. 10  $\text{J}/\text{cm}^2$ ) onto a  $\text{SiO}_2$ -

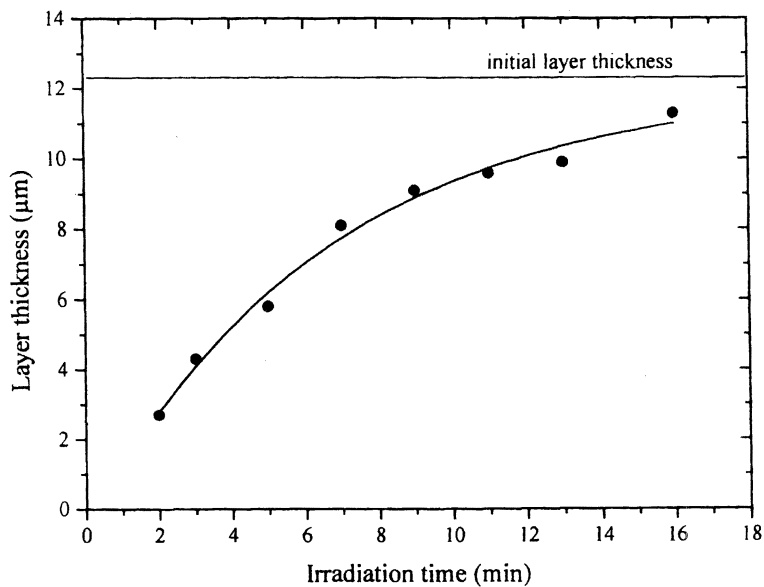


Figure 4: Growth of layer thickness during irradiation of a film of photopolymer A (21)

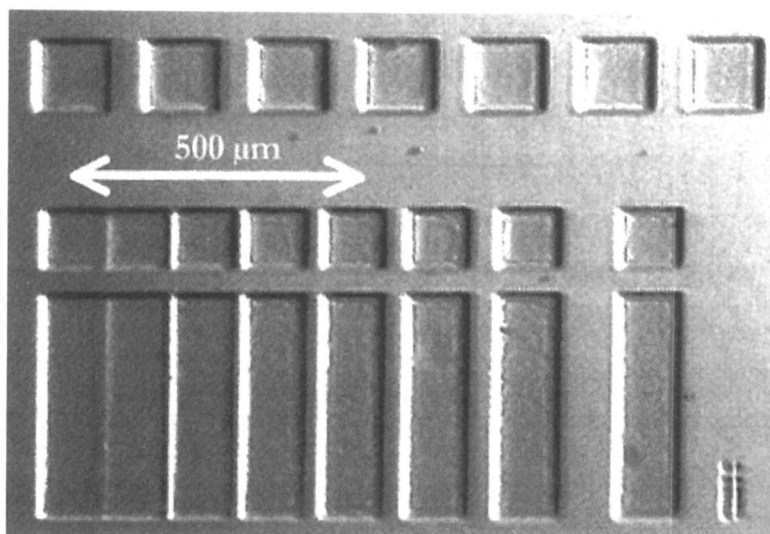


Figure 5: Results of photopatterning using photopolymer A (Reproduced with permission from reference 28. Copyright 1999 Elsevier.)

surface shear strengths of 3 to 4 N/mm<sup>2</sup> and at SiO<sub>2</sub>-surfaces initially deposited with HMDS of 4 to 7 N/mm<sup>2</sup> were obtained.

## Swelling

The swelling behaviour determines the actuator performance, therefore it is the basic property for actuator design. The swelling of patterned hydrogels with dot-like shapes was investigated for HMDS-treated SiO<sub>2</sub> surfaces. The base area was (250 × 250) μm<sup>2</sup>, the height varied depending on crosslinking ratio, i.e. exposure.

The thermal control of the swelling is of importance for the desired actuator performance. The phase temperature in pure PNIPAAm has been determined to be approx. 32 °C (22) and is decreased for the photo-crosslinkable copolymers to approx. 18 °C and 27 °C.

For the investigation of the temperature dependent swelling behaviour of micropatterned features swollen gel dots were immersed in cold water and the bath temperature was increased while observing the gel dot dimensions from a 90° side view. The swelling ratio  $q$  is determined from the quotient of the dot thickness in the swollen state at a certain temperature and the thickness in the dry state. The change of polymer chain conformation with temperature results in a

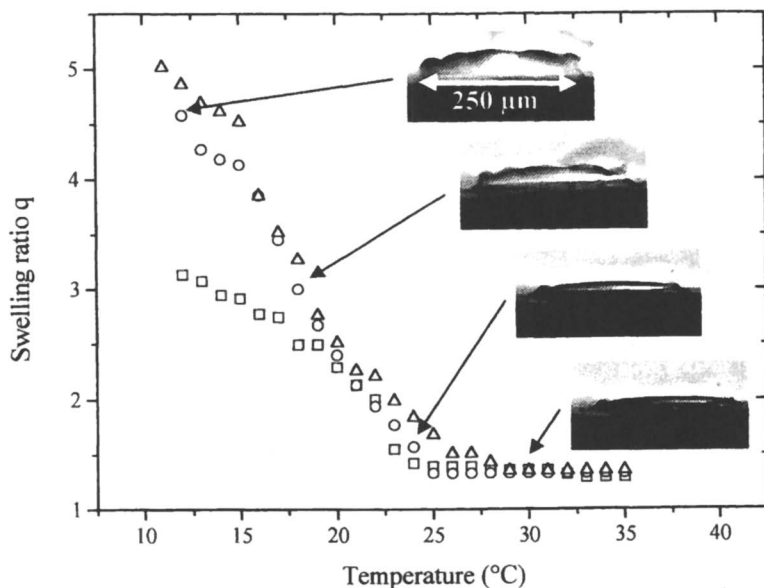


Figure 6: Temperature dependent swelling behaviour of gel dots of photopolymer A with different irradiation times ((Δ) 7 min, (O) 10 min, (□) 16 min) (28)

(Reproduced with permission from reference 28. Copyright 1999 Elsevier.)

temperature dependency of the swelling. The swelling ratio above the transition temperature ( $q_{min}$ ) was determined to be ca. 1.3. It does not significantly depend on the crosslinking ratio. Below the transition temperature swelling ratios ( $q_{max}$ ) varying with the crosslinking ratio were observed. Swelling ratios of 3.1 after 16 min, 4.7 after 10 min and 5.5 after 7 min exposure times were obtained.

The swelling kinetics were measured at temperatures below the transition temperature. The behaviour can be described with an exponential fit of the swelling ratio according to diffusion with time and a time constant determined by the diffusion coefficient, dimensions and boundary conditions. The time constant obtained varies between 6 to 8 s with crosslinking ratio at processes below the transition temperature. In accordance with the diffusion law, the miniaturization of hydrogel features yields a dramatic acceleration of the swelling process. Even porous PNIPAAm hydrogels do not obtain such low time constants (29). Up to now it was not possible to measure time constants for the transition from the swollen to the shrunken state or vice versa, because the heat transfer was limited by the heat capacity of the test chambers. Hence the time constant can only be estimated to be significantly smaller than 6 s.

## Conclusions

Water-soluble, thermosensitive photocrosslinkable polymers were synthesized through the radical copolymerization of NIPAAm with a carboxylic bearing monomer followed by polymer analogous modification with chromophores. Hydrogels with micropatterned features can be formed using these photocrosslinkable PNIPAAm-based copolymers. The properties of these polymers reveal their applicability as the functional material in microactuators. By choosing a suitable chromophore (in this comparison the acridinium salt) it is possible to obtain a fast crosslinking reaction, a good chromophore content in the photopolymer, and a critical temperature above room temperature, which is indispensable for microsystem technology due to the lack of possibilities for cooling the microsystems. Micropatterns of smart crosslinked polymers from smooth films with film thicknesses  $> 10 \mu\text{m}$ , sufficiently high resolutions and good adhesion to the substrate can be obtained when using HMDS as adhesion promoter. The dry thickness as well as the maximum swelling ratio of the micropattern can be adjusted by the irradiation process. Swelling ratios perpendicular to the substrate surface of 300 to 550 % were obtained below the transition temperature. The main advantages of these systems is that the transitions are very fast (time constants for the volume phase transition are significantly smaller than 6 s) and the time constants of the phase transition are no longer limited by the diffusion processes of the gel but by the heat capacity of the test chamber.

## Acknowledgement

The DFG (Deutsche Forschungsgemeinschaft) are gratefully acknowledged for their financial support of this work within the "Sonderforschungsbereich 287 – Reaktive Polymere" and the "Graduiertenkolleg - Struktur-Eigenschafts-Beziehungen bei Heterocyclen".

## References

1. Hoffman, A. S. *Macromol. Symp.* **1995**, *98*, 645-664.
2. Gehrke, S. H. *Adv. Polym. Sci.* **1993**, *110*, 81-144.
3. Shibayama, M.; Tanaka, T. *Adv. Polym. Sci.* **1993**, *109*, 1-62.
4. Hirotsu, S. *Adv. Polym. Sci.* **1993**, *110*, 1-26.
5. Schild, H. G. *Prog. Polym. Sci.* **1992**, *17*, 163-249.
6. Zhou, S.; Wu, C. *Macromolecules* **1996**, *29*, 4998-5001.
7. Yoshioka, H.; Mikami, M.; Mori, Y.; Tsuchida, E. *Polym. Adv. Technol.* **1993**, *4*, 519-521.
8. Nakayama, Y.; Matsuda, T. *J. Polym. Sci. A, Polym. Chem.* **1992**, *30*, 2451-2457.
9. Chujo, Y.; Sada, K.; Saegusa, T. *Macromolecules* **1990**, *23*, 2693-2696.
10. Williams, J. L. R.; Borden, D. G. *Makromol. Chem.* **1964**, *73*, 203-214.
11. Ichimura, K. *Heterog. Chem. Rev.* **1996**, *3*, 419-441.
12. Shindo, Y.; Katagiri, N.; Ebisuno, T.; Hasegawa, M.; Mitsuda, M. *Angew. Makromol. Chem.* **1996**, *240*, 231-239.
13. Cockburn, E. S.; Davidson, R. S.; Pratt, J. E. *J. Photochem. Photobiol. A: Chem.* **1996**, *94*, 83-88.
14. Chen, G.; Imanishi, Y.; Ito, Y. *Macromolecules* **1998**, *31*, 4379-4381.
15. Chen, G.; Ito, Y.; Imanishi, Y. *Macromolecules* **1997**, *30*, 7001-7003.
16. Ito, Y.; Chen, G.; Guan, Y.; Imanishi, Y. *Langmuir* **1997**, *13*, 2756-2759.
17. Lesho, M. J.; Sheppard, N. F. *Sens. Actuators B* **1996**, *37*, 61-66.
18. Hoffmann, J.; Plötner, M.; Kuckling, D.; Fischer, W.-J. *Sens. Actuators A* **1999**, *77*, 139-144.
19. Kuckling, D.; Adler, H.-J.; Arndt, K.-F.; Hoffmann, J.; Plötner, M.; Wolff, T. *Polym. Adv. Technol.* **1999**, *10*, 345-352.
20. Schinner, R.; Wolff, T.; Kuckling, D. *Ber. Bunsenges. Phys. Chem.* **1998**, *102*, 1710-1714.
21. Kuckling, D.; Adler, H.-J.; Arndt, K.-F.; Wolff, T.; Hoffmann, J.; Fischer, W.-J. *Macromol. Symp.* **1999**, *142*, 111-120.
22. Kuckling, D.; Adler, H.-J.; Arndt, K.-F.; Ling, L.; Habicher, W. D. *Macromol. Chem. Phys.* **2000**, *201*, 273-280.

23. Kuckling, D.; Ivanova, I. G.; Adler, H.-J.; Arndt, K.-F.; Wolff, T. *Polym. Prepr.* **2000**, *41*, 714-715.
24. Ichimura, K. *J. Polym. Sci., Polym. Chem. Ed.* **1984**, *22*, 2817-2828.
25. Chapman, O. L.; Lura, R. D. *J. Am. Chem. Soc.* **1970**, *92*, 6352-6354.
26. Nees, D.; Wolff, T. *Langmuir* **1996**, *12*, 4960-4965.
27. Ivanova, I. G.; Kuckling, D.; Adler, H.-J.; Wolff, T.; Arndt, K.-F. *Desig. Monom. Polym.* **2000**, *3*, 447-462.
28. Reprinted from Sensors and Actuators A, Physical 77, J. Hoffmann, M. Plötner, D. Kuckling, W.-J. Fischer, "Photopatterning of thermally sensitive hydrogels useful for microactuators", 139-144, 1999, with permission from Excerpta Medica Inc.
29. Yan, Q.; Hoffman, A. S. *Polymer* **1995**, *36*, 887-889.



## Chapter 22

# Various Interactions of Drugs with Cross-Linked Hyaluronate Gel

Chikako Yomota and Satoshi Okada

National Institute of Health Sciences Osaka, Hoenzaka 1-1-43, Chuo-ku,  
Osaka 540-0006, Japan

Hyaluronate(HA) is a biopolymer composed of repeating disaccharide subunits of N-acetyl-D-glucosamine and D-glucuronate. HA is extensively distributed in connective tissue, synovial fluid of joints and in vitreous humor of the eye. It has been extensively used as a therapeutic agent in osteoarthritis and ophthalmic surgery. Thus hyaluronate is one of the natural polymers successfully applicable to the biomedical use. The basic properties of crosslinked HA gel have been reported(1) and there are several reports of applying the HA gel to medical devices(2,3). However it is reported that due to the high swelling, the ability of the HA gel to retain other substances is not strong enough to use as a pharmaceutical reservoir(2)

Previously we noted the reports that some anionic polymer gels bind cationic surfactants(4,5). We have already reported that dodecyltrimethylammonium bromide(DOTMA) binds HA in solution cooperatively and that the binding constant is much smaller than those of other anionic polysaccharides such as chondroitin sulfate(6). Furthermore the crosslinked HA gel was observed to shrink with time in addition of DOTMA, and the weight of the gel decreased by only 2-4% of the initial weight(7). On the other hand, it is well known that many kinds of drugs have properties of surfactants, and self association (micelle) in aqueous solution have been investigated(8-13). Therefore as cationic surfactants, some drugs were expected to cause the shrinking of the HA gel. The interactions of the crosslinked HA gel with several kinds of cationic drugs were investigated, and the release of incorporated substances was measured.

## Experimental

### Materials

Hyaluronate(HA) produced by microbial fermentation using *Streptococcus zooepidemicus* was supplied by Kibun Food Chemifa Co., Ltd. as a dry powder.

The molecular weight of HA is about  $200 \times 10^4$ . Ethyleneglycol diglycidylether(EGDGE, Nippon Oil&Fats Co., Ltd.) was used as a cross-linking reagent as reported previously. All other chemicals were used without further purification. The structures of all pharmaceuticals used in this study were shown in the next page.

### Preparation of the HA gel

The HA gel was prepared as reported elsewhere. HA at 1g was dissolved in 5ml of 1N NaOH. To this solution 1.46g EGDGE in 1ml ethanol was mixed and heated at 60°C for 15 min. The obtained gel was placed into a mixture of water/ethanol (1:1v/v) and neutralized by the addition of 1N HCl, then washed with excess distilled water and stored in the refrigerator. The gel was opaque and water content was 99.8% in distilled water.

### Measurements

A cube of HA gel(2-4g) was immersed in the cationic drug solutions at 25°C, and the shrinking behavior was followed by measuring the wet weight of the gels. The contraction % of the gel was calculated by the ratio of the weight of contracted gels to that of the initial gels. The bound amount of cationic substances was calculated from their concentration in the surrounding solution. The drug concentrations were measured by RP-HPLC.

## Results and Discussion

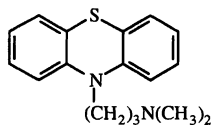
### Effect of phenothiazines on HA gel

When HA gel was immersed in the promazine solution, one of the surface active drugs, a strong contraction of the gel was observed at concentrations over 0.008M promazine, which is far below the cmc(critical micelle concentration) of promazine(0.036M)(Figure 1). As also seen in Figure 1, the presence of NaCl(0.01, 0.1M) seems to cause an increase in the minimum concentration at which the HA gel started to drastically decrease in volume. The gel reached a constant weight after 4-5 days. These findings are quite similar to those for the interactions of DOTMA and HA gel(7).

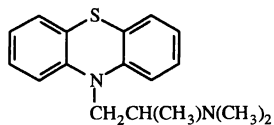
## Structure formulae of drugs

### Phenothiazines(Major tranquillizers)

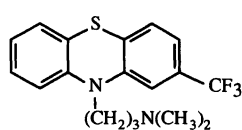
Promazine



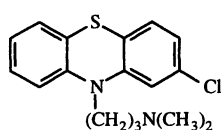
Promethazine



Triflupromazine

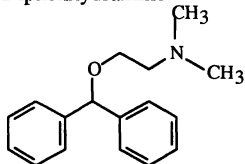


Chlorpromazine

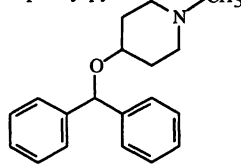


### Atihistamines

Diphenhydramine

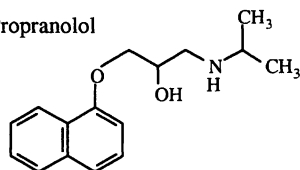


Diphenylpyraline



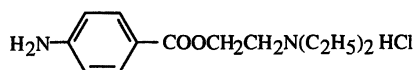
### β-Blokker

Propranolol

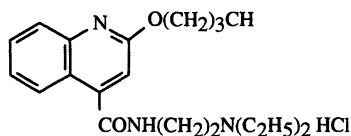


## Anaesthetics

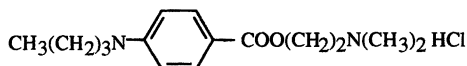
Procaine HCl



Dibcaine HCl

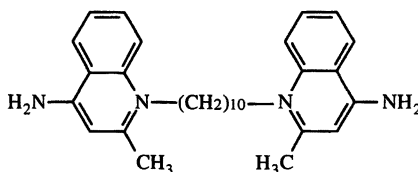


Tetracaine HCl



## Antibiotics

Dequalinium



A photo of the gels, the initial HA gel (A) and shrunk gel(B) was shown in Figure 2. The water content was decreased to be 71.4% from 99.9% as shrinking.

The interaction of polyelectrolytes with oppositely charged surfactants has been characterized to be a highly cooperative process<sup>(4,5,14,15,16)</sup>. The coulombic interaction is important in the initial step of such interactions, and the following hydrophobic interactions between the bound amphiphilic ions play a considerable role in the cooperative binding.

To elucidate the effects of drug hydrophobicity, 4 other kinds of phenothiazines, including chlorpromazine, trifluoromazine, promazine, promethazine, were also investigated according to the protocol, and the results are shown in Figure 3. The minimum drug concentration necessary to cause

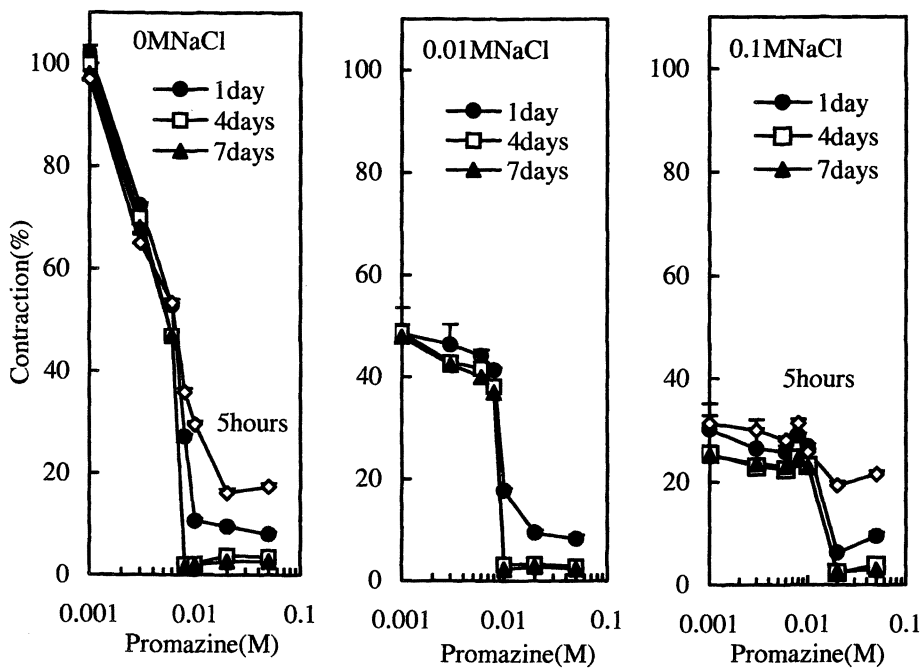


**Figure 1.** Volume contraction of the HA gel by addition of promazine.

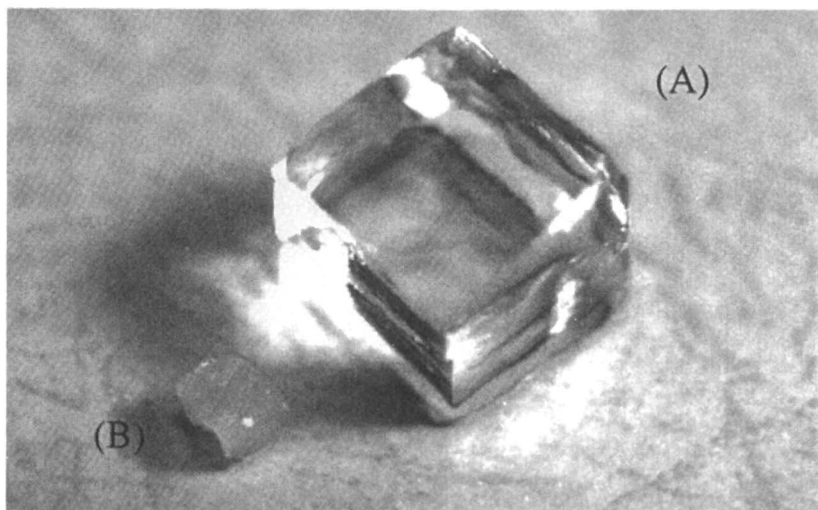


**Figure 2.** HA gels before(A) and after 7 days(B) immersed in 0.01M promazine solution.

shrinkage of the gel was highly variable among the 4 phenothiazines. Their physicochemical properties have been well studied(8,12), and the values of cmc obtained by pH measurement are listed in Table I with the minimum concentration for contraction of the HA gel(cc). As seen in Table I, the values of cmc in phenothiazines are well correlated to those for cc. From these findings, it is clear that hydrophobic interactions are also important in the contraction of the HA gel in addition to the coulombic force.

Recently the binding of chlorpromazine to 4 other anionic polysaccharides( $\kappa$ -carrageenan, dextran sulfate, alginate, and hyaluronate) was investigated by dialysis equilibrium method(17). It was noted that cooperativity in the binding was observed in all cases except for hyaluronate, which showed weak adsorption isotherms. The isotherms of chlorpromazine for hyaluronate were only below 2mM chlorpromazine and were similar to those of DOTMA for hyaluronate reported previously(6) in the low concentration range. However, in the case of DOTMA a steep increase in the binding curve for the HA solution was observed over  $4 \times 10^{-2}$ M, and that concentration corresponded to cc of DOTMA for the HA gel. Considering these finding with the fact that gel contraction was observed over in 2mM chlorpromazine as shown in Figure 3, cooperative behavior in the HA solution may be observed in over 2mM chlorpromazine.

### Effect of other cationic drugs on HA gel

Other cationic drugs that have self-association properties such as local antihistamines, anaesthetic drugs and  $\beta$ -blockers were also investigated. The findings for the addition of two antihistamines are shown in Figure 4. For comparison, the effect of NaCl was also plotted in Figure 4. In the case of diphenylpyraline, similar gel contraction to that induced by phenothiazines was observed, while the degree of shrinkage by diphenhydramine was almost equal to that by NaCl due only to the increase in ionic strength. The micelle properties of some diphenylmethane derivatives have been investigated by light scattering by Attwood et al(9), and the values of cmc for diphenhydramine and diphenylpyraline were reported to be 0.132M and 0.086M, respectively.

The results for  $\beta$ -blocker and local anesthetic drugs are shown in Figure 5. Self-association of  $\beta$ -adrenoreceptor blocking agents(10) and local anesthetic drugs(11) in water have been examined. Attwood et al reported the values of cmc for propranolol, 0.095M. As for local anaesthetic drugs, dibucaine was clearly reported to associate above 0.06M in water and the limited association of tetracaine was described using a co-operative stepwise association model(11). And no association could be detected for procaine. As can be seen in Figure 5, propranolol, tetracaine and dibucaine have the ability to interact strongly with HA gel.

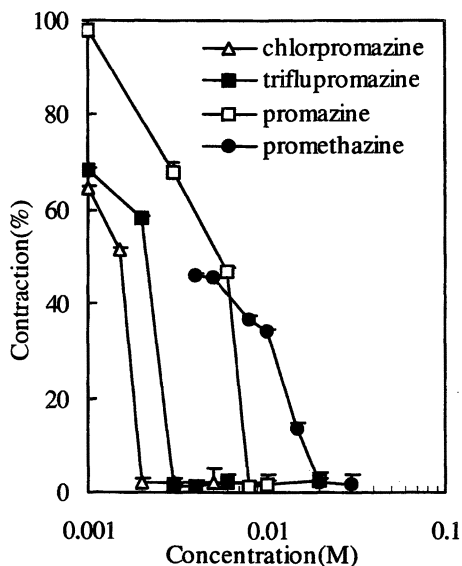


**Figure 3.** Volume contraction of the HA gel by addition of 4 kinds of phenothiazine.

**Table 1. Critical Micelle Concentration(cmc) of phenothiazines and minimum phenothiazine concentration to contract the HA gel(cc)**

phenothiazines	cmc(M)	cc(M)	cc/cmc
chlorpromazine	0.0175	0.0012	0.069
triflupromazine	0.0185	0.0028	0.151
promazine	0.036	0.0065	0.181
promethazine	0.046	0.0153	0.333

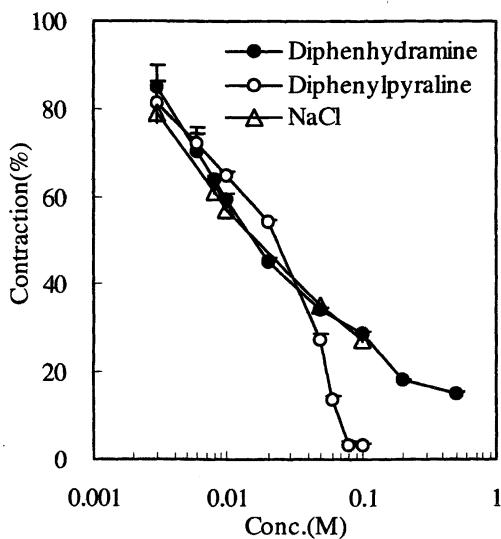


**Figure 4.** Volume contraction of the HA gel by addition of antihistamines and NaCl.

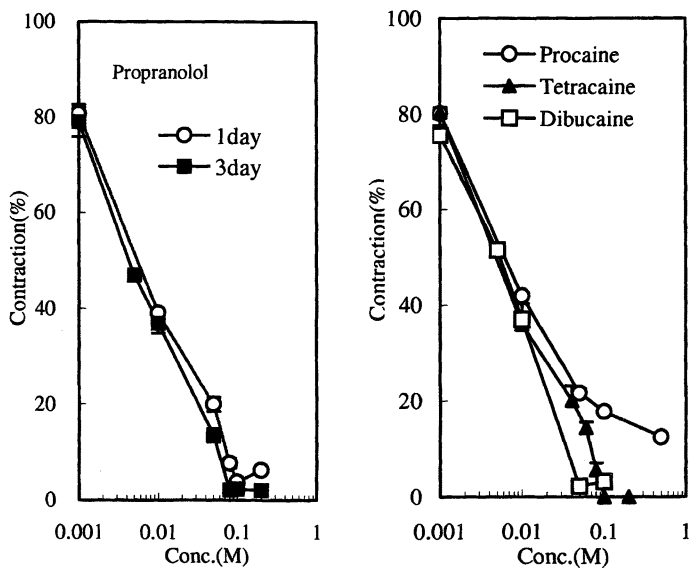


**Figure 5.** Volume contraction of the HA gel by addition of  $\beta$ -blocker and anaesthetic drugs.



## Effect of bolaform drugs to the HA gel

A series of dicationic drugs with structures resembling those of the bolaform electrolytes was also examined. The drugs are symmetrical molecules with two charge centers separated by a relatively large distance. The drugs investigated include, demecarium, distigmine and dequinium. In solution of these three drugs, HA gels were immersed, and only shrank markedly in the case of dequinium. The results obtained for dequinium are shown in Figure 6. As seen in the Figure the gel contracted at much lower drug concentrations than for other examined drugs, and the time required to finish shrinking was shorter than for any other drugs in this study. Attwood et al. have reported the properties of these drugs and determined the values of cmc for demecarium and dequinium to be  $9 \times 10^{-3}$  and  $4 \times 10^{-3}$  mol kg<sup>-1</sup>, respectively(13). However no significant association of distigmine could be detected. By comparing the cmc, dequinium can bind stronger and cause contraction of the gel faster than other drugs, due to the large hydrophobic areas. Additionally, dicationic charges in the molecule may play some role in the shrinkage. Recently it was reported that dequinium forms liposome-like aggregates upon sonication in water, and the size of vehicle was between 70-700nm(18). Dequinium has seen to have a fairly strong surface activity.

## Relationship between the hydrophobicity of drugs and the gel contraction

The structures of the drugs used in this study are very different, however considering findings on phenothiazines in Table 1, the reported values of cmc were used to estimate the hydrophobicity of the drugs (9-13). The ratios of cc/cmc for drugs that cause contraction of the HA gel in this study were plotted against the values of cmc(Figure 7). It was found that in the case of various cationic drugs, even if the electrostatic interactions are the dominant, the cooperative effect in the binding of drug to the HA gel is governed to a large degree by hydrophobic interactions among bound drug molecules, as well as between hydrophobic parts of the gel.

## Binding of promazine to the HA gel

By measuring the free concentration of promazine in the surrounding solutions by HPLC, the amount of drug bound to HA gel was calculated. The maximum amount of promazine was absorbed by the gel at a concentration of 0.008M, which corresponds to the minimum concentration needed to cause

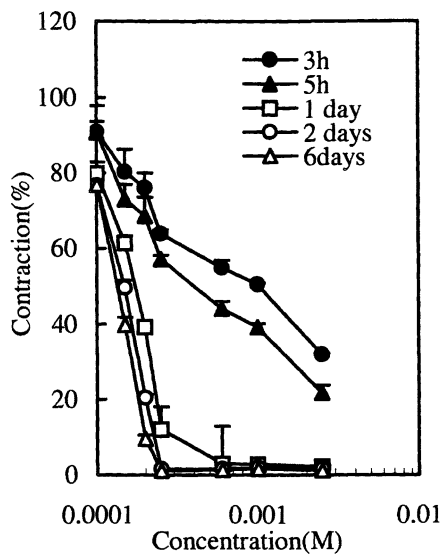


**Figure 6.** Effect of dequiniium chloride to the HA gel.

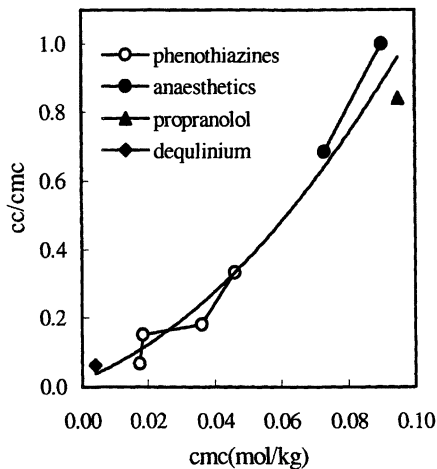


**Figure 7.** Relationship between cmc and cc/cmc.

strong gel contraction (Figure 1). The loading was almost complete after 5 hours at any concentration, and as the gel shrank some amount of drug appeared to be released.

### Release of promazine from HA gel

To clarify the effect of strong contraction of the HA gel on its retention of drugs, the release of promazine from two kinds of gel was measured. When the highly contracted HA gel loaded in over 0.01M promazine was transferred to water, only 7-10% of the absorbed promazine was released in 2 days, whereas 50-60% of trapped promazine was released from the more swollen gel obtained for lower concentrations of promazine. The strongly contracted gel is a better reservoir for cationic, small molecular weight drugs. In other words, drugs that can strongly contract the HA gel are retained well over the critical concentration necessary to contract the HA gel.

In figure 8(A), the release of promazine in several concentration of NaCl is shown. With increasing NaCl concentration, the degree of release over 20 hours increased. After 20 hours, all gel was transferred into BSA (Phosphate Buffered Saline) solution, and immediately almost 80% of the absorbed promazine was released by the change in the ionic strength. Furthermore, Figure 8(B) indicates the subsequent changes in the degree of contraction relative to the initial weight of HA gel in the experiment shown in Fig8(A). As releasing drug, the gel swelled slightly again, but only up to 13% of the initial weight in 0.01M NaCl solution, and 8-10% of that in 0.1M NaCl. As shown in Figure 3, the HA gel shrank to 50-60% in 0.01M NaCl solution, and to 20% in 0.15M NaCl solution. Therefore the contracted gel did not seem able to recover to the initial state after releasing most of the bound drug. It is suggested that some irreversible interactions in the gel may take place such as hydrophobic interactions within the HA gel network.

## Conclusions

From these findings, it was clarified that contracted HA gel can retain pharmaceuticals having the properties of cationic surfactants and release them with increases in ionic strength of the surrounding medium. The crosslinked HA gel investigated in this study was degraded by hyaluronidase and the contracted gel required a longer time for enzymatic degradation. Thus, crosslinked HA gel may be a useful biodegradable pharmaceutical reservoir.

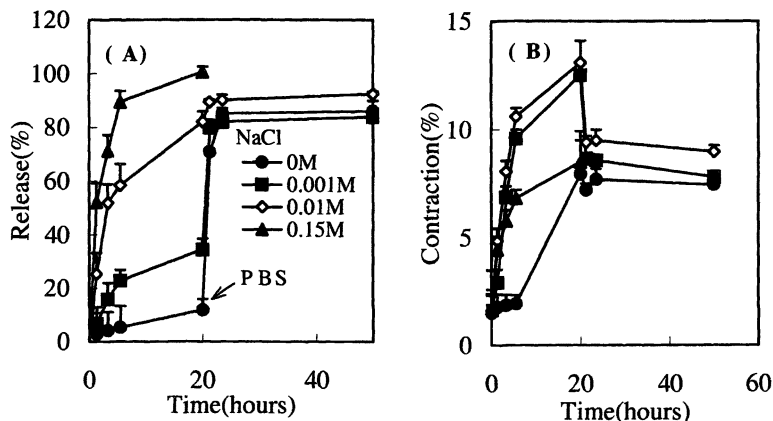


**Figure 8.** Release of promazine from the contracted HA gel(A) and corresponding gel swelling behavior(B) abruptly by switch of the ionic strength.

#### Acknowledgment.

Financial support was provided by the Japan Health Sciences Foundation.

#### References

- (1) Shah, C.B.; Barnett, S.M. *ACS Symp. Ser.*, **1992**, 480, 116
- (2) Yui, N.; Okano, T.; Sakurai, Y. *J. Controlled Release* **1992**, 22, 105.
- (3) Yui, N.; Nihira, J.; Okano, T.; Sakurai, Y. *J. Controlled Release* **1993**, 25, 133.
- (4) Okuzaki, H.; Osada, Y. *Macromolecules* **1994**, 27, 502.
- (5) Okuzaki, H.; Osada, Y. *Macromolecules* **1995**, 28, 4554.
- (6) Yomota, C., Okada, S.: Colligative Properties of Hyaluronate as a polyelectrolyte. "Biomedical Functions and Biotechnology of Natural and Artificial Polymers", Yalpani, M.; Ed.; ATL press: Shrewsbury, MA, **1996**; pp91-102.
- (7) Yomota, C., Okada, S.: Strong contraction of crosslinked hyaluronate gel by cationic drugs. "HYDROCOLLOIDS 2: FUNDAMENTALS AND APPLICATIONS IN FOOD, BIOLOGY, AND MEDICINE", Nishinari, K.; Ed.; Elsevier: Amsterdam, **1999**; pp337-342.
- (8) Nakagaki, M.; Okada, S. *Yakugakuzasshi* **1987**, 98, 1311.
- (9) Attwood, D.; Udeala, K. *J. Pharm. Pharmacol.* **1975**, 27, 395.
- (10) Attwood, D.; Fletcher, P. *J. Pharm. Pharmacol.* **1979**, 31, 392.
- (11) Attwood, D.; Fletcher, P. *J. Pharm. Pharmacol.* **1986**, 38, 494.
- (12) Attwood, D.; Fletcher, P. *J. Phys. Chem.* **1990**, 94, 6034.
- (13) Attwood, D.; Natarajan, R. *J. Pharm. Pharmacol.* **1979**, 32, 460.

- (14) Yomota, C, Ito, Y., Nakagaki, M. *Chem. Pharm. Bull.* **1987**, 35, 798.
- (15) Hayakawa, K.; Kwak, J.C.T. *J. Phys. Chem.* **1982**, 86, 3866.
- (16) Shirahama, K.; Sato, S.; Niino, M.; Takisawa, N. *Colloids and Surfaces* **1996**, 112, 233.
- (17) Caram-Lelham N.; Sundelöf L. *Biopolymers* **1997**, 41, 765.
- (18) Weissig, V.; Lasch, J.; Erdos, G.; Meyer, H. W.; Rowe, T. C.; Hughes, J. *Pharm. Res.* **1998**, 15, 334.

# Author Index

- Adler, Hans-Jürgen P., 312  
Allcock, Harry R., 82  
Ambrosio, Archel, 82  
Amiel, C., 262  
Argüelles-Monal, Waldo, 102  
Arndt, Karl-Friedrich, 312  
Bertozzi, Carolyn R., 163  
Bimendina, L. A., 137  
Bohidar, Himadri B., xi  
Busse, Karsten, 122  
Didukh, A. G., 149  
Dubin, Paul, xi  
Dutta, Naba K., 190  
Eloundou, Jean Pascal, 205  
Evans, Christopher E. B., 175  
Fenyvesi, G., 290  
Frank, Curtis W., 2  
Geissler, Erik, xv  
Gérard, Jean François, 205  
Gitsov, Ivan, 218  
Goycoolea, Francisco M., 102  
Harmon, Marianne E., 2  
Hashidzume, Akihito, 12  
Higuera-Ciapara, Inocencio, 102  
Hirata, Yoshitaka, 70  
Höring, Siegfried, 122  
Ikeda, Yuko, 70  
Kajiwara, Kanji, 70  
Kannan, P., 233  
Kennedy, J. P., 290  
Keszler, B., 290  
Kim, Sung Wan, 300  
Kim, Young Jin, 300  
Kohjiya, Shinzo, 70  
Kressler, Jörg, 122  
Kuckling, Dirk, 312  
Kudaibergenov, S. E., 137, 149  
Kulbaba, Kevin, 175  
Kushner, Aaron M., 163  
Lindemann, Brigitte, 37  
Lizardi, Jaime, 102  
Lys, Thomas, 218  
MacLachlan, Mark J., 175  
Manners, Ian, 175  
Markovic, Nov, 190  
Matisons, Jani, 190  
Mitra, A., 233  
Moldakarimov, S. B., 149  
Morishima, Yotaro, 12  
Mukkamala, Ravi, 163  
Na, S., 290  
Noda, Tetsuya, 12  
Okada, Satoshi, 325  
Oppermann, Wilhelm, 37  
Osada, Yoshihito, xi  
Pascault, Jean Pierre, 205  
Peniche, Carlos, 102  
Porcar, I., 262  
Pouliquen, G., 262  
Ravi, N., 233  
Rosenthal, K. S., 290  
Ross-Murphy, Simon B., 51  
Sigitov, V. B., 149  
Smith, Steven D., 248  
Spontak, Richard J., 248  
Szabó, B. A., 233

- Tribet, C., 262  
Urakawa, Hiroshi, 70  
van Eck, Dirk, 122  
Vögerl, Bettina, 37  
White, Scott A., 248  
Wilder, Elizabeth A., 248
- Williams, David R. G., 190  
Yomota, Chikako, 325  
Yuguchi, Yoshiaki, 70  
Zhang, L., 233  
Zhu, Chao, 218  
Zhumadilova, G. T., 137

# Subject Index

## A

Acrylates. *See* Poly(ethylene glycol)-acrylate hydrogels

Acrylic acid (AA) copolymers. *See* Interpolymer complexes (IPC)

Acrylic acid, sodium salt (AANA). *See* Polyampholyte gels

Adhesion promoter, hexamethyl disilazane, 320

Aggregation number

plot vs. molar concentration of surfactant unit in copolymers, 19, 20*f*

polymer-bound micelles, 17, 19, 21

*See also* Transient network of random copolymers

Alkali chitin. *See* Chitin

Alkylthio acrylates. *See* Hydrogel polymers from alkylthio acrylates

Aluminum soaps

gelator for hydrocarbons, 192–193  
linear assembly, 196, 197*f*

*See also* Hydrocarbon gels

Amine-epoxy systems. *See* Epoxy-amine systems

Amino-terminated tridendrons

procedure for synthesis, 221–222  
synthesis, 222–224

*See also* Amphiphilic hydrogels

Amphiphilic block copolymers in water

AFM (atomic force microscopy) and transmission electron microscopy (TEM), 124

AFM measurements on cast films, 128*f*

alkaline treatment, 127*f*

analyzing water soluble species, 129–130

applications, 122

assumption of spherical core-shell behavior, 133

corrected intensity distributions  
divided by concentration from small angle X-ray scattering (SAXS), 132*f*

dilute samples for dynamic light scattering, 131*f*

dynamic light scattering, 126  
experimental, 123–126

fluorine-19 and proton NMR measurements, 124

gold particles, 130

intensity distributions of aqueous solution of, and Ornstein–Zernicke approximation, 133*f*

intensity versus  $s$  and correlation function by SAXS, 129*f*

linear correlation function  $K(z)$ , 124, 126

2-(*N*-methylperfluorobutane-sulfamido)ethyl methacrylate (FMA) and *t*-butyl methacrylate (tBMA), 125*f*

micelles, 130, 132

monomers for sequential anionic polymerization, 125*f*

polymerization method, 123–124

preparation of aqueous polymer solutions, 124

reduced viscosity of aqueous solution of, vs. polymer concentration, 134*f*  
rheology and Wilhelmy plate method, 126

sequential block copolymerization, 127*f*



- size exclusion chromatography (SEC) measurements, 124
- size of micelles in water at 25°C by SAXS, 133*t*
- small angle X-ray scattering (SAXS), 124, 126
- solvents for casting films, 128
- surface tension of block copolymers in water at room temperature, 130*f*
- synthesis of di- and triblock copolymers, 127*f*
- synthesized di- and triblock copolymers of FMA and tBMA, 125*t*
- TEM pictures of micelle and polymer covered gold colloid, 131*f*
- thermal treatment, 127*f*
- thermolyses, 124
- transformation mechanism into water soluble species, 126, 127*f*
- triblock copolymers, 123
- Amphiphilic gels for insulin delivery
- biocompatibility, 293
  - correlation between  $M_{c,hydrophilic}$  and Stokes radius, 296*f*
  - correlation between  $M_{c,hydrophilic}$  (molecular weight of hydrophilic segment) and molecular weight cut-off, 296*f*
  - diffusion and permeability of glucose and insulin through tubular networks, 297*t*
  - experimental, 293–294
  - immunobarrier membrane synthesis, 291
  - immunoisulatory amphiphilic networks preparation, 291–292
  - methacrylate ditelechelic polyisobutylene (MA–PIB–MA) synthesis, 293
  - microarchitecture of amphiphilic networks, 292*f*
  - molecular weight cut-offs and pore size ranges, 295*t*
  - network synthesis, 293
  - permeability and diffusion studies, 295
  - permeability and diffusion studies procedure, 294
  - physical-chemical-mechanical-biological properties, 292
  - pore size determination, 294–295
  - pore size diameter method, 293–294
- Amphiphilic hydrogels
- biocompatibility of poly(ethylene glycol) (PEG), 218–219
  - characterization of hydrogels, 228–230
  - dendritic macromolecules as crosslinking agents, 219–220
  - differential scanning calorimetry (DSC) traces of dendrimer, PEG, and crosslinked product, 231*f*
  - experimental, 220–222
  - formation of poly(ethylene glycol) (PEG) hydrogels, 219
  - FT-IR spectra, 226*f*, 227*f*
  - <sup>1</sup>H NMR spectra, 224*f*
  - <sup>1</sup>H NMR spectra of dendrimer, PEG, and crosslinked product, 229*f*
  - instrumentation, 220
  - interaction of hydrophilic linear PEG with hydrophobic dendritic poly(benzyl ether), 225
  - materials, 220
  - preparation of protected monomer, 220–221
  - procedure for gel synthesis, 222
  - procedure for synthesis of amino-terminated tridendrons, 221–222
  - procedure for synthesis of cyano-terminated tridendrons, 221
  - procedure for synthesis of dendritic benzyl bromides, 221
  - swelling ratio of hydrogels from amino-terminated tridendron and PEG-diisocyanate, 230*t*

swelling ratio of hydrogels from amino-terminated tridendron and PEG-isocyanate, 230*t*  
 synthesis of amino-terminated tridendrons, 222–224  
 synthesis of hydrogels, 224, 228  
 Amphoteric macromolecules. *See* Polyampholyte gels  
 Anaesthetic drugs  
 effect on hyaluronate (HA) gel, 330  
 structures, 328  
 volume contraction of HA gel, 332*f*  
 Anionic polymerization. *See* Amphiphilic block copolymers in water  
 Antibiotics  
 effect on hyaluronate (HA) gel, 333, 334*f*  
 structure, 328  
 Antihistamines  
 effect on hyaluronate (HA) gel, 330  
 structures, 327  
 volume contraction of HA gel, 332*f*  
 Artificial tear fluid (ATF)  
 incubation of mixed hydrogels, 169–170  
 preparation, 169  
 protein absorption study, 165–166  
*See also* Hydrogel polymers from alkylthio acrylates  
 Association. *See* Photoresponsive thickening in polyamphiphile-based physical gels  
 Association behavior. *See* Amphiphilic block copolymers in water  
 Associative thickeners. *See* Transient network of random copolymers  
 Atomic force microscopy (AFM)  
 cast films of amphiphilic block copolymers, 128*f*  
 method, 124  
 microphase separation of block copolymers, 126

Azo-modified polymers. *See* Photoresponsive thickening in polyamphiphile-based physical gels

## B

Bioerosion, hydrogels, 95, 99*t*  
 Biomaterials, hydrogels, 234  
 Biomedical applications. *See* Hydrogel polymers from alkylthio acrylates  
 Biopolymers. *See* Thermoreversible and irreversible physical gels  
 Biosensors, copolymer gels, 176  
 Block copolymer solutions  
 bidisperse copolymer solutions, 254–260  
 dependence of moduli on temperature for SI/SIS solutions, 260*f*  
 dependence of steady-state viscosity ( $\eta$ ) at two shear stresses vs. concentration of copolymer in solution, 251*f*  
 dependence of  $\eta$  on shear stress ( $\tau$ ) for bidisperse SI/SIS block copolymer gels, 254, 255*f*  
 dynamic rheological measurements of SI copolymer solutions, 251  
 dynamic storage moduli as function of  $\tau$  for SIS copolymer/MO solutions, 252*f*  
 dynamic stresses identifying linear viscoelastic regime and yield as function of SIS concentration, 253*f*  
 experimental, 249  
 nanostructures, 248–249  
 network development in bidisperse mixtures, 259  
 physical gel, 249  
 poly(styrene-*b*-isoprene-*b*-styrene) (SIS) triblock and poly(styrene-*b*-isoprene) (SI) diblock preparation, 249

pure copolymer solutions, 250–252  
 steady-state viscosity ( $\eta$ ) as function  
 of  $\tau$  for SI diblock/MO solutions,  
 250*f*  
 stress dependence of dynamic moduli  
 for SI/SIS copolymer gels with  
 different concentration, 257*f*,  
 258*f*  
 temperature as function of blend  
 composition, 260, 261*f*  
 thermal response of bidisperse  
 solutions, 260  
 transmission electron micrograph of  
 micellar SIS copolymer gel  
 containing mineral oil (MO), 249*f*  
 variation of  $\eta$  with SI/SIS blend  
 composition, 254, 256  
 variation of storage moduli from  
 frequency and  $\tau$  with SIS  
 concentration, 253*f*  
 variation of storage modulus with  
 blend composition for bidisperse  
 SI/SIS solutions, 258, 259*f*  
 Block copolymers. *See* Amphiphilic  
 block copolymers in water  
 $\beta$ -Blocker  
 effect on hyaluronate (HA) gel, 330  
 structure, 327  
 volume contraction of HA gel, 332*f*  
 Bolaform drugs, effect on hyaluronate  
 (HA) gel, 333, 334*f*  
 Bond percolation model, gel point,  
 206  
 Bovine serum albumin (BSA)  
 photoresponsive viscosity in BSA-  
 based systems, 279–281  
*See also* Photoresponsive thickening  
 in polyamphiphile-based physical  
 gels  
 Broyden–Fletcher–Goldfarb–Shanno  
 (BFGS), formula, 238  
*t*-Butyl methacrylate (tBMA). *See*  
 Amphiphilic block copolymers in  
 water

## C

Carboxylate, polyphosphazenes, 92  
 Cation charge, swelling dependence  
 on, 97*f*, 98*f*  
 Chemical networks. *See* Chitosan  
 Chitin  
 alkali chitin in aqueous solution at  
 20°C, 104*f*  
 break point in Arrhenius-type plots,  
 104  
 cloud point, 104  
 cloud point curve for alkali chitin,  
 106*f*  
 estimating cloud point from  
 viscoelastic oscillatory  
 measurements, 104–105  
 gels, 103–106  
 lower critical separation phenomena,  
 106  
 lower critical solution temperature  
 (LCST), 106  
 phase separation-gelation on heating  
 to 70°C, 104*f*  
 scientific and economic interest,  
 102  
 structure, 103*f*  
 supply, 102  
 variation in optical density, ratio of  
 intensities of pyrene fluorescence  
 and complex viscosity for alkali  
 chitin, 105*f*  
 Chitosan  
 chemical networks, 107–109  
 chitosan-carrageenan PEC gels, 118–  
 120  
 critical power-law parameters at  
 rheological gel point for  $\iota$ -  
 carrageenan and  $\iota$ -  
 carrageenan/chitosan gels, 115*t*  
 critical rheological gel point, 110  
 G' and G'' of gels for  $\kappa$ -carrageenan  
 alone and in complexes, 112*f*  
 gelation curves, 107

- gel polyelectrolyte complexes (PEC), 109
- $\iota$ -carrageenan in 0.03 M KCl, 117
- $\iota$ -carrageenan in 0.25 M NaCl, 113–115
- $\kappa$ -carrageenan in 0.03 M KCl, 112–113
- $\kappa$ -carrageenan in 0.25 M NaCl, 109–112
- kinetics and rheological properties of chemically crosslinked, 109
- mechanism in association of two polyelectrolytes, 118–119
- power law relaxation behavior, 116*f*
- preparation, 102
- scientific and economic interest, 102
- spectra of gels with increasing crosslinking, 108*f*
- structure, 103*f*
- temperature dependence of  $G'$  for  $\iota$ -carrageenan in NaCl and complexes, 116*f*
- temperature dependence of  $G'$  for  $\kappa$ -carrageenan in KCl alone and in complexes, 113*f*
- temperature dependence of storage modulus ( $G'$ ) for  $\kappa$ -carrageenan in NaCl alone and in complexes with chitosan, 110*f*
- variation of  $G'$  and  $G''$  with frequency for  $\iota$ -carrageenan alone and complexes at critical gel point, 116*f*
- variation of  $G'$  on cooling and heating for  $\kappa$ -carrageenan alone and complex, 111*f*
- variation of  $\tan \delta$  with temperature on cooling at varying oscillation frequency for  $\iota$ -carrageenan in 0.25 M NaCl alone and in complexes, 114*f*
- Cloud point
- chitin gels, 104
- curve for alkali chitin, 106*f*
- estimation from viscoelastic oscillatory measurements, 104–105
- Cold set gelatin gels
- biopolymers, 62, 65
- melting behavior of mammalian and fish samples, 64*f*
- Collapse, polymer gels, 137–138
- Complexes
- confirmation, 140
- See also* Interpolymer complexes (IPC)
- Complex viscosity, alkali chitin, 105*f*
- Copolymers. *See* Amphiphilic block copolymers in water; Block copolymer solutions; Interpolymer complexes (IPC); Poly(*N*-isopropylacrylamide) copolymers; Transient network of random copolymers; Triblock copolymers for drug delivery
- Correlation length ( $\xi$ )
- influence of network density on, 39–42
- See also* Network inhomogeneities
- Creep
- hydrocarbon gels, 201, 202*f*
- See also* Poly(ethylene glycol)-acrylate hydrogels
- Critical gels. *See* Thermoreversible and irreversible physical gels
- Critical micelle concentration (cmc)
- cmc of phenothiazines and minimum concentration to contract hyaluronate gel, 331*t*
- polymer-bound micelles, 15, 17
- thickening, 269–270
- Crosslinked polymers
- smart gels, 176
- See also* Interpolymer complexes (IPC); Stimuli-responsive gels
- Crosslinking
- ceramic yield of polymer, 182
- See also* Photocrosslinking
- Crosslinks

- formation of poly(ethylene glycol) hydrogels, 219  
 free radical mechanism, 89*f*  
 polysaccharides, 57, 59  
 spectra of chitosan gels with increasing, 107, 108*f*  
 synthetic polymer gels, 51–52  
 time dependent growth, 59  
*See also* Amphiphilic hydrogels; Chitosan; Photoresponsive thickening in polyamphiphile-based physical gels; Transient network of random copolymers
- Cyano-terminated tridendrons  
 procedure for synthesis, 221  
*See also* Amphiphilic hydrogels
- Cyclodextrin polymer systems  
 features of water solutions of, at viscosity maximum, 282*t*  
 index of responsiveness, 283, 285  
 photoresponsive thickening, 281–285  
*See also* Photoresponsive thickening in polyamphiphile-based physical gels
- D**
- Dashpot. *See* Viscoelastic elements
- Debye–Bueche analysis  
 light scattering experiments, 39  
*See also* Network inhomogeneities
- Debye–Bueche model, weakly charged polymer gel, 156
- Dendritic macromolecules  
 crosslinking agents, 219–220  
 procedure for synthesis of dendritic benzyl bromides, 221  
*See also* Amphiphilic hydrogels
- Dequiniun, effect on hyaluronate (HA) gel, 333, 334*f*
- Deswelling. *See N*-Isopropylacrylamide gel
- Diblock copolymers. *See* Block copolymer solutions
- Diffusion  
 constants, 6*t*  
 experiments for *N*-isopropylacrylamide gels, 4–5  
 polymer chains within gel, 5–6  
*See also N*-Isopropylacrylamide gel
- Diglycidyl ether of 1,4-butanediol (DGEBD). *See* Epoxy-amine systems
- Diglycidyl ether of bisphenol A (DGEBA). *See* Epoxy-amine systems
- Drug delivery. *See* Amphiphilic gels for insulin delivery; Poly(*N*-isopropylacrylamide) copolymers; Triblock copolymers for drug delivery
- Dynamic light scattering  
 dilute samples of amphiphilic block copolymers, 131*f*  
 method, 126
- E**
- Electrical analogy, critical exponents, 210*t*
- Electric field. *See* Polyampholyte gels
- Electrochemical studies,  
 poly(ferrocenyldimethylsilane) network, 184–185, 186*f*
- Electrolyte effect, network inhomogeneities, 47–48
- Enthalpy change on mixing, theory, 179–180
- Epoxy-amine systems  
 Arrhenius plot of gel times, 214*f*  
 behavior at gel point, 213–214  
 behavior near gel point, 214, 215*f*  
 chemical gels, 205–206

critical exponents in percolation and classical or mean field theory, 207*t*  
 experimental curves, 211–213  
 experimental procedures, 211  
 loss factor vs. time curves, 212*f*, 213*f*  
 moduli  $G'$  and  $G''$  vs. time curves, 212*f*, 213*f*  
 percolation model for gel point, 206  
 real part of complex viscosity vs. time, 212*f*  
 relations between static and dynamic exponents, 209–210  
 rheological behavior, 207–209  
 structural parameters, 206–207  
 temperatures greater than  $T_{g\infty}$  (gelation only), 211–212, 214, 216  
 temperatures lower than  $T_{g\infty}$  (gelation and vitrification), 212–213, 216–217  
 theoretical background for gel point, 206–210  
 viscosity vs. time, 212*f*  
 Equilibrium water content (EWC). *See* Hydrogel polymers from alkylthio acrylates  
 Eye, hydrogels, 234

## F

### Fish

cold set gelatin gels, 62, 65  
 melting behavior of gels, 64*f*  
 Flory, Paul, gels and gelation, 51  
 Flory–Stockmayer model, polyfunctional polycondensation, 73, 74*f*

## G

### Gelation

chitosan gels, 107  
 reversible, 268  
*See also* Epoxy-amine systems

Gelator. *See* Hydrocarbon gels  
 Gel point  
 percolation model, 206  
 relations between static and dynamic exponents, 209–210  
 rheological behavior, 207–209  
 structural parameters, 206–207  
 theory, 206–210  
*See also* Epoxy-amine systems

### Gels

chitin and chitosan, 102  
 classification, 51–52  
 formation, 51–52  
*See also* Block copolymer solutions; Chitin; Chitosan; Hyaluronate (HA) gel; Hydrocarbon gels; Inorganic/organic hybrid gel; *N*-Isopropylacrylamide gel; Photoresponsive thickening in polyamphiphile-based physical gels; Polyampholyte gels; Stimuli-responsive gels; Thermoreversible and irreversible physical gels  
 Gibbs free energy change on mixing, theory, 179–180  
 Globular proteins, heat set gels, 65–66  
 Glucose  
 diffusion and permeability through tubular amphiphilic networks, 297*t*  
 method for permeability and diffusion studies, 294  
 permeability and diffusion studies, 295  
*See also* Amphiphilic gels for insulin delivery  
 Glucose biosensors, copolymer gels, 176  
 Grafts, hydrogel films on polymer surface, 90*f*

## H

Heat set gels, globular proteins, 65–66  
 Hexamethyl disilazane, adhesion promoter, 320

- Hildebrand solubility parameter, theory, 179
- Hyaluronate (HA) gel  
 before and after immersion in promazine solution, 329*f*  
 binding of promazine to, 333, 335  
 critical micelle concentration (cmc) of phenothiazines and minimum phenothiazine concentration to contract, 331*f*  
 effect of bolaform drugs, 333, 334*f*  
 effect of cationic drugs on, 330  
 effect of phenothiazines on, 326, 328, 330  
 experimental, 325–326  
 measurements, 326  
 preparation, 326  
 relationship between hydrophobicity of drugs and gel contraction, 333, 334*f*  
 release of promazine from, 335, 336*f*  
 structures of drugs, 327, 328  
 volume contraction by addition of antihistamines and NaCl, 332*f*  
 volume contraction by addition of  $\beta$ -blocker and anaesthetic drugs, 332*f*  
 volume contraction by addition of four kinds of phenothiazine, 331*f*  
 volume contraction of, by addition of promazine, 329*f*
- Hybrid gel. *See* Inorganic/organic hybrid gel
- Hydrocarbon gels  
 aluminum soap of mixed organic acids (ALSP), 192  
 assemblies of ALSP by hydrogen bonding, 196  
 contamination, 196  
 creep measurements, 201, 202*f*  
 determining effect of contamination, 192–193  
 dynamic oscillation measurements, 196, 198
- effect of addition of polar co-solvents on viscosity of 2% ALSP/HCF (hydrocarbon fuel) gels, 199*f*  
 effect of ALSP concentration on flow properties of ALSP/HCF gels, 194*f*  
 effect of ALSP concentration on storage modulus of ALSP/HCF gels, 200*f*  
 effect of ALSP concentration on viscosity of ALSP/HCF gels, 194*f*  
 effect of ALSP concentration on zero shear and infinite shear viscosity, 197*f*  
 effect of polar contaminants, 198, 200*f*  
 effect of temperature on elasticity of gels, 201, 202*f*  
 experimental, 192–193  
 hydrogen bonding of aluminum soaps, 192  
 linear assembly of aluminum soap molecules, 196  
 managing flammable fuels, 191  
 organo-gelators, 191  
 proposed supramolecular structure of ALSP in gels, 197*f*  
 recovery of storage modulus with time, 203*f*  
 reversibility, 201, 203  
 rheological investigation, 193  
 sample preparation, 192–193  
 steady shear measurements, 193–196  
 storage modulus as function of ALSP concentration and frequency, 198, 199*f*
- Hydrodynamic size, polymers crosslinked by micelles, 21, 22*f*
- Hydrogel polymers from alkylthio acrylates  
 acrylates monomers 1–4, sulfur-containing, 165  
 artificial tear fluid (ATF), 169–170  
 biomedical applications, 163–164

- concentration of 1, 3, or 4 in pre-polymer mix vs. protein absorption in ATF, 172*f*
- concentration of 1 in pre-polymer mix vs. equilibrium water content (EWC) and protein absorption, 169*f*
- concentration of 1 (sulfoxide), 3 (sulfide) or 4 (sulfone) in pre-polymer mix vs. EWC, 171*f*
- concentration of monomer 1 or 2 in pre-polymer mix vs. EWC, 167*f*
- copolymerization of 2-hydroxyethyl methacrylate (HEMA) with ionic or polar monomers, 164
- effect of sulfur oxidation state on hydrogel properties, 170–172
- equilibrium water content (EWC), 166
- experimental, 165–166
- materials and methods, 165
- poly(HEMA) hydrogels, 164
- protein absorption on surface, 168–169
- protein absorption study, 165–166
- static contact angles of diiodomethane on hydrated HEMA hydrogel surfaces under water, 168*t*, 171*t*
- sulfur-containing polymers, 164–165
- surface atomic concentrations of mixed hydrogels of HEMA and 1 or 2 by XPS, 168*t*
- surface properties and biocompatibility, 166–167
- surfaces and bioadhesion, 167–168
- X-ray photoelectron spectroscopy (XPS), 167–168
- Hydrogels**
- bioerosion, 95, 99*t*
- biomaterials, 234
- biomedical and pharmaceutical applications, 301
- inhomogeneities, 38
- uses of polymer, 138
- See also* Amphiphilic hydrogels; Interpolymer complexes (IPC); Network inhomogeneities; Poly(ethylene glycol)-acrylate hydrogels; Poly(*N*-isopropylacrylamide) copolymers; Poly(organophosphazene) hydrogels
- Hydrogen bonding-**
- aluminum soaps, 192
- assembly of aluminum soaps, 196
- confirmation, 140
- See also* Interpolymer complexes (IPC)
- Hydrophilic polymers**
- classification, 6
- See also* *N*-Isopropylacrylamide gel
- Hydrophobe-bearing polymers (HP)**
- thickening efficiency, 262–263
- See also* Photoresponsive thickening in polyamphiphile-based physical gels
- Hydrophobically modified water soluble polymers (HMWSP)**
- applications, 122
- See also* Amphiphilic block copolymers in water
- Hydrophobic dendrimers.** *See* Amphiphilic hydrogels
- Hydrophobic hydrogels.** *See* Poly(ethylene glycol)-acrylate hydrogels
- 2-Hydroxyethyl methacrylate (HEMA)**
- copolymerization with ionic or polar monomers, 164
- structure, 165
- See also* Hydrogel polymers from alkylthio acrylates

## I

Inhomogeneities. *See* Network inhomogeneities



- Inorganic/organic hybrid gel**  
 analysis of scattering profiles, 75, 77  
 concentration of each component in reaction mixture, 72*t*  
 ET–PTMO (triethoxysilyl-terminated poly(oxytetramethylene)) and TEOS (tetraethoxysilane), 71  
 evaluated parameters as function of reaction time, 76*f*  
 evaluated parameters by curve fitting, 77  
 Flory–Stockmayer model, 73  
 network formation by small-angle X-ray scattering (SAXS), 70–71  
 observed SAXS and calculated profiles vs. reaction time, 76*f*  
 preparation of hybrid gel, 71, 72*f*  
 SAXS method, 72–73  
 scattering intensity, 73  
 schematic structure of PTMO/TEOS gel, 78*f*  
 sol-gel process, 71*f*  
 theoretical background, 73–74  
 time-resolved SAXS profiles from ET–PTMO/TEOS mixtures, 74–75  
 tree-like model for *f*-functional polycondensation and corresponding stochastic process, 74*f*
- Insulin**  
 association with zinc, 309  
 bioartificial pancreas, 290  
 characteristics of implantable biohybrid device, 290–291  
 cumulative release from ReGel™, 309*f*  
 daily release from ReGel™, 308*f*  
 delivery from triblock copolymer, 308–309  
 diabetes, 306  
 diffusion and permeability through tubular amphiphilic networks, 297*t*
- See also* Amphiphilic gels for insulin delivery; Triblock copolymers for drug delivery
- Intelligent polymer systems, interpolymer complexes, 137**
- Interpolymer complexes (IPC)**  
 acrylic acid and vinylbutyl ether (AA–VBE) copolymer preparation, 138  
 behavior of crosslinked poly(*N*-vinylpyrrolidone) and poly(acrylic acid) (CPVP and CPAA) hydrogels, 144  
 collapse phenomenon, 137–138  
 complex formation for AA/VBE and linear PVP LPVP in ethanol and DMF, 144  
 complex formation reactions, 140–141  
 composition of polyacrylic acid-crosslinked poly-*N*-vinylcaprolactam (PAA–CPVCL) complexes, 146, 147*f*  
 confirmation of complexation, 140  
 copolymer of 1,2,5-trimethyl-4-vinylethynylpiperidinol-4 and *N*-vinylpyrrolidone (TMVEP–VP), 138  
 CPVCL behavior in chloroform mixtures, 146, 147*f*  
 crosslinked and linear poly(acrylic acid) (CPAA and LPAA), 138–139  
 crosslinked and linear poly(*N*-vinylpyrrolidone) (CPVP and LPVP), 138  
 crosslinked poly(*N*-vinylcaprolactam) (CPVCL), 139  
 dependencies of reduced and intrinsic viscosities of [AA–VBE]/[LPVP] on AA content, 142*f*  
 dependencies of reduced viscosity and swelling coefficient on

- ionization degree for [AA–VBE]/[LPVP] and [AA–VBE]/[CPVP], 144, 145*f*
- dependencies of swelling coefficients and binding degree on concentration of linear [AA–VBE], 141, 142*f*
- dependencies of swelling coefficients and intrinsic viscosities of [AA–VBE]/[CPVP] and [TMVEP–VP]/[LPAA], 141, 143*f*
- dependencies of swelling coefficients of CPAA, [TMVEP–VP]/[CPAA] complexes and reduced viscosity of [TMVEP–VP]/[LPAA] on ionization degree, 144, 145*f*
- destruction and degree of ionization, 144
- destruction of polymer-polymer and gel-polymer complexes, 144
- experimental materials, 138–139
- formation of H-bonds, 140
- instrumentation, 139–140
- intelligent polymer systems, 137
- interaction of AA/VBE with CPVP in ethanol, 144, 146
- ionic bond formation, 141, 144
- polymer-polymer and gel-polymer systems, 138
- stability in water-DMSO mixtures, 141, 143, 144
- structures, 139
- uses of polymer hydrogels, 138
- Intrinsic viscosity. *See* Interpolymer complexes (IPC)
- Ionic bonds, formation in complexes, 141, 144
- Ionic strength, swelling dependence on, 97*f*, 98*f*
- Irradiation. *See* Photoresponsive thickening in polyamphiphile-based physical gels; Poly(*N*-isopropylacrylamide) copolymers
- Irreversible gels. *See* Thermoreversible and irreversible physical gels
- Isocyanate groups. *See* Amphiphilic hydrogels
- Isoprene. *See* Block copolymer solutions
- N*-Isopropylacrylamide gel
- deswelling and swelling kinetics, 6, 8
- deswelling kinetics vs. free polymer chains added, 7*f*
- diffusion constants, 6*t*
- diffusion experiments, 4–5
- diffusion of polymer chains within gel, 5–6
- experimental materials, 3
- free polymer samples, 4*t*
- gel kinetics for samples containing acrylamide (AAm) free polymer, 7*f*
- gel kinetics for samples containing NIPAAm free polymer, 9*f*
- gel synthesis, 4
- hydrophilic and thermoresponsive polymers, 6
- incorporation of free polymer chains, 10
- kinetic experiments, 4
- kinetics of fastest systems, 9–10
- NIPAAm free polymers in, 8–9
- polymer remaining in gel vs. time, 5*f*
- polymer synthesis, 3
- swelling kinetics vs. free polymer chains added, 8*f*
- volume phase transition, 3
- ## K
- Kelvin models
- combinations of viscoelastic elements, 242
- hydrophobic hydrogels, 242, 244–245

*See also* Poly(ethylene glycol)-acrylate hydrogels  
 Ketoprofen  
 release from triblock copolymers, 303–305  
 structure, 304*f*  
*See also* Triblock copolymers for drug delivery  
 Kinetics  
 deswelling and swelling of gels with free polymer chains, 6, 8  
 experiments for *N*-isopropylacrylamide gels, 4  
*N*-isopropylacrylamide (NIPAAm) free polymers in NIPAAm gel, 8–9  
 physical gels, 56–57  
*See also* *N*-Isopropylacrylamide gel

## L

Lens of eye, hydrogels, 234  
 Light scattering experiments. *See* Network inhomogeneities  
 Linear polymers. *See* Interpolymer complexes (IPC)  
 Lower critical solution temperature (LCST)  
 behavior in hydrogels, 86, 92  
 chitin, 106  
*N*-isopropylacrylamide gels, 3

## M

Macromolecules, transient associations, 262  
 Maxwell model, storage and loss modulus, 30  
 Mean field theory  
 critical exponents, 207*t*  
 structural parameters, 206–207  
 Medicine, hydrogels, 234

Methacrylate, ethylene oxide substituted  
 copolymer with sodium 2-(acrylamido)-2-methylpropanesulfonate (AMPS), 13, 16  
*See also* Transient network of random copolymers  
 Methacrylate ditelechelic polyisobutylene (MA-PIB-MA) immunobarrier membrane, 291  
 synthesis, 293  
*See also* Amphiphilic gels for insulin delivery  
 4,4'-Methylenebis[3-chloro,2,6-diethylaniline] (MCDEA). *See* Epoxy-amine systems  
 2-(*N*-Methylperfluorobutanesulfamido)ethyl methacrylate (FMA) copolymerization with *t*-butyl methacrylate (tBMA), 123–124, 125*t*  
 structure, 125*f*  
*See also* Amphiphilic block copolymers in water  
 Micelles. *See* Transient network of random copolymers  
 Microactuators, design, 313–314  
 Microencapsulation, carboxylate-bearing polyphosphazenes, 92, 94*f*  
 Micropattern, adhesion at substrate, 320, 322  
 Mooney–Rivlin equation, 237

## N

Natural polymers, gels, 102  
 Network inhomogeneities  
 correlation length ( $\xi$ ) and refractive index fluctuation ( $\langle \eta^2 \rangle$ ) vs. network density, 42*f*  
 Debye–Bueche analysis, 39

Debye–Bueche plot of data, 41f  
 Debye–Bueche plot of gels at different degrees of swelling, 45f  
 degree of swelling and NaCl concentration in swelling solution, 47, 48f  
 dependence of  $\xi$  and  $\langle \eta^2 \rangle$  on degree of swelling, 45, 46f  
 excess scattering intensity, 39  
 experimental, 38–39  
 hydrogels, 37–38  
 influence of network density on correlation length  $\xi$  and refractive index fluctuation  $\langle \eta^2 \rangle$ , 39–42  
 influence of swelling, 43, 45, 47  
 inspection of electrolyte effect, 47–48  
 light scattering experiments, 38–39  
 Raleigh ratio of gels at different degrees of swelling, 44f  
 Raleigh ratio of solutions from gels at different degrees of swelling, 44f  
 Raleigh ratio  $R(q)$ , 38–39  
 Raleigh ratio vs.  $q^2$  ( $q$  = scattering vector amplitude), 41f  
 scattering power of gels, 47, 49f  
 shear modulus  $G$  vs. nominal network density  $v_{th}$ , 40f  
 variation in degree of swelling and shear modulus with salt content of swelling solution, 43f  
 Networks. *See* Block copolymer solutions; Chitosan; Transient network of random copolymers  
 NIPAAm. *See* *N*-Isopropylacrylamide gel; Poly(*N*-isopropylacrylamide) copolymers

## O

Optical density  
 alkali chitin, 105f

*See also* Cloud point  
 Ordered block copolymers. *See* Block copolymer solutions  
 Organophosphazenes. *See* Poly(organophosphazene) hydrogels  
 Ornstein–Zernike model, weakly charged polymer gel, 154, 156  
 Oscillatory shear measurements, physical gels, 52–56

## P

Pancreas, bioartificial, 290  
 Particles. *See* Photoresponsive thickening in polyamphiphile-based physical gels  
 Patterning  
 growth of layer thickness during irradiation of photopolymer, 321f  
 poly(*N*-isopropylacrylamide) copolymers, 320–322  
 Percolation model  
 critical exponents, 207t  
 gel point, 206  
 relations between static and dynamic exponents, 209–210  
 rheological behavior, 207–208  
 structural parameters, 206–207  
*See also* Epoxy-amine systems  
 Persistent chain model, polyampholyte gels, 154, 157t  
 Phase diagram, gelation temperature vs. concentration, 66, 67f  
 Phase separation, chitin, 104  
 Phase transitions. *See* Interpolymer complexes (IPC)  
 Phenothiazines  
 critical micelle concentration (cmc) and minimum concentration to contract hyaluronate (HA) gel, 331t  
 effect on HA gel, 326, 328, 330  
 structures, 327

- volume contraction of HA gel, 331 *f*  
*See also* Hyaluronate (HA) gel;  
 Promazine
- pH gradient  
 formation under action of DC electric field, 156, 158  
 measurement, 152, 153 *f*  
 pH oscillation of amphoteric gel  
 induced by DC electric field, 160, 161 *f*  
*See also* Polyampholyte gels
- Phosphazenes. *See*  
 Poly(organophosphazene)  
 hydrogels
- Photocrosslinking  
 general structure of  
 photocrosslinkable temperature sensitive polymers, 315 *f*  
 hydrophilic polymers, 314  
*See also* Poly(*N*-isopropylacrylamide) copolymers
- Photoresponsive thickening in polyamphiphile-based physical gels  
 affinity of pendant groups for particles, 270, 272  
 associating water soluble polymers, 273, 275  
 associations of macromolecules, 262  
 breakage of connectivity, 270  
 change upon irradiation of UV-visible spectrum of azo-modified poly(acrylic acid) in water, 276 *f*  
 composition of azo-modified poly(acrylic acid) by NMR and UV-vis, 274 *t*  
 critical micellar concentration (CMC), 269  
 disruption of association, 270  
 examples of pendant groups/particle molar ratios at optimum thickening and disruption of connectivity, 271 *t*  
 features of modified polymer water solutions with  $\beta$ -cyclodextrin ( $\beta$ CD)-EP particles at viscosity maximum, 282 *t*  
 hydrophobe-bearing polymers (HP), 262–263  
 index of photoresponsiveness, 283, 285  
 irradiation by UV or visible light, 275, 277  
 low-shear viscosity of hydrophobically modified polymer/crosslinkers mixtures, 266 *f*, 267 *f*  
 optimal thickening efficiency, 269  
 particle/polymer stoichiometry, 268–273  
 photoresponsive and associating polymers, 273–279  
 photoresponsive viscosity in bovine serum albumin (BSA)- or sodium dodecyl sulfate (SDS)-based systems, 279–281  
 polymer/particle associations, 263–264  
 possible scenario of gelation in mixed particle/polymer systems, 265 *f*  
 relative amplitude of variation of viscosity upon irradiation as function of  $\beta$ CD-EP/polymer ratio, 284 *f*  
 reptation approach, 272–273  
 reversible gelation demands, 268  
 structure of azo-modified polymer, 276 *f*  
 supplementing azo-modified polymer solutions with connector particles, 277, 279  
 systems containing  $\beta$ -CD polymers, 281–285  
 thickening and molar ratio of crosslinker hosts/pendant guest groups, 270, 272  
 thickening scenario, 264, 268  
 transient associations, 262

- transient network approach, 272–273
- UV absorption of azo-modified poly(acrylic acid) solution in water vs. irradiation time, 278*f*
- variation of viscosity as function of irradiation time, 280*f*
- variation of viscosity at constant polymer concentration as function of colloid/azo-modified polymer ratio, 278*f*
- variations of viscosity of azo-modified polymer solutions as function of  $\beta$ CD-EP/polymer ratio, 282*f*
- pH response
- swelling dependence on, 97*f*, 98*f*
  - See also* Poly(organophosphazene) hydrogels
- Physical gels. *See* Photoresponsive thickening in polyamphiphile-based physical gels
- Poly(acrylic acid) (PAA). *See* Interpolymer complexes (IPC); Photoresponsive thickening in polyamphiphile-based physical gels
- Polyamphiphile-based physical gels. *See* Photoresponsive thickening in polyamphiphile-based physical gels
- Polyampholyte gels
- acid and base content in copolymer gels, 153*t*
  - collapsing-swelling behavior, 150
  - correlation lengths by fitting model to experimental curves, 156, 159*t*
  - Debye–Bueche model, 156
  - dependence of pH on distance for glass electrodes on cathode or anode, 159*f*
  - dualistic behavior, 150
  - experimental, 150–152
  - external electric current application, 150
  - formation of pH gradient under acid of DC electric field, 156, 158
  - FTIR spectra, 152
  - internal structure as function of pH, 156
  - measurement of pH gradient, 152, 153*f*
  - model for weakly charged polymer gel, 154, 156
  - model of persistent chains, 154, 157*t*
  - Ornstein–Zernike model, 154, 156
  - oscillation of mass in applied external DC electric field, 158, 160
  - pH oscillation of, induced by DC electric field, 160, 161*f*
  - possible application for protein separation and purification, 160, 162
  - power law behavior, 154
  - purification and identification of VAEE (vinyl-2-aminoethyl ether), 150–151
  - small-angle X-ray scattering, 155*f*
  - structure, 152, 154, 156
  - synthesis and characterization of crosslinked (co)polymers, 151–152
  - wide angle X-ray spectroscopy (WAXS) vs. pH, 155*f*
  - zones of gel specimen, 159*f*
- Poly(benzyl ether) dendrimers. *See* Amphiphilic hydrogels
- Polycondensation, Flory–Stockmayer model, 73, 74*f*
- Poly(DL-lactide-*co*-glycolide) (PLGA). *See* Triblock copolymers for drug delivery
- Polyelectrolyte complexes (PEC)
- chitosan-carrageenan PEC gels, 118–120
  - $\iota$ -carrageenan in 0.03 M KCl, 117
  - $\iota$ -carrageenan in 0.25 M NaCl, 113–115
  - $\kappa$ -carrageenan in 0.03 M KCl, 112–113
  - $\kappa$ -carrageenan in 0.25 M NaCl, 109–112

- See also* Chitosan
- Polyelectrolytes, hydrophobically modified, associative properties, 13
- Poly(ethylene glycol)-acrylate hydrogels  
 biocompatibility, 234–235  
 Broyden–Fletcher–Goldfarb–Shanno (BFGS) formula, 238  
 characterization of hydrogels, 236–237  
 characterization of monomers, 235  
 combinations of viscoelastic elements, 242  
 creep experimental data of hydrogel sample HG-98-00-02, 243*f*  
 determination of elastic modulus ( $E$ ), 240*f*  
 determination of mechanical properties, 237–238  
 determination of shear modulus ( $G$ ), 241*f*  
 experimental, 235–238  
 four parameter model for hydrophobic hydrogels, 245*t*  
 generalized linear viscoelastic model, 237–238  
 hydrogel preparation, 235–236  
 materials, 235  
 mechanical properties, 239, 242, 244–245  
 Mooney–Rivlin equation, 237  
 Mooney Rivlin plot for HG-98-00-02, 241*f*  
 Raman spectra of monomer and hydrogels, 238–239, 240*f*  
 Raman spectroscopy method, 237  
 synthesis of hydrophobic hydrogels, 236  
 viscoelastic elements fitted to creep data for HG-98-00-02, 244*t*
- Poly(ethylene glycol) (PEG)  
 formation of hydrogels, 219
- See also* Amphiphilic hydrogels;  
 Triblock copolymers for drug delivery
- Polyferrocenes. *See* Stimuli-responsive gels
- Polyferrocenylsilanes  
 crosslinked networks, 180–182  
 solubility parameter of poly(ferrodimethylsilane), 182–183  
 solubility parameter range, 180  
 synthesis of poly(ferrocenyldimethylsilane)-polycarbosilane network, 178  
 synthesis of poly(ferrocenyl-*n*-propylsilane)-polycarbosilane network, 179  
 thermal copolymerization, 177  
*See also* Stimuli-responsive gels
- Polymer gels  
 collapse, 137–138  
*See also* Network inhomogeneities
- Polymer networks  
 incorporation of transition metals, 176  
 swelling characteristics, 184  
 viscoelastic behavior, 27, 30, 33  
*See also* Transient network of random copolymers
- Polymer/particle association  
 photoresponsive thickening, 263–264  
*See also* Photoresponsive thickening in polyamphiphile-based physical gels
- Polymerization, anionic. *See* Amphiphilic block copolymers in water
- Poly(*N,N*-dimethylacrylamide)-1-polyisobutylene. *See* Amphiphilic gels for insulin delivery
- Poly(*N*-isopropylacrylamide) copolymers  
 adhesion of micropatterned features at substrate, 320, 322

- balance between
  - hydrophobic/hydrophilic interactions, 314
- chromophore of photopolymers, 316
- composition and thermal properties of prepolymers and photopolymers, 316*t*
- development of micropatterns, 320, 321*f*
- general structure of
  - photocrosslinkable temperature sensitive polymers, 315*f*
- growth of layer thickness during irradiation of photopolymer film, 321*f*
- influence of solvent on crosslinking behavior, 319*t*
- microsystem technology, 313–314
- patterning, 320–322
- photocrosslinking, 316–317, 319
- prepolymer preparation, 314–315
- relative UV absorption vs. irradiation time of photopolymers, 319*f*
- smart hydrogels, 313
- swelling, 322–323
- swelling kinetics, 323
- synthesis, 314–316
- temperature dependent swelling
  - behavior of gel dots of photopolymer with different irradiation times, 322*f*
- thermal properties of photopolymers, 316
- variation of UV absorption spectrum during photoinduced gelation of photopolymer films, 318*f*
- Poly(*N*-vinylcaprolactam) (PVCL).
  - See* Interpolymer complexes (IPC)
- Poly(organophosphazene) hydrogels
  - alkyl ether-substituted polymers, 86, 92
  - background, 82–86
  - bioerosion, 95, 99*t*
  - carboxylate-bearing
    - polyphosphazenes, 92
    - combination hydrogel synthesis, 96
    - combination hydrogel system, 92, 95
    - combination of two systems, 83*f*, 84*f*, 85*f*
    - crosslinking by free radical mechanism, 89*f*
    - degree of swelling vs. degree of crosslinking, 91*f*
    - dependence of swelling on pH, cation charge, and ionic strength of medium, 97*f*, 98*f*
    - grafting thin films of hydrogels to polymer surfaces, 90*f*
    - hydrolysis sensitizing side groups, 99*t*
    - lower critical solution temperature (LCST) behavior, 86
    - microencapsulating human cells or proteins, 94*f*
    - molecular structure of
      - polyphosphazene platform, 86
    - poly(carboxyphenoxyposphazene) (PCPP), 92
    - polymer types using sodium salts of alkyl ether alcohols, 86, 88*t*
    - preparation technique, 86, 87
    - purpose, 82
    - reactions for preparing carboxylate-bearing polyphosphazenes, 93
  - Poly(oxytetramethylene) (PTMO). *See* Inorganic/organic hybrid gel
  - Polysaccharides, chemical
    - crosslinking, 57, 59
  - Poly(styrene-*b*-isoprene) (SI)
    - copolymers
    - dynamic rheological measurements of SI solution, 251
    - preparation, 249
    - See also* Block copolymer solutions
  - Poly(styrene-*b*-isoprene-*b*-styrene) (SIS) copolymers
    - dynamic rheological measurements of SIS solution, 251–252, 253*f*
    - preparation, 249



transmission electron micrograph of  
SIS gel, 249*f*  
*See also* Block copolymer solutions  
Power law behavior, polyampholyte  
gels, 154  
Promazine  
binding to hyaluronate (HA) gel,  
333, 335  
effect on HA gel, 326, 328, 330  
HA gels before and after immersion  
in, 329*f*  
release from HA gel, 335, 336*f*  
structure, 327  
volume contraction of HA gel by  
addition of, 329*f*  
*See also* Hyaluronate (HA) gel  
Protein absorption. *See* Hydrogel  
polymers from alkylthio acrylates  
Protein deposition, material surfaces,  
168–169  
Protein separation, amphoteric gels,  
160, 162  
Proteins, heat set gels from globular,  
65–66

## R

Raleigh ratio  
light scattering experiments, 38–39  
*See also* Network inhomogeneities  
Raman spectroscopy  
method, 237  
spectra of monomers and  
poly(ethylene glycol)-acrylate  
hydrogels, 238–239, 240*f*  
Random copolymers. *See* Transient  
network of random copolymers  
Reduced viscosity. *See* Interpolymer  
complexes (IPC)  
Refractive index fluctuation  $\langle \eta^2 \rangle$   
influence of network density on, 39–  
42  
*See also* Network inhomogeneities

Reptation, thickening of  
particle/polymer, 272–273  
Responsive gels. *See* Stimuli-  
responsive gels  
Reversibility, hydrocarbon gels, 201,  
203  
Rheology  
theory, 207–209  
*See also* Block copolymer solutions;  
Epoxy-amine systems;  
Hydrocarbon gels  
Ring-opening polymerization (ROP)  
polyferrocenes, 176  
*See also* Stimuli-responsive gels  
Rouse model  
critical exponents, 210*t*  
relations between static and dynamic  
exponents, 209–210  
rheological behavior, 207–208  
theory vs. experimental, 215–216  
*See also* Epoxy-amine systems  
Rubber elasticity theory, extension to  
transient networks, 30

## S

Salt  
crosslinking junctions, 33  
*See also* Transient network of  
random copolymers  
Scattering experiments. *See* Network  
inhomogeneities  
Shear rate dependent solution  
viscosity, polymers crosslinked by  
micelles, 24, 27  
Small-angle X-ray scattering (SAXS)  
corrected intensity distributions  
divided by concentration for  
amphiphilic copolymers by SAXS,  
132*f*  
intensity vs. scattering vector  $s$  and  
correlation function of amphiphilic  
block copolymer, 129*f*

- method, 72–73, 124, 126  
network formation, 70–71  
size of micelles, 132, 133*t*  
time-resolved profiles during sol-gel process, 75*f*  
*See also* Amphiphilic block copolymers in water;  
Inorganic/organic hybrid gel
- Smart gels  
crosslinked networks, 176  
design of microactuators, 313–314  
microsystems, 313  
*See also* Poly(*N*-isopropylacrylamide) copolymers
- Sodium 2-(acrylamide)-2-methylpropanesulfonate (AMPS) copolymers with substituted methacrylate, 13, 16  
*See also* Transient network of random copolymers
- Sodium dodecyl sulfate (SDS) photoresponsive viscosity in SDS-based systems, 279–281  
*See also* Photoresponsive thickening in polyamphiphile-based physical gels
- Sol-gel process  
preparation of hybrid gel, 71, 72*f*  
schematic, 71*f*  
time-resolved small angle X-ray scattering, 75*f*  
*See also* Inorganic/organic hybrid gel
- Sol-gel transition  
copolymer (triblock) of poly(ethylene glycol) (PEG) and poly(DL-lactide-*co*-glycolide) (PLGA) (PEG–PLGA–PEG), 302–303  
PLGA–PEG–PLGA triblock, 306–308
- Solubility parameter  
determination technique, 180  
poly(ferrocenyldimethylsilane), 182–183  
theory, 179–180  
*See also* Stimuli-responsive gels
- Solution viscosity, shear rate dependent, polymers crosslinked by micelles, 24, 27
- Spironolactone  
release from triblock copolymers, 303–305  
structure, 304*f*  
*See also* Triblock copolymers for drug delivery
- Spring. *See* Viscoelastic elements
- Steady shear solution viscosity, polymers crosslinked by micelles, 21, 24
- Stimuli-responsive gels  
controlled potential electrolysis of network, 177–178  
crosslinked  
poly(ferrocenyldimethylsilane) networks, 180–182  
electrochemical studies of 5b, 184–185  
enthalpy change on mixing, 179–180  
experimental, 177–179  
experimental details for preparation of polymer networks, 178*t*  
Gibbs free energy change of mixing, 179–180  
Hildebrand solubility parameter, 179  
incorporation of transition metals into polymer networks, 176  
monomer preparation, 177  
oxidation of network, 186*f*  
poly(ferrocenyldimethylsilane), 177  
relationship between swelling ratio of poly(ferrocenyldimethylsilane) and solubility parameter of solvents, 183*f*  
ring-opening polymerization of ring-tilted [1]ferrocenophanes, 176  
smart gels, 176  
solubility parameter determination technique, 180

solubility parameter of  
poly(ferrocenyldimethylsilane),  
182–183

swelling studies of 6, 184

synthesis of  
poly(ferrocenyldimethylsilane)-  
polycarbosilane network 5a,  
178

synthesis of poly(ferrocenyldi-*n*-  
propylsilane)-polycarbosilane  
network 6, 179

theory, 179–180

thermogravimetric analysis traces of  
homopolymer and crosslinked  
networks, 182*f*

Styrene. *See* Block copolymer  
solutions

Sulfur containing monomers. *See*  
Hydrogel polymers from alkylthio  
acrylates

Surfactant moieties  
sodium 2-(acrylamido)-2-  
methylpropanesulfonate (AMPS)  
with, 13, 16  
*See also* Transient network of  
random copolymers

Swelling  
degree in hydrogel vs. degree of  
crosslinking, 91*f*  
dependence of hydrogels, on pH,  
cation charge, and ionic strength  
of medium, 95, 97*f*, 98*f*  
influence on network  
inhomogeneities, 43, 45, 47  
polymer networks, 184  
poly(*N*-isopropylacrylamide)  
copolymers, 322–323  
swelling ratio of hydrogels from  
amino-terminated tridendron with  
poly(ethylene glycol)-isocyanates,  
230*t*  
*See also* *N*-Isopropylacrylamide gel

Swelling coefficients. *See*  
Interpolymer complexes (IPC)

## T

Temperature  
dependence of moduli on, for block  
copolymer solutions, 260  
effect on elasticity of hydrocarbon  
gels, 201, 202*f*  
transition, as function of blend  
composition, 260, 261*f*

Tetraethoxysilane (TEOS). *See*  
Inorganic/organic hybrid gel

Thermoresponsive gels  
classification, 6  
*See also* *N*-Isopropylacrylamide gel

Thermoreversible and irreversible  
physical gels  
balance between linear and branched  
chain growth, 65  
chemical crosslinking of  
polysaccharides, 57, 59  
cold set gelatin gels from alternative  
sources, 62, 65  
critical gels, 57, 59–62  
cusp-like discontinuity for linear  
viscoelastic strain at gel point, 63*f*  
dynamic shear rheometry vs. time,  
66  
frequency spectra, 60*f*, 61*f*  
gel classification, 51–52  
 $G'$  vs. time kinetic behavior, 58*f*  
heat set gels from globular proteins,  
65–66  
kinetic aspects, 56–57  
low frequency plateau of storage  
modulus  $G'$ , 53, 54*f*  
mechanical spectrum of biopolymer  
hydrogel, 55*f*  
melting and gelling temperature and  
proportion of imino acid residues,  
62  
melting behavior for mammalian and  
fish samples, 64*f*  
phase diagram of gelation  
temperature vs. concentration, 67*f*

- rheological characterization by oscillatory shear measurements, 52–56
- rheological gel point, 57
- strain dependence of strong and weak gels, 56
- stress relaxation modulus at gel point, 57
- terminal zone, 53
- time dependent growth of crosslinking, 59
- viscosity and entanglements, 53
- Thermosensitive polymers. *See* Poly(*N*-isopropylacrylamide) copolymers
- Thickening
- hydrophobe-bearing polymers (HP), 262–263
- See also* Photoresponsive thickening in polyamphiphile-based physical gels
- Transient network, thickening of particle/polymer, 272–273
- Transient network of random copolymers
- absorption maximum for pyrene ratio of 337 to 334 nm, 16*f*
- aggregation numbers ( $N_{\text{agg}}$ ) for polymer-bound micelles, 19, 21
- AMPS (sodium 2-(acrylamido)-2-methylpropanesulfonate) and methylacrylate substituted with  $\text{HO}(\text{CH}_2\text{CH}_2\text{O})_m\text{C}_{12}\text{H}_{25}$  ( $\text{C}_{12}\text{E}_m$ ) ( $\text{DEmMA}$ ), 13, 16
- apparent critical micelle concentration (cmc) and aggregation number for polymer-bound micelles, 15–21
- associative thickener (AT) polymers, 12–13
- balance of intra- and interpolymer associations, 13
- characteristics of AMPS– $\text{DEmMA}$  copolymers, 14*t*
- cmc and  $K_v$  values vs. surfactant comonomer contents, 18*f*
- cmc definition, 15
- crosslinking junctions and salt concentrations, 33
- dependence of viscosity on shear rate at varying salt concentrations, 26*f*
- determining aggregation numbers of dodecyl groups, 17, 19
- estimating plateau modulus ( $G^0$ ) and terminal relaxation time ( $\lambda$ ) as function of salt concentration, 31*f*, 32*f*
- experimental, 14–15
- fluorescence decay method, 15
- fluorescence decay profiles, 17, 19
- $G^0$  and  $\lambda$ , 30
- hydrodynamic size of polymers crosslinked by micelles, 21, 22*f*
- Maxwell model, 30
- measurement methods, 15
- $N_{\text{agg}}$  vs. molar concentration of surfactant unit in copolymers, 20*f*
- polymer synthesis and characterization methods, 14
- quasielastic light scattering (QELS) method, 15
- ratio of pyrene concentration in micellar and aqueous phases vs. polymer concentration, 18*f*
- relaxation time distributions in QELS, 22*f*
- reversible crosslinking, 27
- reversible disruption and reformation of crosslinks under shear, 28*f*
- rheological measurement method, 15
- rubber elasticity theory extending to, 30
- salt-dependent viscosity, 21, 24
- shear rate-dependent solution viscosities of polymers crosslinked by micelles, 24, 27
- solutions behaving as viscoelastic liquid, 27, 30

- spacer between hydrophobe and polymer backbone, 13
- steady shear solution viscosities of polymers crosslinked by micelles, 21, 24
- steady-state fluorescence method, 15
- storage ( $G'$ ) and loss ( $G''$ ) moduli vs. angular frequency, 29*f*
- viscoelastic behavior, 27, 30, 33
- zero shear viscosities for copolymers at varying polymer concentrations vs. salt concentration, 25*f*
- zero-shear viscosity, 21, 24
- zero shear viscosity at 25°C vs. polymer concentration, 23*f*
- zero shear viscosity in relation to  $G^0$  and  $\lambda$ , 30, 33
- Transition metals, incorporation into polymer networks, 176
- Transmission electron microscopy (TEM)  
method, 124
- micelle of amphiphilic block copolymers, 131*f*
- polymer covered gold colloid, 131*f*
- Triblock copolymers. *See* Amphiphilic block copolymers in water; Block copolymer solutions
- Triblock copolymers for drug delivery  
ABA of polyethylene glycol (PEG) and poly(DL-lactide-*co*-glycolide) (PLGA) (PEG-PLGA-PEG), 301–302
- BAB triblock of PLGA-PEG-PLGA (ReGel™), 306
- biomedical and pharmaceutical applications, 301
- cumulative insulin release from ReGel™, 309*f*
- daily insulin release from ReGel™, 308*f*
- drug delivery by PLGA-PEG-PLGA, 308–309
- drug hydrophobicity and release profile, 305
- drug release of ketoprofen and spironolactone, 303–305
- insulin, 306
- insulin association with zinc, 309
- insulin delivery by PLGA-PEG-PLGA, 308–309
- ketoprofen release from PEG-PLGA-PEG hydrogel, 305*f*
- schematic of hydrogel formation in PLGA-PEG-PLGA, 307*f*
- sol-gel transition curve of ReGel™ aqueous solution by UV spectrometer, 307*f*
- sol-gel transition for ABA triblock, 302–303
- sol-gel transition of PLGA-PEG-PLGA, 306, 308
- spironolactone release from PEG-PLGA-PEG hydrogel, 305*f*
- structures of ketoprofen and spironolactone, 304*f*
- 1,2,5-Trimethyl-4-vinylethynylpiperidinol-4 (TMVEP) copolymers. *See* Interpolymer complexes (IPC)
- Tubules. *See* Amphiphilic gels for insulin delivery
- U**
- Ultraviolet irradiation. *See* Photoresponsive thickening in polyamphiphile-based physical gels
- V**
- 1-Vinyl-2-aminoethyl ether (VAEE) purification and identification, 150–151
- See also* Polyampholyte gels

- Vinylbutyl ether (VBE) copolymers.  
*See* Interpolymer complexes (IPC)
- N*-Vinylpyrrolidone (VP) copolymers.  
*See* Interpolymer complexes (IPC)
- Viscoelastic behavior  
polymer networks, 27, 30, 33  
*See also* Poly(ethylene glycol)-  
acrylate hydrogels; Transient  
network of random copolymers
- Viscoelastic elements  
combinations, 242  
creep data for hydrophobic hydrogel,  
244*t*  
hydrophobic hydrogels, 244–245  
*See also* Poly(ethylene glycol)-  
acrylate hydrogels
- Viscosities. *See* Interpolymer  
complexes (IPC)
- Viscosity, complex, alkali chitin,  
105*f*
- Visible light irradiation. *See*  
Photoresponsive thickening in  
polyamphiphile-based physical  
gels
- Vitrification. *See* Epoxy-amine  
systems
- Volume phase transition. *See N*-  
Isopropylacrylamide gel
- X**
- X-ray photoelectron spectroscopy  
(XPS)  
surface analysis, 167–168  
surface atomic concentrations of  
mixed hydrogels, 168*t*  
*See also* Hydrogel polymers from  
alkylthio acrylates
- Z**
- Zero shear viscosity  
polymers crosslinked by micelles,  
21, 24, 25*f*  
*See also* Transient network of  
random copolymers